

**Charles University in Prague**  
**Faculty of Science**  
Department of Cell Biology  
Study program: Developmental and Cell Biology



## **Modulation of the STING signalling pathway**

*Modulace STING signální dráhy*

**Ing. et Ing. Lenka Vaneková**

DOCTORAL THESIS

Scientific Supervisor: doc. Ing. Václav Veverka, Ph.D.

Consultants: Ing. Andrea Brázdová, Ph.D.

Mgr. Gabriel Birkuš, Ph.D.

Prague 2022





This dissertation describes my original work except where acknowledgement is made in the text. It is not substantially the same as any work that has been or is being submitted to any other university for any degree, diploma, or any other qualification.

Prague, 14.11.2022

.....

Ing. et Ing. Lenka Vaneková



## ACKNOWLEDGEMENTS

First and foremost, I would like to sincerely thank my supervisor doc. Ing. Václav Veverka, Ph.D. for his insightful advice, support, and guidance during my Ph.D. study.

My deepest gratitude belongs to my mentor Ing. Andrea Brázdová, Ph.D. for her infinite unwavering support, patience, and guidance regardless of the day and time. Her immense knowledge and experience have encouraged me countless times during my academic research. Without her enthusiasm, passion, and her belief in me I would have never finished this thesis.

I wish to extend my thanks also to Mgr. Gabriel Birkuš, Ph.D. for introducing me to drug discovery, giving me the opportunity to be part of his multidisciplinary team working on interesting and current topics, his counsel and for acquiring funding for such financially demanding research. This thesis was supported by Gilead Sciences, Inc. (Targeting STING for Treatment of CHB and Cancer, Gilead Sciences Research Center (GSRC-3), 2016 – 2021, Birkus G.) and the European Regional Development Fund, OP RDE (Project “Chemical biology for drugging undruggable targets” Chem-BioDrug, No.CZ.02.1.01/0.0/0.0/16\_019/0000729).

I would also like to express my many thanks to HBV Cure team at Institute of Organic Chemistry and Biochemistry of the Czech Academy of Sciences, especially a few of my favourite colleagues and fellow students Ing. Zdeněk Vavřina for (not only) his mathematical, statistical, and biochemical support, Mgr. Markéta Pimková Polidarová, Ph.D. and Mgr. Barbora Novotná for their help, support, and valuable insights to our research.

My sincere thanks also belong to my physiotherapist and dear friend Mgr. Tereza Macková for her support and tremendous knowledge of human body. Without her

magic fingers, I would not be physically able to finish half of this thesis. My gratitude continues with my dear friends Ing. Petra Soušková and Ing. Šárka Císařová for always being my rocks. Finally, I am deeply grateful to my beloved parents Ing. Marie Vaneková and Ing. Karol Vanek, my brother soon-to-be-attorney-at-law Martin Vanek and my partner Ing. Pavel Pícha for their endless love, patience, support, and encouragement at all times.

## ABSTRACT

cGAS-STING signalling pathway plays the key role in the host immune defence in diverse pathologies including, autoimmune and autoinflammatory diseases, cancer, senescence and ageing, pathogen infection, i.e., bacterial, viral infection, such as hepatitis B (HBV). HBV infection can result in either an acute or a chronic type (CHB), both of wide range of immune invading mechanism potentially leading to liver cirrhosis, steatosis, or hepatocellular carcinoma. Currently, two available CHB therapies are approved, both of which rarely result in the complete cure and often require life-long application.

The development and validation of novel CHB therapeutics relies on suitable CHB animal models. The main goal of this theses was to develop a mouse model reflecting CHB based on hydrodynamic injection suitable for robust preclinical testing of novel CHB therapeutics. Two delivery systems were compared, adeno-associated plasmid vector (pAAV) and minicircle construct, encoding HBV genomes of two genotypes (A or D) with introduced point mutation in the START codon of the polymerase in two immunocompetent mouse strains, C57Bl/6 and C3H/HeN. Persisting expression of viral antigens was observed only in the C3H/HeN mice when using pAAV construct encoding HBV genome of genotype A with introduced T2308C point mutation in the START codon of the polymerase preventing formation of viral progeny. Developed mouse model reflecting CHB was used to study and identify the most effective CHB therapeutics based on natural cyclic dinucleotide - STING interaction and activation together with immune response induction. Our lead compound chosen based on *in vitro* screening from a large library of novel STING agonists exclusively prepared at the Institute of Organic Chemistry and Biochemistry

of the Czech Academy of Sciences showed outstanding results in CHB mouse model as monotherapy which makes it interesting for clinical studies.

## ABSTRAKT

cGAS-STING signální dráha hraje klíčovou roli v imunitní obraně hostitele proti různým patologiím včetně autoimunitních a autozánětlivých onemocnění, rakoviny, senescenci a patogenních infekcí, a to jak bakteriálních, tak virových (např. virus hepatitidy B (HBV)). Infekce virem HBV může vyústit buď v akutní či chronickou formu (CHB) s širokým rozsahem imunitních invazivních mechanismů vedoucích až k jaterní cirhóze, steatóze nebo hepatocelulárnímu karcinomu. V současné době jsou schváleny dvě CHB terapie, z nichž obě zřídka vedou k úplnému vyléčení a často vyžadují celoživotní aplikaci.

Vývoj a validace nových CHB terapeutik závisí na výběru vhodného *in vivo* modelu. Hlavním cílem této práce bylo vyvinout CHB myší model vhodný pro robustní preklinické testování nových terapeutik založený na hydrodynamické injekci. Byly porovnávány dva transportní systémy, adeno-asociovaný plazmidový vektor (pAAV) a minikruhový konstrukt kódující HBV genomy dvou genotypů (A nebo D) se zavedenou bodovou mutací ve START kodonu polymerázy u dvou imunokompetentních myších kmenů, C57Bl/6 a C3H/HeN. Přetrvávající exprese virových antigenů byla pozorována pouze u myšího kmene C3H/HeN při použití pAAV konstruktů kódujícího HBV genom genotypu A se zavedenou bodovou mutací T2308C ve START kodonu polymerázy bránící tvorbě virového potomstva. Vyvinutý CHB myší model byl použit následně ke studiu a identifikaci nejúčinnějších CHB terapeutik založených na aktivaci STING proteinu přirozeným cyklickým dinukleotidem. Naše hlavní sloučenina vybraná na základě *in vitro* testování velké knihovny nových agonistů STING exkluzivně připravených na Ústavu organické chemie a biochemie AV ČR vykazovala skvělé výsledky v CHB myším modelu jako monoterapie, proto by mohla být vhodným kandidátem pro klinické studie.

## **ABBREVIATIONS**

<b>AAV</b>	adeno-associated virus
<b>AGS</b>	Aicardi-Goutières syndrome
<b>AIM2</b>	absent in melanoma 2
<b>AMP</b>	adenosine monophosphate
<b>Banf1</b>	barrier-to-autointegration factor 1
<b>BAX</b>	IRF3 - BCL-2 associated X gene
<b>BRCA2</b>	breast cancer gene 2
<b>CARD</b>	caspase recruitment domain
<b>cccDNA</b>	covalently closed circular DNA
<b>CDN</b>	cyclic dinucleotides
<b>cGAS</b>	cyclic GMP-AMP synthase
<b>CHB</b>	chronic hepatitis B
<b>CLR</b>	C-type lectin receptor
<b>CpG</b>	cytosine-phosphate-guanine
<b>DAMP</b>	damage-associated molecular pattern
<b>dsDNA/RNA</b>	double stranded DNA/RNA
<b>DSF</b>	differential scanning fluorimetry
<b>EC<sub>50</sub></b>	half maximal effective concentration
<b>EMA</b>	European Medicines Agency
<b>ENPP1</b>	ectonucleotide pyrophosphatase/phosphodiesterase 1
<b>ER</b>	endoplasmic reticulum
<b>ERGIC</b>	ER-Golgi intermediate compartment
<b>ERIS</b>	endoplasmic reticulum interferon stimulator
<b>FC</b>	flow cytometry
<b>FDA</b>	U.S. Food and Drug Administration



<b>G3BP1</b>	Ras-GTPase - activating protein binding protein 1
<b>GA</b>	Golgi apparatus
<b>GMP</b>	guanosine monophosphate
<b>HBc/s/eAg</b>	HBV core/surface/e antigen
<b>HBsAb</b>	antibody against HBsAg
<b>HBV</b>	hepatitis B
<b>HDI</b>	hydrodynamic injection
<b>i.p.</b>	intraperitoneal
<b>IFN</b>	interferon
<b>IFNAR</b>	interferon- $\alpha$ receptor
<b>IHC</b>	immunohistochemistry
<b>IKK<math>\epsilon</math></b>	inhibitor of NF- $\kappa$ B kinase $\epsilon$
<b>IRF3</b>	IFN regulatory factor 3
<b>KRAS</b>	Kirsten rat sarcoma
<b>MHC</b>	major histocompatibility complex
<b>MITA</b>	mediator of IRF3 activations
<b>mtDNA</b>	mitochondrial DNA
<b>NET</b>	neutrophil extracellular trap
<b>NF-<math>\kappa</math>B</b>	nuclear factor kappa B
<b>NK cells</b>	natural killer cells
<b>NLR</b>	NOD-like receptor
<b>NLRC3</b>	NLR family CARD-containing 3
<b>NOD</b>	nucleotide-binding oligomerization domain
<b>NPC</b>	non-parenchymal cells
<b>NTCP</b>	sodium taurocholate co-transporting polypeptide
<b>pAAV</b>	adeno-associated plasmid vector

<b>PAMP</b>	pathogen-associated molecular pattern
<b>PBMC</b>	peripheral blood mononuclear cells
<b>pgRNA</b>	pregenomic RNA
<b>pMC</b>	minicircle
<b>PRR</b>	pattern recognition receptor
<b>RA</b>	rheumatoid arthritis
<b>rcDNA</b>	relaxed circular DNA
<b>RLR</b>	retinoic acid-inducible gene I-like receptor
<b>RNASEH2</b>	RNase H2 endonuclease
<b>SAMHD1</b>	SAM domain and HD domain-containing protein 1
<b>SASP</b>	senescence-associated secretory phenotype
<b>SAVI</b>	STING-associated vasculopathy
<b>SCAP</b>	sterol regulatory element-bindingprotein cleavage-activation protein
<b>SEM</b>	standard error of the mean
<b>SLE</b>	systemic lupus erythematosus
<b>STING</b>	stimulator of interferon genes
<b>TBK1</b>	TANK-binding kinase 1
<b>TFAM</b>	mitochondrial transcription factor A
<b>TLR</b>	toll-like receptor
<b>TM173</b>	transmembrane protein 173
<b>TNF</b>	tumour necrosis factor
<b>TREX1</b>	three prime repair exonuclease 1
<b>TRIM38</b>	tripartite motif-containing protein 38
<b>ZZCHC3</b>	CCHC-type zinc-finger protein

## LIST OF PUBLICATIONS

### Publications included in doctoral thesis

Novotná, B., **Vaneková, L.**, Zavřel, M., Buděšínský, M., Dejmek, M., Smola, M., Gutten, O., Tehrani, Z. A., Pimková Polidarová, M., Brázdová, A., Liboska, R., Štěpánek, I., Vavřina, Z., Jandušík, T., Nencka, R., Rulíšek, L., Bouřa, E., Brynda, J., Páv, O., & Birkuš, G. (2019). Enzymatic Preparation of 2'-5',3'-5'-Cyclic Dinucleotides, Their Binding Properties to Stimulator of Interferon Genes Adaptor Protein, and Structure/Activity Correlations. *Journal of medicinal chemistry*, 62(23), 10676–10690. <https://doi.org/10.1021/acs.jmedchem.9b01062>

Dejmek, M., Šála, M., Brazdova, A., **Vanekova, L.**, Smola, M., Klíma, M., Břehová, P., Buděšínský, M., Dračínský, M., Procházková, E., Zavřel, M., Šimák, O., Páv, O., Boura, E., Birkuš, G., & Nencka, R. (2022). Discovery of isonucleotidic CDNs as potent STING agonists with immunomodulatory potential. *Structure (London, England: 1993)*, 30(8), 1146–1156.e11. <https://doi.org/10.1016/j.str.2022.05.012>

Vavřina, Z., Perlíková, P., Milisavljević, N., Chevrier, F., Smola, M., Smith, J., Dejmek, M., Havlíček, V., Buděšínský, M., Liboska, R., **Vaneková, L.**, Brynda, J., Boura, E., Řezáčová, P., Hocek, M., & Birkuš, G. (2022). Design, Synthesis, and Biochemical and Biological Evaluation of Novel 7-Deazapurine Cyclic Dinucleotide Analogues as STING Receptor Agonists. *Journal of medicinal chemistry*, 65(20), 14082–14103. <https://doi.org/10.1021/acs.jmedchem.2c01305>

**Vanekova L**, Polidarova M, Charvat V, Vavrina Z, Veverka V, Birkus G, Brazdova A. (2022) Development and characterisation of a chronic hepatitis B murine model with a mutation in the START codon of an HBV polymerase. *Physiological research*, doi:10.33549/physiolres.934979 – accepted 9.11.2022

**Vanekova, L.**, Polidarova, M. P., Veverka, V., Birkus, G., & Brazdova, A. (2022). Multiparametric Flow Cytometry-Based Immunophenotyping of Mouse Liver Immune Cells. *Methods and protocols*, 5(5), 70. <https://doi.org/10.3390/mps5050070>

## TABLE OF CONTENTS

ACKNOWLEDGEMENTS .....	5
ABSTRACT .....	7
ABSTRAKT .....	9
ABBREVIATIONS .....	10
LIST OF PUBLICATIONS .....	13
TABLE OF CONTENTS.....	14
1. INTRODUCTION .....	16
1.1. cGAS.....	18
1.2. STING.....	24
1.3. cGAS-STING pathway downstream signalling.....	29
1.4. cGAS-STING signalling pathway regulation.....	32
1.5. cGAS-STING signalling pathway in disease context.....	35
1.5.1. Autoinflammatory and autoimmune diseases.....	35
1.5.2. Senescence and ageing.....	41
1.5.3. Cancer .....	41
1.6. HBV .....	44
2. AIMS .....	51
3. METHODS .....	52
3.1. <i>In vivo</i> studies .....	52
3.1.1. <i>In vivo</i> mouse model HDI induction.....	52
3.1.2. HBV antigen secretion analysis.....	53
3.1.3. HBcAg immunohistochemistry .....	53
3.1.4. Flow cytometry (FC)-based T cell activation analysis .....	53
3.1.5. <i>In vivo</i> efficacy of lead compound.....	53
3.1.6. <i>In vivo</i> IFN- $\alpha$ receptor (IFNAR) blockade.....	54
4. RESULTS .....	55
4.1. <i>In vitro</i> characterisation of compounds and selection of lead compound using biochemical and cell-based assays.....	55
4.1.1. Background and motivation.....	56
4.1.2. Results.....	58
4.1.3. Conclusion .....	62
4.2. Development and characterisation of <i>in vivo</i> murine model reflecting CHB based on hydrodynamic injection .....	63
4.2.1. Background and motivation.....	63
4.2.2. Results.....	64
4.2.3. Conclusion .....	75

4.3.	<i>In vivo</i> preclinical evaluation of lead compound to determine its CHB therapeutic potential.....	76
4.3.1.	Background and motivation.....	76
4.3.2.	Results.....	77
4.3.1.	Conclusion .....	87
4.4.	Suggestions for additional therapy outcome evaluation .....	88
4.4.1.	Background and motivation.....	88
4.4.2.	Methodology for suggested additional evaluation.....	89
4.4.3.	Conclusion .....	92
5.	DISCUSSION.....	93
6.	CONCLUSION.....	102
7.	REFERENCES .....	104
8.	SUPPLEMENTS .....	134
8.1.	Supplement S1: Enzymatic Preparation of 2'-5', 3'-5'-Cyclic Dinucleotides, Their Binding Properties to Stimulator of Interferon Genes Adaptor Protein, and Structure/Activity Correlations.....	134
8.2.	Supplement S2: Discovery of isonucleotidic CDNs as potent STING agonists with immunomodulatory potential.....	183
8.3.	Supplement S3: Design, Synthesis, and Biochemical and Biological Evaluation of Novel 7-Deazapurine Cyclic Dinucleotide Analogues as STING Receptor Agonists .....	246
8.4.	Supplement S4: Development and characterisation of a chronic hepatitis B murine model with a mutation in the START codon of an HBV polymerase .....	290
8.5.	Supplement S5: Multiparametric Flow Cytometry-based Immunophenotyping of Mouse Liver Immune Cells .....	311

## 1. INTRODUCTION

Innate immune responses are crucial first line defence in humans against various pathogen infections, cell damage, cellular stress and/or cancer (Q. Chen et al., 2016; S. Pandey et al., 2015). Innate immune system directly recognizes pathogens via limited number of pattern recognition receptors (PRRs) resulting in general defence mechanisms (D. Cohen et al., 2019; D. Walsh et al., 2013). Subsequently in the late phase of the infection, acquired adaptive along with innate immune system is involved in pathogen clearance and is responsible for generation of immunological memory. Adaptive immunity is characterised by targeted defences highly specific to the particular agents. Yet, the innate immune system and the adaptive immune system work together to successfully eliminate threat. (A. Abbas et al., 2016; D. Schenten & R. Medzhitov, 2011)

The detection of pathogens by the innate immune system relies on sensor proteins, known as PRRs (C. A. Janeway & R. Medzhitov, 2002; H. Kumar et al., 2011; G. Mitchell & R. R. Isberg, 2017; S. Pandey et al., 2015; D. Walsh et al., 2013), interacting with molecular components referred to as molecular patterns related to pathogen (pathogen-associated molecular patterns, PAMPs) (C. A. Janeway & R. Medzhitov, 2002) or cell damage (damage-associated molecular patterns, DAMPs) (P. Matzinger, 1994). There are several types of PRRs (S. Pandey et al., 2015; D. Walsh et al., 2013), such as Toll-like receptors (TLRs), nucleotide-binding oligomerization domain (NOD)-like receptors (NLRs), retinoic acid-inducible gene I-like receptors (RLRs), C-type lectin receptors (CLRs), etc. Each PRR recognizes different PAMPs or DAMPs (C. A. Janeway & R. Medzhitov, 2002; H. Kumar et al., 2011; G. Mitchell & R. R. Isberg, 2017). TLRs, for instance, can be divided into several 12 subfamilies based on their primary sequences (S. Pandey et al., 2015). Each subfamily recognizes

distinct ligands (S. R. El-Zayat et al., 2019; T. Kawasaki & T. Kawai, 2014; R. Medzhitov, 2001; A. S. Sameer & S. Nissar, 2021) such as nucleic acids (double stranded (ds)RNA (TLR3), ssRNA (TLR7, TLR8), DNA containing cytosine-phosphate-guanine (CpG) (TLR9), flagellin (TLR5), lipopeptides (TLR1, TLR2, TLR6) or bacterial polysaccharide or viral coat proteins (TLR4). The activation of PRRs results in inducing various signalling pathways leading to the cell autonomous defence mechanisms and production of downstream immune mediators such as type I interferons (IFNs) and/or inflammatory cytokines (A. Abbas et al., 2016; C. A. Janeway & R. Medzhitov, 2002; H. Kumar et al., 2011; G. Mitchell & R. R. Isberg, 2017; D. Schenten & R. Medzhitov, 2011). Furthermore, type I IFNs play a key role primarily in anti-viral and anti-tumour defence. (A. Decout et al., 2021; X. Feng et al., 2020; T. Gong et al., 2019; K. Zhang et al., 2021)

Under physiologic conditions in eukaryotic cells, DNA occurs in nucleus and mitochondria and is absent from the cytoplasm. DNA in cytosol (viral, leaked self-DNA (Z. Dou et al., 2017; S. Glück et al., 2017; S. M. Harding et al., 2017; K. J. MacKenzie et al., 2017) or mitochondrial DNA (J. S. Riley et al., 2018)) is recognized by cytoplasmic PRR, i.e., cyclic guanosine monophosphate (GMP) – adenosine monophosphate (AMP) synthase (cGAS). Activation of cGAS results in production of 2'-5', 3'-5' cyclic guanosine monophosphate – adenosine monophosphate (2'3'-cGAMP) from ATP and GTP. 2'3'-cGAMP, the second messenger in cGAS-STING signalling pathway. cGAMP then activates stimulator of interferon genes (STING) which leads to TANK-binding kinase 1 (TBK1) recruitment, its phosphorylation and STING oligomerization inducing STING translocation from endoplasmic reticulum (ER) to Golgi apparatus (GA) via ER-Golgi intermediate compartment (ERGIC). Activation of cGAS-STING signalling induces various downstream signalizations,

such as activation of IFN regulatory factor 3 (IRF3), nuclear factor kappa B (NF- $\kappa$ B), induction of autophagy, lysosomal degradation, etc. Therefore, cGAS-STING pathway is crucial in antiviral, antibacterial and/or antitumour defence. Furthermore, malfunction of cGAS-STING signalling pathway is associated with various autoimmune and inflammatory diseases, such as Aicardi-Goutières syndrome, systemic lupus erythematosus or STING-associated vasculopathy of infancy. (X. Cai et al., 2014; K. P. Hopfner & V. Hornung, 2020) cGAS-STING pathway has, hence, become a promising immunotherapeutic target (X. Tian et al., 2022).

### **1.1. cGAS**

cGAS consists of a flexible highly basic ~160-amino-acid N-terminal domain and ~360-amino-acid C-terminal catalytic domain (L. Sun et al., 2013) containing two lobes with a zinc (Zn)-thumb sequence and an active site in their interface (Fig. 1) (F. Civril et al., 2013). Lobe I has a highly twisted core scaffold with a two alpha-helices on the outside and catalytic residues of beta-sheet nucleotidyltransferase NTases on the inside. Lobe II consists of a series of alpha-helices connected to lobe I by a spine, two linker helices and by a loop connecting lobe I outside alpha helices and beta-sheet of NTase (Fig. 1A). Zn-thumb inserted in-between lobes I and II consists of one histidine and three cysteines coordinating  $Zn^{2+}$  ion (Fig. 1B). (F. Civril et al., 2013; P. J. Kranzusch et al., 2013; X. Li et al., 2013; L. Sun et al., 2013)



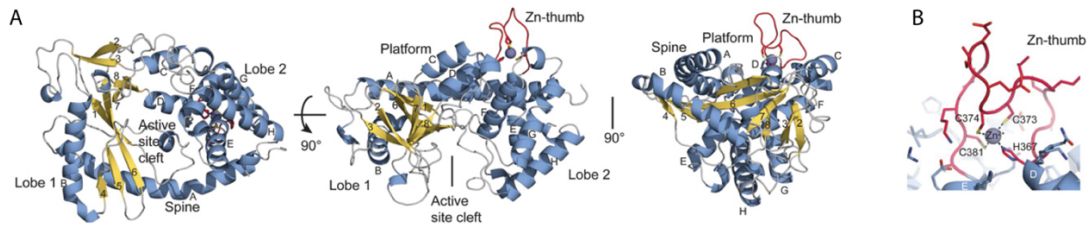


**Fig. 1: cGAS structure.** (A) side and top views of cGAS. Ribbon representation of Lobe I and II with their secondary structures, alpha-helices (blue) and beta-sheets (yellow) and a Zn-thumb (red) position in-between lobes. (B) Close view of Zn-thumb. Adapted from Civril et al., 2013.

The catalytic active site points to the outside in unbound cGAS (apo-cGAS). Once cGAS recognizes DNA, DNA binding residues of alpha-helices bind to DNA (Fig. 2). This causes conformational switch of an active site allowing further binding of the positive charged residues of alpha-helices to the phosphate-sugar backbone DNA strand and an optimal interaction with substrate (X. Zhang et al., 2014). Meanwhile, Zn-thumb mediates forming of 2:2 DNA-cGAS complex by binding each DNA to two cGAS protomers (X. Zhang et al., 2014). Then, cGAS dimers further assemble into oligomers in ladder-like networks along >40bp long dsDNA independently on sequence (R. M. Hooy & J. Sohn, 2018). Crosslink of the cGAS dimer and DNA stabilizes the active conformation of the enzyme. Activated cGAS catalyses the synthesis of 2'3'-cGAMP through utilizing ATP and GTP from substrate (A. Ablasser et al., 2013). In 2'3'-cGAMP, phosphodiester bond is located between 3'-hydroxyl group of AMP and the 5'-phosphoric group of GMP, or between the 5'-phosphoric group of AMP and the 3'-hydroxyl group of GMP (S. Srikanth et al., 2019). The 2'3'-cGAMP acts as a second messenger for STING activation. (A. Ablasser et al., 2013; E. J. Diner et al., 2013; P. Gao et al., 2013)

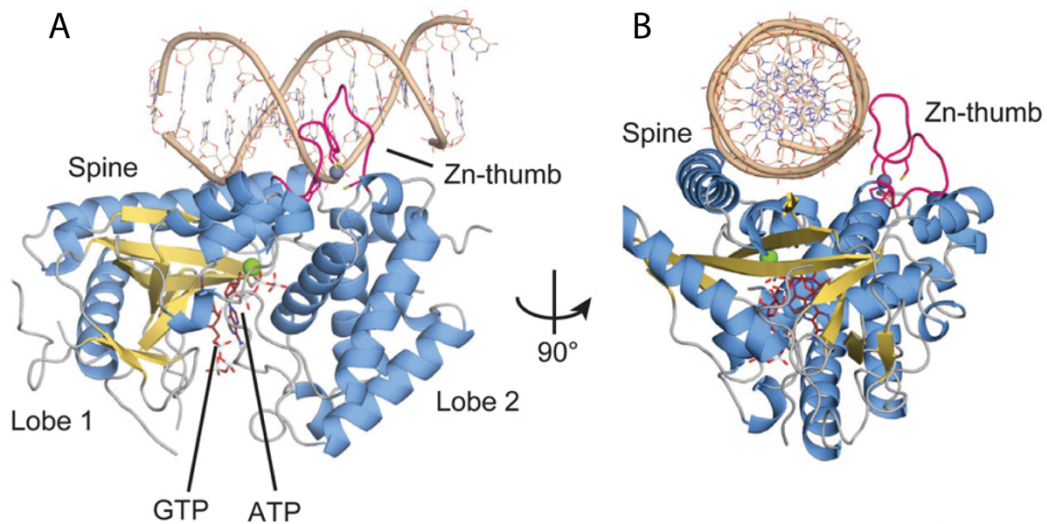


**Fig. 2: cGAS-DNA complex.** (A) Side view of complex cGAS-dsDNA utilizing ATP and GTP from substrate. DNA visualized as brown, alpha-helices of cGAS (blue) and beta-sheets (yellow) and a Zn-thumb (red) position in-between lobes. (B) Top view of dsDNA binding along the platform of cGAS between spine and Zn-thumb. Adapted from Civril et al., 2013.

cGAS was initially (F. Civril et al., 2013; P. Gao et al., 2013; X. Li et al., 2013) suggested to be a monomeric in the inactive state and dimerization of cGAS along with cGAS-DNA complex formation could be effective only when the DNA is larger than 16bp. However, later studies showed that human and mouse cGAS can form a DNA-free dimer promoted by N-terminal domain (W. Xie et al., 2019).

Sun et al., 2013 detected cGAS in cytosol and barely in nucleus. Therefore, it was presumed that cGAS is cytosolic DNA sensor with specificity mostly towards non-self-DNA with an access to nuclear or mitochondrial DNA being restricted by membranes of organelles. More recent studies (M. Gentili et al., 2019; H. E. Volkman et al., 2019; Y. Wu et al., 2022; H. Yang et al., 2017) showed that cGAS can also constitutively and perhaps preferentially reside in the nucleus and be sequestered to chromatin (Fig. 3). Furthermore, N-terminal domain of cytosolic cGAS appears to be sequestered to the inner leaflet of the plasma membrane in the steady state (Fig. 3) (K.

C. Barnett et al., 2019). The nuclear localization of cGAS was observed during mitosis and interphase after disruption of nuclear envelop (B. L. Uhlorn et al., 2020; L. Zhong et al., 2020), as well as when the N-terminal domain is disturbed (K. C. Barnett et al., 2019; M. Gentili et al., 2019). The interaction with the histones H2A-H2B of the nucleosome prevents cGAS dimerization and activation in the nucleus (J. Bai & F. Liu, 2022). Hence, the self-DNA detection is not prevented through the compartmentalization, but through the sequestering to the chromatin or plasma membrane (K. C. Barnett et al., 2019). It has also been reported that the cytosolic DNA sensing requires the export of nuclear cGAS to cytosol (H. Sun et al., 2021). However, it has not been clarified, yet how cGAS migrates between cytosol and the nucleus and more studies are of need to thoroughly describe and further clarify cGAS cellular localization and transport together with the mechanism of inactivation of nuclear cGAS while interacting with DNA (Y. Wu et al., 2022).

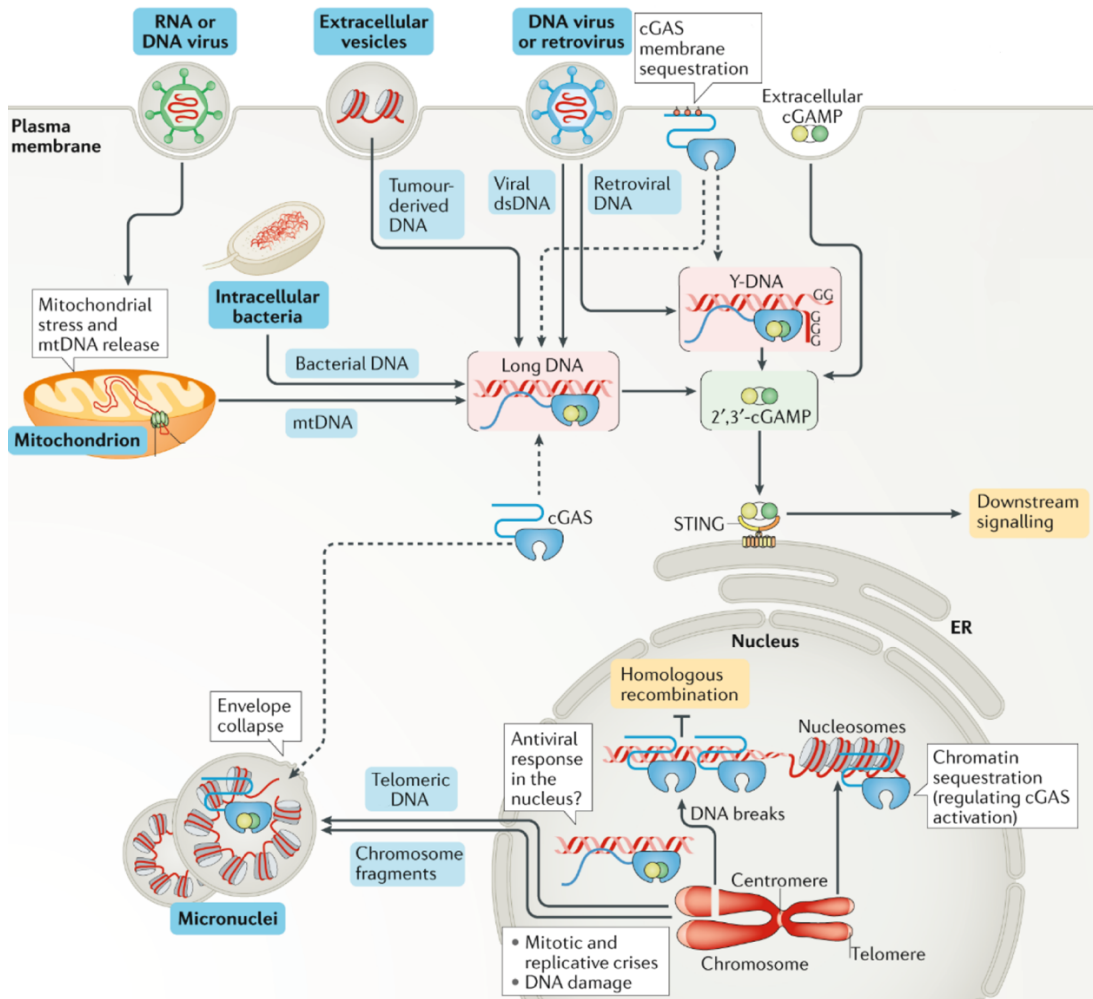


**Fig. 3: cGAS localization and activation.** cGAS is activated by various DNA of viral-, bacterial- or endogenous self-origin, mostly comprising long double-stranded (ds) DNA or other (e.g., Y-form DNA, mtDNA, chromatin fragments, micronuclei). cGAS recognizes DNA in the cytosol, however cGAS is also sequestered at the plasma membrane on the inner leaflet allowing more efficient detection of viral DNA entering the cell. In the nucleus, inactive cGAS is sequestered to chromatin in steady state raising the possibility of viral DNA sensing right in the nucleus. Additionally, nuclear cGAS may inhibit DNA repair resulting in cGAS activation. Activated cGAS catalyses the synthesis of 2'3'-cGAMP, which activates STING triggering downstream signalling. Adapted from Hopfner and Hornung, 2020.

As mentioned above, cGAS can be activated by wide range of DNAs from long dsDNA to RNA-DNA hybrids of viral-, bacterial- or endogenous self-origin (increased cell death, disturbed phagocytic digestion, leaking mitochondrial DNA (mtDNA), defective cell cycle) (Fig. 3) (L. Andreeva et al., 2017; A. M. Herzner et al., 2015; H. Konno et al., 2013; S. Luecke et al., 2017). However, with the recent discovery of cGAS nuclear localization, the pathogens might also be detected in nucleus as many viruses replicate there, which makes the viral DNA more accessible to cGAS (K. P. Hopfner & V. Hornung, 2020). Extracellular self-DNA could enter the cytosol during the above-mentioned cell death, disturbed phagocytic digestion or then via extracellular vesicles (K. P. Hopfner & V. Hornung, 2020). mtDNA leakage into the cytoplasm and activation of cGAS-STING signalling may occur when mitochondrial membrane is disturbed (Fig. 3) (J. S. Riley et al., 2018). However, the cGAS is antagonized by the effector caspases and the mtDNA leakage does not result in activation of cGAS during apoptosis (A. Rongvaux et al., 2014; M. J. White et al., 2014). Interestingly, it has been observed (A. P. West et al., 2015) that cGAS can be activated by mtDNA before the release of cytochrome c and the resulting apoptotic cell death. This mechanism could play a role in antimicrobial defence when pathogen can indirectly trigger cGAS-STING signalling pathway through leaked mtDNA by the induced mitochondrial stress (A. P. West et al., 2015). Another important source of self-DNA are cytosolic micronuclei, cytosolic chromatin and DNA from defective replication, repair, and mitosis (Fig. 3) (Z. Dou et al., 2017; S. Glück et al., 2017; S. M. Harding et al., 2017; K. J. MacKenzie et al., 2017). Moreover, cGAS also detects self-DNA from dysfunctional telomeres (Y. A. Chen et al., 2017) originating in e.g., precancerous, ageing, or senescent cells.

## 1.2. STING

STING, also known as transmembrane protein 173 (TM173), mediator of IRF3 activations (MITA) or endoplasmic reticulum interferon (IFN) stimulator (ERIS), is a transmembrane protein localized on ER (H. Ishikawa & G. N. Barber, 2008). Human population is highly heterogenous for *STING* gene. Major STING allelic variant is *WT* (*R232*) and other most common minor allelic variants with single or multiple amino acid changes are *REF* (*R232H*), *HAQ* (*R71H*, *G230A*, *R293Q*), *AQ* (*G230A*, *R293Q*), and *Q* (*R293Q*) with a wide variability across continents. (S. Patel & L. Jin, 2018) Interestingly, ~ 16% of East Asians are *HAQ/HAQ* contrary to ~ 3% of Europeans and 0% of Africans. On the other hand, ~ 4% Africans are *AQ/AQ* which is unique among ethnic populations. (R. Schumann et al., 2022) The responsiveness of allelic forms of STING towards cyclic dinucleotides (CDN) differs, e.g., STING *R232H* and *R293Q* is responsive towards 2'3'-cGAMP but not to bacterial 3'3'-CDN. Also, G230A change in *HAQ* allelic form may modify the lid region of STING and increase the stability of the STING – cyclic 3'3' di-guanosine monophosphate (3'3'-c-di-GMP) interaction. (A. Decout et al., 2021)

STING protein is composed of a short cytosolic N-terminal tail, four-span transmembrane domain, connector region, ligand binding domain, and a cytosolic C-terminal tail containing IRF3 and NF- $\kappa$ B binding sites (Fig. 4) (S. Ouyang et al., 2012; S. Qi et al., 2022).

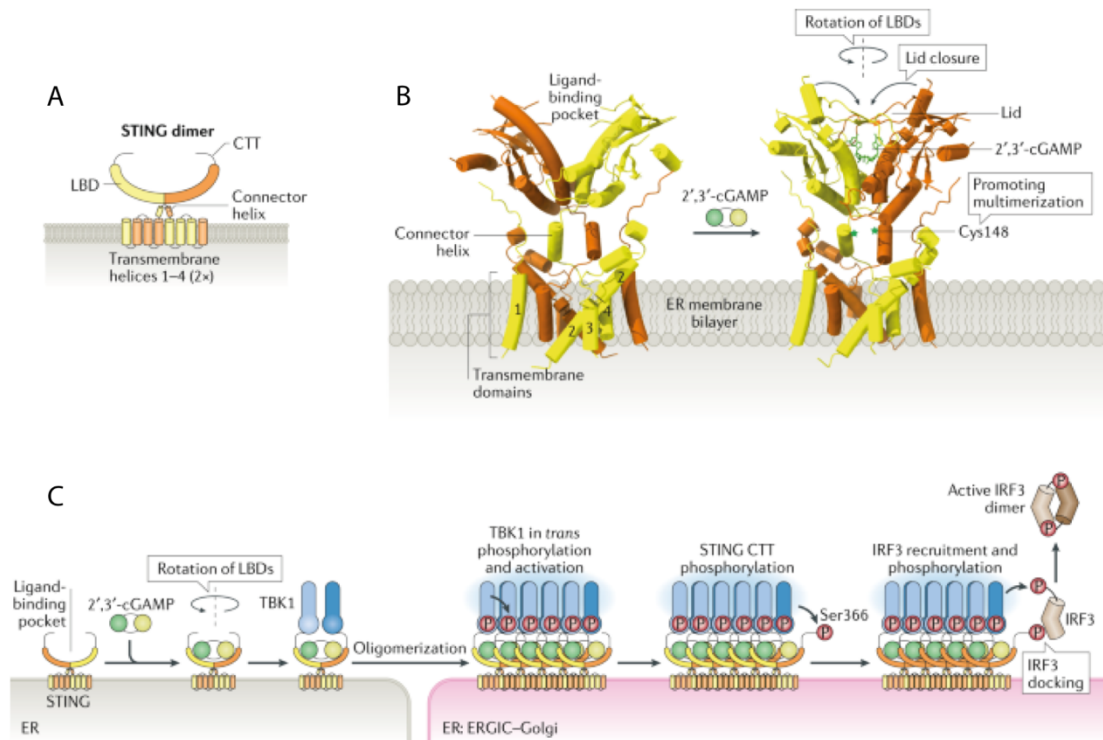


**Fig. 4: Mechanism of STING activation.** (A) Membrane-bound STING dimer with structural domains. (B) Structure of ligand-free and ligand-bound STING dimer. Binding of 2'3'-cGAMP results in the closure of the lid, rotation of ligand-binding domains and STING oligomerization. (C) Schema of the activation and translocation of STING protein. After STING binds 2'3'-cGAMP to ligand-binding pocket, extensive conformational changes occur leading to TBK1 association and STING oligomerization. Oligomerization promotes TBK1 phosphorylation and STING translocation from ER to ERGIC and GA. C-terminal tail phosphorylation and subsequent IRF3 recruitment, triggers its dimerization, and phosphorylation. Activated IRF3 is then involved in downstream signalization. Adapted from Hopfner and Hornung, 2020.

STING forms a butterfly-shaped homodimer even in the absence of ligand, ligand binding domains of both STING homodimers generate a V-shaped ligand binding pocket (Y. H. Huang et al., 2012; S. Ouyang et al., 2012; G. Shang et al., 2012; S. Srikanth et al., 2019; Q. Yin et al., 2012; X. Zhang et al., 2013). The transmembrane helices form integrated, domain-swapped architecture. The connector helices link transmembrane and ligand binding domains of STING and form a crossover in STING dimer resulting in close intermolecular interactions at the junction (S. L. Ergun et al., 2019). The cytosolic C-terminal tail contains a highly conserved TBK1-binding motif (S. Ouyang et al., 2012; B. Zhao et al., 2019), adjacent to the LxIS motif providing a docking site for IRF3 (S. Liu et al., 2015; B. Zhao et al., 2016). It was also suggested that significant amount of TBK1 is already present in the proximity of an inactive STING dimer, but phosphorylation of TBK1 may be limited only to the *cis* conformation (K. Zhang et al., 2021). Therefore, upon 2'3'-cGAMP binding to the STING protein, massive conformational switch leading to its 180° clockwise rotation, relieves the connector helices crossover and the lid structure around 2'3'-cGAMP is closed (Fig. 4) (Y. H. Huang et al., 2012; G. Shang et al., 2012). In the absence of upstream signalization, the ligand binding domain of STING can bind to C-terminal tail and provides a sophisticated autoinhibition for the signalling domain, which could be unlocked by binding of 2'3'-cGAMP (S. Qi et al., 2022). The conformational switch also makes C-terminal tail of STING more accessible to TBK1. After recruitment of TBK1 by a specific TBK1-binding motif in STING C-terminal tail, the *cis* TBK1 molecules are positioned to the close proximity of *trans* TBK1 molecules. This makes *trans* TBK1 more accessible to the catalytic centre of the *cis* TBK1 molecule leading to phosphorylation and activation of *trans* TBK1. Activated TBK1 then phosphorylates the C-terminal tail of adjacent STING dimer (S. Liu et al., 2015; G.



Shang et al., 2019; B. Zhao et al., 2019). Another important prerequisite for STING signal transduction promoted by conformational switch is the lateral oligomerization of several STING dimers. The STING oligomerization leads to induction of translocation of STING-cGAMP complex from ER to GA via ERGIC (Fig. 4) along with post-translational modifications in GA (Fig. 5) (e.g., palmytoilation of cysteine residues (S. L. Ergun et al., 2019; K. Mukai et al., 2016a), ubiquitination (Q. Li et al., 2018; T. Tsuchida et al., 2010)) (S. L. Ergun et al., 2019; G. Shang et al., 2019). The STING translocation depends on canonical coat protein complex II (COPII) anterograde transport (X. Gui et al., 2019). Interestingly, it has also been suggested (S. Qi et al., 2022) that STING could also recruit other signalling molecules than from ER or GA.

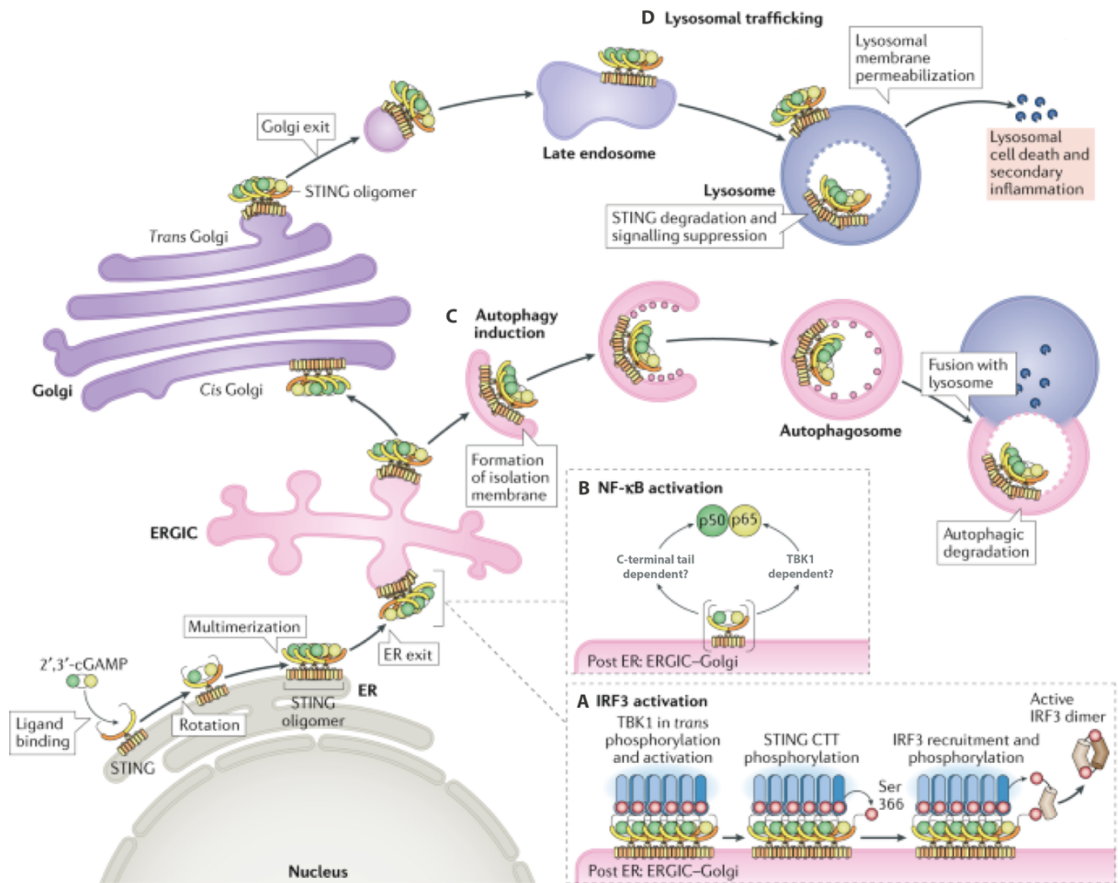


**Fig. 5: cGAS-STING signalling pathway.** As shown previously (Fig. 4), after activation of STING protein, oligomerized STING translocates to ERGIC. (A) As soon as STING reaches ERGIC, STING recruits TBK1 which phosphorylates C-terminal tail of STING. All of this leads to IRF3 recruitment and phosphorylation resulting in formation of active IRF3 dimer. (B) Another downstream signalization triggered by STING activation is unconventional signalling of NF- $\kappa$ B pathway, however it remains unknown whether TBK1 activates IKK complex or whether C-terminal tail region is responsible. (C) STING is also involved in induction of autophagy. ERGIC containing STING serve as a membrane source for autophagosome biogenesis. (D) From ERGIC STING translocates to Golgi apparatus (GA) and then through late endosomes to the lysosome designated for degradation. In some cell lines, accumulation of STING in lysosomes leads to lysosome-dependent cell death and secondary inflammatory response. Adapted from Hopfner and Hornung, 2020.

### 1.3. cGAS-STING pathway downstream signalling

The phosphorylation of C-terminal tail of STING, namely conserved residue Ser366, leads to IRF3 recruitment (J. J. Wu et al., 2020), subsequent IRF3 phosphorylation and dimerization as soon as STING oligomers reach ERGIC (Fig. 5A) (Q. Chen et al., 2016; K. P. Hopfner & V. Hornung, 2020). Activated IRF3 dimers enter the nucleus and triggers transcription of type I IFN as well as proinflammatory cytokines.

It has been reported that STING activation also triggers unconventional signalling pathway of NF- $\kappa$ B activation (Fig. 5B) (C. C. de Oliveira Mann et al., 2019), however the exact mechanism of activation remains unknown (S. Qi et al., 2022). It has been shown, that TBK1 and inhibitor of NF- $\kappa$ B kinase  $\epsilon$  (IKK $\epsilon$ ) activate the IKK complex leading by the activation of the transcription factor NF- $\kappa$ B (T. Abe & G. N. Barber, 2014; R. Fang et al., 2017). However, Qi et al. (S. Qi et al., 2022) identified a region of C-terminal tail (AA 345-357) responsible specifically for activation of NF- $\kappa$ B downstream signalling and suggested that TBK1 is not required. The unresolved question is how NF- $\kappa$ B STING region interacts with IKK for NF- $\kappa$ B activation. Alternatively, it has also been observed that STING can activate NF- $\kappa$ B downstream signalization independently of cGAS via alternative STING-p53-TNF receptor associated factor 6 (TRAF6) complex (G. Dunphy et al., 2018).

Another important STING-dependent downstream signalling separate from IFN production is an autonomous cell defence mechanism, autophagy. The autophagy together with type I IFNs play an important role in regulation of pathogen clearance, tissue damage, and immune response. STING triggers autophagy from the ERGIC and subsequently formats an autophagosome. The autophagosome than fuses with the lysosome followed by degradation (X. Gui et al., 2019). Autophagy also plays an

important role in regulation of cGAS-STING signalling activation, for instance by degradation of cGAS or STING, binding to adaptor proteins or regulation the post-transcriptional modifications of key molecules (K. Zhang et al., 2021). Damaged autophagy may lead to uncontrolled inflammation and cell death. (Q. Hu et al., 2019)

cGAS-STING pathway is involved in various types of cell death, such as apoptosis (Y. Kato et al., 2018), pyroptosis (S. Christgen et al., 2020), necroptosis (M. Brault et al., 2018; D. Chen et al., 2018), PANoptosis (S. Christgen et al., 2020; J. M. Gullett et al., 2022; Y. Messaoud-Nacer et al., 2022), lysosomal or autophagy dependent cell death (P. D. Adams et al., 2013; Q. Hu et al., 2019), all of which induce various cellular signalling pathways.

In certain cell types, STING activation can also induce a lytic cell death programme. It has been observed in human myeloid cells (M. M. Gaidt et al., 2017), that STING activation leads to its translocation to lysosomes, where the accumulation of STING triggers subsequent permeabilization of lysosomal membranes, release of lysosomal hydrolases resulting in cell death. Meanwhile, the secondary inflammatory response is triggered. Loss of plasma membrane and cellular K<sup>+</sup> efflux mediate the activation of inflammasome, and inflammatory cytokines are released (M. M. Gaidt & V. Hornung, 2018). Otherwise, it has been reported (V. K. Gonugunta et al., 2017; X. Gui et al., 2019), that STING signalization is regulated by lysosomal trafficking and degradation. STING translocates to the lysosome after exiting the GA via late endosome independently from TBK1 activation or C-terminal tail phosphorylation. Preventing this trafficking or lysosomal degradation leads to increased STING levels and antiviral gene expression.

cGAS-STING signalling pathway is engaged also in apoptosis through mitochondrial apoptosis pathway dependent on the formation of complex IRF3 - BCL-

2 associated X gene (*BAX*) (A. Sze et al., 2013). It was also described (S. Chattopadhyay et al., 2010; S. Liu et al., 2015), that IRF3-mediated apoptosis is independent on IRF3 phosphorylation, however, TBK1 phosphorylation of STING is required for IRF3 recruitment. After TBK1 phosphorylates STING and STING-TBK1 complex activates ubiquitination of IRF3, the IRF3-BAX complex is formed and the mitochondrial apoptosis pathway is induced (Y. Cui et al., 2016; K. McArthur et al., 2018). Leakage of mtDNA, in turn, activates STING-mediated inflammatory responses (S. Chattopadhyay et al., 2016; A. Sze et al., 2013). Finally, type I IFN secreted by activation of cGAS-STING, can stimulate the expression of tumour necrosis factor (TNF)-related apoptosis. (Q. Zhu et al., 2018).

Other studies reported (M. Brault et al., 2018; S. N. Schock et al., 2017), that another type of programmed immunogenic cell death dependent on STING signalling is DNA-induced necroptosis in mouse fibroblasts and bone marrow-derived macrophages. This DNA-induced necroptosis is dependent on coregulation by STING-induced TNF and type I IFN or other TNF/type I IFN-inducing stimuli (M. Brault et al., 2018; S. N. Schock et al., 2017).

Recently, a new unique concept of inflammatory cell death linking pyroptosis, apoptosis and necroptosis components called PANoptosis was described (R. K. S. Malireddi et al., 2019). All those components act simultaneously and affect each other to induce relevant host immune response related to pathogen infection (S. Christgen et al., 2020). Intervention targeting one of PANoptosis pathways may lead to compensatory response of mutual regulatory mechanisms (P. H. Ding et al., 2020). PANoptosis has been involved in various pathologies, such as bacterial or viral infection, cancer, or STING-dependent inflammatory diseases (J. M. Gullett et al., 2022; Y. Messaoud-Nacer et al., 2022).

#### 1.4. cGAS-STING signalling pathway regulation

cGAS-STING signalization can be regulated in multiple parts of the signalling pathway, starting at the regulation of the mRNA level, cGAS, production of cGAMP, regulation of STING or downstream signalling affecting cGAS-STING signalization.

Disturbed DNA replication may lead to abnormal DNA damage response and DNA accumulation in cytoplasm (R. Kreienkamp et al., 2018). DNA replication and double-strand break repair is affected, among others, by breast cancer gene 2 (*BRCA2*) tumour suppressor (X. Lai et al., 2017; T. Reisländer et al., 2019; J. Zimmer et al., 2016). The mutation in *BRCA2* gene causes DNA damage, instability of the replication fork and degradation of nucleolysis which results in the activation of innate immunity by cGAS-STING signalization. Two responses to *BRCA2* gene mutation were observed (T. Reisländer et al., 2019), early acute resulting in the cell cycle arrest and downregulation of the DNA replication and upregulation of DNA repair genes and the late response leading to the upregulation of the transcription of IFN-stimulated genes. The degradation or unwinding of DNA is regulated by three prime repair exonuclease 1 (*TREX1*) gene, coding 3'-5' DNA nucleic acid exonuclease (T. B. H. Geijtenbeek, 2010; Y. Y. Lan et al., 2014; D. B. Stetson et al., 2008; S.-S. Tao et al., 2019). *TREX1* is mainly responsible for preventing of DNA accumulation in dead cells causing autoimmune response (S.-S. Tao et al., 2019). Lysosomal degradation of DNA is regulated by both, *TREX1* and *DNase2* endonuclease. If *TREX1* or *DNase2* are damaged, DNA accumulates in the cytoplasm which results in overactivation of the cGAS-STING signalling (T. B. H. Geijtenbeek, 2010; Y. Y. Lan et al., 2014; D. B. Stetson et al., 2008). It has also been reported (C. T. Campbell et al., 2012) that mitochondrial transcription factor A (*TFAM*) maintains mtDNA functional stability and its deletion causes aberrant mtDNA accumulation in cytosol leading to induction

of inflammatory responses by the activation of cGAS-STING (K. W. Chung et al., 2019; A. P. West et al., 2015). Furthermore, inactivation of disulfide-bond-A oxidoreductase-like protein which maintains the mitochondria functional stability and integrity, also leads to mtDNA release and cGAS-STING activation (J. Bai et al., 2017). Cytosolic accumulation of dsDNA may also be caused by mutation of barrier-to-autointegration factor 1 (Banf1) which recognizes DNA and modulate basal cell-intrinsic immunity leading to expression of IFN-stimulated genes (N. Ibrahim et al., 2011; H. Ma et al., 2020).

The activity of cGAS is regulated through post-translational modification such as phosphorylation, acetylation, ubiquitination, SUMOylation, mono- or poly-glutamylated (Q. Chen et al., 2016; M. Motwani et al., 2019). The tripartite motif-containing protein 38 (TRIM38) is known as an inhibitor of the innate immune and inflammatory responses (M. M. Hu et al., 2016; M.-M. Hu et al., 2015; M. M. Hu et al., 2014). It was also reported (M. Chen et al., 2016) that upregulation of protein p62 causes K48-linked cGAS ubiquitination, as well as TRIM38 induce polyubiquitination of cGAS to induce cGAS degradation triggering immune responses. Deubiquitination of cGAS protein induced by TRIM 14, interferon-activated gene highly expressed during viral infection, leads to cGAS degradation. TRIM 38 is also responsible for stabilization of murine cGAS by SUMOylation to prevent its degradation due to viral infection (M. M. Hu et al., 2016; M.-M. Hu et al., 2015; M. M. Hu et al., 2014). cGAS can be degraded by deSUMOylation by SUMO-specific protease 2 or apoptotic caspases. cGAMP synthesis can be inhibited by apoptosis-associated speck protein (AIM2) inflammasome composed of AIM2 and caspase 1 (L. Corrales et al., 2016; V. Kumar, 2019), or by autophagy protein Beclin1 (H. Ishikawa & G. N. Barber, 2008). The presence of Beclin1 protein not only induces the inhibition of cGAMP synthesis,

moreover, increases degradation of cytoplasmic DNA. It has also been reported that cGAS is regulated by Ras-GTPase - activating protein binding protein 1(G3BP1) protein with nucleic acid helicase activity (Z. S. Liu et al., 2019). Mutation in G3BP1 negatively affects cGAMP synthesis and blocks cGAS condensation (Z. S. Liu et al., 2019). Cytoplasmic DNA recognition by cGAS protein is inhibited when the deficiency in CCHC-type zinc-finger protein (ZZCHC3) occurs (H. Lian et al., 2018). ZZCHC3 is responsible for interaction with various types of dsDNAs to activate cGAS; moreover, ZZCHC3 directly interacts with cGAS and modulates its oligomerization (H. Lian et al., 2018).

The cGAS-STING activation can also be inhibited by exo-nucleotide pyrophosphatase/phosphodiesterase family member 1 (ENPP1) which can hydrolyse extracellular ATP or 2',5'phosphodiester bond and 3',5'phosphodiester bond and thus reduce cGAMP levels (K. Kato et al., 2018; L. Li et al., 2014).

STING protein can be regulated through various post-translation modification, most importantly phosphorylation and ubiquitination (J. K. Lee et al., 2020; M. Motwani et al., 2019). TBK1 phosphorylates STING at Ser358 and 366 which leads to its activation (B. Zhong et al., 2008). However, the recruitment of TBK1 by insulin-induced gene 1 and E3 ubiquitin ligase complex leads to its polyubiquitination and degradation (Q. Li et al., 2018; Y. Wang et al., 2015; B. Zhong et al., 2009). Dimerization of STING can be enhanced by ER-associated palmitoyl transferase (Q. Zhou et al., 2014). IRF3 recruitment is affected by sterol regulatory element-binding protein cleavage-activation protein (SCAP) which interacts with STING (W. Chen et al., 2016). Poly-ubiquitination of STING by TRIM29 or TRIM30 $\alpha$  leads to STING degradation (Q. Li et al., 2018; Y. Wang et al., 2015). On the contrary, STING can be stabilized by removal of K48-linked ubiquitin chains by deubiquitinase and the



degradation can be impeded by induced SUMOylation of STING (W. Chen et al., 2016). STING palmytoilation can be inhibited by covalent modification of STING by nitro fatty acids caused by viral infection and caspase recruitment domain (CARD) of NLR family CARD-containing 3 (NLRC3) inflammatory protein can bind to STING C-terminal tail and N terminus of TBK1 leading to inhibition of STING signalization (A. L. Hansen et al., 2018a; M. Nascimento et al., 2019; L. Zhang et al., 2014; B. Zhong et al., 2009).

### **1.5. cGAS-STING signalling pathway in disease context**

The complexity of cGAS-STING signalling pathway plays the key role of the host immune defence in diverse pathologies including, autoimmune or autoinflammatory diseases, cancer, senescence and ageing or pathogen infection. The modulation of cGAS-STING signalization might represent a promising strategy in their treatment (Tab. 1, Tab. 2, Tab. 3).

#### **1.5.1. Autoinflammatory and autoimmune diseases**

Monogenic autoinflammatory diseases such as Aicardi-Goutières syndrome (AGS) or STING-associated vasculopathy (SAVI) are associated with mutations in genes that participate in DNA maintenance. AGS is a rare genetic disease associated with nucleic acid sensing or metabolism. (Y. J. Crow & N. Manel, 2015) AGS mainly affects nervous, immune system and the skin. It is characterised by early onset of encephalomyelitis. Other symptoms may include skin lesions (chilblains), joint and muscle spasticity, involuntary muscle twisting and contractions, microcephaly, or inflammation in the cerebrospinal fluid (A. Shapson-Coe et al., 2019). Mutations of *TREX1* and genes encoding RNase H2 endonuclease subunits (RNASEH2A, RNASEH2C, SAM domain and HD domain-containing protein 1 (SAMHD1)) leading to loss of gene function are associated with failure of self-DNA metabolism and

overactivation of cGAS-STING signalling pathway (M. Benitez-Guijarro et al., 2018; A. Cristini et al., 2022; A. Shapson-Coe et al., 2019). Deficiency in AGS-associated genes in mice showed that inhibition of cGAS-STING activity or knock-out of STING genes reverses the pathogenesis (A. Gall et al., 2012; D. Gao et al., 2015; E. E. Gray et al., 2015). Elevated type I IFN levels were also observed in DNase2 knock-out mice which results in severe anaemia and embryonic death of animal (M. P. Rodero et al., 2017). DNA is recognized by TLR9 in the phagosome and cGAS-STING pathway is activated, which results in the prevention of disease onset and development in cGAS or STING and DNase2 double knock-out mice (J. Ahn et al., 2012; D. Gao et al., 2015).

Self-activation of STING can be caused by gain-of function mutations. SAVI is a severe autoinflammatory disease with onset in infancy caused by the mutation in STING. The clinical manifestation includes ulcerative skin lesions, fever, and interstitial lung disease. (S. Balci et al., 2020; N. Jeremiah et al., 2014; B. Lin et al., 2020) Six mutated residues were discovered in SAVI patients localized to the dimerization interface (N154S, V155M, V147L, G207E, R281Q, R284G, R284S) (S. L. Ergun et al., 2019; N. Jeremiah et al., 2014; S. Keskitalo et al., 2019; H. Konno et al., 2018; Y. Liu et al., 2014; I. Melki et al., 2017; R. G. Saldanha et al., 2018). In the absence of the ligand, STING mutants may be activated either by inducing spontaneous rotation of the ligand binding domain along the connector helix loop or spontaneous polymerization of STING (S. L. Ergun et al., 2019; G. Shang et al., 2019). These mutations also cause spontaneous trafficking of STING to GA and activation of the downstream signalization; however, mutants N154S, V155M, V147L are located in perinuclear membrane which enables STING direct access to TBK1 and subsequent IRF3 phosphorylation (N. Riteau et al., 2022).

Another mutation involved in cGAS-STING signalization leading to monogenic autoimmune disorder is caused by mutation in *COPA* gene encoding the COP $\alpha$  protein of the COPI complex. COPI complex mediates the binding, sorting and transport of proteins from GA to the ER and engages in intra-GA transport. The mutation in *COPA* gene causes defects in proteins retrieval to ER leading to an aggregation and spontaneous ligand-independent activation of STING in GA. (Z. Deng et al., 2020; S. Volpi et al., 2018; L. B. Watkin et al., 2015) Patients suffering from COPA syndrome have symptoms similar to SAVI, such as increased type I IFN levels in blood (A. Lepelley et al., 2020). It has been shown that crossing COPA mutant mouse with STING-deficient mice blocks type I IFN-driven inflammation and reduces embryonic lethality of COPA<sup>-/-</sup> mice. It has also been reported that either genetic or pharmacological interference with STING can reduce the type I IFN levels. (Z. T. Al-Salama & L. J. Scott, 2018; M. C. Genovese et al., 2016; S. Krutzke et al., 2020)

The self-DNA recognition and type I IFN secretion can associate cGAS-STING signalling pathway with chronic system autoimmune diseases such as systemic lupus erythematosus (SLE) or rheumatoid arthritis (RA). The aberrant cGAS-STING signalling engages in SLE through various pathological mechanisms such as dysregulation of endogenous retroelements, defects in extracellular removal of apoptotic cells, replication of mtDNA defects or accumulation of neutrophil extracellular traps (NETs) from dying neutrophils (E. D. Batu, 2018). It has been reported that overreaction of cGAS-STING activity leading to the increased levels of type I IFNs may accelerate the symptoms such as systemic inflammation, mucosal ulceration or liver and kidney damage (Y. Kato et al., 2018). Additionally, many patients with mutant-type allele of *TREX1* suffering from SLE have increased levels of cGAMP in blood cells (J. An et al., 2017; Y. J. Crow et al., 2006; A. Gall et al.,

2012; B. Namjou et al., 2011). However, the cGAS-STING pathway engagement in SLE is variable and mouse models reflecting SLE need to consider the heterogeneity of the disease. Mice with deletion of lupus susceptibility gene *Fcgr2b* and without deletion of *Sting1* gene showed improved survival and disease symptoms when (A. Thim-uam et al., 2020). On the other hand, the deletion of STING in the MRL.Fas<sup>lpr</sup> mice, homozygous for the lymphoproliferation spontaneous mutation (*FAS<sup>lpr</sup>*) showing systemic autoimmunity, worsen the symptoms (S. Sharma et al., 2015). The patients with SLE have been also diagnosed with the mutations of DNase1 and other mutations in genes involved in DNA degradation which also leads to overactivation of cGAS-STING signalling (K. Yasutomo et al., 2001).

In RA patients the accumulation of cytoplasmic dsDNA has been observed and probably participates in inflammatory synovitis and other autoimmune diseases (N. Bottini & G. S. Firestein, 2012). Consistently, knock out of cGAS or STING causes inhibition of dsDNA-induced activation of IRF3 and NF- $\kappa$ B and decrease of proinflammatory cytokines in mouse models of RA (J. Wang et al., 2019).

Variety of therapeutical strategies in cGAS/STING-related autoimmune and autoinflammatory diseases have been developed. Yet, inhibiting activation of cGAS and STING has promising therapeutic potential. Inhibitors of cGAS and STING involved in cGAS/STING-related autoimmune and autoinflammatory diseases treatment together with their mechanism of action are summarized (Tab. 1, Fig. 6).

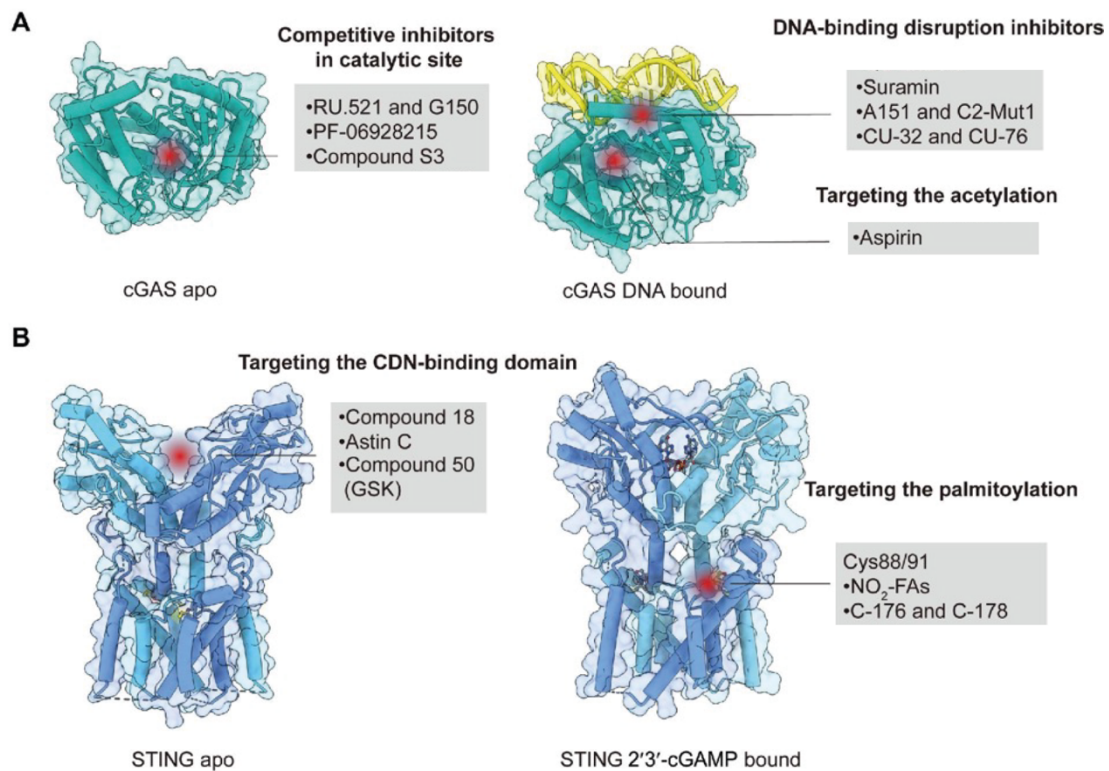


**Fig. 6: Mechanism of cGAS and STING inhibitors.** (A) competitive inhibitors of cGAS catalytic pocket, inhibitors disrupting the DNA-binding to cGAS and inducer of cGAS acetylation; (B) STING inhibitors targeting CDN-binding domain and STING inhibitors impeding palmytoylation. Adapted from (Z. Hong et al., 2022).

**Tab. 1:** Therapeutic intervention for cGAS-STING-related diseases

<b>cGAS inhibitor</b>	<b>Mechanism of inhibition</b>	<b>Reference</b>
aspirin	acetylation of cGAS protein	(J. Dai et al., 2019; M. R. Shakespear et al., 2011)
AMD	dsDNA binding, occupying cGAS binding site	(J. An et al., 2015)
ODN A151	competition with DNA	(F. Steinhagen et al., 2018)
RU.521	competition with ATP, occupying cGAS catalytic site	(J. Vincent et al., 2017)
Suramin	cGAS prevention of binding dsDNA, TLR3 interaction	(M. Wang et al., 2018)
CU-32; CU-76	inhibition of dimer formation	(R. Padilla-Salinas et al., 2020)
G150	occupying cGAS catalytic site	(L. Lama et al., 2019)
Compound S3	mimicking the 2'3'-cGAMP – cGAS interaction	(W. Zhao et al., 2020)
PF-06928215	not known	(W. Zhao et al., 2020)
C2-Mut1	inactive competitors of DNA binding in a sequence-dependent manner	(R. Valentin et al., 2021)
<b>STING inhibitor</b>	<b>mechanism of inhibition</b>	<b>reference</b>
C-178; H-151	bond with N-terminal domain, blocking palmitoylation	(S. M. Haag et al., 2018)
NO <sub>2</sub> -Fas	bond with N-terminal domain, blocking palmitoylation	(A. L. Hansen et al., 2018b)
Astin C	occupying cGAMP binding pocket	(S. Li et al., 2018)
Cys88/91	palmitoylation of STING	(K. Mukai et al., 2016b)
Compound 50	competition with 2'3'-cGAMP binding	(Fosbenner D.T. et al., 2018)
Compound 18	targeting the CDN-binding domain (CBD)	(T. Siu et al., 2019)

### **1.5.2. Senescence and ageing**

The increased release of proinflammatory cytokines associated with cGAS-STING signalization have been described in senescent cells. During ageing, the mechanisms maintaining tissue and cellular homeostasis are disrupted, further increasing inflammation. Senescent cells are crucial in this inflammation-ageing process due to, among others, the lost proliferation capacity and remarkable secretory activity, referred to as a senescence-associated secretory phenotype (SASP). (J. M. van Deursen, 2014) It has been suggested that cGAS-STING signalling pathway, specifically cGAS, is crucial for secretion of SASP components which can activate and regulate immune cells (Z. Dou et al., 2017; S. Glück et al., 2017; H. Yang et al., 2017). The source of senescent cell activation may be cytosolic DNA derived from ruptured micronuclei, disrupted nuclear envelope or the accumulation of cytosolic chromatin. It then increases cGAS concentration and activation in senescent cells (P. D. Adams et al., 2013; S. M. Harding et al., 2017; K. J. MacKenzie et al., 2017). The depletion or inhibition of senescent cells can improve the ageing related cell disfunction and prolonged the lifespan *in vivo* (D. J. Baker et al., 2016).

### **1.5.3. Cancer**

cGAS-STING pathway plays an important and a complex role in cancer immunotherapy due to the induction of innate immunity and bridging it to adaptive type, all of which leads to tumor growth suppression or direct eradication. The genome instability in cancer cells leads to the formation of micronuclei in a cell cycle-dependent manner and the rupture of the envelope of micronuclei leads to genome DNA detection by cGAS (S. M. Harding et al., 2017; K. J. MacKenzie et al., 2017). Moreover, the mitochondrial dysfunction in cancer cells leads to mtDNA leakage and activation of cGAS (S. Kitajima et al., 2019). It has been observed that several skin

melanoma cell lines (T. Xia et al., 2016b), colorectal adenocarcinoma cell lines (T. Xia et al., 2016a) or Kirsten rat sarcoma (KRAS)-mutated lung cancer (S. Kitajima et al., 2019) has inhibited or disturbed STING expression. Therefore, STING deficiency and downregulation of cGAS-STING signalization can reduce induction of antitumoral immunity (Y. S. Tan et al., 2018). The activation of the cGAS-STING signalling pathway may either result in antitumour or pro-tumorigenesis processes. Cytokine production can positively regulate multiple steps in tumour immunity such as boosting natural killer (NK) cells and priming cytotoxic T cells (A. Marcus et al., 2018; S. R. Woo et al., 2014) or induction of cancer cell senescence (Z. Dou et al., 2017) via secretion of SASP components (J. P. Coppé et al., 2008; Z. Dou et al., 2017; H. Yang et al., 2017) leading to tumorigenesis restriction (S. Glück et al., 2017; H. Yang et al., 2017). On the other hand, metastatic tumour cells present high genome instability leading to chronic activation of cGAS-STING signalling pathway to facilitate cellular invasion mediated by STING-dependent noncanonical NF- $\kappa$ B signalization (S. F. Bakhoun et al., 2018). Interestingly, STING agonists show promising results in cancer therapies (Tab. 2) due to CD8<sup>+</sup> T cell priming and NK cell activation and might represent a promising role in cancer therapy (L. Corrales et al., 2015; T. Nakamura et al., 2015).



**Tab. 2: STING agonists in clinical trials for cancer therapy**

<b>Compound</b>	<b>Cancer type</b>	<b>Phase</b>	<b>Reference</b>
ADU-S100 (MIW815)	Head and neck cancer	Phase 2	(Inc. Chinook Therapeutics, 2022)
ADU-S100 (MIW815) +/- Ipilimumab	Solid tumors/lymphomas	Phase 1	(Novartis Pharmaceuticals, 2022)
ADU-S100 (MIW815) + PDR001	Solid tumors/lymphomas	Phase 1	(Novartis Pharmaceuticals, 2022)
E7766	Urinary bladder neoplasms	Phase 1	(Eisai Inc., 2022)
E7766	Lymphoma/advanced solid tumors	Phase 1	(Eisai Inc., 2022)
GSK3745417	Neoplasms	Phase 1	(GlaxoSmithKline, 2022)
MK-1454	Solid tumors/lymphomas	Phase 1	(Merck Sharp & Dohme LLC, 2022a)
MK-1454 + pembrolizumab	Head and neck squamous cell carcinoma	Phase 2	(Merck Sharp & Dohme LLC, 2022b)
BMS-986301	Solid cancers	Phase 1	(Bristol-Myers Squibb, 2022)
SB 11285	Solid tumor	Phase 1	(Inc. F-star Therapeutics, 2020)

## 1.6. HBV

cGAS-STING signalization plays a crucial role in detection of viral DNA and viral clearance, such as hepatitis B (HBV). HBV is a small, enveloped DNA virus belonging to the *Hepadnaviridae* family (P. A. Revill et al., 2020) selectively targeting hepatocytes.

The genome of HBV virus consists of partially double-stranded relaxed circular DNA (rcDNA) which is stored in an icosahedral capsid. The reverse transcriptase is covalently linked to the 5' end of the complete (-) strand of DNA. The incomplete strand is mostly made of DNA, however short segment of RNA remains at the 5' end. The capsid consists of core proteins (HBcAg) and is covered with a lipoprotein membrane containing surface antigens (HBsAg). Antigen E (HBeAg) occurs only in the replication phase of the viral cycle and is secreted by the cell. HBsAg recognizes the receptor, which is exposed on the surface of the hepatocytes, then virus is bound and enter the cell using sodium taurocholate co-transporting polypeptide (NTCP) (Fig. 7). The virus loses lipid membrane during entry; therefore, the viral capsid is released to the cytoplasm. The capsid then interacts with nuclear pore proteins and releases rcDNA into the hepatocyte nucleus. In the nucleus, the synthesis of rcDNA is completed by replication enzymes to form covalently closed circular DNA (cccDNA), which is used as a template for the transcription of viral RNA. Long strands of RNA are transcribed, the longest strand serves as pregenomic RNA (pgRNA) and at the same time as the template for reverse transcriptase synthesis. Other shorter RNA molecules serve as mRNA for synthesis of HBsAg, HBcAg and HBxAg (regulator of transcription). Formed pgRNA together with the polymerase is encapsulated and is reverse-transcribed into (-) DNA. This is followed by degradation of the cap and part of pgRNA 5' end, the remaining part is used as a primer for the incomplete synthesis

of the second strand of DNA. After circularization and elongation of (+) DNA, the capsid in the ER is coated with a lipid membrane containing HBsAg and subsequently the virions are released from the cell. (Eric. Freed & M. Martin, 2013; D. Glebe & A. König, 2014; J.-H. Kao & D.-S. Chen, 2006; R. J. Lamontagne et al., 2016; S. Locarnini, 2004; W. H. Mason, W.S.Gerlich et al., 2012; P. A. Revill et al., 2019)

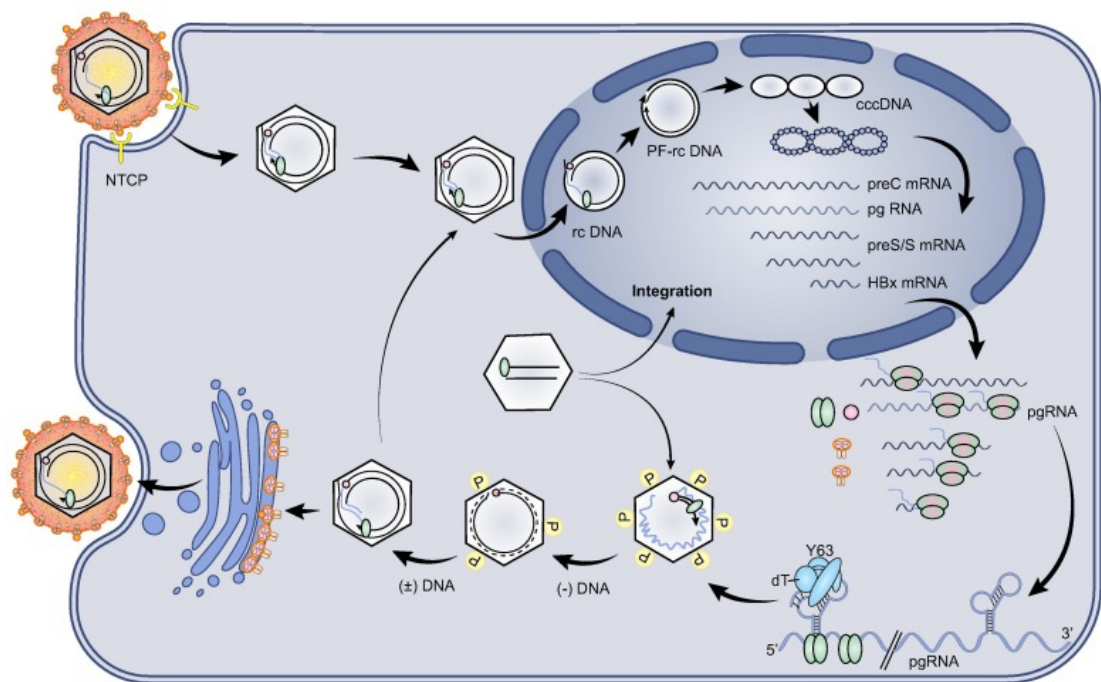


**Fig. 7: HBV replication cycle.** HBV DNA is partially double stranded forming a relaxed circular DNA genome. The virus enters the cytoplasm by receptor-mediated endocytosis involving sodium taurocholate co-transporting polypeptide (NTCP) receptor. After endocytosis and fusion of HBV envelope and plasma membrane, covalently closed circular DNAs (cccDNA) are formed from rcDNA. These cccDNAs produce HBV RNAs of different lengths which are translated into various proteins involved further in capsid formation and virus assembly. Adapted from (S. Tong & P. Revill, 2016).

HBV virus has wide range of immune evading mechanisms (A. Kuiper et al., 2020) such as active inhibition of STING-mediated signalization including decreased expression levels of cGAS, STING and/or TBK1 (L. Lauterbach-Rivière et al., 2020; Y. Liu et al., 2015; E. R. Verrier et al., 2018). Thus cGAS-STING signalization is essential for modulating susceptibility to CHB. The crucial role of cGAS-STING was confirmed *in vivo* (H. Dansako et al., 2019; M. K. Thomsen et al., 2016), where the lack of DNA-sensing or disruption of STING impaired the ability to control HBV, contrary to the STING induction which led to reduced viral gene expression and replication.

Lacking strong innate immune responses lead to convenient transformation of HBV to CHB resulting in liver cirrhosis, steatosis, or hepatocellular carcinoma. (H. L. Ha et al., 2010; M. Krajden et al., 2005) Approximately 5 % of adults, 30 % of children under 5 years and up to 95 % of neonates develop CHB. The possibility of vaccination in early childhood contributes to the overall reduction of new cases, however, mortality among CHB patients is rising. (World Health Organization, 2017)

The human HBV virus can chronically infect only humans and chimpanzees (S. F. Wieland, 2015), transiently tree shrew (J. Xiao et al., 2017). Human HBV-like family of viruses (woodchuck (J. Summers et al., 1978), domestic duck (W. S. Mason et al., 1980), Beechey ground squirrel (P. L. Marion et al., 1980)) could be used for *in vivo* CHB models, however, stringent ethical, administration and handling procedures and lack of research tools (S. F. Wieland, 2015; J. Xiao et al., 2017) make murine models of CHB essential for researchers and pharmaceutical companies.

First, transgenic mouse model with integrated HBV DNA into mouse genome was described (F. v Chisari et al., 1986). This model supports viral replication including particle production and infectious virion release; therefore, it is useful for

studying of molecular virus-host interactions and the biology of HBV-related immunology and pathogenesis (G. Ebert et al., 2011; J. G. Julander et al., 2003; C. Klein et al., 2003; O. Weber et al., 2002). Transgenic models can be separated into single HBV-protein (F. v. Chisari et al., 1985; L. G. Guidotti et al., 1994; C. M. Kim et al., 1991; D. R. Milich et al., 1990) or full-genome transgenic mice (L. G. Guidotti et al., 1995). However, all HBV transgenic mice developed tolerance to viral antigens, therefore the HBV-related liver diseases including liver cirrhosis cannot be developed (L. G. Guidotti et al., 1996). Another limitation is the transgenic origin itself. The model is lacking HBV entry and does not have the potential of viral clearance (F. A. Lempp et al., 2016).

Human chimeric mouse model was developed in order to study entire replication cycle including hepatocyte infection and cccDNA synthesis and intrahepatic spread. The mouse model is generated by engraftment of primary human hepatocytes in immunodeficient mice. (L. Allweiss & M. Dandri, 2016) However, the negative aspects of these models are health risks (kidney disorders/failure) and mouse immunodeficiency status which does not allow the study of adaptive immune responses and immunotherapeutic strategies. (H. Azuma et al., 2007; K.-D. Bissig et al., 2010; M. Dandri et al., 2001; M. Grompe et al., 1993; E. Ilan et al., 1999; P. Meuleman et al., 2005; M. Tsuge et al., 2005) To overcome these limitations, double chimeric mouse models using immunocompetent human liver-chimeric mice with immune cells and hepatocytes of human origin were developed (M. T. Bility et al., 2014, 2012; A. Irudayaswamy et al., 2018; M. L. Washburn et al., 2011), yet it is still a major challenge to generate this animal model.

Therefore, immunocompetent mouse models mimicking CHB infection based on the *in vivo* transduction via intravenous application of 1.2mer – 1.3mer of

HBV genome integrated into the adeno-associated virus (AAV) (Y. Du et al., 2021; Y. H. Huang et al., 2011; D. Yang et al., 2014) or adenovirus (S. Dion et al., 2013; L. R. Huang et al., 2012; M. F. Sprinzl et al., 2001; M. Suzuki et al., 2017) genome. This model has a relatively long virus replication time (3 months – 1 year) (L. R. Huang et al., 2012; M. John Von Freyend et al., 2011; H. T. Tzeng et al., 2013), however, adenoviral transduction can lead to direct immune response against the adenovirus itself making it challenging to clarify the HBV-related immune response and pathogenesis (V. J. Cavanaugh et al., 1998; S. Dion et al., 2013; Z. C. Hartman et al., 2007; L. R. Huang et al., 2012; D. Yang et al., 2014).

The immune response against the viral vector can be prevented by injecting plasmid containing HBV genome via pressurized delivery through the tail vein, hydrodynamic injection (HDI). Injecting of vehicle containing HBV DNA in a volume equivalent to 8-10% of the mouse weight in the limited time (5-10s) (S. P. Preston et al., 2016) allows HBV DNA specifically to transfect the hepatocytes (L. R. Huang et al., 2012). The pathogenesis of the infection and the host immune response can be monitored during both, acute and persistent HBV replication. The success of this model depends on the correct choice of mouse strain, sex, age, and plasmid sequence (H. H. Chou et al., 2015; L. R. Huang et al., 2006; X. H. Peng et al., 2015; P. L. Yang et al., 2002). HDI mouse models are widely used for host immune interactions and viral persistence or clearance, preclinical evaluation of anti-viral therapies, immune therapeutic strategies, or anti-viral effects against mutated HBV. (X. Li et al., 2016; S. R. Lin et al., 2014; A. P. McCaffrey et al., 2003; B. Qin et al., 2013)

Currently, two available CHB therapies are approved, interferon  $\alpha$ -based therapy and nucleos(t)ide analogues, both of which rarely result in the complete cure and often require life-long application (S. M. F. Akbar et al., 2022) with serious side

effects (W. Leowattana & T. Leowattana, 2022). Therefore, due to the severity of the disease and lack of 100% effective treatment the development of novel therapies is needed. Several approaches based on viral interference have been undergoing clinical trials (Tab. 3). However, we specifically focused on the activation of STING signalization as the induction of immune responses by *in vitro* and *in vivo* targeting of cGAS-STING using synthetic cGAMP or 5,6-dimethylxanthenone-4-acetic acid (DMXAA) led to inhibition of viral replication (F. Guo et al., 2017, 2015; J. He et al., 2016). As CDN-based STING agonists have already become an important medicinal chemistry tool as an effective anti-tumour therapeutic intervention (Tab. 2) (Inc. Chinook Therapeutics, 2022; C. M. Downey et al., 2014; A. Marcus et al., 2018; S. Vyskocil et al., 2021; A. H. Zaidi et al., 2021) and cGAS-STING signalization is essential for modulating susceptibility to CHB (H. Dansako et al., 2016; M. Pimková Polidarová, 2022), we focused on the CHB treatment based on the STING pathway activation using CDN-based STING agonists.

**Tab. 3:** Therapeutic approaches for CHB in clinical trials.

<b>Mechanism</b>	<b>Drug</b>	<b>Characteristics</b>	<b>Phase</b>	<b>References</b>
HBV entry inhibitors	Hepcludex	Blocking HBV binding to NTCP receptor	I Ib	(H. Wedemeyer et al., 2019)
Targeting viral transcripts	JNJ-3989	siRNAs	I Ib	(E. Gane et al., 2020)
	VIR-2218	siRNAs	II	(Gane et al., 2021)
Capsid assembly inhibitors	ABI-H0731	New capsid assembly inhibitor	II	(S. Fung et al., 2020; M.-F. Yuen et al., 2020)
HBsAg secretion inhibitors	REP2139	A nucleic acid polymer	II	(M. Bazinet et al., 2017)
TLR agonists	GS-9620	TLR-7 agonist	II	(H. L. A. Janssen et al., 2018)
	GS-9688	TLR-8 agonist	I	(H. L. A. Janssen et al., 2021)
Therapeutic vaccine	GS-4774	Expressing HBsAg, HBcAg, and HBx	II	(C. Boni et al., 2019)
	ABX-203	Expressing HBsAg and HBcAg	III	(G. Fernández et al., 2018)
	BRII-179	Induction of Th1 immune response	I	(Ma et al., 2021)
Immune checkpoint inhibitors	Nivolumab	Anti-PD-1/PD-L1	Ib/IIa	(E. Gane et al., 2019)
Monoclonal antibodies	GC1102	HBsAg monoclonal antibody	II	(Lee HW et al., 2018)
	VIR-3434	RNA gene silencer	II	(K. Agarwal et al., 2021)
Other immune approaches	IMC-I109V	Immune mobilizing monoclonal T cell receptors against the virus	I	(S. Bourgeois et al., 2022)



## 2. AIMS

The main objective of this doctoral thesis was the development of immunocompetent murine model reflecting CHB suitable for robust preclinical testing of novel CHB therapeutics based on activation of STING pathway using novel set of CDNs exclusively prepared by our group HBV Cure at Institute of Organic Chemistry and Biochemistry of the Czech Academy of Sciences.

Specific research aims:

- 2.1. *In vitro* characterisation of cyclic dinucleotides prepared by the group HBV Cure at the Institute of Organic Chemistry and Biochemistry of the Czech Academy of Sciences and selection of the lead compound using biochemical and cell-based assays
- 2.2. Development and characterisation of *in vivo* murine model reflecting CHB based on hydrodynamic injection
- 2.3. *In vivo* preclinical evaluation of lead compound to determine its therapeutic potential

### **3. METHODS**

This chapter briefly summarize methods important for understanding the results described in this thesis. Detailed method description is a part of the enclosed publications.

#### **3.1. *In vivo* studies**

All animal procedures were approved by institutional and national committees for the care and use of laboratory animals. All experiments were performed in accordance with the Directive 2010/63/EU of the European Parliament and of the Council of 22 September 2010 on the protection of animals used for scientific purposes (CAS 77/2018, CAS 79/2019, MSMT 29416/2020-7, Czech Republic). All mice were housed in specific, pathogen-free conditions in an individually ventilated cage-system with food and water ad libitum under controlled temperature and light settings and monitored regularly for morbidity and general appearance (weight, fur ruffling, and mobility/ activity).

##### **3.1.1. *In vivo* mouse model HDI induction**

The HDI model was induced in male C3H/HeN and C57Bl/6 mice (aged 4-6 weeks, purchased from the Charles River Laboratories) by tail vein injection of 10 µg of endotoxin free pAAV/1.2HBV plasmid DNA or 5 µg of endotoxin free minicircle DNA (pMC/1.0HBV) in a tempered saline solution within 5-8 s in a volume equal to 10% of the mouse body weight. Blood samples were collected into lithium heparin tubes every 1-3 weeks for up to 30 weeks. The mice were housed in specific, pathogen-free conditions in an individually ventilated cage-system with food and water ad libitum under controlled temperature and light settings and monitored regularly for morbidity and general appearance (weight, fur ruffling, and mobility/ activity).

### **3.1.2. HBV antigen secretion analysis**

The blood levels of the HBV surface, the HBV envelope-relevant antigens (HBsAg and HBeAg), and the antibody against HBsAg (HBsAb) were determined using an ELISA kit according to the adapted manufacturer's protocol. The absorbance was measured on a Spark reader. The internally established positivity threshold was determined as five times the mean of HDI controls for HB-Ag markers and as three times the mean of HDI controls for the HBsAb marker.

### **3.1.3. HBcAg immunohistochemistry**

The liver was preserved in 4% paraformaldehyde for 24-48 h and kept in 70% ethanol (Penta s.r.o.) until immunohistochemistry analysis. Liver tissue was stained with polyclonal rabbit anti-HBcAg antibody (DAKO-Agilent). HBcAg positivity was defined as a percentage of positive cells in the entire sample.

### **3.1.4. Flow cytometry (FC)-based T cell activation analysis**

Blood immune cells were prestained with live/dead marker Zombie-NIR for 20 min, at room temperature in dark, and then stained with rat anti-mouse monoclonal antibodies CD3, CD4, CD8, CD69 for 30 min, at room temperature in dark. Data were acquired on BD LSR Fortessa Cytometer with FACS DIVA software and analysed using FlowJo software. First debris, doublets and dead cells were excluded. Population of interest was gated on CD3 positive CD4 or CD8 positive T cells and expressed as a frequency of various subsets in the parent population.

### **3.1.5. *In vivo* efficacy of lead compound**

Plasma cytokine profiling (IFN $\alpha$ , IFN $\beta$ , IFN $\gamma$  and TNF $\alpha$ ) in reaction to intraperitoneal (i.p.) administration of 0.5, 1.5 and 5 mg/kg CDN-L in tempered saline solution was analyzed using ProcartaPlex Assays according to the adapted manufacturer's protocol. Data was measured on MAGPIX system. Blood samples

were collected into lithium heparin tubes in 1h, 4h, 8h, overnight (OVN). Vehicle group was injected i.p. only with tempered 0.9% saline solution.

CDN-L was injected intraperitoneally (i.p.) only into mice reflecting CHB with 1.5 and 5 mg/kg CDN-L in tempered saline solution biweekly for one month (8 applications in total, Fig. 16) and with 0.15 and 0.5 mg/kg CDN-L per mouse in tempered 0.9% saline solution biweekly for two months (16 applications in total, Fig. 16). Vehicle group was injected (i.p.) only with tempered 0.9% saline solution with a same schema as therapeutic compound, biweekly for up to two months (16 applications in total). Blood samples were collected into lithium heparin tubes every 1-3 weeks for up to 30 weeks. The HBV atigens secretion was measured as previously described (3.1.2) and the internally established positivity threshold was determined as five times the mean of HDI controls for HB-Ag markers.

### **3.1.6. *In vivo* IFN- $\alpha$ receptor (IFNAR) blockade**

For IFNAR blockade, mice were i.p. injected with 12.5 mg/kg of anti-mouse IFNAR monoclonal antibody, 12.5 mg/kg of relevant isotype control antibody, combination of 12.5 mg/kg of anti-mouse IFNAR monoclonal antibody and 2.5 mg/kg CDN-L, combination of 12.5 mg/kg of relevant isotype control antibody and 2.5 mg/kg CDN-L, 2.5 mg/kg of CDN-L or vehicle (tempered 0.9 % saline solution). Mice were treated biweekly for one month (8 applications in total, Fig. 19). Blood samples were collected into lithium heparin tubes every 1-3 weeks for up to 30 weeks.

## 4. RESULTS

### 4.1. *In vitro* characterisation of compounds and selection of lead compound using biochemical and cell-based assays

Results from this chapter were published:

Novotná, B., **Vaneková, L.**, Zavřel, M., Buděšínský, M., Dejmek, M., Smola, M., Gutten, O., Tehrani, Z. A., Pimková Polidarová, M., Brázdová, A., Liboska, R., Štěpánek, I., Vavřina, Z., Jandušík, T., Nencka, R., Rulišek, L., Bouřa, E., Brynda, J., Páv, O., & Birkuš, G. (2019). Enzymatic Preparation of 2'-5',3'-5'-Cyclic Dinucleotides, Their Binding Properties to Stimulator of Interferon Genes Adaptor Protein, and Structure/Activity Correlations. *Journal of medicinal chemistry*, 62(23), 10676–10690. <https://doi.org/10.1021/acs.jmedchem.9b01062>

My contribution:

Development and establishment of 293T reporter cell lines stably expressing five most abundant STING haplotypes (*WT*, *HAQ*, *REF*, *AQ*, *Q*), and optimization of screening methods using these cell lines (permeant one for direct STING activation using digitonin and standard one with an active uptake of compound). Development of differential scanning fluorimetry (DSF) method using *WT* STING protein and participation in manuscript preparation.

Dejmek, M., Šála, M., Brazdova, A., **Vanekova, L.**, Smola, M., Klíma, M., Břehová, P., Buděšínský, M., Dračínský, M., Procházková, E., Zavřel, M., Šimák, O., Páv, O., Boura, E., Birkuš, G., & Nencka, R. (2022). Discovery of isonucleotidic CDNs as potent STING agonists with immunomodulatory potential. *Structure (London, England : 1993)*, 30(8), 1146–1156.e11. <https://doi.org/10.1016/j.str.2022.05.012>

My contribution:

*In vitro* screening of tested CDNs using established DSF and cell-based *in vitro* assays, data evaluation and interpretation, participation in manuscript preparation.

Vavřina, Z., Perlíková, P., Milisavljević, N., Chevrier, F., Smola, M., Smith, J., Dejmek, M., Havlíček, V., Buděšínský, M., Liboska, R., **Vaneková, L.**, Brynda, J., Boura, E., Řezáčová, P., Hocek, M., & Birkuš, G. (2022). Design, Synthesis, and Biochemical and Biological Evaluation of Novel 7-Deazapurine Cyclic Dinucleotide Analogues as STING Receptor Agonists. *Journal of medicinal chemistry*, 65(20), 14082–14103. <https://doi.org/10.1021/acs.jmedchem.2c01305>

My contribution:

*In vitro* screening of tested CDNs using established DSF and cell-based *in vitro* assays, data evaluation and interpretation, participation in manuscript preparation.

Nonpublished results: biological characteristic of lead compound (referred to as a CDN-L, a STING agonist based on CDN structure).

#### **4.1.1. Background and motivation**

cGAS, a DNA sensor activated by dsDNA in cytosol, is responsible for the synthesis of a natural STING agonist 2'3'-cGAMP (Fig. 8) which acts as a second messenger in cGAS-STING signalization. However, STING also can be activated by other CDN STING agonists (3'3'-cGAMP; 3'3'-c-diAMP; 3'3'-c-di-GMP; Fig. 8) produced by various bacteria or by synthetically prepared CDNs (Birkus, 2018; G. Birkus et al., 2020; M. Dejmek et al., 2022; B. Novotná et al., 2021, 2019; M. Pimková Polidarová et al., 2021). Owing to the important role of STING in the control of cancer and pathogen infections, CDNs became an important medicinal chemistry tool with potential of therapeutic application in various diseases (e.g., CHB, HIV, cancer, etc.).

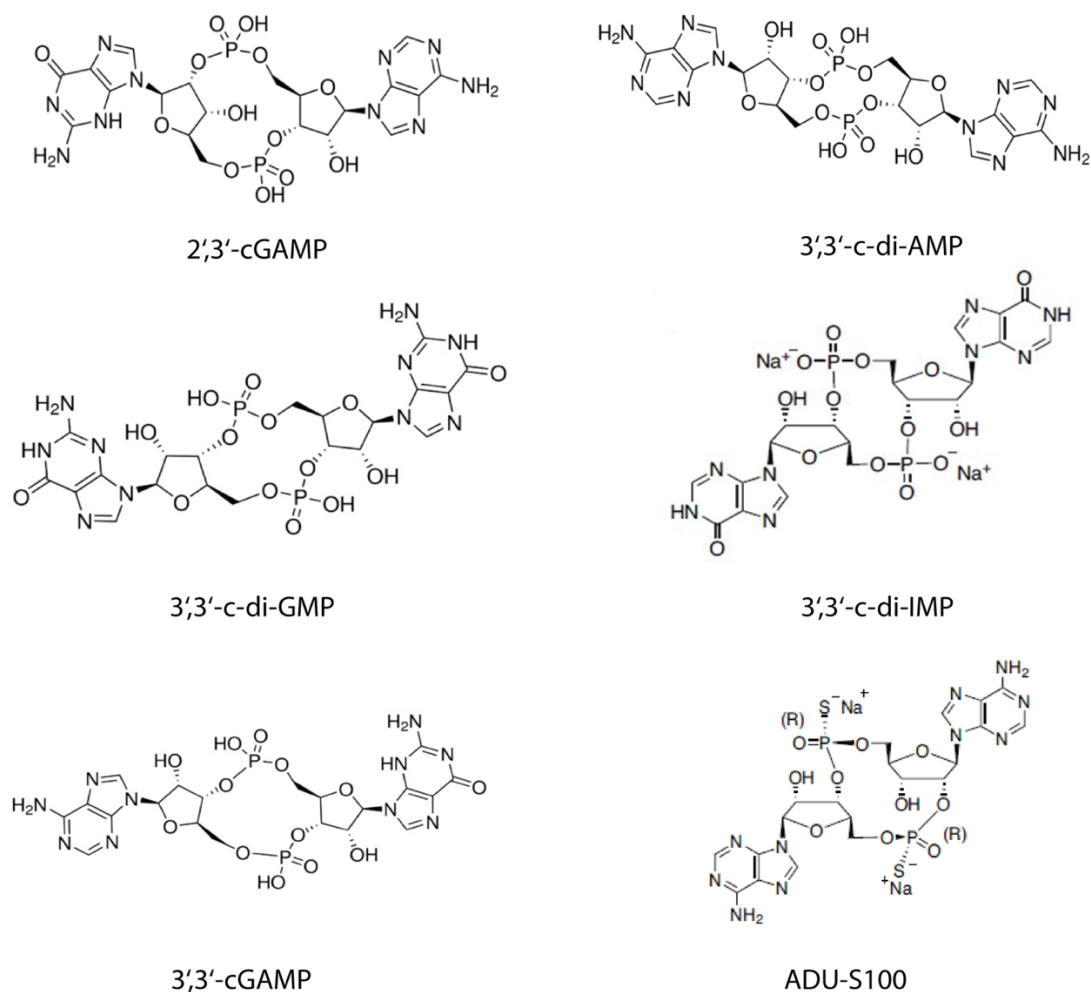


**Fig. 8:** Examples of cyclic dinucleotides structures activating STING protein.

The objective of this thesis was to identify a novel STING agonist with optimal pharmacokinetic profile for CHB and cancer therapy. At the Institute of Organic Chemistry and Biochemistry of the Czech Academy of Sciences, the HBV Cure group led by Mgr. Gabriel Birkuš, Ph.D. prepared a large library of modified CDNs. They were prepared by enzymatic and synthetic approach and contained modifications of nucleobase, sugar, and the phosphate groups. We determined and compared the affinity of these CDNs towards five STING haplotypes in biochemical and cell-based

assays and translated the results into the cytokine and chemokine induction in human peripheral blood mononuclear cells (PBMCs).

#### 4.1.2. Results

A set of simple yet effective biochemical and cell-based assays was prepared to routinely profile the activity of CDNs based on the interaction of CDN – STING protein. At first, differential scanning fluorimetry (DSF) determined the CDN binding affinity to STING protein via difference between melting temperature of STING apo-protein and STING – CDN complex ( $\Delta T_m$ ). As demonstrated in Tab. 4, newly prepared CDNs (enzymatically prepared 2'3'-CDNs (B. Novotná et al., 2019), isonucleosidic CDNs (M. Dejmek et al., 2022) and our lead compound CDN-L) had similar or even higher binding affinity to STING than control CDNs such as 3'3'-c-di-AMP or STING agonist ADU-S100, the clinical candidate terminated in the Phase II clinical trial (Inc. Chinook Therapeutics, 2022). In comparison with 2'3'-cGAMP ( $\Delta T_m = 15.29$  °C), the natural second messenger of cGAS-STING signalling pathway, only a few of our enzymatically prepared 2'3'-CDNs had higher binding affinity ( $\Delta T_m < 20.5$  °C) to *WT* STING protein (B. Novotná et al., 2019). Chemically synthesized isonucleosidic 3'3'-CDNs ( $\Delta T_m < 13.5$  °C, Dejmek et al., 2022) and our lead compound CDN-L ( $\Delta T_m = 8.6$  °C), had slightly lower  $\Delta T_m$  to *WT* STING protein compared to 2'3'-cGAMP suggesting lower binding affinity to *WT* haplotype.

To profile the biological activity of our CDNs, a cell-based reporter assay using HEK293T ISRE reporter cell line stably transfected with various STING haplotypes (*WT*, *HAQ*, *REF*, *AQ* or *Q*) was prepared. The reporter cell line is based on expression of firefly luciferase from a reporter plasmid with four ISRE sites placed upstream of the firefly luciferase reporter gene minimum promoter. The expression is induced by the activation of IRF3 as a consequence of a CDN binding to STING. We employed



two assay formats for five STING haplotypes with different CDNs binding capacity (*WT*, *HAQ*, *REF*, *AQ*, *Q*) to determine the activity of our CDNs towards STING haplotypes present in human population: so called digitonin assay, in the presence of digitonin A (detergent permeabilizing cell membranes allowing the charged CDN to easily enter the cell), and standard assay, with an active uptake of compound reflecting the physiological conditions. Half-maximal effective concentration ( $EC_{50}$ ) values were then determined.

All enzymatically prepared 2'3'-CDNs had 10-100x better or comparable  $EC_{50}$  values than control 3'3'-CDNs in the digitonin assay (Tab. 4), however only a few of them showed better or similar activity towards all five STING haplotypes as 2'2'-cGAMP and 2'3'-cGAMP (Tab. 4). Interestingly, many of our enzymatically prepared 2'3'-CDNs had better activity towards *HAQ* ( $<0.1 \mu\text{M}$ ), *REF* ( $<2 \mu\text{M}$ ), *AQ* ( $<0.17 \mu\text{M}$ ) and *Q* ( $<0.7 \mu\text{M}$ ) STING haplotypes than ADU-S100 (0.26  $\mu\text{M}$ ; 1.64  $\mu\text{M}$ ; 0.23  $\mu\text{M}$ ; 1.01  $\mu\text{M}$ , respectively), the clinical candidate CDN (Tab. 4). Most of our enzymatically prepared 3'3' – CDNs had much higher activities (up to 40x) than ADU-S100 or natural STING agonists (Tab. 4). Isonucleosidic CNDs, on the other hand, showed more promising results using *WT* ( $<1.35 \mu\text{M}$ ), *HAQ* ( $<0.77 \mu\text{M}$ ) and *AQ* STING ( $<0.68 \mu\text{M}$ ) haplotypes than with *REF* ( $>45 \mu\text{M}$ ) and *Q* ( $<26.90 \mu\text{M}$ ). Our lead compound, CDN-L had similar  $EC_{50}$  value as 2'2'-cGAMP and 2'3'-cGAMP for *WT* STING (0.02  $\mu\text{M}$ ) and *AQ* STING (0.09  $\mu\text{M}$ ) and much lower  $EC_{50}$  values for all STING haplotypes except *REF* compared with ADU-S100 (Tab. 4). Standard assay with an active uptake of the compound was performed on *WT* STING. Only CDN-L (0.8  $\mu\text{M}$ ) and some of enzymatically prepared 3'3' – CDNs ( $>2,58 \mu\text{M}$ ) had much lower  $EC_{50}$  value than natural STING agonists ( $>9.83 \mu\text{M}$ ) or ADU-S100 (3.32  $\mu\text{M}$ ).

Cytokine production is the primary response to the activation of cGAS-STING pathway, therefore, *in vitro* therapeutic efficacy of CDNs was tested using human PBMCs reflecting physiologically relevant *in vitro* cell-based model. The production of IFN $\gamma$ , TNF- $\alpha$ , IFN $\alpha$  was measured as proinflammatory cytokine TNF- $\alpha$  and IFN $\alpha$  represent the primary and IFN $\gamma$  the late onset response to the activation of cGAS-STING signalling pathway. All data obtained from the PBMC assay correlated with previously measured DSF and 293T assays. CDN-L, our lead compound had much lower EC<sub>50</sub> value for TNF- $\alpha$  (2.73  $\mu$ M) and IFN $\gamma$  (1.02  $\mu$ M) than all naturally occurring STING agonists as well as clinical candidate ADU-S100, unlike IFN $\alpha$ , where CDN-L had slightly higher EC<sub>50</sub> (28.53  $\mu$ M) than all control compounds. Interestingly, ADU-S100 had the highest EC<sub>50</sub> values (>140  $\mu$ M) for all cytokines measured (Tab. 4).

**Tab. 4: Summary of *in vitro* biochemical and cell-based evaluation of part of newly prepared CDNs.**

Compound	DSF	DIGITONIN assay					Standard assay	PBMC		
	$\Delta T_m$ (°C)	EC <sub>50</sub> (μM)					EC <sub>50</sub> (μM)	EC <sub>50</sub> (μM)		
	<i>WT</i>	<i>WT</i>	<i>HAQ</i>	<i>REF</i>	<i>AQ</i>	<i>Q</i>	<i>WT</i>	IFN $\gamma$	TNF $\alpha$	IFN $\alpha$
3'3'-c-diAMP	2.48	0.26	0.19	>45	0.17	7.09	>150	8.98	7.54	9.25
3'3'-cGAMP	5.12	0.12	0.12	4.26	0.26	2.06	68.37	5.45	14.50	8.48
2'2'-cGAMP	11.57	0.03	0.02	0.21	0.03	0.17	9.83	11.64	23.12	22.15
2'3'-cGAMP	15.29	0.02	0.02	0.07	0.04	0.05	28.37	13.45	37.16	18.26
ADU - S100	9.30	0.08	0.26	1.64	0.23	1.01	3.32	140.00	150.00	150.00
2'3'-CDNs	-7 – 20.5	0.01 – 0.20	0.01 – 0.1	0.01 – 2.00	0.01 – 0.17	0.02 – 0.70	10.07 - >150	0.53 – 35.03	0.59 – 57.34	1.27 – 183.63
3'3'-CDNs	0 – 13.5	0.01 - >45	0.06 - >45	0.19 - >45	0.08 - >45	0.18 - >45	2.58 - >150	0.87 – 85.20	1.43 - >200	2.80 - >200
Isonuc- CDNs	1.8 – 11.0	0.01 – 1.35	0.06 – 0.77	0.40 - >45	0.06 – 0.68	0.20 – 26.90	4.93 - >150	0.66 – 58.83	1.29 - 195.00	3.09 - >200
CDN-L	8.60	0.02	0.11	7.60	0.09	0.20	0.8	1.02	2.73	28.53

#### 4.1.3. Conclusion

We performed series of biochemical and biological screenings to determine the binding affinity of CDNs to STING and their activity *in vitro* using reporter cell line and PBMC assays. Some of the introduced modifications of CDN structures resulted in similar or even higher *in vitro* activity of our CDNs towards all STING haplotypes compared to the natural STING agonist 2'3'-cGAMP. We also compared our results with the clinical candidate ADU-S100, which was terminated in Phase II clinical trials due to the lack of the substantial anti-tumour activity. The potency of our CDNs trended from enzymatically prepared 2'3'-CDNs being best, followed by isonucleosidic CDNs and enzymatically prepared 3'3'-CDNs. Based on the biochemical and biological testing of the newly prepared CDN library, we chose CDN-L as the lead compound with the optimal activity in all *in vitro* assays and improved *in vitro* plasma stability.

## **4.2. Development and characterisation of *in vivo* murine model reflecting CHB based on hydrodynamic injection**

Results from this chapter were accepted 9.11.2022 for publication in Physiological research:

*Vanekova L, Polidarova M, Charvat V, Vavrina Z, Veverka V, Birkus G, Brazdova A. (2022) Development and characterisation of a chronic hepatitis B murine model with a mutation in the START codon of an HBV polymerase. Physiological research, doi:10.33549/physiolres.934979*

My contribution:

Development, establishment, and characterisation of HDI induced mouse model, data evaluation and interpretation, manuscript preparation.

### **4.2.1. Background and motivation**

Preclinical safety and efficacy of novel CHB therapeutics relies on animal models. However, the human HBV virus can only infect humans and chimpanzees. Human HBV-like family of viruses (woodchuck, domestic duck, Beechey ground squirrel) could be used for *in vivo* CHB models, but stringent ethical, handling, and administrative procedures and the lack of research tools for studying host-virus immune interactions make it unsuitable. On the other hand, murine CHB models are well established and much simpler to use. Several murine HBV models have been described, such as transgenic and chimeric HBV mouse models based on tail vein delivery of adeno-associated virus (AAV), or models based on HDI of plasmid vector carrying replication-competent DNA genome. However, CHB model sustainability based on HDI induction depends on the selected mouse strain as three different genotypes of major histocompatibility complex (MHC) associated with immune

response to HBsAg are defined: high ( $H-2^{d,g}$ ), intermediate ( $H-2^a>H-2^b>H-2^k$ ), and low/non-responders ( $H-2^{s,f}$ ).

Therefore, we aimed to develop a mouse model based on HDI reflecting CHB suitable for robust preclinical testing of novel CHB therapeutics. We compared two different plasmid systems (adeno-associated plasmid vector (pAAV) and minicircle (pMC)) encoding HBV genomes of genotype A and D with introduced point mutation in the START codon of the polymerase in two different immunocompetent mouse strains, C57Bl/6 and C3H/HeN. The model sustainability was evaluated based on viral markers, HBsAg and HBeAg, as HBsAg is considered a general marker of HBV in both mouse and human plasma (J.-H. Kao, 2014), regardless of acute or chronic infection. HBeAg is considered as a marker of HBV replication and infectivity and its presence is associated with elevated levels of HBV DNA (M. A. Konerman & A. S. Lok, 2018).

#### 4.2.2. Results

Male mice, C3H/HeN and C57Bl/6 were hydrodynamically injected with either 10 $\mu$ g (L. R. Huang et al., 2006; L. Li et al., 2017) of pAAV/1.2HBV (Fig. 9A, B) or 5 $\mu$ g (X. Guo et al., 2016; Z. Yan et al., 2017) of pMC/1.0HBV (Fig. 9C, D) plasmids with the point mutation T2308C, more specifically pAAV/1.2HBV genotype A and D, pMC/1.0HBV genotype D with pre-C (encoding HBeAg) and pre-S (encoding envelope proteins) residual recombination sites (plasmid preparation and verification described in Pimková Polidarová, 2022). Briefly, both plasmid constructs carrying the replication-competent HBV DNA genome (wt pAAV (L. R. Huang et al., 2006), wt pMC (Z. Yan et al., 2017) ) or the HBV DNA genome with a mutation of the START codon of the polymerase (T2308C (Z. Yan et al., 2017)) were tested for the *in vitro/in vivo* quality, purity, and functionality (M. Pimková Polidarová, 2022) (Fig. 10). The

T2308C point mutation was effectively introduced and had a non-significant effect on the *in vitro* expression of HB-Ag when compared to the wt plasmid using an *in vitro* HepG2-NTCP infection system (M. Pimková Polidarová, 2022; Y. Sun et al., 2017) (Fig. 10). The absence of HBV virions using plasmids with a point mutation in the START codon of polymerase was verified in mouse plasma by quantitative polymerase chain reaction (qPCR), showing that HBV DNA was below the limit of detection.

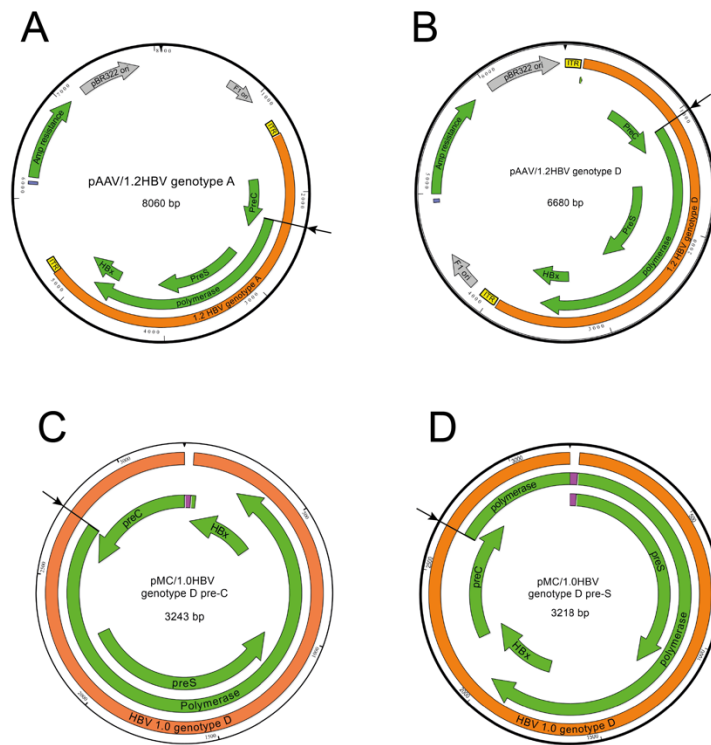


**Fig. 9: Plasmid maps:** pAAV/1.2HBV genotype A (A) and D (B), pMC/1.0HBV genotype D pre-C (C) and pre-S (D); mutation T2308C eliminating the START codon of the HBV polymerase pointed as an arrow; the orange bar represents the HBV sequence; green represents open reading frames encoding the polymerase, HBx = HBV X protein, pre-C region encoding HBeAg and HBcAg, pre-S domain encoding 3 forms of HBsAg; grey represents the bacterial origin of replication; yellow represents inverted terminal repeats from AAV2 virus; blue represents promoter, and purple represents the ATT recombination site (resulting from a minicircle preparation from the parental plasmid).



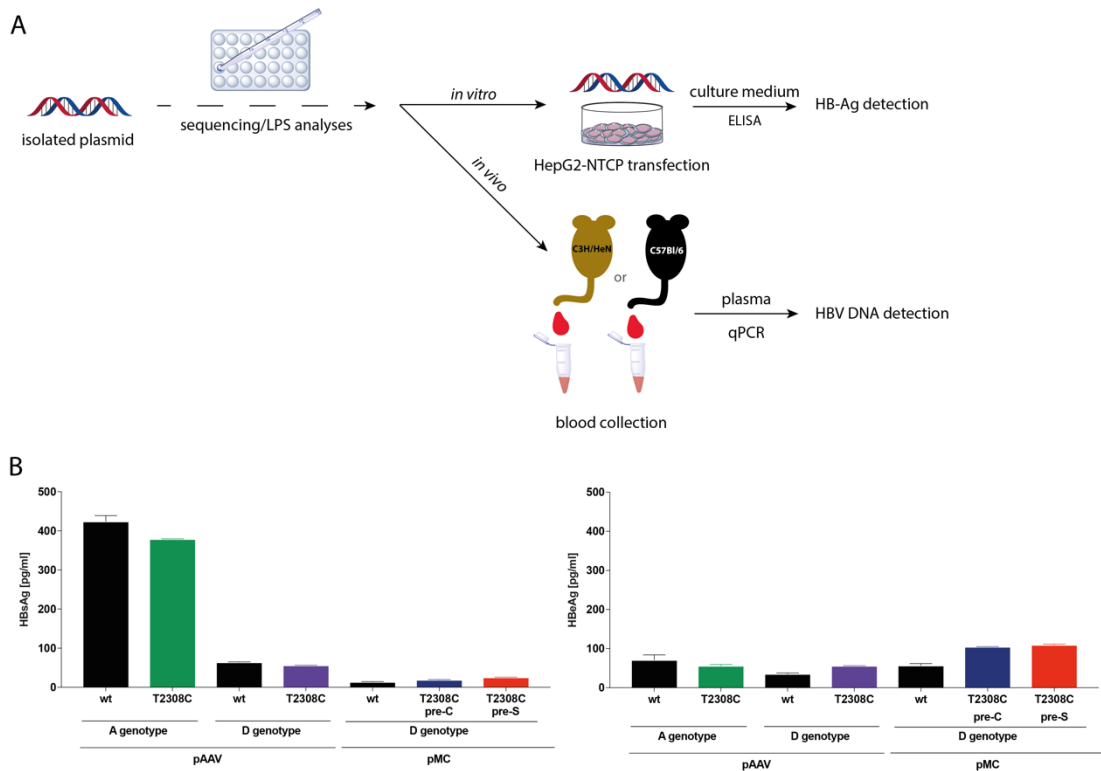


**Fig. 10: Quality control of plasmids.** (A) Schema of the experiment. (B) Production of HB-Ag secreted into media by HepG2-NTCP cells transfected with non-mutated (L. R. Huang et al., 2006) (wt) and mutated (T2308C (Z. Yan et al., 2017)) plasmids of prepared constructs (M. Pimková Polidarová, 2022). Data from 2 independent measurements expressed as a mean  $\pm$  standard error of the mean (SEM). No HBV DNA was detected in mouse plasma.

## **Injection of both constructs into C57Bl/6 mice results in transient expression of viral proteins.**

The models were evaluated based on the plasma levels of viral HB-Ag and host immune antiviral response was determined by seroconversion by the presence of anti-HBsAg antibodies (HBsAb) in blood (Fig. 11, Fig. 12, Fig. 13) and confirmed by HBcAg expression in the liver (Fig. 14).

In C57Bl/6 mice, the HBsAg and HBeAg positivity started decreasing within the first week post HDI. Mice injected with pAAV/1.2HBV genotype D showed a rapid loss of HBsAg (no animal was positive by D35, Fig. 11) and HBeAg (20% positive by D21, Fig. 11), and 80% of mice seroconverted by D35 (Fig. 13). Due to the rapid clearance of HB-Ag and the very low HBV persistence rate the minicircle construct (Z. Yan et al., 2017) of genotype D was prepared. pMC/1.0HBV pre-C genotype D injection into C57Bl/6 mice resulted in a relatively fast clearance of HBsAg (only 10% positive mice by D35, Fig. 11) with sustained 10% HBsAg positivity up to D105 (Fig. 11). HBeAg positivity decreased from 70% (D7) to 10% (D77) and sustained to the terminal point of experiment (D105, Fig. 11). HBsAb were detected within 4 weeks post HDI, and by the end of the study, up to 40% animals had seroconverted (Fig. 13). Mice injected with pMC/1.0HBV pre-S genotype D and pAAV/1.2HBV genotype A showed a mild decrease of HBsAg-related positivity (10-20% loss every week by D21, Fig. 11). However, HBsAg-related positivity rapidly dropped to 10% (D35) and sustained to D49 in the term of pMC/1.0HBV pre-S genotype D (Fig. 11), while HBeAg positivity decreased gradually to 20% (D49, Fig. 11). Up to 50% animals seroconverted by D28 (Fig. 13). Mice injected with pAAV/1.2HBV genotype A showed the most promising results, however, all animals

showed total loss of HBsAg and HBeAg by D49 (Fig. 11), while HBsAg seroconversion rapidly increased to 90% within 2-3 weeks post HDI (Fig. 13).

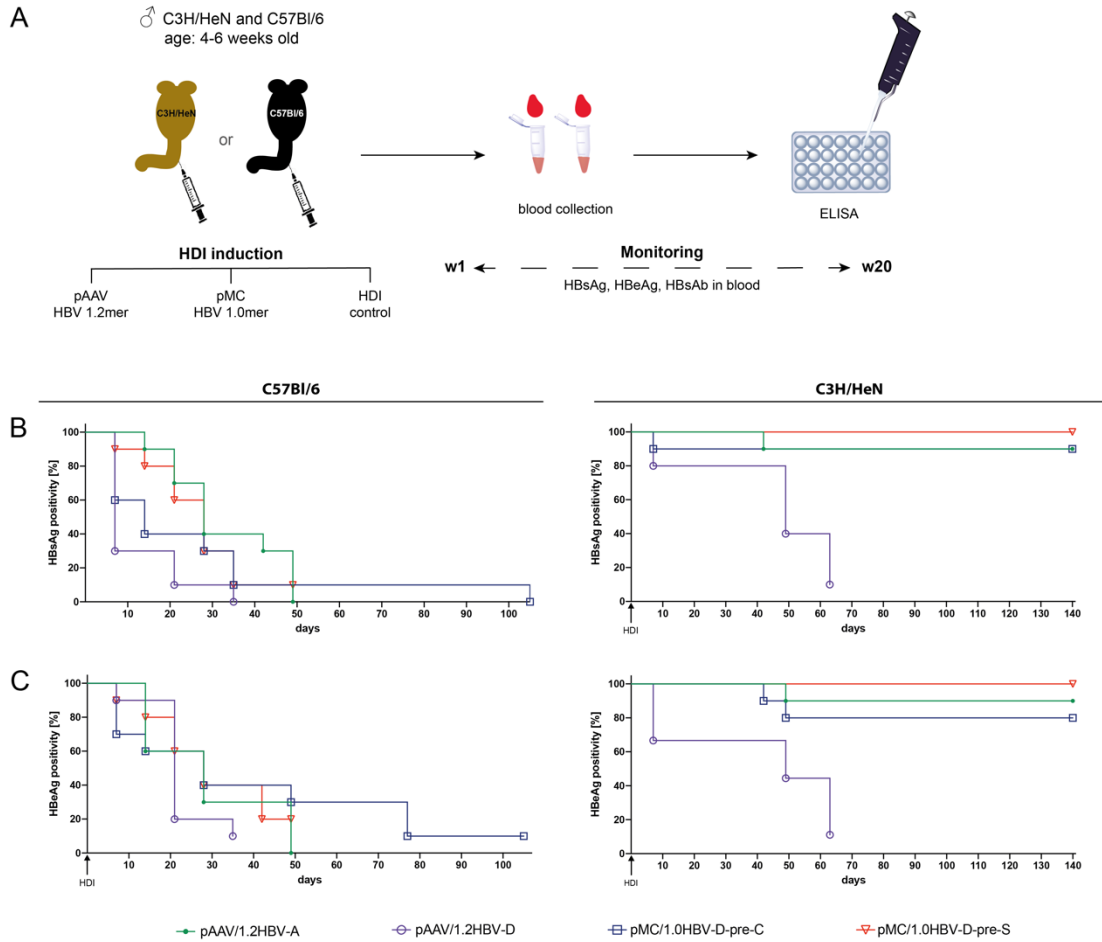


**Fig. 11: CHB *in vivo* model establishment and characterisation in C57Bl/6 and C3H/HeN mice:** (A) scheme of the experiment and continuous monitoring of HBsAg (B), HBeAg (C) blood levels; the positivity proportions of all induction systems (pAAV/1.2HBV genotype A and D, pMC/1.0HBV genotype D pre-C and pre-S) were shown as Kaplan-Meier curves; n=5-20 mice/group.

**Hydrodynamic injection of pAAV/1.2HBV genotype A with a point mutation in the START codon of polymerase into C3H/HeN mice leads to a persistent expression of viral proteins.**

HDI injection of both plasmid constructs into the C3H/HeN mouse strain led to a more consistent and sustainable expression of viral proteins. More than 80% of animals remained HB-Ag positive up to the end of the study (D140, the study endpoint) when using pMC/1.0HBV pre-C genotype D, pMC/1.0HBV pre-S genotype D, and pAAV/1.2HBV genotype A (Fig. 11, 12). However, pAAV/1.2HBV genotype D induced only a transient expression of viral proteins (10% positivity by D62) (Fig. 11, 12). Only 10% of the mice injected with pAAV/1.2HBV genotype D developed HBsAb (Fig. 13). Contrary to pAAV/1.2HBV genotype D, both pAAV/1.2HBV genotype A and pMC/1.0HBV genotype D (pre-C and pre-S) showed a similar chronic expression of HB-Ag (>80% positivity up to study endpoint, Fig. 11, 12). We also observed differences in the average values of detected HB-Ag between constructs. The minicircle constructs had low HBsAg levels (<500 ng/ml, Fig. 12), while pAAV/1.2HBV genotype A had >40x higher average values of HBsAg (<20000 ng/ml, Fig. 12). On the other hand, the plasma endpoint levels of HBeAg were significantly higher when using the minicircle constructs (120-200 ng/ml, Fig. 12) than when using pAAV/1.2HBV genotype A (<30 ng/ml, Fig. 12).

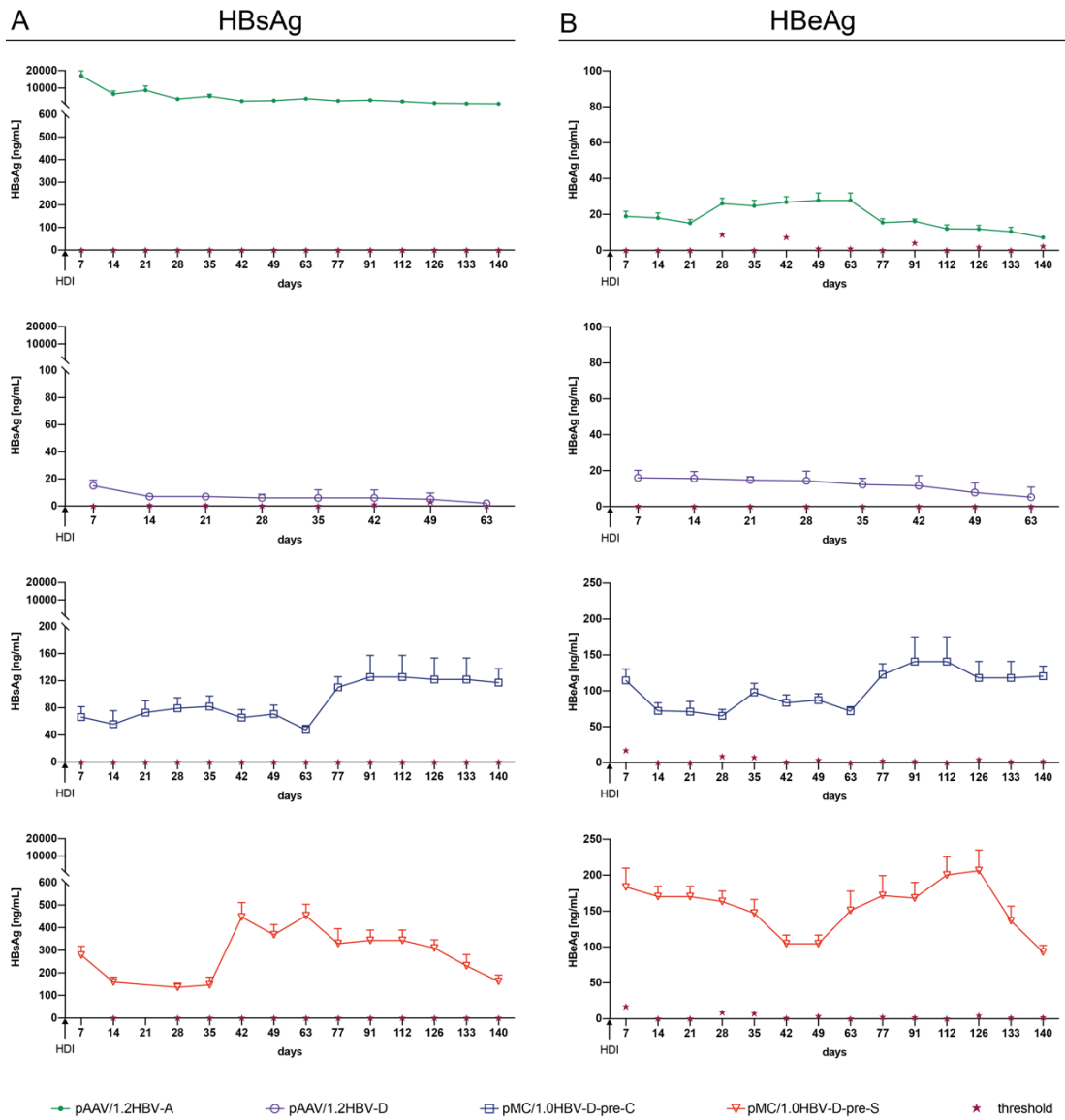


**Fig. 12: HBV marker levels in C3H/HeN mice;** HBsAg (A) and HBeAg (B) were monitored in animals hydrodynamically injected with plasmids. Data were expressed as mean  $\pm$  standard error of mean (SEM) per group. (a, b) n=5-20 mice/group

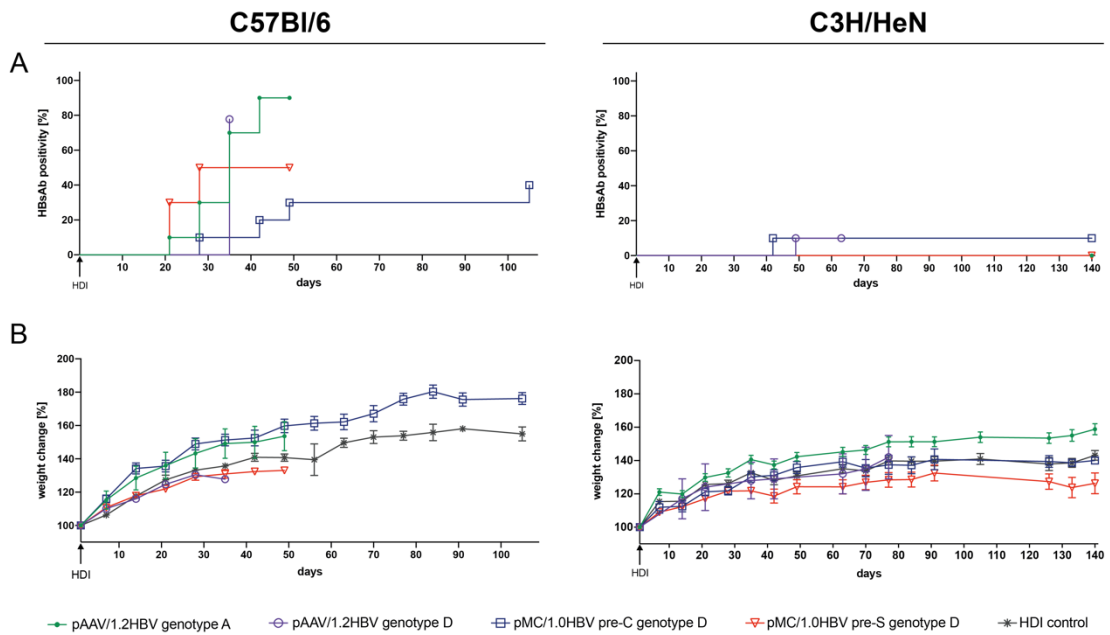


**Fig. 13: Characterisation of mouse model reflecting CHB.** *In vivo* model establishment in C57Bl/6 and C3H/HeN mice. (A) Continuous monitoring of HBsAb blood levels. Positivity proportion related to all induction systems (pAAV/1.2HBV genotype A and D, pMC/1.0HBV genotype D pre-C and pre-S) shown as Kaplan-Meier curves. (B) Weight as stratified by induction system groups for both mouse strains. Data were expressed as mean value per group  $\pm$  standards error of mean (SEM). n=5-20 mice/group.

**HBcAg was detected only in C3H/HeN mice regardless of induction system at the terminal point of the experiment.**

The expression of HBcAg in mouse hepatocytes was determined by immunohistochemical analysis of liver tissue on D7 post HDI and at the terminal point of the experiment. IHC confirmed the presence of HBcAg positive cells on D7 post HDI regardless of HBV construct (10-25%, Fig. 14) in C57Bl/6 mice, however not a single liver tissue showed the presence of HBcAg at the end of the study (Fig. 14). D7 post HDI, C3H/HeN mice showed 20-25% HBcAg positive hepatocytes for pAAV/1.2HBV genotype A and 10-15% HBcAg positive hepatocytes for genotype D regardless of plasmid induction system. However, the HBcAg-related positivity of the genotype D decreased to <10% by the terminal point of the experiment regardless of construct used. HBcAg positivity remained unchanged when using pAAV/1.2HBV genotype A in C3H/HeN mice. Mice injected only with physiologic solution (HDI control) were HBcAg negative throughout the experiment (Fig. 14).

Regardless of mouse strain or HBV genotype, HBV transduction was latent. In both mouse strains, none of the induction systems affected physiology, as confirmed by the absence of weight changes (Fig. 13). The mice were also monitored regularly for general appearance (fur ruffling, mobility, and activity), showing no pathologic changes.

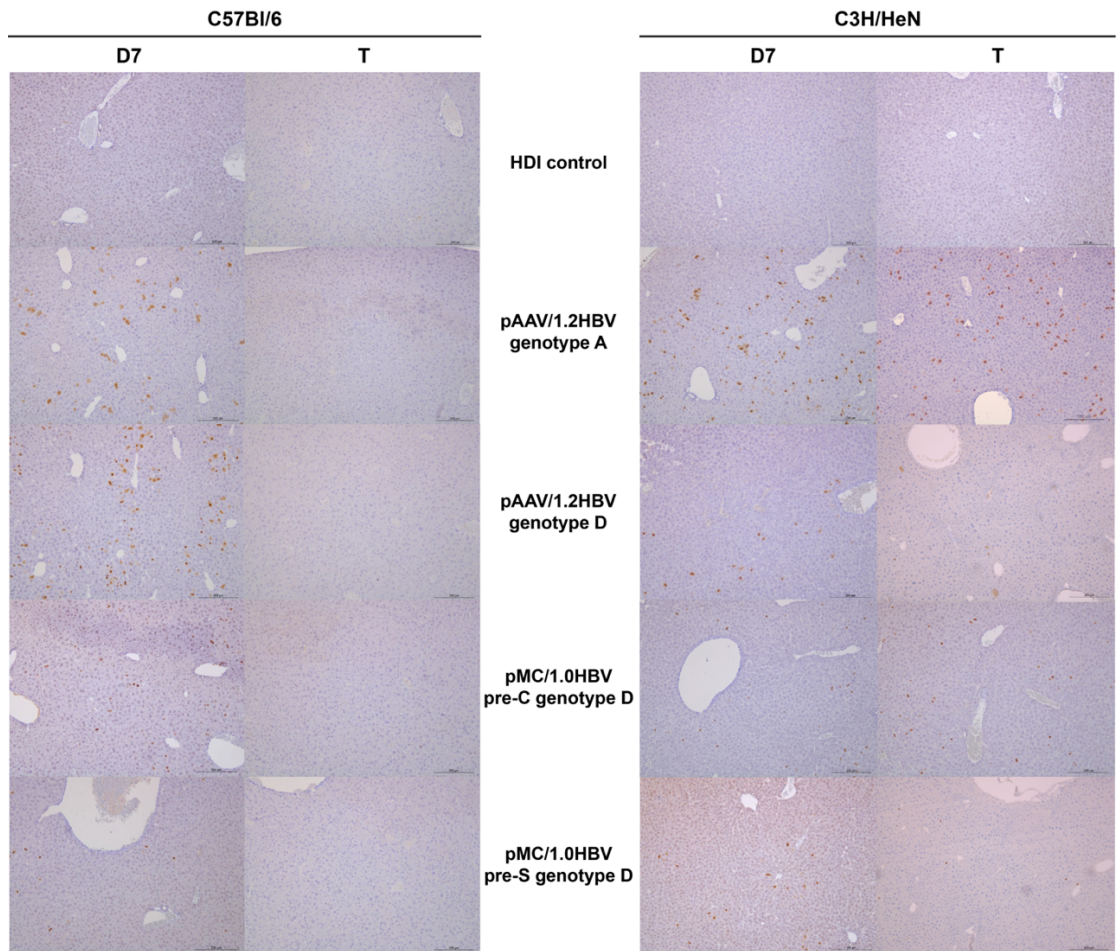


**Fig. 14: HBcAg expression in liver sections of C57BL/6 and C3H/HeN mice detected by immunohistochemistry:** HBcAg detected on day 7 (D7) post HDI and at the terminal point of the experiment (T; C57Bl/6: D35 pAAV/1.2HBV D genotype, D49 pAAV/1.2HBV A genotype and pMC/1.0HBV pre-S D genotype, D105 pMC/1.0HBV pre-C D genotype; C3H/HeN: D62 pAAV/1.2HBV D genotype, D140 pAAV/1.2HBV A genotype, pMC/1.0HBV pre-C D genotype and pMC/1.0HBV pre-S D genotype); representative results of HBcAg (brown spots) per induction system group



### 4.2.3. Conclusion

The C3H/HeN mouse strain is more suitable for developing a long-term *in vivo* model reflecting CHB than C57Bl/6. Hydrodynamic injection of pAAV/1.2HBV genotype A and pMC/1.0HBV pre-S genotype D, both with a T2308C point mutation of the polymerase START codon, results in persisting HB-Ag (Fig. 11, 12) expression for up to 20 weeks. Based on the pAAV/1.2HBV genotype A-associated HBsAg levels we believe that the pAAV induction system is more suitable for assessing the efficacy of potential therapeutics. Thanks to the T2308C (Z. Yan et al., 2017) point mutation of the polymerase START codon and the resulting lack of virion progeny (Fig. 10); such *in vivo* testing can be routinely performed in a Biosafety Level 2 animal facility. Our model provides several advantages, including its accessibility, convenience, and affordability.

### **4.3. *In vivo* preclinical evaluation of lead compound to determine its CHB therapeutic potential**

This chapter contains non-published preclinical results of lead compound CDN-L (STING agonist based on CDN structure).

#### **4.3.1. Background and motivation**

Currently, only two available CHB therapies are approved by US. Food and Drug Administration (FDA) and European Medicines Agency (EMA), interferon  $\alpha$ -based therapy and nucleos(t)ide analogues. Both therapies rarely result in complete cure and require life-long application (S. M. F. Akbar et al., 2022) with many side effects (W. Leowattana & T. Leowattana, 2022). There are many compounds for CHB therapy in clinical trials (Tab. 3) with different anti-HBV strategies, such as modulators of HBV life cycle: inhibitors of HBV entry (phase II), modulators of nucleocapsid assembly (phase II), inhibitors of HBV transcription (phase I-II) or HBsAg release (phase II clinical trial), etc.; or modulators of immune system: TLR agonists (phase I-II), immune checkpoint inhibitors (phase II), therapeutic vaccines (phase III), etc.

We explored utility of CDN-L, the lead compound chosen based on *in vitro* screening (chapter 4.1), in the treatment of CHB based on its ability to induce innate immunity via cGAS-STING pathway. The compound was tested, at first, in naïve C3H/HeN male mice to determine cytokine production, immune activation and dose response. Then therapeutic potential of CDN-L was determined using C3H/HeN HDI murine model reflecting CHB (chapter 4.2).

### 4.3.2. Results

#### **The induction of immune response is dependent on CDN-L dose.**

At first, cytokine production and innate immune system activation in naïve mice was tested. The CDN-L was intraperitoneally injected into C3H/HeN male mice in three different doses: 0.5, 1.5 and 5 mg/kg. The plasma cytokine profile was determined by multiplex ELISA assays and T cell activation using flow cytometry after 1h, 4h, 8h and overnight (OVN) post i.p. application (Fig. 15). The kinetics of cytokine response was determined in all timepoints. One hour post application no differences in production of cytokines compared to vehicle occurred. However, at 4h timepoint post application, increased IFN $\alpha$ , IFN $\beta$  and TNF- $\alpha$  levels were detected (Fig. 15). Compared to the vehicle group, cytokine response was CDN-L dose dependent with up to 8-, 20- and 40-fold increase, respectively. Interestingly, slightly increased IFN $\gamma$  occurred after 4h post injection at 1.5 and 5 mg/kg CDN-L. Eight hours post CDN-L application, the decrease of IFN $\alpha$ , IFN $\beta$  and TNF- $\alpha$  plasma levels was observed. However, IFN $\gamma$  levels reached peak at 8 hours post i.p. (up to 70x higher in case of 5 mg/kg CDN-L application compared to vehicle). OVN timepoint showed decrease of all observed cytokines to the vehicle levels.

At 4h and OVN timepoint post CDN-L administration, activation of T cells was investigated by determining CD69 activation marker expression on these cells. Again, the strongest activation of both CD8<sup>+</sup> and CD4<sup>+</sup> T cells was observed in mice injected with 5 mg/kg CDN-L followed by 1.5 mg/kg and 0.5 mg/kg dose of the injected compound. Interestingly, compared to 4h, OVN timepoint showed slightly increased CD8<sup>+</sup> T cell activation using all dosages of CDN and decreased CD4<sup>+</sup> T cell activation.

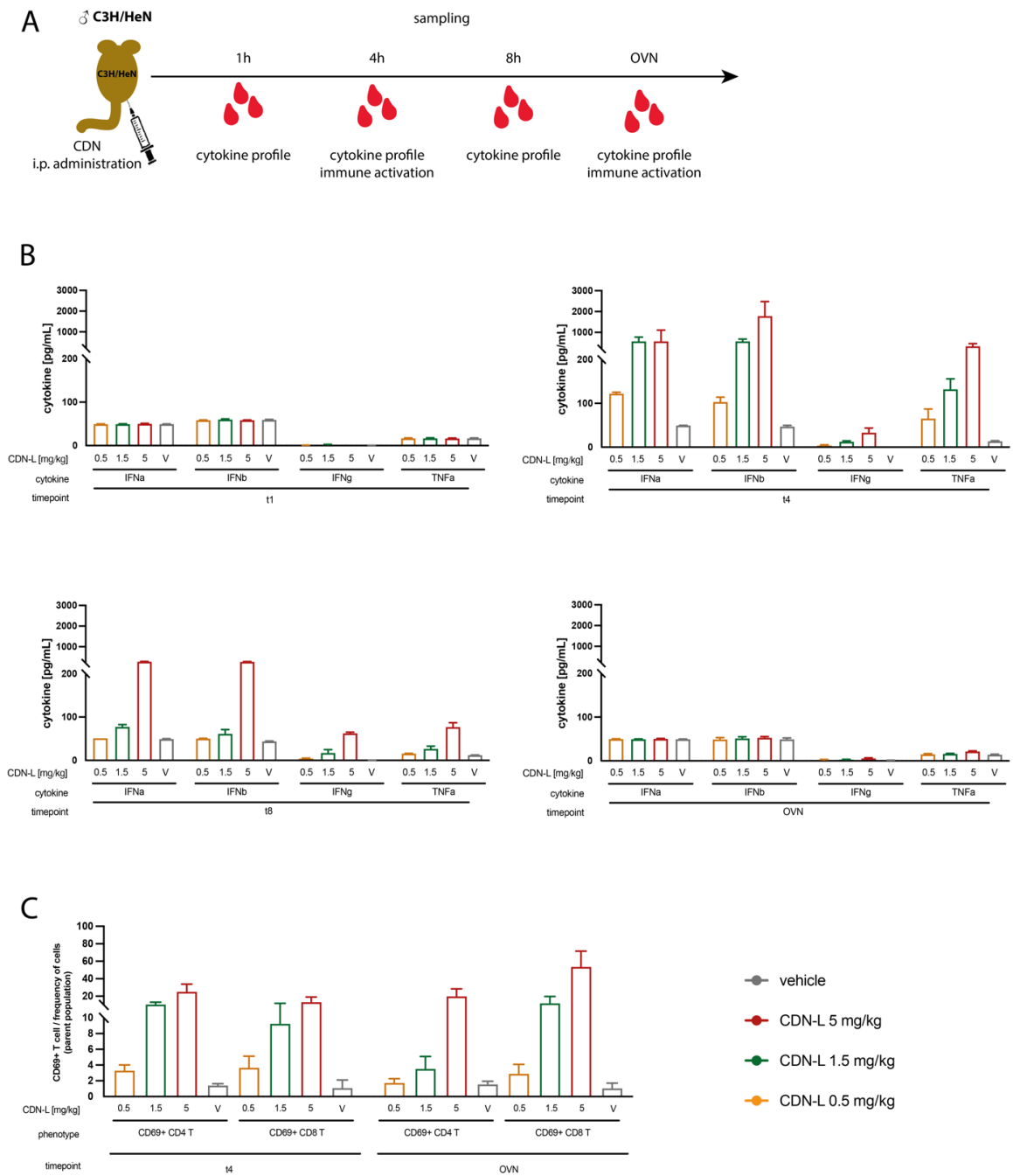


**Fig. 15: *in vivo* immune response of naïve C3H/HeN mice to CDN-L compound:** (A) schema of the experiment, (B) cytokine production, (C) CD4<sup>+</sup> and CD8<sup>+</sup> T cell activation, (B,C) in particular timepoints. Data were expressed as mean  $\pm$  standard error of mean (SEM) per group. V = vehicle, OVN = overnight incubation; n=5-10 mice/group

**Intraperitoneal application of CDN-L starting at dose 0.5 mg/kg leads to viral proteins clearance.**

C3H/HeN male mice (aged 4-6 weeks) were hydrodynamically injected with 10 µg pAAV/1.2HBV genotype A plasmid containing mutation in the START codon of the polymerase (chapter 4.2). The animals participating in the study were selected based on the high, stable level expression of HB-Ags for the first 5 weeks post HDI (Fig. 16). Animals reflecting CHB were treated intraperitoneally (i.p.) with CDN-L in 0.9% saline solution in 2 different therapeutic schemes. Treatment with higher doses of CDN-L, 1.5 and 5 mg/kg, was injected biweekly for one month (8 applications in total, Fig. 16) and lower doses, 0.15 and 0.5 mg/kg, were applied biweekly for two months (16 applications in total, Fig. 16). Vehicle group was injected i.p. only with 0.9% saline solution in the same schedule as therapeutic compound (16 applications in total). Efficacy results were evaluated as a relative fold of HB-Ag to week 5 as it serves as a determination and randomization point for CHB model.

After just two applications of 5 mg/kg CDN-L, the average HB-Ag levels dropped to <60% of the baseline level at week 5. After next three CDN-L applications, HBsAg levels dropped to <20% and sustained up to terminal point of the experiment (week 21). Average HBeAg levels dropped to <30% of the baseline level after six applications of CDN-L and sustained up to terminal point of experiment. On the contrary, first two applications of 1.5 mg/kg CDN-L led to milder decrease of HB-Ag, <80% of HBsAg and <60% of HBeAg compared to their baseline level at week 5. After 8 applications of 1.5 mg/kg CDN-L, HB-Ag levels dropped to <30% and sustained low up to terminal point of the experiment.

Mice injected with 0.5 mg/kg CDN-L started decreasing HBeAg compared to the baseline levels after 4 i.p. applications (<50%) and HBsAg levels after 6

applications (<70%). Slower kinetics of HB-Ag decrease led us to extend the treatment of the animals for up to two months. After 10 applications of 0.5 mg/kg CDN-L HBsAg levels dropped to <50% and HBeAg levels dropped to <30% and, both, the HBsAg and HBeAg levels sustained up to terminal point of the experiment. The first two application of the lowest dose 0.15 mg/kg CDN-L, only mildly affected the HBsAg levels, however the increase of HBsAg levels (<110%) appeared. The decrease of HBsAg occurred after 6 applications of 0.15 mg/kg CDN-L and dropped to <50% after completing treatment schema (16 applications) and sustained up to terminal point of the experiment.

Vehicle group, on the other hand, was increasing HBsAg levels up to w10 post HDI (>150%), then mildly dropped to <120% (w12) and sustained up to the terminal point of experiment. HBeAg levels in vehicle group mildly increased up to w10 post HDI and started dropping w12 post HDI to <80%. None of animals spontaneously cleared HB-Ag by the end of the study.

First measurable post treatment timepoint, week 15, showed the decrease of HBsAg positivity (Fig. 16) in dose dependent manner in terms of 5 mg/kg > 1.5 mg/kg > 0.5 mg/kg > 0.15 mg/kg. HBeAg positivity (Fig. 16) decrease showed in dose dependent manner as a trend of 5 mg/kg ~ 1.5 mg/kg > 0.5 mg/kg > 0.15 mg/kg. Both HB-Ag reflected effectivity trend.

None of the dosage affected physiology, as confirmed by the absence of weight changes (Fig. 17). The mice were also monitored regularly for general appearance (fur ruffling, mobility, and activity), showing no pathologic changes.

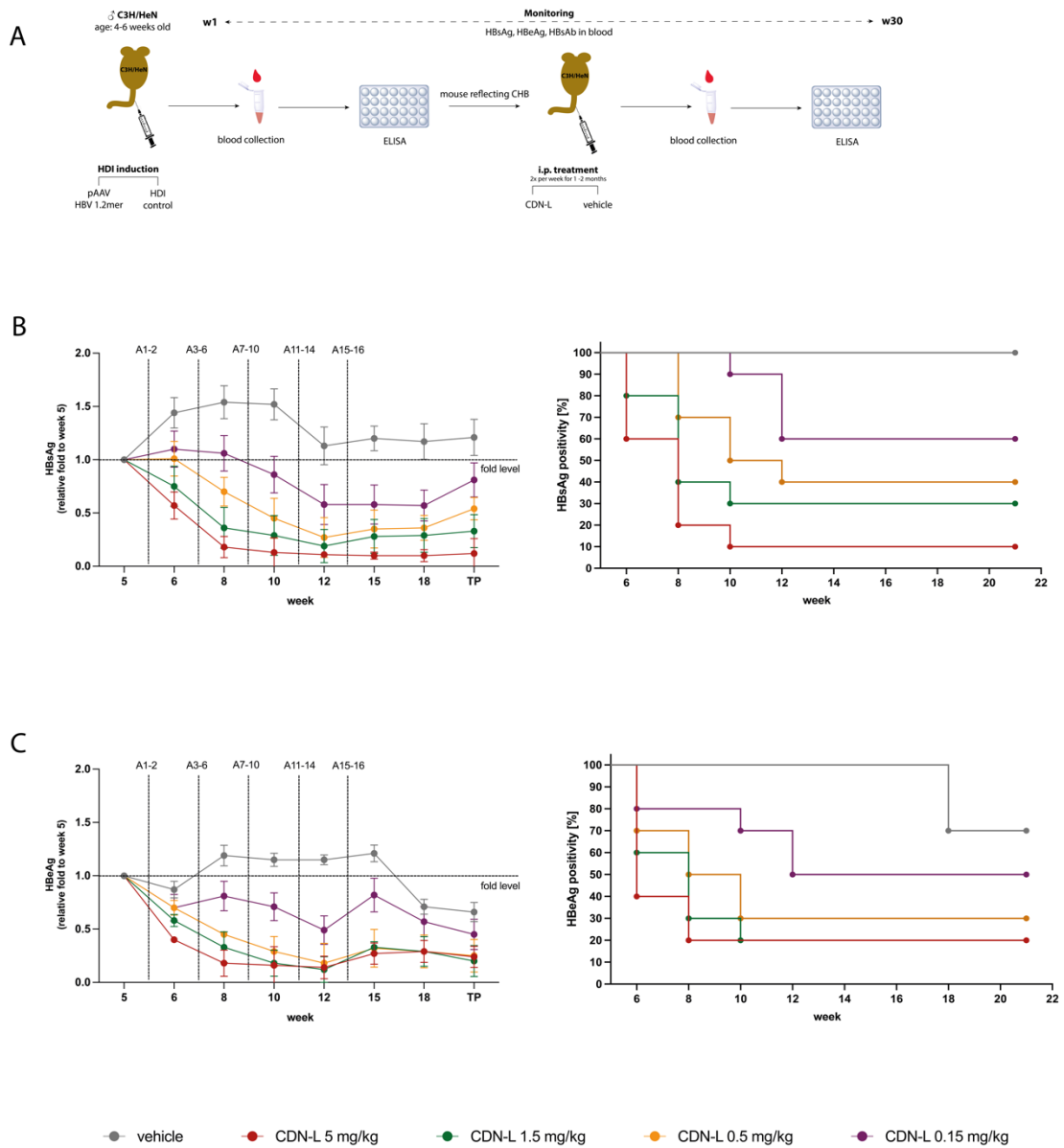


**Fig. 16: *in vivo* efficacy of CDN-L compound using C3H/HeN CHB murine model:** (A) schema of the experiment and continuous monitoring of HBsAg (B), HBeAg (C) blood levels. Data were expressed as a relative fold of HB-Ag to week 5 (mean  $\pm$  standard error of the mean (SEM)), the positivity proportions of all treatment groups were shown as Kaplan-Meier curves. A1-16 = administration of the compound 1-16; n=5-10 mice/group

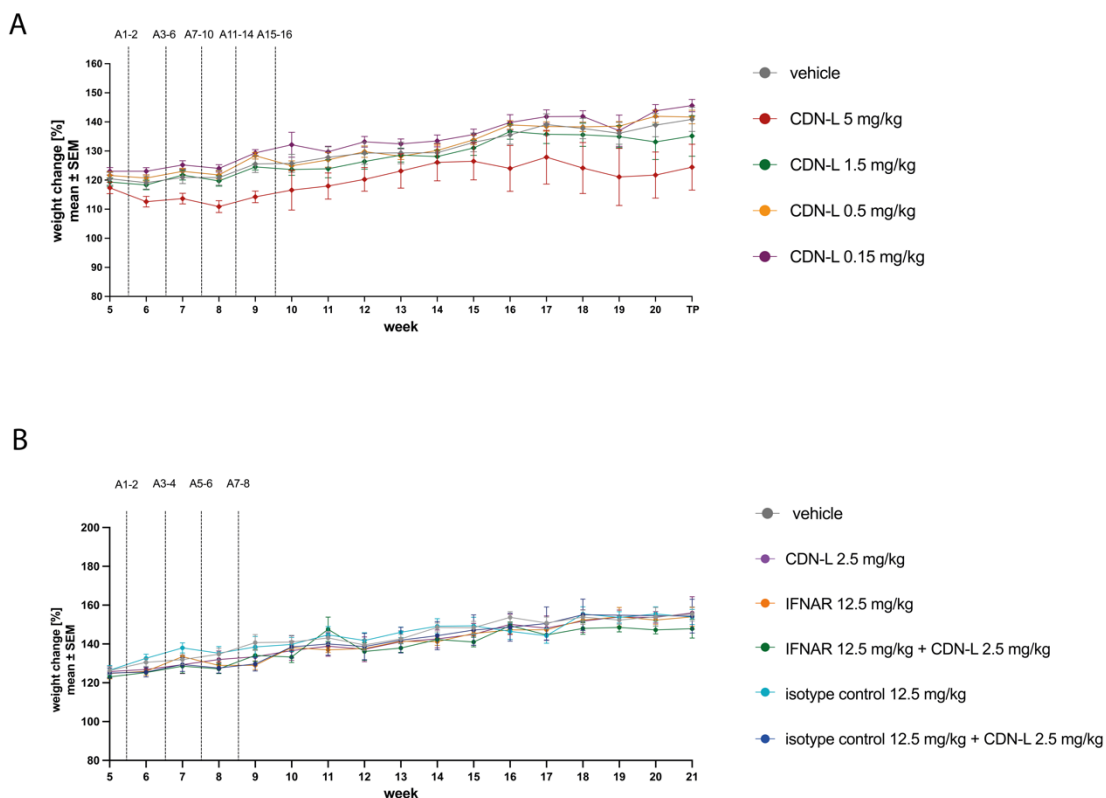


**Fig. 17: Characterisation of *in vivo* efficacy.** Weight as stratified by treatment groups for CDN-L efficacy (A) and interferon- $\alpha$  receptor (IFNAR) based CDN-L study (B), data were expressed as a mean  $\pm$  standard error of the mean (SEM); A1-16 = administration of the compound 1-16; n=5-20 mice/group.

**CDN-L treatment resulted in decrease of HBcAg positivity at the terminal point of the experiment.**

The expression of HBcAg in mouse hepatocytes was determined by immunohistochemical analysis of liver tissue at the terminal point of the experiment. IHC confirmed the presence of <25% of HBcAg positive cells in vehicle group at the terminal point of experiment (Fig. 18). Mice injected with CDN-L showed decrease of HBcAg positive cells to <10%, namely 0.15 mg/kg CDN-L and 0.5 mg/kg CDN-L (<10% HBcAg positivity), 1.5 mg/kg CDN-L (most cells negative to HBcAg) and 5 mg/kg CDN-L (very rare HBcAg positivity). Control mice (HDI control) were HBcAg negative throughout the experiment (Fig. 18).



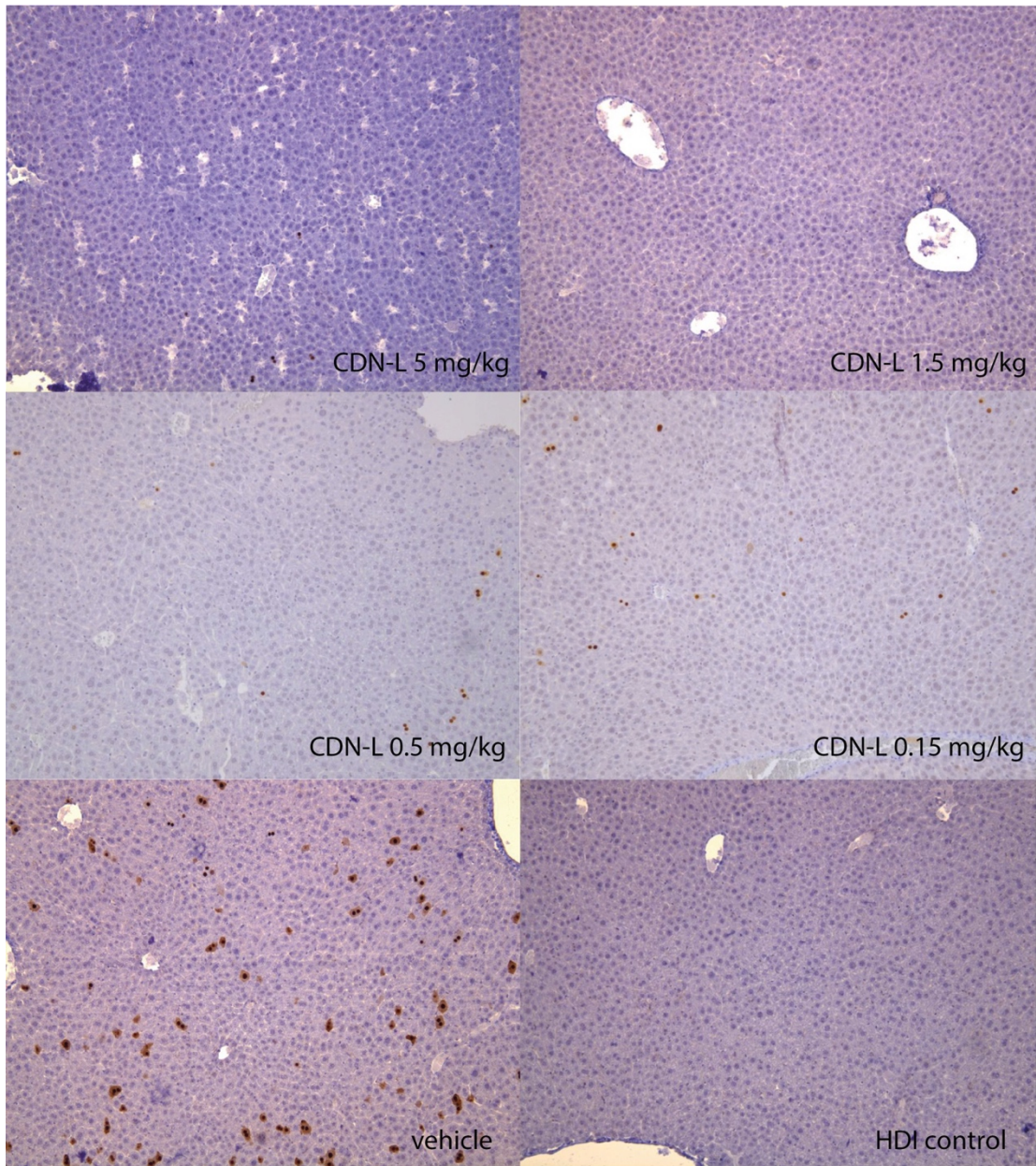


**Fig. 18: HBcAg expression in liver sections of C3H/HeN mice detected by immunohistochemistry:** HBcAg detected in CHB mice after treatment with different doses of CDN-L at the terminal point of the experiment; representative results of HBcAg (brown spots) per group. Vehicle = CHB mice injected with physiologic solution, HDI control = HDI delivery of physiologic solution.

### **Signalling through interferon- $\alpha$ receptor is required for optimal CDN-L effectivity.**

To determine the role of type I IFN during the treatment of our lead compound, we performed a combination therapy using anti-mouse interferon- $\alpha$  receptor (IFNAR) monoclonal antibody together with our lead compound CDN-L in animals reflecting CHB. Mice were subjected to the treatment with CDN-L, anti-mouse IFNAR antibody, combination of CDN-L and anti-mouse IFNAR antibody, relevant isotype control antibody, combination of CDN-L and relevant isotype control antibody biweekly for up to 8 applications (Fig. 19). The dose 2.5 mg/kg of CDN-L was determined as an optimal based on the previously established therapeutic window, dosage of anti-mouse IFNAR antibody (12.5 mg/kg) and relevant isotype control (12.5 mg/kg) was used as previously published (A. Dangi et al., 2018). Blocking of IFNAR receptor *in vivo* counteracted the potency of lead compound which led to the similar trend of HBsAg increase (>200% increase of HBsAg levels after 4 applications, Fig. 19) as in mice injected only with vehicle (200% increase of HBsAg levels, Fig. 19) or isotype control antibody (>200% increase of HBsAg levels, Fig. 19). IFNAR blockade itself did not affect the sustainability of the model and comparable HBsAg levels were observed during the experiment to vehicle group (250% increase of HBsAg levels after first 4 applications, Fig. 19). Slight decrease of HBeAg levels (40%, Fig. 19) was observed after 4 applications of anti-mouse IFNAR antibody, anti-mouse IFNAR antibody in combination with CDN-L, relevant isotype control antibody and vehicle group. On the contrary, the rapid decrease of both HBsAg and HBeAg levels was observed using 2.5 mg/kg of CDN-L or in combination with isotype control antibody. After first 4 applications, 20% and 70% decrease of HBsAg and HBeAg levels was observed. After 8 applications, HBsAg levels dropped to 20% (Fig. 19). In terms of positivity, vehicle,

isotype control antibody, anti-mouse IFNAR antibody and anti-mouse IFNAR antibody in combination with CDN-L maintained >80% of HBsAg positive animals up to the terminal point of experiment (w21, Fig. 19) counter to 20% of HBsAg positive animals in both, CDN-L and CDN-L in combination with isotype control antibody groups. HBeAg positivity dropped to 30-40% in vehicle, isotype control antibody, anti-mouse IFNAR antibody and anti-mouse IFNAR antibody in combination with CDN-L group, whereas CDN-L and CDN-L in combination with isotype control antibody showed only 20% HBeAg positivity. These data suggest that the activation of immunity through IFNAR is required for an optimal effectivity of CDN-L.

None of the treatment affected physiology, as confirmed by the absence of weight changes (Fig. 17). The mice were also monitored regularly for general appearance (fur ruffling, mobility, and activity), showing no pathologic changes.

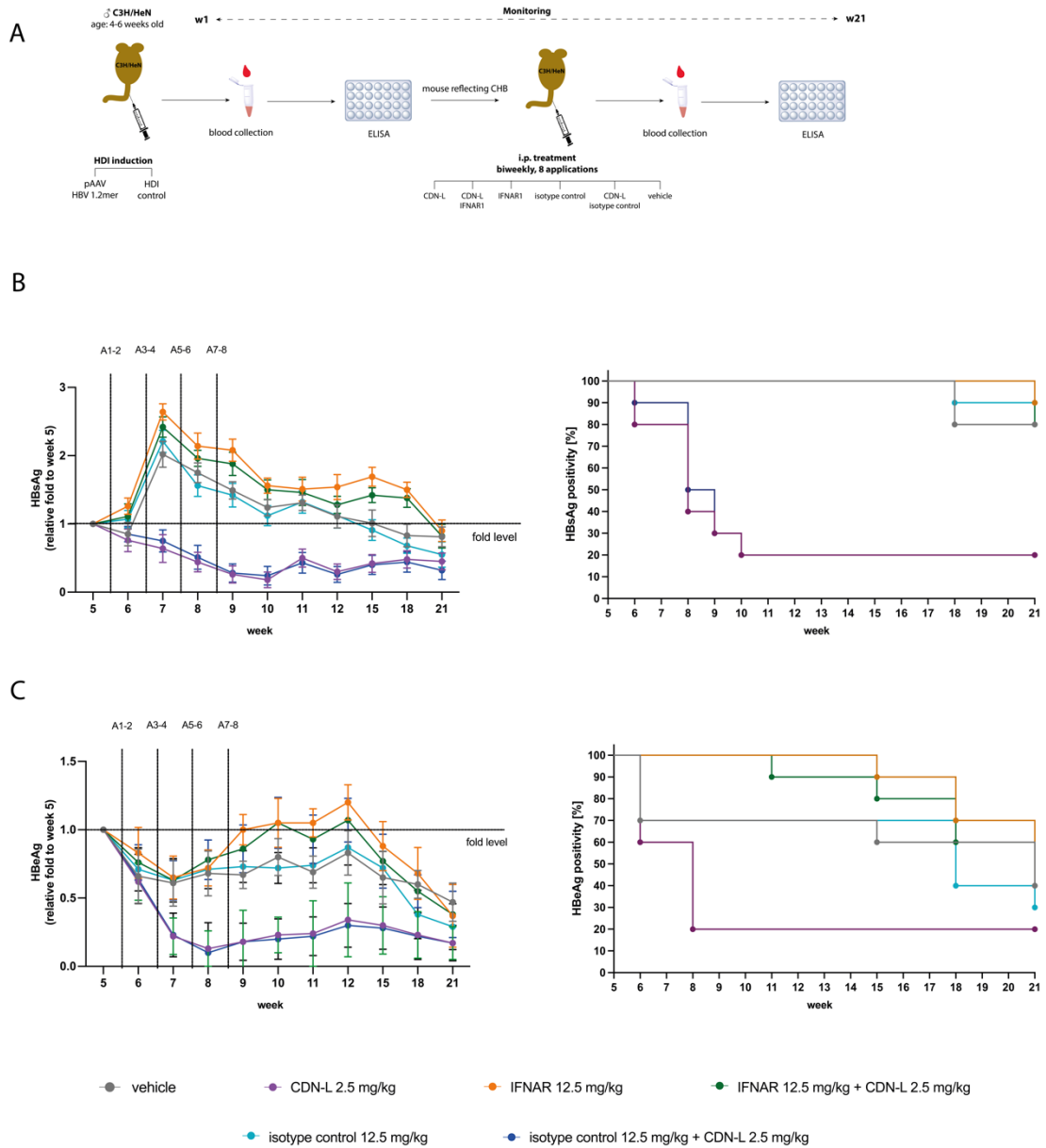


**Fig. 19: *in vivo* CDN-L efficacy dependent on interferon- $\alpha$  receptor using C3H/HeN CHB murine model:** (A) schema of the experiment and continuous monitoring of HBsAg (B), HBeAg (C) blood levels. Data were expressed as a relative fold of HB-Ag to week 5 (mean  $\pm$  standard error of the mean (SEM)), the positivity proportions of all treatment groups were shown as Kaplan-Meier curves. IFNAR = anti-mouse IFN- $\alpha$  receptor antibody; A1-16 = administration of the compound 1-16; n=5-10 mice/group

#### **4.3.1. Conclusion**

The therapeutic potential of CDN-L was verified using a C3H/HeN mouse model reflecting CHB based on HDI induction of pAAV/1.2HBV genotype A with a point mutation in START codon of polymerase (chapter 4.2). As anticipated, we observed dose dependent effect of CDN-L on viral HB-Ags in the CHB model. Application (i.p.) of CDN-L at lowest dose (0.15 mg/kg) induced slow decrease of viral HB-Ag levels; however, even 16 applications of 0.15 mg/kg CDN-L per mouse did not result in HB-Ag disappearance even though xyz animals responded to the treatment. Nevertheless, 1.5 and 5 mg/kg CDN-L led to the fast decrease of the viral proteins. Importantly, plasma HBsAg and HBeAg did not rebound after the secession of the treatment. The follow up study on the role of type I interferons induced by CDN-L using anti-IFNAR monoclonal antibody clearly indicate the essential role of type I interferons in antiviral activity of the compound. would result in long-term remission of CHB even in lower dosage (0.5 mg/kg), however, repetitive administration would be needed. Hence, we firmly believe that CDN-L has high therapeutic potential for CHB treatment. Based on our results, we conclude that treatment with CDN-L would result in long-term remission of CHB even in lower dosage (0.5 mg/kg), however, repetitive administration would be needed. Hence, we firmly believe that CDN-L has high therapeutic potential for CHB treatment.

#### **4.4. Suggestions for additional therapy outcome evaluation**

Methodology was published:

*Vanekova, L., Polidarova, M. P., Veverka, V., Birkus, G., & Brazdova, A. (2022). Multiparametric Flow Cytometry-Based Immunophenotyping of Mouse Liver Immune Cells. Methods and protocols, 5(5), 70. <https://doi.org/10.3390/mps5050070>*

My contribution:

Methodology development and validation, data analysis, manuscript preparation.

##### **4.4.1. Background and motivation**

Liver is a complex organ involved in many types of metabolisms and cellular processes, including immune processes. Therefore, the outcome of many liver pathologies, such as CHB, is affected by the liver-tissue-associated immunity. Characterisation of liver immune microenvironment may provide a better understanding of immune signalling as well as mechanisms of specific immune responses to different treatments which could be beneficial for preclinical evaluation of novel therapies. (D. P. Bogdanos et al., 2013; M. Haque et al., 2020; F. Heymann & F. Tacke, 2016; F. Tacke & H. W. Zimmermann, 2014; M. Zheng & Z. Tian, 2019)

Several immunophenotyping methods are available, including conventional and spectral flow cytometry (L. Ferrer-Font et al., 2020; F. Gondois-Rey et al., 2012), cytometry by time-of-flight (B. A. David et al., 2017), automated parallel RNA single-cell sequencing combining fluorescence-activated cell sorting techniques (A. Giladi et al., 2018) or massive multiplexing RNA sequencing (D. A. Jaitin et al., 2014). However, the cost and instrumental setup of most of the described methods allowing multiparametric analysis of more than 20 colours in one panel make it rarely available in regular academic laboratory conditions.

#### 4.4.2. Methodology for suggested additional evaluation

In order to further evaluate liver specific immune response after CDN-L therapy, we developed a robust yet low-cost, fast, and straightforward procedure for isolation of single cell suspension of high yield of mouse liver non-parenchymal cells (NPC) while still preserving antigen/epitope profiles in order to characterise multiple intrahepatic immune populations. The procedure combines *in situ* perfusion with PBS via portal vein (F. Cabral et al., 2018), *ex vivo* liver tissue dissociation combining mechanical disruption and enzymatic digestion using Miltenyi Biotec kit (Miltenyi Biotec, 2021), Percoll density gradient-based cell purification (M. Aparicio-Vergara et al., 2017; K. G. Blom et al., 2009; P. zhi Li et al., 2014; R. W. Lynch et al., 2018; I. Mohar et al., 2015; W. Shi et al., 2020) and thorough conventional FC-based immunophenotyping (Fig. 20, Fig. 21, Fig. 22).

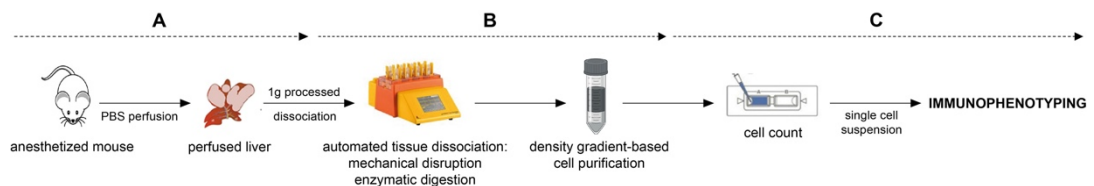


**Fig. 20:** Workflow as a schematic description. (A) *in vivo* manipulation part, (B) liver processing, (C) downstream procedure.

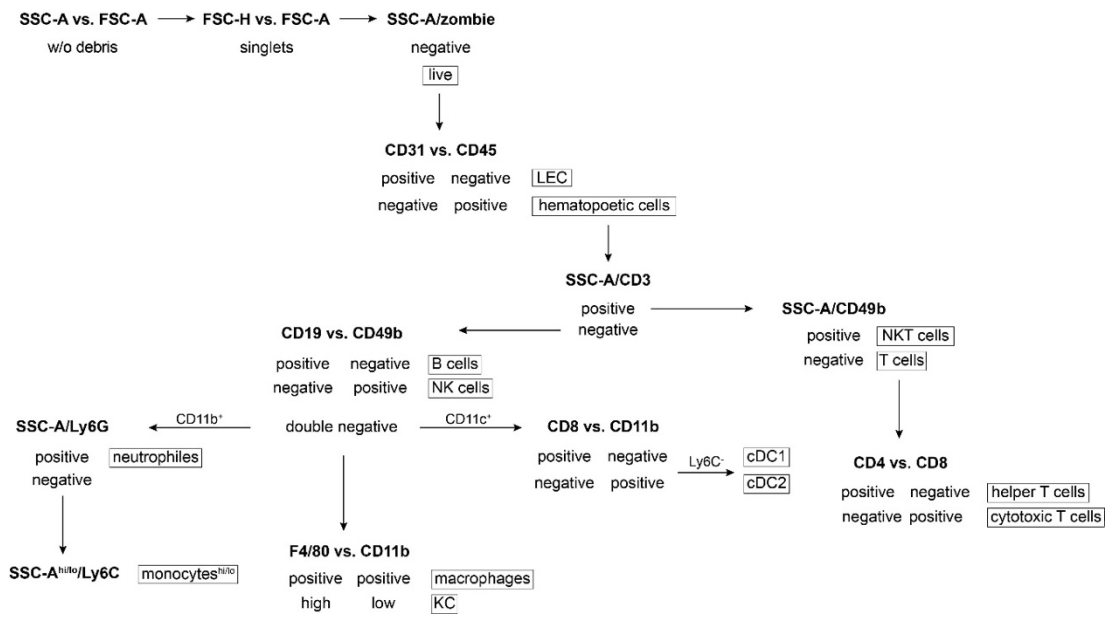


**Fig. 21:** Schema of gating strategy for flow cytometry data acquisition.

The gating strategy for the presented multicolor FC panel (Fig. 21, 22) is based on the gradual elimination of unwanted populations and further identification of targeted subsets. To monitor the overall changes of many immune subsets, we show the simple approach of gating the inflammatory (or classical) Ly6C<sup>high</sup> monocytes and reparative (patrolling, non-classical) Ly6C<sup>low</sup> monocytes (Fig. 21, Fig. 22). However, the additional combination of immune profiling can expand the obtained datasets and alternative gating strategies, such as gating particular (sub)phenotypes of NK or NKT subsets, can provide supplementary information of ongoing immune reactions (Z. Li et al., 2019; C. Wang et al., 2015). Accordingly, the further gating of functional cells could be a useful approach in the therapeutic studies.



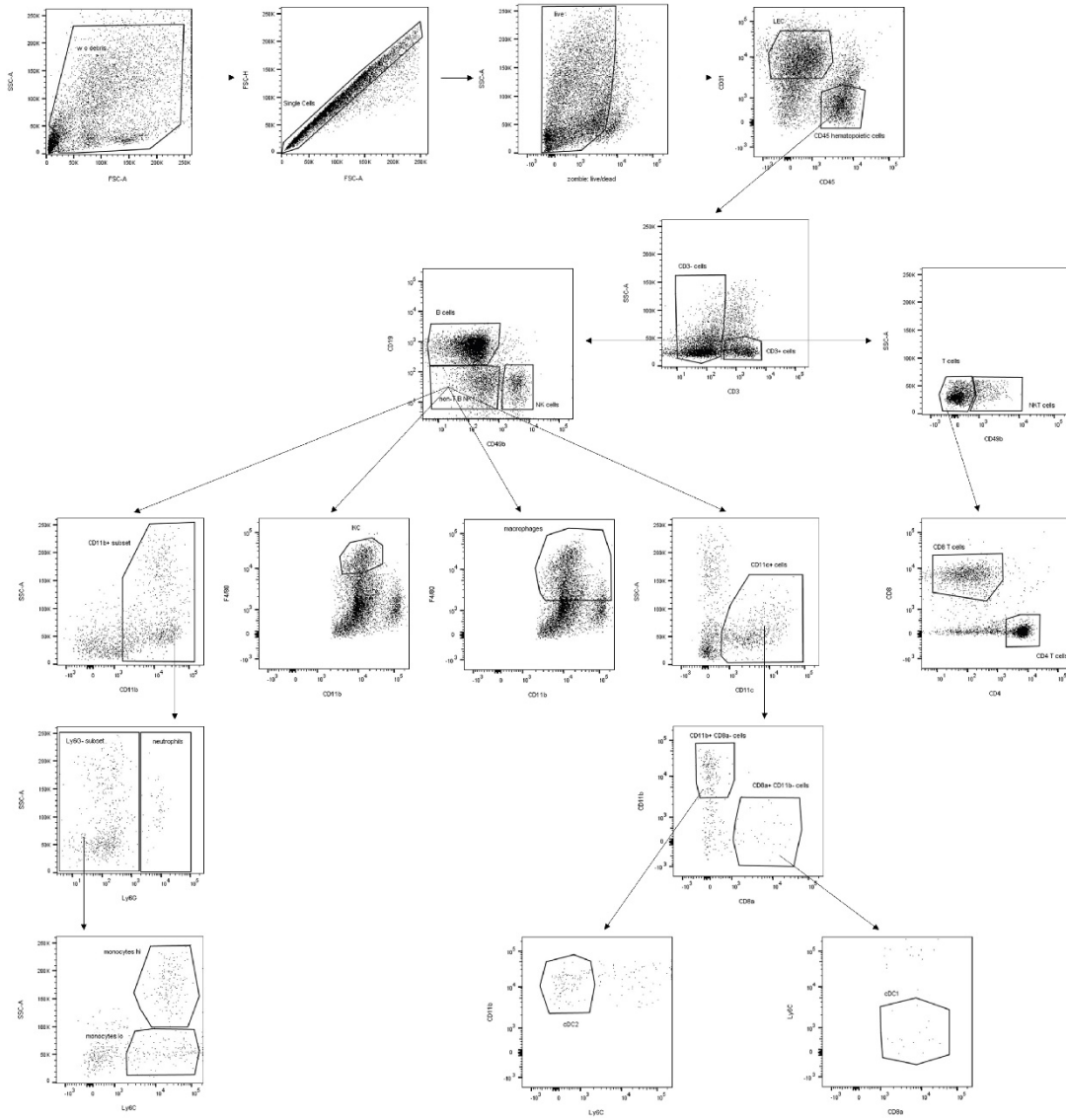


**Fig. 22:** Illustration of gating strategy for individual immune populations. (Shown images represent a composition of three independent measurements).

#### **4.4.3. Conclusion**

The suggested additional therapy outcome evaluation based on the thorough immunophenotyping protocol using conventional FC allows detection and quantification of various intrahepatic immune populations (LEC, T cells (helper and cytotoxic), B cells, NK cells, NKT cells, neutrophils, monocytes (reparative and inflammatory), dendritic cells (including their subsets), macrophages and Kupffer cells (KC)) in one single sample (Fig. 22). The presented FC gating strategy is, though, not limited by the determination of basic populations as it can be extended to monitoring expression of a particular marker or subphenotypes within the population of interest. This method can provide supplementary information on ongoing immune reactions in further CDN-L *in vivo* studies focusing on the characterisation of the liver immune response to CDN-L therapy in murine model reflecting CHB.

## 5. DISCUSSION

The cGAS-STING signalling pathway plays a major role in host immune reactions involved in many pathologies including cancer (C. Gravekamp & D. Chandra, 2015), senescence (J. M. van Deursen, 2014; H. Yang et al., 2017), and ageing (J. M. van Deursen, 2014), autoimmune or autoinflammatory diseases (D. Gao et al., 2015; V. Kumar, 2019; S. Sharma et al., 2015) and pathogen infection (H. Kumar et al., 2011; G. Mitchell & R. R. Isberg, 2017). Thus, cGAS-STING signalization became a promising therapeutic target and both, STING agonists and antagonists became intensively studied as a relatively new therapeutic strategy in diverse pathologies (X. Feng et al., 2020; C. Gravekamp & D. Chandra, 2015; X. Tian et al., 2022; J. J. Wu et al., 2020). We specifically focused on the development of CHB therapy, as only two available therapies are currently approved (interferon  $\alpha$ -based therapy and nucleos(t)ide analogues). Unfortunately, they often require life-long application as the therapy rarely result in the complete cure (S. M. F. Akbar et al., 2022). Unlike inhibitors of HBV entry (H. Wedemeyer et al., 2019), viral transcripts (Gane et al., 2020, 2021), capsid assembly (S. Fung et al., 2020; M.-F. Yuen et al., 2020) or HBsAg secretion (M. Bazinet et al., 2017), we aimed at innate immune system activation to eliminate the viral infection. To the best of our knowledge, only few immune modulators are currently in clinical trials with various mechanisms of action, among others, agonists of TLR receptors (H. L. A. Janssen et al., 2021, 2018) or immune checkpoint inhibitors (E. Gane et al., 2019).

Unlike already available drugs in clinical trials, we focused on the activation of STING protein to trigger downstream signalization leading to type I interferon-based immunomodulation. Large library of CDNs based on STING natural agonists, 2'3'-CDNs or 3'3'-CDNs, was prepared in the HBV Cure group at Institute of Organic

Chemistry and Biochemistry of the Czech Academy of Sciences using both enzymatic and synthetic approach (Birkus, 2018; G. Birkus et al., 2020; M. Dejmek et al., 2022; B. Novotná et al., 2021, 2019; M. Pimková Polidarová et al., 2021; Z. Vavrina et al., 2022; Z. Vavřina et al., 2021). To better evaluate and understand the potency of our newly prepared compounds, we compared their *in vitro* activity relatively to the set of control CDNs, such canonical STING agonist 2'3'-cGAMP or ADU-S100, the CDN-based STING agonist terminated in Phase II clinical trials in cancer (Inc. Chinook Therapeutics, 2022; L. Corrales et al., 2015). Our results strongly suggests that newly prepared CDNs are involved in direct binding to the STING protein. To support this paradigm and rationalize the interactions of the ligands to STING protein, the thermal shift assay using DSF method was performed. The enhancement of STING-CDN stability of our lead compound is considerable compared to natural 3'3'-CDNs or ADU-S100. Unlike (S. Vyskocil et al., 2021), we employed biological testing using HEK293T reporter cell line stably transfected with all STING haplotypes to understand the lead CDN activity towards all described STING allelic forms as different binding capacity among described STING allelic forms (*WT*, *HAQ*, *REF*, *R293Q* and *Q*) was observed (G. Yi et al., 2013). Understanding the allele-associated STING activation and such uniformly acting STING agonists would eliminate genotyping of CHB patients given the variable frequency of human polymorphism in STING protein in the population (G. Yi et al., 2013), all of which would simplify CHB therapy and would importantly contribute to the applicability of lead STING agonist as potential therapeutics. The *in vitro* activity of newly prepared CDNs is also influenced by the efficiency of their active uptake into the cell (M. Dejmek et al., 2022; B. Novotná et al., 2021, 2019; M. Pimková Polidarová et al., 2021; Z. Vavrina et al., 2022; Z. Vavřina et al., 2021). Our results show increase in the activity more than 100x

in the presence of digitonin, where the polar, charged CDNs freely diffused into cells. However, to avoid an obstacle of active cell uptake for polar CDNs, a lipophilic prodrug of CDNs could help efficiently deliver the active CDNs into the cell (M. Dejmek et al., 2022; R. P. Iyer et al., 2019; M. Pimková Polidarová et al., 2021). The vast majority of our newly prepared CDNs had comparable or even lower EC<sub>50</sub> values compared to canonical 2'3'-cGAMP or ADU-S100 using all STING allelic forms. Moreover, our lead compound CDN-L had 10x higher potency compared to recently described STING agonists (C. R. Ager et al., 2019; W. Chang et al., 2022; S. Vyskocil et al., 2021) or even nucleic acid analogues (S. Stazzoni, 2020). In order to confirm the CDNs efficacy *in vitro* in physiologically relevant system, the STING-dependent cytokine production in response to the stimulation of PBMCs was measured. We focused mainly on the production of TNF- $\alpha$ , IFN $\alpha$ , an early onset immune response, and IFN $\gamma$ , late onset reaction. Our results support previously published data on STING-based cytokine stimulation in PBMC using CDN-agonists (F. Borriello et al., 2017; D. K. R. Karaolis et al., 2007; D. Lirussi et al., 2017), dsDNA (K. Kis-Toth et al., 2011) or diABZI (J. M. Ramanjulu et al., 2018). The CDN-based secretion of cytokines using our lead compound showed >10x higher potency than canonical 2'3'-cGAMP or clinical candidate ADU-S100.

Taken all together, our newly prepared CDNs *in vitro* activate innate immune response through STING-dependent signalization with a specificity towards majority of STING haplotypes. Our lead compound (CDN-L) was selected based on multiple factors, such as the *in vitro* activity towards STING haplotypes, induction of cytokines in PBMC assay, human/mouse plasma stability, mouse pharmacokinetics, *in vitro* anti-HBV activity etc. Furthermore, CDN-L showed superior activity in all screening assay relative to the clinical candidate ADU-S100 used in anti-tumour therapy.

In order to validate lead compound efficacy *in vivo*, we developed immunocompetent CHB mouse model based on HDI delivery of plasmid vector carrying HBV genome (A. M. Ortega-Prieto et al., 2019) leading to stable expression of the viral markers HBsAg and HBeAg for 20 weeks without induction of viral progeny. Research in this field has recently led to the development of several other murine models, such as transgenic (L. G. Guidotti et al., 1995) and chimeric (M. Grompe et al., 1993) mouse models, as well as models based on tail vein delivery of viral vectors carrying HBV DNA genome (L. L. Wu et al., 2017). However, all of them have some limitations (Y. Du et al., 2021), including requiring Biosafety Level 3 animal facilities. We used HDI induction system based on tail vein delivery of viral vector carrying HBV genome as its main advantage lies in the variability of HBV genotypes or mutants used (B. Qin et al., 2013). We chose two different induction systems, pAAV (L. R. Huang et al., 2006; L. Li et al., 2017) and pMC (Z. Yan et al., 2017) plasmid vectors carrying 1.2mer and 1.0mer HBV DNA genome (genotype A and D) with a T2308C (Z. Yan et al., 2017) point mutation of the START codon of the polymerase. The performed mutation prevents the production of infectious HBV progeny (Z. Yan et al., 2017) without affecting HBV transcription and antigen expression. Therefore, mouse model reflecting CHB using these plasmid vectors with this particular point mutation allows us to operate in a Biosafety Level 2 animal facility.

As suggested by Milich and Leroux-Roels, 2003 mouse strains differ in MHC class-based immune response, therefore, we decided to use C57Bl/6 and C3H/HeN mouse strain to compare the persistence of CHB model focusing on HB-Ag as the CHB pathogenesis is a consequence of persistent expression of various HBV antigens (H. J. Alter & F. v. Chisari, 2019; P. A. Revill et al., 2019). HBsAg is considered a general marker of HBV in both mouse and human plasma (J.-H. Kao, 2014), regardless

of acute or chronic infection and has been shown to inhibit host immune reactions by various mechanisms (A. Bertolotti & C. Ferrari, 2016; C. Dembek et al., 2018; S. N. Mueller & R. Ahmed, 2009). As the seroconversion of HBsAg to HBsAb stands as a marker of the host recovery and cure of CHB, we evaluated our model based on the decrease of HBsAg. Since HBsAb production is affected by S region-encoding MHC class III complement components, including C<sup>4</sup> and C<sup>2</sup> (D. R. Milich & G. G. Leroux-Roels, 2003), we tested mouse strains from an intermediate MHC genotype group with different haplotypes, i.e., C57Bl/6 (haplotype *b*) and C3H/HeN (haplotype *k*).

Unlike other studies (L. R. Huang et al., 2006; L. Li et al., 2017), where HB-Ag expression persisted for more than 6 months when using replication-competent HBV genome in C57Bl/6 mice, we demonstrated that the C57Bl/6 mouse strain bearing the S<sup>b</sup> region with a sufficient response to HBsAg leads to HB-Ag clearance resulting in only an acute HBV model which, on the other hand, corresponds with Peng, et al. (X. H. Peng et al., 2015). This result could be explained by differences in positivity threshold settings.

In agreement with Peng et al., 2015 and Yan et al., 2017, who presented non-mutated pAAV/1.2HBV and pMC/1.0HBV in the C3H/HeN mouse strain, we observed markedly increased and sustained viral antigen expression. Based on MHC class of C3H/HeN mice, we assume that the insufficient response to HBsAg reflects its persisting levels and the low levels of seroconversion.

Considering the plasma levels of the viral markers, the efficacy of the induction systems in both C57Bl/6 and C3H/HeN mice was reflected as a trend of pAAV/1.2HBV genotype A  $\geq$  pMC/1.0HBV pre-S genotype D  $>$  pMC/1.0HBV pre-C genotype D  $\gg$  pAAV/1.2HBV genotype D. In contrast to genotype A, genotype D has a 33-nucleotide deletion in the N terminus of the PreS1 region (A. Kramvis, 2014)

which changes the ratio of the three S antigen forms and affects their secretion (S. Sengupta et al., 2007). It may thus explain why the HBsAg levels were significantly lower in mice induced with HBV genotype D. The differences in HBeAg levels among plasmids in both mouse strains might be associated with the use of different induction systems. The pMC HDI induction system was primarily developed to address cccDNA *in vivo* (Z. Yan et al., 2017). As previously described (T. Zhou et al., 2006), HBeAg secretion and cccDNA formation may be correlated; if so, significantly higher HBeAg levels should be found when using minicircle constructs. However, the point mutation of the START codon of the polymerase adversely affected the viral replication cycle. Nevertheless, HBeAg persistence is variable even among CHB patients and thus not a definitive CHB marker (The World Health Organisation, 2017).

Immunocompetent HDI mouse models reflecting CHB are widely used for research of novel therapies aiming to restore the host innate immune antiviral function. For instance, TLR3 ligand, Polyinosinic:polycytidylic acid [poly(I:C)], led to HBV clearance associated with increased CD8<sup>+</sup> T cell infiltration (J. Wu et al., 2014), then similar results were observed using NOD1 ligand acting by promoting HBV-specific CD8<sup>+</sup> T cells leading to HBV clearance (S. Huang et al., 2018). We addressed the activation of CD8<sup>+</sup> T cells, yet not HBV specific, *in vivo* after CDN-L application in the naïve C3H/HeN mice and dose response T cell activation was observed. As CD69 represents early activation marker (D. Cibrián & F. Sánchez-Madrid, 2017), the activation was proportional in both counterparts, CD4<sup>+</sup> and CD8<sup>+</sup> T cells, yet CD69<sup>+</sup> CD8<sup>+</sup> T cells are more profound in time relaps of 24h. Pathogenesis of CHB is characterised by exhaustion of HBV-specific CD8<sup>+</sup> T cells leading to weaken CD8<sup>+</sup> T cell responses (B. Rehermann, 2013; B. Rehermann & M. Nascimbeni, 2005; Q. Wang et al., 2018) and as we show CDN-associated T cell activation in naïve C3H/HeN mice,



we assume that CHB therapy using CDN-L could benefit from induced T cell mediated HBV clearance (F. v. Chisari & C. Ferrari, 1995; P. L. Yang et al., 2010). Based on the previous reports on inflammatory and antiviral processes (F. v. Chisari & C. Ferrari, 1995; S. Huang et al., 2018; B. Rehermann, 2013; B. Rehermann & M. Nascimbeni, 2005; Q. Wang et al., 2018; J. Wu et al., 2014; P. L. Yang et al., 2010), it seems crucial to modulate the type I IFN response together with the activation of adaptive immune responses such as activation of CD8<sup>+</sup> T cells. The STING agonist CDN-L triggers sufficient antiviral responses via cGAS-STING pathway as it represents the major signalization for antiviral immunity.

As clearance of HBsAg is considered as a crucial step for restoring host immunity and cure of CHB (A. Bertolotti & C. Ferrari, 2016; C. Dembek et al., 2018; S. N. Mueller & R. Ahmed, 2009), the main goal for CDN-L treatment was the induction of effective host immune response via STING signalization resulting in the rapid decrease of the HBsAg levels. Our results demonstrate the rapid decrease of HBsAg levels after single high dose injection with CDN-L. However, for the effective CHB cure in term of lasting lowered HBsAg levels, repeated application biweekly for up to two months based on the dosing of the compound was required. As previously described in CDN-based anti-tumour therapy research (C. Pantelidou et al., 2022; C. Song et al., 2022), repeated CDN administration is mandatory for successful therapeutic outcome. Notwithstanding, CDN-L itself showed promising results in anti-CHB therapy *in vivo*. We speculate that the increased efficacy using combined therapy of our lead compound with for instance HBsAb infusion or HBsAg vaccination could be achieved as it was previously reported for the TLR9 agonist (D. Zhu et al., 2016). It should also be mentioned that combination of IFN-based therapy and nucleos(t)ide analogues for CHB was already addressed in several clinical trials with promising

results. However, the loss of HBsAg increased only in a few CHB patients (H. L. Y. Chan et al., 2019; Q. Ning et al., 2014). Moreover, benefits of combined therapy using CDNs have already been reported (C. Pantelidou et al., 2022) in anti-tumour therapy using clinical candidate ADU-S100 with poly (ADP-ribose) polymerase inhibitors, immune checkpoint anti-PD1 therapy (K. E. Sivick et al., 2018), immune checkpoint PD-L1 therapy (J.-J. Lee et al., 2022; M. Yi et al., 2022) or CTLA-4 therapy (S. Dorta-Estremera et al., 2019).

The type I interferons dependent mechanism of HBV inhibition by CDN-L was confirmed using anti-mouse interferon- $\alpha$  receptor (IFNAR) monoclonal antibody. Our results are in accordance with an observed anti-HBV activity using first line CHB treatment option, pegylated-IFN $\alpha$  (A. S. J. Woo et al., 2017). Moreover, previously described ADU-S100 treatment in tumour models (K. E. Sivick et al., 2018) or other STING agonists (L. Corrales et al., 2015; O. Demaria et al., 2015) was inhibited by IFNAR blocking, pointing to important role of type I interferons in inducing antitumoral adaptive immunity.

Lastly, we also suggest additional therapy outcome evaluation based on the thorough immunophenotyping of intrahepatic immune cells using conventional FC. The developed methodology allows the detection and quantification of various intrahepatic immune populations in one single sample which makes it useful in regular small research as well as large-scale screening focusing on the characterisation of the liver immune cells in mouse models of human pathologies, or in studies of the liver immune response to different treatments. It should be noted, that using multiparametric conventional FC-based immunophenotyping requires a precise compensation matrix due to the high spillover signals. It is crucial to define a proper gating and non-specific antibody binding using relevant controls (such as fluorescence minus one (FMO),

relevant antibody isotype control, positive control for live/dead marker). To overcome this limitation, the spectral FC could be used as it measures full range of emission spectrum of each fluorochrome across all lasers (L. Ferrer-Font et al., 2020) or cytometry by time-of-flight as it uses unique isotope-conjugated markers without need of compensation (B. A. David et al., 2017).

Taken all together, our lead compound (CDN-L) showed outstanding results in CHB mouse model based on HDI delivery of HBV genome as monotherapy. We believe that the combination therapy using our lead compound might eliminate the burden of recurrent application which would make it more interesting for clinical studies. On top of that, assuming ADU-S100 results and other CDN based anticancer therapeutic outcome, we speculate that our lead compound might have remarkable results also in cancer therapy *in vivo*, as STING agonists are highly assessed in anticancer immunity in current literature (C. Pantelidou et al., 2022; C. Song et al., 2022; S. Stazzoni et al., 2022; S. Vyskocil et al., 2021; A. H. Zaidi et al., 2021). Thus, outstanding results in CHB therapy using CDN-L together with diverse therapeutical applications makes our compound highly interesting for pharmaceutical industry. Moreover, we confirmed that our mouse model reflecting CHB can be used in preclinical validation of novel CHB therapies.

## 6. CONCLUSION

This doctoral thesis was focused on the CHB therapy, mainly the development of immunocompetent mouse model reflecting CHB which would be suitable for robust preclinical evaluation of potential novel CHB therapeutics. Moreover, set of STING agonists exclusively prepared at the Institute of Organic Chemistry and Biochemistry of the Czech Academy of Sciences in the group HBV Cure led by Mgr. Gabriel Birkuš, Ph.D. were tested *in vitro* whereas the lead compound was evaluated *in vivo* for anti-CHB effect.

We developed series of biochemical and biological screening methods to determine the *in vitro* binding affinity towards STING protein and related activity using five most abundant STING haplotypes, *WT*, *HAQ*, *AQ*, *REF*, *Q*. We compared our results with natural STING agonist 2'3'-cGAMP and CDN-based STING agonist ADU-S100, the clinical candidate for cancer treatment terminated in the Phase II clinical trials (Inc. Chinook Therapeutics, 2022). Based on the *in vitro* testing of novel CDNs, we chose the lead compound with promising results in all performed *in vitro* tests and towards all STING haplotypes, CDN-L.

An accessible, convenient, and affordable long-term *in vivo* model reflecting CHB using hydrodynamic injection of pAAV/1.2HBV genotype A with a T2308C point mutation of the polymerase START codon was developed in C3H/HeN mouse strain. The expression of viral markers lasted for all screened 20-week experimental *in vivo* setting, however, based on the pAAV/1.2HBV genotype A-associated HBsAg levels, we believe that the persistence could last much longer. Thanks to the T2308C point mutation of the polymerase START codon and the resulting lack of virion progeny; such *in vivo* testing can be routinely performed in a Biosafety Level 2 animal facility.

The therapeutic potential of our lead compound, CDN-L, was verified using developed mouse model reflecting CHB. Based on our results, we conclude that continuous monotherapy with CDN-L would result in long-term remission of CHB even in lower doses (0.5 mg/kg). As of yet, the detailed liver specific immune response to CDN-L therapy remain unclear, therefore, we suggest additional CDN-L therapy outcome evaluation based on the developed FC-immunophenotyping method. Besides, considering other CND-based anticancer therapies, ADU-S100 and our preliminary *in vivo* data (not shown), we believe that our lead compound might have remarkable results also in cancer therapy, as STING agonists are highly associated with anti-tumour therapy.

Taken all together, accessible, convenient, and affordable immunocompetent mouse model reflecting CHB suitable for *in vivo* preclinical validation of novel CHB therapeutics was developed. Outstanding results were obtained regarding CHB therapy using our hit-to-lead compound, CDN-L. We believe that our monotherapy might be highly interesting for pharmaceutical industry.

## 7. REFERENCES

- Abbas A, Lichtman A, Pillai S. Cellular and Molecular Immunology 9th edition. Elsevier 2016:608.
- Abe T, Barber GN. Cytosolic-DNA-Mediated, STING-Dependent Proinflammatory Gene Induction Necessitates Canonical NF- $\kappa$ B Activation through TBK1. *J Virol* 2014;88:5328–41. [https://doi.org/10.1128/JVI.00037-14/SUPPL\\_FILE/ZJV999098989SO1.PDF](https://doi.org/10.1128/JVI.00037-14/SUPPL_FILE/ZJV999098989SO1.PDF).
- Ablasser A, Goldeck M, Cavlar T, Deimling T, Witte G, Röhl I, et al. cGAS produces a 2'-5'-linked cyclic dinucleotide second messenger that activates STING. *Nature* 2013;498:380. <https://doi.org/10.1038/NATURE12306>.
- Adams PD, Ivanov A, Pawlikowski J, Manoharan I, Tuyn J van, Nelson DM, et al. Lysosome-mediated processing of chromatin in senescence. *Journal of Cell Biology* 2013;202:129–43. <https://doi.org/10.1083/JCB.201212110/VIDEO-1>.
- Agarwal K, Yuen M-F, Wedemeyer H, Cloutier D, Shen L, Arizpe A, et al. A phase 1 study evaluating the neutralizing, vaccinal monoclonal antibody VIR-3434 in participants with chronic hepatitis B virus infection 2021.
- Ager CR, Zhang H, Wei Z, Jones P, Curran MA, di Francesco ME. Discovery of IACS-8803 and IACS-8779, potent agonists of stimulator of interferon genes (STING) with robust systemic antitumor efficacy. *Bioorg Med Chem Lett* 2019;29:126640. <https://doi.org/10.1016/J.BMCL.2019.126640>.
- Ahn J, Gutman D, Saijo S, Barber GN. STING manifests self DNA-dependent inflammatory disease. *Proc Natl Acad Sci U S A* 2012;109:19386–91. [https://doi.org/10.1073/PNAS.1215006109/SUPPL\\_FILE/PNAS.201215006SI.PDF](https://doi.org/10.1073/PNAS.1215006109/SUPPL_FILE/PNAS.201215006SI.PDF).
- Akbar SMF, Al Mahtab M, Aguilar JC, Yoshida O, Khan S, Penton E, et al. The Safety and Efficacy of a Therapeutic Vaccine for Chronic Hepatitis B: A Follow-Up Study of Phase III Clinical Trial. *Vaccines (Basel)* 2022;10. <https://doi.org/10.3390/VACCINES10010045>.
- Allweiss L, Dandri M. Experimental in vitro and in vivo models for the study of human hepatitis B virus infection. *J Hepatol* 2016;64:S17–31. <https://doi.org/10.1016/J.JHEP.2016.02.012>.
- Al-Salama ZT, Scott LJ. Baricitinib: A Review in Rheumatoid Arthritis. *Drugs* 2018 78:7 2018;78:761–72. <https://doi.org/10.1007/S40265-018-0908-4>.
- Alter HJ, Chisari F v. Is Elimination of Hepatitis B and C a Pipe Dream or Reality? *Gastroenterology* 2019;156:294–6. <https://doi.org/10.1053/j.gastro.2018.12.015>.
- An J, Durcan L, Karr RM, Briggs TA, Rice GI, Teal TH, et al. Expression of Cyclic GMP-AMP Synthase in Patients With Systemic Lupus Erythematosus. *Arthritis and Rheumatology* 2017;69:800–7. <https://doi.org/10.1002/ART.40002>.
- An J, Woodward JJ, Sasaki T, Minie M, Elkon KB. Cutting Edge: Antimalarial Drugs Inhibit IFN- $\beta$  Production through Blockade of Cyclic GMP-AMP Synthase–DNA Interaction. *The Journal of Immunology* 2015;194:4089–93. <https://doi.org/10.4049/JIMMUNOL.1402793/-/DCSUPPLEMENTAL>.
- Andreeva L, Hiller B, Kostrewa D, Lässig C, de Oliveira Mann CC, Jan Drexler D, et al. cGAS senses long and HMGB/TFAM-bound U-turn DNA by forming protein–

- DNA ladders. *Nature* 2017 549:7672 2017;549:394–8.  
<https://doi.org/10.1038/nature23890>.
- Aparicio-Vergara M, Tencerova M, Morgantini C, Barreby E, Aouadi M. Isolation of Kupffer Cells and Hepatocytes from a Single Mouse Liver. *Methods Mol Biol* 2017;1639:161–71. [https://doi.org/10.1007/978-1-4939-7163-3\\_16](https://doi.org/10.1007/978-1-4939-7163-3_16).
- Azuma H, Paulk N, Ranade A, Dorrell C, Al-Dhalimy M, Ellis E, et al. Robust expansion of human hepatocytes in Fah<sup>-/-</sup>/Rag2<sup>-/-</sup>/Il2rg<sup>-/-</sup> mice. *Nat Biotechnol* 2007;25:903–10. <https://doi.org/10.1038/nbt1326>.
- Bai J, Cervantes C, Liu J, He S, Zhou H, Zhang B, et al. DsbA-L prevents obesity-induced inflammation and insulin resistance by suppressing the mtDNA release-activated cGAS-cGAMP-STING pathway. *Proc Natl Acad Sci U S A* 2017;114:12196–201. <https://doi.org/10.1073/PNAS.1708744114>.
- Bai J, Liu F. Nuclear cGAS: sequestration and beyond. *Protein Cell* 2022;13:90–101. <https://doi.org/10.1007/S13238-021-00869-0/FIGURES/6>.
- Baker DJ, Childs BG, Durik M, Wijers ME, Sieben CJ, Zhong J, et al. Naturally occurring p16Ink4a-positive cells shorten healthy lifespan. *Nature* 2016 530:7589 2016;530:184–9. <https://doi.org/10.1038/nature16932>.
- Bakhoun SF, Ngo B, Laughney AM, Cavallo JA, Murphy CJ, Ly P, et al. Chromosomal instability drives metastasis through a cytosolic DNA response. *Nature* 2018 553:7689 2018;553:467–72. <https://doi.org/10.1038/nature25432>.
- Balci S, Ekinci RMK, de Jesus AA, Goldbach-Mansky R, Yilmaz M. Baricitinib experience on STING-associated vasculopathy with onset in infancy: A representative case from Turkey. *Clinical Immunology* 2020;212:108273. <https://doi.org/10.1016/J.CLIM.2019.108273>.
- Barnett KC, Coronas-Serna JM, Zhou W, Ernandes MJ, Cao A, Kranzusch PJ, et al. Phosphoinositide interactions position cGAS at the plasma membrane to ensure efficient distinction between self- and Viral DNA. *Cell* 2019;176:1432-1446.e1411. <https://doi.org/10.1016/j.cell.2019.01.049>.
- Batu ED. Monogenic systemic lupus erythematosus: insights in pathophysiology. *Rheumatology International* 2018 38:10 2018;38:1763–75. <https://doi.org/10.1007/S00296-018-4048-7>.
- Bazinet M, Pântea V, Cebotarescu V, Cojuhari L, Jimbei P, Albrecht J, et al. Safety and efficacy of REP 2139 and pegylated interferon alfa-2a for treatment-naïve patients with chronic hepatitis B virus and hepatitis D virus co-infection (REP 301 and REP 301-LTF): a non-randomised, open-label, phase 2 trial. *Lancet Gastroenterol Hepatol* 2017;2:877–89. [https://doi.org/10.1016/S2468-1253\(17\)30288-1](https://doi.org/10.1016/S2468-1253(17)30288-1).
- Benitez-Guijarro M, Lopez-Ruiz C, Tarnauskaitė Ž, Murina O, Mohammad MM, Williams TC, et al. RNase H2, mutated in Aicardi-Goutières syndrome, promotes LINE-1 retrotransposition. *EMBO J* 2018;37. <https://doi.org/10.15252/EMBJ.201798506>.
- Bertoletti A, Ferrari C. Adaptive immunity in HBV infection. *J Hepatol* 2016;64:S71–83. <https://doi.org/10.1016/J.JHEP.2016.01.026>.
- Bility MT, Cheng L, Zhang Z, Luan Y, Li F, Chi L, et al. Hepatitis B virus infection and immunopathogenesis in a humanized mouse model: induction of human-specific

- liver fibrosis and M2-like macrophages. *PLoS Pathog* 2014;10. <https://doi.org/10.1371/JOURNAL.PPAT.1004032>.
- Bility MT, Zhang L, Washburn ML, Curtis TA, Kovalev GI, Su L. Generation of a humanized mouse model with both human immune system and liver cells to model hepatitis C virus infection and liver immunopathogenesis. *Nat Protoc* 2012;7:1608–17. <https://doi.org/10.1038/NPROT.2012.083>.
- Birkus. 3'3' cyclic dinucleotides with phosphonate bond activating the sting adaptor protein 2018.
- Birkus G, Brehova P, Dejmek M, Nencka R, Pav O, Sala M. 3'3'-cyclic dinucleotide analogue comprising a cyclopentanyl modified nucleotide as STING modulator, 2020.
- Bissig K-D, Wieland SF, Tran P, Isogawa M, Le TT, Chisari F v, et al. Human liver chimeric mice provide a model for hepatitis B and C virus infection and treatment. *J Clin Invest* 2010;120:924–30. <https://doi.org/10.1172/JCI40094>.
- Blom KG, Rahman Qazi M, Noronha Matos JB, Nelson BD, DePierre JW, Abedi-Valugerdi M. Isolation of murine intrahepatic immune cells employing a modified procedure for mechanical disruption and functional characterization of the B, T and natural killer T cells obtained. *Clin Exp Immunol* 2009;155:320–9. <https://doi.org/10.1111/J.1365-2249.2008.03815.X>.
- Bogdanos DP, Gao B, Gershwin ME. Liver immunology. *Compr Physiol* 2013;3:567–98. <https://doi.org/10.1002/CPHY.C120011>.
- Boni C, Janssen HLA, Rossi M, Yoon SK, Vecchi A, Barili V, et al. Combined GS-4774 and Tenofovir Therapy Can Improve HBV-Specific T-Cell Responses in Patients With Chronic Hepatitis. *Gastroenterology* 2019;157:227-241.e7. <https://doi.org/10.1053/j.gastro.2019.03.044>.
- Borriello F, Pietrasanta C, Lai JCY, Walsh LM, Sharma P, O'Driscoll DN, et al. Identification and characterization of stimulator of interferon genes as a robust adjuvant target for early life immunization. *Front Immunol* 2017;8:1772. <https://doi.org/10.3389/FIMMU.2017.01772/FULL>.
- Bottini N, Firestein GS. Duality of fibroblast-like synoviocytes in RA: passive responders and imprinted aggressors. *Nature Reviews Rheumatology* 2012 9:1 2012;9:24–33. <https://doi.org/10.1038/nrrheum.2012.190>.
- Bourgeois S, Lim Y-S, Gane E, Lee H, Cheng W, Heo J, et al. IMC-I109V, a novel T cell receptor (TCR) bispecific (ENVxCD3) designed to eliminate HBV-infected hepatocytes in chronic HBV patients: initial data from a first-in-human study. Poster Presentation (SAT437) 2022.
- Brault M, Olsen TM, Martinez J, Stetson DB, Oberst A. Intracellular Nucleic Acid Sensing Triggers Necroptosis through Synergistic Type I IFN and TNF Signaling. *The Journal of Immunology* 2018;200:2748–56. <https://doi.org/10.4049/JIMMUNOL.1701492/-/DCSUPPLEMENTAL>.
- Bristol-Myers Squibb. An Investigational Immunotherapy Study of BMS-986301 Alone or in Combination With Nivolumab, and Ipilimumab in Participants With Advanced Solid Cancers - Full Text View - ClinicalTrials.gov 2022.



- Cabral F, Miller CM, Kudrna KM, Hass BE, Daubendiek JG, Kellar BM, et al. Purification of Hepatocytes and Sinusoidal Endothelial Cells from Mouse Liver Perfusion. *J Vis Exp* 2018;2018. <https://doi.org/10.3791/56993>.
- Cai X, Chiu YH, Chen ZJ. The cGAS-cGAMP-STING pathway of cytosolic DNA sensing and signaling. *Mol Cell* 2014;54:289–96. <https://doi.org/10.1016/j.molcel.2014.03.040>.
- Campbell CT, Kolesar JE, Kaufman BA. Mitochondrial transcription factor A regulates mitochondrial transcription initiation, DNA packaging, and genome copy number. *Biochimica et Biophysica Acta (BBA) - Gene Regulatory Mechanisms* 2012;1819:921–9. <https://doi.org/10.1016/J.BBAGRM.2012.03.002>.
- Cavanaugh VJ, Guidotti LG, Chisari F v. Inhibition of hepatitis B virus replication during adenovirus and cytomegalovirus infections in transgenic mice. *J Virol* 1998;72:2630–7. <https://doi.org/10.1128/JVI.72.4.2630-2637.1998>.
- Chan HLY, Chan FWS, Hui AJ, Li MKK, Chan KH, Wong GLH, et al. Switching to peginterferon for chronic hepatitis B patients with hepatitis B e antigen seroconversion on entecavir - A prospective study. *J Viral Hepat* 2019;26:126–35. <https://doi.org/10.1111/JVH.13000>.
- Chang W, Altman MD, Lesburg CA, Perera SA, Piesvaux JA, Schroeder GK, et al. Discovery of MK-1454: A Potent Cyclic Dinucleotide Stimulator of Interferon Genes Agonist for the Treatment of Cancer. *J Med Chem* 2022. <https://doi.org/10.1021/ACS.JMEDCHEM.1C02197>.
- Chattopadhyay S, Kuzmanovic T, Zhang Y, Wetzel JL, Sen GC. Ubiquitination of the Transcription Factor IRF-3 Activates RIPA, the Apoptotic Pathway that Protects Mice from Viral Pathogenesis. *Immunity* 2016;44:1151–61. <https://doi.org/10.1016/J.IMMUNI.2016.04.009/ATTACHMENT/06FBA50C-B9C4-4E82-8E77-383961628F41/MMC1.PDF>.
- Chattopadhyay S, Marques JT, Yamashita M, Peters KL, Smith K, Desai A, et al. Viral apoptosis is induced by IRF-3-mediated activation of Bax. *EMBO J* 2010;29:1762. <https://doi.org/10.1038/EMBOJ.2010.50>.
- Chen D, Tong J, Yang L, Wei L, Stolz DB, Yu J, et al. PUMA amplifies necroptosis signaling by activating cytosolic DNA sensors. *Proc Natl Acad Sci U S A* 2018;115:3930–5. [https://doi.org/10.1073/PNAS.1717190115/SUPPL\\_FILE/PNAS.201717190SI.PDF](https://doi.org/10.1073/PNAS.1717190115/SUPPL_FILE/PNAS.201717190SI.PDF).
- Chen M, Meng Q, Qin Y, Liang P, Tan P, He L, et al. TRIM14 Inhibits cGAS Degradation Mediated by Selective Autophagy Receptor p62 to Promote Innate Immune Responses. *Mol Cell* 2016;64:105–19. <https://doi.org/10.1016/J.MOLCEL.2016.08.025>.
- Chen Q, Sun L, Chen ZJ. Regulation and function of the cGAS–STING pathway of cytosolic DNA sensing. *Nature Immunology* 2016 17:10 2016;17:1142–9. <https://doi.org/10.1038/ni.3558>.
- Chen W, Li S, Yu H, Liu X, Huang L, Wang Q, et al. ER Adaptor SCAP Translocates and Recruits IRF3 to Perinuclear Microsome Induced by Cytosolic Microbial DNAs. *PLoS Pathog* 2016;12. <https://doi.org/10.1371/JOURNAL.PPAT.1005462>.

Chen YA, Shen YL, Hsia HY, Tiang YP, Sung TL, Chen LY. Extrachromosomal telomere repeat DNA is linked to ALT development via cGAS-STING DNA sensing pathway. *Nature Structural & Molecular Biology* 2017 24:12 2017;24:1124–31. <https://doi.org/10.1038/nsmb.3498>.

Chinook Therapeutics Inc. Efficacy and Safety Trial of ADU-S100 and Pembrolizumab in Head and Neck Cancer - Full Text View - [ClinicalTrials.gov](https://clinicaltrials.gov) 2022.

Chisari F v., Ferrari C. Hepatitis B virus immunopathogenesis. *Annu Rev Immunol* 1995;13:29–60. <https://doi.org/10.1146/ANNUREV.IY.13.040195.000333>.

Chisari F v, Filippi P, McLachlan A, Milich DR, Riggs M, Lee S, et al. Expression of hepatitis B virus large envelope polypeptide inhibits hepatitis B surface antigen secretion in transgenic mice. *J Virol* 1986;60:880–7. <https://doi.org/10.1128/JVI.60.3.880-887.1986>.

Chisari F v., Pinkert CA, Milich DR, Filippi P, Mclachlan A, Palmiter RD, et al. A transgenic mouse model of the chronic hepatitis B surface antigen carrier state. *Science* 1985;230:1157–60. <https://doi.org/10.1126/SCIENCE.3865369>.

Chou HH, Chien WH, Wu LL, Cheng CH, Chung CH, Horng JH, et al. Age-related immune clearance of hepatitis B virus infection requires the establishment of gut microbiota. *Proc Natl Acad Sci U S A* 2015;112:2175–80. <https://doi.org/10.1073/pnas.1424775112>.

Christgen S, Zheng M, Kesavardhana S, Karki R, Malireddi RKS, Banoth B, et al. Identification of the PANoptosome: A Molecular Platform Triggering Pyroptosis, Apoptosis, and Necroptosis (PANoptosis). *Front Cell Infect Microbiol* 2020;10:237. <https://doi.org/10.3389/FCIMB.2020.00237/BIBTEX>.

Chung KW, Dhillon P, Huang S, Sheng X, Shrestha R, Qiu C, et al. Mitochondrial Damage and Activation of the STING Pathway Lead to Renal Inflammation and Fibrosis. *Cell Metab* 2019;30:784-799.e5. <https://doi.org/10.1016/J.CMET.2019.08.003>.

Cibrián D, Sánchez-Madrid F. CD69: from activation marker to metabolic gatekeeper. *Eur J Immunol* 2017;47:946. <https://doi.org/10.1002/EJI.201646837>.

Civril F, Deimling T, de Oliveira Mann CC, Ablasser A, Moldt M, Witte G, et al. Structural mechanism of cytosolic DNA sensing by cGAS. *Nature* 2013;498:332. <https://doi.org/10.1038/NATURE12305>.

Cohen D, Melamed S, Millman A, Shulman G, Oppenheimer-Shaanan Y, Kacen A, et al. Cyclic GMP–AMP signalling protects bacteria against viral infection. *Nature* 2019;574:691–5. <https://doi.org/10.1038/S41586-019-1605-5>.

Coppé JP, Patil CK, Rodier F, Sun Y, Muñoz DP, Goldstein J, et al. Senescence-Associated Secretory Phenotypes Reveal Cell-Nonautonomous Functions of Oncogenic RAS and the p53 Tumor Suppressor. *PLoS Biol* 2008;6:e301. <https://doi.org/10.1371/JOURNAL.PBIO.0060301>.

Corrales L, Glickman LH, McWhirter SM, Kanne DB, Sivick KE, Katibah GE, et al. Direct Activation of STING in the Tumor Microenvironment Leads to Potent and Systemic Tumor Regression and Immunity. *Cell Rep* 2015;11:1018–30. <https://doi.org/10.1016/j.celrep.2015.04.031>.

- Corrales L, Woo S-R, Williams JB, McWhirter SM, Dubensky TW, Gajewski TF. Antagonism of the STING Pathway via Activation of the AIM2 Inflammasome by Intracellular DNA. *J Immunol* 2016;196:3191–8. <https://doi.org/10.4049/JIMMUNOL.1502538>.
- Cristini A, Tellier M, Constantinescu F, Accalai C, Albuлесcu LO, Heiringhoff R, et al. RNase H2, mutated in Aicardi-Goutières syndrome, resolves co-transcriptional R-loops to prevent DNA breaks and inflammation. *Nature Communications* 2022 13:1 2022;13:1–14. <https://doi.org/10.1038/s41467-022-30604-0>.
- Crow YJ, Hayward BE, Parmar R, Robins P, Leitch A, Ali M, et al. Mutations in the gene encoding the 3'-5' DNA exonuclease TREX1 cause Aicardi-Goutières syndrome at the AGS1 locus. *Nature Genetics* 2006 38:8 2006;38:917–20. <https://doi.org/10.1038/ng1845>.
- Crow YJ, Manel N. Aicardi–Goutières syndrome and the type I interferonopathies. *Nature Reviews Immunology* 2015 15:7 2015;15:429–40. <https://doi.org/10.1038/nri3850>.
- Cui Y, Zhao D, Sreevatsan S, Liu C, Yang W, Song Z, et al. Mycobacterium bovis induces endoplasmic reticulum stress mediated-apoptosis by activating IRF3 in a murine macrophage cell line. *Front Cell Infect Microbiol* 2016;6:182. <https://doi.org/10.3389/FCIMB.2016.00182/XML/NLM>.
- Dai J, Huang YJ, He X, Zhao M, Wang X, Liu ZS, et al. Acetylation Blocks cGAS Activity and Inhibits Self-DNA-Induced Autoimmunity. *Cell* 2019;176:1447-1460.e14. <https://doi.org/10.1016/j.cell.2019.01.016>.
- Dandri M, Burda MR, Török E, Pollok JM, Iwanska A, Sommer G, et al. Repopulation of mouse liver with human hepatocytes and in vivo infection with hepatitis B virus. *Hepatology* 2001;33:981–8. <https://doi.org/10.1053/jhep.2001.23314>.
- Dangi A, Zhang L, Zhang X, Luo X. Murine CMV induces type 1 IFN that impairs differentiation of MDSCs critical for transplantation tolerance. *Blood Adv* 2018;2:669–80. <https://doi.org/10.1182/BLOODADVANCES.2017012187>.
- Dansako H, Imai H, Ueda Y, Satoh S, Shimotohno K, Kato N. High-level expression of STING restricts susceptibility to HBV by mediating type III IFN induction. *FASEB Bioadv* 2019;1:67–80. <https://doi.org/10.1096/FBA.1022>.
- Dansako H, Ueda Y, Okumura N, Satoh S, Sugiyama M, Mizokami M, et al. The cyclic GMP-AMP synthetase–STING signaling pathway is required for both the innate immune response against HBV and the suppression of HBV assembly. *FEBS J* 2016;283:144–56. <https://doi.org/10.1111/FEBS.13563>.
- David BA, Rubino S, Moreira TG, Freitas-Lopes MA, Araújo AM, Paul NE, et al. Isolation and high-dimensional phenotyping of gastrointestinal immune cells. *Immunology* 2017;151:56–70. <https://doi.org/10.1111/IMM.12706>.
- Decout A, Katz JD, Venkatraman S, Ablasser A. The cGAS–STING pathway as a therapeutic target in inflammatory diseases. *Nature Reviews Immunology* 2021 21:9 2021;21:548–69. <https://doi.org/10.1038/s41577-021-00524-z>.
- Dejmek M, Šála M, Brazdova A, Vanekova L, Smola M, Klíma M, et al. Discovery of isonucleotidic CDNs as potent STING agonists with immunomodulatory potential. *Structure* 2022;30:1146-1156.e11. <https://doi.org/10.1016/j.str.2022.05.012>.

- Demaria O, de Gassart A, Coso S, Gestermann N, di Domizio J, Flatz L, et al. STING activation of tumor endothelial cells initiates spontaneous and therapeutic antitumor immunity. *Proc Natl Acad Sci U S A* 2015;112:15408–13. [https://doi.org/10.1073/PNAS.1512832112/SUPPL\\_FILE/PNAS.201512832SI.PDF](https://doi.org/10.1073/PNAS.1512832112/SUPPL_FILE/PNAS.201512832SI.PDF).
- Dembek C, Protzer U, Roggendorf M. Overcoming immune tolerance in chronic hepatitis B by therapeutic vaccination. *Curr Opin Virol* 2018;30:58–67. <https://doi.org/10.1016/J.COVIRO.2018.04.003>.
- Deng Z, Chong Z, Law CS, Mukai K, Ho FO, Martinu T, et al. A defect in COPI-mediated transport of STING causes immune dysregulation in COPA syndrome. *Journal of Experimental Medicine* 2020;217. <https://doi.org/10.1084/JEM.20201045/151981>.
- van Deursen JM. The role of senescent cells in ageing. *Nature* 2014 509:7501 2014;509:439–46. <https://doi.org/10.1038/nature13193>.
- Diner EJ, Burdette DL, Wilson SC, Monroe KM, Kellenberger CA, Hyodo M, et al. The innate immune DNA sensor cGAS produces a non-canonical cyclic-di-nucleotide that activates human STING. *Cell Rep* 2013;3:1355. <https://doi.org/10.1016/J.CELREP.2013.05.009>.
- Ding PH, Yang MX, Wang NN, Jin LJ, Dong Y, Cai X, et al. Porphyromonas gingivalis-Induced NLRP3 Inflammasome Activation and Its Downstream Interleukin-1 $\beta$  Release Depend on Caspase-4. *Front Microbiol* 2020;11:1881. <https://doi.org/10.3389/FMICB.2020.01881/BIBTEX>.
- Dion S, Bourguine M, Godon O, Levillayer F, Michel M-L. Adeno-associated virus-mediated gene transfer leads to persistent hepatitis B virus replication in mice expressing HLA-A2 and HLA-DR1 molecules. *J Virol* 2013;87:5554–63. <https://doi.org/10.1128/JVI.03134-12>.
- Dorta-Estremera S, Hegde VL, Slay RB, Sun R, Yanamandra A v., Nicholas C, et al. Targeting interferon signaling and CTLA-4 enhance the therapeutic efficacy of anti-PD-1 immunotherapy in preclinical model of HPV+ oral cancer. *J Immunother Cancer* 2019;7. <https://doi.org/10.1186/S40425-019-0728-4>.
- Dou Z, Ghosh K, Vizioli MG, Zhu J, Sen P, Wangenstein KJ, et al. Cytoplasmic chromatin triggers inflammation in senescence and cancer. *Nature* 2017 550:7676 2017;550:402–6. <https://doi.org/10.1038/nature24050>.
- Downey CM, Aghaei M, Schwendener RA, Jirik FR. DMXAA causes tumor site-specific vascular disruption in murine non-small cell lung cancer, and like the endogenous non-canonical cyclic dinucleotide STING agonist, 2'3'-cGAMP, induces M2 macrophage repolarization. *PLoS One* 2014;9:10–2. <https://doi.org/10.1371/journal.pone.0099988>.
- Du Y, Broering R, Li X, Zhang X, Liu J, Yang D, et al. In Vivo Mouse Models for Hepatitis B Virus Infection and Their Application. *Front Immunol* 2021;12. <https://doi.org/10.3389/FIMMU.2021.766534>.
- Dunphy G, Flannery SM, Almine JF, Connolly DJ, Paulus C, Jønsson KL, et al. Non-canonical Activation of the DNA Sensing Adaptor STING by ATM and IFI16 Mediates NF- $\kappa$ B Signaling after Nuclear DNA Damage. *Mol Cell* 2018;71:745. <https://doi.org/10.1016/J.MOLCEL.2018.07.034>.

- Ebert G, Poeck H, Lucifora J, Baschuk N, Esser K, Esposito I, et al. 5' Triphosphorylated small interfering RNAs control replication of hepatitis B virus and induce an interferon response in human liver cells and mice. *Gastroenterology* 2011;141:696–706, 706.e1-3. <https://doi.org/10.1053/j.gastro.2011.05.001>.
- Eisai Inc. Study of Intratumorally Administered Stimulator of Interferon Genes (STING) Agonist E7766 in Participants With Advanced Solid Tumors or Lymphomas - INSTAL-101 - Full Text View - ClinicalTrials.gov 2022.
- El-Zayat SR, Sibaii H, Mannaa FA. Toll-like receptors activation, signaling, and targeting: an overview. *Bulletin of the National Research Centre* 2019 43:1 2019;43:1–12. <https://doi.org/10.1186/S42269-019-0227-2>.
- Ergun SL, Fernandez D, Weiss TM, Li L. STING Polymer Structure Reveals Mechanisms for Activation, Hyperactivation, and Inhibition. *Cell* 2019;178:290-301.e10. <https://doi.org/10.1016/J.CELL.2019.05.036/ATTACHMENT/A346D280-C932-45BF-95AD-6DC3DE979388/MMC1.PDF>.
- Fang R, Wang C, Jiang Q, Lv M, Gao P, Yu X, et al. NEMO–IKK $\beta$  Are Essential for IRF3 and NF- $\kappa$ B Activation in the cGAS–STING Pathway. *The Journal of Immunology* 2017;199:3222–33. <https://doi.org/10.4049/JIMMUNOL.1700699/-/DCSUPPLEMENTAL>.
- Feng X, Liu D, Li Z, Bian J. Bioactive modulators targeting STING adaptor in cGAS-STING pathway. *Drug Discov Today* 2020;25:230–7. <https://doi.org/10.1016/J.DRUDIS.2019.11.007>.
- Fernández G, Sanchez AL, Jerez E, Anillo LE, Freyre F, Aguiar JA, et al. Five-year Follow-up of Chronic Hepatitis B Patients Immunized by Nasal Route with the Therapeutic Vaccine HeberNasvac. *Euroasian J Hepatogastroenterol* 2018;8:133. <https://doi.org/10.5005/JP-JOURNALS-10018-1279>.
- Ferrer-Font L, Pellefigues C, Mayer JU, Small SJ, Jaimes MC, Price KM. Panel Design and Optimization for High-Dimensional Immunophenotyping Assays Using Spectral Flow Cytometry. *Curr Protoc Cytom* 2020;92. <https://doi.org/10.1002/CPCY.70>.
- Fosbenner D.T., Graybill T.L., Kang J., King B.W., Lan Y., Leister L.K., et al. Modulators of stimulator of interferon genes (STING), 2018.
- Freed Eric, Martin M. *Fields Virology*. 2013. <https://doi.org/9781451105636>.
- F-star Therapeutics Inc. Evaluating Safety and Efficacy of SB 11285 Alone and in Combination With Atezolizumab in Patients With Advanced Solid Tumors - Full Text View - ClinicalTrials.gov 2020.
- Fung S, Sulkowski M, Lalezari J, Schiff ER, Dieterich D, Hassanein T, et al. Antiviral activity and safety of the hepatitis B core inhibitor ABI-H0731 administered with a nucleos(t)ide reverse transcriptase inhibitor in patients with HBeAg-negative chronic hepatitis B infection. *J Hepatol* 2020;73:S51–2. [https://doi.org/10.1016/S0168-8278\(20\)30649-8](https://doi.org/10.1016/S0168-8278(20)30649-8).
- Gaidt MM, Ebert TS, Chauhan D, Ramshorn K, Pinci F, Zuber S, et al. The DNA Inflammasome in Human Myeloid Cells Is Initiated by a STING-Cell Death Program Upstream of NLRP3. *Cell* 2017;171:1110-1124.e18. <https://doi.org/10.1016/J.CELL.2017.09.039>.

- Gaidt MM, Hornung V. The NLRP3 Inflammasome Renders Cell Death Pro-inflammatory. *J Mol Biol* 2018;430:133–41. <https://doi.org/10.1016/J.JMB.2017.11.013>.
- Gall A, Treuting P, Elkon KB, Loo YM, Gale M, Barber GN, et al. Autoimmunity initiates in non-hematopoietic cells and progresses via lymphocytes in an interferon-dependent autoimmune disease. *Immunity* 2012;36:120. <https://doi.org/10.1016/J.IMMUNI.2011.11.018>.
- Gane E, Lim Y-S, Cloutier D, Shen L, Cathcart A, Ding X, et al. Safety and antiviral activity of VIR-2218, an X-targeting RNAi therapeutic, in participants with chronic hepatitis B Infection: week 48 follow-up results n.d.
- Gane E, Locarnini S, Lim TH, Strasser S, Sievert W, Cheng W, et al. Short-term treatment with RNA interference therapy, JNJ-3989, results in sustained hepatitis B surface antigen suppression in patients with chronic hepatitis B receiving nucleos(t)ide analogue treatment. *J Hepatol* 2020;73:S20. [https://doi.org/10.1016/S0168-8278\(20\)30597-3](https://doi.org/10.1016/S0168-8278(20)30597-3).
- Gane E, Verdon DJ, Brooks AE, Gaggar A, Nguyen AH, Subramanian GM, et al. Anti-PD-1 blockade with nivolumab with and without therapeutic vaccination for virally suppressed chronic hepatitis B: A pilot study. *J Hepatol* 2019;71:900–7. <https://doi.org/10.1016/j.jhep.2019.06.028>.
- Gao D, Li T, Li XD, Chen X, Li QZ, Wight-Carter M, et al. Activation of cyclic GMP-AMP synthase by self-DNA causes autoimmune diseases. *Proc Natl Acad Sci U S A* 2015;112:E5699–705. <https://doi.org/10.1073/PNAS.1516465112>.
- Gao P, Ascano M, Wu Y, Barchet W, Gaffney BL, Zillinger T, et al. Cyclic [G(2',5')pA(3',5')p] Is the Metazoan Second Messenger Produced by DNA-Activated Cyclic GMP-AMP Synthase. *Cell* 2013;153:1094. <https://doi.org/10.1016/J.CELL.2013.04.046>.
- Geijtenbeek TBH. Host DNase TREX1 hides HIV from DNA sensors. *Nat Immunol* 2010;11:979–80. <https://doi.org/10.1038/NI1110-979>.
- Genovese MC, Kremer J, Zamani O, Ludivico C, Krogulec M, Xie L, et al. Baricitinib in patients with refractory rheumatoid arthritis. *Journal Fur Mineralstoffwechsel* 2016;23:60–1. [https://doi.org/10.1056/NEJMOA1507247/SUPPL\\_FILE/NEJMOA1507247\\_DISCLOSURES.PDF](https://doi.org/10.1056/NEJMOA1507247/SUPPL_FILE/NEJMOA1507247_DISCLOSURES.PDF).
- Gentili M, Lahaye X, Nadalin F, Nader GPF, Lombardi EP, Herve S, et al. The N-terminal domain of cGAS determines preferential association with centromeric DNA and innate immune activation in the nucleus. *Cell Rep* 2019;26:3798. <https://doi.org/10.1016/j.celrep.2019.03.049>.
- Giladi A, Paul F, Herzog Y, Lubling Y, Weiner A, Yofe I, et al. Single-cell characterization of haematopoietic progenitors and their trajectories in homeostasis and perturbed haematopoiesis. *Nat Cell Biol* 2018;20:836–46. <https://doi.org/10.1038/S41556-018-0121-4>.
- GlaxoSmithKline. Phase 1 First Time in Human (FTIH), Open Label Study of GSK3745417 Administered to Participants With Advanced Solid Tumors - Full Text View - [ClinicalTrials.gov](https://clinicaltrials.gov) 2022.

- Glebe D, König A. Molecular Virology of Hepatitis B Virus and Targets for Antiviral Intervention. *Intervirology* 2014;57:134–40. <https://doi.org/10.1159/000360946>.
- Glück S, Guey B, Gulen MF, Wolter K, Kang TW, Schmacke NA, et al. Innate immune sensing of cytosolic chromatin fragments through cGAS promotes senescence. *Nature Cell Biology* 2017 19:9 2017;19:1061–70. <https://doi.org/10.1038/ncb3586>.
- Gondois-Rey F, Granjeaud S, Kieu SLT, Herrera D, Hirsch I, Olive D. Multiparametric cytometry for exploration of complex cellular dynamics. *Cytometry A* 2012;81:332–42. <https://doi.org/10.1002/CYTO.A.22016>.
- Gong T, Liu L, Jiang W, Zhou R. DAMP-sensing receptors in sterile inflammation and inflammatory diseases. *Nature Reviews Immunology* 2019 20:2 2019;20:95–112. <https://doi.org/10.1038/s41577-019-0215-7>.
- Gonugunta VK, Sakai T, Pokatayev V, Yang K, Wu J, Dobbs N, et al. Trafficking-Mediated STING Degradation Requires Sorting to Acidified Endolysosomes and Can Be Targeted to Enhance Anti-tumor Response. *Cell Rep* 2017;21:3234–42. <https://doi.org/10.1016/J.CELREP.2017.11.061/ATTACHMENT/D7C39CA6-CD38-40D1-88C7-D24072124AE8/MMC5.MP4>.
- Gravekamp C, Chandra D. Targeting STING pathways for the treatment of cancer. *Oncoimmunology* 2015;4:29–31. <https://doi.org/10.4161/2162402X.2014.988463>.
- Gray EE, Treuting PM, Woodward JJ, Stetson DB. cGAS is required for lethal autoimmune disease in the *Trex1*-deficient mouse model of Aicardi-Goutieres Syndrome. *J Immunol* 2015;195:1939. <https://doi.org/10.4049/JIMMUNOL.1500969>.
- Grompe M, Al-Dhalimy M, Finegold M, Ou CN, Burlingame T, Kennaway NG, et al. Loss of fumarylacetoacetate hydrolase is responsible for the neonatal hepatic dysfunction phenotype of lethal albino mice. *Genes Dev* 1993;7:2298–307. <https://doi.org/10.1101/gad.7.12a.2298>.
- Gui X, Yang H, Li T, Tan X, Shi P, Li M, et al. Autophagy induction via STING trafficking is a primordial function of the cGAS pathway. *Nature* 2019 567:7747 2019;567:262–6. <https://doi.org/10.1038/s41586-019-1006-9>.
- Guidotti LG, Ishikawa T, Hobbs M v, Matzke B, Schreiber R, Chisari F v. Intracellular Inactivation of the Hepatitis B Virus by Cytotoxic T Lymphocytes. *Immunity* 1996;4:25–36. [https://doi.org/10.1016/S1074-7613\(00\)80295-2](https://doi.org/10.1016/S1074-7613(00)80295-2).
- Guidotti LG, Martinez V, Loh YT, Rogler CE, Chisari F v. Hepatitis B virus nucleocapsid particles do not cross the hepatocyte nuclear membrane in transgenic mice. *J Virol* 1994;68:5469–75. <https://doi.org/10.1128/JVI.68.9.5469-5475.1994>.
- Guidotti LG, Matzke B, Schaller H, Chisari F v. High-level hepatitis B virus replication in transgenic mice. *J Virol* 1995;69:6158–69.
- Gullett JM, Tweedell RE, Kanneganti TD. It's All in the PAN: Crosstalk, Plasticity, Redundancies, Switches, and Interconnectedness Encompassed by PANoptosis Underlying the Totality of Cell Death-Associated Biological Effects. *Cells* 2022;11. <https://doi.org/10.3390/CELLS11091495>.
- Guo F, Han Y, Zhao X, Wang J, Liu F, Xu C, et al. Sting agonists induce an innate antiviral immune response against hepatitis B virus. *Antimicrob Agents Chemother*

2015;59:1273–81. <https://doi.org/10.1128/AAC.04321-14/ASSET/7C0D8A85-3AFC-4F36-923D-CC0761EEC150/ASSETS/GRAPHIC/ZAC0021537300008.JPEG>.

Guo F, Tang L, Shu S, Sehgal M, Sheraz M, Liu B, et al. Activation of stimulator of interferon genes in hepatocytes suppresses the replication of hepatitis B virus. *Antimicrob Agents Chemother* 2017;61. <https://doi.org/10.1128/AAC.00771-17/ASSET/B127CCC6-AB08-44B7-8C44-AF62660D7941/ASSETS/GRAPHIC/ZAC0101765380008.JPEG>.

Guo X, Chen P, Hou X, Xu W, Wang D, Wang TY, et al. The recombined cccDNA produced using minicircle technology mimicked HBV genome in structure and function closely. *Scientific Reports* 2016 6:1 2016;6:1–10. <https://doi.org/10.1038/srep25552>.

Ha HL, Shin HJ, Feitelson MA, Yu DY. Oxidative stress and antioxidants in hepatic pathogenesis. *World J Gastroenterol* 2010;16:6035–43. <https://doi.org/10.3748/wjg.v16.i48.6035>.

Haag SM, Gulen MF, Reymond L, Gibelin A, Abrami L, Decout A, et al. Targeting STING with covalent small-molecule inhibitors. *Nature* 2018 559:7713 2018;559:269–73. <https://doi.org/10.1038/s41586-018-0287-8>.

Hansen AL, Buchan GJ, Rühl M, Mukai K, Salvatore SR, Ogawa E, et al. Nitro-fatty acids are formed in response to virus infection and are potent inhibitors of STING palmitoylation and signaling. *Proc Natl Acad Sci U S A* 2018a;115:E7768–75. <https://doi.org/10.1073/PNAS.1806239115>.

Hansen AL, Buchan GJ, Rühl M, Mukai K, Salvatore SR, Ogawa E, et al. Nitro-fatty acids are formed in response to virus infection and are potent inhibitors of STING palmitoylation and signaling. *Proc Natl Acad Sci U S A* 2018b;115:E7768–75. [https://doi.org/10.1073/PNAS.1806239115/SUPPL\\_FILE/PNAS.1806239115.SAPP.PDF](https://doi.org/10.1073/PNAS.1806239115/SUPPL_FILE/PNAS.1806239115.SAPP.PDF).

Haque M, Lei F, Xiong X, Ren Y, Kumar A, Das JK, et al. Stem Cell-Derived Viral Antigen-Specific T Cells Suppress HBV Replication through Production of IFN- $\gamma$  and TNF- $\alpha$ . *IScience* 2020;23:101333. <https://doi.org/10.1016/J.ISCI.2020.101333>.

Harding SM, Benci JL, Irianto J, Discher DE, Minn AJ, Greenberg RA. Mitotic progression following DNA damage enables pattern recognition within micronuclei. *Nature* 2017 548:7668 2017;548:466–70. <https://doi.org/10.1038/nature23470>.

Hartman ZC, Kiang A, Everett RS, Serra D, Yang XY, Clay TM, et al. Adenovirus infection triggers a rapid, MyD88-regulated transcriptome response critical to acute-phase and adaptive immune responses in vivo. *J Virol* 2007;81:1796–812. <https://doi.org/10.1128/JVI.01936-06>.

He J, Hao R, Liu D, Liu X, Wu S, Guo S, et al. Inhibition of hepatitis B virus replication by activation of the cGAS-STING pathway. *Journal of General Virology* 2016;97:3368–78. <https://doi.org/10.1099/JGV.0.000647/CITE/REFWORKS>.

Herzner AM, Hagmann CA, Goldeck M, Wolter S, Kübler K, Wittmann S, et al. Sequence-specific activation of the DNA sensor cGAS by Y-form DNA structures as found in primary HIV-1 cDNA. *Nature Immunology* 2015 16:10 2015;16:1025–33. <https://doi.org/10.1038/ni.3267>.



- Heymann F, Tacke F. Immunology in the liver--from homeostasis to disease. *Nat Rev Gastroenterol Hepatol* 2016;13:88–110. <https://doi.org/10.1038/NRGASTRO.2015.200>.
- Hong Z, Mei J, Guo H, Zhu J, Wang C. Intervention of cGAS–STING signaling in sterile inflammatory diseases. *J Mol Cell Biol* 2022;14:5. <https://doi.org/10.1093/JMCB/MJAC005>.
- Hooy RM, Sohn J. The allosteric activation of cGAS underpins its dynamic signaling landscape. *Elife* 2018;7. <https://doi.org/10.7554/ELIFE.39984>.
- Hopfner KP, Hornung V. Molecular mechanisms and cellular functions of cGAS–STING signalling. *Nature Reviews Molecular Cell Biology* 2020 21:9 2020;21:501–21. <https://doi.org/10.1038/s41580-020-0244-x>.
- Hu M-M, Xie X-Q, Yang Q, Liao C-Y, Ye W, Lin H, et al. TRIM38 Negatively Regulates TLR3/4-Mediated Innate Immune and Inflammatory Responses by Two Sequential and Distinct Mechanisms. *J Immunol* 2015;195:4415–25. <https://doi.org/10.4049/JIMMUNOL.1500859>.
- Hu MM, Yang Q, Xie XQ, Liao CY, Lin H, Liu TT, et al. Sumoylation Promotes the Stability of the DNA Sensor cGAS and the Adaptor STING to Regulate the Kinetics of Response to DNA Virus. *Immunity* 2016;45:555–69. <https://doi.org/10.1016/J.IMMUNI.2016.08.014>.
- Hu MM, Yang Q, Zhang J, Liu SM, Zhang Y, Lin H, et al. TRIM38 inhibits TNF $\alpha$ - and IL-1 $\beta$ -triggered NF- $\kappa$ B activation by mediating lysosome-dependent degradation of TAB2/3. *Proc Natl Acad Sci U S A* 2014;111:1509–14. <https://doi.org/10.1073/PNAS.1318227111>.
- Hu Q, Knight PH, Ren Y, Ren H, Zheng J, Wu X, et al. The emerging role of stimulator of interferons genes signaling in sepsis: Inflammation, autophagy, and cell death. *Acta Physiologica* 2019;225:e13194. <https://doi.org/10.1111/APHA.13194>.
- Huang LR, Gäbel YA, Graf S, Arzberger S, Kurts C, Heikenwalder M, et al. Transfer of HBV genomes using low doses of adenovirus vectors leads to persistent infection in immune competent mice. *Gastroenterology* 2012;142. <https://doi.org/10.1053/J.GASTRO.2012.03.006>.
- Huang LR, Wu HL, Chen PJ, Chen DS. An immunocompetent mouse model for the tolerance of human chronic hepatitis B virus infection. *Proc Natl Acad Sci U S A* 2006;103:17862–7. <https://doi.org/10.1073/pnas.0608578103>.
- Huang S, Zou S, Chen M, Gao X, Chen L, Yang X, et al. Local Stimulation of Liver Sinusoidal Endothelial Cells with a NOD1 Agonist Activates T Cells and Suppresses Hepatitis B Virus Replication in Mice. *J Immunol* 2018;200:3170–9. <https://doi.org/10.4049/JIMMUNOL.1700921>.
- Huang YH, Fang CC, Tsuneyama K, Chou HY, Pan WY, Shih YM, et al. A murine model of hepatitis B-associated hepatocellular carcinoma generated by adeno-associated virus-mediated gene delivery. *Int J Oncol* 2011;39:1511–9. <https://doi.org/10.3892/IJO.2011.1145>.
- Huang YH, Liu XY, Du XX, Jiang ZF, Su XD. The structural basis for the sensing and binding of cyclic di-GMP by STING. *Nat Struct Mol Biol* 2012;19:728–30. <https://doi.org/10.1038/nsmb.2333>.

- Ibrahim N, Wicklund A, Wiebe MS. Molecular Characterization of the Host Defense Activity of the Barrier to Autointegration Factor against Vaccinia Virus. *J Virol* 2011;85:11588–600. <https://doi.org/10.1128/JVI.00641-11/ASSET/A3D6FCB3-0FCE-43DB-92A1-E48DE481DE2A/ASSETS/GRAPHIC/ZJV9990951930009.JPEG>.
- Ilan E, Burakova T, Dagan S, Nussbaum O, Lubin I, Eren R, et al. The hepatitis B virus-trimera mouse: a model for human HBV infection and evaluation of anti-HBV therapeutic agents. *Hepatology* 1999;29:553–62. <https://doi.org/10.1002/hep.510290228>.
- Irudayaswamy A, Muthiah M, Zhou L, Hung H, Jumat NHB, Haque J, et al. Long-Term Fate of Human Fetal Liver Progenitor Cells Transplanted in Injured Mouse Livers. *Stem Cells* 2018;36:103–13. <https://doi.org/10.1002/STEM.2710>.
- Ishikawa H, Barber GN. STING is an endoplasmic reticulum adaptor that facilitates innate immune signalling. *Nature* 2008 455:7213 2008;455:674–8. <https://doi.org/10.1038/nature07317>.
- Iyer RP, Meher G, Sheri A, Zhou S, Challa S, Gimi RH, et al. Compounds compositions, and methods for the treatment of disease, 2019.
- Jaitin DA, Kenigsberg E, Keren-Shaul H, Elefant N, Paul F, Zaretsky I, et al. Massively parallel single cell RNA-Seq for marker-free decomposition of tissues into cell types. *Science* 2014;343:776. <https://doi.org/10.1126/SCIENCE.1247651>.
- Janeway CA, Medzhitov R. Innate immune recognition. *Annu Rev Immunol* 2002;20:197–216. <https://doi.org/10.1146/ANNUREV.IMMUNOL.20.083001.084359>.
- Janssen HLA, Brunetto MR, Kim YJ, Ferrari C, Masetto B, Nguyen AH, et al. Safety, efficacy and pharmacodynamics of vesatolimod (GS-9620) in virally suppressed patients with chronic hepatitis B. *J Hepatol* 2018;68:431–40. <https://doi.org/10.1016/J.JHEP.2017.10.027>.
- Janssen HLA, Lim Y-S, Kim HJ, Tseng C-H, Coffin CS, Elkashab M, et al. Safety and efficacy of oral TLR8 agonist, selgantolimod, in viremic adult patients with chronic hepatitis B. *J Hepatol* 2021;75:S757–8.
- Jeremiah N, Neven B, Gentili M, Callebaut I, Maschalidi S, Stolzenberg MC, et al. Inherited STING-activating mutation underlies a familial inflammatory syndrome with lupus-like manifestations. *J Clin Invest* 2014;124:5516. <https://doi.org/10.1172/JCI79100>.
- John Von Freyend M, Untergasser A, Arzberger S, Oberwinkler H, Drebber U, Schirmacher P, et al. Sequential control of hepatitis B virus in a mouse model of acute, self-resolving hepatitis B. *J Viral Hepat* 2011;18:216–26. <https://doi.org/10.1111/J.1365-2893.2010.01302.X>.
- Julander JG, Colonno RJ, Sidwell RW, Morrey JD. Characterization of antiviral activity of entecavir in transgenic mice expressing hepatitis B virus. *Antiviral Res* 2003;59:155–61. [https://doi.org/10.1016/s0166-3542\(03\)00109-8](https://doi.org/10.1016/s0166-3542(03)00109-8).
- Kao J-H. Diagnosis of hepatitis B virus infection through serological and virological markers. [Http://DxDoiOrg/101586/1747412424553](http://DxDoiOrg/101586/1747412424553) 2014;2:553–62. <https://doi.org/10.1586/17474124.2.4.553>.

- Kao J-H, Chen D-S. HBV genotypes: Epidemiology and implications regarding natural history. *Curr Hepat Rep* 2006;5:5–13. <https://doi.org/10.1007/s11901-006-0017-9>.
- Karaolis DKR, Means TK, Yang D, Takahashi M, Yoshimura T, Muraille E, et al. Bacterial c-di-GMP Is an Immunostimulatory Molecule. *The Journal of Immunology* 2007;178:2171–81. <https://doi.org/10.4049/JIMMUNOL.178.4.2171>.
- Kato K, Nishimasu H, Oikawa D, Hirano S, Hirano H, Kasuya G, et al. Structural insights into cGAMP degradation by Ecto-nucleotide pyrophosphatase phosphodiesterase 1. *Nat Commun* 2018;9. <https://doi.org/10.1038/S41467-018-06922-7>.
- Kato Y, Park J, Takamatsu H, Konaka H, Aoki W, Aburaya S, et al. Apoptosis-derived membrane vesicles drive the cGAS–STING pathway and enhance type I IFN production in systemic lupus erythematosus. *Ann Rheum Dis* 2018;77:1507–15. <https://doi.org/10.1136/ANNRHEUMDIS-2018-212988>.
- Kawasaki T, Kawai T. Toll-like receptor signaling pathways. *Front Immunol* 2014;5:461. <https://doi.org/10.3389/FIMMU.2014.00461/BIBTEX>.
- Keskitalo S, Haapaniemi E, Einarsdottir E, Rajamäki K, Heikkilä H, Ilander M, et al. Novel TMEM173 Mutation and the Role of Disease Modifying Alleles. *Front Immunol* 2019;10:2770. <https://doi.org/10.3389/FIMMU.2019.02770/BIBTEX>.
- Kim CM, Koike K, Saito I, Miyamura T, Jay G. HBx gene of hepatitis B virus induces liver cancer in transgenic mice. *Nature* 1991;351:317–20. <https://doi.org/10.1038/351317A0>.
- Kis-Toth K, Szanto A, Thai T-H, Tsokos GC. Cytosolic DNA-activated Human Dendritic Cells are Potent Activators of the Adaptive Immune Response. *J Immunol* 2011;187:1222. <https://doi.org/10.4049/JIMMUNOL.1100469>.
- Kitajima S, Ivanova E, Guo S, Yoshida R, Campisi M, Sundararaman SK, et al. Suppression of STING associated with lkb1 loss in KRAS-driven lung cancer. *Cancer Discov* 2019;9:34–45. <https://doi.org/10.1158/2159-8290.CD-18-0689/42860/AM/SUPPRESSION-OF-STING-ASSOCIATED-WITH-LKB1-LOSS-IN>.
- Klein C, Bock CT, Wedemeyer H, Wüstefeld T, Locarnini S, Dienes HP, et al. Inhibition of hepatitis B virus replication in vivo by nucleoside analogues and siRNA. *Gastroenterology* 2003;125:9–18. [https://doi.org/10.1016/s0016-5085\(03\)00720-0](https://doi.org/10.1016/s0016-5085(03)00720-0).
- Konerman MA, Lok AS. Epidemiology, Diagnosis, and Natural History of Hepatitis B. *Zakim and Boyer's Hepatology* 2018:474-484.e4. <https://doi.org/10.1016/B978-0-323-37591-7.00032-X>.
- Konno H, Chinn IK, Hong D, Orange JS, Lupski JR, Mendoza A, et al. Pro-inflammation Associated with a Gain-of-Function Mutation (R284S) in the Innate Immune Sensor STING. *Cell Rep* 2018;23:1112–23. <https://doi.org/10.1016/J.CELREP.2018.03.115/ATTACHMENT/8E55AD84-69A1-40F3-9E95-2EF3E2287E86/MMC1.PDF>.
- Konno H, Konno K, Barber GN. Cyclic Dinucleotides Trigger ULK1 (ATG1) Phosphorylation of STING to Prevent Sustained Innate Immune Signaling. *Cell* 2013;155:688–98. <https://doi.org/10.1016/J.CELL.2013.09.049>.

- Krajden M, McNabb G, Petric M. The laboratory diagnosis of hepatitis B virus. *Canadian Journal of Infectious Diseases and Medical Microbiology* 2005;16:65–72. <https://doi.org/10.1155/2005/450574>.
- Kramvis A. Genotypes and genetic variability of hepatitis B virus. *Intervirology* 2014;57:141–50. <https://doi.org/10.1159/000360947>.
- Kranzusch PJ, Lee ASY, Berger JM, Doudna JA. Structure of human cGAS reveals a conserved family of second-messenger enzymes in innate immunity. *Cell Rep* 2013;3:1362. <https://doi.org/10.1016/J.CELREP.2013.05.008>.
- Kreienkamp R, Graziano S, Coll-Bonfill N, Bedia-Diaz G, Cybulla E, Vindigni A, et al. A Cell-Intrinsic Interferon-like Response Links Replication Stress to Cellular Aging Caused by Progerin. *Cell Rep* 2018;22:2006–15. <https://doi.org/10.1016/J.CELREP.2018.01.090>.
- Krutzke S, Rietschel C, Horneff G. Baricitinib in therapy of COPA syndrome in a 15-year-old girl. *Eur J Rheumatol* 2020;7:S78. <https://doi.org/10.5152/EURJRHEUM.2019.18177>.
- Kuiper A, Gehring AJ, Isogawa M. Mechanisms of HBV immune evasion. *Antiviral Res* 2020;179:104816. <https://doi.org/10.1016/J.ANTIVIRAL.2020.104816>.
- Kumar H, Kawai T, Akira S. Pathogen recognition by the innate immune system. *Int Rev Immunol* 2011;30:16–34. <https://doi.org/10.3109/08830185.2010.529976>.
- Kumar V. A STING to inflammation and autoimmunity. *J Leukoc Biol* 2019;106:171–85. <https://doi.org/10.1002/JLB.4MIR1018-397RR>.
- Lai X, Broderick R, Bergoglio V, Zimmer J, Badie S, Niedzwiedz W, et al. MUS81 nuclease activity is essential for replication stress tolerance and chromosome segregation in BRCA2-deficient cells. *Nat Commun* 2017;8. <https://doi.org/10.1038/NCOMMS15983>.
- Lama L, Adura C, Xie W, Tomita D, Kamei T, Kuryavyi V, et al. Development of human cGAS-specific small-molecule inhibitors for repression of dsDNA-triggered interferon expression. *Nature Communications* 2019 10:1 2019;10:1–14. <https://doi.org/10.1038/s41467-019-08620-4>.
- Lamontagne RJ, Bagga S, Bouchard MJ. Hepatitis B virus molecular biology and pathogenesis. *Hepatoma Res* 2016;2:163. <https://doi.org/10.20517/2394-5079.2016.05>.
- Lan YY, Londoño D, Bouley R, Rooney MS, Hachohen N. Dnase2a deficiency uncovers lysosomal clearance of damaged nuclear DNA via autophagy. *Cell Rep* 2014;9:180–92. <https://doi.org/10.1016/j.celrep.2014.08.074>.
- Lauterbach-Rivière L, Bergez M, Mönch S, Qu B, Riess M, Vondran FWR, et al. Hepatitis B Virus DNA is a Substrate for the cGAS/STING Pathway but is not Sensed in Infected Hepatocytes. *Viruses* 2020;12:592. <https://doi.org/10.3390/V12060592>.
- Lee HW, Park JY, Hong T, Park MS, Ahn SH. A Prospective, Open-label, Dose-escalation, Single-center, Phase I Trial to Explore the Tolerability, Safety and Pharmacokinetics/Pharmacodynamics of GC1102 (Recombinant Hepatitis B Human Immunoglobulin) - AdisInsight. *Hepatology* 2018.

- Lee J-J, Kim SY, Kim SH, Choi S, Lee B, Shin J-S. STING mediates nuclear PD-L1 targeting-induced senescence in cancer cells. *Cell Death & Disease* 2022;13:9 2022;13:1–11. <https://doi.org/10.1038/s41419-022-05217-6>.
- Lee JK, Kim JE, Park BJ, Song YJ. Human cytomegalovirus IE86 protein aa 136-289 mediates STING degradation and blocks the cGAS-STING pathway. *J Microbiol* 2020;58:54–60. <https://doi.org/10.1007/S12275-020-9577-6>.
- Lempp FA, Mutz P, Lipps C, Wirth D, Bartenschlager R, Urban S. Evidence that hepatitis B virus replication in mouse cells is limited by the lack of a host cell dependency factor. *J Hepatol* 2016;64:556–64. <https://doi.org/10.1016/J.JHEP.2015.10.030>.
- Leowattana W, Leowattana T. Chronic hepatitis B: New potential therapeutic drugs target. *World J Virol* 2022;11:57. <https://doi.org/10.5501/WJV.V11.I1.57>.
- Lepelley A, Martin-Niélós MJ, Bihan M le, Marsh JA, Ugenti C, Rice GI, et al. Mutations in COPA lead to abnormal trafficking of STING to the Golgi and interferon signaling. *Journal of Experimental Medicine* 2020;217. <https://doi.org/10.1084/JEM.20200600/151983>.
- Li L, Li S, Zhou Y, Yang L, Zhou D, Yang Y, et al. The dose of HBV genome contained plasmid has a great impact on HBV persistence in hydrodynamic injection mouse model. *Virol J* 2017;14:1–12. <https://doi.org/10.1186/s12985-017-0874-6>.
- Li L, Yin Q, Kuss P, Maliga Z, Millán JL, Wu H, et al. Hydrolysis of 2'3'-cGAMP by ENPP1 and design of nonhydrolyzable analogs. *Nat Chem Biol* 2014;10:1043–8. <https://doi.org/10.1038/NCHEMBIO.1661>.
- Li P zhi, Li J zheng, Li M, Gong J ping, He K. An efficient method to isolate and culture mouse Kupffer cells. *Immunol Lett* 2014;158:52–6. <https://doi.org/10.1016/J.IMLET.2013.12.002>.
- Li Q, Lin L, Tong Y, Liu Y, Mou J, Wang X, et al. TRIM29 negatively controls antiviral immune response through targeting STING for degradation. *Cell Discovery* 2018 4:1 2018;4:1–13. <https://doi.org/10.1038/s41421-018-0010-9>.
- Li S, Hong Z, Wang Z, Li F, Mei J, Huang L, et al. The Cyclopeptide Astin C Specifically Inhibits the Innate Immune CDN Sensor STING. *Cell Rep* 2018;25:3405-3421.e7. <https://doi.org/10.1016/j.celrep.2018.11.097>.
- Li X, Liu G, Chen M, Yang Y, Xie Y, Kong X. A Novel Hydrodynamic Injection Mouse Model of HBV Genotype C for the Study of HBV Biology and the Anti-Viral Activity of Lamivudine. *Hepat Mon* 2016;16. <https://doi.org/10.5812/HEPATMON.34420>.
- Li X, Shu C, Yi G, Chaton CT, Shelton CL, Diao J, et al. Cyclic GMP-AMP Synthase is Activated by Double-stranded DNA-Induced Oligomerization. *Immunity* 2013;39:1019–31. <https://doi.org/10.1016/J.IMMUNI.2013.10.019>.
- Li Z, Wu Y, Wang C, Zhang M. Mouse CD8+NKT-like cells exert dual cytotoxicity against mouse tumor cells and myeloid-derived suppressor cells. *Cancer Immunol Immunother* 2019;68:1303–15. <https://doi.org/10.1007/S00262-019-02363-3>.
- Lian H, Wei J, Zang R, Ye W, Yang Q, Zhang XN, et al. ZCCHC3 is a co-sensor of cGAS for dsDNA recognition in innate immune response. *Nat Commun* 2018;9. <https://doi.org/10.1038/S41467-018-05559-W>.

- Lin B, Berard R, al Rasheed A, Aladba B, Kranzusch PJ, Henderlight M, et al. A novel STING1 variant causes a recessive form of STING-associated vasculopathy with onset in infancy (SAVI). *J Allergy Clin Immunol* 2020;146:1204. <https://doi.org/10.1016/J.JACI.2020.06.032>.
- Lin SR, Yang HC, Kuo YT, Liu CJ, Yang TY, Sung KC, et al. The CRISPR/Cas9 System Facilitates Clearance of the Intrahepatic HBV Templates In Vivo. *Mol Ther Nucleic Acids* 2014;3:e186. <https://doi.org/10.1038/MTNA.2014.38>.
- Lirussi D, Ebensen T, Schulze K, Trittel S, Duran V, Liebich I, et al. Type I IFN and not TNF, is Essential for Cyclic Di-nucleotide-elicited CTL by a Cytosolic Cross-presentation Pathway. *EBioMedicine* 2017;22:100. <https://doi.org/10.1016/J.EBIOM.2017.07.016>.
- Liu S, Cai X, Wu J, Cong Q, Chen X, Li T, et al. Phosphorylation of innate immune adaptor proteins MAVS, STING, and TRIF induces IRF3 activation. *Science (1979)* 2015;347. [https://doi.org/10.1126/SCIENCE.AAA2630/SUPPL\\_FILE/LIU.SM.REVISION.1.PDF](https://doi.org/10.1126/SCIENCE.AAA2630/SUPPL_FILE/LIU.SM.REVISION.1.PDF).
- Liu Y, Jesus AA, Marrero B, Yang D, Ramsey SE, Montealegre Sanchez GA, et al. Activated STING in a Vascular and Pulmonary Syndrome. *N Engl J Med* 2014;371:507. <https://doi.org/10.1056/NEJMOA1312625>.
- Liu Y, Li J, Chen J, Li Y, Wang W, Du X, et al. Hepatitis B Virus Polymerase Disrupts K63-Linked Ubiquitination of STING To Block Innate Cytosolic DNA-Sensing Pathways. *J Virol* 2015;89:2287–300. <https://doi.org/10.1128/JVI.02760-14/ASSET/2D733823-E812-45EA-B75A-D93B0A1B5F23/ASSETS/GRAPHIC/ZJV9990900560006.JPEG>.
- Liu ZS, Cai H, Xue W, Wang M, Xia T, Li WJ, et al. G3BP1 promotes DNA binding and activation of cGAS. *Nat Immunol* 2019;20:18–28. <https://doi.org/10.1038/S41590-018-0262-4>.
- Locarnini S. Molecular Virology of Hepatitis B Virus. *Semin Liver Dis* 2004;24:3–10. <https://doi.org/10.1055/s-2004-828672>.
- Luecke S, Holleufer A, Christensen MH, Jønsson KL, Boni GA, Sørensen LK, et al. cGAS is activated by DNA in a length-dependent manner. *EMBO Rep* 2017;18:1707. <https://doi.org/10.15252/EMBR.201744017>.
- Lynch RW, Hawley CA, Pellicoro A, Bain CC, Iredale JP, Jenkins SJ. An efficient method to isolate Kupffer cells eliminating endothelial cell contamination and selective bias. *J Leukoc Biol* 2018;104:579–86. <https://doi.org/10.1002/JLB.1TA0517-169R>.
- Ma H, Lim TH, Leerapun A, Weltman M, Jia J, Lim Y-S, et al. Restoration of HBV-specific immune responses with therapeutic vaccine BR11-179 (VBI-2601) in chronic HBV patients in a phase 1b/2a study n.d.
- Ma H, Qian W, Bambouskova M, Collins PL, Porter SI, Byrum AK, et al. Barrier-to-Autointegration Factor 1 Protects against a Basal cGAS-STING Response. *MBio* 2020;11. <https://doi.org/10.1128/MBIO.00136-20>.
- MacKenzie KJ, Carroll P, Martin CA, Murina O, Fluteau A, Simpson DJ, et al. cGAS surveillance of micronuclei links genome instability to innate immunity. *Nature* 2017 548:7668 2017;548:461–5. <https://doi.org/10.1038/nature23449>.

- Malireddi RKS, Kesavardhana S, Kanneganti TD. ZBP1 and TAK1: Master Regulators of NLRP3 Inflammasome/Pyroptosis, Apoptosis, and Necroptosis (PANoptosis). *Front Cell Infect Microbiol* 2019;9:406. <https://doi.org/10.3389/FCIMB.2019.00406/BIBTEX>.
- Marcus A, Mao AJ, Lensink-Vasan M, Wang LA, Vance RE, Raulet DH. Tumor-Derived cGAMP Triggers a STING-Mediated Interferon Response in Non-tumor Cells to Activate the NK Cell Response. *Immunity* 2018;49:754-763.e4. <https://doi.org/10.1016/j.immuni.2018.09.016>.
- Marion PL, Oshiro LS, Regnery DC, Scullard GH, Robinson WS. A virus in Beechey ground squirrels that is related to hepatitis B virus of humans. *Proc Natl Acad Sci U S A* 1980;77:2941. <https://doi.org/10.1073/PNAS.77.5.2941>.
- Mason WS, Seal G, Summers J. Virus of Pekin ducks with structural and biological relatedness to human hepatitis B virus. *J Virol* 1980;36:829. <https://doi.org/10.1128/jvi.36.3.829-836.1980>.
- Mason, W.S.Gerlich WH, Taylor JM, Kann M, Mizokami T, Loeb D, Sureau C, et al. Hepadnaviridae. *Virus Taxonomy*, Elsevier; 2012, p. 445–55. <https://doi.org/10.1016/B978-0-12-384684-6.00041-0>.
- Matzinger P. Tolerance, danger, and the extended family. *Annu Rev Immunol* 1994;12:991–1045. <https://doi.org/10.1146/ANNUREV.IY.12.040194.005015>.
- McArthur K, Whitehead LW, Heddleston JM, Li L, Padman BS, Oorschot V, et al. BAK/BAX macropores facilitate mitochondrial herniation and mtDNA efflux during apoptosis. *Science (1979)* 2018;359. [https://doi.org/10.1126/SCIENCE.AAO6047/SUPPL\\_FILE/AAO6047\\_MCARTHUR\\_SM.PDF](https://doi.org/10.1126/SCIENCE.AAO6047/SUPPL_FILE/AAO6047_MCARTHUR_SM.PDF).
- McCaffrey AP, Nakai H, Pandey K, Huang Z, Salazar FH, Xu H, et al. Inhibition of hepatitis B virus in mice by RNA interference. *Nat Biotechnol* 2003;21:639–44. <https://doi.org/10.1038/NBT824>.
- Medzhitov R. Toll-like receptors and innate immunity. *Nature Reviews Immunology* 2001 1:2 2001;1:135–45. <https://doi.org/10.1038/35100529>.
- Melki I, Rose Y, Uggenti C, van Eyck L, Frémond ML, Kitabayashi N, et al. Disease-associated mutations identify a novel region in human STING necessary for the control of type I interferon signaling. *Journal of Allergy and Clinical Immunology* 2017;140:543-552.e5. <https://doi.org/10.1016/J.JACI.2016.10.031>.
- Merck Sharp & Dohme LLC. Study of Ulevostinag (MK-1454) Alone or in Combination With Pembrolizumab (MK-3475) in Participants With Advanced/Metastatic Solid Tumors or Lymphomas (MK-1454-001) - Full Text View - ClinicalTrials.gov 2022a.
- Merck Sharp & Dohme LLC. Study of Intratumoral (IT) Ulevostinag (MK-1454) in Combination With Intravenous (IV) Pembrolizumab (MK-3475) Compared to IV Pembrolizumab Alone as the First Line Treatment of Metastatic or Unresectable, Recurrent Head and Neck Squamous Cell Carcinoma (HNSCC) (MK-1454-002) - Full Text View - ClinicalTrials.gov 2022b.
- Messaoud-Nacer Y, Culerier E, Rose S, Maillet I, Rouxel N, Briault S, et al. STING agonist diABZI induces PANoptosis and DNA mediated acute respiratory distress

- syndrome (ARDS). *Cell Death & Disease* 2022 13:3 2022;13:1–17. <https://doi.org/10.1038/s41419-022-04664-5>.
- Meuleman P, Libbrecht L, de Vos R, de Hemptinne B, Gevaert K, Vandekerckhove J, et al. Morphological and biochemical characterization of a human liver in a uPA-SCID mouse chimera. *Hepatology* 2005;41:847–56. <https://doi.org/10.1002/hep.20657>.
- Milich DR, Jones JE, Hughes JL, Price J, Raney AK, Mclachlan A. Is a function of the secreted hepatitis B e antigen to induce immunologic tolerance in utero? *Proc Natl Acad Sci U S A* 1990;87:6599–603. <https://doi.org/10.1073/PNAS.87.17.6599>.
- Milich DR, Leroux-Roels GG. Immunogenetics of the response to HBsAg vaccination. *Autoimmun Rev* 2003;2:248–57. [https://doi.org/10.1016/S1568-9972\(03\)00031-4](https://doi.org/10.1016/S1568-9972(03)00031-4).
- Miltenyi Biotec. Liver Dissociation Kit Mouse Protocol 2021.
- Mitchell G, Isberg RR. Innate Immunity to Intracellular pathogens: balancing microbial elimination and inflammation. *Cell Host Microbe* 2017;22:166. <https://doi.org/10.1016/J.CHOM.2017.07.005>.
- Mohar I, Brempelis KJ, Murray SA, Ebrahimkhani MR, Crispe IN. Isolation of Non-parenchymal Cells from the Mouse Liver. *Methods Mol Biol* 2015;1325:3–17. [https://doi.org/10.1007/978-1-4939-2815-6\\_1](https://doi.org/10.1007/978-1-4939-2815-6_1).
- Motwani M, Pesiridis S, Fitzgerald KA. DNA sensing by the cGAS-STING pathway in health and disease. *Nat Rev Genet* 2019;20:657–74. <https://doi.org/10.1038/S41576-019-0151-1>.
- Mueller SN, Ahmed R. High antigen levels are the cause of T cell exhaustion during chronic viral infection. *Proc Natl Acad Sci U S A* 2009;106:8623. <https://doi.org/10.1073/PNAS.0809818106>.
- Mukai K, Konno H, Akiba T, Uemura T, Waguri S, Kobayashi T, et al. Activation of STING requires palmitoylation at the Golgi. *Nature Communications* 2016 7:1 2016a;7:1–10. <https://doi.org/10.1038/ncomms11932>.
- Mukai K, Konno H, Akiba T, Uemura T, Waguri S, Kobayashi T, et al. Activation of STING requires palmitoylation at the Golgi. *Nature Communications* 2016 7:1 2016b;7:1–10. <https://doi.org/10.1038/ncomms11932>.
- Nakamura T, Miyabe H, Hyodo M, Sato Y, Hayakawa Y, Harashima H. Liposomes loaded with a STING pathway ligand, cyclic di-GMP, enhance cancer immunotherapy against metastatic melanoma. *Journal of Controlled Release* 2015;216:149–57. <https://doi.org/10.1016/J.JCONREL.2015.08.026>.
- Namjou B, Kothari PH, Kelly JA, Glenn SB, Ojwang JO, Adler A, et al. Evaluation of the TREX1 gene in a large multi-ancestral lupus cohort. *Genes & Immunity* 2011 12:4 2011;12:270–9. <https://doi.org/10.1038/gene.2010.73>.
- Nascimento M, Gombault A, Lacerda-Queiroz N, Panek C, Savigny F, Sbeity M, et al. Self-DNA release and STING-dependent sensing drives inflammation to cigarette smoke in mice. *Sci Rep* 2019;9. <https://doi.org/10.1038/S41598-019-51427-Y>.
- Ning Q, Han M, Sun Y, Jiang J, Tan D, Hou J, et al. Switching from entecavir to PegIFN alfa-2a in patients with HBeAg-positive chronic hepatitis B: a randomised



open-label trial (OSST trial). *J Hepatol* 2014;61:777–84.  
<https://doi.org/10.1016/J.JHEP.2014.05.044>.

Novartis Pharmaceuticals. Study of the Safety and Efficacy of MIW815 With PDR001 in Patients With Advanced/Metastatic Solid Tumors or Lymphomas - Full Text View - [ClinicalTrials.gov](https://clinicaltrials.gov) 2022.

Novotná B, Holá L, Staš M, Gutten O, Smola M, Zavřel M, et al. Enzymatic Synthesis of 3'-5', 3'-5' Cyclic Dinucleotides, Their Binding Properties to the Stimulator of Interferon Genes Adaptor Protein, and Structure/Activity Correlations. *Biochemistry* 2021;60:3714–27. <https://doi.org/10.1021/ACS.BIOCHEM.1C00692>.

Novotná B, Vaneková L, Zavřel M, Buděšínský M, Dejmek M, Smola M, et al. Enzymatic Preparation of 2'-5',3'-5'-Cyclic Dinucleotides, Their Binding Properties to Stimulator of Interferon Genes Adaptor Protein, and Structure/Activity Correlations. *J Med Chem* 2019;62:10676–90.  
[https://doi.org/10.1021/ACS.JMEDCHEM.9B01062/SUPPL\\_FILE/JM9B01062\\_SI\\_003.CSV](https://doi.org/10.1021/ACS.JMEDCHEM.9B01062/SUPPL_FILE/JM9B01062_SI_003.CSV).

de Oliveira Mann CC, Orzalli MH, King DS, Kagan JC, Lee ASY, Kranzusch PJ. Modular Architecture of the STING C-Terminal Tail Allows Interferon and NF- $\kappa$ B Signaling Adaptation. *Cell Rep* 2019;27:1165-1175.e5.  
<https://doi.org/10.1016/J.CELREP.2019.03.098/ATTACHMENT/AD1FEDC1-C23A-4046-BD72-A2FBF290DE2C/MMC5.XLSX>.

Ortega-Prieto AM, Cherry C, Gunn H, Dorner M. In Vivo Model Systems for Hepatitis B Virus Research. *ACS Infect Dis* 2019;5:688–702.  
<https://doi.org/10.1021/acsinfecdis.8b00223>.

Ouyang S, Song X, Wang Y, Ru H, Shaw N, Jiang Y, et al. Structural Analysis of the STING Adaptor Protein Reveals a Hydrophobic Dimer Interface and Mode of Cyclic di-GMP Binding. *Immunity* 2012;36:1073–86.  
<https://doi.org/10.1016/J.IMMUNI.2012.03.019/ATTACHMENT/379407B6-9EA1-44B8-949D-E12721B70AFE/MMC1.PDF>.

Padilla-Salinas R, Sun L, Anderson R, Yang X, Zhang S, Chen ZJ, et al. Discovery of Small-Molecule Cyclic GMP-AMP Synthase Inhibitors. *Journal of Organic Chemistry* 2020;85:1579–600.  
[https://doi.org/10.1021/ACS.JOC.9B02666/SUPPL\\_FILE/JO9B02666\\_SI\\_001.PDF](https://doi.org/10.1021/ACS.JOC.9B02666/SUPPL_FILE/JO9B02666_SI_001.PDF).

Pandey S, Kawai T, Akira S. Microbial Sensing by Toll-Like Receptors and Intracellular Nucleic Acid Sensors. *Cold Spring Harb Perspect Biol* 2015;7:a016246.  
<https://doi.org/10.1101/CSHPERSPECT.A016246>.

Pantelidou C, Jadhav H, Kothari A, Liu R, Wulf GM, Guerriero JL, et al. STING agonism enhances anti-tumor immune responses and therapeutic efficacy of PARP inhibition in BRCA-associated breast cancer. *Npj Breast Cancer* 2022 8:1 2022;8:1–6. <https://doi.org/10.1038/s41523-022-00471-5>.

Patel S, Jin L. TMEM173 variants and potential importance to human biology and disease. *Genes & Immunity* 2018 20:1 2018;20:82–9.  
<https://doi.org/10.1038/s41435-018-0029-9>.

Peng XH, Ren XN, Chen LX, Shi BS, Xu CH, Fang Z, et al. High persistence rate of hepatitis B virus in a hydrodynamic injection-based transfection model in C3H/HeN

- mice. *World J Gastroenterol* 2015;21:3527–36. <https://doi.org/10.3748/wjg.v21.i12.3527>.
- Pimková Polidarová M. Protein STING targeting for chronic hepatitis B treatment. 2022.
- Pimková Polidarová M, Břehová P, Kaiser MM, Smola M, Dračinský M, Smith J, et al. Synthesis and Biological Evaluation of Phosphoester and Phosphorothioate Prodrugs of STING Agonist 3',3'-c-Di(2'F,2'dAMP). *J Med Chem* 2021;64:7596–616. [https://doi.org/10.1021/ACS.JMEDCHEM.1C00301/SUPPL\\_FILE/JM1C00301\\_SI\\_002.CSV](https://doi.org/10.1021/ACS.JMEDCHEM.1C00301/SUPPL_FILE/JM1C00301_SI_002.CSV).
- Preston SP, Pellegrini M, Ebert G. Hydrodynamic Injection as a Method of Gene Delivery in Mice: A Model of Chronic Hepatitis B Virus Infection, 2016, p. 109–15. [https://doi.org/10.1007/978-1-4939-3581-9\\_9](https://doi.org/10.1007/978-1-4939-3581-9_9).
- Qi S, Wang C, Zhang R, Zhu J, Hou X, Jiang Y, et al. Human STING Is Regulated by an Autoinhibitory Mechanism for Type I Interferon Production. *J Innate Immun* 2022;14:518–31. <https://doi.org/10.1159/000521734>.
- Qin B, Budeus B, Cao L, Wu C, Wang Y, Zhang X, et al. The amino acid substitutions rtP177G and rtF249A in the reverse transcriptase domain of hepatitis B virus polymerase reduce the susceptibility to tenofovir. *Antiviral Res* 2013;97:93–100. <https://doi.org/10.1016/J.ANTIVIRAL.2012.12.007>.
- Ramanjulu JM, Pesiridis GS, Yang J, Concha N, Singhaus R, Zhang SY, et al. Design of amidobenzimidazole STING receptor agonists with systemic activity. *Nature* 2018 564:7736 2018;564:439–43. <https://doi.org/10.1038/s41586-018-0705-y>.
- Rehermann B. Pathogenesis of chronic viral hepatitis: differential roles of T cells and NK cells. *Nat Med* 2013;19:859–68. <https://doi.org/10.1038/NM.3251>.
- Rehermann B, Nascimbeni M. Immunology of hepatitis B virus and hepatitis C virus infection. *Nat Rev Immunol* 2005;5:215–29. <https://doi.org/10.1038/NRI1573>.
- Reisländer T, Lombardi EP, Groelly FJ, Miar A, Porru M, di Vito S, et al. BRCA2 abrogation triggers innate immune responses potentiated by treatment with PARP inhibitors. *Nat Commun* 2019;10. <https://doi.org/10.1038/S41467-019-11048-5>.
- Revell PA, Chisari F v., Block JM, Dandri M, Gehring AJ, Guo H, et al. A global scientific strategy to cure hepatitis B. *Lancet Gastroenterol Hepatol* 2019;4:545. [https://doi.org/10.1016/S2468-1253\(19\)30119-0](https://doi.org/10.1016/S2468-1253(19)30119-0).
- Revell PA, Tu T, Netter HJ, Yuen LKW, Locarnini SA, Littlejohn M. The evolution and clinical impact of hepatitis B virus genome diversity 2020. <https://doi.org/10.1038/s41575-020-0296-6>.
- Riley JS, Quarato G, Cloix C, Lopez J, O'Prey J, Pearson M, et al. Mitochondrial inner membrane permeabilisation enables mtDNA release during apoptosis. *EMBO J* 2018;37:e99238. <https://doi.org/10.15252/EMBJ.201899238>.
- Riteau N, Alves-Filho JC, David C, Frémond M-L. Lung Inflammation in STING-Associated Vasculopathy with Onset in Infancy (SAVI). *Cells* 2022, Vol 11, Page 318 2022;11:318. <https://doi.org/10.3390/CELLS11030318>.

Rodero MP, Tesser A, Bartok E, Rice GI, della Mina E, Depp M, et al. Type I interferon-mediated autoinflammation due to DNase II deficiency. *Nature Communications* 2017 8:1 2017;8:1–15. <https://doi.org/10.1038/s41467-017-01932-3>.

Rongvaux A, Jackson R, Harman CCD, Li T, West AP, de Zoete MR, et al. Apoptotic caspases prevent the induction of type I interferons by mitochondrial DNA. *Cell* 2014;159:1563–77. <https://doi.org/10.1016/J.CELL.2014.11.037/ATTACHMENT/6C326845-1431-4248-B680-3D2B94780B83/MMC2.PDF>.

Saldanha RG, Balka KR, Davidson S, Wainstein BK, Wong M, Macintosh R, et al. A mutation outside the dimerization domain causing atypical STING-associated vasculopathy with onset in infancy. *Front Immunol* 2018;9:1535. <https://doi.org/10.3389/FIMMU.2018.01535/XML/NLM>.

Sameer AS, Nissar S. Toll-Like Receptors (TLRs): Structure, Functions, Signaling, and Role of Their Polymorphisms in Colorectal Cancer Susceptibility. *Biomed Res Int* 2021;2021. <https://doi.org/10.1155/2021/1157023>.

Schenten D, Medzhitov R. The control of adaptive immune responses by the innate immune system. *Adv Immunol* 2011;109:87–124. <https://doi.org/10.1016/B978-0-12-387664-5.00003-0>.

Schock SN, Chandra N v., Sun Y, Irie T, Kitagawa Y, Gotoh B, et al. Induction of necroptotic cell death by viral activation of the RIG-I or STING pathway. *Cell Death & Differentiation* 2017 24:4 2017;24:615–25. <https://doi.org/10.1038/cdd.2016.153>.

Schumann R, Opitz B, Lei J, Mansouri J, Sebastian Ruiz-Moreno L, Hamann RS, et al. Is a Null Allele TMEM173 The Common R71H-G230A-R293Q Human 2022. <https://doi.org/10.4049/jimmunol.1601585>.

Sengupta S, Rehman S, Durgapal H, Acharya SK, Panda SK. Role of surface promoter mutations in hepatitis B surface antigen production and secretion in occult hepatitis B virus infection. *J Med Virol* 2007;79:220–8. <https://doi.org/10.1002/JMV.20790>.

Shakespeare MR, Halili MA, Irvine KM, Fairlie DP, Sweet MJ. Histone deacetylases as regulators of inflammation and immunity. *Trends Immunol* 2011;32:335–43. <https://doi.org/10.1016/j.it.2011.04.001>.

Shang G, Zhang C, Chen ZJ, Bai X chen, Zhang X. Cryo-EM structures of STING reveal its mechanism of activation by cyclic GMP–AMP. *Nature* 2019 567:7748 2019;567:389–93. <https://doi.org/10.1038/s41586-019-0998-5>.

Shang G, Zhu D, Li N, Zhang J, Zhu C, Lu D, et al. Crystal structures of STING protein reveal basis for recognition of cyclic di-GMP. *Nat Struct Mol Biol* 2012;19:725–7. <https://doi.org/10.1038/nsmb.2332>.

Shapson-Coe A, Valeiras B, Wall C, Rada C. Aicardi–Goutières Syndrome associated mutations of RNase H2B impair its interaction with ZMYM3 and the CoREST histone-modifying complex. *PLoS One* 2019;14:e0213553. <https://doi.org/10.1371/JOURNAL.PONE.0213553>.

Sharma S, Campbell AM, Chan J, Schattgen SA, Orłowski GM, Nayar R, et al. Suppression of systemic autoimmunity by the innate immune adaptor STING. *Proc*

Natl Acad Sci U S A 2015;112:E710–7.  
[https://doi.org/10.1073/PNAS.1420217112/SUPPL\\_FILE/PNAS.201420217SI.PDF](https://doi.org/10.1073/PNAS.1420217112/SUPPL_FILE/PNAS.201420217SI.PDF).

Shi W, Wang Y, Zhang C, Jin H, Zeng Z, Wei L, et al. Isolation and purification of immune cells from the liver. *Int Immunopharmacol* 2020;85.  
<https://doi.org/10.1016/J.INTIMP.2020.106632>.

Siu T, Altman MD, Baltus GA, Childers M, Ellis JM, Gunaydin H, et al. Discovery of a Novel cGAMP Competitive Ligand of the Inactive Form of STING. *ACS Med Chem Lett* 2019;10:92–7.  
[https://doi.org/10.1021/ACSMEDCHEMLETT.8B00466/SUPPL\\_FILE/ML8B00466\\_SI\\_001.PDF](https://doi.org/10.1021/ACSMEDCHEMLETT.8B00466/SUPPL_FILE/ML8B00466_SI_001.PDF).

Sivick KE, Desbien AL, Glickman LH, Reiner GL, Corrales L, Surh NH, et al. Magnitude of Therapeutic STING Activation Determines CD8+ T Cell-Mediated Anti-tumor Immunity. *Cell Rep* 2018;25:3074-3085.e5.  
<https://doi.org/10.1016/J.CELREP.2018.11.047>.

Song C, Liu D, Liu S, Li D, Horecny I, Zhang X, et al. SHR1032, a novel STING agonist, stimulates anti-tumor immunity and directly induces AML apoptosis. *Scientific Reports* 2022 12:1 2022;12:1–12. <https://doi.org/10.1038/s41598-022-12449-1>.

Sprinzl MF, Oberwinkler H, Schaller H, Protzer U. Transfer of hepatitis B virus genome by adenovirus vectors into cultured cells and mice: crossing the species barrier. *J Virol* 2001;75:5108–18. <https://doi.org/10.1128/JVI.75.11.5108-5118.2001>.

Srikanth S, Woo JS, Wu B, El-Sherbiny YM, Leung J, Chupradit K, et al. The Ca<sup>2+</sup> sensor STIM1 regulates the type I interferon response by retaining the signaling adaptor STING at the endoplasmic reticulum. *Nature Immunology* 2019 20:2 2019;20:152–62. <https://doi.org/10.1038/s41590-018-0287-8>.

Stazzoni S. Design and Synthesis of Clickable Nucleic Acid Analogues for Cancer Therapy and Diagnosis 2020.

Stazzoni S, Böhmer DFR, Hernichel F, Özdemir D, Pappa A, Drexler D, et al. Novel Poxin Stable cGAMP-Derivatives Are Remarkable STING Agonists. *Angewandte Chemie International Edition* 2022;61:e202207175.  
<https://doi.org/10.1002/ANIE.202207175>.

Steinhagen F, Zillinger T, Peukert K, Fox M, Thudium M, Barchet W, et al. Suppressive oligodeoxynucleotides containing TTAGGG motifs inhibit cGAS activation in human monocytes. *Eur J Immunol* 2018;48:605–11.  
<https://doi.org/10.1002/EJI.201747338>.

Stetson DB, Ko JS, Heidmann T, Medzhitov R. Trex1 prevents cell-intrinsic initiation of autoimmunity. *Cell* 2008;134:587–98.  
<https://doi.org/10.1016/J.CELL.2008.06.032>.

Summers J, Smolec JM, Snyder R. A virus similar to human hepatitis B virus associated with hepatitis and hepatoma in woodchucks. *Proc Natl Acad Sci U S A* 1978;75:4533. <https://doi.org/10.1073/PNAS.75.9.4533>.

Sun H, Huang Y, Mei S, Xu F, Liu X, Zhao F, et al. A Nuclear Export Signal Is Required for cGAS to Sense Cytosolic DNA. *Cell Rep* 2021;34:108586.  
<https://doi.org/10.1016/j.celrep.2020.108586>.

- Sun L, Wu J, Du F, Chen X, Chen ZJ. Cyclic GMP-AMP Synthase is a Cytosolic DNA Sensor that Activates the Type-I Interferon Pathway. *Science* 2013;339:786–91. <https://doi.org/10.1126/SCIENCE.1232458>.
- Sun Y, Qi Y, Peng B, Li W. NTCP-Reconstituted In Vitro HBV Infection System. *Methods in Molecular Biology* 2017;1540:1–14. [https://doi.org/10.1007/978-1-4939-6700-1\\_1](https://doi.org/10.1007/978-1-4939-6700-1_1).
- Suzuki M, Kondo S, Yamasaki M, Matsuda N, Nomoto A, Suzuki T, et al. Efficient genome replication of hepatitis B virus using adenovirus vector: a compact pregenomic RNA-expression unit. *Sci Rep* 2017;7. <https://doi.org/10.1038/SREP41851>.
- Sze A, Belgnaoui SM, Olganier D, Lin R, Hiscott J, van Grevenynghe J. Host restriction factor SAMHD1 limits human T cell leukemia virus type 1 infection of monocytes via STING-mediated apoptosis. *Cell Host Microbe* 2013;14:422–34. <https://doi.org/10.1016/J.CHOM.2013.09.009/ATTACHMENT/F06632A9-F7EF-465D-B1BC-45F97CC7D4E8/MMC1.PDF>.
- Tacke F, Zimmermann HW. Macrophage heterogeneity in liver injury and fibrosis. *J Hepatol* 2014;60:1090–6. <https://doi.org/10.1016/J.JHEP.2013.12.025>.
- Tan YS, Sansanaphongpricha K, Xie Y, Donnelly CR, Luo X, Heath BR, et al. Mitigating SOX2-potentiated Immune Escape of Head and Neck Squamous Cell Carcinoma with a STING-inducing Nanosatellite Vaccine. *Clinical Cancer Research* 2018;24:4242–55. <https://doi.org/10.1158/1078-0432.CCR-17-2807/87543/AM/MITIGATING-SOX2-POTENTIATED-IMMUNE-ESCAPE-OF-HEAD>.
- Tao S-S, Wu G-C, Zhang Q, Zhang T-P, Leng R-X, Pan H-F, et al. TREX1 As a Potential Therapeutic Target for Autoimmune and Inflammatory Diseases. *Curr Pharm Des* 2019;25:3239–47. <https://doi.org/10.2174/1381612825666190902113218>.
- The World Health Organisation. Guidelines on hepatitis B and C testing. vol. 66. 2017.
- Thim-uam A, Prabakaran T, Tansakul M, Makjaroen J, Wongkongkathep P, Chantaravisoot N, et al. STING Mediates Lupus via the Activation of Conventional Dendritic Cell Maturation and Plasmacytoid Dendritic Cell Differentiation. *IScience* 2020;23. <https://doi.org/10.1016/J.ISCI.2020.101530>.
- Thomsen MK, Nandakumar R, Stadler D, Malo A, Valls RM, Wang F, et al. Lack of immunological DNA sensing in hepatocytes facilitates hepatitis B virus infection. *Hepatology* 2016;64:746–59. <https://doi.org/10.1002/HEP.28685/SUPPINFO>.
- Tian X, Xu F, Zhu Q, Feng Z, Dai W, Zhou Y, et al. Medicinal chemistry perspective on cGAS-STING signaling pathway with small molecule inhibitors. *Eur J Med Chem* 2022;244:114791. <https://doi.org/10.1016/J.EJMECH.2022.114791>.
- Tong S, Revill P. Overview of hepatitis B viral replication and genetic variability. *J Hepatol* 2016;64:S4–16. <https://doi.org/10.1016/j.jhep.2016.01.027>.
- Tsuchida T, Zou J, Saitoh T, Kumar H, Abe T, Matsuura Y, et al. The ubiquitin ligase TRIM56 regulates innate immune responses to intracellular double-stranded DNA. *Immunity* 2010;33:765–76.

<https://doi.org/10.1016/J.IMMUNI.2010.10.013/ATTACHMENT/EF6EDF57-23AD-4D3D-A105-3D11D7D59E9F/MMC1.PDF>.

Tsuge M, Hiraga N, Takaishi H, Noguchi C, Oga H, Imamura M, et al. Infection of human hepatocyte chimeric mouse with genetically engineered hepatitis B virus. *Hepatology* 2005;42:1046–54. <https://doi.org/10.1002/hep.20892>.

Tzeng HT, Hsu PN, Chen PJ. Immunocompetent nontransgenic mouse models for studying hepatitis B virus immune responses. *J Gastroenterol Hepatol* 2013;28 Suppl 1:116–9. <https://doi.org/10.1111/JGH.12035>.

Uhlorn BL, Gamez ER, Li S, Campos SK. Attenuation of cGAS/STING activity during mitosis. *Life Sci Alliance* 2020;3. <https://doi.org/10.26508/LSA.201900636>.

Valentin R, Wong C, Alharbi AS, Pradeloux S, Morros MP, Lennox KA, et al. Sequence-dependent inhibition of cGAS and TLR9 DNA sensing by 2'-O-methyl gapmer oligonucleotides. *Nucleic Acids Res* 2021;49:6082–99. <https://doi.org/10.1093/NAR/GKAB451>.

Vavřina Z, Gutten O, Smola M, Zavřel M, Aliakbar Tehrani Z, Charvát V, et al. Protein-Ligand Interactions in the STING Binding Site Probed by Rationally Designed Single-Point Mutations: Experiment and Theory. *Biochemistry* 2021;60:607–20. [https://doi.org/10.1021/ACS.BIOCHEM.0C00949/SUPPL\\_FILE/BI0C00949\\_SI\\_002.ZIP](https://doi.org/10.1021/ACS.BIOCHEM.0C00949/SUPPL_FILE/BI0C00949_SI_002.ZIP).

Vavrina Z, Perlíková P, Milisavljevic N, Chevri er F, Smola M, Smith J, et al. Design, Synthesis, and Biochemical and Biological Evaluation of Novel 7-Deazapurine Cyclic Dinucleotide Analogues as STING Receptor Agonists. *J Med Chem* 2022;65:14082. [https://doi.org/10.1021/ACS.JMEDCHEM.2C01305/SUPPL\\_FILE/JM2C01305\\_SI\\_002.CSV](https://doi.org/10.1021/ACS.JMEDCHEM.2C01305/SUPPL_FILE/JM2C01305_SI_002.CSV).

Verrier ER, Yim SA, Heydmann L, el Saghire H, Bach C, Turon-Lagot V, et al. Hepatitis B Virus Evasion From Cyclic Guanosine Monophosphate–Adenosine Monophosphate Synthase Sensing in Human Hepatocytes. *Hepatology* 2018;68:1695–709. <https://doi.org/10.1002/HEP.30054>.

Vincent J, Adura C, Gao P, Luz A, Lama L, Asano Y, et al. Small molecule inhibition of cGAS reduces interferon expression in primary macrophages from autoimmune mice. *Nature Communications* 2017 8:1 2017;8:1–13. <https://doi.org/10.1038/s41467-017-00833-9>.

Volkman HE, Cambier S, Gray EE, Stetson DB. Tight nuclear tethering of cGAS is essential for preventing autoreactivity. *Elife* 2019;8. <https://doi.org/10.7554/ELIFE.47491>.

Volpi S, Tsui J, Mariani M, Pastorino C, Caorsi R, Sacco O, et al. Type I interferon pathway activation in COPA syndrome. *Clinical Immunology* 2018;187:33–6. <https://doi.org/10.1016/J.CLIM.2017.10.001>.

Vyskocil S, Cardin D, Ciavarri J, Conlon J, Cullis C, England D, et al. Identification of Novel Carbocyclic Pyrimidine Cyclic Dinucleotide STING Agonists for Antitumor Immunotherapy Using Systemic Intravenous Route. *J Med Chem* 2021;64:6902–23.

[https://doi.org/10.1021/ACS.JMEDCHEM.1C00374/SUPPL\\_FILE/JM1C00374\\_SI\\_002.PDB](https://doi.org/10.1021/ACS.JMEDCHEM.1C00374/SUPPL_FILE/JM1C00374_SI_002.PDB).

Walsh D, McCarthy J, O'Driscoll C, Melgar S. Pattern recognition receptors—Molecular orchestrators of inflammation in inflammatory bowel disease. *Cytokine Growth Factor Rev* 2013;24:91–104.

<https://doi.org/10.1016/J.CYTOGFR.2012.09.003>.

Wang C, Liu X, Li Z, Chai Y, Jiang Y, Wang Q, et al. CD8(+)NKT-like cells regulate the immune response by killing antigen-bearing DCs. *Sci Rep* 2015;5.

<https://doi.org/10.1038/SREP14124>.

Wang J, Li R, Lin H, Qiu Q, Lao M, Zeng S, et al. Accumulation of cytosolic dsDNA contributes to fibroblast-like synoviocytes-mediated rheumatoid arthritis synovial inflammation. *Int Immunopharmacol* 2019;76:105791.

<https://doi.org/10.1016/J.INTIMP.2019.105791>.

Wang M, Soorshjani MA, Mikek C, Opoku-Temeng C, Sintim HO. Suramin potently inhibits cGAMP synthase, cGAS, in THP1 cells to modulate IFN- $\beta$  levels. *Future Med Chem* 2018;10:1301–17.

<https://doi.org/10.4155/FMC-2017-0322/ASSET/IMAGES/LARGE/FIGURE8.JPEG>.

Wang Q, Pan W, Liu Y, Luo J, Zhu D, Lu Y, et al. Hepatitis B Virus-Specific CD8<sup>+</sup> T Cells Maintain Functional Exhaustion after Antigen Reexposure in an Acute Activation Immune Environment. *Front Immunol* 2018;9.

<https://doi.org/10.3389/FIMMU.2018.00219>.

Wang Y, Lian Q, Yang B, Yan S, Zhou H, He L, et al. TRIM30 $\alpha$  Is a Negative-Feedback Regulator of the Intracellular DNA and DNA Virus-Triggered Response by Targeting STING. *PLoS Pathog* 2015;11.

<https://doi.org/10.1371/JOURNAL.PPAT.1005012>.

Washburn ML, Bility MT, Zhang L, Kovalev GI, Buntzman A, Frelinger JA, et al. A humanized mouse model to study hepatitis C virus infection, immune response, and liver disease. *Gastroenterology* 2011;140:1334–44.

<https://doi.org/10.1053/J.GASTRO.2011.01.001>.

Watkin LB, Jessen B, Wiszniewski W, Vece TJ, Jan M, Sha Y, et al. COPA mutations impair ER-Golgi transport and cause hereditary autoimmune-mediated lung disease and arthritis. *Nature Genetics* 2015 47:6 2015;47:654–60.

<https://doi.org/10.1038/ng.3279>.

Weber O, Schlemmer K-H, Hartmann E, Hagelschuer I, Paessens A, Graef E, et al. Inhibition of human hepatitis B virus (HBV) by a novel non-nucleosidic compound in a transgenic mouse model. *Antiviral Res* 2002;54:69–78.

[https://doi.org/10.1016/s0166-3542\(01\)00216-9](https://doi.org/10.1016/s0166-3542(01)00216-9).

Wedemeyer H, Schöneweis K, Bogomolov PO, Voronkova N, Chulanov V, Stepanova T, et al. GS-13-Final results of a multicenter, open-label phase 2 clinical trial (MYR203) to assess safety and efficacy of myrcludex B in cwith PEG-interferon Alpha 2a in patients with chronic HBV/HDV co-infection. *J Hepatol* 2019;70:e81. [https://doi.org/10.1016/S0618-8278\(19\)30141-0](https://doi.org/10.1016/S0618-8278(19)30141-0).

West AP, Khoury-Hanold W, Staron M, Tal MC, Pineda CM, Lang SM, et al. Mitochondrial DNA stress primes the antiviral innate immune response. *Nature* 2015 520:7548 2015;520:553–7. <https://doi.org/10.1038/nature14156>.

- White MJ, McArthur K, Metcalf D, Lane RM, Cambier JC, Herold MJ, et al. Apoptotic caspases suppress mtDNA-induced STING-mediated type I IFN production. *Cell* 2014;159:1549–62. <https://doi.org/10.1016/j.cell.2014.11.036>/ATTACHMENT/65854558-F35C-4B38-BDEB-2F95F89BFF01/MMC2.XLSX.
- Wieland SF. The Chimpanzee Model for Hepatitis B Virus Infection. *Cold Spring Harb Perspect Med* 2015;5:a021469–a021469. <https://doi.org/10.1101/cshperspect.a021469>.
- Woo ASJ, Kwok R, Ahmed T. Alpha-interferon treatment in hepatitis B. *Ann Transl Med* 2017;5. <https://doi.org/10.21037/ATM.2017.03.69>.
- Woo SR, Fuertes MB, Corrales L, Spranger S, Furdyna MJ, Leung MYK, et al. STING-dependent cytosolic DNA sensing mediates innate immune recognition of immunogenic tumors. *Immunity* 2014;41:830–42. <https://doi.org/10.1016/j.immuni.2014.10.017>.
- World Health Organization. Global hepatitis report, 2017. 2017. <https://doi.org/ISBN978-92-4-156545-5>.
- Wu J, Huang S, Zhao X, Chen M, Lin Y, Xia Y, et al. Poly(I:C) treatment leads to interferon-dependent clearance of hepatitis B virus in a hydrodynamic injection mouse model. *J Virol* 2014;88:10421–31. <https://doi.org/10.1128/JVI.00996-14>.
- Wu JJ, Zhao L, Hu HG, Li WH, Li YM. Agonists and inhibitors of the STING pathway: Potential agents for immunotherapy. *Med Res Rev* 2020;40:1117–41. <https://doi.org/10.1002/MED.21649>.
- Wu LL, Wang HY, Chen PJ. Hydrodynamic HBV Transfection Mouse Model. *Methods in Molecular Biology* 2017;1540:227–35. [https://doi.org/10.1007/978-1-4939-6700-1\\_19](https://doi.org/10.1007/978-1-4939-6700-1_19).
- Wu Y, Song K, Hao W, Li J, Wang L, Li S. Nuclear soluble cGAS senses double-stranded DNA virus infection. *Communications Biology* 2022 5:1 2022;5:1–13. <https://doi.org/10.1038/s42003-022-03400-1>.
- Xia T, Konno H, Ahn J, Barber GN. Deregulation of STING Signaling in Colorectal Carcinoma Constrains DNA Damage Responses and Correlates With Tumorigenesis. *Cell Rep* 2016a;14:282–97. <https://doi.org/10.1016/j.celrep.2015.12.029>.
- Xia T, Konno H, Barber GN. Recurrent loss of STING signaling in melanoma correlates with susceptibility to viral oncolysis. *Cancer Res* 2016b;76:6747–59. <https://doi.org/10.1158/0008-5472.CAN-16-1404/652459/AM/RECURRENT-LOSS-OF-STING-SIGNALING-IN-MELANOMA>.
- Xiao J, Liu R, Chen C-S. Tree shrew (*Tupaia belangeri*) as a novel laboratory disease animal model. *Zool Res* 2017;38:127–37. <https://doi.org/10.24272/j.issn.2095-8137.2017.033>.
- Xie W, Lama L, Adura C, Tomita D, Glickman JF, Tuschl T, et al. Human cGAS catalytic domain has an additional DNA-binding interface that enhances enzymatic activity and liquid-phase condensation. *Proc Natl Acad Sci U S A* 2019;116:11946–55. [https://doi.org/10.1073/PNAS.1905013116/SUPPL\\_FILE/PNAS.1905013116.SAPP.PDF](https://doi.org/10.1073/PNAS.1905013116/SUPPL_FILE/PNAS.1905013116.SAPP.PDF).



- Yan Z, Zeng J, Yu Y, Xiang K, Hu H, Zhou X, et al. HBVcircle: A novel tool to investigate hepatitis B virus covalently closed circular DNA. *J Hepatol* 2017;66:1149–57. <https://doi.org/10.1016/J.JHEP.2017.02.004>.
- Yang D, Liu L, Zhu D, Peng H, Su L, Fu Y-X, et al. A mouse model for HBV immunotolerance and immunotherapy. *Cell Mol Immunol* 2014;11:71–8. <https://doi.org/10.1038/cmi.2013.43>.
- Yang H, Wang H, Ren U, Chen Q, Chena ZJ. CGAS is essential for cellular senescence. *Proc Natl Acad Sci U S A* 2017;114:E4612–20. [https://doi.org/10.1073/PNAS.1705499114/SUPPL\\_FILE/PNAS.1705499114.SM01.AVI](https://doi.org/10.1073/PNAS.1705499114/SUPPL_FILE/PNAS.1705499114.SM01.AVI).
- Yang PL, Althage A, Chung J, Chisari F v. Hydrodynamic injection of viral DNA: a mouse model of acute hepatitis B virus infection. *Proc Natl Acad Sci U S A* 2002;99:13825–30. <https://doi.org/10.1073/pnas.202398599>.
- Yang PL, Althage A, Chung J, Maier H, Wieland S, Isogawa M, et al. Immune effectors required for hepatitis B virus clearance. *Proc Natl Acad Sci U S A* 2010;107:798–802. <https://doi.org/10.1073/PNAS.0913498107>.
- Yasutomo K, Horiuchi T, Kagami S, Tsukamoto H, Hashimura C, Urushihara M, et al. Mutation of DNASE1 in people with systemic lupus erythematosus. *Nature Genetics* 2001 28:4 2001;28:313–4. <https://doi.org/10.1038/91070>.
- Yi G, Brendel VP, Shu C, Li P, Palanathan S, Cheng Kao C. Single nucleotide polymorphisms of human STING can affect innate immune response to cyclic dinucleotides. *PLoS One* 2013;8:e77846. <https://doi.org/10.1371/journal.pone.0077846>.
- Yi M, Niu M, Wu Y, Ge H, Jiao D, Zhu S, et al. Combination of oral STING agonist MSA-2 and anti-TGF- $\beta$ /PD-L1 bispecific antibody YM101: a novel immune cocktail therapy for non-inflamed tumors. *J Hematol Oncol* 2022;15:142. <https://doi.org/10.1186/S13045-022-01363-8/FIGURES/8>.
- Yin Q, Tian Y, Kabaleeswaran V, Jiang X, Tu D, Eck MJ, et al. Cyclic di-GMP Sensing via the Innate Immune Signaling Protein STING. *Mol Cell* 2012;46:735–45. <https://doi.org/10.1016/j.molcel.2012.05.029>.
- Yuen M-F, Agarwal K, Ma X, Nguyen T, Schiff ER, Hann H-W, et al. Antiviral activity and safety of the hepatitis B core inhibitor ABI-H0731 administered with a nucleos(t)ide reverse transcriptase inhibitor in patients with HBeAg-positive chronic hepatitis B infection in a long-term extension study. *J Hepatol* 2020;73:S140. [https://doi.org/10.1016/S0168-8278\(20\)30790-X](https://doi.org/10.1016/S0168-8278(20)30790-X).
- Zaidi AH, Kelly RJ, Gorbunova A, Omstead AN, Salvitti MS, Zheng P, et al. Intratumoral immunotherapy with STING agonist, ADU-S100, induces CD8<sup>+</sup> T-cell mediated anti-tumor immunity in an esophageal adenocarcinoma model. *Oncotarget* 2021;12:292. <https://doi.org/10.18632/ONCOTARGET.27886>.
- Zhang K, Wang S, Gou H, Zhang J, Li C. Crosstalk Between Autophagy and the cGAS–STING Signaling Pathway in Type I Interferon Production. *Front Cell Dev Biol* 2021;9. <https://doi.org/10.3389/FCELL.2021.748485>.
- Zhang L, Mo J, Swanson K v., Wen H, Petrucelli A, Gregory SM, et al. NLRC3, a member of the NLR family of proteins, is a negative regulator of innate immune

- signaling induced by the DNA sensor STING. *Immunity* 2014;40:329–41.  
<https://doi.org/10.1016/J.IMMUNI.2014.01.010>.
- Zhang X, Shi H, Wu J, Zhang X, Sun L, Chen C, et al. Cyclic GMP-AMP containing mixed Phosphodiester linkages is an endogenous high-affinity ligand for STING. *Mol Cell* 2013;51:226–35. <https://doi.org/10.1016/j.molcel.2013.05.022>.
- Zhang X, Wu J, Du F, Xu H, Sun L, Chen Z, et al. The Cytosolic DNA Sensor cGAS Forms An Oligomeric Complex with DNA and Undergoes Switch-like Conformational Changes in the Activation Loop. *Cell Rep* 2014;6:421.  
<https://doi.org/10.1016/J.CELREP.2014.01.003>.
- Zhao B, Du F, Xu P, Shu C, Sankaran B, Bell SL, et al. A conserved PLPLRT/SD motif of STING mediates the recruitment and activation of TBK1. *Nature* 2019 569:7758 2019;569:718–22. <https://doi.org/10.1038/s41586-019-1228-x>.
- Zhao B, Shu C, Gao X, Sankaran B, Du F, Shelton CL, et al. Structural basis for concerted recruitment and activation of IRF-3 by innate immune adaptor proteins. *Proc Natl Acad Sci U S A* 2016;113:E3403–12.  
[https://doi.org/10.1073/PNAS.1603269113/SUPPL\\_FILE/PNAS.201603269SI.PDF](https://doi.org/10.1073/PNAS.1603269113/SUPPL_FILE/PNAS.201603269SI.PDF).
- Zhao W, Xiong M, Yuan X, Li M, Sun H, Xu Y. In Silico Screening-Based Discovery of Novel Inhibitors of Human Cyclic GMP-AMP Synthase: A Cross-Validation Study of Molecular Docking and Experimental Testing. *J Chem Inf Model* 2020;60:3265–76.  
[https://doi.org/10.1021/ACS.JCIM.0C00171/SUPPL\\_FILE/CI0C00171\\_SI\\_001.PDF](https://doi.org/10.1021/ACS.JCIM.0C00171/SUPPL_FILE/CI0C00171_SI_001.PDF)
- .
- Zheng M, Tian Z. Liver-Mediated Adaptive Immune Tolerance. *Front Immunol* 2019;10. <https://doi.org/10.3389/FIMMU.2019.02525>.
- Zhong B, Yang Y, Li S, Wang YY, Li Y, Diao F, et al. The adaptor protein MITA links virus-sensing receptors to IRF3 transcription factor activation. *Immunity* 2008;29:538–50. <https://doi.org/10.1016/J.IMMUNI.2008.09.003>.
- Zhong B, Zhang L, Lei C, Li Y, Mao AP, Yang Y, et al. The ubiquitin ligase RNF5 regulates antiviral responses by mediating degradation of the adaptor protein MITA. *Immunity* 2009;30:397–407. <https://doi.org/10.1016/J.IMMUNI.2009.01.008>.
- Zhong L, Hu MM, Bian LJ, Liu Y, Chen Q, Shu HB. Phosphorylation of cGAS by CDK1 impairs self-DNA sensing in mitosis. *Cell Disco* 2020;6:26.  
<https://doi.org/10.1038/s41421-020-0162-2>.
- Zhou Q, Lin H, Wang S, Wang S, Ran Y, Liu Y, et al. The ER-associated protein ZDHHC1 is a positive regulator of DNA virus-triggered, MITA/STING-dependent innate immune signaling. *Cell Host Microbe* 2014;16:450–61.  
<https://doi.org/10.1016/J.CHOM.2014.09.006>.
- Zhou T, Guo H, Guo JT, Cuconati A, Mehta A, Block TM. Hepatitis B virus e antigen production is dependent upon covalently closed circular (ccc) DNA in HepAD38 cell cultures and may serve as a cccDNA surrogate in antiviral screening assays. *Antiviral Res* 2006;72:116–24.  
<https://doi.org/10.1016/J.ANTIVIRAL.2006.05.006>.
- Zhu D, Liu L, Yang D, Fu S, Bian Y, Sun Z, et al. Clearing Persistent Extracellular Antigen of Hepatitis B Virus: An Immunomodulatory Strategy To Reverse Tolerance

for an Effective Therapeutic Vaccination. *J Immunol* 2016;196:3079–87. <https://doi.org/10.4049/JIMMUNOL.1502061>.

Zhu Q, Man SM, Karki R, Malireddi RKS, Kanneganti TD. Detrimental Type I Interferon Signaling Dominates Protective AIM2 Inflammasome Responses during *Francisella novicida* Infection. *Cell Rep* 2018;22:3168–74. <https://doi.org/10.1016/J.CELREP.2018.02.096/ATTACHMENT/D586F606-6A7C-48D6-8BD5-8A9372B7E232/MMC1.PDF>.

Zimmer J, Tacconi EMC, Folio C, Badie S, Porru M, Klare K, et al. Targeting BRCA1 and BRCA2 Deficiencies with G-Quadruplex-Interacting Compounds. *Mol Cell* 2016;61:449–60. <https://doi.org/10.1016/J.MOLCEL.2015.12.004>.

## 8. SUPPLEMENTS

### 8.1. Supplement S1: Enzymatic Preparation of 2'-5', 3'-5'-Cyclic Dinucleotides, Their Binding Properties to Stimulator of Interferon Genes Adaptor Protein, and Structure/Activity Correlations

Novotná, B., **Vaneková, L.**, Zavřel, M., Buděšínský, M., Dejmek, M., Smola, M., Gutten, O., Tehrani, Z. A., Pimková Polidarová, M., Brázdová, A., Liboska, R., Štěpánek, I., Vavřina, Z., Jandušík, T., Nencka, R., Rulišek, L., Bouřa, E., Brynda, J., Páv, O., & Birkuš, G. (2019). Enzymatic Preparation of 2'-5',3'-5'-Cyclic Dinucleotides, Their Binding Properties to Stimulator of Interferon Genes Adaptor Protein, and Structure/Activity Correlations. *Journal of medicinal chemistry*, 62(23), 10676–10690. <https://doi.org/10.1021/acs.jmedchem.9b01062>

My contribution:

Development and establishment of 293T reporter cell lines stably expressing five most abundant STING haplotypes (*WT*, *HAQ*, *REF*, *AQ*, *Q*), and optimization of screening methods using these cell lines (permeant one for direct STING activation using digitonin and standard one with an active uptake of compound). Development of differential scanning fluorimetry (DSF) method using *WT* STING protein and participation in manuscript preparation.

## Enzymatic Preparation of 2′–5′,3′–5′-Cyclic Dinucleotides, Their Binding Properties to Stimulator of Interferon Genes Adaptor Protein, and Structure/Activity Correlations

Barbora Novotná,<sup>†,‡</sup> Lenka Vaneková,<sup>†,‡</sup> Martin Zavřel,<sup>†</sup> Miloš Buděšínský,<sup>†</sup> Milan Dejmek,<sup>†</sup> Miroslav Smola,<sup>†</sup> Ondřej Gutten,<sup>†</sup> Zahra Aliakbar Tehrani,<sup>†</sup> Markéta Pimková Polidarová,<sup>†,‡</sup> Andrea Brázdová,<sup>†</sup> Radek Liboska,<sup>†</sup> Ivan Štěpánek,<sup>†</sup> Zdeněk Vavřina,<sup>†,‡</sup> Tomáš Jandušík,<sup>‡,§</sup> Radim Nencka,<sup>†</sup> Lubomír Rulišek,<sup>†</sup> Evžen Bouřa,<sup>†</sup> Jiří Brynda,<sup>†</sup> Ondřej Páv,<sup>†</sup> and Gabriel Birkuš<sup>\*,†,‡</sup>

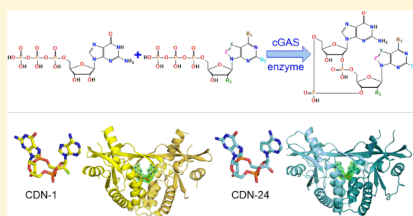
<sup>†</sup>Institute of Organic Chemistry and Biochemistry of the Czech Academy of Sciences and Gilead Sciences Research Centre at IOCB, Flemingovo nám. 2, Prague 16610, Czech Republic

<sup>‡</sup>Faculty of Science, Charles University, Prague 110 00, Czech Republic

<sup>§</sup>Faculty of Food and Biochemical Technology, University of Chemistry and Technology, Prague 166 28, Czech Republic

### Supporting Information

**ABSTRACT:** Cyclic dinucleotides are second messengers in the cyclic GMP–AMP synthase (cGAS)–stimulator of interferon genes (STING) pathway, which plays an important role in recognizing tumor cells and viral or bacterial infections. They bind to the STING adaptor protein and trigger expression of cytokines via TANK binding kinase 1 (TBK1)/interferon regulatory factor 3 (IRF3) and inhibitor of nuclear factor- $\kappa$ B (I $\kappa$ B) kinase (IKK)/nuclear factor- $\kappa$ B (NF $\kappa$ B) signaling cascades. In this work, we describe an enzymatic preparation of 2′–5′,3′–5′-cyclic dinucleotides (2′3′CDNs) with use of cyclic GMP–AMP synthases (cGAS) from human, mouse, and chicken. We profile substrate specificity of these enzymes by employing a small library of nucleotide-5′-triphosphate (NTP) analogues and use them to prepare 33 2′3′CDNs. We also determine affinity of these CDNs to five different STING haplotypes in cell-based and biochemical assays and describe properties needed for their optimal activity toward all STING haplotypes. Next, we study their effect on cytokine and chemokine induction by human peripheral blood mononuclear cells (PBMCs) and evaluate their cytotoxic effect on monocytes. Additionally, we report X-ray crystal structures of two new CDNs bound to STING protein and discuss structure–activity relationship by using quantum and molecular mechanical (QM/MM) computational modeling.



### INTRODUCTION

Cyclic dinucleotides (CDNs) play an important role as second messengers in vertebrates and prokaryotes.<sup>1–3</sup> They are naturally synthesized from NTPs by cyclic dinucleotide synthases. Prokaryotic and vertebrate CDNs differ in the type of phosphodiester linkages connecting two nucleotide monophosphates together. While bacteria produce 3′3′CDNs (e.g., 3′3′c-diGMP, 3′3′c-diAMP, 3′3′cGAMP) with two 3′–5′ phosphodiester bonds,<sup>4–6</sup> only one CDN with mixed 2′–5′ and 3′–5′ phosphodiester linkage (2′3′cGAMP) is found in mammalian cells.<sup>7</sup>

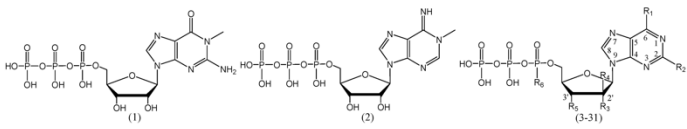
2′3′cGAMP is a product of cyclic-GMP–AMP (cGAMP) synthase, which is evolutionarily conserved from fish to human.<sup>2,8,9</sup> The enzyme belongs to a family of DNA sensors and detects dsDNA released into cytosol during pathogen infection or disruption of host homeostasis.<sup>10</sup> Binding of dsDNA to cGAS occurs in a sequence-independent manner and induces a conformational change ultimately allowing

synthesis of 2′3′cGAMP from ATP and GTP.<sup>11</sup> The 2′3′ and 3′3′CDNs bind to an adaptor protein called stimulator of interferon genes (STING, also denoted as TMEM173, MITA, or ERI5) residing in endoplasmic reticulum.<sup>12</sup> STING is a 379 amino acid long protein consisting of an N-terminal transmembrane domain, a C-terminal ligand-binding domain, and a C-terminal tail (CTT).<sup>11,13</sup> Upon CDN binding, STING homodimer transforms from an open to closed conformation and forms oligomers.<sup>8</sup> This conformational change leads to the recruitment of TBK1 kinase, transphosphorylation of the CTT of STING, and subsequent recruitment and phosphorylation of the transcription factor IRF3.<sup>14–17</sup> IRF3 then forms homodimers that translocate to the nucleus where they trigger expression of type I and III interferons. In parallel, a crosstalk

Received: July 2, 2019

Published: November 12, 2019

Table 1. Substrate Specificity of Human, Mouse, and Chicken cGAS toward NTP Analogues 1–31



NTP	R <sub>1</sub>	R <sub>2</sub>	R <sub>3</sub>	R <sub>4</sub>	R <sub>5</sub>	R <sub>6</sub>	reaction conversion <sup>a</sup> (%)					
							GTP			ATP		
							hcGAS	mcGAS	ccGAS	hcGAS	mcGAS	ccGAS
1							<i>b</i>	<i>b</i>	<i>b</i>	29	45	18
2							6	5	0	<i>b</i>	<i>b</i>	<i>b</i>
3	NH <sub>2</sub>	NH <sub>2</sub>	OH	H	OH	OH	90	54	47	0	31	0
4	NH <sub>2</sub>	OH	OH	H	OH	OH	74	50	36	0	52	0
5	NH <sub>2</sub>	F	H	OH	OH	OH	22	60	0	<i>b</i>	<i>b</i>	<i>b</i>
6	NH <sub>2</sub>	Cl	H	H	OH	OH	0	29	0	<i>b</i>	<i>b</i>	<i>b</i>
7	SH	H	OH	H	OH	OH	78	73	19	<i>b</i>	<i>b</i>	<i>b</i>
8	Cl	H	H	H	OH	OH	0	0	0	<i>b</i>	<i>b</i>	<i>b</i>
9	NHCH <sub>3</sub>	H	OH	H	OH	OH	67	91	9	<i>b</i>	<i>b</i>	<i>b</i>
10	SCH <sub>3</sub>	H	OH	H	OH	OH	100	95	67	<i>b</i>	<i>b</i>	<i>b</i>
11	H	NH <sub>2</sub>	OH	H	OH	OH	90	82	48	6	6	0
12	SH	NH <sub>2</sub>	OH	H	OH	OH	<i>b</i>	<i>b</i>	<i>b</i>	0	0	0
13	Cl	NH <sub>2</sub>	OH	H	OH	OH	91	100	71	0	5	0
14	OH	OH	OH	H	OH	OH	0	26	0	66	78	0
15	OH	H	OH	H	OH	OH	0	0	0	2	6	0
16	OCH <sub>3</sub>	NH <sub>2</sub>	OH	H	OH	OH	<i>b</i>	<i>b</i>	<i>b</i>	50	1	13
17	SCH <sub>3</sub>	NH <sub>2</sub>	OH	H	OH	OH	70	67	34	0	0	23
18	NH <sub>2</sub>	H	H	OH	OH	OH	25	51	14	<i>b</i>	<i>b</i>	<i>b</i>
19	NH <sub>2</sub>	H	H	F	OH	OH	0	0	0	<i>b</i>	<i>b</i>	<i>b</i>
20	NH <sub>2</sub>	H	H	H	OH	OH	0	57	0	<i>b</i>	<i>b</i>	<i>b</i>
21	NH <sub>2</sub>	H	NH <sub>2</sub>	H	OH	OH	9	20	0	<i>b</i>	<i>b</i>	<i>b</i>
22	NH <sub>2</sub>	H	F	H	OH	OH	0	38	0	<i>b</i>	<i>b</i>	<i>b</i>
23	NH <sub>2</sub>	F	F	H	OH	OH	12	47	0	<i>b</i>	<i>b</i>	<i>b</i>
24	NH <sub>2</sub>	H	Cl	H	OH	OH	0	0	0	<i>b</i>	<i>b</i>	<i>b</i>
25	NH <sub>2</sub>	H	Br	H	OH	OH	0	0	0	<i>b</i>	<i>b</i>	<i>b</i>
26	NH <sub>2</sub>	H	I	H	OH	OH	0	0	0	<i>b</i>	<i>b</i>	<i>b</i>
27	NH <sub>2</sub>	H	OH	H	OCH <sub>3</sub>	OH	0	0	0	<i>b</i>	<i>b</i>	<i>b</i>
28	OH	NH <sub>2</sub>	OH	H	H	OH	<i>b</i>	<i>b</i>	<i>b</i>	0	17	0
29	OH	NH <sub>2</sub>	OH	H	F	OH	<i>b</i>	<i>b</i>	<i>b</i>	3	72	34
30	OH	NH <sub>2</sub>	OH	H	OH	SH	0	0	0	28	48	45
31	NH <sub>2</sub>	H	OH	H	OH	SH	0	52	0	<i>b</i>	<i>b</i>	<i>b</i>

<sup>a</sup>ATP or GTP (1 mM) was reacted with 1 mM NTP analogue in the presence of 5  $\mu$ M human, mouse, or chicken full-length cGAS for 16 h at 37 °C in 20  $\mu$ L volume. Reaction conversions were determined by HPLC using UV detection at 260 nm. Conversions are defined as follows: a ratio of AUC of a CDN over the sum of AUCs of the CDN, NTPs, and NDPs. <sup>b</sup>Not determined.

between TBK1 and IKK $\beta$  kinases leads to NF $\kappa$ B activation and TNF $\alpha$  and IL-6 expression.<sup>18</sup>

The cGAS–STING pathway plays an essential role in host defense against invading pathogens and in immune surveillance of tumor cells.<sup>12,19</sup> Its importance from the perspective of drug discovery is highlighted by the fact that two cyclic dinucleotides, ADU-S100 and MK-1454, are currently undergoing evaluation in phase I clinical trials for the treatment of cancer.<sup>20,21</sup> Moreover CDNs could also find utility in the treatment of viral infections such as chronic hepatitis B or human immunodeficiency virus (HIV) infection or as adjuvants in vaccines.<sup>22,23</sup>

Several synthetic routes for 2'3'- and 3'3'-CDN preparations have been established.<sup>24–26</sup> However, these are usually complex multistep syntheses. Meanwhile, an elegant idea of using dinucleotide synthases for CDN preparation was

pursued, and a few 3'3'- and 2'3'-CDNs were thus enzymatically prepared from the commercially available ATP and GTP analogues.<sup>7,27–30</sup>

The objective of this study is to identify the most suitable enzyme for synthesis of 2'3'-CDNs, characterize binding properties of prepared CDNs toward STING adaptor protein, and determine structure–activity relations between STING and CDNs. To achieve this goal, we profile substrate specificity of chicken, mouse, and human cGAS using a library of 41 NTP analogues and describe preparation of 33 2'3'-CDNs. We characterize affinity of prepared CDNs toward five STING haplotypes in cell-based and biochemical assays. We also study their effect on induction of cytokines and chemokines by employing human peripheral blood mononuclear cells (PBMCs) and evaluate their cytotoxic effect specifically on monocytes. Finally, we also discuss a structure–activity

Table 2. Substrate Specificity of Human, Mouse, and Chicken cGAS toward NTP Analogues 32–41

NTP	R <sub>1</sub>	R <sub>2</sub>	X	Y	Z	reaction conversion <sup>a</sup> (%)					
						GTP			ATP		
						hcGAS	mcGAS	ccGAS	hcGAS	mcGAS	ccGAS
32	NH <sub>2</sub>	H	CH	CH	N	94	96	83	<i>b</i>	<i>b</i>	<i>b</i>
33	OH	NH <sub>2</sub>	CH	CH	N	<i>b</i>	<i>b</i>	<i>b</i>	<i>b</i>	<i>b</i>	<i>b</i>
34	OH	NH <sub>2</sub>	N-CH <sub>3</sub>	CH	N	<i>b</i>	<i>b</i>	<i>b</i>	0	0	0
35	NH <sub>2</sub>	H	N	N	N	29	58	24	<i>b</i>	<i>b</i>	<i>b</i>
36	NH <sub>2</sub>	H	N	C-N <sub>3</sub>	N	0	0	0	<i>b</i>	<i>b</i>	<i>b</i>
37	NH <sub>2</sub>	H	N	C-OH	N	37	0	0	<i>b</i>	<i>b</i>	<i>b</i>
38	OH	NH <sub>2</sub>	N	C-OH	N	<i>b</i>	<i>b</i>	<i>b</i>	0	0	0
39	OH	NH <sub>2</sub>	C	CH	C	<i>b</i>	<i>b</i>	<i>b</i>	24	62	41
40						16	45	23	<i>b</i>	<i>b</i>	<i>b</i>
41						24	51	31	0	33	0

<sup>a</sup>ATP or GTP (1 mM) was reacted with 1 mM NTP analogue in the presence of 5 μM human, mouse, or chicken full-length cGAS for 16 h at 37 °C in 20 μL volume. Reaction conversions were determined by HPLC using UV detection at 260 nm. Conversions are defined as follows: a ratio of AUC of a CDN over the sum of AUCs of the CDN, NTPs, and NDPs. <sup>b</sup>Not determined.

relationship (SAR) between prepared molecules and their biological activity by employing state-of-the-art methods of computational chemistry, such as QM/MM calculations.

## RESULTS

**Substrate Specificity of Human, Mouse, and Chicken cGAS.** Binding of DNA to cGAS triggers rearrangement of its active site and catalysis of 2'-5' phosphodiester bond formation between the 2'-OH of GTP and the α-phosphate of ATP.<sup>11,29</sup> The formed intermediate AMP-2'-GTP flips in the active site of the enzyme, and a 3'-5' phosphodiester bond between the 3'-OH group of AMP and the α-phosphate of GTP is formed.<sup>11,29</sup> Despite being responsible for the synthesis of the same product, cGAS from different species have relatively low amino acid homology. For example, human and mouse or human and chicken cGAS share 56% and 51% amino acid identity, respectively, based on BLAST alignment<sup>31</sup> of amino acid sequences Q8C6L5, Q8N884 (UNIPROT), and XP\_419881.4 (NCBI). Because of low homology of cGAS enzymes from these three species, we decided to express them and profile their substrate specificity with a goal to identify the most suitable enzyme for synthesis of CDNs. We performed a small-scale synthesis of CDNs in such a way that one of the NTPs was always either ATP or GTP and the other was an NTP analogue 1–41 (Tables 1 and 2).

For the arbitrarily chosen cutoff of >25% reaction conversion, 28 CDNs could be prepared using mouse cGAS (mcGAS) compared to 16 and 11 CDNs that could be made with human (hcGAS) and chicken (ccGAS) cGAS, respectively (Tables 1 and 2). Thus, mouse cGAS shows the lowest substrate specificity and is the most suited for enzymatic synthesis of CDNs. Nevertheless, human and chicken cGAS should not be disregarded. For example, human cGAS more efficiently catalyzed the reaction of GTP with 2-amino-adenosine-5'-triphosphate (3) or isoguanosine-5'-triphosphate (4), and the conversion of ATP with O<sup>6</sup>-methylguanosine-5'-

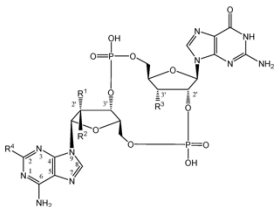
triphosphate (16) to the appropriate CDN was only possible with human cGAS (Table 1).

As shown in Table 1, N<sup>1</sup>-methylguanosine-5'-triphosphate (1) was a mcGAS substrate but N<sup>1</sup>-methyladenosine-5'-triphosphate (2) was not. Nucleotide triphosphates with 2-amino (3), 2-hydroxy (4), 2-fluoro (5 and 23), and 2-chloro (6) substitutions of adenosine were tolerated by mcGAS as well as NTPs with 6-mercaptapurine (7), 6-N-methyladenine (9), and 6-methylthiopurine (10) nucleobases; however, 2'-deoxy-6-chloropurine-5'-triphosphate (8) was not a mcGAS substrate. NTPs with 2-aminopurine (11), 6-thioguanine (12), 2-amino-6-chloropurine (13), xanthine (14), hypoxanthine (15), and 2-amino-6-methylthiopurine (17) nucleobases were good mcGAS substrates. As mentioned above mcGAS did not tolerate O<sup>6</sup>-methyl-guanosine-5'-triphosphate (16).

It was also possible to prepare CDNs by employing 7-deazaadenosine-5'-triphosphate (32) and 7-deazaguanosine-5'-triphosphate (33), but not by the use of N<sup>7</sup>-methylguanosine-5'-triphosphate (34) (Table 2). 8-Azaadenosine-5'-triphosphate (35) was a substrate for mcGAS, but 8-azido-adenosine-5'-triphosphate (36), 8-oxo-adenosine-5'-triphosphate (37), and 8-oxo-guanosine-5'-triphosphate (38) were not. Interestingly, mcGAS could also catalyze synthesis of CDNs from thienoguanosine-5'-triphosphate (39), ribavirin 5'-triphosphate (40), and 5-aminoimidazole-4-carboxamide-1-β-D-ribofuranosyl-5'-triphosphate (AICAR-5'-triphosphate) (41).

Ara-adenosine-5'-triphosphate (18), 2'-deoxy-adenosine-5'-triphosphate (20), and 2'-amino-2'-deoxy- (21) and 2'-fluoro-2'-deoxy-adenosine-5'-triphosphates (22) were also good mcGAS substrates; however, 2'-fluoro-2'-deoxy-ara-adenosine-5'-triphosphate (19) and 2'-chloro- (24), 2'-bromo- (25), and 2'-iodo-2'-deoxyadenosine-5'-triphosphates (26) were not accepted. Similarly, 3'-deoxy- (28) and 3'-fluoro-3'-deoxy-guanosine-5'-triphosphate (29) were mcGAS substrates

Table 3. Activity of 2'-OH and 3'-OH Substituted 2'3'CDNs in Biochemical and Cell-Based Assays



compd	R <sub>1</sub>	R <sub>2</sub>	R <sub>3</sub>	R <sub>4</sub>	DSF $\Delta T_m$ <sup>a</sup> (°C)		std assay EC <sub>50</sub> (μM) <sup>b</sup>		digitonin assay EC <sub>50</sub> (μM) <sup>c</sup>			
					WT	WT	WT	HAQ	REF	AQ	Q	
CDN-1	F	H	OH	H	20.5	13.8	0.01	0.01	0.01	0.03	0.02	0.02
CDN-2	F	H	F	H	20.3	13.3	0.02	0.05	0.02	0.09	0.01	0.20
CDN-3	OH	H	F	H	16.2	16.7	0.02	0.02	0.07	0.01	0.04	0.04
CDN-4	F	H	H	H	17.4	10.7	0.02	0.05	0.04	0.04	0.18	0.18
CDN-5	H	H	F	H	16.6	15.1	0.01	0.04	0.07	0.02	0.06	0.06
CDN-6	H	H	F	F	10.7	>300	0.05	0.10	2.00	0.17	0.70	0.70
CDN-7	F	H	OH	F	14.7	11.0	0.02	0.08	0.07	0.03	0.08	0.08
CDN-8	F	H	OH	NH <sub>2</sub>	14.4	27.6	0.02	0.04	0.17	0.03	0.13	0.13
CDN-9	NH <sub>2</sub>	H	OH	H	9.4	107.5	0.02	0.03	1.40	0.02	0.24	0.24
CDN-10	H	OH	OH	H	17.0	<i>d</i>	0.04	0.08	0.40	0.04	0.09	0.09
CDN-11	H	OH	OH	F	12.3	186.8	0.20	0.1	6.40	0.06	0.60	0.60
CDN-12	H	H	OH	H	15.8	31.9	0.02	0.06	0.14	0.03	0.34	0.34
CDN-13	H	H	H	H	13.5	75.4	0.06	0.03	3.30	0.03	0.04	0.04
CDN-14	OH	H	H	H	13.2	21.6	0.01	0.03	0.40	0.03	0.12	0.12
CDN-15	H	H	OH	Cl	9.5	58.2	0.07	0.08	4.70	0.09	0.96	0.96
2'3'-cGAMP					15.3	13.7	0.02	0.02	0.07	0.04	0.05	0.05
2'2'-cGAMP					11.6	39.2	0.03	0.02	0.21	0.03	0.17	0.17
3'3'-cGAMP					5.1	70.1	0.12	0.12	4.30	0.26	2.06	2.06
3'3'-c-diAMP					2.5	14.9	0.3	0.2	>45	0.2	7.1	7.1
3'3'-c-diGMP					2.4	184.2	4.5	0.9	8.40	1.1	>45	>45

<sup>a</sup>Results of differential scanning fluorimetry assay performed with WT STING haplotype.  $\Delta T_m$  values are the mean of two independent double determinations. <sup>b</sup>Results of standard assay in 293T reporter cells expressing WT STING haplotype. EC<sub>50</sub> values are the mean of two independent experiments measured in triplicate with standard deviations <50% of EC<sub>50</sub> values. <sup>c</sup>Results of digitonin assay in 293T reporter cells expressing different STING haplotypes. EC<sub>50</sub> values are the mean of two independent experiments measured in triplicate with standard deviations <50% of EC<sub>50</sub> values. <sup>d</sup>Not determined.

as were guanosine-5'-O-(1-thiotriphosphate) (30) and adenosine-5'-O-(1-thiotriphosphate) (31) (Table 1).

**Large Scale Synthesis of CDNs and Profiling of Their Activity.** Next, we initiated a larger scale synthesis of CDNs from NTP analogues. We attempted to prepare about 2 μmol of CDNs, which was a sufficient amount for their downstream biological and physicochemical characterization. Some of the CDNs from nucleotide-5'-triphosphates listed in Tables 1 and 2 could not be prepared in sufficient purity since nucleotide-5'-diphosphates or linear intermediates often coeluted with CDNs. In the end, we prepared 33 CDNs enzymatically, and in order to get more complete SAR, we also prepared four CDNs (CDN-29 and -35–37) through chemical synthesis (Tables 3, 4, 5, and 7; for more details on synthesis of CDN-29 and -35–37, see Supporting Information).

To profile the activity of CDNs, we employed cell based reporter assays. These assays are based on CDN/STING dependent expression of firefly luciferase from a reporter plasmid with four ISRE sites placed upstream of the firefly luciferase reporter gene minimum promoter. The luciferase expression is induced by IRF3 transcription factor as a result of STING signaling cascade activation.<sup>32</sup> We have developed the

reporter assays for five STING haplotypes that are present in humans<sup>33</sup> and run them in two assay formats. In the digitonin assay, we performed permeabilization of cellular membranes with a detergent (digitonin A). As a consequence, the uptake of negatively charged CDNs into cells was not the limiting step in STING activation. In the standard assay, the detergent was absent, and the activity of CDNs was therefore influenced by efficiency of their cellular uptake. Finally, our biochemical assay (differential scanning fluorimetry, DSF) determined the difference between melting temperature of STING protein with and without ligand ( $\Delta T_m$ ) and was an indirect measure of CDN binding affinity to STING protein.  $\Delta T_m$  values from the DSF assay correlated better with log EC<sub>50</sub> values from digitonin (Pearson  $r = -0.73$ ,  $P$  (two-tailed) < 0.0001) than with log EC<sub>50</sub> values from standard assay (Pearson  $r = -0.56$ ,  $P$  (two-tailed) 0.001) (SI Figure S1). EC<sub>50</sub> values were calculated from dose–response curves of individual CDN treated cells in digitonin or standard assay. Representative dose–response curves are shown in Figure S2. To compare results of presented cell-based and biochemical assays for all prepared CDNs, see Tables 3, 4, 5, and 7.



**Structure and Conformation of CDNs in Water Solution.** All prepared CDNs (CDN 1–37) were characterized by  $^1\text{H}$ ,  $^{31}\text{P}$ , and  $^{19}\text{F}$  NMR spectra and high-resolution MS. The NMR data are summarized in Tables S1a, S1b, S2, S3, S4, and S5.  $^{31}\text{P}$  chemical shifts clearly distinguished the presence of thiophosphate group ( $\delta$  52–57 ppm in CDNs 33–37) from phosphate group ( $\delta$  +1.5 to –1.5 ppm in all other CDNs 1–32).  $^{19}\text{F}$  signals in the range  $\delta$  –196 to –200 ppm proved fluorine substituent on the furanose ring (CDNs 1–8), while signal around  $\delta$  –50 showed CDNs with fluorine substituent in position 2 of the nucleobase (CDNs 6 and 7). Basic conformation features of CDNs can be derived from vicinal coupling constants and observed homonuclear NOEs. Furanose rings of CDNs with ribose sugar units and a 2'-phosphate group adopted *C2'-endo* conformation (characterized by large  $J(1',2') = 7$ –9 Hz and small  $J(3',4') = 0$ –1.5 Hz), while rings with 3'-phosphate group preferred *C3'-endo* conformation (manifested by very small  $J(1',2') = 0$ –1.5 Hz and large  $J(3',4') = 7$ –9 Hz). Orientation of the nucleobase was found to be *anti*- throughout the whole series of our CDNs as indicated by characteristics observed from NOE contacts: between H-8 and protons H-1' and H-2' in 2'-phosphate units and between H-8 and protons H-1', H-2', and H-3' in 3'-phosphate units. The structure modifications of the nucleobase had only a very small effect on the conformation of furanose ring. For conformation analysis of phosphate and thiophosphate linkages of CDNs, there was not a complete set of proper NMR parameters accessible. While torsion angles  $\beta$  and  $\epsilon$  were still related to vicinal heteronuclear couplings  $J(\text{P,H})$  observable in  $^1\text{H}$  NMR spectra and  $J(\text{P,C})$  obtainable from  $^{13}\text{C}$  NMR spectra, for torsion angles  $\alpha$  and  $\zeta$ , such usable couplings were missing.

**2'- and 3'-Substituted 2'3'CDNs.** We were able to prepare 15 2'3'CDNs with substitutions at 2'-position of adenosine or 3'-position of guanosine monophosphate units (Table 3). Compared to the parent 2'3'cGAMP, all but one CDN (CDN-11) had less than 5-fold shift in  $\text{EC}_{50}$  values in the digitonin reporter assay using cells expressing WT, HAQ, and AQ STING haplotypes (Table 3). The important difference appeared in the case of REF STING haplotype that is present in about 13% of humans.<sup>33,34</sup> 2'3'CDNs with 2'-amino-2'-deoxyadenosine (CDN-9), ara-adenosine (CDN-10), and some with deoxyribonucleotides (CDN-13, -14) were at least 10-fold less active against REF than WT STING haplotype (Table 3). Similarly, fluoro (CDN-6, CDN-11) or chloro (CDN-15) substitutions at  $\text{C}_2$  position of adenine resulted in decreased activity against the REF STING.

Despite log  $\text{EC}_{50}$  values from digitonin and  $\Delta T_m$  values from DSF assay correlating well (Figure S1), clear outliers could be found (e.g., CDN-1 and -2 vs 2'3'cGAMP). This is probably due to differences in efflux or intra- or extracellular stability of these CDNs that are captured in digitonin cell-based assay but not in DSF assay.

We also determined activities of the prepared CDNs in the standard assay using WT STING 293T reporter cells (Tables 3, 4, 5, and 7). Due to the dramatic effect of the cellular uptake on the activity of CDNs,  $\text{EC}_{50}$  values for all prepared CDNs were more than 100-fold higher compared to  $\text{EC}_{50}$  values from the digitonin assay (Tables 3, 4, 5, and 7).

Throughout the study, we attempted to explain all experimentally observed binding affinities of CDNs with STING by employing crystallography and computational modeling. For relative comparison of binding affinity of

CDNs to STING, we used  $\Delta T_m$  values from our biochemical DSF assay. In order to highlight changes brought about by individual modifications of a ligand, we discuss  $\Delta\Delta T_m$ , defined as the difference between  $\Delta T_m$  of a ligand X and a reference ligand specified in the text below. Positive values of  $\Delta\Delta T_m$  (X) indicate higher stability of protein–ligand complex than in the case of a reference ligand.

Several modifications of the sugar ring on both nucleotides have been examined. For the 3' nucleotide, these modifications include substitution of the 2'-hydroxyl with 2'-fluorine (CDN-1), hydrogen (i.e., deoxyribose, CDN-12), or amine group (CDN-9) or changed stereochemistry of the 2' carbon (i.e., arabinose, CDN-10).

Of these modifications, CDN-9 forms the least stable ligand–protein complex. The amine group of the unbound ligand is expected to be protonated. However, it is improbable that the binding site would favor the presence of a positively charged substituent. Thus, binding of this ligand is expected to incur a desolvation penalty, which in turn leads to decreased thermal stability of the protein–ligand complex ( $\Delta T_m(\text{CDN-9}) = +9.4$  °C; that is,  $\Delta\Delta T_m = -5.9$  °C with respect to 2'3'cGAMP (see Table 3)).

According to QM/MM models, the arabinose modification (CDN-10) leads to the 2' hydroxyl interaction with Arg238. This differs from 2'3'cGAMP–STING complex where this amino acid is primarily in contact with the phosphate group.<sup>8</sup> In the case of CDN-10, the phosphate is displaced and interacts with Arg232 and the 2' hydroxyl via intramolecular hydrogen bonding. Thus, the arabinose modification is well tolerated by WT STING, which is reflected by  $\Delta\Delta T_m(\text{CDN-10}) = +1.7$  °C with respect to 2'3'cGAMP.

In the crystal structure of 2'3'cGAMP with STING, the environment surrounding 2'-hydroxyl includes both hydrophobic and hydrophilic residues and a nearby water molecule (Figure 1). The amphipathic character of this region contributes to the ability of the protein to accommodate less hydrophilic substitutions of 2'-hydroxyl, for example, hydrogen (i.e., deoxyribose,  $\Delta\Delta T_m(\text{CDN-12}) = +0.5$  °C, or fluorine,  $\Delta\Delta T_m(\text{CDN-1}) = +5.2$  °C, both with respect to 2'3'cGAMP).

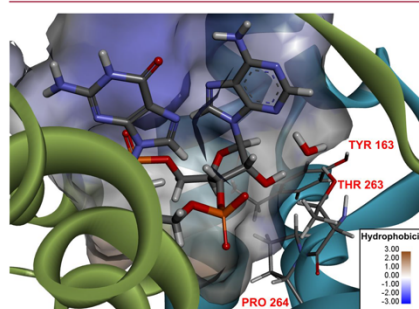
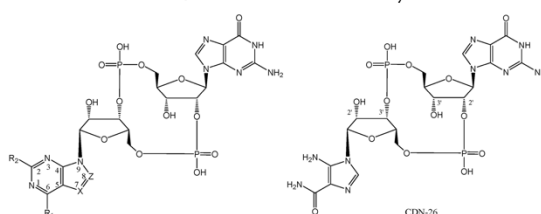


**Figure 1.** Amphipathic pocket around the 2' position of 3' nucleotide. Environment includes both hydrophobic (Tyr163 and Pro264) and hydrophilic residues (Thr263) and a water molecule. Hydrophobicity visualized by BIOVIA Discovery Studio.<sup>35</sup> Structure obtained from a QM/MM model based on PDB 6T1X. Only the relevant residues and the ligand are shown in stick representation.

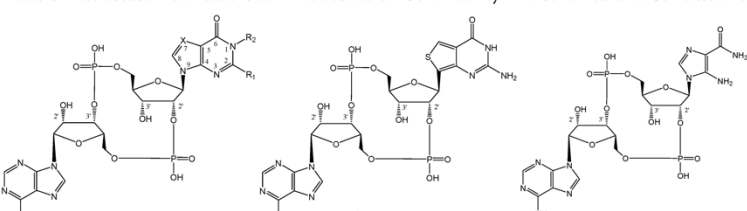
Table 4. Effects of Nucleobase Modifications at 3'-Nucleotide on CDN Activity in Biochemical and Cell-Based Assays



compd	R <sub>1</sub>	R <sub>2</sub>	X	Z	DSF $\Delta T_m^a$ (°C)		std assay EC <sub>50</sub> <sup>b</sup> (μM)		digitonin assay EC <sub>50</sub> <sup>c</sup> (μM)			
					WT	WT	WT	HAQ	REF	AQ	Q	
CDN-16	NH <sub>2</sub>	NH <sub>2</sub>	N	CH	10.0	35.9	0.02	0.05	1.10	0.04	0.31	
CDN-17	NHCH <sub>3</sub>	H	N	CH	9.0	63.7	0.02	0.06	0.70	0.06	1.20	
CDN-18	OH	H	N	CH	8.8	148.8	0.05	0.30	2.10	0.14	2.20	
CDN-19	OH	OH	N	CH	2.4	>300	1.80	1.70	20.9	2.00	32.8	
CDN-20	SH	H	N	CH	7.3	182.1	0.30	0.20	1.70	0.15	8.30	
CDN-21	H	NH <sub>2</sub>	N	CH	9.2	53.9	0.02	0.04	1.60	0.04	0.70	
CDN-22	SCH <sub>3</sub>	NH <sub>2</sub>	N	CH	3.5	>300	0.30	0.48	27.6	0.24	8.50	
CDN-23	SCH <sub>3</sub>	H	N	CH	8.3	13.3	0.01	0.06	2.30	0.06	1.23	
CDN-24	NH <sub>2</sub>	H	CH	CH	11.5	66.4	0.01	0.02	0.28	0.01	0.16	
CDN-25	NH <sub>2</sub>	H	N	N	3.9	>300	0.23	0.31	34.2	0.21	5.72	
CDN-26					1.7	>300	0.32	0.21	>45	0.21	45.3	
2'3'-cGAMP					15.3	13.7	0.02	0.02	0.07	0.04	0.05	

<sup>a</sup>Results of differential scanning fluorimetry assay performed with WT STING haplotype.  $\Delta T_m$  values are the mean of two independent double determinations. <sup>b</sup>Results of standard assay in 293T reporter cells expressing WT STING haplotype. EC<sub>50</sub> values are the mean of two independent experiments measured in triplicate with standard deviations <50% of EC<sub>50</sub> values. <sup>c</sup>Results of digitonin assay in 293T reporter cells expressing different STING haplotypes. EC<sub>50</sub> values are the mean of two independent experiments measured in triplicate with standard deviations <50% of EC<sub>50</sub> values.

Table 5. Effects of Nucleobase Modifications at 2'-Nucleotide on CDN Activity in Biochemical and Cell-Based Assays



compd	R <sub>1</sub>	R <sub>2</sub>	X	DSF $\Delta T_m^a$ (°C)		std assay EC <sub>50</sub> <sup>b</sup> (μM)		digitonin assay EC <sub>50</sub> <sup>c</sup> (μM)			
				WT	WT	WT	HAQ	REF	AQ	Q	
CDN-27	OH	H	NH	7.6	>300	0.13	0.19	5.80	0.18	0.72	
CDN-28	NH <sub>2</sub>	CH <sub>3</sub>	NH	9.0	40.0	0.02	0.04	0.90	0.04	0.78	
CDN-29	H	H	NH	16.1	29.9	0.02	0.03	0.04	0.01	0.02	
CDN-30	NH <sub>2</sub>	H	CH	6.6	40.4	0.04	0.10	3.50	0.06	1.10	
CDN-31				2.8	240.6	0.11	0.25	6.00	0.05	3.00	
CDN-32				0.6	>300	0.83	0.40	>45	0.42	47.20	
2'3'-cGAMP				15.3	13.7	0.02	0.02	0.07	0.04	0.05	

<sup>a</sup>Results of differential scanning fluorimetry assay performed with WT STING haplotype.  $\Delta T_m$  values are the mean of two independent double determinations. <sup>b</sup>Results of standard assay in 293T reporter cells expressing WT STING haplotype. EC<sub>50</sub> values are the mean of two independent experiments measured in triplicate with standard deviations <50% of EC<sub>50</sub> values. <sup>c</sup>Results of digitonin assay in 293T reporter cells expressing different STING haplotypes. EC<sub>50</sub> values are the mean of two independent experiments measured in triplicate with standard deviations <50% of EC<sub>50</sub> values.

On the other hand, the environment around the 3'-hydroxyl of the 2'-nucleotide is significantly more hydrophilic. Thus, the

same modifications (i.e., hydrogen or fluorine substitution in the 3'-position of the 2'-nucleotide) are less favorable than

their 2'-position counterparts, with  $\Delta\Delta T_m(\text{CDN-3}) = +0.9$  °C and  $\Delta\Delta T_m(\text{CDN-14}) = -1.8$  °C compared to 2'3'-cGAMP (Table 3).

While the above explanations help to rationalize some of the observed differences, it is remarkable that the 2'-fluorine (CDN-1) and arabinose (CDN-10) modifications actually lead to higher  $\Delta T_m$  with respect to the native ligand. One can speculate that this improvement in STING binding is not due to their specific interaction with the protein but an inherently lower energetic cost for these ligands to adapt the STING bound conformation.

By combining QM/MM models and conformational sampling of these two ligands, we can estimate this energetic penalty (see Experimental Section). Indeed, it turns out that both CDN-1 and CDN-10 require 4.7 and 4.6 kcal·mol<sup>-1</sup> less (free) energy, respectively, than 2'3'-cGAMP to change the conformation from unbound state in solvent to that found in the protein. These estimates are qualitative but serve to illustrate that the ligand may be optimized not only by its interactions with the protein but also via minimizing its conformational strain.

The 2'- and 3'-hydroxyl groups of the native ligand are more than 7 Å apart. Based on the crystal structure of CDN-1 with WT STING, substituting 2' hydroxyl with fluorine does not lead to any significant change in the binding mode. We presume the same is the case for substitution with hydrogen (CDN-12) and analogous substitutions of the 3' hydroxyl (CDN-3 and CDN-14). Thus, it is not surprising that combined modifications result in additive changes of  $\Delta\Delta T_m$ . Indeed, measurement of  $\Delta\Delta T_m$  for disubstituted ligands CDN-2, CDN-4, CDN-5, and CDN-13 give values that can also be estimated by simply summing up the  $\Delta\Delta T_m$  values of monosubstituted ligands. The error of such estimate is within 1.1 °C, which is within the 3 times standard deviation of DSF measurement. Further examples of such additivity or lack thereof will be discussed below and may be used as an argument for cooperative effects of substitutions in different parts of a ligand.

**2'3'CDNs with Substituted Nucleobases.** 2'3'CDNs with guanosine subunit combined with 2-aminoadenosine (CDN-16), N<sup>6</sup>-methyladenosine (CDN-17), inosine (CDN-18), 2-aminopurineriboside (CDN-21), or 7-deazaadenosine (CDN-24) (Table 4) and 2'3'CDNs with adenosine subunit combined with N<sup>1</sup>-methylguanosine (CDN-28), inosine (CDN-29), 7-deazaguanosine (CDN-30), and thienoguanosine (CDN-31) (Table 5) retained comparable activities in WT, HAQ and AQ STING digitonin reporter assays as 2'3'-cGAMP. Compared to 2'3'-cGAMP, 2'3'CDN with xanthosine-MP (CDN-19), 6-thio-IMP (CDN-20), 6-methylthio-GMP (22), 8-aza-AMP (CDN-25), and AICAR-MP (CDN-26 and -32) had substantially diminished activity against all STING haplotypes (Tables 4 and 5). Moreover, with the exception of CDN-29, all prepared 2'3'CDNs had significantly impaired activity toward REF STING haplotype in digitonin assays (Tables 4 and 5). Similar to 2'- and 3'-substituted 2'3'CDNs, CDN-16–32 were at least 2 orders of magnitude less potent in standard than in digitonin assay (Tables 4 and 5).

CDNs are anchored to STING protein through Arg238 and Tyr167 which stack via  $\pi$ - $\pi$  and cation- $\pi$  interactions from both sides of the nucleobases (Figure 2). The functional groups at C<sub>6</sub> position on CDNs are without direct contacts with the protein. Instead, their interactions with STING are

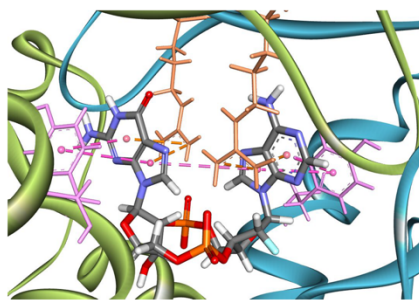


**Figure 2.** Interactions of purine bases. Purine bases of a CDN stack with Tyr167 and Arg238 residues. Detail from the structure of CDN-1 with human WT STING (PDB 6S27). The  $\pi$ - $\pi$  interaction is shown in dashed-pink line, and cation- $\pi$  interaction is shown in dashed-orange line.

mediated through a network of water molecules to backbone groups of residues 238 to 241, which are located in the lid region (Figure 3) of STING protein. This water network might be crucial for understanding the effect of base modification on the activity of CDNs.

Information about the positions of water molecules is difficult to interpret due to symmetry considerations. A 2',3'-cyclic dinucleotide allows for two equivalent binding modes to a symmetric STING homodimer. Even if the water molecules are resolved in a crystal structure, the averaging of their

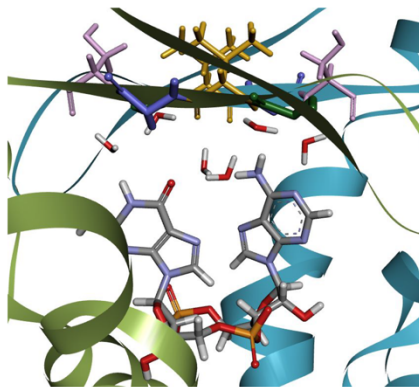


**Figure 3.** Proposed local water network near position 6 of 2'3'-cGAMP. Water-mediated hydrogen bond network between the purine bases of 2'3'-cGAMP and the lid region backbone groups of residues 238 (green), 239 (yellow), 240 (purple), and 241 (pink) located in  $\beta$ 3/ $\beta$ 4 strands of human WT STING's lid domain. Four water molecules together with position 6 substituents of purine bases form an asymmetrical chain of hydrogen donors and acceptors. Structure was obtained from a QM/MM model based on PDB 6T1X. Only the relevant residues and the ligand are shown in stick representation.

positions poses a challenge for a fundamentally asymmetric ligand interpretation. In the following, we rely on the ability of QM/MM calculations to provide detailed structural information concerning water positions. Moreover, most of the ligands presented herein contain modification of the adenine base (with respect to the native 2′3′cGAMP ligand), and hence, the discussion of water environment is focused on this region.

Figure 3 shows the proposed network of water molecules. This configuration not only provides an ideal number of interactions for all water molecules in the network but also accommodates the asymmetry of the ligand, that is, hydrogen bond acceptor at position 6 of guanine and hydrogen bond donor at position 6 of adenine. This configuration agrees well with water molecules resolved in a crystal structure of STING in complex with CDN-24. There is one less water molecule in the QM/MM model in the vicinity of position 2 of the 3′ nucleotide due to a different orientation of the Ile235 side chain in the crystal structure and in the QM/MM model.

We speculate that this ideal setup is sensitive to modification of nearby functional groups. Changing a substituent at the position 6 of adenine to an electron acceptor, such as oxygen (CDN-18) or sulfur (CDN-20), leads to  $\Delta\Delta T_m \approx -7$  °C with respect to 2′3′cGAMP. Bulkier substituents like 6-methylamino (CDN-17) and 6-methylthio (CDN-23) are also disruptive, probably due to the decreasing number of water molecules around these ligands. Regardless of the nature of the methylated substituent, this disruption also leads to  $\Delta\Delta T_m \approx -7$  °C. On the other hand, substitution of the NH<sub>2</sub> group with hydrogen is accommodated without incurring a penalty to  $\Delta T_m$  (compare CDN-16 and CDN-21).

Shifting the focus to substitutions on position 2, it seems that any substituent other than the native hydrogen incurs a penalty of a  $\Delta\Delta T_m \approx -5$  °C relative to an unsubstituted CDN, as evidenced by a number of cases, including amine substituents (compare  $\Delta T_m$  values of CDN-16 and 2′3′cGAMP; CDN-22 and CDN-23; CDN-1 and CDN-8), oxygen (compare  $\Delta T_m$  values of CDN-18 and CDN-19), fluorine (compare  $\Delta T_m$  values of CDN-10 and CDN-11, CDN-1 and CDN-7, CDN-5 and CDN-6), and chlorine (CDN-15 and CDN-12).

Note the approximate penalties mentioned in the previous paragraphs, that is,  $\Delta\Delta T_m \approx -7$  °C for an electron acceptor or methylated substituent in position 6 and  $\Delta\Delta T_m \approx -5$  °C for any substituent at position 2 of the 3′ nucleotide. These two very simple rules are sufficient to estimate measured  $\Delta T_m$  of all 14 ligands with substituted purine base of 3′ nucleotide in our set for which  $\Delta T_m$  span from +2.4 to +14.9 °C to within 1.3 °C (with mean absolute deviation of 0.7 °C), which is well within the experimental error. The above QSAR analysis is summed up in Table 6.

**Thiophosphate 2′3′CDNs.** We were able to prepare enzymatically two thiophosphate 2′3′CDNs. Monothiophosphate 2′3′CDN (CDN-33) is about 3–7-fold less active against all STING haplotypes than 2′3′cGAMP. On the other hand, bis-thiophosphate CDN (CDN-34) retains similar activity toward all STING haplotypes as the parent 2′3′cGAMP (Table 7). Since the enzymatic cyclization afforded only one diastereomer out of four possible, we prepared bis-thiophosphate versions of 2′3′cGAMP through chemical synthesis, which is detailed in Supplementary Methods. As shown in Table 7, none of the prepared compounds had activity profile similar to the enzymatically prepared CDN-34. Moreover, <sup>1</sup>H NMR data of CDN-34

Table 6. QSAR of Ligand Modifications

position	native substituent	modified substituent	DSF $\Delta\Delta T_m^a$ (°C)
6 (3′nucleotide)	NH <sub>2</sub>	hydrogen-bond acceptor	-7
6 (3′nucleotide)	NH <sub>2</sub>	methylated	-7
2 (3′nucleotide)	H	any	-5
2′ (3′nucleotide)	OH	F	+5
2′ (3′nucleotide)	OH	H	+0.5
3′ (2′nucleotide)	OH	F	+1
3′ (2′nucleotide)	OH	H	-2

<sup>a</sup> $\Delta\Delta T_m$  defined as the difference between  $\Delta T_m$  of a ligand X and reference ligand.

differed from those for the chemically prepared diastereomers CDN-35, -36, and -37, indicating that CDN-34 is the diastereomer that was not obtained during chemical synthesis of CDN-35, -36, and -37.

QM/MM modeling of CDN-34 and its diastereoisomers (CDN-35, CDN-36, and CDN-37) reveals very few differences. The native ligand (phosphate) and R configuration of the thiophosphate exhibit identical binding modes. In case of S-configuration of the thiophosphate (i.e., P=S bond pointing in direction of Arg238), the interaction is shared with both Arg232 and Arg238. Hence, we speculate that (S,S) configuration is the one that would be most affected in REF variant of the protein (i.e., R232H allelic form). However, this difference alone is not sufficient to explain all the observed differences in activities.

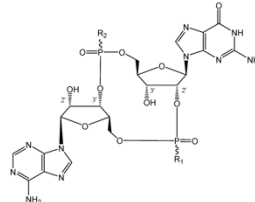
**The Structures of WT STING with CDN-1 and -24.** By employing our optimized protocol,<sup>36</sup> we were able to obtain crystal structures of human WT STING in complex with CDN-1 and -24 with final resolutions of 3 Å (*I*/ $\sigma$  = 2) and 2.2 Å (*I*/ $\sigma$  = 2), respectively. The crystal of STING in complex with CDN-1 belonged to the tetragonal P4<sub>1</sub>2<sub>1</sub>2 and that in complex with CDN-24 to the orthorhombic P2<sub>1</sub>2<sub>1</sub>2 space group (Tables S6 and S7). The alignment of the structure of the WT STING in complex with CDN-1 or CDN-24 with structure of STING in complex with 2′3′cGAMP (PDB entry 4KSY) revealed slight differences in protein conformation (the RMSD over Ca 0.57 and 0.78, respectively), and the protein structures can be therefore considered virtually identical (Figure 4B and 5B). The binding mode and conformation of the CDN-1 and CDN-24 correspond well to the binding mode and conformation of 2′3′cGAMP (Figure 4C and 5C).

The water network chain in the vicinity of position 6 of purine bases coincides with those used in QM/MM calculation, which *a posteriori* confirms the validity of our previous structural considerations on water networks. However, compared to the QM/MM model, both X-ray structures show an extra water molecule near position 1 due to different orientation of the Ile235 side chain. Also, both crystal structures lack one water molecule near position 3, which is present in the QM/MM model (Figure 1).

**Effect of 2′3′CDNs on Cytokine Induction and Monocytes.** Activation of cGAS–STING pathway results in the induction of interferons and TNF secretion.<sup>37</sup> Consistently, PBMCs treated with CDNs prepared within this study induced high levels of IFN $\alpha$ , IFN $\gamma$ , and TNF $\alpha$  secretion into cultivation medium (Table 8, Table S8). Since CDNs were reported to induce monocyte cytotoxicity in a A2a G $\alpha$ s protein-coupled receptor dependent manner,<sup>37</sup> we tested the effect of CDNs 1–37 on viability of monocytes in PBMCs

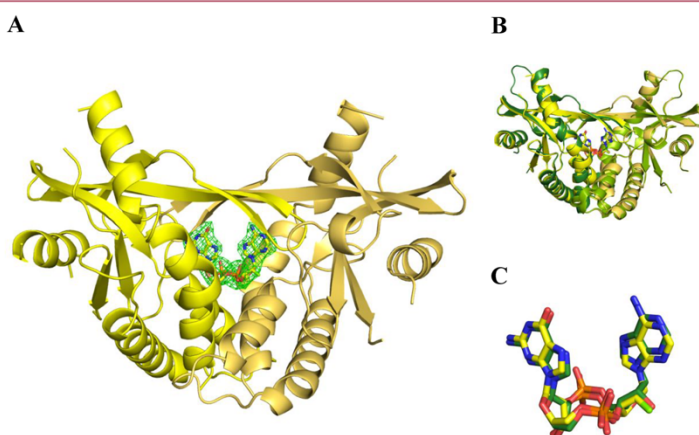


Table 7. Activity of Thiophosphate 2'3'CDNs in Biochemical and Cell-Based Assays



compd	R <sub>1</sub>	R <sub>2</sub>	DSF $\Delta T_m$ <sup>a</sup> (°C)		std assay EC <sub>50</sub> <sup>b</sup> ( $\mu$ M)		digitonin assay EC <sub>50</sub> <sup>c</sup> ( $\mu$ M)				
			WT	<i>d</i>	WT	<i>d</i>	WT	HAQ	REF	AQ	Q
CDN-33	OH	SH	13.8				0.06	0.11	0.6	0.12	0.14
CDN-34	SH	SH	14.6				0.03	0.02	0.01	0.03	0.03
CDN-35	SH	SH	13.6				0.09	0.13	0.7	0.14	0.19
CDN-36	SH	SH	15.1				0.02	0.02	0.2	0.03	0.07
CDN-37	SH	SH	14.8				0.03	0.03	0.15	0.03	0.08
2'3'-cGAMP			15.3				0.02	0.02	0.07	0.04	0.05

<sup>a</sup>Results of differential scanning fluorimetry assay performed with WT STING haplotype.  $\Delta T_m$  values are the mean of two independent double determinations. <sup>b</sup>Results of standard assay in 293T reporter cells expressing WT STING haplotype. EC<sub>50</sub> values are the mean of two independent experiments measured in triplicate with standard deviations <50% of EC<sub>50</sub> values. <sup>c</sup>Results of digitonin assay in 293T reporter cells expressing different STING haplotypes. EC<sub>50</sub> values are the mean of two independent experiments measured in triplicate with standard deviations <50% of EC<sub>50</sub> values. <sup>d</sup>Not determined.



**Figure 4.** Structure of human WT STING in complex with CDN-1 (6S27) and its comparison to the structure of STING in complex with its natural ligand 2'3'cGAMP (4KSY). (A) Structure of human WT STING in complex with CDN-1 (6S27). The  $F_o - F_c$  map is contoured at  $1/\sigma = 3$ . (B) Alignment of 6S27 and 4KSY (the RMSD over  $C\alpha = 0.5690$ ). (C) Comparison of 2'3'cGAMP and CDN-1 bound to STING. Coloring: nitrogen, blue; oxygen, red; fluorine, bright green; phosphate, orange; carbon, yellow (CDN-1) or dark green (2'3'cGAMP).

using a single concentration of 12.5  $\mu$ M. Similar to the published data, the majority of the prepared compounds caused profound monocytic cytotoxicity without affecting the CD3<sup>+</sup> T cell population (Table 8, Table S8).

#### DISCUSSION AND CONCLUSIONS

In this study, we show that 2'3'CDNs can easily be prepared from NTP analogues by employing vertebrate cyclic

dinucleotide synthase cGAS. We profiled substrate specificity of human, mouse, and chicken cGAS, and we developed a general protocol for enzymatic synthesis of CDNs. With few exceptions (e.g., *O*<sup>6</sup>-methyl-guanosine-triphosphate (16), which was an exclusive substrate of human cGAS), the mouse enzyme turned out to be the most promiscuous and was used for preparation of 34 CDNs. Principally, it should be possible to prepare more CDNs from our small library of

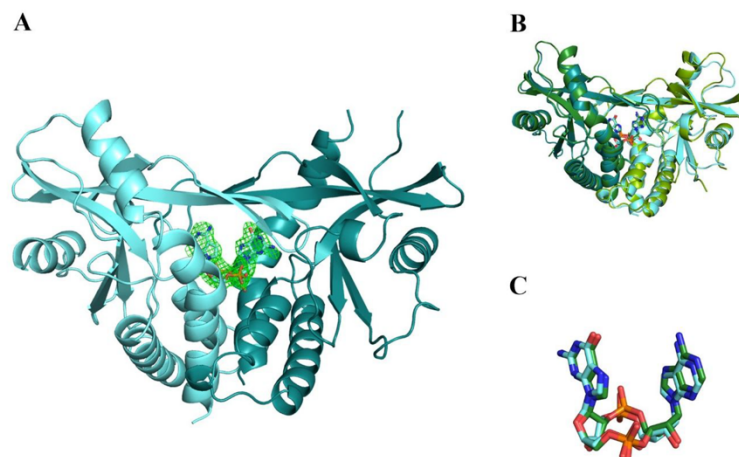


**Figure 5.** Structure of human WT STING in complex with CDN-24 (6S26) and its comparison to the structure of STING in complex with its natural ligand 2'3'cGAMP (4KSY). (A) Structure of human WT STING in complex with CDN-24 (6S26). The  $F_o - F_c$  map is contoured at  $1/\sigma = 3$ . (B) Alignment of 6S26 and 4KSY (the RMSD over  $C\alpha = 0.7833$ ). (C) Comparison of 2'3'cGAMP and CDN-24 bound to STING. Coloring: nitrogen, blue; oxygen, red; phosphate, orange; carbon, light blue (CDN-24) or dark green (2'3'cGAMP).

NTPs. The majority of CDNs in this study contained either AMP as the 3' nucleotide or GMP as 2' nucleotide, and more CDNs where both nucleotides are analogues, such as CDN-2, -4, and -5, can be envisioned.

During our efforts to identify novel STING agonists,<sup>38</sup> we were guided rather by the digitonin than the standard assay. As mentioned above, activity of CDNs is influenced by the efficiency of their uptake into cells in the latter assay. Consequently,  $EC_{50}$  values for the same CDN are at least 100-fold higher in the standard than in the digitonin assay (Tables 3, 4, 5, and 7). The uptake issue can be ultimately solved by synthesis of lipophilic prodrugs of CDNs as presented in recent patent literature.<sup>35</sup>

An ideal CDN for clinical use should have similar activity toward all STING haplotypes, thus eliminating the need for genotyping of patients. CDNs with adenine 3' nucleotide and guanine 2' nucleotide containing 2'-F or 3'-F substitutions or both (CDN-1, -2, and -3), 2'-F and 3'-deoxy groups (CDN-4) or 2'-deoxy and 3'-F substitutions (CDN-5) showed good activity across all STING haplotypes. In contrast to the general notion, not all 2'3'CDNs are good REF STING agonists.<sup>33,34,40</sup> CDNs with ara-adenosine or 2'-amino-2'-deoxy-adenosine as 3' nucleotide and some of CDNs with 2'-deoxyribonucleotides had diminished potency against REF STING. Substitutions of nucleobases almost always resulted in impaired activation of REF STING haplotype with the only exception being CDN-29 where 2' nucleotide guanosine was replaced for inosine.

All prepared CDNs stimulated human PBMCs to secrete  $IFN\alpha$ ,  $IFN\gamma$ , and  $TNF\alpha$ , consistently with their ability to activate cGAS–STING pathway. In agreement with previously published data,<sup>37</sup> CDNs decreased viability of monocytes in PBMC cultures without affecting T-lymphocytes (Table 8, S8).

However, we cannot exclude that some other factors such as PBMC purification, cell density, or cultivation conditions could exacerbate the negative effect of CDNs on monocytes. Monocytic cytotoxicity seemed to be somewhat proportional to the levels of induced cytokines (Table 8, S8). Unfortunately, no CDN inducing high levels of cytokines and low monocytic cytotoxicity was identified (Table 8, S8).

We used DSF measurements to rationalize interactions of CDN ligands with human WT STING. Crystal structures and docking calculations highlight large binding mode similarities of examined ligands. This suggests that the effects of modifications on  $\Delta T_m$  values will be dictated primarily by local environment. This notion is further supported by the additivity of  $\Delta\Delta T_m$  values of ligands with multiple modifications. As a result, the inferred structure–activity relationships show good agreement with measured  $\Delta T_m$  values in all cases.

A crucial element for understanding these relationships is the network of water molecules, which was obtained by combining information from X-ray crystallography and computational modeling. Furthermore, estimates of differences in conformational strain of various ligands highlight that changes to the ligand affect not only its interactions with the protein but the ease of adopting the necessary conformation as well.

In summary, an enzymatic synthesis of 2'3'CDNs turned out to be an efficient way of generating SAR for CDNs and STING and can be employed beyond ribonucleotides as exemplified in a recently published patent.<sup>38</sup>

## EXPERIMENTAL SECTION

**Materials.** Adenosine-5'-O-(1-thiotriphosphate), 2-aminoadenosine-5'-triphosphate, 2-amino-6-chloropurine-5'-triphosphate, 2'-amino-2'-deoxy-adenosine-5'-triphosphate, 2-aminopurine-riboside-

10685

DOI: 10.1021/acs.jmedchem.9b01062  
J. Med. Chem. 2019, 62, 10676–10690

**Table 8. Effect of CDNs on Monocyte Viability and Cytokine Induction in PBMC Assay**

compd	monocyte viability <sup>a</sup> (%)	cytokines <sup>b</sup>		
		INF $\gamma$	TNF $\alpha$	IFN $\alpha$
CDN-1	1.7	1.3	0.6	0.9
CDN-2	0.4	5.1	4.3	0.5
CDN-3	0.7	4	0.8	0.6
CDN-4	0.7	6.2	4.4	0.3
CDN-5	0.5	5.6	4.2	0.3
CDN-6	0.2	0.1	2.3	0
CDN-7	0.4	4.6	3.2	0.4
CDN-8	2.5	3.1	0.7	0.8
CDN-9	3.0	2.7	3.7	0.4
CDN-10	5.2	3.2	2.6	1
CDN-11	3.0	3.2	3.4	2.4
CDN-12	2.3	3.3	4.1	0.5
CDN-13	1.6	1.6	0.6	1.3
CDN-14	3.3	5	1.9	0.6
CDN-15	0.1	0.8	4.3	0.1
CDN-16	1.5	3.6	4.3	0.7
CDN-17	0.8	3.3	4.1	0.5
CDN-18	17	0.5	0.2	0.8
CDN-19	45	0	0	0
CDN-20	10	1.8	0.7	0.7
CDN-21	0.6	2.4	4.1	0.5
CDN-22	4.8	1.1	3.2	0
CDN-23	0.4	1.7	4.2	0.2
CDN-24	0.7	1.2	3.3	0.3
CDN-25	2.3	2.9	3.8	0.1
CDN-26	83	0	0	0
CDN-27	8.3	3	0.6	0.7
CDN-28	2.0	3.3	0.5	0.7
CDN-29	1.0	1.2	0.4	1.9
CDN-30	0.9	5.9	3.5	0.3
CDN-31	0.9	4	1.6	2.4
CDN-32	87	0	0	0
CDN-33	9.4	2.2	1.6	1.2
CDN-34	2.1	2.4	1.3	2
CDN-35	1.8	1	0.2	0.6
CDN-36	0.3	3.9	0.4	1.2
CDN-37	0.8	0.2	0.5	0.1
2'2'-cGAMP	2.8	1.8	0.2	0.6
3'3'-cGAMP	17	1	0.3	1.4
3'3'-diGAMP	32	0	0	0
2'3'-cGAMP	1.1	1	1	1

<sup>a</sup>Viability of monocytes in PBMC culture treated with 12.5  $\mu$ M CDN for 16 h. Viability of monocytes in untreated control equals 100%. Values are the mean of three independent determinations from one PBMC donor. <sup>b</sup>Fold of 2'3'-cGAMP induced cytokines. Levels of INF  $\alpha$ , INF  $\gamma$ , and TNF  $\alpha$  secreted by PBMCs treated with 12.5  $\mu$ M CDN for 16 h relative to levels secreted by PBMCs treated with 12.5  $\mu$ M 2'3'-cGAMP. Values are the mean of three independent determinations from the same PBMC donor as in monocyte cytotoxicity assay. Amount of cytokines induced by 2'3'-cGAMP treatment: interferon  $\gamma$ , 5570 pg/mL; TNF $\alpha$ , 5552 pg/mL; interferon  $\alpha$ , 648 pg/mL.

5'-triphosphate, ara-adenosine-5'-triphosphate, 8-azaadenosine-5'-triphosphate, 8-azidoadenosine-5'-triphosphate, 7-deazaadenosine-5'-triphosphate, 7-deazaguanosine-5'-triphosphate, 2'-deoxyadenosine-5'-triphosphate, 2'-fluoro-2'-deoxyadenosine-5'-triphosphate, guanosine-5'-O-(1-thiotriphosphate), isoguanosine-5'-triphosphate, N<sup>6</sup>-methyladenosine-5'-triphosphate, 3'-O-methyladenosine-5'-triphos-

phate, N<sup>1</sup>-methyl-adenosine-5'-triphosphate, O<sup>6</sup>-methylguanosine-5'-triphosphate, 8-oxoadenosine-5'-triphosphate, 8-oxoguanosine-5'-triphosphate, thienoguanosine-5'-triphosphate, and xanthosine-5'-triphosphate were purchased from TriLink Biotechnologies (San Diego, CA, USA). AICAR triphosphate, 2'-bromo-2'-deoxyadenosine-5'-triphosphate, 2'-chloro-2'-deoxyadenosine-5'-triphosphate, 3'-deoxyguanosine-5'-triphosphate, 2-fluoro-ara-adenosine-5'-triphosphate, 2'-iodo-2'-deoxyadenosine-5'-triphosphate, 6-mercaptopurineriboside-5'-triphosphate, 6-methylthioguanosine-5'-triphosphate, 6-methylthioinosine-5'-triphosphate, and 6-thioguanosine-5'-triphosphate were from Jena Bioscience (Jena, Germany). 2-Fluoro-ara-adenosine-5'-triphosphate, 2'-deoxy-2-chloroadenosine-5'-triphosphate, 2'-deoxy-2,2'-difluoroadenosine 5'-triphosphate, and 2'-deoxy-2-fluoro-adenosine-5'-triphosphate were obtained from Metkinen Chemistry (Kuopio, Finland). Inosine-5'-triphosphate and 7-methylguanosine-5'-triphosphate were from Sigma-Aldrich (Prague, Czech Republic). The other NTPs were prepared from commercially available nucleosides following a standard protocol.<sup>16</sup> SeQuant ZIC-pHILIC column was from Merck Millipore (Prague, Czech Republic). Luna column (5  $\mu$ m C18 250 mm  $\times$  10 mm) was purchased from Phenomenex (Torrance, CA, USA). Zombie NIR Fixable Viability Kit and BD Cytotoxicity Fixation Buffer were supplied by BioLegend (San Diego, CA, USA). ProcartaPlex Assays and SYPRO Orange originated from Thermo Fisher Scientific (Waltham, MA, USA).

Generation of 293T reporter cell lines stably expressing WT, HAQ, REF, AQ, and Q STING haplotypes and purification of human, chicken, and mouse cGAS protein and human WT STING protein are detailed in Supporting Information.

**Enzymatic Synthesis of CDNs.** Nucleoside triphosphates (final concentration 1 mM) were incubated in 20 mM Tris-HCl buffer, pH 8.0, containing 20 mM MgCl<sub>2</sub>, 5  $\mu$ M mouse, chicken, or human cGAS, and 0.1 mg/mL herring testes DNA at 37  $^{\circ}$ C overnight in a shaker. The reaction mixtures were then spun at 25000g for 20 min, and supernatants were passed through Pierce Protein Concentrators PES, 3000 MWCO, 0.5 mL (Thermo Fisher Scientific, Prague, Czech Republic). In small scale reactions, the samples were directly analyzed by methods mentioned below. Reaction conversions were determined by HPLC using UV detection at 260 nm. Conversions are defined as follows: a ratio of AUC of a CDN over the sum of AUCs of the CDN, NTPs, and NDPs.

In the case of large scale CDN synthesis, triethylammonium bicarbonate buffer (pH 8.5) was added to the flow-through fractions to 0.1 M final concentration, and CDNs were purified on semipreparative C18 column (Luna 5  $\mu$ m C18 250 mm  $\times$  10 mm) using 50 min gradient at flow rate 3 mL/min of 0–10% acetonitrile in 0.1 M TEAB buffer (pH 8.5). TEAB was removed from the collected fractions by 3 cycles of evaporation/dissolution in 50% methanol, and triethylammonium ion was exchanged for Na<sup>+</sup> ion by slowly passing aqueous solution of the TEA<sup>+</sup> salt through a DOWEX 50 (Na<sup>+</sup> cycle) column and freeze-drying appropriate eluted fractions. The identification of CDNs was performed on ACQUITY UPLC H-Class PLUS chromatographic system with MS SQ Detector 2 (Waters, Milford, USA) using iHILIC-Fusion column SS 50 mm  $\times$  2.1 mm, 1.8  $\mu$ m (HILICON AB, Sweden), and 20 mM ammonium acetate buffer, pH 6.8, with a linear gradient of acetonitrile (85% to 50% in 4 min; flow rate 0.32 mL/min). Positive ESI method was used for ionization. Alternatively, CDNs were identified on Waters UPLC H-Class Core chromatographic system with MS QDa Detector (Waters, Milford, MA, USA) using Acquity UPLC BEH C18 column 50 mm  $\times$  2.1 mm, 1.7  $\mu$ m (Waters, Milford, MA, USA), and 0.1% formic acid in water with linear gradient of acetonitrile (0 to 100% in 7 min, flow rate 0.5 mL/min). Negative ESI method was used for ionization. Identification of CDNs was also performed on Waters UPLC chromatographic system with Q-TOF MS detector (Waters, Milford, MA, USA) using SeQuant ZIC-pHILIC column 5 mm, polymeric, 50 mm  $\times$  2.1 mm (Merck, Darmstadt, Germany), and 10 mM ammonium acetate buffer, pH 6.8, with linear gradient of acetonitrile (10% to 60% in 7 min, flow rate 0.3 mL/min). Negative ESI method was used for ionization. Purity of all final compounds was >95% as determined by methods mentioned above. Large scale

synthesis conversion rates of NTPs to CDNs and the enzymes used for reaction can be found in SI in Table S5.

**NMR Spectroscopy and High Resolution Mass Spectrometry Analysis.** Proton NMR spectra (1D, 2D-<sup>1</sup>H-<sup>1</sup>H-COSY, and 2D-<sup>1</sup>H-<sup>1</sup>H-ROESY) were measured on a Bruker 600 AVANCE III HD instrument (<sup>1</sup>H at 600 MHz) equipped with 5 mm cryoprobe in D<sub>2</sub>O at 25 °C. Chemical shifts were referenced to dioxane (added as internal standard) and recalculated to  $\delta$ -scale using  $\delta_{\text{H}}(\text{dioxane}) = 3.75$  ppm. The <sup>31</sup>P and <sup>19</sup>F NMR spectra were measured in D<sub>2</sub>O at 25 °C on a Bruker 500 AVANCE III HD instrument (<sup>31</sup>P at 202.4 MHz and <sup>19</sup>F at 470.4 MHz frequency) in 5 mm cryoprobe and referenced to H<sub>3</sub>PO<sub>4</sub> (<sup>31</sup>P) and CFCl<sub>3</sub> (<sup>19</sup>F) as external standards.

High resolution mass spectrometry analysis of prepared CDNs was performed on LTQ Orbitrap XL ETD Hybrid Ion Trap-Orbitrap Mass Spectrometer (Thermo Fisher Scientific). Negative ESI method was used for ionization.

**Digitonin Assay with 293T Reporter Cells.** The 293T reporter cells stably expressing different STING protein haplotypes (WT, HAQ, REF, AQ, or Q) were seeded at density of 250 000 cells per cm<sup>2</sup> onto 96 well white poly(D-lysine) coated plates in 100  $\mu$ L of DMEM with high glucose supplemented with 10% heat inactivated FBS. The medium was removed the next day, and 3-fold serial dilutions of compounds in digitonin buffer containing 50 mM HEPES (pH 7.0), 100 mM KCl, 3 mM MgCl<sub>2</sub>, 0.1 mM DTT, 85 mM sucrose, 0.2% (w/w) BSA, 1 mM ATP, 0.1 mM GTP, and 10  $\mu$ g/mL digitonin A were added to the cells. After 30 min incubation at 37 °C with 5% CO<sub>2</sub>, the digitonin buffer was removed, cells were washed once with 100  $\mu$ L of cultivation medium, and 100  $\mu$ L of fresh medium was added to each well. The plates with cells were further incubated for 5 h at 37 °C with 5% CO<sub>2</sub>. Thereafter 50  $\mu$ L of the medium was removed, and 30  $\mu$ L of Bright-Glo Luciferase Assay System reagent was added to each well. Luminescence was measured on Spark (TECAN, Grödig, Austria), and GraphPad Prism (La Jolla, USA) was used to calculate the 50% effective concentration (EC<sub>50</sub>) from an 8-point dose–response curve. Representative dose–response curves are shown in Figure S2. Nonlinear regression curve fit with standard slope was used for EC<sub>50</sub> value calculations. The EC<sub>50</sub> value represents CDN concentration that gives half-maximal response of firefly luciferase in the 293T reporter assay. Maximum fold of firefly luciferase induction in 293T reporter assay did not differ among tested CDNs by more than 30% compared to the natural STING ligand 2'3'cGAMP.

**Standard Assay Using 293T Reporter Cells.** The 293T reporter cells stably expressing WT STING protein haplotype were seeded at density of 250 000 cells per cm<sup>2</sup> onto 96 well white poly(D-lysine) coated plates in 100  $\mu$ L of DMEM with high glucose supplemented with 10% heat inactivated FBS. The next day, medium was removed, and 30  $\mu$ L of serially diluted compounds in the cultivation medium were added to wells. After 7 h of incubation at 37 °C with 5% CO<sub>2</sub>, 20  $\mu$ L of incubation medium and 30  $\mu$ L of Bright-Glo Luciferase Assay System reagent were added to wells. Luminescence measurement and EC<sub>50</sub> calculations were performed as described above.

**Differential Scanning Fluorimetry with WT STING.** WT STING protein was diluted to the final concentration 0.1 mg/mL in 100 mM Tris-HCl buffer, pH 7.4, containing 150 mM NaCl, 1:500 (v/v) SYPRO Orange, and 150  $\mu$ M CDN or water. Solutions (20  $\mu$ L) of the reaction mixtures were pipetted in triplicate into 96 well optical plates, and thermal denaturation of samples was performed on real time PCR cycler (LightCycler 480 Instrument II, Roche, Basel, Switzerland). The first derivative of the thermal denaturation curves was performed to calculate melting temperatures ( $T_m$ ) of STING–CDN complexes and STING protein alone. The thermal shift ( $\Delta T_m$ ) for each CDN was calculated by subtracting the average denaturing temperature of STING without CDN from the average denaturing temperature of STING–CDN complex.

**Peripheral Blood Mononuclear Cell Assay.** Buffy coats from healthy individuals were obtained from the Institute of Hematology and Blood Transfusion (Prague, Czech Republic). Informed written consent was obtained from each individual enrolled. PBMCs were isolated from fresh buffy coats using Ficoll density gradient

centrifugation (Ficoll Paque Plus, GE Healthcare) in SepMate tubes (SepMate PBMC Isolation Tubes, Stemcell Technologies). Freshly isolated PBMCs were washed with PBS containing 2 mM EDTA, and 500 000 cells were seeded into a well in RPMI 1640 medium supplemented with 10% (v/v) fetal bovine serum in U-shaped 96 well plates ( $5 \times 10^5$  cells/mL). CDNs were added to the final concentration of 12.5  $\mu$ M, and after a 16 h incubation time at 37 °C in 5% CO<sub>2</sub> atmosphere, culture medium was collected for cytokine analyses. The levels of secreted INF $\alpha$ , INF $\gamma$ , and TNF $\alpha$  were determined with ProcartaPlex Assays using MAGPIX System (Merck KGaA, Darmstadt, Germany) according to manufacturer's instruction. Culture medium served as a negative control, and values are represented as a fold of 2'3'cGAMP induced cytokine values. Cells were then harvested, and flow cytometry was performed for phenotype determination. PBMCs were prestained with live/dead marker Zombie-NIR at 1:100 dilution for 20 min at room temperature. Specific staining was carried out with the following mouse anti-human monoclonal antibodies: CD3-APC (1:100 dilution, OKT3 clone, Tonbo Biosciences) and CD14-PE (1:50 dilution, clone 61D3, Tonbo Biosciences). Cells were incubated with the antibody mixture or appropriate isotype controls for 30 min at 4 °C in PBS supplemented with 0.5% BSA. Then they were fixed with BD Cytotfix Fixation Buffer and kept at 4 °C until assayed. Data were acquired on a BD LSR Fortessa cytometer (BD Biosciences) using FACS Diva software (version 7, BD Biosciences). Debris were excluded by forward and side scatter gating followed by doublet and dead cell exclusion. Population of interest was gated on specific CD3 negative CD14 positive monocytes or CD3 positive T-lymphocytes in live population. Data were analyzed using FlowJo software (version 10, FlowJo LLC, Ashland, OR, USA).

**Crystallization and Crystallographic Analysis.** Sitting drop vapor diffusion protocol was used for setting up drops of the mixture of 1 mM WT STING and 0.5 mM CDN-1 or CDN-24 supplemented with 10 mM EDTA. The crystals grew in drops consisting of 1:1 mixture of protein/ligand complexes and well solution consisting of 0.2 M CaCl<sub>2</sub> and 20% (w/v) PEG 3350 in the case of CDN-1 or 1.6 M NaH<sub>2</sub>PO<sub>4</sub>/0.4 M K<sub>2</sub>HPO<sub>4</sub> and 0.1 M phosphate-citrate buffer, pH 4.2, for CDN-24. Crystals were cryoprotected in the mother liquor supplemented with 20% (v/v) glycerol and flash frozen in liquid nitrogen. A single frozen crystal was used for X-ray data set collection using the home-source or BESSY ID 14-2.<sup>42</sup> Processing of the data sets (integration and scaling) was done by XDS.<sup>43</sup> The structures were solved using the program Phaser<sup>44</sup> of the CCP4 package and molecular replacement strategy (MR) with structure of STING (pdb code 4KSY) as a search model. Ligands were placed in their electron densities by Coot.<sup>45</sup> The structures were refined using Phenix (XYZ coordinates and real-space refinement),<sup>46</sup> and figures were generated using PyMol software.<sup>47</sup> The structures were deposited in the Protein Data Bank, ([www.pdb.org](http://www.pdb.org)) under accession codes 6S27 and 6S26.

**Conformational Sampling.** The ligands were sampled using PRIME algorithm<sup>48</sup> (employing “thorough” setting) as implemented in Schrödinger 2019-1 suite.<sup>49</sup> Obtained structures were subjected to optimization using the Becke-Perdew 86 (BP86) exchange–correlation functional,<sup>50–52</sup> Ahlrichs' def-TZVP basis set,<sup>53</sup> the empirical dispersion correction with zero-damping<sup>54</sup> (denoted as D3), and conductor-like screening model (COSMO) for implicit solvation, with  $\epsilon_r = 80$  corresponding to dielectric constant of water. The single-point energies were calculated using the BP86-D3 and the def2-TZVPD basis set. Both structure optimizations and single-point energies were obtained with TurboMole 7.2 program suite.<sup>55</sup> Solvation (free) energies were calculated using COSMO-RS method<sup>56,57</sup> (conductor-like screening model for realistic solvation) as implemented in COSMOthermX17,<sup>58</sup> employing “BP\_TZVPD\_FINE\_C30\_1701.ctd” parametrization file and FINE cavities (Scosmo\_isorad keyword) with  $\epsilon_r = \infty$  (ideal conductor). The conformational (strain) energy was obtained as difference between the total energy (i.e., sum of single-point and solvation energies) of the bound structure (obtained from QM/MM) and the lowest total free energy of all conformers obtained from conformational sampling.



**QM/MM Methods. Protein Setup.** For QM/MM modeling, we employed the X-ray structure of the STING protein complexes with cyclic [FdA(3',5')pFdA(3',5')p] deposited in the Protein Data Bank ([www.pdb.org](http://www.pdb.org)) under accession code 6T1X, applying appropriate symmetry operation from raw X-ray data. An initial model was built within the YASARA modeling package.<sup>59</sup> H atoms were added to the protein to mimic neutral pH, and their positions were optimized. The glycerol and water molecules were removed from the model. The parameter set used for the protein was AMBER ff03.<sup>60</sup> The ligand was optimized in a vacuum and partial charges on its atoms were obtained by a restrained fit to the electrostatic potential (RESP) at the AM1BCC level.<sup>61</sup>

The YASARA refined model was further equilibrated within the water solvation shell of  $R = 41 \text{ \AA}$  and subjected to simulated annealing and minimization according to standard protocols mentioned in detail in the Supporting Information. The quantum system consisted of approximately 600 atoms (~70 atoms of the ligands, 18 water molecules, and 486 atoms of the STING protein, which included all interacting residues in the vicinity of the ligand; the 3-D structures of the QM systems in QM/MM calculations for studied ligands are deposited in the Supporting Information in PDB format).

In the QM/MM calculations, the standard hydrogen-link atom approach was used; the quantum system was treated at the BP86-D3/DZVP-DFT level, while the MM system was described by the same force field as used in the YASARA (Amber ff03). The QM/MM calculations were done employing ComQum software.<sup>62</sup> Further details are mentioned in the Supporting Information.

## ■ ASSOCIATED CONTENT

### Supporting Information

The Supporting Information is available free of charge at <https://pubs.acs.org/doi/10.1021/acs.jmedchem.9b01062>.

Cloning of pUNO1-hSTING-AQ<sub>2</sub>-Q<sub>2</sub> and -REF plasmids, cloning of pGL64.27-4xSRE plasmid, development of 293T reporter cells, cloning and expression of WT STING protein, cloning of cGAS enzymes, expression and purification of cGAS enzymes, synthesis of CDN-29, synthesis of CDN-35, -36, and -37, molecular docking, details of QM/MM calculations, <sup>1</sup>H, <sup>31</sup>P, and <sup>19</sup>F NMR data of 2',3'CDNs 1–3 and 7–11 and 2',3'-deoxy-CDNs 4–6 and 12–15 in D<sub>2</sub>O, <sup>1</sup>H and <sup>31</sup>P NMR data of 2',3'CDNs 16–26 and 27–32 in D<sub>2</sub>O, <sup>1</sup>H and <sup>31</sup>P NMR data of 2',3'CDNs with thiophosphate groups, 33–37, in D<sub>2</sub>O, yields of CDNs from enzymatic preparation and their HRMS data for prepared CDN analysis, crystallography data collection and processing and structure solution and refinement, effect of CDNs on CD14+ monocyte and CD3+ T-cell populations and cytokine induction in PBMC assay (donor 2), correlation of  $\Delta T_m$  values from DSF assay and EC<sub>50</sub> values from standard or digitonin assay of prepared CDNs, and representative dose–response curves of 5 CDNs from digitonin assay on WT or REF STING haplotypes (PDF)

Structures obtained from computational modeling (ZIP)  
Molecular formula strings (CSV)

### Accession Codes

PDB codes for human STING with bound CDN-1 and CDN-24 are 6S27 and 6S26, respectively.

## ■ AUTHOR INFORMATION

### Corresponding Author

\*Email: [Gabriel.Birkus@uochb.cas.cz](mailto:Gabriel.Birkus@uochb.cas.cz). Phone: (+420) 770-125-014.

## ORCID

Gabriel Birkus: 0000-0002-9850-2150

## Notes

The authors declare no competing financial interest.

## ■ ACKNOWLEDGMENTS

The work was supported by Gilead Sciences, Inc., from European Regional Development Fund, OP RDE; Project “Chemical biology for drugging undruggable targets” (ChemBioDrug, No. CZ.02.1.01/0.0/0.0/16\_019/0000729), and the Grant Agency of the Czech Republic (grant 20-08772S). Computational resources were provided by the IT4Innovations National Supercomputing Center (project LM2015070) and CESNET MetaCentrum (project LM2015042). Our special thanks belong to Kvetoslava Kertisová for her kind assistance with HRMS spectra and Hana Prouzová for help with biochemical assays. We also thank Kamil Hercík for providing us with the plasmid construct used for production of STING protein for crystallographic analysis. We thank HZB for the allocation of synchrotron radiation beamtime.

## ■ ABBREVIATIONS USED

2D-H,H-COSY, two-dimensional homonuclear correlation spectroscopy; 2D-H,H-ROESY, two-dimensional homonuclear rotating Overhauser effect spectroscopy; AMP, adenosine monophosphate; AUC, area under the curve; BSA, bovine serum albumin; CDN, cyclic dinucleotide; DCA, dichloroacetic acid; DCM, dichloromethane; dsDNA, double stranded DNA; DSF, differential scanning fluorimetry; FBS, fetal bovine serum; cGAS, cyclic guanosine adenosine synthase; GMP, guanosine monophosphate; IFN, interferon; IL-6, interleukin 6; IRE3, interferon regulatory factor 3; PBMC, peripheral blood mononuclear cell; PBS, phosphate-buffered saline; STING, stimulator of interferon genes; MP, monophosphate; MS, mass spectroscopy; NDP, nucleotide-5'-diphosphate; NFκB, nuclear factor kappa-light-chain-enhancer of activated B cells; NOE, nuclear Overhauser effect; NTP, nucleotide-5'-triphosphate; PEG, poly(ethylene glycol); TBK1, TANK binding kinase 1; TEAB, triethylammonium bicarbonate; TNFα, tumor necrosis factor α

## ■ REFERENCES

- (1) Danilchanka, O.; Mekalanos, J. J. Cyclic Dinucleotides and the Innate Immune Response. *Cell* **2013**, *154* (5), 962–970.
- (2) Sun, L.; Wu, J.; Du, F.; Chen, X.; Chen, Z. J. Cyclic GMP-AMP Synthase Is a Cytosolic DNA Sensor That Activates the Type-I Interferon Pathway. *Science* **2013**, *339* (6121), 786–791.
- (3) Römmling, U.; Galperin, M. Y.; Gomelsky, M. Cyclic Di-GMP: The First 25 Years of a Universal Bacterial Second Messenger. *Microbiol. Mol. Biol. Rev. MMBR* **2013**, *77* (1), 1–52.
- (4) Corrigan, R. M.; Abbott, J. C.; Burhenne, H.; Kaever, V.; Gründling, A. C-Di-AMP Is a New Second Messenger in *Staphylococcus Aureus* with a Role in Controlling Cell Size and Envelope Stress. *PLoS Pathog.* **2011**, *7* (9), e1002217.
- (5) Davies, B. W.; Bogard, R. W.; Young, T. S.; Mekalanos, J. J. Coordinated Regulation of Accessory Genetic Elements Produces Cyclic Di-Nucleotides for *V. Cholerae* Virulence. *Cell* **2012**, *149* (2), 358–370.
- (6) Ross, P.; Weinhouse, H.; Aloni, Y.; Michaeli, D.; Weinberger-Ohana, P.; Mayer, R.; Braun, S.; de Vroom, E.; van der Marel, G. A.; van Boom, J. H.; Benziman, M. Regulation of Cellulose Synthesis in *Acetobacter Xylinum* by Cyclic Diguanylic Acid. *Nature* **1987**, *325* (6101), 279–281.

- (7) Ablasser, A.; Goldeck, M.; Cavar, T.; Deimling, T.; Witte, G.; Röhl, L.; Hopfner, K.-P.; Ludwig, J.; Hornung, V. cGAS Produces a 2'-5'-Linked Cyclic Dinucleotide Second Messenger That Activates STING. *Nature* **2013**, *498* (7454), 380–384.
- (8) Zhang, X.; Shi, H.; Wu, J.; Zhang, X.; Sun, L.; Chen, C.; Chen, Z. J. Cyclic GMP-AMP Containing Mixed Phosphodiester Linkages Is an Endogenous High-Affinity Ligand for STING. *Mol. Cell* **2013**, *51* (2), 226–235.
- (9) Wu, X.; Wu, F.-H.; Wang, X.; Wang, L.; Siedow, J. N.; Zhang, W.; Pei, Z.-M. Molecular Evolutionary and Structural Analysis of the Cytosolic DNA Sensor cGAS and STING. *Nucleic Acids Res.* **2014**, *42* (13), 8243–8257.
- (10) Gallucci, S.; Maffei, M. E. DNA Sensing across the Tree of Life. *Trends Immunol.* **2017**, *38* (10), 719–732.
- (11) Gao, P.; Ascano, M.; Wu, Y.; Barchet, W.; Gaffney, B. L.; Zillinger, T.; Serganov, A. A.; Liu, Y.; Jones, R. A.; Hartmann, G.; Tuschl, T.; Patel, D. J. Cyclic [G(2',5')PA(3',5')p] Is the Metazoan Second Messenger Produced by DNA-Activated Cyclic GMP-AMP Synthase. *Cell* **2013**, *153* (5), 1094–1107.
- (12) Ishikawa, H.; Barber, G. N. STING Is an Endoplasmic Reticulum Adaptor That Facilitates Innate Immune Signalling. *Nature* **2008**, *455* (7213), 674–678.
- (13) Tsuchiya, Y.; Jounai, N.; Takeshita, F.; Ishii, K. J.; Mizuguchi, K. Ligand-Induced Ordering of the C-Terminal Tail Primes STING for Phosphorylation by TBK1. *EBioMedicine* **2016**, *9*, 87–96.
- (14) Liu, S.; Cai, X.; Wu, J.; Cong, Q.; Chen, X.; Li, T.; Du, F.; Ren, J.; Wu, Y.-T.; Grishin, N. V.; Chen, Z. J. Phosphorylation of Innate Immune Adaptor Proteins MAVS, STING, and TRIF Induces IRF3 Activation. *Science* **2015**, *347* (6227), aar2630.
- (15) Shang, G.; Zhang, C.; Chen, Z. J.; Bai, X.-C.; Zhang, X. Cryo-EM Structures of STING Reveal Its Mechanism of Activation by Cyclic GMP-AMP. *Nature* **2019**, *567* (7748), 389–393.
- (16) Zhang, C.; Shang, G.; Gui, X.; Zhang, X.; Bai, X.-C.; Chen, Z. J. Structural Basis of STING Binding with and Phosphorylation by TBK1. *Nature* **2019**, *567* (7748), 394–398.
- (17) Zhao, B.; Du, F.; Xu, P.; Shu, C.; Sankaran, B.; Bell, S. L.; Liu, M.; Lei, Y.; Gao, X.; Fu, X.; Zhu, F.; Liu, Y.; Laganowsky, A.; Zheng, X.; Ji, J.-Y.; West, A. P.; Watson, R. O.; Li, P. A Conserved PLPLRT/SD Motif of STING Mediates the Recruitment and Activation of TBK1. *Nature* **2019**, *569* (7758), 718–722.
- (18) Fang, R.; Wang, C.; Jiang, Q.; Lv, M.; Gao, P.; Yu, X.; Mu, P.; Zhang, R.; Bi, S.; Feng, J.-M.; et al. NEMO-IKK $\beta$  Are Essential for IRF3 and NF- $\kappa$ B Activation in the cGAS-STING Pathway. *J. Immunol.* **2017**, *199* (9), 3222–3233.
- (19) Musella, M.; Manic, G.; De Maria, R.; Vitale, I.; Sistigu, A. Type-I-Interferons in Infection and Cancer: Unanticipated Dynamics with Therapeutic Implications. *Oncoimmunology* **2017**, *6* (5), e1314424.
- (20) Study of MK-1454 Alone or in Combination With Pembrolizumab in Participants With Advanced/Metastatic Solid Tumors or Lymphomas (MK-1454-001) - Full Text View - ClinicalTrials.gov <https://clinicaltrials.gov/ct2/show/NCT03010176> (accessed Jun 19, 2019).
- (21) Safety and Efficacy of MIW815 (ADU-S100)  $\pm$  Ipilimumab in Patients With Advanced/Metastatic Solid Tumors or Lymphomas - Full Text View - ClinicalTrials.gov <https://clinicaltrials.gov/ct2/show/NCT02675439> (accessed Jun 19, 2019).
- (22) Li, X.-D.; Wu, J.; Gao, D.; Wang, H.; Sun, L.; Chen, Z. J. Pivotal Roles of cGAS-CGAMP Signaling in Antiviral Defense and Immune Adjuvant Effects. *Science* **2013**, *341* (6152), 1390–1394.
- (23) Barber, G. N. STING: Infection, Inflammation and Cancer. *Nat. Rev. Immunol.* **2015**, *15* (12), 760–770.
- (24) Gaffney, B. L.; Veliath, E.; Zhao, J.; Jones, R. A. One-Flask Syntheses of c-Di-GMP and the [Rp,Rp] and [Rp,Sp] Thiophosphate Analogues. *Org. Lett.* **2010**, *12* (14), 3269–3271.
- (25) Clivio, P.; Coatic-Castex, S.; Guillaume, D. (3'-5')-Cyclic Dinucleotides: Synthetic Strategies and Biological Potential. *Chem. Rev.* **2013**, *113* (10), 7354–7401.
- (26) Gillis, E. P.; Eastman, K. J.; Hill, M. D.; Donnelly, D. J.; Meanwell, N. A. Applications of Fluorine in Medicinal Chemistry. *J. Med. Chem.* **2015**, *58* (21), 8315–8359.
- (27) Launer-Felty, K. D.; Strobel, S. A. Enzymatic Synthesis of Cyclic Dinucleotide Analogs by a Promiscuous Cyclic-AMP-GMP Synthetase and Analysis of Cyclic Dinucleotide Responsive Riboswitches. *Nucleic Acids Res.* **2018**, *46* (6), 2765–2776.
- (28) Li, F.; Cimdins, A.; Rohde, M.; Jänsch, L.; Kaefer, V.; Nimtz, M.; Römling, U. DncV Synthesizes Cyclic GMP-AMP and Regulates Biofilm Formation and Motility in *Escherichia Coli* ECOR31. *mBio* **2019**, *10* (2), e02492–02418.
- (29) Kranzusch, P. J.; Lee, A. S. Y.; Wilson, S. C.; Solovkyh, M. S.; Vance, R. E.; Berger, J. M.; Doudna, J. A. Structure-Guided Reprogramming of Human cGAS Dinucleotide Linkage Specificity. *Cell* **2014**, *158* (5), 1011–1021.
- (30) Li, L.; Yin, Q.; Kuss, P.; Maliga, Z.; Millán, J. L.; Wu, H.; Mitchison, T. J. Hydrolysis of 2'3'-CGAMP by ENPP1 and Design of Nonhydrolyzable Analogs. *Nat. Chem. Biol.* **2014**, *10* (12), 1043–1048.
- (31) Altschul, S. F.; Gish, W.; Miller, W.; Myers, E. W.; Lipman, D. J. Basic Local Alignment Search Tool. *J. Mol. Biol.* **1990**, *215* (3), 403–410.
- (32) Khari, S.; Lucas-Hourani, M.; Nisole, S.; Smith, N.; Helynick, O.; Bourguin, M.; Ruffié, C.; Herbeval, J.-P.; Munier-Lehmann, H.; Tangy, F.; Vidalain, P.-O. Identification of a Small Molecule That Primes the Type I Interferon Response to Cytosolic DNA. *Sci. Rep.* **2017**, *7*, 2561.
- (33) Yi, G.; Brendel, V. P.; Shu, C.; Li, P.; Palanathan, S.; Cheng Kao, C. Single Nucleotide Polymorphisms of Human STING Can Affect Innate Immune Response to Cyclic Dinucleotides. *PLoS One* **2013**, *8* (10), e77846.
- (34) Patel, S.; Jin, L. TMEM173 Variants and Potential Importance to Human Biology and Disease. *Genes Immun.* **2019**, *20* (1), 82–89.
- (35) Dassault Systèmes BIOVIA. *Discovery Studio*; 2017 R2; Dassault Systèmes: San Diego, 2017.
- (36) Smola, M.; Birkus, G.; Boura, E. No Magnesium Is Needed for Binding of the Stimulator of Interferon Genes to Cyclic Dinucleotides. *Acta Crystallogr., Sect. F: Struct. Biol. Commun.* **2019**, *75*, 593–598.
- (37) Tosolini, M.; Pont, F.; Bétoux, D.; Ravet, E.; Ligat, L.; Lopez, F.; Pouput, M.; Poirot, M.; Pérouzel, E.; Tiraby, G.; Verhoeyen, E.; Fournié, J.-J. Human Monocyte Recognition of Adenosine-Based Cyclic Dinucleotides Unveils the A2a Gas Protein-Coupled Receptor Tonic Inhibition of Mitochondrially Induced Cell Death. *Mol. Cell Biol.* **2015**, *35* (2), 479–495.
- (38) Birkus, G.; Páv, O.; Jandušik, T.; Rosenberg, I.; Nencka, R. 2'3' Cyclic Dinucleotides with Phosphonate Bond Activating the STING Adaptor Protein. U.S. PatentUS20190185510, June 20, 2019.
- (39) Iyer, R. P.; Sheri, A.; Padmanabhan, S.; Meher, G.; Zhou, S.; Challa, S.; Gimi, R. H.; Cleary, D. Compounds, Compositions, and Methods for the Treatment of Disease. International Patent-WO2018009652A1, August 29, 2019.
- (40) Diner, E. J.; Burdette, D. L.; Wilson, S. C.; Monroe, K. M.; Kellenberger, C. A.; Hyodo, M.; Hayakawa, Y.; Hammond, M. C.; Vance, R. E. The Innate Immune DNA Sensor cGAS Produces a Noncanonical Cyclic Dinucleotide That Activates Human STING. *Cell Rep.* **2013**, *3* (5), 1355–1361.
- (41) Gillerman, I.; Fischer, B. An Improved One-Pot Synthesis of Nucleoside 5'-Triphosphate Analogues. *Nucleosides, Nucleotides Nucleic Acids* **2010**, *29* (3), 245–256.
- (42) Mueller, U.; Darowski, N.; Fuchs, M. R.; Förster, R.; Hellmig, M.; Paithankar, K. S.; Pühringer, S.; Steffen, M.; Zocher, G.; Weiss, M. S. Facilities for Macromolecular Crystallography at the Helmholtz-Zentrum Berlin. *J. Synchrotron Radiat.* **2012**, *19*, 442–449.
- (43) Kabsch, W. XDS. *Acta Crystallogr., Sect. D: Biol. Crystallogr.* **2010**, *66*, 125–132.
- (44) McCoy, A. J.; Grosse-Kunstleve, R. W.; Adams, P. D.; Winn, M. D.; Storoni, L. C.; Read, R. J. Phaser Crystallographic Software. *J. Appl. Crystallogr.* **2007**, *40*, 658–674.

- (45) Debreczeni, J. É.; Emsley, P. Handling Ligands with Coot. *Acta Crystallogr., Sect. D: Biol. Crystallogr.* **2012**, *68*, 425–430.
- (46) Adams, P. D.; Afonine, P. V.; Bunkóczi, G.; Chen, V. B.; Davis, I. W.; Echols, N.; Headd, J. J.; Hung, L.-W.; Kapral, G. J.; Grosse-Kunstleve, R. W.; McCoy, A. J.; Moriarty, N. W.; Oeffner, R.; Read, R. J.; Richardson, D. C.; Richardson, J. S.; Terwilliger, T. C.; Zwart, P. H. PHENIX: A Comprehensive Python-Based System for Macromolecular Structure Solution. *Acta Crystallogr., Sect. D: Biol. Crystallogr.* **2010**, *66*, 213–221.
- (47) Schrödinger LLC. PyMOL; The PyMOL Molecular Graphics System, Version 1.3r1; 2010.
- (48) Sindhikara, D.; Spronk, S. A.; Day, T.; Borrelli, K.; Cheney, D. L.; Posy, S. L. Improving Accuracy, Diversity, and Speed with Prime Macrocycle Conformational Sampling. *J. Chem. Inf. Model.* **2017**, *57* (8), 1881–1894.
- (49) Schrödinger LLC. *Maestro*; Schrödinger Release 2019-1; Schrödinger Suites: New York, NY, 2019.
- (50) Becke, A. D. Density-Functional Exchange-Energy Approximation with Correct Asymptotic Behavior. *Phys. Rev. A: At, Mol, Opt. Phys.* **1988**, *38* (6), 3098–3100.
- (51) Vosko, S. H.; Wilk, L.; Nusair, M. Accurate Spin-Dependent Electron Liquid Correlation Energies for Local Spin Density Calculations: A Critical Analysis. *Can. J. Phys.* **1980**, *58* (8), 1200–1211.
- (52) Perdew, J. P. Density-Functional Approximation for the Correlation Energy of the Inhomogeneous Electron Gas. *Phys. Rev. B: Condens. Matter Mater. Phys.* **1986**, *33* (12), 8822–8824.
- (53) Weigend, F.; Ahlrichs, R. Balanced Basis Sets of Split Valence, Triple Zeta Valence and Quadruple Zeta Valence Quality for H to Rn: Design and Assessment of Accuracy. *Phys. Chem. Chem. Phys.* **2005**, *7* (18), 3297–3305.
- (54) Grimme, S.; Antony, J.; Ehrlich, S.; Krieg, H. A Consistent and Accurate Ab Initio Parametrization of Density Functional Dispersion Correction (DFT-D) for the 94 Elements H-Pu. *J. Chem. Phys.* **2010**, *132* (15), 154104.
- (55) TURBOMOLE 7.2 2017, a Development of the University of Karlsruhe and Forschungszentrum Karlsruhe GmbH 1989–2007, TURBOMOLE GmbH since 2007.
- (56) Klamt, A. Conductor-like Screening Model for Real Solvents: A New Approach to the Quantitative Calculation of Solvation Phenomena. *J. Phys. Chem.* **1995**, *99* (7), 2224–2235.
- (57) Klamt, A.; Jonas, V.; Bürger, T.; Lohrenz, J. C. W. Refinement and Parametrization of COSMO-RS. *J. Phys. Chem. A* **1998**, *102* (26), 5074–5085.
- (58) Eckert, F.; Klamt, A. *COSMOthermX17*, Version C3.0, Release 15.01; COSMOlogic GmbH & Co. KG; Leverkusen, Germany, 2014.
- (59) Krieger, E.; Joo, K.; Lee, J.; Lee, J.; Raman, S.; Thompson, J.; Tyka, M.; Baker, D.; Karplus, K. Improving Physical Realism, Stereochemistry, and Side-Chain Accuracy in Homology Modeling: Four Approaches That Performed Well in CASP8. *Proteins: Struct., Funct., Genet.* **2009**, *77*, 114–122.
- (60) Duan, Y.; Wu, C.; Chowdhury, S.; Lee, M. C.; Xiong, G.; Zhang, W.; Yang, R.; Cieplak, P.; Luo, R.; Lee, T.; Caldwell, J.; Wang, J.; Kollman, P. A Point-Charge Force Field for Molecular Mechanics Simulations of Proteins Based on Condensed-Phase Quantum Mechanical Calculations. *J. Comput. Chem.* **2003**, *24* (16), 1999–2012.
- (61) Jakalian, A.; Jack, D. B.; Bayly, C. I. Fast, Efficient Generation of High-Quality Atomic Charges. AM1-BCC Model: II. Parameterization and Validation. *J. Comput. Chem.* **2002**, *23* (16), 1623–1641.
- (62) Ryde, U.; Olsson, M. H. M. Structure, Strain, and Reorganization Energy of Blue Copper Models in the Protein. *Int. J. Quantum Chem.* **2001**, *81* (5), 335–347.

## Supporting Information

# Enzymatic Preparation of 2'-5', 3'-5' Cyclic Dinucleotides, Their Binding Properties to Stimulator of Interferon Genes Adaptor Protein and Structure/Activity Correlations

*Barbora Novotná<sup>1,2</sup>, Lenka Vaneková<sup>1,2</sup>, Martin Zavřel<sup>1</sup>, Miloš Buděšínský<sup>1</sup>, Milan Dejmek<sup>1</sup>,  
Miroslav Smola<sup>1</sup>, Ondřej Gutten<sup>1</sup>, Zahra Aliakbar Tehrani<sup>1</sup>, Markéta Pimková Polidarová<sup>1,2</sup>,  
Andrea Brázdová<sup>1</sup>, Radek Liboska<sup>1</sup>, Ivan Štěpánek<sup>1</sup>, Zdeněk Vavřina<sup>1,2</sup>, Tomáš Jandušík<sup>1,3</sup>,  
Radim Nencka<sup>1</sup>, Lubomír Rulišek<sup>1</sup>, Evžen Bouřa<sup>1</sup>, Jiří Brynda<sup>1</sup>, Ondřej Páv<sup>1</sup> and Gabriel  
Birkuš<sup>1,\*</sup>*

<sup>1</sup>Institute of Organic Chemistry and Biochemistry of the Czech Academy of Sciences and Gilead  
Sciences Research Centre at IOCB, Flemingovo nám. 2, Prague, 16610, Czech Republic

<sup>2</sup>Faculty of Science, Charles University, Prague, 110 00, Czech Republic

<sup>3</sup>Faculty of Food and Biochemical Technology, University of Chemistry and Technology,  
Prague, 166 28, Czech Republic

S1

**Table of Contents:**

## 1. Supplemental materials

## 2. Supplemental methods

Cloning of pUNO1- hSTING-AQ, -Q, and -REF plasmids.

Cloning of pGL64.27-4xISRE plasmid.

Development of 293T reporter cells.

Cloning and expression of *wt* STING protein.

Cloning of cGAS enzymes.

Expression and Purification of cGAS enzymes.

Synthesis of CDN-29.

Synthesis of CDN-35, -36, -37.

Molecular docking.

Details of QM/MM Calculations.

## 3. Supplemental data

**Table S1a.** The  $^1\text{H}$ ,  $^{31}\text{P}$  and  $^{19}\text{F}$  NMR data of 2',3'-CDNs **1 – 3** and **7 – 11** in  $\text{D}_2\text{O}$ .

**Table S1b.** The  $^1\text{H}$ ,  $^{31}\text{P}$  and  $^{19}\text{F}$  NMR data of 2',3'-deoxy CDNs **4 – 6** and **12 – 15** in  $\text{D}_2\text{O}$ .

**Table S2.** The  $^1\text{H}$  and  $^{31}\text{P}$  NMR data of 2',3'-CDNs **16 – 26** in  $\text{D}_2\text{O}$ .

**Table S3.** The  $^1\text{H}$  and  $^{31}\text{P}$  NMR data of 2',3'-CDNs **27 – 32** in  $\text{D}_2\text{O}$ .

**Table S4.** The  $^1\text{H}$  and  $^{31}\text{P}$  NMR data of 2',3'-CDNs with thiophosphate groups **33 – 37** in  $\text{D}_2\text{O}$ .

**Table S5.** Yields of CDNs from enzymatic preparation and their HRMS data for prepared CDNs analysis.

**Table S6.** Crystallography data collection and processing.

**Table S7.** Crystallography structure solution and refinement.

**Table S8.** Effect of CDNs on CD14<sup>+</sup> monocyte and CD3<sup>+</sup> T-cell populations and cytokine induction in PBMC Assay (Donor 2).

**Figure S1.** Correlation of  $\Delta T_m$  values from DSF Assay and  $\text{EC}_{50}$  values from Standard or Digitonin Assay of prepared CDNs.

**Figure S2.** Representative dose response curves of 5 CDNs from Digitonin Assay on WT or REF STING haplotypes.

**Supplementary files**

Structures obtained from computational modeling.

Molecular Formula Strings.

## 1. SUPPLEMENTAL MATERIALS

pUNO1-hSTING-WT, pUNO1-hSTING-HAQ, 3'3'-c-di-GMP, 2'3'-cGAMP, 3'3'-cGAMP, 3'3'-c-di-AMP, 2'2'-cGAMP, and blasticidin were purchased from InvivoGen (San Diego, USA). Lipofectamine 2000, OptiMEM medium, SYPRO Orange and hygromycin were purchased from ThermoFisher (Waltham, USA). STING antibody (cat. #. MAB7169) and Mouse IgG HRP-conjugated Antibody (cat. #. HAF007) were supplied by R&D Systems (Minneapolis, USA). DMEM with high glucose, FBS, poly-D-lysine, Digitonin A, sucrose, DTT, HEPES, BSA, ATP, GTP and other common chemicals were purchased from Sigma Aldrich (Prague, Czech Republic). 293T cells were obtained from ATCC (Manassas, USA). Phusion® High-Fidelity DNA Polymerase, Q5® Site-Directed Mutagenesis Kit, HindIII, BglII, NdeI, NotI and BamHI were delivered by NEB (Ipswich, USA). Luciferase Assay System reagent was purchased from Promega (Madison, USA). Rosetta-gami B (DE3) competent cells, Amicon® Ultra-15 10 K, were from Merck Millipore (Billerica, USA). Ni-NTA resin (cat. # 745400.25 Macherey-Nagel, Düren, Germany).

## 2. SUPPLEMENTAL METHODS

### **Cloning of pUNO1-hSTING-AQ, pUNO1-hSTING-Q and pUNO1-hSTING-REF plasmids**

pUNO1-hSTING-Q and pUNO1-hSTING-REF were prepared by site-directed mutagenesis of pUNO1-hSTING-WT with NEB Q5® Site-Directed Mutagenesis Kit and primers STING\_R293Q\_F (AGACACTTGAGGACATCCTG) and STING\_R293Q\_R (GGCAGAAGAGTTTGGCCTGC) and STING\_R232H\_F (ATGCTGGCATCAAGGATCGG) and STING\_R232H\_R (GGTCACCGGTCTGCTGGGGC). Allelic version AQ was prepared by restriction of plasmids pUNO1-hSTING-WT and pUNO1-hSTING-HAQ with enzymes BgIII and EcoRI (NEB). The smaller fragment from pUNO1-hSTING-HAQ, carrying only the STING AQ mutations, was ligated into pUNO1-hSTING-WT plasmid backbone. This subcloning resulted in plasmid pUNO1-hSTING-AQ. All the constructs were sequenced for verification.

### **Cloning of pGL4.27-4xISRE plasmid**

Two complementary oligonucleotides of the sequence AAAGATCTTGAAAGTGAAACCTTGAAAAACGAAACTGGACAAAGGGAAACTGCA GAAACTGAAACAAAGCTTAA and TTAAGCTTTGTTTCAGTTTCTGCAGTTTCCCTTTGTCCAGTTTCGTTTTCCAAGGTTTC ACTTTCCAAGATCTTT containing four interferon-sensitive response elements (ISRE) were synthesized by Sigma Aldrich (Prague, Czech Republic). The oligonucleotides were mixed in equal molar amounts, hybridized, and cleaved by restriction endonucleases HindIII and BgIII. Ultimately, they were ligated into plasmid pGL4.27 (Promega, Madison, USA) linearized with the same enzymes. As result the sequence with four ISRE sites was placed upstream of the minimum promoter of firefly luciferase reporter gene.

S4

#### **Development of 293T reporter cells**

293T cells were seeded a day before transfection at density 125,000 cells per cm<sup>2</sup> onto poly-D-lysine coated six well plates in antibiotic free DMEM medium with high glucose supplemented with 10% heat inactivated FBS. On the day of transfection, 2.5 µg of the plasmid pUNO1-hSTING-WT, pUNO1- hSTING-HAQ, pUNO1- hSTING-AQ, pUNO1-hSTING-Q or pUNO1-hSTING-REF encoding human WT, HAQ (R71H, G230A and R293Q), AQ (G230A and R293Q), Q (R293Q) or REF STING (R232H)<sup>1</sup> were diluted in 125 µL OptiMEM medium and mixed with 125 µL of the same medium containing 12.5 µL of Lipofectamine 2000. After 5 min incubation at room temperature (RT), 250 µL of the mixture was added dropwise to the cells in one well. Cells were incubated 36 hours at 37 °C with 5% CO<sub>2</sub>, and then detached with 0.05% Trypsin and 0.22 g/L EDTA. Transfected cells were seeded onto poly-D-lysine coated six well plates at density 50,000 cells per 1 cm<sup>2</sup> in DMEM medium with high glucose containing 10% heat inactivated FBS, 30µg/mL blasticidin, 0.06 mg/ml Penicillin G and 0.1mg/ml Streptomycin Sulfate. The medium was replenished every 3 – 4 days until visible colonies of cells resistant to blasticidin were formed. Blasticidin resistant cells stably expressing different variants of STING protein were further transfected with pGL64.27-4xISRE plasmid following the same procedure as described above. The transfected cells were selected for the resistance to 300 µg/mL hygromycin in DMEM with high glucose containing 10% heat inactivated FBS, 30µg/mL blasticidin, 0.06 mg/ml Penicillin G and 0.1 mg/ml Streptomycin Sulfate. Homogeneous culture of stably double transfected cells was prepared by limiting dilution of cells in 96 well plates and wells with cells were selected that originated from a single cell. These cells were expanded, and expression of *wt* STING was confirmed by western blot using monoclonal mouse anti STING antibodies (cat. #. MAB7169, 1:1000 dilution; 2<sup>o</sup> antibody cat. #. HAF007, 1:2000 dilution, both from R&D Systems,



Minneapolis, USA), and by induction of firefly luciferase expression in the presence of 50  $\mu$ M STING agonist 2'3' cGAMP. Genomic DNA from the transfected cells was amplified with primers pUNO1\_Seq\_F (TGCTTGCTCAACTCTACGTC) and pUNO1\_Seq\_R (GTGGTTTGTCCAAACTCATC) that were complementary to pUNO1 plasmids and the presence of correct STING gene variant in the transfected cells was confirmed by DNA sequencing.

#### **Cloning, expression and purification of *wt* STING protein**

Human *wt* STING cDNA was amplified by the use of PCR by employing Phusion® High-Fidelity DNA Polymerase and oligonucleotides hSTING140-BamH-For (GTGGGATCCGCCCGCTGAGATCTCTGCAG) and hSTING379-Not-Rev3 (TATGCGGCGCCTATTACACAGTAACCTCTTCCTTTTC) from pUNO1-hSTING-WT. Purified PCR products were cleaved with restriction enzymes BamHI and NotI and cloned into the pSUMO vector linearized with the identical enzymes. Plasmid pSUMO was created by introducing 8-His-SUMO sequence between NdeI and BamHI sites of pHis-parallel2 plasmid. pSUMO- *wt* STING thus encoded truncated human *wt* STING (amino acid residues 140-343) with N-terminal 8xHis and SUMO tag. The recombinant *wt* STING protein was overexpressed in Rosetta-gami B (DE3) competent cells. Bacterial pellets were re-suspended in ice-cold lysis buffer containing 50 mM Tris-Cl pH 8.0, 300 mM NaCl, 3 mM  $\beta$ -mercaptoethanol, 10% (v/v) glycerol, and 20 mM imidazole using Dounce homogenizer. DNase I and RNase A were added (final concentration 50  $\mu$ g/ml) together with MgCl<sub>2</sub> (final concentration 5 mM) to the homogenate and bacteria were lysed using French Press G-M™ High-Pressure Cell Press Homogenizer (1500 psi, 3 cycles). Lysates were spun 30,000 g for 20 min and supernatant was gently stirred with Ni-NTA resin for 30 min. The resin was poured into a chromatography column, washed with 50 ml buffer A (50 mM Tris-Cl (pH 8.0), 800 mM NaCl, 3 mM  $\beta$ -mercaptoethanol; 10% glycerol; 20 mM imidazole) and 8-His-SUMO tagged STING proteins were eluted with 15 ml buffer A containing 300 mM imidazole. The eluted protein was cleaved with recombinant SUMO protease (80  $\mu$ g/ml of protein solution). STING protein

was further purified by size exclusion chromatography using HiLoad 16/60 Superdex 75 (GE Healthcare Bio-Sciences, Pittsburgh, USA) in 50 mM Tris-Cl buffer pH 7.4 containing 150 mM NaCl, and 10% glycerol. For crystallography experiment, the protein was also passed through ion exchange chromatography on HiTrap™ Q HP (GE Healthcare, Bio-Sciences, Pittsburgh, USA) column (Buffer A: 50 mM NaCl, 50 mM Tris-HCl pH 7.4; buffer B: 1 M NaCl, 50 mM Tris-HCl pH 7.4). Protein was concentrated with Amicon® Ultra-15 10 K device and flash frozen in liquid N<sub>2</sub>.

### **Cloning of cGAS Enzymes**

Exons encoding chicken cGAS were amplified using Q5 polymerase from chicken (*Gallus gallus*) genomic DNA using oligonucleotides:

pET22b\_gcGAS\_Rec\_F (TTTAAGAAGGAGATATACATATGGAGGAGACCGCGCGGG),  
gcGAS\_E1R (CTTGACGTGCTCGTAGTAGC), gcGAS\_E2F  
(GCTACTACGAGCACGTC AAGATATCTGAACCAAATGAGTT), gcGAS\_E2R  
(TTTTAATGTGTTTTAGTTCT), gcGAS\_E3F  
(AGAACTAAAACACATTA AAAATGTGGAAGTAACTGTGAAA), gcGAS\_E3R  
(CTCTTGGGAGCTTTTCTTTT), gcGAS\_E4F  
(AAAAGAAAAGCTCCCAAGAGGAAACACCTGGCGACTCTCT), gcGAS\_E4R  
(CTGCAACACTTCACTCCATC), gcGAS\_E5F  
(GATGGAGTGAAGTGTGCAGGAAAGATTGTCTCAA ACTTC) and gcGAS\_6His\_Rec\_R2  
(TGGTGCTCGAGTGC GCGCCGCCACCTGGTGAAATACTGGGA). All the PCR products  
were pooled together, mixed with NdeI+HindIII restricted plasmid pET-22b(+) and recombined  
using Gibson Assembly® Master Mix (New England Biolabs) according to the manufacturer's  
instructions. Positive clones were sequenced and compared to the database. This resulted in  
plasmid pET-22b(+) gcGAS.

S7

Exons encoding human cGAS were amplified using Q5 polymerase from genomic DNA of HepG2 cells using oligonucleotides pET22b\_hcGAS\_Rec\_F (TTTAAGAAGGAGATATACATATGCAGCCTTGGCACGGAAA), hcGAS\_E1R (CTTCACGTGCTCATAGTAGC), hcGAS\_E2F (GCTACTATGAGCACGTGAAGATTTCTGCACCTAATGAATT), hcGAS\_E2R (CTTTAATGTCGTTAATTTCT), hcGAS\_E3F (AGAAATTAACGACATTAAGATACAGATGTCATCATGAAG), hcGAS\_E3R (CTTGGAACCATTTCTTCC), hcGAS\_E4F (GGAAGGAAATGGTTTCCAAGAAGAAACATGGCG,GCTATCC), hcGAS\_E4R (CTGCAACATTTCTTCTTT), hcGAS\_E5F (AAAGAAGAGAAATGTTGCAGGAAAGATTGTTTAAACTAA) and hcGAS\_6His\_Rec\_R (TGGTGCTCGAGTGCGCCGCAAATTCATCAAAAAGTGGAA). All the PCR products were pooled together, mixed with NdeI+HindIII restricted plasmid pET-22b(+) and recombined using Gibson Assembly® Master Mix (New England Biolabs) according to the manufacturer's instructions. Positive clones were sequenced and compared to the database. This resulted in plasmid pET-22b(+) hcGAS.

Two version of mouse cGAS cDNAs were prepared. Truncated version of *E. coli* codon optimized mouse cGAS, lacking N-terminus and encoding AA 147-507, was chemically synthesized by GenSYS company and cloned into pET-22b(+) between NdeI and XhoI sites (resulting in plasmid pET-22b(+) mcGAS-S). For full-length mouse cGAS, an additional N-terminus has been amplified from BALB/c mouse gut gDNA using Q5 polymerase and oligonucleotides mcGAS\_N-term\_F (TTTAAGAAGGAGATATACATATGGAAGATCCGCGTAGAAG) and mcGAS\_N-term\_R (ACCTTCTCAGTTTATCCGGTTCCTTCCTGGACCCTCGCG). PCR product was

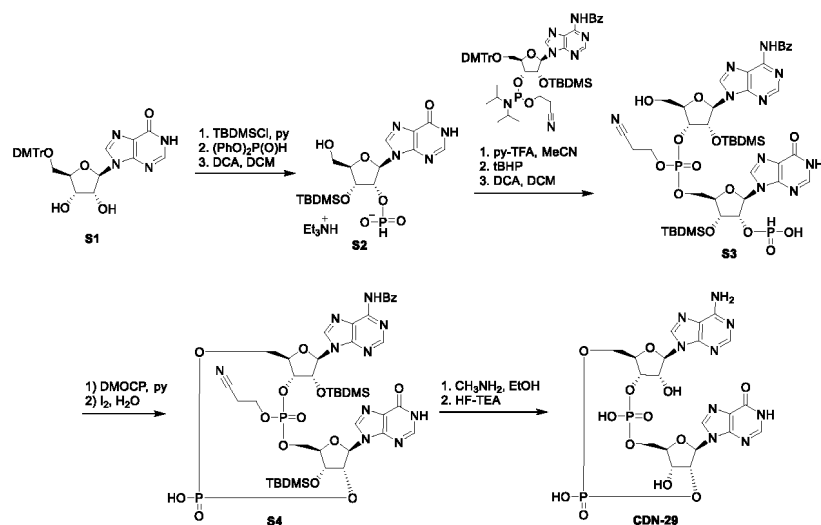
S8

mixed with NdeI restricted plasmid pET-22b(+) mcGAS-S and recombined using Gibson Assembly® Master Mix (New England Biolabs) according to the manufacturer's instructions. Positive clones were sequenced. This resulted in plasmid pET-22b(+) mcGAS-L.

#### **Expression and Purification of cGAS Enzymes**

The protein (chicken, human or murine full-length and truncated cGAS) was overexpressed in *E. coli* BL21 (DE3) (ThermoFisher, Waltham, USA). Bacterial pellet was re-suspended in ice-cold lysis buffer containing 20 mM Phosphate Na buffer (pH 7.4), 500 mM NaCl, 10% glycerol, and 20 mM imidazole using Dounce homogenizer. DNase I and RNase A were added (final concentration 50 µg/ml) together with MgCl<sub>2</sub> (final concentration 5mM) to the homogenate and bacteria were lysed using MSE Soniprep 150 (3 mm Tip Solid Titanium Exponential Probe, 2 min, 50% power, amplitude 12 microns). The lysate was spun at 30,000 x g for 20 min and supernatant was loaded onto 5 mL HisTrap column (GE Healthcare BioSciences, Pittsburgh, USA). The resin was washed with 50 ml lysis buffer and protein was eluted with 15 ml 20 mM Phosphate-Na buffer (pH 7.4) buffer containing 500 mM NaCl; 10% glycerol, and 300 mM imidazole. The protein was further purified by size exclusion chromatography using HiLoad 16/60 Superdex 75 in buffer containing 150 mM NaCl; 50 mM Tris (pH 7.4), and 10% glycerol. The protein buffer was exchanged for 50% glycerol, 50 mM Tris (pH 7.6), 100 mM NaCl, 1 mM DTT, 1 mM EDTA with Amicon® Ultra-15 10 K Device (Merck Millipore Ltd.), and proteins were flash frozen in liquid N<sub>2</sub> and stored at -80°C for further use.

## Synthesis of CDN-29



(2*R*,3*R*,4*R*,5*R*)-4-((tert-butylidimethylsilyl)oxy)-5-(hydroxymethyl)-2-(6-oxo-1,6-dihydro-9*H*-purin-9-yl)tetrahydrofuran-3-yl phosphonate, TEA<sup>+</sup> salt (**S2**):

5'-DMTr inosine **S1** (Carbosynth Ltd., 2 g, 3.5 mmol) was azeotroped with pyridine (2x 10 mL), dissolved in pyridine (40 mL) and then imidazole (479 mg, 7 mmol) followed by TBDMSCl (530 mg, 3.5 mmol) were added. After stirring the reaction mixture at ambient temperature for 12 hours it was diluted with AcOEt (200 mL), washed with saturated aqueous solution of  $\text{NaHCO}_3$  and water. Organic phase was dried over sodium sulfate and evaporated to afford a 1:1 mixture of 2' and 3' silylated products. Small amounts (< 5%) of starting material as well as double silylated compounds were also observed. Isomers were not isolated due to migration of the silyl group.

Crude mixture of silylated intermediates (3 g) was azeotroped with pyridine (2 x 15 mL), dissolved in dry pyridine (10 mL) and diphenyl phosphite (85%, 3 mL) was added in one portion. After stirring at ambient temperature for 20 min, TEA (4 mL) was added followed by water (4 mL) and the reaction was stirred for

further 20 min. Resulting solution was diluted with dichloromethane (200 mL) and washed with saturated aqueous solution of NaHCO<sub>3</sub> (75 mL). Water phase was extracted with dichloromethane (2 x 150 mL). Combined organic phases were dried over sodium sulfate and evaporated. Residue was adsorbed on silica and applied on a FCC column (DCM/1% Et<sub>3</sub>N-MeOH 5 to 30%), where good separation of isomers was achieved and the desired product eluted as the second eluting isomer (1.5 g, 95% purity).

To a solution of this intermediate in dichloromethane (10 mL) was added water (360  $\mu$ L, 20 mmol) followed by a solution of DCA (1.5 mL, 18 mmol) in dichloromethane (4 mL). Reaction mixture was stirred at ambient temperature for 30 min, after which it was quenched with triethylsilane (3.6 mL). Reaction mixture was then stirred for 1 hour and then pyridine (4 mL) was added and all volatiles were evaporated. Purification on reverse phase FCC (ACN in water, 0-30%) afforded **S2** (600 mg, 31% over 3 steps).

<sup>1</sup>H NMR (401 MHz, DMSO-*d*<sub>6</sub>)  $\delta$  8.33 (s, 1H), 8.02 (s, 1H), 6.49 (d, *J* = 591.1 Hz, 1H), 5.96 (d, *J* = 6.6 Hz, 1H), 5.24 (bs, 1H), 5.05 (ddd, *J* = 11.0, 6.6, 4.7 Hz, 1H), 4.42 (dd, *J* = 4.7, 2.6 Hz, 1H), 3.94 (td, *J* = 4.1, 2.5 Hz, 1H), 3.63 (dd, *J* = 11.9, 4.5 Hz, 1H), 3.52 (dd, *J* = 11.9, 3.9 Hz, 1H), 0.90 (s, 9H), 0.13 and 0.13 (s, 3H).

<sup>13</sup>C NMR (101 MHz, DMSO)  $\delta$  156.82, 148.62, 146.18, 139.19, 124.53, 86.80, 86.08 (d, *J* = 5.0 Hz), 74.83 (d, *J* = 4.2 Hz), 72.32 (d, *J* = 2.5 Hz), 61.28, 45.40, 26.06, 18.21, 8.57, -4.17, -4.81.

<sup>31</sup>P NMR (162 MHz, DMSO)  $\delta$  2.08.

(1R,6R,8R,9R,10S,15R,17R,18R)-8-(6-amino-9H-purin-9-yl)-3,9,12,18-tetrahydroxy-17-(6-oxo-6,9-dihydro-1H-purin-9-yl)-2,4,7,11,13,16-hexaoxa-3 $\lambda$ ,5,12 $\lambda$ ,5-diphosphatricyclo[13.2.1.0<sup>6,9</sup>]octadecane-3,12-dione (**CDN-29**)

A mixture of **S2** (55 mg, 0.1 mmol) and pyridinium trifluoroacetate (py-TFA, 29 mg, 0.15 mmol) was codistilled with dry MeCN (3 x 3 mL), suspended in dry MeCN (2 mL) and stirred overnight in a sealed vessel over activated molecular sieves. In a separate flask, *N*-benzoyl-5'-*O*-[bis(4-

S11

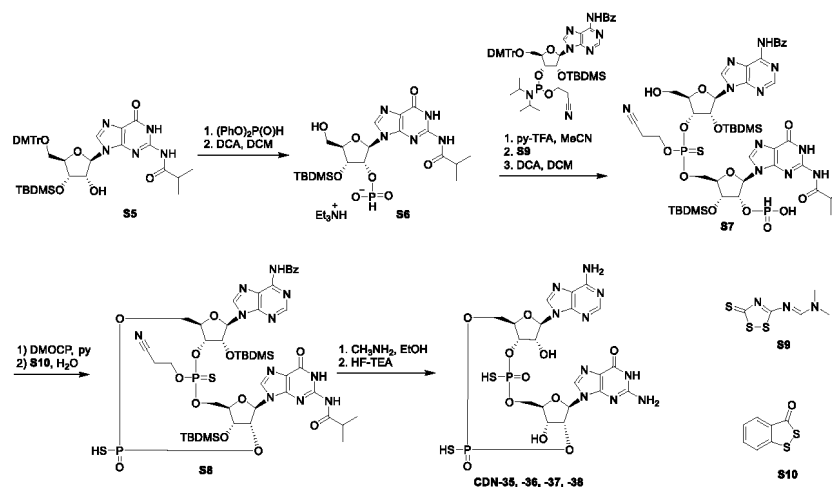
methoxyphenyl)phenylmethyl]-2'-O-[(1,1-dimethylethyl)dimethylsilyl]-adenosine (124 mg, 0.125 mmol, Sigma-Aldrich) was codistilled with dry MeCN (3x 3 mL), dissolved in dry MeCN (1 mL) and stirred overnight in a sealed vessel over activated molecular sieves. A solution of phosphoramidite was transferred *via syringe* to the flask with the suspension of **S2** with py-TFA and the resulting solution was stirred for 1 hour at ambient temperature. tert-Butyl hydroperoxide (tBHP, 5.5M solution in decane, 55  $\mu$ L, 0.3 mmol) was added and the reaction mixture was stirred for further 30 min. Reaction mixture was quenched with NaHSO<sub>3</sub> (39% soln. in water, 54  $\mu$ L, 0.27 mmol), filtered and evaporated. To a solution of the crude tritylated linear dimer in DCM (3 mL) was added water (18  $\mu$ L, 1 mmol) and a solution of DCA (74  $\mu$ L, 0.9 mmol) in DCM (3 mL) dropwise. After stirring the reaction mixture for 30 min, triethylsilane (1.5 mL) was added and the reaction mixture was stirred for further 90 min, after which it was quenched with pyridine (1.5 mL). Volatiles were evaporated and crude **3** was co-distilled with dry pyridine (3x 3 mL) and used in the next reaction without further purification.

To a solution of crude **S3** in pyridine (2 mL) was added DMOCP (65 mg, 0.35 mmol) and reaction mixture was stirred at ambient temperature for 1 hour. Water (59  $\mu$ L, 0.35 mmol) was added followed by iodine (34 mg, 0.13 mmol) and reaction mixture was stirred for 10 min, after which it was cooled down to 0 °C and quenched by the addition of NaHSO<sub>3</sub> (39% soln. in water, 49  $\mu$ L, 0.25 mmol). Purification on reverse phase FCC (MeCN in 50 mM aqueous NH<sub>4</sub>HCO<sub>3</sub> 0-70%) afforded **S4**.

A solution of **S4** in CH<sub>3</sub>NH<sub>2</sub> (33% in ethanol, 1 mL) was stirred at ambient temperature for 3 hours. Volatiles were evaporated and the residue was co-distilled with pyridine (3x 2 mL), dissolved in pyridine-TEA (1:1, v/v, 1 mL) and HF-TEA (160  $\mu$ L, 1 mmol) was added dropwise. Reaction mixture was stirred at 50 °C for 1 hour, quenched with 1M ammonium acetate (2 mL) and purified on preparative HPLC (ACN in 0.1M TEAB, 0-30%). Appropriate fractions were pooled, evaporated, co-distilled with water (3x 5 mL) and methanol (3x 5 mL), dissolved in water (10 mL) and slowly passed through a 2 mL column of Dowex 50 (Na<sup>+</sup> cycle). Freeze-drying the eluent afforded the sodium salt **CDN-29**. NMR and HRMS data can be found in Table S3 and Table S5.

S12

### Synthesis of CDN-35, -36, -37



(2*R*,3*R*,4*R*,5*R*)-4-((tert-butyldimethylsilyl)oxy)-5-(hydroxymethyl)-2-(2-isobutyramido-6-oxo-1,6-dihydro-9*H*-purin-9-yl)tetrahydrofuran-3-yl phosphonate TEA<sup>+</sup> salt (**S6**):

Protected guanosine **S5** (ChemGenes, 2 g, 2.6 mmol) was azeotroped with pyridine (2x 10 mL), dissolved in dry pyridine (10 mL) and diphenyl phosphite (85%, 1.8 mL) was added in one portion. After stirring at ambient temperature for 20 min, TEA (3 mL) was added followed by water (3 mL) and the reaction was stirred for further 20 min. Resulting solution was diluted with dichloromethane (150 mL) and washed with saturated aqueous solution of  $\text{NaHCO}_3$  (60 mL). Water phase was extracted with dichloromethane (2 x 150 mL). Combined organic phases were dried over sodium sulfate and evaporated.

To a solution of this intermediate in dichloromethane (10 mL) was added water (468  $\mu\text{L}$ , 26 mmol) followed by a solution of DCA (2 mL, 24 mmol) in dichloromethane (10 mL). Reaction mixture was stirred at ambient temperature for 30 min, after which it was quenched with triethylsilane (3.6 mL). Reaction mixture was then stirred for 1 hour and then pyridine (4 mL) was added and all volatiles were evaporated. Purification on reverse phase FCC (ACN in water, 0-30%) afforded **S6** (1.2 g, 71% over 2 steps).

S13



<sup>1</sup>H NMR (501 MHz, DMSO-*d*<sub>6</sub>) δ 12.10 (s, 1H), 11.78 (s, 1H), 10.69 (bs, 1H), 8.29 (s, 1H), 6.55 (d, *J* = 595.7 Hz, 1H), 5.88 (d, *J* = 7.4 Hz, 1H), 5.30 (s, 1H), 5.12-5.02 (m, 1H), 4.36 (dd, *J* = 4.8 Hz, *J* = 1.6 Hz, 1H), 3.97-3.88 (m, 1H), 3.55 (ddt, 1H), 2.91 (q, *J* = 7.3 Hz, 6H), 2.76 (hept, *J* = 6.9 Hz, 1H), 1.11 (dd, *J* = 7.3 Hz), 1.07 (t, *J* = 7.3 Hz, 9H), 0.89 (s, 9H), 0.13 and 0.13 (s, 3H).

<sup>13</sup>C NMR (101 MHz, DMSO) δ 180.37, 155.00, 149.39, 148.41, 138.06, 120.16, 87.26, 84.72 (d, *J* = 5.1 Hz), 74.61 (d, *J* = 4.1 Hz), 72.63, 61.25, 45.36, 34.92, 26.00, 19.08, 18.18, 8.50, -4.26, -4.88.

<sup>31</sup>P NMR (202.4 MHz, DMSO-*d*<sub>6</sub>) δ 2.17 (s).

(1R,6R,8R,9R,10S,15R,17R,18R)-17-(2-amino-6-oxo-6,9-dihydro-1H-purin-9-yl)-8-(6-amino-9H-purin-9-yl)-9,18-dihydroxy-3,12-disulfanyl-2,4,7,11,13,16-hexaoxa-3λ<sup>5</sup>,12λ<sup>5</sup>-

diphosphatricyclo[13.2.1.0<sup>6,10</sup>]octadecane-3,12-dione (**CDN-35**, **-36**, **-37**)

A mixture of **S6** (55 mg, 0.1 mmol) and pyridinium trifluoroacetate (29 mg, 0.15 mmol) was codistilled with dry MeCN (3x 3 mL), suspended in dry MeCN (1 mL) and stirred overnight in a sealed vessel over activated molecular sieves. In a separate flask, *N*-benzoyl-5'-*O*-[bis(4-methoxyphenyl)phenylmethyl]-2'-*O*-[(1,1-dimethylethyl)dimethylsilyl]-adenosine (123 mg, 0.125 mmol, CAS # 136834-22-5, purchased from Sigma-Aldrich) was codistilled with dry MeCN (3x 3 mL), dissolved in dry MeCN (1 mL) and stirred overnight in a sealed vessel over activated molecular sieves. A solution of the commercial phosphoramidite was transferred *via syringe* to the flask with the suspension of **S6** with py-TFA and the resulting solution was stirred for 1 hour at ambient temperature. 3-((*N,N*-dimethylaminomethylidene)amino)-3H-1,2,4-dithiazole-5-thione (23 mg, 0.11 mmol) was added and the reaction mixture was stirred for further 30 min. Volatiles were evaporated, residue was dissolved in DCM (3 mL) and water (18 mL, 1 mmol) was added followed by a solution of DCA (74 mL, 0.9 mmol) in DCM (3 mL). After stirring the reaction mixture for 30 min, triethylsilane (1.5 mL) was added and the reaction mixture was stirred for further 90 min, after which it was quenched by the addition of pyridine (1.5 mL). Volatiles were evaporated and crude **S7** was codistilled with dry pyridine (3x 3 mL) and used in the next reaction without further purification.

S14

To a solution of crude **S7** in pyridine (2 mL) was added DMOCP (65 mg, 0.35 mmol) and reaction mixture was stirred at ambient temperature for 1 hour. Water (18 mL, 1 mmol) was added followed by 3*H*-1,2-benzodithiol-3-one (25 mg, 0.15 mmol) and reaction mixture was stirred for 10 min. Volatiles were evaporated and product was isolated on reverse phase FCC (MeCN in 50 mM aqueous NH<sub>4</sub>HCO<sub>3</sub> 0-70%) to afford **S8** as a mixture of diastereomers.

A solution of **S8** (23 mg) in CH<sub>3</sub>NH<sub>2</sub> (33% in ethanol, 1 mL) was stirred at ambient temperature for 3 hours. Volatiles were evaporated and the residue was codistilled with pyridine (3x 2 mL), dissolved in pyridine-TEA (1:1, v/v, 1 mL) and HF-TEA (160 μL, 1 mmol) was added dropwise. Reaction mixture was stirred at 50 °C for 1 hour, quenched with 1M ammonium acetate (2 mL) and purified on preparative HPLC (C18, ACN in 0.1M TEAB, 0-30%). Appropriate fractions were pooled, evaporated, codistilled with water (3x 5 mL) and methanol (3x 5 mL) to afford diastereoisomers **CDN-35**, **-36** and **-37** in approx. 2:3:3:1 ratio, in order of their elution from HPLC, as triethylammonium salts. NMR and HRMS data can be found in Table S4 and Table S5.

#### **Molecular docking.**

We used the DOCK6 algorithm to perform computational docking for selected set of 17 CDN ligands to the wt-STING target protein (4KSY.pdb code). To establish the accuracy of the DOCK algorithm for this system, the native ligand in 4KSY.pdb X-ray structure was re-docked to crystal structures with RMSD = 1.1 Å for docked ligand conformation/native conformation. The DOCK 6.6 calculations<sup>2</sup> were set up within CHIMERA graphical interface<sup>3</sup> according to protocol recommended in official documents of DOCK (including protonation states, molecular surface generation, charge calculation at AM1-BCC level). Rigid ligand docking with optimization and flexible ligand “anchor and grow” was tested with grid scoring of 50 conformers in each run. The ten best scored poses for each complex were further rescored using the amber score.

#### **Details of QM/MM Calculations.**

In our QM/MM approach, the protein and solvent are split into three subsystems: The QM region (system 1) contains most of the atoms relevant for the chemical process under consideration (i.e., the active site and its nearest vicinity) and is relaxed by QM/MM forces. System 2 consists of all residues within 2.5 Å of any atom in system 1 and is relaxed by full MM minimization in each step of the QM/MM geometry optimization. Finally, system 3 contains the remaining part of the protein and surrounding solvent molecules and is kept fixed at the original (crystallographic) coordinates. When there is a bond spanning the boundary of systems 1 and 2 (a junction), the quantum region is reduced to hydrogen atoms (the hydrogen link approach). The total energy is calculated as

$$E_{\text{tot}} = E_{\text{QM}} + E_{\text{MM},123} - E_{\text{MM},1}$$

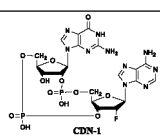
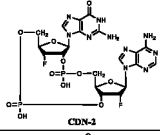
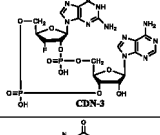
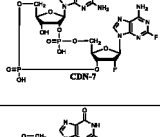
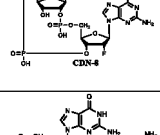
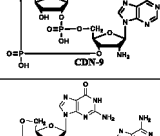
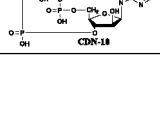
$E_{\text{QM}}$  is the QM energy of the quantum system truncated by hydrogen atoms in the field of the surrounding point charges, but excluding the self-energy of the point charges.  $E_{\text{MM},1}$  is the MM energy of the quantum system, still truncated by hydrogen atoms but without any electrostatic interactions. Finally,  $E_{\text{MM},123}$  is the MM energy of all atoms in the system with original atoms at the junctions and with the charges of the quantum system set to zero (to avoid double counting of the electrostatic interactions). The actual charges used for all atoms can be found in the sample PDB file in the Supporting Information (last column).

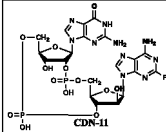
In the quantum chemical calculations, the QM system is represented by a wave function, whereas all of the other atoms are represented by an array of partial point charges, one per atom, taken from Amber libraries (see SI for the actual charges used). Thereby, the polarization of the quantum

chemical system by the surroundings is included in a self-consistent manner. In the MM calculations for the QM/MM forces and energies, all atoms are represented by the Amber force field. When there is a bond spanning the boundary of systems 1 and 2 (a junction), the quantum region is reduced to hydrogen atoms, the positions of which are linearly related to the corresponding carbon atoms in the full system (the hydrogen link approach). In order to avoid over-polarization of the quantum system, point charges on the atoms in the MM region bound to the junction atoms are omitted, and the remaining charges on the truncated amino acid are adjusted to keep the fragment neutral.

### 3. SUPPLEMENTAL DATA

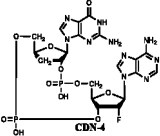
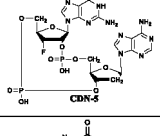
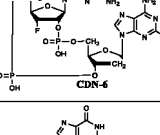
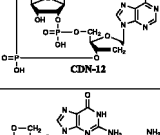
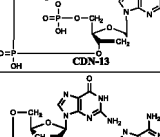
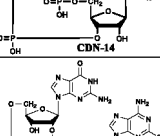
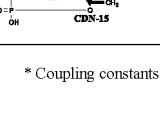
Table S1a. The <sup>1</sup>H and <sup>31</sup>P NMR data of 2',3'-CDNs 1 – 3 and 7 – 11 in D<sub>2</sub>O.\*

Structure	Res.	H-1'	H-2'	H-3'	H-4'	H-5'a	H-5'b	Base	<sup>31</sup> P	<sup>19</sup> F
 CDN-1	G	5.96 d 1,2 = 8.3	5.58 td 2,1 = 8.3 2,3 = 4.3 2,P = 8.4	4.60 d 3,2 = 4.3 3,4 = 0	4.395 q 4,3 = 0 4,5a = 2.6 4,5b = 2.8 4,P = 3.0	4.27 ddd 5a,4 = 2.6 5a,5b = 12.0 5a,P = 4.5	4.25 ddd 5b,4 = 2.8 5b,5a = 12.0 5b,P = 6.3	H-8: 7.86 s	1.18 0.40	...
	A	6.47 d 1,2 = 0 1,F = 15.1	5.60 dd 2,1 = 0 2,3 = 3.7 2,F = 51.5	5.16 dddd 3,2 = 3.7 3,4 = 9.2 3,P = 23.2 3,P = 5.6	4.55 dm 4,3 = 9.2	4.45 ddd 5a,4 = 2.5 5a,5b = 12.1 5a,P = 1.0	4.15 ddd 5b,4 = 1.3 5b,5a = 12.1 5b,P = 3.7	H-2: 8.26 s H-8: 8.24 s		-199.06
 CDN-2	G	6.04 d 1,2 = 8.6	5.73 dddd 2,1 = 8.6 2,3 = 3.4 2,P = 7.2 2,F = 26.7	5.44 dd 3,2 = 3.4 3,4 = 0	4.70 overlap	4.33 m	4.17 dtd 5b,4 = 2.5 5b,5a = 11.8 5b,P = 2.7 5b,F = 1.6	H-8: 7.86 s	0.57 -1.61	-196.28 -199.80
	A	6.46 d 1,2 = 0 1,F = 13.7	5.55 dd 2,1 = 0 2,3 = 3.5 2,F = 51.5	5.11 dddd 3,2 = 3.5 3,4 = 9.5 3,P = 24.0 3,P = 6.5	4.57 dm 4,3 = 9.5	4.52 ddd 5a,4 = 2.3 5a,5b = 12.2 5a,P = 1	4.21 ddd 5b,4 = 1.2 5b,5a = 12.2 5b,P = 3.0	H-2: 8.28 s H-8: 8.25 s		
 CDN-3	G	6.03 d 1,2 = 8.8	5.73 dddd 2,1 = 8.8 2,3 = 3.4 2,P = 6.0 2,F = 37.0	5.45 dd 3,2 = 3.4 3,4 = 0	4.70 dtd 4,3 = 0 4,5a = 3.5 4,5b = 1.5 4,F = 25.6 4,P = 3.4	4.31 ddd 5a,4 = 3.5 5a,5b = 11.7 5a,P = 3.9	4.13 ddd 5b,4 = 1.5 5b,5a = 11.7 5b,P = 2.4 5b,F = 2.3	H-8: 7.86 s	0.42 -1.63	...
	A	6.19 s 1,2 = 0	4.79 d 2,1 = 0 2,3 = 4.1	5.04 ddd 3,2 = 4.1 3,4 = 9.3 3,P = 7.1	4.50 m	4.515 m	4.20 m	H-2: 8.28 s H-8: 8.29 s		
 CDN-7	G	5.96 d 1,2 = 8.4	5.66 td 2,1 = 8.4 2,3 = 4.3 2,P = 8.2	4.585 d 3,2 = 4.3 3,4 = 0	4.40 q 4,3 = 0 4,5a = 2.8 4,5b = 2.3 4,P = 3.1	4.26 ddd 5a,4 = 2.8 5a,5b = 11.8 5a,P = 5.7	4.29 ddd 5b,4 = 2.3 5b,5a = 11.8 5b,P = 3.7	H-8: 7.86 s	0.34 -1.13	...
	2F-A	6.375 d 1,2 = 0 1,F = 14.0	5.52 ddd 2,1 = 0 2,3 = 3.8 2,F = 51.1	5.13 dddd 3,2 = 3.4 3,4 = 9.6 3,F = 23.9 3,P = 5.8	4.55 dm 4,3 = 9.6	4.47 bdd 5a,4 = 2.3 5a,5b = 12.1 5a,P = 1	4.14 ddd 5b,4 = 1.2 5b,5a = 12.1 5b,P = 3.4	H-8: 8.21 s		2F: -49.22 2F: -199.52
 CDN-8	G	5.96 d 1,2 = 8.4	5.66 td 2,1 = 8.6 2,3 = 4.3 2,P = 8.0	4.59 d 3,2 = 4.3 3,4 = 0	4.40 q 4,3 = 0 4,5a = 2.8 4,5b = 2.8 4,P = 2.8	4.32 m	4.28 m	H-8: 7.88 s	1.13 0.40	...
	D&P	6.29 d 1,2 = 0 1,F = 14.5	5.51 dd 2,1 = 0 2,3 = 3.5 2,F = 51.3	5.14 dddd 3,2 = 3.5 3,4 = 9.5 3,F = 24.0 3,P = 5.7	4.51 dm 4,3 = 9.5	4.45 bdd 5a,4 = 2.3 5a,5b = 11.7 5a,P = 1.0	4.13 ddd 5b,4 = 1.2 5b,5a = 11.7 5b,P = 3.5	H-8: 7.96 s		-199.15
 CDN-9	G	5.96 d 1,2 = 8.5	5.60 ddd 2,1 = 8.5 2,3 = 4.1 2,P = 8.0	4.60 d 3,2 = 4.1 3,4 = 0	4.415 ddd 4,3 = 0 4,5a = 2.8 4,5b = 1.8 4,P = 3.4	4.26 dd 5a,4 = 2.8 5a,5b = 11.8 5a,P = 5.1	4.165 ddd 5b,4 = 1.8 5b,5a = 11.8 5b,P = 2.4	H-8: 7.91 s	0.18 -1.00	...
	A	6.11 d 1,2 = 1.6	4.16 dd 2,1 = 1.6 2,3 = 5.2	5.11 ddd 3,2 = 5.2 3,4 = 8.2 3,P = 7.0	4.51 dddd 4,3 = 8.2 4,5a = 3.0 4,5b = 1.5 4,P = 3.4	4.43 dt 5a,4 = 3.0 5a,5b = 12.0 5a,P = 3.2	4.13 ddd 5b,4 = 1.5 5b,5a = 12.0 5b,P = 3.5	H-2: 8.28 s H-8: 8.36 s		
 CDN-18	G	6.04 d 1,2 = 8.5	5.465 td 2,1 = 8.5 2,3 = 4.4 2,P = 8.5	4.97 d 3,2 = 4.4 3,4 = 0	4.41 q 4,3 = 0 4,5a = 2.2 4,5b = 2.1 4,P = 2.7	4.305 ddd 5a,5b = 12.2 5a,4 = 2.2 5a,P = 7.8	4.20 ddd 5b,5a = 12.2 5b,4 = 2.1 5b,P = 3.7	H-8: 8.03 s	0.72 0.00	...
	A	6.50 d 1,2 = 5.0	4.78 overlap	4.97 dt 3,2 = 6.1 3,4 = 8.8 3,P = 5.0	4.39 ddd 4,3 = 4.8 4,5a = 6.0 4,5b = 3.0	4.275 dt 5a,5b = 11.3 5a,4 = 6.0 5a,P = 6.0	4.15 ddd 5b,5a = 11.3 5b,4 = 3.0 5b,P = 5.0	H-2: 8.24 s H-8: 8.37 s		

 CDN-II	G	6.09 d <i>1,2 = 8.5</i>	5.47 td <i>2,1 = 8.5</i> <i>2,3 = 4.4</i> <i>2,4 = 9.0</i>	4.55 d <i>3,2 = 4.4</i> <i>3,4 = 0</i>	4.38 q <i>4,3 = 0</i> <i>4,5a = 2.2</i> <i>4,5b = 2.2</i> <i>4,6 = 2.8</i>	4.30 ddd <i>5a,4 = 2.2</i> <i>5a,5b = 12.1</i> <i>5a,6 = 7.7</i>	4.20 ddd <i>5b,4 = 2.2</i> <i>5b,5a = 12.1</i> <i>5b,6 = 3.9</i>	H-B: 8.02 s	-0.10 0.79	...
	2F-A	6.37 d <i>1,2 = 5.1</i>	4.78 overlap	4.96 dt <i>3,2 = 5.0</i> <i>3,4 = 5.4</i> <i>3,6 = 6.2</i>	4.37 tdd <i>4,3 = 5.4</i> <i>4,5a = 5.6</i> <i>4,5b = 2.8</i> <i>4,6 = 1.5</i>	4.27 dt <i>5a,4 = 5.4</i> <i>5a,5b = 11.3</i> <i>5a,6 = 5.8</i>	4.14 ddd <i>5b,4 = 2.8</i> <i>5b,5a = 11.3</i> <i>5b,6 = 4.8</i>	H-B: 8.29 s		49.79

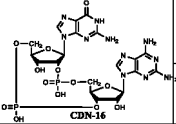
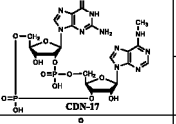
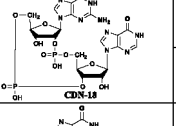
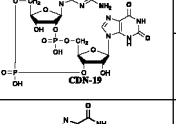
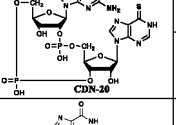
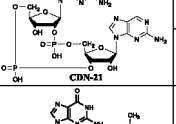
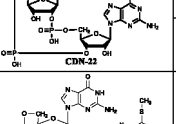
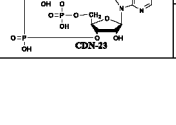
\* Coupling constants are written in italics in a shortened form (e.g. instead  $J(1',2') = 8.6 \text{ Hz}$  we type simply  $1,2 = 8.6$ ).

Table S1b. The <sup>1</sup>H and <sup>31</sup>P NMR data of 3'- or 2'-deoxy- 2',3'-CDNs 4 – 6 and 12 – 15 in D<sub>2</sub>O.\*

Structure	Res.	H-1'	H-2'a	H-2'b	H-3a'	H-3b'	H-4'	H-5'a	H-5'b	Base	<sup>31</sup> P	<sup>19</sup> F
	G	5.85 d <i>1,2 = 6.4</i>	..	5.56 dq <i>2,1 = 6.4</i> <i>2,3 = 9.0</i> <i>2,3b = 6.5</i> <i>2,P = 5.2</i>	2.62 dt <i>3b,2 = 9.0</i> <i>3b,3b = 13.0</i> <i>3b,4 = 8.6</i>	2.49 ddd <i>3,2 = 6.5</i> <i>3b,3a = 13.0</i> <i>3b,4 = 3.4</i>	4.60 m	4.35 m	4.16 m	H-8: 7.84 s	-0.32 -1.14	..
	A	6.47 d <i>1,2 = 0</i> <i>1,F = 14.4</i>	..	5.61 dd <i>2,1 = 0</i> <i>2,3 = 3.5</i> <i>2,F = 51.0</i>	..	5.105 dddd <i>3,2 = 3.5</i> <i>3,4 = 9.5</i> <i>3,F = 23.8</i> <i>3,P = 5.2</i>	4.56 dm <i>4,3 = 9.5</i>	4.49 dd <i>5a,4 = 2.3</i> <i>5a,5b = 12.2</i> <i>5b,P &lt; 1</i>	4.22 ddd <i>5b,4 = 2.1</i> <i>5b,5a = 12.2</i> <i>5b,P = 3.4</i>	H-2: 8.28 s H-8: 8.32 s	-199.33	..
	G	6.05 d <i>1,2 = 8.6</i>	..	5.69 dddd <i>2,1 = 8.6</i> <i>2,3 = 3.4</i> <i>2,P = 7.7</i> <i>2,F = 26.8</i>	..	5.44 dd <i>3,2 = 3.4</i> <i>3,4 = 0</i> <i>3,F = 53.3</i>	4.70 overlap	4.34 dt <i>5a,4 = 3.3</i> <i>5a,5b = 11.5</i> <i>5b,P = 3.3</i>	4.16 ddd <i>5b,4 = 1.3</i> <i>5b,5a = 11.5</i> <i>5b,P = 3.5</i>	H-8: 7.91 s	-196.33	..
	A	6.45 dd <i>1,2a = 6.6</i> <i>1,2b = 2.2</i>	2.80 ddd <i>2a,1 = 6.6</i> <i>2a,2b = 13.5</i> <i>2a,3 = 9.0</i>	2.99 ddd <i>2b,1 = 2.2</i> <i>2b,2a = 13.5</i> <i>2b,3 = 6.4</i>	..	5.17 dq <i>3,2a = 9.0</i> <i>3,2b = 6.4</i> <i>3,4 = 7.0</i> <i>3,P = 6.7</i>	4.31 m	4.30 m	4.17 m	H-8: 8.28 s	-0.10	..
	G	6.05 d <i>1,2 = 8.6</i>	..	5.69 dddd <i>2,1 = 8.6</i> <i>2,3 = 3.4</i> <i>2,P = 7.0</i> <i>2,F = 26.8</i>	..	5.43 dd <i>3,2 = 3.4</i> <i>3,4 = 0</i> <i>3,F = 53.5</i>	4.71 overlap	4.30 ddd <i>5a,4 = 3.2</i> <i>5a,5b = 11.6</i> <i>5b,P = 4.9</i>	4.18 dhd <i>5b,4 = 2.5</i> <i>5b,5a = 11.6</i> <i>5b,P = 1.7</i>	H-8: 7.91 s	-196.28	..
	2F-A	6.34 dd <i>1,2a = 6.6</i> <i>1,2b = 2.2</i>	2.775 ddd <i>2a,1 = 6.6</i> <i>2a,2b = 13.5</i> <i>2a,3 = 8.9</i>	2.96 ddd <i>2b,1 = 2.2</i> <i>2b,2a = 13.5</i> <i>2b,3 = 6.4</i>	..	5.17 dq <i>3,2a = 8.9</i> <i>3,2b = 6.4</i> <i>3,4 = 6.7</i> <i>3,P = 6.7</i>	4.30 m	4.32 dt <i>5a,4 = 3.4</i> <i>5a,5b = 11.3</i> <i>5b,P = 3.4</i>	4.15 ddd <i>5b,4 = 1.1</i> <i>5b,5a = 11.3</i> <i>5b,P = 3.6</i>	H-8: 8.20 s	-0.10	-49.68
	G	5.98 d <i>1,2 = 8.4</i>	..	5.59 td <i>2,1 = 8.4</i> <i>2,3 = 4.2</i> <i>2,P = 8.2</i>	..	4.595 d <i>3,2 = 4.2</i> <i>3,4 = 0</i>	4.42 ddd <i>4,3 = 0</i> <i>4,5a = 2.8</i> <i>4,5b = 2.2</i> <i>4,P = 3.4</i>	4.235 ddd <i>5a,4 = 2.8</i> <i>5a,5b = 11.8</i> <i>5b,P = 5.3</i>	4.21 ddd <i>5b,4 = 2.2</i> <i>5b,5a = 11.8</i> <i>5b,P = 3.5</i>	H-8: 7.93 s	0.28 -0.59	..
	A	6.465 dd <i>1,2a = 6.6</i> <i>1,2b = 2.7</i>	2.81 ddd <i>2a,1 = 6.6</i> <i>2a,2b = 13.6</i> <i>2a,3 = 8.6</i>	3.00 ddd <i>2b,1 = 2.7</i> <i>2b,2a = 13.6</i> <i>2b,3 = 6.3</i>	..	5.19 dq <i>3,2a = 6.3</i> <i>3,2b = 6.3</i> <i>3,4 = 6.5</i> <i>3,P = 6.5</i>	4.32 dddd <i>4,3 = 6.5</i> <i>4,5a = 4.0</i> <i>4,5b = 1.5</i> <i>4,P = 2.5</i>	4.295 ddd <i>5a,4 = 4.0</i> <i>5a,5b = 11.5</i> <i>5b,P = 3.2</i>	4.105 ddd <i>5b,4 = 1.5</i> <i>5b,5a = 11.5</i> <i>5b,P = 4.0</i>	H-2: 8.25 s H-8: 8.30 s	..	..
	G	5.875 d <i>1,2 = 5.8</i>	..	5.46 dq <i>2,1 = 5.8</i> <i>2,3a = 8.1</i> <i>2,3b = 6.2</i> <i>2,P = 5.6</i>	2.65 dt <i>3a,2 = 8.1</i> <i>3a,3b = 13.1</i> <i>3a,4 = 8.2</i>	2.48 ddd <i>3b,2 = 6.2</i> <i>3b,3a = 13.1</i> <i>3b,4 = 4.0</i>	4.61 m	4.19 ddd <i>5a,4 = 3.2</i> <i>5a,5b = 11.8</i> <i>5b,P = 7.7</i>	4.11 ddd <i>5b,4 = 2.2</i> <i>5b,5a = 11.8</i> <i>5b,P = 7.8</i>	H-8: 7.90 s	0.29	..
	A	6.475 dd <i>1,2a = 6.7</i> <i>1,2b = 3.0</i>	2.83 ddd <i>2a,1 = 6.7</i> <i>2a,2b = 13.8</i> <i>2a,3 = 8.1</i>	3.04 ddd <i>2b,1 = 3.0</i> <i>2b,2a = 13.8</i> <i>2b,3 = 6.4</i>	..	5.14 dq <i>3,2a = 8.1</i> <i>3,2b = 6.4</i> <i>3,4 = 6.0</i> <i>3,P = 6.0</i>	4.33 m	4.27 dt <i>5a,4 = 3.9</i> <i>5a,5b = 11.8</i> <i>5b,P = 3.9</i>	4.18 ddd <i>5b,4 = 1.9</i> <i>5b,5a = 11.8</i> <i>5b,P = 4.4</i>	H-2: 8.25 s H-8: 8.34 s	-0.75	..
	G	5.80 d <i>1,2 = 6.8</i>	..	5.58 dtd <i>2,1 = 6.8</i> <i>2,3a = 9.7</i> <i>2,3b = 6.6</i> <i>2,P = 5.9</i>	2.59 ddd <i>3a,2 = 9.7</i> <i>3a,3b = 12.7</i> <i>3a,4 = 8.5</i>	2.51 ddd <i>3b,2 = 6.6</i> <i>3b,3a = 12.7</i> <i>3b,4 = 2.9</i>	4.60 dq <i>4,3a = 8.5</i> <i>4,3b = 2.9</i> <i>4,5a = 3.0</i> <i>4,5b = 2.9</i>	4.14 ddd <i>5a,4 = 3.0</i> <i>5a,5b = 11.6</i> <i>5b,P = 6.3</i>	4.10 ddd <i>5b,4 = 2.9</i> <i>5b,5a = 11.6</i> <i>5b,P = 6.5</i>	H-8: 7.84 s	-0.07 -1.06	..
	A	6.19 s <i>1,2 = 0</i>	..	4.84 d <i>2,1 = 0</i> <i>2,3 = 4.1</i>	..	5.04 ddd <i>3,2 = 4.1</i> <i>3,4 = 9.0</i> <i>3,P = 6.0</i>	4.50 m	4.48 m	4.215 m	H-2: 8.28 s H-8: 8.36 s	..	..
	G	5.985 d <i>1,2 = 8.4</i>	..	5.595 td <i>2,1 = 8.4</i> <i>2,3 = 4.2</i> <i>2,P = 8.4</i>	..	4.59 d <i>3,2 = 4.2</i> <i>3,4 = 0</i>	4.42 ddd <i>4,3 = 0</i> <i>4,5a = 2.7</i> <i>4,5b = 2.2</i> <i>4,P = 3.3</i>	4.24 ddd <i>5a,4 = 2.7</i> <i>5a,5b = 11.8</i> <i>5b,P = 5.3</i>	4.21 ddd <i>5b,4 = 2.2</i> <i>5b,5a = 11.8</i> <i>5b,P = 3.5</i>	H-8: 7.94 s	0.29 -0.65	..
	2Cl-A	6.39 dd <i>1,2a = 6.6</i> <i>1,2b = 2.7</i>	2.80 ddd <i>2a,1 = 6.6</i> <i>2a,2b = 13.7</i> <i>2a,3 = 8.5</i>	2.96 ddd <i>2b,1 = 2.7</i> <i>2b,2a = 13.7</i> <i>2b,3 = 6.4</i>	..	5.19 dq <i>3,2a = 8.5</i> <i>3,2b = 6.4</i> <i>3,4 = 6.5</i> <i>3,P = 6.5</i>	4.31 m	4.29 m	4.10 m	H-8: 8.26 s	..	..

\* Coupling constants are written in italics in a shortened form (e.g. instead  $J(1',2') = 8.6$  Hz we type simply  $1,2 = 8.6$ ).

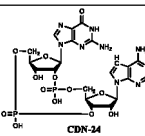
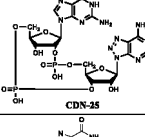
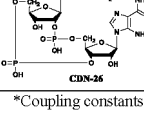
Table S2. The <sup>1</sup>H and <sup>31</sup>P NMR data of 2',3'-CDNs 16 - 26 in D<sub>2</sub>O.\*

Structure	Residue	H-1'	H-2'	H-3'	H-4'	H-5'a	H-5'b	Base	<sup>31</sup> P
	G	5.95 d 1,2 = 8.5	5.65 ddd 2,1 = 8.5 2,3 = 4.2 2,P = 7.6	4.60 d 3,2 = 4.2 3,4 = 0	4.41 ddd 4,3 = 0 4,5a = 3.0 4,5b = 1.9 4,P = 3.6	4.25 ddd 5a,5b = 11.7 5a,4 = 3.0 5a,P = 5.2	4.18 ddd 5b,5a = 11.7 5b,4 = 1.9 5b,P = 2.5	H-8: 7.87 s	-0.21 -1.11
	DIAP	6.01 s 1,2 = 0	4.74 d 2,1 = 0 2,3 = 4.1	5.055 ddd 3,2 = 4.1 3,4 = 9.0 3,P = 6.5	4.44 m	4.44 m	4.13 m	H-8: 7.99 s	
	G	5.935 d 1,2 = 8.5	5.63 ddd 2,1 = 8.5 2,3 = 4.1 2,P = 7.5	4.61 d 3,2 = 4.1 3,4 = 0	4.41 ddd 4,3 = 0 4,5a = 3.2 4,5b = 1.7 4,P = 3.6	4.24 ddd 5a,5b = 11.7 5a,4 = 3.2 5a,P = 4.8	4.15 ddd 5b,5a = 11.7 5b,4 = 1.7 5b,P = 2.3	H-8: 7.86 s	-0.26 -1.26
	6-NMe-A	6.16 s 1,2 = 0	4.775 overlap	5.055 ddd 3,2 = 4.1 3,4 = 8.9 3,P = 6.8	4.49 m	4.49 m	4.16 m	H-2: 8.28 bs H-8: 8.28 bs	
	G	5.97 d 1,2 = 8.4	5.66 td 2,1 = 8.4 2,3 = 4.2 2,P = 8.4	4.59 d 3,2 = 4.2 3,4 = 0	4.395 ddd 4,3 = 0 4,5a = 2.6 4,5b = 2.0 4,P = 3.2	4.25 ddd 5a,4 = 11.8 5a,P = 6.0	4.18 ddd 5b,4 = 2.0 5b,5a = 11.8 5b,P = 3.2	H-8: 7.91 s	-0.81 -0.15
	Hpx	6.195 d 1,2 = 1.0	4.80 overlap	5.06 ddd 3,2 = 4.3 3,4 = 8.6 3,P = 6.8	4.49 ddd 4,3 = 8.6	4.42 dt 5a,4 = 2.4 5a,5b = 11.8 5a,P = 2.0	4.11 ddd 5b,4 = 1.3 5b,5a = 11.8 5b,P = 3.5	H-2: 8.21 s H-8: 8.27 s	
	G	5.95 d 1,2 = 8.4	5.72 td 2,1 = 8.4 2,3 = 4.3 2,P = 8.4	4.58 d 3,2 = 4.3 3,4 = 0	4.39 ddd 4,3 = 0 4,5a = 2.7 4,5b = 2.2 4,P = 3.2	4.25 ddd 5a,4 = 11.8 5a,P = 6.1	4.21 ddd 5b,4 = 2.2 5b,5a = 11.8 5b,P = 3.5	H-8: 7.87 s	-0.77 -0.15
	Xan	5.95 d 1,2 = 1.1	4.70 dd 2,1 = 1.1 2,3 = 4.3	5.04 ddd 3,2 = 4.3 3,4 = 8.8 3,P = 6.1	4.44 dtd 4,3 = 8.6 4,5a = 2.7 4,5b = 1.3 4,P = 2.7	4.38 dt 5a,4 = 2.7 5a,5b = 12.0 5a,P = 1.4	4.08 ddd 5b,4 = 1.3 5b,5a = 11.8 5b,P = 3.6	H-8: 7.855 s	
	G	5.97 d 1,2 = 8.4	5.70 td 2,1 = 8.4 2,3 = 4.2 2,P = 8.1	4.575 d 3,2 = 4.2 3,4 = 0	4.38 ddd 4,3 = 0 4,5a = 2.6 4,5b = 2.2 4,P = 3.0	4.25 ddd 5a,4 = 2.6 5a,5b = 12.0 5a,P = 6.7	4.18 ddd 5b,4 = 2.2 5b,5a = 12.0 5b,P = 3.6	H-8: 7.91 s	-0.61 -0.08
	6-S-Hpx	6.20 s 1,2 = 0	4.81 overlap	5.04 ddd 3,2 = 4.3 3,4 = 8.5 3,P = 6.1	4.50 dtd 4,3 = 8.5 4,5a = 2.5 4,5b = 1.6 4,P = 2.5	4.42 dt 5a,4 = 2.5 5a,5b = 11.7 5a,P = 2.5	4.105 ddd 5b,4 = 1.6 5b,5a = 11.7 5b,P = 3.8	H-2: 8.34 s H-8: 8.40 s	
	G	5.955 d 1,2 = 8.7	5.59 ddd 2,1 = 8.7 2,3 = 4.1 2,P = 7.5	4.62 d 3,2 = 4.1 3,4 = 0	4.42 td 4,3 = 0 4,5a = 3.0 4,5b = 1.7 4,P = 3.6	4.25 ddd 5a,5b = 11.8 5a,4 = 3.0 5a,P = 5.0	4.17 ddd 5b,5a = 11.8 5b,4 = 1.7 5b,P = 2.8	H-8: 7.89 s	-0.18 -1.00
	2-NH <sub>2</sub> -Pur	6.11 d 1,2 = 1.0	4.82 overlap	5.05 ddd 3,2 = 4.1 3,4 = 8.6 3,P = 6.7	4.47 m	4.46 m	4.15 m	H-8: 8.24 s H-6: 8.63 s 5b,5a = 12.2 5b,4 = 1.3 5b,P = 3.4	
	G	5.94 d 1,2 = 8.5	5.64 ddd 2,1 = 8.5 2,3 = 4.1 2,P = 7.0	4.60 d 3,2 = 4.1 3,4 = 0	4.40 td 4,3 = 0 4,5a = 3.0 4,5b = 2.0 4,P = 3.3	4.24 ddd 5a,5b = 11.8 5a,4 = 3.0 5a,P = 5.3	4.16 ddd 5b,5a = 11.8 5b,4 = 2.0 5b,P = 2.6	H-8: 7.87 s	-0.22 -1.10
	6-SMe-2-NH <sub>2</sub> -Pur	6.05 s 1,2 = 0	4.83 d 2,3 = 4.2	5.035 ddd 3,2 = 4.2 3,4 = 9.1 3,P = 6.5	4.47 m	4.47 m	4.16 m	H-8: 8.18 s SMe: 2.67 s	
	G	5.94 d 1,2 = 8.6	5.63 ddd 2,1 = 8.6 2,3 = 4.1 2,P = 6.8	4.61 d 3,2 = 4.1 3,4 = 0	4.40 ddd 4,3 = 0 4,5a = 3.0 4,5b = 1.8 4,P = 3.5	4.235 ddd 5a,5b = 11.8 5a,4 = 3.0 5a,P = 5.0	4.14 ddd 5b,5a = 11.8 5b,4 = 1.8 5b,P = 2.5	H-8: 7.87 s	-0.24 -1.19
	6-SMe-Pur	6.25 s 1,2 = 0	4.89 d 2,1 = 0 2,3 = 4.1	5.04 ddd 3,2 = 4.1 3,4 = 9.2 3,P = 6.6	4.53 m	4.515 dt 5a,4 = 2.9 5a,5b = 10.8 5a,P = 2.9	4.19 ddd 5b,4 = 1.3 5b,5a = 10.8 5b,P = 3.0	H-2: 8.71 s H-8: 8.58 s SMe: 2.76 s	

S21

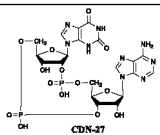
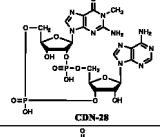
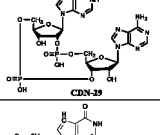
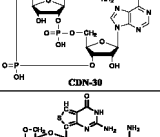
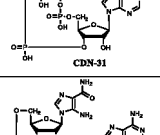
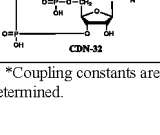


Table S2 - continued. The  $^1\text{H}$  and  $^{31}\text{P}$  NMR data of 2',3'-CDNs 16 - 26 in  $\text{D}_2\text{O}$ .\*

Structure	Res.	H-1'	H-2'	H-3'	H-4'	H-5'a	H-5'b	Base	$^{31}\text{P}$
 <b>CDN-24</b>	G	5.97 d <i>1,2 = 8.4</i>	5.61 ddd <i>2,1 = 8.4</i> <i>2,3 = 4.1</i> <i>2,P = 7.4</i>	4.62 d <i>3,2 = 4.1</i> <i>3,4 = 0</i>	4.44 ddd <i>4,3 = 0</i> <i>4,5a = 3.1</i> <i>4,5b = 1.6</i> <i>4,P = 3.5</i>	4.27 ddd <i>5a,4 = 3.1</i> <i>5a,5b = 11.7</i> <i>5a,P = 5.0</i>	4.21 ddd <i>5b,4 = 1.5</i> <i>5b,5a = 11.7</i> <i>5b,P = 2.5</i>	H:8: 7.91 s	-0.24 -0.92
	7-deaza-A	6.29 d <i>1,2 = 1.0</i>	4.64 dd <i>2,1 = 1.0</i> <i>2,3 = 4.2</i>	5.08 ddd <i>3,2 = 4.2</i> <i>3,4 = 8.6</i> <i>3,P = 6.6</i>	4.42 ddd <i>4,3 = 8.6</i> <i>4,5a = 2.2</i> <i>4,5b = 1.3</i>	4.40 dt <i>5a,4 = 2.2</i> <i>5a,5b = 11.6</i> <i>5a,P = 2.2</i>	4.13 ddd <i>5b,4 = 1.3</i> <i>5b,5a = 11.6</i> <i>5b,P = 3.2</i>	H:2: 8.17 s H:7: 6.24 d <i>7,8 = 3.2</i> H:8: 7.37 d <i>8,7 = 3.2</i>	
 <b>CDN-35</b>	G	6.03 d <i>1,2 = 8.4</i>	5.44 ddd <i>2,1 = 8.4</i> <i>2,3 = 4.3</i> <i>2,P = 8.2</i>	4.62 d <i>3,2 = 4.3</i> <i>3,4 = 0</i>	4.445 ddd <i>4,3 = 0</i> <i>4,5a = 2.4</i> <i>4,5b = 2.0</i> <i>4,P = 3.1</i>	4.32 ddd <i>5a,4 = 2.4</i> <i>5a,5b = 12.0</i> <i>5a,P = 6.7</i>	4.255 ddd <i>5b,4 = 2.0</i> <i>5b,5a = 12.0</i> <i>5b,P = 3.6</i>	H:8: 8.06 s	-0.11 -0.40
	8-aza-A	6.42 d <i>1,2 = 1.9</i>	5.21 dd <i>2,1 = 1.9</i> <i>2,3 = 4.7</i>	5.46 ddd <i>3,2 = 4.7</i> <i>3,4 = 7.4</i> <i>3,P = 6.4</i>	4.50 dddd <i>4,3 = 7.4</i> <i>4,5a = 3.7</i> <i>4,5b = 2.3</i> <i>4,P = 2.8</i>	4.15 dt <i>5a,4 = 3.7</i> <i>5a,5b = 12.4</i> <i>5a,P = 3.8</i>	4.03 ddd <i>5b,4 = 2.3</i> <i>5b,5a = 12.4</i> <i>5b,P = 4.2</i>	H:2: 8.33 s	
 <b>CDN-26</b>	G	5.955 d <i>1,2 = 8.4</i>	5.65 td <i>2,1 = 8.4</i> <i>2,3 = 4.2</i> <i>2,P = 8.1</i>	4.585 d <i>3,2 = 4.2</i> <i>3,4 = 0</i>	4.42 td <i>4,3 = 0</i> <i>4,5a = 3.0</i> <i>4,5b = 1.7</i> <i>4,P = 3.3</i>	4.265 ddd <i>5a,4 = 3.0</i> <i>5a,5b = 11.7</i> <i>5a,P = 5.3</i>	4.21 ddd <i>5b,4 = 1.7</i> <i>5b,5a = 11.7</i> <i>5b,P = 2.7</i>	H:8: 7.87 s	-0.18 -1.12
	AICA	5.77 d <i>1,2 = 0.9</i>	4.67 htd <i>2,1 = 0.9</i> <i>2,3 = 4.4</i>	5.05 ddd <i>3,2 = 4.4</i> <i>3,4 = 9.0</i> <i>3,P = 6.5</i>	4.39 m	4.38 m	4.09 m	H:8: 7.485 s	

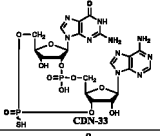
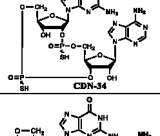
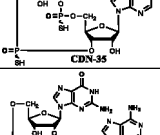
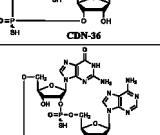
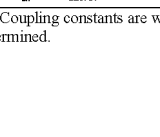
\*Coupling constants are written in italics in a shortened form (e.g. instead  $J(1',2') = 8.6 \text{ Hz}$  we type simply  $1,2 = 8.6$ ).

Table S3. The  $^1\text{H}$  and  $^{31}\text{P}$  NMR data of 2',3'-CDNs **27** - **32** in  $\text{D}_2\text{O}$ .\*

Structure	Residue	H-1'	H-2'	H-3'	H-4'	H-5'a	H-5'b	Base	$^{31}\text{P}$
 <b>CDN-27</b>	Xan	6.075 d <i>1,2 = 8.4</i>	5.08 td <i>2,1 = 8.4</i> <i>2,3 = 4.2</i> <i>2,P = 8.7</i>	4.63 d <i>3,2 = 4.2</i> <i>3,4 = 0</i>	4.42 dt <i>4,3 = 0</i> <i>4,5a = 1.8</i> <i>4,5b = 1.7</i> <i>4,P = 3.2</i>	4.28 ddd <i>5a,4 = 1.8</i> <i>5a,5b = 12.0</i> <i>5a,P = 6.4</i>	4.12 ddd <i>5b,4 = 1.7</i> <i>5b,5a = 12.0</i> <i>5b,P = 3.6</i>	H-8: 8.06 s	0.16 -0.26
	A	6.155 d <i>1,2 = 9.1</i>	4.87 dd <i>2,1 = 3.1</i> <i>2,3 = 4.7</i>	4.925 td <i>3,2 = 4.7</i> <i>3,4 = 6.8</i> <i>3,P = 6.8</i>	4.50 ddt <i>4,3 = 6.8</i> <i>4,5a = 4.5</i> <i>4,5b = 2.5</i> <i>4,P = 2.1</i>	4.34 dt <i>5a,4 = 4.5</i> <i>5a,5b = 11.7</i> <i>5a,P = 4.5</i>	4.165 ddd <i>5b,4 = 2.5</i> <i>5b,5a = 11.7</i> <i>5b,P = 4.4</i>	H-2: 8.25 s H-8: 8.25 s	
 <b>CDN-28</b>	N1-Me-G	5.95 d <i>1,2 = 8.5</i>	5.705 ddd <i>2,1 = 6.5</i> <i>2,3 = 4.2</i> <i>2,P = 7.6</i>	4.61 d <i>3,2 = 4.2</i> <i>3,4 = 0</i>	4.41 td <i>4,3 = 0</i> <i>4,5a = 3.0</i> <i>4,5b = 1.8</i> <i>4,P = 3.6</i>	4.26 ddd <i>5a,4 = 3.0</i> <i>5a,5b = 11.7</i> <i>5a,P = 5.2</i>	4.19 ddd <i>5b,4 = 1.8</i> <i>5b,5a = 11.7</i> <i>5b,P = 2.7</i>	H-8: 7.85 s N-Me: 2.89 s	-1.18 -0.11
	A	6.21 s <i>1,2 = 0</i>	4.77 overlap	5.12 ddd <i>3,2 = 4.1</i> <i>3,4 = 9.2</i> <i>3,P = 6.5</i>	4.495 tdd <i>4,3 = 5.4</i> <i>4,5a = 5.6</i> <i>4,5b = 2.8</i> <i>4,P = 3.0</i>	4.47 m	4.15 m	H-2: 8.27s H-8: 8.29 s	
 <b>CDN-29</b>	Hpx	6.225 d <i>1,2 = 8.2</i>	5.905 td <i>2,1 = 8.2</i> <i>2,3 = 4.2</i> <i>2,P = 8.4</i>	4.695 d <i>3,2 = 4.2</i> <i>3,4 = 0</i>	4.50 q <i>4,3 = 0</i> <i>4,5a = 2.0</i> <i>4,5b = 1.9</i> <i>4,P = 3.0</i>	4.35 ddd <i>5a,4 = 2.0</i> <i>5a,5b = 12.0</i> <i>5a,P = 6.6</i>	4.22 ddd <i>5b,4 = 1.9</i> <i>5b,5a = 12.0</i> <i>5b,P = 3.7</i>	H-2: 7.96 s H-8: 8.40 s	1.43 0.97
	A	6.02 d <i>1,2 = 2.2</i>	4.79 dd <i>2,1 = 2.2</i> <i>2,3 = 4.7</i>	4.995 td <i>3,2 = 4.7</i> <i>3,4 = 7.0</i> <i>3,P = 7.0</i>	4.50 m	4.41 dt <i>4,3 = 3.5</i> <i>4,5a = 12.0</i> <i>4,5b = 3.5</i>	4.19 ddd <i>5b,4 = 2.0</i> <i>5b,5a = 12.0</i> <i>5b,P = 4.2</i>	H-2: 8.01 s H-8: 8.10 s	
 <b>CDN-30</b>	7-deaza-G	5.96 d <i>1,2 = 8.6</i>	5.48 ddd <i>2,1 = 8.6</i> <i>2,3 = 4.2</i> <i>2,P = 7.2</i>	4.60 d <i>3,2 = 4.2</i> <i>3,4 = 0</i>	4.375 ddd <i>4,3 = 0</i> <i>4,5a = 2.7</i> <i>4,5b = 3.1</i> <i>4,P = 2.2</i>	4.24 ddd <i>5a,4 = 2.7</i> <i>5a,5b = 11.8</i> <i>5a,P = 5.0</i>	4.16 ddd <i>5b,4 = 3.1</i> <i>5b,5a = 11.8</i> <i>5b,P = 1.8</i>	H-7: 6.27 d <i>7,8 = 3.7</i> H-8: 6.98 d <i>8,7 = 3.7</i>	-0.16 -1.01
	A	6.17 d <i>1,2 = 1.2</i>	4.83 dd <i>2,1 = 1.2</i> <i>2,3 = 4.2</i>	5.00 ddd <i>3,2 = 4.2</i> <i>3,4 = 8.6</i> <i>3,P = 6.6</i>	4.495 dtd <i>4,3 = 8.6</i> <i>4,5a = 3.0</i> <i>4,5b = 11.5</i> <i>4,P = 3.0</i>	4.445 ddd <i>5a,4 = 3.0</i> <i>5a,5b = 11.8</i> <i>5a,P = 2.0</i>	4.185 ddd <i>5b,4 = 1.5</i> <i>5b,5a = 11.8</i> <i>5b,P = 3.5</i>	H-2: 8.275 s H-8: 8.26 s	
 <b>CDN-31</b>	8-5,7,9-deaza-G	nd	nd	4.575 d <i>3,2 = 4.2</i> <i>3,4 = 0</i>	4.34 um	4.275 br	4.125 vbd	--	-0.32 -1.14
	A	6.14 d <i>1,2 = 1.0</i>	4.885 overlap	nd	4.495 dddd <i>4,3 = 8.5</i> <i>4,5a = 3.0</i> <i>4,5b = 1.5</i> <i>4,P = 3.0</i>	4.44 ddd <i>5a,4 = 3.0</i> <i>5a,5b = 12.0</i> <i>5a,P = 1.7</i>	4.215 ddd <i>5b,4 = 1.5</i> <i>5b,5a = 12.0</i> <i>5b,P = 3.5</i>	H-2: 8.25 s H-8: 8.20 s	
 <b>CDN-32</b>	AICA	5.94 d <i>1,2 = 8.6</i>	5.095 ddd <i>2,1 = 8.6</i> <i>2,3 = 4.3</i> <i>2,P = 7.8</i>	4.61 d <i>3,2 = 4.3</i> <i>3,4 = 0</i>	4.42 dt <i>4,3 = 0</i> <i>4,5a = 1.7</i> <i>4,5b = 1.6</i>	4.30 ddd <i>5a,4 = 1.7</i> <i>5a,5b = 12.0</i> <i>5a,P = 5.6</i>	4.14 ddd <i>5b,4 = 1.6</i> <i>5b,5a = 12.0</i> <i>5b,P = 3.4</i>	H-2: 7.51 s	-0.60 -0.80
	A	6.16 d <i>1,2 = 2.0</i>	4.78 overlap	5.015 ddd <i>3,2 = 4.7</i> <i>3,4 = 7.7</i> <i>3,P = 6.7</i>	4.48 dtd <i>4,3 = 7.7</i> <i>4,5a = 3.0</i> <i>4,5b = 1.9</i> <i>4,P = 3.6</i>	4.40 ddd <i>5a,4 = 3.0</i> <i>5a,5b = 11.9</i> <i>5a,P = 3.2</i>	4.20 ddd <i>5b,4 = 4.0</i> <i>5b,5a = 11.9</i> <i>5b,P = 4.0</i>	H-2: 8.25 s H-8: 8.26 s	

\*Coupling constants are written in italics in a shortened form (e.g. instead  $J(I',2') = 8.6 \text{ Hz}$  we type simply  $1,2 = 8.6$ ); nd, not determined.

Table S4. The <sup>1</sup>H and <sup>31</sup>P NMR data of 2',3'-CDNs with thiophosphate groups **33** - **37** in D<sub>2</sub>O.\*

Structure	Res.	H-1'	H-2'	H-3'	H-4'	H-5'a	H-5'b	Base	<sup>31</sup> P
 CDN-33	G	5.97 d <i>1,2 = 8.6</i>	5.44 ddd <i>2,1 = 8.6</i> <i>2,3 = 4.0</i> <i>2,P = 7.6</i>	4.62 d <i>3,2 = 4.3</i> <i>3,4 = 0</i>	4.46 dd <i>4,3 = 0</i> <i>4,5a = 3.3</i> <i>4,5b = 1.3</i>	4.25 ddd <i>5a,4 = 3.3</i> <i>5a,5b = 11.7</i> <i>5a,P = 4.8</i>	4.17 ddd <i>5b,4 = 1.3</i> <i>5b,5a = 11.7</i> <i>5b,P = 3.2</i>	H-8: 8.03 s	-1.22 53.59
	A	6.20 s <i>1,2 = 0</i>	5.09 d <i>2,1 = 0</i> <i>2,3 = 4.3</i>	5.04 td <i>3,2 = 4.3</i> <i>3,4 = 8.9</i> <i>3,P = 8.9</i>	4.49 m	4.47 m	4.16 bdd <i>5b,4 = 1</i> <i>5b,5a = 11.0</i> <i>5b,P = 3.0</i>	H-2: 8.27 s H-8: 8.24 s	
 CDN-34	G	5.96 d <i>1,2 = 8.6</i>	5.51 td <i>2,1 = 8.6</i> <i>2,3 = 3.9</i> <i>2,P = 8.5</i>	4.78 overlap <i>3,2 = 4.3</i> <i>3,4 = 0</i>	4.47 dd <i>4,3 = 0</i> <i>4,5a = 3.3</i> <i>4,5b = 1.3</i> <i>4,P = 3.4</i>	4.25 ddd <i>5a,4 = 3.3</i> <i>5a,5b = 11.8</i> <i>5a,P = 5.1</i>	4.17 ddd <i>5b,4 = 1.3</i> <i>5b,5a = 11.8</i> <i>5b,P = 3.1</i>	H-8: 8.025 s	52.88 53.56
	A	6.20 d <i>1,2 = 0.8</i>	5.095 dd <i>2,1 = 0.8</i> <i>2,3 = 4.3</i>	5.05 td <i>3,2 = 4.3</i> <i>3,4 = 8.9</i> <i>3,P = 8.9</i>	4.53 m	4.52 m	4.19 m	H-2: 8.27 s H-8: 8.26 s	
 CDN-35	G	6.04 d <i>1,2 = 8.5</i>	5.46 ddd <i>2,1 = 8.5</i> <i>2,3 = 4.0</i> <i>2,P = 12.4</i>	4.59 d <i>3,2 = 4.0</i> <i>3,4 = 0</i>	4.44 td <i>4,3 = 0</i> <i>4,5a = 2.7</i> <i>4,5b = 1.8</i> <i>4,P = 2.8</i>	4.26 ddd <i>5a,4 = 2.7</i> <i>5a,5b = 11.8</i> <i>5a,P = 5.7</i>	4.18 ddd <i>5b,4 = 1.8</i> <i>5b,5a = 11.8</i> <i>5b,P = 4.0</i>	H-8: 8.29 s	53.36 56.08
	A	6.18 d <i>1,2 = 3.7</i>	5.10 dd <i>2,1 = 3.7</i> <i>2,3 = 4.4</i>	5.29 ddd <i>3,2 = 4.4</i> <i>3,4 = 5.8</i> <i>3,P = 10.2</i>	4.54 ddd <i>4,3 = 5.8</i> <i>4,5a = 6.0</i> <i>4,5b = 2.2</i> <i>4,P = 1.0</i>	4.49 ddd <i>5a,4 = 6.0</i> <i>5a,5b = 11.2</i> <i>5a,P = 7.2</i>	4.06 ddd <i>5b,4 = 2.2</i> <i>5b,5a = 11.2</i> <i>5b,P = 4.1</i>	H-2: 8.26 s H-8: 8.44 s	
 CDN-36	G	6.00 d <i>1,2 = 8.4</i>	5.665 ddd <i>2,1 = 8.4</i> <i>2,3 = 4.2</i> <i>2,P = 11.7</i>	4.55 d <i>3,2 = 4.2</i> <i>3,4 = 0</i>	4.44 t <i>4,3 = 0</i> <i>4,5a = 2.7</i> <i>4,5b = 2.8</i>	4.42 ddd <i>5a,4 = 2.7</i> <i>5a,5b = 11.7</i> <i>5a,P = 8.0</i>	4.11 ddd <i>5b,4 = 2.8</i> <i>5b,5a = 11.7</i> <i>5b,P = 1.3</i>	H-8: 7.97 s	56.67 56.98
	A	6.20 d <i>1,2 = 2.4</i>	4.86 dd <i>2,1 = 2.4</i> <i>2,3 = 4.2</i>	5.30 ddd <i>3,2 = 4.2</i> <i>3,4 = 7.0</i> <i>3,P = 8.3</i>	4.53 ddt <i>4,3 = 7.0</i> <i>4,5a = 5.0</i> <i>4,5b = 1.7</i> <i>4,P = 1.7</i>	4.47 ddd <i>5a,4 = 5.0</i> <i>5a,5b = 11.4</i> <i>5a,P = 5.4</i>	4.06 ddd <i>5b,4 = 1.7</i> <i>5b,5a = 11.4</i> <i>5b,P = 3.8</i>	H-2: 8.27 s H-8: 8.51 s	
 CDN-37	G	6.01 d <i>1,2 = 8.5</i>	5.39 td <i>2,1 = 8.5</i> <i>2,3 = 3.9</i> <i>2,P = 8.8</i>	4.81 d <i>3,2 = 3.9</i> <i>3,4 = 0</i>	4.46 td <i>4,3 = 0</i> <i>4,5a = 2.8</i> <i>4,5b = 1.5</i> <i>4,P = 3.4</i>	4.235 ddd <i>5a,4 = 2.8</i> <i>5a,5b = 11.6</i> <i>5a,P = 4.7</i>	4.18 ddd <i>5b,4 = 1.5</i> <i>5b,5a = 11.6</i> <i>5b,P = 4.2</i>	H-8: 8.16 s	53.38 55.12
	A	6.18 d <i>1,2 = 2.0</i>	5.11 dd <i>2,1 = 2.0</i> <i>2,3 = 4.4</i>	5.08 ddd <i>3,2 = 4.4</i> <i>3,4 = 9.6</i> <i>3,P = 7.4</i>	4.56 ddd <i>4,3 = 9.6</i> <i>4,5a = 4.3</i> <i>4,5b = 2.0</i>	4.43 dt <i>5a,4 = 4.3</i> <i>5a,5b = 11.8</i> <i>5a,P = 4.9</i>	4.22 ddd <i>5b,4 = 2.0</i> <i>5b,5a = 11.8</i> <i>5b,P = 4.9</i>	H-2: 8.25 s H-8: 8.22 s	

\*Coupling constants are written in italics in a shortened form (e.g. instead  $J(1',2') = 8.6 \text{ Hz}$  we type simply  $1,2 = 8.6$ ); nd, not determined.

**Table S5.** Yields of CDNs from enzymatic preparation and their HRMS data for prepared CDNs analysis.

Compound	Enzyme used for CDN preparation	Relative conversion of NTP to CDN [%]	Calculated Mass [M-H]	Measured Mass [M-H]
CDN-1	mouse cGAS-TR	45	675.08834	675.08820
CDN-2	mouse cGAS-TR	59,5	677.08400	677.08278
CDN-3	mouse cGAS-FL	76	675.08834	675.08734
CDN-4	mouse cGAS-TR	55	659.09343	659.09297
CDN-5	mouse cGAS-TR	28	659.09343	659.09259
CDN-6	mouse cGAS-TR	44	677.08400	677.08372
CDN-7	mouse cGAS-TR	74	693.07892	693.07934
CDN-8	mouse cGAS-TR	53	690.09924	690.09967
CDN-9	mouse cGAS-FL	74	672.10866	672.10803
CDN-10	mouse cGAS-TR	43	673.09268	673.09142
CDN-11	mouse cGAS-FL	86	691.08326	691.08289
CDN-12	mouse cGAS-FL	50	657.09776	657.09652
CDN-13	mouse cGAS-FL	43	642.4185	nd
CDN-14	mouse cGAS-FL	85	657.09776	657.09747
CDN-15	mouse cGAS-FL	38	691.05879	691.05764
CDN-16	mouse cGAS-FL	65	688.10358	688.10255
CDN-17	mouse cGAS-TR	45	687.10833	687.10823
CDN-18	mouse cGAS-TR	53	674.07669	674.07623
CDN-19	mouse cGAS-FL	94	690.07161	690.07072
CDN-20	mouse cGAS-TR	70	690.05385	690.05287
CDN-21	human cGAS-TR	77	673.09268	673.09210
CDN-22	human cGAS-TR	56	719.08040	719.07920
CDN-23	mouse cGAS-TR	94	704.06950	704.06919
CDN-24	mouse cGAS-TR	93	672.09743	672.09589
CDN-25	mouse cGAS-TR	58	674.08793	674.08681
CDN-26	mouse cGAS-FL	54	664.09234	664.09209
CDN-27	mouse cGAS-FL	87	674.07669	674.07557
CDN-28	mouse cGAS-TR	73	687.10833	687.10727
CDN-29	*	*	658.08178	658.08061
CDN-30	mouse cGAS-FL	96	672.09743	672.09596
CDN-31	mouse cGAS-FL	78	689.05860	689.05747
CDN-32	mouse cGAS-FL	59	648.09743	648.09582
CDN-33	mouse cGAS-TR	64,5	689.06983	689.06894
CDN-34	mouse cGAS-TR	58	705.04699	705.04568
CDN-35	*	*	705.04699	705.04688
CDN-36	*	*	705.04699	705.04644
CDN-37	*	*	705.04699	705.04674

cGAS-TR, truncated version of cGAS, cGAS-FL, full length version of cGAS \*CDNs prepared by organic synthesis; nd, not determined. Reaction conversions were determined by HPLC using UV detection at 260 nm. Conversions are defined as follows; a ratio of AUC of a CDN over the sum of AUCs of the CDN, NTPs and NDPs.

**Table S6.** Crystallography data collection and processing

<b>Crystal</b>	<b>wf STING_CDN-1</b>	<b>wf STING_CDN-24</b>
<b>Diffraction source</b>	Rotating Anode, Rigaku Micromax-007 HF	BESSY ID 14-2
<b>Detector</b>	Pixel, Dectris Pilatus 200K	Pixel, Dectris Pilatus 2M
<b>Space group</b>	P4 <sub>1</sub> 2 <sub>1</sub> 2	P 2 <sub>1</sub> 2 <sub>1</sub> 2
<b>Resolution (Å)</b>	2.8	2.05
<b>R<sub>sym</sub> (deg)*</b>	0.1567	0.1350
<b>Completeness (%)</b>	99.62	99.17
<b>a (Å)</b>	111.441	93.776
<b>b (Å)</b>	111.441	116.478
<b>c (Å)</b>	35.24	35.845

\* $R_{\text{sym}} = \frac{\sum_{hkl} \sum_j |I_{hkl,j} - \langle I_{hkl} \rangle|}{\sum_{hkl} \sum_j I_{hkl,j}}$  where  $\langle I_{hkl} \rangle$  is the average symmetry-related observations of a unique reflection.

**Table S7.** Crystallography structure solution and refinement

Crystal	wtSTING_CDN-1	wtSTING_CDN-24
<b>Resolution</b>	35.24 - 2.802*	33.48 - 2.05*
<b>R<sub>cryst</sub><sup>#</sup></b>	0.2037	0.1958
<b>R<sub>free</sub></b>	0.2761	0.2431
<b>RMS deviation bond length (Å)</b>	0.012	0.014
<b>RMS deviation bond angle (deg)</b>	1.54	1.51
<b>PDB code</b>	6S27	6S26

\* It has been proven that including data with mean  $I/\sigma(I) < 2.0$  leads to improved electron density maps.<sup>4</sup> We have decided to cut the data at 2.8 Å leading to  $I/\sigma(I) = 1.89$  in the highest resolution shell for **wtSTING\_CDN-1** and 2.05 Å leading to  $I/\sigma(I) = 1.21$  in the highest resolution shell for **wtSTING\_CDN-24**.  $I/\sigma(I) = 2$  in case of **wtSTING\_CDN-1** corresponds to 3 Å resolution and in case of for **wtSTING\_CDN-24** corresponds to 2.2 Å.

<sup>#</sup> $R_{\text{cryst}} = \frac{\sum_{\text{hkl}} |F_{\text{hkl}}^{\text{obs}} - F_{\text{hkl}}^{\text{calc}}|}{\sum_{\text{hkl}} F_{\text{hkl}}^{\text{obs}}}$  where F is the structure factor. R<sub>free</sub> differs from R<sub>cryst</sub> in the set of reflections, which were used for its calculation (for R<sub>free</sub> usually 10% of working set).

**Table S8.** Effect of CDNs on CD14+ monocyte and CD3+ T-cell populations and cytokine induction in PBMC Assay (Donor 2).

Compound	Monocyte viability <sup>a</sup>	T-lymphocyte viability <sup>b</sup>	Cytokines (fold of 2'3'cGAMP induced cytokines) <sup>c</sup>		
			INF $\gamma$	TNF $\alpha$	IFN $\alpha$
CDN-1	2.1%	101.3%	1.30	1.75	2.48
CDN-2	1.5%	106.0%	0.74	1.37	1.81
CDN-3	1.0%	108.7%	1.05	1.50	1.70
CDN-4	1.95%	97.0%	0.93	1.38	1.97
CDN-5	5.5%	103.3%	1.28	2.48	0.23
CDN-6	0.3%	106.7%	0.11	0.67	0.08
CDN-7	0.5%	109.2%	1.35	1.73	0.71
CDN-8	2.3%	102.9%	1.10	1.37	1.45
CDN-9	21.3%	109.2%	1.14	1.91	1.25
CDN-10	3.9%	100.4%	1.71	2.60	2.10
CDN-11	7.8%	107.3%	2.01	2.33	1.79
CDN-12	6.1%	113.7%	1.82	2.84	1.23
CDN-13	nd	nd	n.d.	n.d.	n.d.
CDN-14	3.0%	112.0%	1.14	1.34	1.16
CDN-15	0.4%	97.0%	1.13	2.41	0.34
CDN-16	3.2%	105.7%	1.84	3.80	0.88
CDN-17	3.6%	106.0%	1.55	1.84	1.05
CDN-18	nd	nd	n.d.	n.d.	n.d.
CDN-19	85.8%	102.2%	0.05	0.08	0.03
CDN-20	6.4%	106.5%	1.59	1.53	0.69
CDN-21	2.5%	108.4%	1.25	1.76	0.46
CDN-22	28.2%	112.6%	1.08	2.00	0.05
CDN-23	nd	nd	n.d.	n.d.	n.d.
CDN-24	4.0%	100.2%	0.94	2.01	0.45
CDN-25	nd	nd	n.d.	n.d.	n.d.
CDN-26	29.1%	106.4%	0.49	0.27	0.36
CDN-27	35.0%	110.2%	0.33	0.20	0.13
CDN-28	2.7%	98.5%	0.91	1.05	0.61
CDN-29	4.7%	109.5%	1.10	1.12	1.28
CDN-30	1.3%	110.0%	1.13	1.63	0.56
CDN-31	1.0%	100.8%	1.83	1.60	1.58
CDN-32	39.8%	110.6%	0.67	0.12	0.70
CDN-33	7.6%	103.6%	1.48	1.42	1.19
CDN-34	1.5%	98.9%	1.44	1.80	3.80
CDN-35	4.7%	107.0%	1.12	0.94	0.64
CDN-36	0.7%	99.8%	0.31	1.08	0.34
CDN-37	1.0%	95.8%	1.06	0.81	1.61

S28

2'2'cGAMP	1.6%	105.3%	1.21	1.40	1.42
3'3'c-diGMP	106.5%	104.1%	0.00	0.02	0.02
3'3'cGAMP	3.4%	109.5%	1.05	1.03	0.78
2'3'cGAMP	5.6%	110.5%	1.00	1.00	1.00

<sup>a</sup> Viability of monocytes in PBMC culture treated with 12.5µM CDN for 16 h. Values are the mean of three independent determinations from one PBMC donor. Viability of monocytes in untreated control equals 100%.

<sup>b</sup> Viability of CD3 T-lymphocytes in PBMC culture treated with 12.5µM CDN for 16 h. Values are the mean of three independent determinations from one PBMC donor. Viability of T-lymphocytes in untreated control equals 100%.

<sup>c</sup> Levels of INF α, INF γ and TNFα secreted by PBMC treated with 12.5µM CDN for 16 h relative to levels secreted by PBMC treated with 12.5µM 2'3'cGAMP. Values are the mean of three independent determinations from the same PBMC donor as in monocyte/CD3 T-lymphocyte cytotoxicity assay; Amount of cytokines induced by 2'3'cGAMP treatment: Interferon γ: 28579 pg/ml, TNFα: 5340 pg/ml, Interferon α: 295 pg/ml. nd, not determined



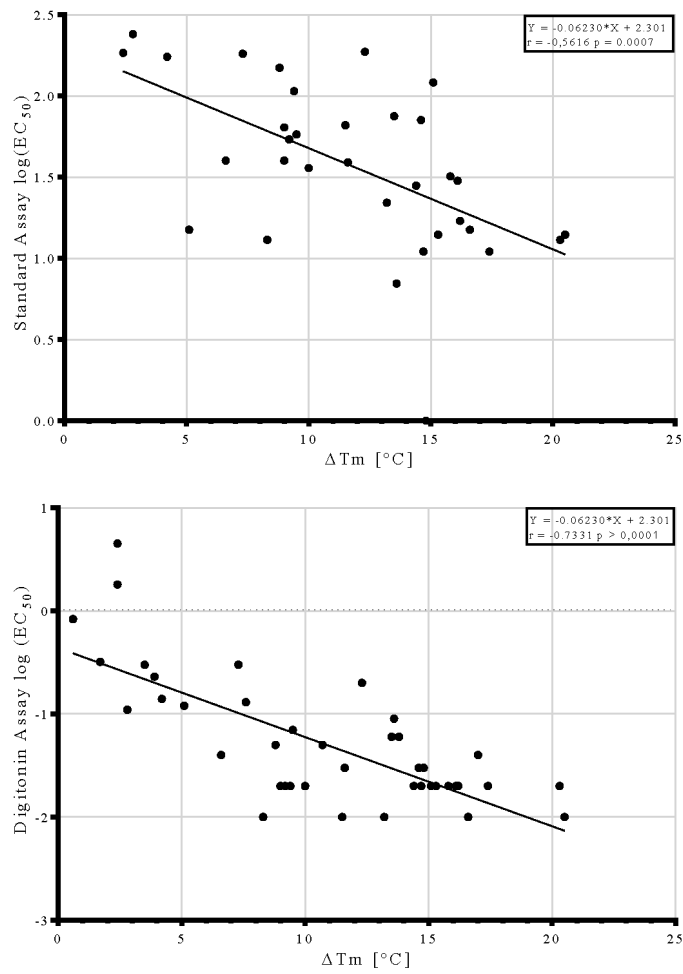


**Figure S1.** Correlation of  $\Delta T_m$  values from DSF Assay and log  $EC_{50}$  values from Standard or Digitonin Assay of prepared CDNs.

S30

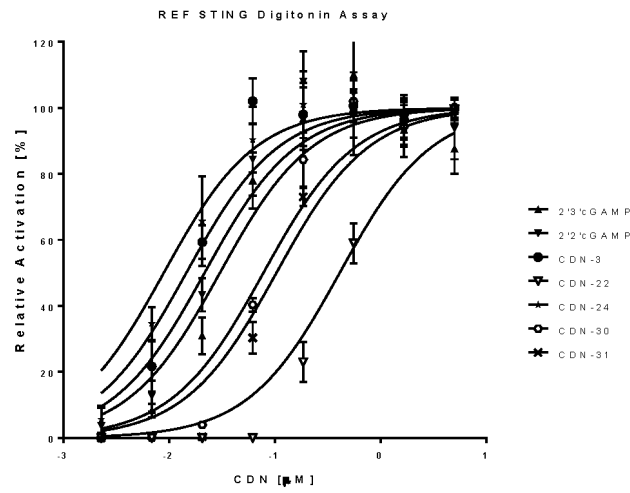
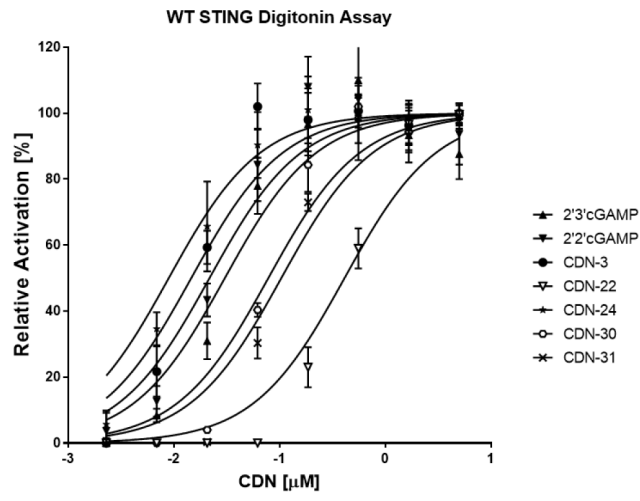


**Figure S2.** Representative dose response curves of 5 CDNs from Digitonin Assay on WT or REF STING haplotypes.

S31

### Supplementary files

Structures obtained from computational modeling are provided in file jm9b01062\_si\_002.zip, which contains three folders:

confsampl: structures of ligands identified by conformational sampling as global minima and those obtained from QM/MM calculation

QMMM: QM/MM structures for a series of ligands. Full system with 2'3'cGAMP is provided. Only the QM region is provided for the other ligands (non-QM region was kept identical). These include CDN-1, CDN-10, and four diastereoisomers of CDN-34.

docking: selected CDNs docked into 4KSY pdb structure

Molecular formula strings can be found in SI file jm9b01062\_si\_003.csv

## REFERENCES

- (1) Yi, G.; Brendel, V. P.; Shu, C.; Li, P.; Palanathan, S.; Cheng Kao, C. Single Nucleotide Polymorphisms of Human STING Can Affect Innate Immune Response to Cyclic Dinucleotides. *PLoS ONE* **2013**, *8* (10), e77846. <https://doi.org/10.1371/journal.pone.0077846>.
- (2) Lang, P. T.; Brozell, S. R.; Mukherjee, S.; Pettersen, E. F.; Meng, E. C.; Thomas, V.; Rizzo, R. C.; Case, D. A.; James, T. L.; Kuntz, I. D. DOCK 6: Combining Techniques to Model RNA–Small Molecule Complexes. *RNA* **2009**, *15* (6), 1219–1230. <https://doi.org/10.1261/rna.1563609>.
- (3) Pettersen, E. F.; Goddard, T. D.; Huang, C. C.; Couch, G. S.; Greenblatt, D. M.; Meng, E. C.; Ferrin, T. E. UCSF Chimera--a Visualization System for Exploratory Research and Analysis. *J Comput Chem* **2004**, *25* (13), 1605–1612. <https://doi.org/10.1002/jcc.20084>.
- (4) Karplus, P. A.; Diederichs, K. Linking Crystallographic Model and Data Quality. *Science* **2012**, *336* (6084), 1030–1033. <https://doi.org/10.1126/science.1218231>.

## **8.2. Supplement S2: Discovery of isonucleotidic CDNs as potent STING agonists with immunomodulatory potential**

*Dejmek, M., Šála, M., Brazdova, A., **Vanekova, L.**, Smola, M., Klíma, M., Břehová, P., Buděšínský, M., Dračínský, M., Procházková, E., Zavřel, M., Šimák, O., Páv, O., Boura, E., Birkuš, G., & Nencka, R. (2022). Discovery of isonucleotidic CDNs as potent STING agonists with immunomodulatory potential. *Structure (London, England : 1993)*, 30(8), 1146–1156.e11. <https://doi.org/10.1016/j.str.2022.05.012>*

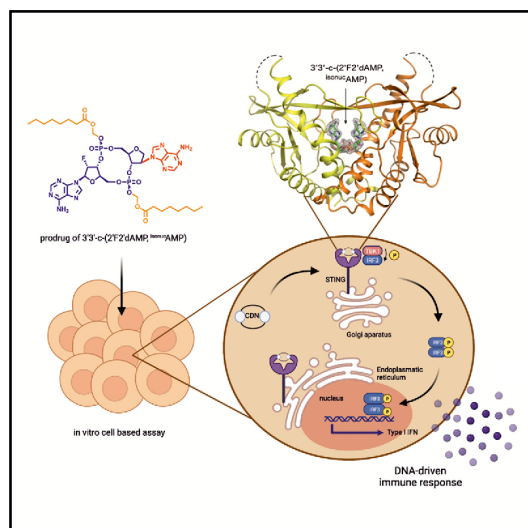
My contribution:

*In vitro* screening of tested CDNs using established DSF and cell-based *in vitro* assays, data evaluation and interpretation, participation in manuscript preparation.

# Structure

## Discovery of isonucleotidic CDNs as potent STING agonists with immunomodulatory potential

### Graphical abstract



### Authors

Milan Dejmek, Michal Šála, Andrea Brazdova, ..., Evzen Boura, Gabriel Birkuš, Radim Nencka

### Correspondence

nencka@uochb.cas.cz

### In brief

Stimulator of interferon genes (STING) is an adaptor protein of the cGAS-STING signaling pathway mediating host immunity. Dejmek et al. present a class of STING agonists: isonucleotidic cyclic dinucleotides (CDNs) and their prodrugs. These molecules display unprecedented efficiency in agonizing STING and proved to be potent inducers of immune response.

### Highlights

- Preparation of previously unknown class of cyclic dinucleotides is reported
- Isonucleotidic CDNs and their prodrugs display exceptional STING agonistic properties
- X-ray structure of the lead CDN with 3',3'-c-(2'F,2'dAMP, isonucAMP) is presented
- Compounds show excellent performance in cytokine secretion

Dejmek et al., 2022, *Structure* 30, 1–11  
 August 4, 2022 © 2022 Elsevier Ltd.  
<https://doi.org/10.1016/j.str.2022.05.012>



Article

# Discovery of isonucleotidic CDNs as potent STING agonists with immunomodulatory potential

Milan Dejmejk,<sup>1</sup> Michal Sála,<sup>1</sup> Andrea Brazdova,<sup>1</sup> Lenka Vanekova,<sup>1,2</sup> Miroslav Smola,<sup>1</sup> Martin Klíma,<sup>1</sup> Petra Břehová,<sup>1</sup> Miloš Buděšínský,<sup>1</sup> Martin Dračínský,<sup>1</sup> Eliška Procházková,<sup>1</sup> Martin Zavřel,<sup>1</sup> Ondřej Šimák,<sup>1</sup> Ondřej Páv,<sup>1</sup> Evzen Boura,<sup>1</sup> Gabriel Birkus,<sup>1</sup> and Radim Nencka<sup>1,3,\*</sup>

<sup>1</sup>Institute of Organic Chemistry and Biochemistry of the Czech Academy of Sciences, 16610 Prague, Czech Republic

<sup>2</sup>Faculty of Science, Charles University, 128 00 Prague, Czech Republic

<sup>3</sup>Lead contact

\*Correspondence: [nencka@uochb.cas.cz](mailto:nencka@uochb.cas.cz)

<https://doi.org/10.1016/j.str.2022.05.012>

## SUMMARY

Stimulator of interferon genes (STING) is an adaptor protein of the cGAS-STING signaling pathway involved in the sensing of cytosolic DNA. It functions as a receptor for cyclic dinucleotides (CDNs) and, upon their binding, mediates cytokine expression and host immunity. Besides naturally occurring CDNs, various synthetic CDNs, such as ADU-S100, have been reported to effectively activate STING and are being evaluated in clinical trials for the treatment of cancer. Here, we describe the preparation of a unique new class of STING agonists: isonucleotidic cyclic dinucleotides and the synthesis of their prodrugs. The presented CDNs stimulate STING with comparable efficiency to ADU-S100, whereas their prodrugs demonstrate activity up to four orders of magnitude better due to the improved cellular uptake. The compounds are very potent inducers of inflammatory cytokines by peripheral blood mononuclear cells (PBMCs). We also report the X-ray crystal structure of the lead inhibitor bound to the wild-type (WT) STING.

## INTRODUCTION

Sensing of nucleic acids in the cytosolic compartment of cells is an important component of the innate immunity of mammals, including humans. The cyclic GMP-AMP synthase-stimulator of interferon genes (cGAS-STING) signaling pathway plays an important role in the detection of cytosolic DNA derived from pathogens such as bacteria and viruses as well as host DNA released from the nucleus or mitochondria under various stress conditions such as a malignant transformation of cells (Hopfner and Hornung, 2020; Cheng et al., 2020) (Figure 1). cGAS is a DNA-sensing receptor responsible for the detection of double-stranded DNA in cytosol. When cGAS binds to DNA, it is activated and begins the synthesis of the 2',3'-cGAMP (2',3'-cGAMP, **1**) (Figure 2), which acts as a natural agonist of STING (Gao et al., 2013; Novotna et al., 2019; Pimková Polidarová et al., 2021). STING can also be activated by bacterial 3',3'-cyclic dinucleotide (CDN) agonists (Kalia et al., 2013) (e.g. 3',3'-cGAMP, **2**), synthetic CDNs (Birkus et al., 2020, 2019; Dubensky and Kanne, 2014; Kim et al., 2021; Pan et al., 2020; Pimková Polidarová et al., 2021; Vyskocil et al., 2021) (e.g., ADU-S100, **3**) or non-CDN STING agonists (Motwani et al., 2019; Ramanjulu et al., 2018).

Inactive STING is a dimeric transmembrane protein located in the endoplasmic reticulum (ER) that adopts a V-shaped, opened conformation. When STING binds 2',3'-cGAMP, it changes to

the closed conformation, translocates from the ER to the ER-Golgi intermediate compartment, and then moves through the Golgi apparatus to the perinuclear regions (Hopfner and Hornung, 2020). Subsequently, activated STING recruits TANK-binding kinase 1 (TBK1). TBK1 phosphorylates both itself and STING by binding to activated STING. The complex of STING and TBK1 binds interferon regulatory factor 3 (IRF3), whereas TBK1 phosphorylates IRF3 (pIRF3). After its phosphorylation, IRF3 dissociates from STING-TBK1 complex, and, in the nucleus, it induces the expression of type I interferon (IFN) genes. TBK1 also activates the nuclear factor  $\kappa$ B (NF- $\kappa$ B), which can also be activated by the kinase I $\kappa$ B epsilon (IKK $\epsilon$ ), through which it contributes to the expression of cytokines and chemokines (Hopfner and Hornung, 2020; Balka et al., 2020; Flood et al., 2019; Du and Su, 2017).

The canonical STING agonist 2',3'-cGAMP consists of 5'-AMP connected via its phosphate to the 2' position of 5'-GMP, which is cyclized through its phosphate to the 3' position of the aforementioned 5'-AMP (Figure 2). The analogous derivatives are therefore called 2',3'-CDNs. Nevertheless, STING can be also activated by the above-mentioned 3',3'-CDNs that are produced by bacteria, namely 3',3'-cGAMP, 3',3'-c-di-AMP, and 3',3'-c-di-GMP (Kalia et al., 2013). Recently, CDNs have become one of the extremely active fields in medicinal chemistry due to their potential application in the therapy of solid tumors (Flood et al., 2019;

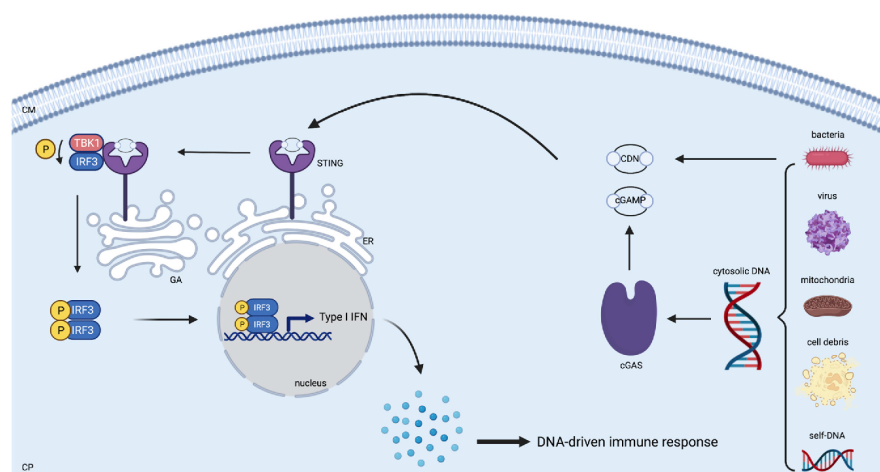


**Figure 1. Depiction of the cyclic GMP-AMP synthase (cGAS)-stimulator of interferon genes (STING) signaling pathway**  
CDNs, cyclic dinucleotides; cGAMP, 2',3'-cyclic GMP-AMP; CM, cell membrane; CP, cytoplasm; ER, endoplasmic reticulum; GA, Golgi apparatus; IFNs, interferons; TBK1, TANK-binding kinase 1; IRF3, interferon regulatory factor 3 transcription factor; P, phosphorylation. Figure adapted from Motwani et al. (2019) and Zheng et al. (2020) and modified and created with BioRender.com.

Sivick et al., 2018) and several viral diseases, e.g., chronic hepatitis B (Guo et al., 2017; Pimkova Polidarova et al., 2022). A comprehensive review of CDN modifications was written by Zhang and coworkers (Zhang et al., 2020). There are several conclusions that one can derive from the contemporary knowledge of these compounds. Firstly, many modifications of the natural nucleobases do not affect the biological activity of CDNs. Secondly, the substitutions of free hydroxy groups on the sugar moieties by fluorine, hydrogen, and several other substituents either retain or increase their affinity to the STING protein. Natural phosphate linkers can be substituted by phosphorothioates and masked by certain type of prodrugs (Birkus et al., 2020; Pimkova Polidarova et al., 2021).

Despite this extensive research driven mostly by the pharmaceutical industry, all the contemporarily unveiled CDN-based STING agonists bear the nucleobase or its bioisostere in the 1' position of the sugar or pseudosugar moiety. Here, to the best of our knowledge, we report on the first example of CDN in which one nucleoside is substituted by an isonucleosidic derivative, a nucleoside that bears the nucleobase in the 2' position, resulting in isonucleotidic CDNs (IsoCDNs). We performed physicochemical and biological characterizations of the novel compounds, proving that these compounds are able to effectively bind to STING variants and induce the production of type I (IFN $\alpha$ ) or II (IFN $\gamma$ ) IFNs, together with tumor necrosis factor alpha (TNF- $\alpha$ ). We also demonstrated the superiority of prepared prodrugs based on their cell-based activity compared with the parent CDNs. This is due to vastly improved cellular uptake of the otherwise charged and rather polar nature

of CDNs. We were also able to solve a crystal structure of wild-type STING in complex with one of our IsoCDNs, which clearly explains the binding mode of these compounds and shows why even this unusually positioned nucleobase is well accepted by the protein.

## RESULTS AND DISCUSSION

### Rational design of isonucleosidic CDNs and their synthesis

Isonucleosides are modified derivatives of nucleosides whose first representatives were synthesized almost half a century ago. During this time, they have been used in both medicinal chemistry for targeting viral diseases (Jiang et al., 2007; Purdy et al., 1994) and as building blocks for the synthesis of linear dinucleotides that possess HIV integrase inhibitory activity (Chi et al., 2004; Taktakishvili et al., 2000). In neither of these applications, however, did isonucleosides see any major success. This can be attributed to the rather significantly altered geometry of the nucleoside, which seems to prevent their proper recognition by the proteins they target. In extensive efforts to understand how the STING protein is able to recognize particular modifications on CDNs (Novotna et al., 2019; Simola et al., 2021; Vavrina et al., 2021), certain modifications of the nucleobase, sugar, and the phosphate part of CDNs have been shown to be tolerated. Therefore, we decided to incorporate CDN modifications in the design of new derivatives that should significantly alter their overall geometry: we selected isonucleosides as appropriate candidates (Figure 3).



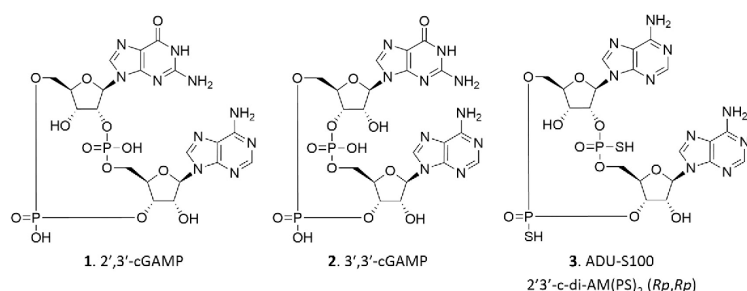


Figure 2. Examples of naturally occurring and synthetic CDNs acting as STING agonists

The synthesis of isonucleosides usually consists of the reduction of a suitably protected ribose to afford anhydro-ribose, which is followed by a nucleobase introduction (Bera et al., 1999; Kakefuda et al., 1994; Montgomery and Thomas, 1978). This operation can be achieved by the nucleophilic displacement of a 2'-hydroxymethylate or by a nucleobase construction on a previously introduced amino group. However, we instead found it more convenient to use the Mitsunobu reaction for the transformation, and thus we prepared isonucleosidic adenosine **6** (IsoA). Adenine nucleobase was subsequently protected (benzoyl and pentenyl [PNT], respectively), and an H-phosphonate and a phosphoramidite, respectively, were introduced as phosphate precursor groups (Figure 4). Guanine-based isonucleoside **S6** (IsoG) was synthesized in the same manner as the adenine-based one, and the experimental details are described in the supplemental information.

These monomers were subsequently combined with commercially available phosphoramidites (of 2'-fluoro-2'-deoxy-adenosine, 2'-deoxy-adenosine, or guanosine) to form CDNs. We decided to focus mainly on the fluorinated monomers because of our recently published discoveries in which the fluorinated CDNs were always more active than their OH-containing analogs (Smola et al., 2021). We used a pyridine-trifluoroacetate-mediated coupling of a phosphoramidite-containing unit to a free 5'-OH group of an H-phosphonate-containing unit. The obtained

linear dinucleotide was then cyclized via DMOC-induced macrocycle closure. Phosphorus(III) groups were either oxidized into phosphates using tBHP and iodine, respectively, or sulfurized to phosphorothioates using xanthane hydride and Beaucage reagent, respectively. Final cleavage of the acyl protection of nucleobases, together with the cyanoethyl protection of the phosphate OH group, was performed using methylamine solution in ethanol (Figure 5). Synthesized CDNs were isolated by reverse phase chromatography (high-performance liquid chromatography [HPLC] or medium-pressure liquid chromatography [MPLC]) with TEAB as a mobile phase modifier. As expected, phosphorothioate **20** was obtained as a mixture of 4 diastereomers, where the amounts of the two most polar were negligible, and the third and fourth were separable by HPLC and characterized and tested separately. Meticulous analysis of nuclear magnetic resonance (NMR) data led us to believe that the IsoA-3'-phosphorothioate sulfur atom points almost exclusively below the plane of the macrocycle, whereas the 2'-fluoro-2'-deoxy-adenosine phosphorothioate group was formed as a 1:1 mixture. The analysis is further described in detail in the STAR Methods.

#### Evaluation of biological activity of the parent CDNs

The biological activity of the prepared compounds was evaluated using the reporter HEK 293T ISRE cell lines in the

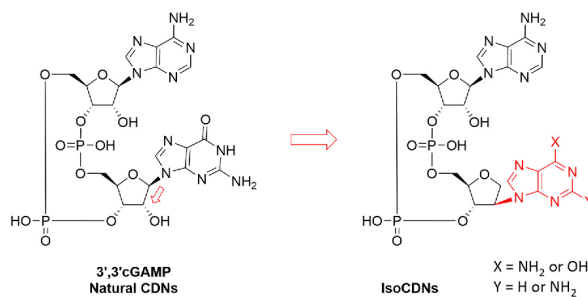
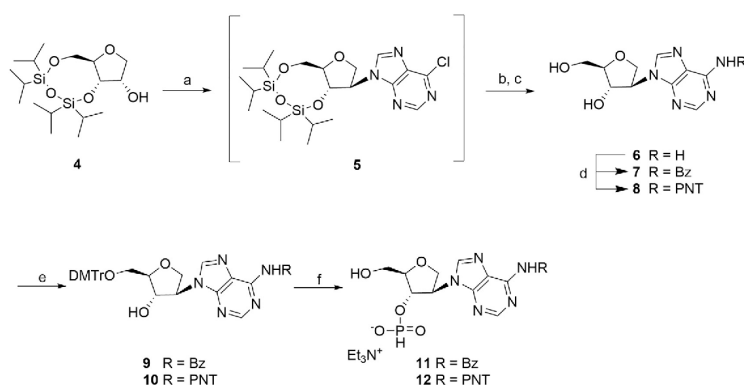


Figure 3. Design of IsoCDNs as potential STING agonists



**Figure 4. Synthesis of the isonucleotidic H-phosphonate monomer**  
(a–f) Reagents and conditions are as follows: (a) 6-chloropurine, PPh<sub>3</sub>, DIAD, THF; (b) NH<sub>2</sub>-EtOH, dioxane, 90°C, 24 h; (c) 80% FA, 65°C, 18 h; (d) TMSCl, BzCl, py or TMSCl, PNT<sub>2</sub>O, py; (e) DMTrCl, py; and (f) (1) diphenyl phosphite, py, RT, 40 min and (2) DCA, DCM, RT, 30 min.

presence of a mild detergent, digitonin A (Figure 6). In this format, CDNs freely diffuse into cells without the need of an active uptake, and the assay predicts the activity of optimized prodrugs of these CDNs in the absence of the detergent (Novotna et al., 2019; Pimková Polidarová et al., 2021). Furthermore, direct binding of CDNs to STING was determined by the means of differential scanning fluorimetry (DSF) (Novotna et al., 2019; Vavrina et al., 2021). The human STING has been described in five major allelic variants, which were annotated as wild type (WT), HAQ (R71H-G230A-R293Q), REF (H232R), G230A-AQ (R293Q), and Q (R293Q). These forms display different binding capacity for CDNs, as, for example, the REF STING binds the 3'3'-CDNs less efficiently (Novotna

et al., 2021). Even though this particular single-nucleotide mutation is not very strongly populated (Lubbers et al., 2021), it is vital to evaluate the ability of the IsoCDNs to stimulate all allelic forms of STING.

Outstanding results of the STING agonistic properties of 19 were revealed, which prompted us to synthesize an additional seven CDNs and draw a relatively straightforward SAR (structure-activity relationship). The most active compounds, 19 and 21, contained the nucleoside 6 (IsoA) and a 2'-fluorinated 2'-deoxyribonucleoside (A or G) as a partner. The inverse combination 22, with the IsoG S6 (synthesis described in the supplemental information) as a monomer, resulted in a 2- to 4-fold decrease of potency compared with the lead compound.

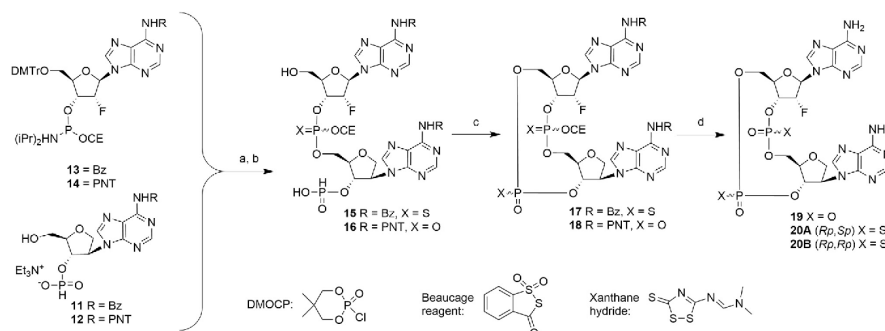
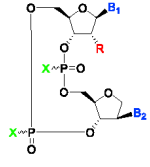


**Figure 5. Synthesis of 3'3'-c-(2F2 dAMP, isonucAMP), typical example of isoCDN preparation**  
(a–d) Reagents and conditions are as follows: (a) py-TFA, tBHP or xanthane hydride, ACN; (b) DCA, DCM; (c) DMOCP, l<sub>2</sub> or Beaucage reagent, py; and (d) CH<sub>3</sub>NH<sub>2</sub>, EtOH.



					DSF $\Delta T_m$ ( $^{\circ}\text{C}$ ) <sup>a</sup> ( $\pm$ SEM)		Digitonin assay - $\text{EC}_{50}$ ( $\mu\text{M}$ ) <sup>b</sup> ( $\pm$ SEM)				
	B <sub>1</sub>	B <sub>2</sub>	R	X	WT	AQ	WT	HAQ	REF	AQ	Q
1	2',3'-cGAMP				15.3 ( $\pm$ 0.17)	22.7 ( $\pm$ 0.19)	0.02 ( $\pm$ 0.004)	0.02 ( $\pm$ 0.003)	0.07 ( $\pm$ 0.02)	0.04 ( $\pm$ 0.01)	0.05 ( $\pm$ 0.02)
2	3',3'-cGAMP				5.1 ( $\pm$ 0.14)	13.2 ( $\pm$ 0.16)	0.12 ( $\pm$ 0.03)	0.12 ( $\pm$ 0.01)	4.26 ( $\pm$ 0.49)	0.26 ( $\pm$ 0.09)	2.06 ( $\pm$ 0.36)
3	ADU-S100				9.3 ( $\pm$ 0.18)	17.1 ( $\pm$ 0.20)	0.08 ( $\pm$ 0.01)	0.26 ( $\pm$ 0.05)	1.64 ( $\pm$ 0.28)	0.23 ( $\pm$ 0.03)	1.01 ( $\pm$ 0.19)
19	A	A	F	O	5.6 ( $\pm$ 0.50)	13.3 ( $\pm$ 0.40)	0.02 ( $\pm$ 0.01)	0.10 ( $\pm$ 0.03)	7.30 ( $\pm$ 1.00)	0.08 ( $\pm$ 0.02)	0.79 ( $\pm$ 0.10)
20A	A	A	F	S	8.5 ( $\pm$ 0.30)	17.2 ( $\pm$ 0.03)	0.01 ( $\pm$ 0.00)	0.065 ( $\pm$ 0.015)	1.65 ( $\pm$ 0.75)	0.08 ( $\pm$ 0.02)	0.26 ( $\pm$ 0.07)
20B	A	A	F	S	11.0 ( $\pm$ 0.40)	20.0 ( $\pm$ 0.17)	0.01 ( $\pm$ 0.006)	0.06 ( $\pm$ 0.03)	1.50 ( $\pm$ 0.00)	0.055 ( $\pm$ 0.035)	0.20 ( $\pm$ 0.13)
21	G	A	F	O	8.5 ( $\pm$ 0.05)	16.9 ( $\pm$ 0.05)	0.025 ( $\pm$ 0.005)	0.095 ( $\pm$ 0.035)	0.75 ( $\pm$ 0.25)	0.075 ( $\pm$ 0.025)	0.40 ( $\pm$ 0.20)
22	A	G	F	O	6.8 ( $\pm$ 0.10)	15.8 ( $\pm$ 0.30)	0.08 ( $\pm$ 0.00)	0.20 ( $\pm$ 0.00)	3.85 ( $\pm$ 1.05)	0.20 ( $\pm$ 0.00)	2.03 ( $\pm$ 1.58)
23	A	A	H	O	1.8 ( $\pm$ 0.30)	9.3 ( $\pm$ 0.30)	0.28 ( $\pm$ 0.015)	0.30 ( $\pm$ 0.20)	>45	0.14 ( $\pm$ 0.02)	13.90 ( $\pm$ 8.1)
24	A	G	H	O	2.9 ( $\pm$ 0.08)	11.5 ( $\pm$ 0.10)	0.28 ( $\pm$ 0.05)	0.40 ( $\pm$ 0.09)	0.40 ( $\pm$ 0.08)	0.26 ( $\pm$ 0.07)	11.40 ( $\pm$ 2.00)
25 <sup>c</sup>	A	G	H	O	2.4 ( $\pm$ 0.05)	10.7 ( $\pm$ 0.40)	1.35 ( $\pm$ 0.35)	0.77 ( $\pm$ 0.33)	>45	0.68 ( $\pm$ 0.02)	26.90 ( $\pm$ 22.1)

**Figure 6. Activities of CDNs in the digitonin HEK 293T cell-based reporter assay**

<sup>a</sup>The values of the melting temperature ( $\Delta T_m$ ) obtained by differential scanning fluorimetry (DSF) performed with different STING haplotypes.  $\Delta T_m$  values expressed as mean value  $\pm$  standard error of mean (SEM) of at least two independent experiments.

<sup>b</sup>Results from the digitonin assay using 293T reporter cells expressing different STING protein haplotypes.  $\text{EC}_{50}$  values expressed as mean values  $\pm$  SEM of at least two independent experiments measured in triplicate.

<sup>c</sup>Compound **25** has both units isonucleosidic.

Omitting the fluorine atom and using 2'-deoxyribosides diminished the activity even more (compounds **23** and **24**), and using isonucleotides as both CDN units resulted in the poorly active molecule **25**. As expected, diastereoisomeric molecules **20A** and **20B** containing thiophosphate linkages exerted similar agonistic potency as the phosphate-linked analogue.

#### Crystallographic analysis of the STING-19 interaction

To uncover the atomic details of the STING-19 interaction, we performed a crystallographic analysis of the STING/19 complex. The STING/19 crystals diffracted to 2.6 Å resolution and belonged to the tetragonal P4<sub>1</sub>2<sub>1</sub>2 space group. The structure was subsequently solved by molecular replacement using the

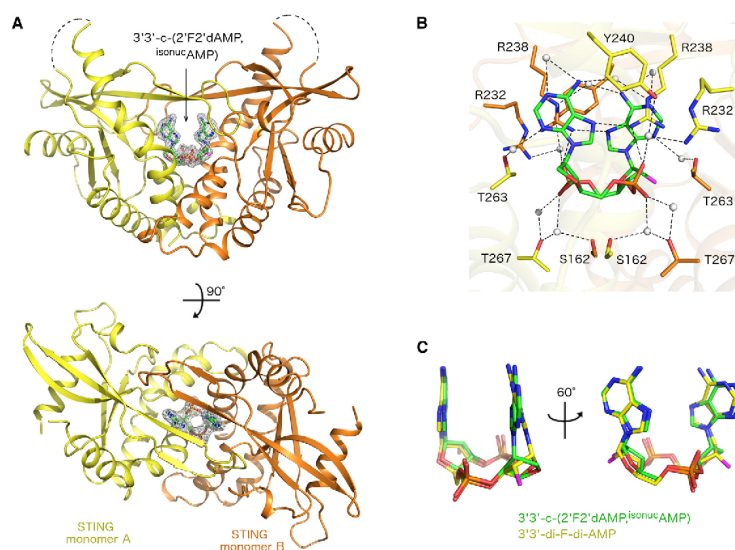


**Figure 7. Crystal structure of human STING in complex with 19**

(A) Overall view of the STING/19 complex. The protein backbone is shown in cartoon representation; the two STING monomers are depicted in yellow and orange. The 19 ligand is shown in stick representation and colored according to elements: carbon, green; nitrogen, blue; oxygen, red; phosphorus, orange; fluorine, magenta. The unbiased *F<sub>o</sub>-F<sub>c</sub>* omit map contoured at 3 $\sigma$  is shown around the ligand 19.

(B) Detailed view of the 19-ligand binding site. The ligand and side chains of selected STING amino-acid residues are shown in stick representation with carbon atoms colored according to the protein assignment and other elements colored as in (A). Water molecules are shown as gray spheres; hydrogen atoms are not shown. Selected hydrogen bonds involved in the STING-19 interaction are presented as dotted black lines.

(C) Superposition of 3',3'-c-GAMP (2, PDB: 6YDZ [Smola et al., 2021]) and 3',3'-c-(2'F<sub>2</sub>'dAMP, isonucAMP) (19, PDB: 7Q3B, from this publication) bound to STING. The ligands are shown in stick representation with carbon atoms colored in yellow (2) or green (19), and other elements colored as in (A). The STING protein molecules are not shown.

crystal structure of the STING/cGAMP complex as a search model (PDB: 4KSY [Zhang et al., 2013]). The structure was further refined to  $R_{\text{free}} = 23.17\%$  and  $R_{\text{work}} = 19.46\%$  (Supplementary Tables 1 and 2). One molecule of STING per one asymmetric unit and one molecule of the 19 ligand per two asymmetric units were present, thereby confirming the usual protein:ligand 2:1 stoichiometry of the complexes formed by STING and CDNs. We were able to trace the polypeptide chain of STING from Asn154 to Glu336 except for one short intrinsically disordered loop between residues Tyr186 and Gly192 (Figure 7A). The binding of 19 to STING was mediated by multiple interactions, including both direct (via Arg238) and indirect water-mediated hydrogen bonds (via Ser162, Arg232, Tyr240, Thr263, or Thr267) (Figure 7B). We compared our structure of STING in a complex with 19 with the recently published structure of STING in a complex with naturally occurring 3',3'-c-GAMP 2 (PDB: 6YDZ [Smola et al., 2021]). This comparison revealed a slightly modified position of the 2'-linked adenine base, although it was still in an almost parallel orientation with the second 1'-linked adenine base of the 19 ligand (Figure 7C), while the overall conformation of the STING protein remained unchanged.

The shift of the nucleobase from the 1' to the 2' position represents a substantial change in the chemical structure compared with natural nucleosides. We show here that, despite this change, the isonucleosidic CDNs bind to the dimer of STING almost identically as the natural CDNs. It is also apparent from this crystal structure that the position shift of the nucleobases is compensated for by the shift of the sugar moieties (Figure 7C).

#### Preparation of CDN prodrugs and their evaluation in cell-based assays

In order to validate the potency of our ligands in cell-based assays without the digitonin permeabilization, we were highly motivated to synthesize a prodrug of our lead compound and thus circumvent the poor cellular uptake of the charged CDNs. As a promoiety of first choice, we employed a pivaloyloxymethyl (POM) group, known from marketed phosphonate-based drugs (Fosfomycin, Adefovir Dipivoxil [De Clercq, 2003]) as well as CDNs recently reported by our group (Pimková Polidarová et al., 2021). Based on our previous experience, we selected iodomethyl pivalate 27a (Maiti et al., 2013), iodomethyl *tert*-

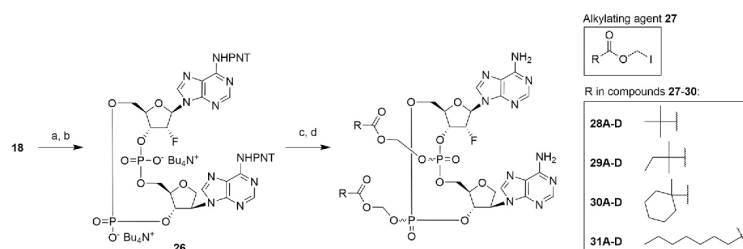


**Figure 8. Synthesis of prodrugs derived from 19**

(a–d) Reagents and conditions are as follows: (a)  $t\text{BuNH}_2$ , 20 min; (b) DOWEX 50 (TBA<sup>+</sup>); (c) **27a–d**, ACN, RT; and (d) NIS, ACN.

pentanoate **27b**, iodomethyl 1-methylcyclohexanoate **27c**, and iodomethyl octanoate **27d** as alkylating agents. These alkylating reagents were prepared immediately before use from corresponding chlorides using the Finkelstein reaction (Maiti et al., 2013). Despite our best efforts, our attempts at a direct introduction of the POM groups in the same manner unfortunately resulted in rich mixtures of side products containing only traces of the desired molecule. Different UV characteristics of the products indicated changes on the nucleobase, and it seemed necessary to protect the exocyclic amino groups prior to the alkylation step. Because the deprotection of commonly used acyl groups under basic conditions proved to be incompatible with the POM pro-moieties, we used a PNT group that could be cleaved with N-iodosuccinimide (NIS) under neutral conditions, with good results (Figure 8; Wu et al., 1988). Here, all four diastereomers were formed in a similar ratio and were separated relatively easily by HPLC.

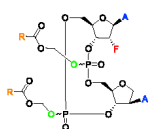
To confirm prodrug superiority in the STING pathway activation, this first prodrug molecule of **19**, compound **28**, and its parent CDN were examined for their activity in the standard assay using HEK 293T reporter cells expressing WT STING haplotype, i.e., without the digitonin permeabilization. Half-maximal effective concentration ( $\text{EC}_{50}$ ) values were recorded after a 30-min pulse compared with a continuous 7-h incubation in order to elucidate the effect of maximized CDN delivery into cells and the pro-moiety cleavage. Comparing the  $\text{EC}_{50}$  of the parent CDN in the digitonin and in the standard assay ( $\sim 400$  times higher in the permeabilized cells; Figures 6 and 9) as well as comparing the  $\text{EC}_{50}$  of the lipophilic prodrug with the  $\text{EC}_{50}$  of the polar, free CDN (3,400 times higher activity of the prodrug; Figure 9) confirmed that delivery to cells is the decisive factor for the CDN activities. Excellent results of **28** in the standard assay prompted us to explore other more lipophilic POM-like groups that could further enhance the STING agonistic properties by accelerating the cellular uptake and their intracellular metabolism. The results of these experiments exceeded our expectations (summarized in the Figure 9). **31**, with the pivaloyl group substituted with *n*-octanoyl, displayed potency below 1 nM with an improvement over the parent CDN 13,000–57,000 $\times$ . The activity of *tert*-pentanoyl-based prodrug **29** and 1-methylcyclohexanoyl-based prodrug **30** remained the same or slightly increased compared with **28**.

To estimate the implicated therapeutic efficacy of our candidate compounds, we tested the cytokine production rate in response to the cGAS-STING pathway activation in a physiologically relevant system, based on human peripheral blood mononuclear cells (PBMCs). STING-dependent cytokine production is of high importance in triggering the innate antimicrobial and anti-viral immune defense and in amplifying and broadening the adaptive immune defense to generate a robust, tumor-specific T cell response (Barber, 2015; Sivick et al., 2018). The most lipophilic diastereomer of each prodrug type was employed in the determination of the values for the production of  $\text{IFN}_\gamma$ ,  $\text{TNF-}\alpha$ ,  $\text{IFN}\alpha$ .  $\text{IFN}\alpha$  and  $\text{TNF-}\alpha$  secretions are primary responses to the STING pathway activation, and  $\text{IFN}_\gamma$  production is a late onset reaction. Thus, the CDN treatment was performed for a continuous 16 h (Pimková Polidarová et al., 2021) to measure both the initial and later reactions. The obtained data reflected a higher potency of lipophilic prodrugs over the related CDNs already shown in the 293T cell reporter standard assay. Thus, the activity profile differed from 300 times to 13,000 times compared with the parent CDN **19**. The *n*-octanoyloxymethyl prodrug **31** stood above all other pro-moieties, as this modification made an  $\sim 2,000$  times difference in the  $\text{EC}_{50}$  values for  $\text{IFN}_\gamma$ , 3,000 times for  $\text{TNF-}\alpha$ , and even 13,000 times for  $\text{IFN}\alpha$  secretion relative to the parent **19**. In terms of cytokine-associated  $\text{EC}_{50}$  values, the potency of the acyloxymethyl type prodrugs displayed a trend of *n*-octanoyl **31**  $\gg$  1-methylcyclohexanoyl **30** > *tert*-pentanoyl **29** > pivaloyl **28** in  $\text{IFN}_\gamma$  secretion, octanoyl **31** > methylcyclohexanoyl **30** > *tert*-pentanoyl **29** > pivaloyl **28** in  $\text{TNF-}\alpha$  secretion, and *n*-octanoyl **31**  $\gg$  pivaloyl **28** > *tert*-pentanoyl **29** > methylcyclohexanoyl **30** in  $\text{IFN}\alpha$  production. Figure 9 also shows a comparison of the isonucleosidic CDN prodrugs with the canonical 2'3'-cGAMP and the clinical candidate ADU-S100. The improvement of our lipophilic molecules over the polar, charged CDNs is about 4 orders of magnitude in the 293T cell reporter standard assay and 3 orders of magnitude in the cytokine production tested in the PBMC assay.

### Conclusion

The STING pathway stands at the forefront of scientific interests for the development of innovative anti-viral, -cancer, and -inflammatory therapies. This has resulted in very intensive research of STING agonists over the past few years. In this work, we focused on highly modified STING ligands derived from their natural



	Standard assay - EC <sub>50</sub> (μM) <sup>a</sup>				PBMC assay, cytokines - EC <sub>50</sub> (μM) <sup>b</sup>		
	30 minutes		7 hours		IFN <sub>γ</sub>	TNF <sub>α</sub>	IFN <sub>α</sub>
	EC <sub>50</sub> (± SEM)	EC <sub>50</sub> parent/prodrug	EC <sub>50</sub> (± SEM)	EC <sub>50</sub> parent/prodrug			
1 (2',3'-cGAMP)	233.00 (±34.79)		36.91 (±8.02)		50 (±17)	216 (±64)	93 (±38)
3 (ADU-S100)	24.18 (±2.67)		3.32 (±0.43)		140 (±10.3)	150 (±21.0)	150 (±133)
<b>19</b>	67.73 (±4.23)		15.14 (±2.48)		33 (±0.2)	129 (±13.7)	527 (±368)
<b>28A</b>	0.13 (±0.05)	496	0.087 (±0.011)	173			
<b>28B</b>	0.096 (±0.009)	705	0.077 (±0.008)	197			
<b>28C</b>	0.054 (±0.008)	1380	0.052 (±0.007)	289			
<b>28D</b>	0.027 (±0.005)	2726	0.028 (±0.003)	540	0.12 (±0.039)	0.33 (±0.098)	0.18 (±0.104)
<b>29A</b>	0.138 (±0.020)	491	0.032 (±0.006)	478			
<b>29B</b>	0.055 (±0.021)	1 233	0.018 (±0.007)	826			
<b>29C</b>	0.062 (±0.044)	1 088	0.013 (±0.0014)	1 195			
<b>29D</b>	0.026 (±0.010)	2 594	0.014 (±0.008)	1 094	0.08 (±0.005)	0.21 (±0.002)	0.26 (±0.004)
<b>30A</b>	3.395 (±1.1)	20	0.285 (±0.19)	53			
<b>30B</b>	0.220 (±0.035)	308	0.044 (±0.021)	342			
<b>30C</b>	0.123 (±0.022)	551	0.021 (±0.008)	733			
<b>30D</b>	0.193 (±0.033)	304	0.051 (±0.020)	297	0.05 (±0.012)	0.16 (±0.015)	0.33 (±0.063)
<b>31A</b>	0.0050 (±0.0025)	13 567	0.005 (±0.0023)	2 839			
<b>31B</b>	0.0012 (±0.0006)	57 486	0.0005 (±0.0002)	29 686			
<b>31C</b>	0.0030 (±0.0012)	22 611	0.0019 (±0.0011)	7 865			
<b>31D</b>	0.0022 (±0.0010)	30 610	0.0017 (±0.0007)	8 883	0.02 (±0.00)	0.04 (±0.015)	0.04 (±0.01)

(legend on next page)

agonists, i.e., CDNs. The main modification is moving the nucleobase of one of the CDN nucleotides from the canonical 1' position to the 2' position. Our data show that the STING dimer is able to tolerate this rather fundamental structural change, and CDNs modified in this way show marked STING agonism on both isolated proteins and in cell-based assays. Our X-ray structural analysis answered the question of how it is possible that even such significantly modified CDNs are recognized as STING agonists. The structural data show that the position of the nucleobase and phosphate parts of the molecule is particularly crucial for agonistic activity, and these positions were almost identical in IsoCDNs when compared with the nucleobases and phosphates in 3',3' natural CDNs. Even the limited flexibility of the CDN macrocycle was shown to be able to compensate for the nucleobase shift and thereby retain the IsoCDN efficient binding to STING. From a practical point of view, the cell permeability of CDNs is crucial for the activity of STING agonists derived from CDNs, which is severely limited by the charged character of natural CDNs. Therefore, we also prepared a series of IsoCDN prodrugs that are able to efficiently deliver the active species into cells. In particular, we confirmed the vast superiority of prodrugs over the parent CDNs as well as over the canonical CDNs and the clinical candidate—ADU-S100—in various cell-based assays. IsoCDNs and their prodrugs represent a new, attractive type of STING agonists that display excellent *in vitro* activity and may therefore be suitable candidates for preclinical testing.

#### STAR★METHODS

Detailed methods are provided in the online version of this paper and include the following:

- KEY RESOURCES TABLE
- RESOURCE AVAILABILITY
  - Lead contact
  - Materials availability
  - Data and code availability
- EXPERIMENTAL MODEL AND SUBJECT DETAILS
- METHOD DETAILS
  - Differential scanning fluorimetry (DSF)
  - Activity of CDN in *in vitro* cell-based assay
  - Activity of CDN in PBMC assay
  - Crystallography methods
  - DFT calculation and NMR-assisted determination of the 20A and 20B configuration
  - Chemistry methods
  - Description of synthetic experiments
- QUANTIFICATION AND STATISTICAL ANALYSIS

#### SUPPLEMENTAL INFORMATION

Supplemental information can be found online at <https://doi.org/10.1016/j.str.2022.05.012>.

#### Figure 9. Biological evaluation of prodrugs in a standard HEK 293T WT STING cell-based reporter assay

<sup>a</sup>Results from the standard assay using HEK 293T reporter cells expressing different STING haplotypes. EC<sub>50</sub> values expressed as mean values ± SEM of 1–3 independent experiments measured in triplicates.

<sup>b</sup>Physiologically relevant cell system using peripheral blood mononuclear cells (PBMCs) isolated from the buffy coats of healthy donors. EC<sub>50</sub> values expressed as mean values ± SEM of a representative experiment measured in triplicates.

#### ACKNOWLEDGMENTS

The work was supported by the European Regional Development Fund, OP RDE (project “Chemical biology for drugging undruggable targets,” ChemBioDrug no. Z.02.1.01/0.0/0.0/16.019/0000729), Ministry of Health of the Czech Republic (grant NU20-05-00472), the Czech Academy of Sciences (RVO: 61388963), and by Gilead Sciences, Inc. Our special thanks belong to Hana Prouzová for her help with digitonin assays and Tamara Jenkins for English proofreading.

#### AUTHORS CONTRIBUTIONS

M. Dejmeek and M. Šála designed and synthesized all parent CDNs and prodrugs. P.B. designed the prodrug preparation. L.V. and M.Z. carried out the measurements of biological activity. G.B. designed and coordinated biological assays. A.B. and G.B. interpreted the obtained biological data. O.Š. and O.P. designed the PNT protection and validated its usability. M. Smola, M.K., and E.B. performed crystallization of the CDN with WT STING, resolved the crystal structure, and analyzed the X-ray data. M.B., M. Dračinský, and E.P. measured NMR spectra and analyzed the data. M. Dračinský carried out the density functional theory (DFT) calculations and NMR-assisted determination of the thiophosphate configurations. M. Dejmeek, A.B., G.B., and R.N. designed the study and wrote the manuscript. G.B. and R.N. acquired the funding that enabled this study.

#### DECLARATION OF INTERESTS

A patent application has been filed for this work and the filing process was completed in March 2022. No patent has been, however, granted yet, and the application itself will be published later in 2022. Part of this work was sponsored by Gilead Sciences, Inc.

Received: February 9, 2022

Revised: April 19, 2022

Accepted: May 17, 2022

Published: June 10, 2022

#### REFERENCES

- Adams, P.D., Afonine, P.V., Bunkóczi, G., Chen, V.B., Davis, I.W., Echols, N., Headd, J.J., Hung, L.-W., Kapral, G.J., Grosse-Kunstleve, R.W., et al. (2010). PHENIX: a comprehensive Python-based system for macromolecular structure solution. *Acta Crystallogr. D Biol. Crystallogr.* 66, 213–221. <https://doi.org/10.1107/S0907444909052925>.
- Afonine, P.V., Grosse-Kunstleve, R.W., Echols, N., Headd, J.J., Moriarty, N.W., Mustyakimov, M., Terwilliger, T.C., Urzhumtsev, A., Zwart, P.H., and Adams, P.D. (2012). Towards automated crystallographic structure refinement with phenix.refine. *Acta Crystallogr. D* 68, 352–367. <https://doi.org/10.1107/S0907444912001308>.
- Balka, K.R., Louis, C., Saunders, T.L., Smith, A.M., Calleja, D.J., D'Silva, D.B., Moghaddas, F., Tailler, M., Lawlor, K.E., Zhan, Y., et al. (2020). TBK1 and IKKε act redundantly to mediate STING-induced NF-κB responses in myeloid cells. *Cell Rep.* 31, 107492. <https://doi.org/10.1016/j.celrep.2020.03.056>.
- Barber, G.N. (2015). STING: infection, inflammation and cancer. *Nat. Rev. Immunol.* 15, 760–770. <https://doi.org/10.1038/nri3921>.
- Barone, V., and Cossi, M. (1998). Quantum calculation of molecular energies and energy gradients in solution by a conductor solvent model. *J. Phys. Chem.* 102, 1995–2001. <https://doi.org/10.1021/jp9716997>.
- Becke, A.D. (1993). Density-functional thermochemistry. III. The role of exact exchange. *J. Chem. Phys.* 98, 5648–5652. <https://doi.org/10.1063/1.464913>.



- Bera, S., Mickle, T., and Nair, V. (1999). Synthesis and antiviral studies of unsaturated analogues of isomeric dideoxynucleosides. *Nucleosides Nucleotides* 18, 2379–2395. <https://doi.org/10.1080/07328319908044614>.
- Birkus, G., Brehova, P., Dejmek, M., Nencka, R., Pav, O., and Sala, M. (2020). 3′,3′-Cyclic Dinucleotide Analogue Comprising a Cyclopentanyl Modified Nucleotide as Sting Modulator. Patent WO2020178768A1, Patent Application IB2020051883W, 2020/09/10/, and granted 2020-09-10 (Institute of Organic Chemistry and Biochemistry ASCR, V.V.I.).
- Birkus, G., Pav, O., Jandusik, T., Rosenberg, I., and Nencka, R. (2019). 3′,3′-Cyclic Dinucleotides with Phosphonate Bond Activating the Sting Adaptor Protein. patent WO2019123340A1, Patent Application IB2018060383W, 2019/06/27/, and granted 2019-06-27 (Institute of Organic Chemistry and Biochemistry ASCR, V.V.I.).
- Cossi, M., Rega, N., Scalmani, G., and Barone, V. (2003). Energies, structures, and electronic properties of molecules in solution with the C-PCM solvation model. *J. Comput. Chem.* 24, 669–681. <https://doi.org/10.1002/jcc.10189>.
- De Clercq, E. (2003). Potential of acyclic nucleoside phosphonates in the treatment of DNA virus and retrovirus infections. *Expert Rev. Anti-Infect. Ther.* 7, 21–43. <https://doi.org/10.1586/14787210.1.1.21>.
- Du, X.X., and Su, X.D. (2017). Detection of cyclic dinucleotides by STING. *Methods Mol. Biol.* 1657, 59–69. [https://doi.org/10.1007/978-1-4939-7240-1\\_6](https://doi.org/10.1007/978-1-4939-7240-1_6).
- Dubensky, J.T.W., and Kanne, D.B. (2014). Compositions and Methods for Inhibiting “Stimulator of Interferon Gene”-Dependent Signalling. Patent US2014341976 (A1), Patent Application US201414280668 20140519, 2014/11/20/, and granted 2014-11-20 (Aduro Biotech Inc).
- Emmsley, P., and Cowtan, K. (2004). Coot: model-building tools for molecular graphics. *Acta Crystallogr. D* 60, 2126–2132. <https://doi.org/10.1107/S0907444904019158>.
- Flood, B.A., Higgs, E.F., Li, S., Luke, J.J., and Gajewski, T.F. (2019). STING pathway agonism as a cancer therapeutic. *Immunol. Rev.* 290, 24–38. <https://doi.org/10.1111/imr.12765>.
- Frisch, M.J., Trucks, G.W., Schlegel, H.B., Scuseria, G.E., Robb, M.A., Cheeseman, J.R., Scalmani, G., Barone, V., Petersson, G.A., Nakatsuji, H., et al. (2016). Gaussian 16 Rev. C.01 (Gaussian, Inc.).
- Gao, P., Asciano, M., Wu, Y., Barchet, W., Gaffney, B.L., Zillinger, T., Serganov, A.A., Liu, Y., Jones, R.A., Hartmann, G., et al. (2013). Cyclic [G(2′,5′)pA(3′,5′)p] is the metazoan second messenger produced by DNA-activated cyclic GMP-AMP synthesis. *Cell* 153, 1094–1107. <https://doi.org/10.1016/j.cell.2013.04.046>.
- Guo, F., Tang, L., Shu, S., Sehgal, M., Sheraz, M., Liu, B., Zhao, Q., Cheng, J., Zhao, X., Zhou, T., et al. (2017). Activation of stimulator of interferon genes in Hepatocytes Suppresses the replication of hepatitis B virus. *Antimicrob. Agents Chemother.* 61, e00771–00717. <https://doi.org/10.1128/AAC.00771-17>.
- Hopfner, K.-P., and Horning, V. (2020). Molecular mechanisms and cellular functions of cGAS-STING signalling. *Nat. Rev. Mol. Cell Biol.* 21, 501–521. <https://doi.org/10.1038/s41580-020-0244-x>.
- Cheng, Z., Dai, T., He, X., Zhang, Z., Xie, F., Wang, S., Zhang, L., and Zhou, F. (2020). The interactions between cGAS-STING pathway and pathogens. *Signal Transduct. Targeted Ther.* 5, 91. <https://doi.org/10.1038/s41392-020-0198-7>.
- Chi, G., Neamati, N., and Nair, V. (2004). Inhibition of the strand transfer step of HIV-1 integrase by non-natural dinucleotides. *Bioorg. Med. Chem. Lett* 14, 4815–4817. <https://doi.org/10.1016/j.bmcl.2004.07.050>.
- Jiang, C., Li, B., Guan, Z., Yang, Z., Zhang, L., and Zhang, L. (2007). Synthesis and recognition of novel isonucleoside triphosphates by DNA polymerases. *Bioorg. Med. Chem.* 15, 3019–3025. <https://doi.org/10.1016/j.bmc.2007.02.003>.
- Kabsch, W. (2010). Xds. *Acta Crystallogr. D Biol. Crystallogr.* 66, 125–132. <https://doi.org/10.1107/S0907444909047337>.
- Kakefuda, A., Shuto, S., Nagahata, T., Seki, J.-i., Sasaki, T., and Matsuda, A. (1994). Nucleosides and nucleotides. 132. Synthesis and biological evaluations of ring-expanded oxetanocin analogues: purine and pyrimidine analogues of 1,4-anhydro-2-deoxy-D-arabitol and 1,4-anhydro-2-deoxy-3-hydroxymethyl-D-arabitol. *Tetrahedron* 50, 10167–10182. [https://doi.org/10.1016/S0040-4020\(01\)81749-X](https://doi.org/10.1016/S0040-4020(01)81749-X).
- Kalia, D., Merey, G., Nakayama, S., Zheng, Y., Zhou, J., Luo, Y., Guo, M., Roembke, B.T., and Sintim, H.O. (2013). Nucleotide, C-Di-GMP, C-Di-AMP, cGMP, cAMP(p)Nucleotide, c-di-GMP, c-di-AMP, cGMP, cAMP, (pppGpp) signaling in bacteria and implications in pathogenesis. *Chem. Soc. Rev.* 42, 305–341. <https://doi.org/10.1039/c2cs35206k>.
- Kim, D.-S., Endo, A., Fang, F.G., Huang, K.-C., Bao, X., Choi, H.-w., Majumder, U., Shen, Y.Y., Mathieu, S., Zhu, X., et al. (2021). E7766, a macrocycle-bridged stimulator of interferon genes (STING) agonist with potent pan-genotypic activity. *ChemMedChem* 16, 1741–1744. <https://doi.org/10.1002/cmcc.202100068>.
- Lee, C., Yang, W., and Parr, R.G. (1988). Development of the Colle-Salvetti correlation-energy formula into a functional of the electron density. *Phys. Rev. B Condens. Matter.* 37, 785–789. <https://doi.org/10.1103/physrevb.37.785>.
- Lubbers, J.M., Koopman, B., de Klerk-Stuis, J.M., van Rooij, N., Plat, A., Pijper, H., Koopman, T., van Hemel, B.M., Hollema, H., Wisman, B., et al. (2021). Association of homozygous variants of STING1 with outcome in human cervical cancer. *Cancer Sci.* 112, 61–71. <https://doi.org/10.1111/cas.14680>.
- Maiili, M., Persoons, L., Andrei, G., Snoeck, R., Balzarini, J., and Herdewijn, P. (2013). Synthesis and anti-herpetic activity of phosphoramidate ProTides. *ChemMedChem* 8, 985–993. <https://doi.org/10.1002/cmcc.201300035>.
- McCoy, A.J., Grosse-Kunstleve, R.W., Adams, P.D., Winn, M.D., Storoni, L.C., and Read, R.J. (2007). Phaser crystallographic software. *J. Appl. Crystallogr.* 40, 658–674. <https://doi.org/10.1107/S0021889607021206>.
- Montgomery, J.A., and Thomas, H.J. (1978). Isonucleosides. 2. Purine and pyrimidine derivatives of 1,4-anhydro-2-deoxy-D-arabinitol. *J. Org. Chem.* 43, 541–544. <https://doi.org/10.1021/jo00398a003>.
- Motwani, M., Pesiridis, S., and Fitzgerald, K.A. (2019). DNA sensing by the cGAS-STING pathway in health and disease. *Nat. Rev. Genet.* 20, 657–674. <https://doi.org/10.1038/s41576-019-0151-1>.
- Novotná, B., Holá, L., Staš, M., Gutten, O., Smola, M., Zavrlel, M., Vavrina, Z., Buděšínský, M., Liboska, R., Chevner, F., et al. (2021). Enzymatic synthesis of 3′-5′, 3′-5′ cyclic dinucleotides, their binding properties to the stimulator of interferon genes adaptor protein, and structure/activity correlations. *Biochemistry* 60, 3714–3727. <https://doi.org/10.1021/acs.biochem.1c00692>.
- Novotná, B., Vanekova, L., Zavrlel, M., Buděšínský, M., Dejmek, M., Smola, M., Gutten, O., Tehrani, Z.A., Pimkova Polidarova, M., Brazdova, A., et al. (2019). Enzymatic preparation of 2′-5′,3′-5′-cyclic dinucleotides, their binding properties to stimulator of interferon genes adaptor protein, and structure/activity correlations. *J. Med. Chem.* 62, 10676–10690. <https://doi.org/10.1021/acs.jmedchem.9b01062>.
- Pan, B.-S., Perera, S.A., Plesvaux, J.A., Prestland, J.P., Schroeder, G.K., Cumming, J.N., Trotter, B.W., Altman, M.D., Buevich, A.V., Cash, B., et al. (2020). An orally available non-nucleotide STING agonist with antitumor activity. *Science* 369, ea66098. <https://doi.org/10.1126/science.aba6098>.
- Pimkova Polidarova, M., Brehová, P., Dejmek, M., Birkus, G., and Brazdova, A. (2022). STING agonist-mediated cytokine secretion is accompanied by monocyte apoptosis. *ACS Infect. Dis.* 8, 463–471. <https://doi.org/10.1021/acinfed.1c00554>.
- Pimková Polidarová, M., Brehová, P., Kaiser, M.M., Smola, M., Dračinský, M., Smith, J., Marek, A., Dejmek, M., Šála, M., Gutten, O., et al. (2021). Synthesis and biological evaluation of phosphoester and phosphorothioate prodrugs of STING agonist 3′,3′-c-Di[2′,5′-dAMP]. *J. Med. Chem.* 64, 7596–7616. <https://doi.org/10.1021/acs.jmedchem.1c00301>.
- Policarová, M.P., Brehová, P., Kaiser, M.M., Smola, M., Dračinský, M., Smith, J., Marek, A., Dejmek, M., Šála, M., Gutten, O., et al. (2021). Synthesis and biological evaluation of phosphoester and phosphorothioate prodrugs of STING agonist 3′,3′-c-Di[2′,5′-dAMP]. *J. Med. Chem.* 64, 7596–7616. <https://doi.org/10.1021/acs.jmedchem.1c00301>.
- Purdy, D.F., Zintek, L.B., and Nair, V. (1994). Synthesis of isonucleosides related to AZT and AZU. *Nucleosides Nucleotides* 13, 109–126. <https://doi.org/10.1080/15257779408013230>.
- Ramanjulu, J.M., Pesiridis, G.S., Yang, J., Concha, N., Singhaus, R., Zhang, S.Y., Tran, J.L., Moore, P., Lehmann, S., Eberl, H.C., et al. (2018). Design of amidobenzimidazole STING receptor agonists with systemic activity. *Nature* 564, 439–443. <https://doi.org/10.1038/s41586-018-0705-y>.



- Scheuer-Larsen, C., Rosenbohm, C., Joergensen, T.J.D., and Wengel, J. (1997). Introduction of a universal solid support for oligonucleotide synthesis. *Nucleosides Nucleotides* 16, 67–80.
- Sivick, K.E., Desbien, A.L., Glickman, L.H., Reiner, G.L., Corrales, L., Surh, N.H., Hudson, T.E., Vu, U.T., Francica, B.J., Banda, T., et al. (2018). Magnitude of therapeutic STING activation determines CD8(+) T cell-mediated anti-tumor immunity. *Cell Rep.* 25, 3074–3085.e5. <https://doi.org/10.1016/j.celrep.2018.11.047>.
- Smola, M., Birkus, G., and Boura, E. (2019). No magnesium is needed for binding of the stimulator of interferon genes to cyclic dinucleotides. *Acta Crystallogr. F Struct. Biol. Commun.* 75, 593–598. <https://doi.org/10.1107/S2053230X19010999>.
- Smola, M., Gutten, O., Dejmek, M., Kozíšek, M., Evangelidis, T., Tehrani, Z.A., Novotná, B., Nencka, R., Birkus, G., Rulíšek, L., and Boura, E. (2021). Ligand strain and its conformational complexity is a major factor in the binding of cyclic dinucleotides to STING protein. *Angew. Chem. Int. Ed.* 60, 10172–10178. <https://doi.org/10.1002/anie.202016805>.
- Taktakishvili, M., Neamati, N., Pommier, Y., Pal, S., and Nair, V. (2000). Recognition and inhibition of HIV integrase by novel dinucleotides. *J. Am. Chem. Soc.* 122, 5671–5677. <https://doi.org/10.1021/ja992528d>.
- The PyMOL Molecular Graphics System (2015). The PyMOL Molecular Graphics System, Version 1.8 (Schrodinger, LLC).
- Vavřina, Z., Gutten, O., Smola, M., Zavřel, M., Aliakbar Tehrani, Z., Charvát, V., Kozíšek, M., Boura, E., Birkus, G., and Rulíšek, L. (2021). Protein-ligand interactions in the STING binding site probed by rationally designed single-point mutations: experiment and theory. *Biochemistry* 60, 607–620. <https://doi.org/10.1021/acs.biochem.0c00949>.
- Vyskocil, S., Cardin, D., Ciavarrì, J., Conlon, J., Cullis, C., England, D., Gershman, R., Gigstad, K., Gipson, K., Gould, A., et al. (2021). Identification of novel carbocyclic pyrimidine cyclic dinucleotide STING agonists for anti-tumor immunotherapy using systemic intravenous route. *J. Med. Chem.* 64, 6902–6923. <https://doi.org/10.1021/acs.jmedchem.1c00374>.
- Wu, Z., Mootoo, D.R., and Fraser-Reid, B. (1988). Protecting groups that incorporate a 4-pentenyl acetal moiety can be cleaved under neutral conditions. *Tetrahedron Lett.* 29, 6549–6551. [https://doi.org/10.1016/S0040-4039\(00\)82394-1](https://doi.org/10.1016/S0040-4039(00)82394-1).
- Zhang, H., You, Q.-D., and Xu, X.-L. (2020). Targeting stimulator of interferon genes (STING): a medicinal chemistry perspective. *J. Med. Chem.* 63, 3785–3816. <https://doi.org/10.1021/acs.jmedchem.9b01039>.
- Zhang, X., Shi, H., Wu, J., Zhang, X., Sun, L., Chen, C., and Chen, Z.J. (2013). Cyclic GMP-AMP containing mixed phosphodiester linkages is an endogenous high-affinity ligand for STING. *Mol Cell* 51, 226–235. <https://doi.org/10.1016/j.molcel.2013.05.022>.
- Zheng, J., Mo, J., Zhu, T., Zhuo, W., Yi, Y., Hu, S., Yin, J., Zhang, W., Zhou, H., and Liu, Z. (2020). Comprehensive elaboration of the cGAS-STING signaling axis in cancer development and immunotherapy. *Mol. Cancer* 19, 133. <https://doi.org/10.1186/s12943-020-01250-1>.



## STAR METHODS

### KEY RESOURCES TABLE

REAGENT or RESOURCE	SOURCE	IDENTIFIER
<b>Bacterial and virus strains</b>		
<i>Escherichia coli</i> BL21 DE3 NiCo strain	New England Biolabs	C2529H
<b>Biological samples</b>		
Buffy coats from healthy donors	IHBT Prague, Czech Republic	Evidence# 13/06/2012
<b>Chemicals, peptides, and recombinant proteins</b>		
HisPur Ni-NTA Superflow Agarose	Thermo Fisher Scientific	25216
STING (WT, G230-R293Q (AQ))	(Vavrina et al., 2021)	<a href="https://doi.org/10.1021/acs.biochem.0c00949">https://doi.org/10.1021/acs.biochem.0c00949</a>
Ficoll®-Paque Plus	GE Healthcare	Cat#17-1440-03
DMT-2' Fluoro-dG(b) Phosphoramidite	Sigma-Aldrich	Cat#G211230
DMT-2' Fluoro-dA(bz) Phosphoramidite	Sigma-Aldrich	Cat#A211230
DMT-dA(bz) Phosphoramidite	Sigma-Aldrich	Cat#A111050
DMOCP	Sigma-Aldrich	Cat#541508
3H-1,2-Benzodithiol-3-one	Sigma-Aldrich	Cat#375462
Xanthane Hydride	TCI	Cat#X0001
<b>Critical commercial assays</b>		
TNF $\alpha$ Human ProcartaPlex™ Simplex Kit	ThermoFisher Scientific	EPX01A-10223-901
IFN $\alpha$ Human ProcartaPlex™ Simplex Kit	ThermoFisher Scientific	EPX01A-10216-901
IFN $\gamma$ Human ProcartaPlex™ Simplex Kit	ThermoFisher Scientific	EPX01A-10228-901
ProcartaPlex™ Human Basic Kit	ThermoFisher Scientific	EPX010-10420-901
Bright-Glo Luciferase Assay System	Promega (eastport)	Cat#E2650
<b>Deposited data</b>		
STING(3',3'-c-(2'F,2'dAMP) <sup>1500H4</sup> AMP) structure	This paper	PDB: 7Q3B
<b>Experimental models: Organisms/strains</b>		
HEK 293T ISRE wt STING	(Novotna et al., 2019)	N/A
HEK 293T ISRE R293Q STING	(Novotna et al., 2019)	N/A
HEK 293T ISRE R232H STING	(Novotna et al., 2019)	N/A
HEK 293T ISRE G230A-R293Q STING	(Novotna et al., 2019)	N/A
HEK 293T ISRE R71H-G230A-R293Q STING	(Novotna et al., 2019)	N/A
<b>Recombinant DNA</b>		
Plasmid pSUMO-STING	(Smola et al., 2021)	N/A
<b>Software and algorithms</b>		
XDS	(Kabsch, 2010)	<a href="https://xds.mr.mpg.de/">https://xds.mr.mpg.de/</a>
Phenix	(Adams et al., 2010)	<a href="https://phenix-online.org/">https://phenix-online.org/</a>
Coot	(Emsley and Cowtan, 2004)	<a href="https://www2.mrc-lmb.cam.ac.uk/personal/pemsley/coot/">https://www2.mrc-lmb.cam.ac.uk/personal/pemsley/coot/</a>
PyMol	Schrödinger, LLC	<a href="https://pymol.org/">https://pymol.org/</a>
Prism 7.05	GraphPad Software	<a href="https://www.graphpad.com/">https://www.graphpad.com/</a>

### RESOURCE AVAILABILITY

#### Lead contact

Further information and requests for resources and reagents should be directed to and will be fulfilled by the Lead contact, Radim Nencka ([nencka@uochb.cas.cz](mailto:nencka@uochb.cas.cz)).

e1 Structure 30, 1–11.e1–e11, August 4, 2022

#### Materials availability

All unique/stable reagents generated in this study will be made available on request, but we may require a payment and/or a completed materials transfer agreement if there is potential for commercial application.

#### Data and code availability

Data Deposition: The structural restraints and structure coordinates have been deposited with accession code PDB: 7Q3B.

This paper does not report original code.

Copies of LCMS traces and  $^1\text{H}$  and  $^{13}\text{C}$  NMR spectra of final compounds are included in the [supplementary information](#) document. Any additional information required to reanalyze the data reported in this paper is available from the [lead contact](#) upon request.

#### EXPERIMENTAL MODEL AND SUBJECT DETAILS

All proteins used for biochemical studies were recombinantly expressed in *Escherichia coli* BL21 DE3 NiCo strain. All cell lines for cell-based assay studies were performed using commercially available HEK 293T and buffy coats from healthy donors.

#### METHOD DETAILS

##### Differential scanning fluorimetry (DSF)

To determine the stability of protein-ligand complex, the DSF was performed as previously described (Novotna et al., 2019; Vavrina et al., 2021). Briefly, the DSF was run in 96-well optical plates (LightCycler® 480 Multiwell Plate 96 white, Roche). STING protein WT and AQ allelic forms were used. Thermal denaturation of samples was performed on a LightCycler 480 Instrument II (Roche). The first derivative of fluorescence intensity referring to thermal denaturation of the protein was determined as melting temperatures ( $T_m$ ) and the thermal shift ( $\Delta T_m$ ) was calculated as the difference of  $T_m$  of ligand-free and protein in complex with CDN (Novotna et al., 2019; Vavrina et al., 2021; Vyskocil et al., 2021).

##### Activity of CDN in *in vitro* cell-based assay

The activity of tested CDNs was determined using reporter HEK 293T ISRE cell lines expressing various STING protein haplotypes in digitonin (R232 (WT), R293Q (Q), R232H (REF), G230A-R293Q (AQ), R71H-G230A-R293Q (HAQ) allelic forms) and standard (WT allelic form) reporter assays as previously described (Novotna et al., 2019; Pimková Polidarová et al., 2021). Digitonin Assay with 293T Reporter Cells: Briefly, the 293T reporter cells stably expressing different STING protein haplotypes were seeded into poly(D-lysine)-coated 96 white plates. Next day, the cells were treated with serial dilutions of compounds in digitonin buffer. After 30 min incubation, the digitonin buffer was removed, cells were washed and fresh medium was added for the following incubation time of 5h. The luminescence was assessed using Bright-Glo Luciferase Assay System reagent measured on Spark (TECAN, Grödig, Austria). GraphPad Prism (La Jolla, USA) was used to calculate the 50% effective concentration ( $EC_{50}$ ).

Standard Assay Using 293T Reporter Cells: Briefly, the 293T reporter cells stably expressing WT STING protein haplotype were seeded into poly(D-lysine)-coated 96 white plates. The next day, the cells were treated with serially diluted compounds in cell culture medium. The cells were incubated for 30 min, washed and incubated for further 6.5h or incubated for complete period of 7h. After the incubation time, cells were washed and incubated for additional 6.5h, or of complete 7h, the luminescence was measured using Bright-Glo Luciferase Assay System reagent and the  $EC_{50}$  values were calculated.

All incubations were performed at standard conditions (37 °C, 5% CO<sub>2</sub> atmosphere).

##### Activity of CDN in PBMC assay

Buffy coats from healthy individuals were obtained from the Institute of Hematology and Blood Transfusion (IHBT, Prague, Czech Republic). Informed written consent was obtained from each individual enrolled. The study was approved by the institutional review board of IHBT, with evidence number 13/06/2012. Peripheral blood mononuclear cells (PBMC) were isolated from buffy coats using SepMate™-50 (Stem Cell Technologies), based on Ficoll® Paque Plus (GE Healthcare) density gradient centrifugation, according to the manufacturer's protocol and treated as previously described (Pimková Polidarová et al., 2021). Briefly, the cells were incubated with compounds for 60 min, the medium was removed, the cells were washed twice with fresh medium. The cells were further incubated in fresh medium for the following 15 h. The levels of human IFN $\alpha$ , IFN $\gamma$  and TNF $\alpha$  secreted into the cell culture medium were assessed with ProcartaPlex™ assays (Invitrogen; ThermoFisher Scientific) using a Magpix Luminex Instrument (Merck), according to the manufacturer's instruction. Compound-associated  $EC_{50}$  values were calculated using GraphPad Prism (La Jolla) (Novotna et al., 2019; Pimková Polidarová et al., 2021).

##### Crystallography methods

###### Protein expression and purification

The cytosolic domain of human STING (i.e. residues 140-343, hereafter referred to as "STING protein") was expressed as a fusion protein with an *N*-terminal 8x histidine (His<sub>8</sub>) purification tag, followed by a SUMO solubility and folding tag. The protein was expressed in the *E. coli* BL21 DE3 NiCo bacterial strain (New England Biolabs) in the autoinduction ZY-5052 medium. Bacterial cells were harvested by centrifugation and lysed using the French Press Cell Disruptor instrument (Thermo Fisher Scientific) at 1,000

Psi in the lysis buffer (50 mM Tris pH 8, 300 mM NaCl, 3 mM  $\beta$ -mercaptoethanol, 30 mM imidazole, 10% glycerol). The lysate was precleared with centrifugation for 30 min at 30,000 g and incubated with the HisPur Ni-NTA Superflow agarose (Thermo Fisher Scientific) for 30 min. Then, the agarose beads were extensively washed with the lysis buffer, and the protein of interest was eluted with the elution buffer (50 mM Tris pH 8, 300 mM NaCl, 3 mM  $\beta$ -mercaptoethanol, 300 mM imidazole, 10% glycerol). The His<sub>6</sub>-SUMO tag was removed by overnight cleavage with the recombinant yeast Ulp1 protease. The STING protein was purified using size exclusion chromatography at the HiLoad 16/600 Superdex 75 prep grade column (GE Healthcare) in the buffer A (50 mM Tris pH 7.4, 50 mM NaCl), followed by anion exchange chromatography at the HiTrap Q HP column (GE Healthcare) using a gradient from buffer A to buffer B (50 mM Tris pH 7.4, 1 M NaCl). The purified protein was concentrated to 20 mg/mL, aliquoted, flash frozen in liquid nitrogen, and stored at 193 K.

#### Crystallization and crystallographic analysis

We used our established protocol for STING crystallization (Smola et al., 2019). Briefly, the STING protein was supplemented with 10 mM EDTA and 0.5 mM 3',3'-c-(2'F,2'dAMP<sup>iso</sup>AMP), (19). The protein crystals were obtained at 291 K in sitting drops using the vapor diffusion method. They were cryoprotected in a mother liquor supplemented with 20% (v/v) glycerol, flash cooled in liquid nitrogen, and analyzed by X-ray crystallography. The dataset was collected from a single cooled crystal using the home source, Rigaku MicroMax-007 HF rotating anode, equipped with the Dectris Pilatus 200K pixel detector. The data was integrated and scaled using XDS (Kabsch, 2010). The structure of the STING/19 complex was solved by molecular replacement using the structure of the STING/cGAMP complex (pdb entry 4KSY (Zhang et al., 2013)) as a search model. The initial model was obtained with Phaser (McCoy et al., 2007) from the Phenix package (Adams et al., 2010). The model was further improved using automatic model refinement with Phenix.refine (Afonine et al., 2012) from the Phenix package (Adams et al., 2010) and manual model building with Coot (Emsley and Cowtan, 2004). Structural figures were generated with PyMol (The PyMOL Molecular Graphics System, 2015). The atomic coordinates and structural factors were deposited in the Protein Data Bank (<https://www.rcsb.org>).

The starting structure for the computations was the X-ray diffraction structure of compound 19 in complex with human STING. The protein and water molecules were deleted and the phosphate oxygen atoms were substituted with sulfur so that four different diastereomers of compound 20 were created. The resulting structures were subjected to geometry optimization at the DFT level, using the B3LYP functional (Becke, 1993; Lee et al., 1988) (no dispersion correction) with the standard 6-31+G (2d,p) basis set and the polarizable continuum model used for implicit water solvation (Barone and Cossi, 1998; Cossi et al., 2003). The vibrational frequencies and free energies were calculated for all of the optimized structures, and the stationary point (minimum) character was thus confirmed. The Gaussian16 program package (Frisch et al., 2016) was used in these calculations.

#### DFT calculation and NMR-assisted determination of the 20A and 20B configuration

In our previous work (Polidarová et al., 2021) we observed a good correlation between experimental and calculated chemical shifts of cyclic dinucleotide phosphonates and phosphorothioates that enabled unequivocal determination of the configuration of the chiral phosphorus atoms. We also observed that the hydrogen atom H2', which is close in space to the thiophosphate sulfur atom, has a significantly higher chemical shift (by 0.4 ppm) than H2' close to the thiophosphate oxygen. Here, we applied the same methodology for getting an insight into the configuration of phosphorothioates 20A and 20B.

The largest <sup>1</sup>H chemical-shift difference (0.3 ppm) between compounds 20A (5.78 ppm) and 20B (5.48 ppm) can be observed for atom H2' in the 2'-fluoro-2'-deoxy unit. This indicates (by analogy with our previous study) that the sulfur atom in the phosphorothioate group in position 3' of the 2'-fluoro-2'-deoxy unit of compound 20A is in  $\beta$  position (on the same side of the macrocycle as the bases, supplementary information). This was also confirmed by the DFT calculations, which provided the H2' chemical shift difference of 0.4 ppm). Therefore, we strongly believe that the structural difference between compounds 20A and 20B is the configuration of the phosphorus atom in position 3' of the 2'-fluoro-2'-deoxy unit and that the configuration of the other phosphorus atom is the same in both compounds.

We plotted the experimental proton and carbon chemical shifts of compounds 20A and 20B versus the calculated nuclear shieldings and a slightly better linear correlation was observed for the structures with the sulfur atom in position 3' of the iso-A unit in  $\alpha$  position. We therefore tentatively conclude that the configuration of compound 20A is *RpSp* and the configuration of 20B is *RpRp*.

#### Chemistry methods

Unless stated otherwise, solvents were evaporated at 40 °C at 2 kPa, and prepared compounds were dried at 30 °C at 2 kPa. Starting compounds and reagents were purchased from commercial suppliers (Sigma-Aldrich, Fluorochem, Acros Organics, Carbosynth) and used without further purification. Acetonitrile was dried using activated 3A molecular sieves. Analytical TLC was performed on silica gel-precoated aluminum plates with a fluorescent indicator (Merck 60 F254). Column chromatography (both normal and reverse phase) was performed on a 40-60  $\mu$ m silica gel using an ISCO flash chromatography system.

Analytical HPLC, mass spectra, UV absorbance and purity of compounds were measured on Waters UPLC-MS system consisting of a Waters UPLC H-Class Core System, UPLC PDA detector and Mass spectrometer Waters SQD2. The MS method used was ESI+ and/or ESI-, cone voltage = 15 V, and mass detector range 200–1000 Da or 200–1250 Da. Two sets of HPLC conditions were used as indicated: (a) C18 (column: Waters Acquity UPLC BEH C18 column, 1.7 mm, 2.1  $\times$  100 mm; LC method: H<sub>2</sub>O/CH<sub>3</sub>CN, 0.1% formic acid as modifier, gradient 0–100%, run length 7 min, flow 0.5 mL/min) and (b) HILIC (column: Hilicon - Fusion iHILIC, 1.8  $\mu$ m, 50  $\times$  2.1 mm; LC method: CH<sub>3</sub>CN/0.01M aqueous ammonium acetate gradient 10–60%, run length 7 min, flow 0.3 mL/min).

The final products (CDNs and CDN prodrugs) were purified by semi-preparative HPLC (Luna, 5  $\mu$ m, C18 250  $\times$  21 mm or 150  $\times$  10 mm). In the preparation of free CDNs, triethylammonium bicarbonate (TEAB) was used as a modifier. TEAB was removed from the collected fractions by 3 cycles of co-evaporation with methanol. The concentrations of CDNs and the respective prodrugs were measured using an Implen NanoPhotometer N60 Touch system. The purity of all prepared compounds was higher than 95% unless stated otherwise.

NMR spectra were recorded on Bruker Avance III HD machines ( $^1\text{H}$  at 400, 500 or 600 MHz), using a solvent signal as a reference. *Tert*-butyl alcohol was used as an internal standard in  $\text{D}_2\text{O}$  solutions. Chemical shifts ( $\delta$ ) and coupling constants ( $J$ ) were expressed in ppm and Hz, respectively. All structures were confirmed, and  $^1\text{H}$  and  $^{13}\text{C}$  signals were assigned by a combination of 1D and 2D NMR (H,H-COSY, H,C-HSQC, H,C-HMBC) techniques. Standard pulse programs from the spectrometer library were used; gradient selection was used in the 2D experiments. Mass spectra were measured on an LTQ Orbitrap XL using electrospray ionization (ESI).

#### Description of synthetic experiments

**6-Chloro-9-((6aR,9R,9aS)-2,2,4,4-tetraisopropyltetrahydro-6H-furo[3,2-f][1,3,5,2,4]trioxadisilocin-9-yl)-9H-purine (5)**  
A mixture of **4** (1.9 g, 5.05 mmol) (Scheuer-Larsen et al., 1997), 6-chloropurine (1.169 g, 7.58 mmol) and triphenylphosphine (2.66 g, 10.1 mmol) in THF (66 mL) was cooled to 0°C, and DIAD (2.02 mL, 10.1 mmol) was added dropwise for 10 min. After 30 min at ambient temperature, the reaction mixture was heated to 65°C (bath) for 20 h. Volatiles were evaporated, and the residue was purified by flash chromatography on a silica gel (ethyl acetate in cyclohexane, 0–35%). Product was contaminated by triphenylphosphine oxide and was used without further purification in the next step. ESI MS  $m/z$  (%): 513.2 (100) [M+H].

**(2R,3S,4R)-4-(6-Amino-9H-purin-9-yl)-2-(hydroxymethyl)tetrahydrofuran-3-ol (6)**  
Intermediate **5** was suspended in a mixture of ethanolic ammonia (60 mL, 4 M) and dioxane (30 mL), and this mixture was heated in a sealed tube at 90 °C for 24 h. Volatiles were evaporated, and the residue was azeotroped with dioxane (2  $\times$  75 mL). The oily intermediate was dissolved in aq. HCOOH (110 mL, 80%), and the reaction mixture was heated to 65°C for 18 h. Volatiles were evaporated, residue was azeotroped with ethanol (3  $\times$  150 mL), and then dissolved in a mixture of ethanol (70 mL) and aq. ammonia (35 mL, 25%). The resulting solution was stirred for 3 h, volatiles were evaporated, and the residue was azeotroped with ethanol (3  $\times$  150 mL). Nucleoside **6** was purified by chromatography on silica gel (ethyl acetate to ethyl acetate:acetone:ethanol:water 36:6:5:3, 0–100%) to afford **3** (981 mg, 77%, over two steps).  $^1\text{H}$  NMR (400 MHz, DMSO- $d_6$ )  $\delta$  8.19 (s, 1H, H-8), 8.15 (s, 1H, H-2), 7.23 (s, 2H, NH<sub>2</sub>), 5.77 (s, 1H, 3'-OH), 4.91 (s, 1H, 5'-OH), 4.86 (m, 1H, H-2'), 4.39 (m, 1H, H-3'), 4.17 (dd,  $J_{gem} = 9.7$ ,  $J_{1'a,2'} = 6.6$  Hz, 1H, H-1'a), 4.09 (dd,  $J_{gem} = 9.7$ ,  $J_{1'b,2'} = 5.0$  Hz, 1H, H-1'b), 3.69 (m, 1H, H-4'), 3.65–3.51 (dm, 2H, H-5').  $^{13}\text{C}$  NMR (101 MHz, DMSO- $d_6$ )  $\delta$  156.20 (C-6), 152.54 (C-2), 149.61 (C-4), 139.36 (C-8), 118.91 (C-5), 86.06 (C-4'), 75.86 (C-3'), 69.72 (C-1'), 62.11 (C-2'), 61.05 (C-5'). HRMS ESI (C<sub>10</sub>H<sub>13</sub>N<sub>5</sub>O<sub>3</sub>) calculated 252.1097, found: 252.1091.

#### **N-(9-((3R,4S,5R)-4-Hydroxy-5-(hydroxymethyl)tetrahydrofuran-3-yl)-9H-purin-6-yl)benzamide (7)**

**6** (498 mg, 1.98 mmol) was azeotroped with pyridine (3  $\times$  20 mL), dissolved in pyridine (15 mL), cooled to 0°C, and TMSCl (1.89 mL, 14.7 mmol) was added dropwise for 3 min. The reaction mixture was stirred at 0°C for 20 min, and then at ambient temperature for 1.5 h. Benzoyl chloride (0.45 mL, 3.9 mmol) was slowly added at 0°C, and the resulting solution was stirred overnight at ambient temperature. The reaction mixture was cooled to 0°C, quenched with water (1.6 mL), and after 15 min, aq. ammonia (4 mL, 25%). After a further 15 min at 0°C and 20 min at ambient temperature, all volatiles were evaporated, the residue was extracted with an ethyl acetate:ethanol:mixture (50 mL, 2:1), and solids were filtered-off on a celite pad. The product was purified on a silica gel (ethyl acetate to ethyl acetate:acetone:ethanol:water 36:6:5:3, 0–100%) to afford **580** mg (83%) of **7** as white solid.  $^1\text{H}$  NMR (400 MHz, DMSO- $d_6$ )  $\delta$  11.17 (s, 1H, NH), 8.75 (s, 1H, H-2), 8.54 (s, 1H, H-8), 8.09–8.01 (m, 2H, Bz-*o*), 7.64 (m, 1H, Bz-*p*), 7.60–7.51 (m, 2H, Bz-*m*), 5.82 (d,  $J_{OH,3'} = 5.4$  Hz, 1H, 3'-OH), 5.03 (m, 1H, H-2'), 4.93 (t,  $J_{OH,5'} = 5.6$  Hz, 1H, 5'-OH), 4.45 (m, 1H, H-3'), 4.22 (dd,  $J_{gem} = 9.9$ ,  $J_{1'a,2'} = 6.3$  Hz, 1H, H-1'a), 3.74 (m, 1H, H-4'), 3.65 (ddd,  $J_{gem} = 12.0$ ,  $J_{5'a-OH} = 5.5$ ,  $J_{5'a-4'} = 3.2$  Hz, 1H, H-5'a), 3.59 (m, 1H, H-5'b).  $^{13}\text{C}$  NMR (101 MHz, DMSO- $d_6$ )  $\delta$  166.0 (CON), 152.47 (C-4), 151.50 (C-2), 150.37 (C-6), 143.16 (C-8), 133.63 (Bz-*i*), 132.57 (Bz-*p*), 128.63 (Bz-*o*, Bz-*m*), 125.57 (C-5), 86.15 (C-4'), 75.90 (C-3'), 69.59 (C-1'), 62.44 (C-2'), 60.92 (C-5'). HRMS ESI (C<sub>17</sub>H<sub>17</sub>N<sub>5</sub>O<sub>4</sub>) calculated 356.1359, found: 356.1360.

#### **N-(9-((3R,4S,5R)-5-((Bis(4-methoxyphenyl)(phenyl)methoxy)methyl)-4-hydroxytetrahydrofuran-3-yl)-9H-purin-6-yl)benzamide (9)**

Compound **7** (559 mg, 1.57 mmol) was azeotroped with pyridine (2  $\times$  20 mL), dissolved in pyridine (15 mL), and DMTrCl (556 mg, 1.73 mmol) was added in one portion at 0°C. The reaction mixture was stirred at ambient temperature for 15 h, quenched with satd. aq. NaHCO<sub>3</sub> (8 mL), and evaporated. The residue was dissolved in ethyl acetate (400 mL) and washed with a saturated aqueous solution of NaHCO<sub>3</sub> (2  $\times$  150 mL) and brine (150 mL). The organic phase was dried over sodium sulfate and evaporated. The product was purified by chromatography (acetone in toluene 50–70%) on a TEA-deactivated silica to afford **5** (882 mg, 85%) as a white foam.  $^1\text{H}$  NMR (400 MHz, DMSO- $d_6$ )  $\delta$  11.19 (bs, 1H, NH), 8.75 (s, 1H, H-2), 8.50 (s, 1H, H-8), 8.07–8.03 (m, 2H, Bz-*o*), 7.65 (m, 1H, Bz-*p*), 7.58–7.52 (m, 2H, Bz-*m*), 7.43–7.38 (m, 2H, DMTr-*o*), 7.33–7.19 (m, 7H, DMTr-*m,p*, DMTr-2), 6.91–6.86 (m, 4H, DMTr-3), 5.82 (d, 1H,  $J_{OH,3'} = 5.7$  Hz, OH), 5.05 (dt, 1H,  $J_{2',1'b} = 7.2$ ,  $J_{2',1'a} = J_{2',3'} = 6.0$  Hz, H-2'), 4.56 (dt, 1H,  $J_{3',4'} = 6.8$ ,  $J_{3',2'} = 5.6$  Hz, H-3'), 4.37 (dd, 1H,  $J_{gem} = 9.6$ ,  $J_{1'a,2'} = 6.1$  Hz, H-1'a), 4.30 (dd, 1H,  $J_{gem} = 9.6$ ,  $J_{1'b,2'} = 7.2$  Hz, H-1'b), 3.94 (dt, 1H,  $J_{4',3'} = 6.9$ ,  $J_{4',5'} = 4.5$  Hz, H-4'), 3.73 (s, 6H, DMTr-OCH<sub>3</sub>), 3.19 (d, 2H,  $J_{5',4'} = 4.4$  Hz, H-5').  $^{13}\text{C}$  NMR (101 MHz, DMSO- $d_6$ )  $\delta$  165.62 (CON), 158.23 (DMTr-4), 152.55 (C-4), 151.51 (C-2), 150.49 (C-6), 145.06 (DMTr-*i*), 143.37 (C-8), 135.82 and 135.79 (DMTr-1), 133.63 (Bz-*i*), 132.61 (Bz-*p*), 129.90 (DMTr-2),

128.66 and 128.65 (Bz-*o,m*), 128.00 and 127.92 (DMTr-*o,m*), 126.83 (DMTr-*p*), 125.88 (C-5), 113.36 (DMTr-3), 85.51 (DMTr-C), 83.49 (C-4'), 75.20 (C-3'), 68.74 (C-1'), 63.71 (C-5'), 62.32 (C-2'), 55.21 (DMTr-OCH<sub>3</sub>). ESI MS *m/z* (%): 658.3 (100) [M + H]; HRMS ESI (C<sub>38</sub>H<sub>38</sub>N<sub>6</sub>O<sub>8</sub>) calculated: 658.2666; found: 658.2661.

**(2R,3S,4R)-4-(6-Benzamido-9H-purin-9-yl)-2-(hydroxymethyl)tetrahydrofuran-3-yl hydrogen phosphonate (11)**

Compound 9 (403 mg, 0.61 mmol) was azeotroped with pyridine (2 × 10 mL), dissolved in pyridine (10 mL), and diphenyl phosphite (85%, 417 μL, 1.9 mmol) was added in one portion. After stirring at ambient temperature for 20 min, TEA (0.92 mL) was added, followed by water (0.92 mL), and the reaction was stirred for a further 20 min. The resulting solution was diluted with DCM (200 mL) and washed with a saturated aqueous solution of NaHCO<sub>3</sub> (2 × 75 mL). The organic layer was dried over sodium sulfate and evaporated. The resulting intermediate was purified on FCC (DCM/1% Et<sub>3</sub>N-MeOH 0-30%). Water (200 μL, 11.1 mmol) was added to a solution of obtained intermediate in DCM (10 mL), followed by a solution of DCA (457 μL, 5.6 mmol) in DCM (5.1 mL). The reaction mixture was stirred at ambient temperature for 30 min, and the volatiles were evaporated. Purification on reverse phase FCC (ACN in 50 mM aqueous NH<sub>4</sub>HCO<sub>3</sub>, 0-30%) afforded 6 (192 mg, 75%, ammonium salt). <sup>1</sup>H NMR (400 MHz, DMSO-*d*<sub>6</sub>) δ 11.17 (s, 1H, NH), 8.74 (s, 1H, H-2), 8.63 (s, 1H, H-8), 8.07–8.02 (m, 2H, Bz-*o*), 7.64 (m, 1H, Bz-*p*), 7.58–7.52 (m, 2H, Bz-*m*), 6.48 (d, 1H, J<sub>1,2</sub> = 588.2 Hz, PH), 5.20 (dt, 1H, J<sub>2',1'a</sub> = 6.8, J<sub>2',1'b</sub> = J<sub>2',3'</sub> = 5.2 Hz, H-2'), 4.90 (ddd, 1H, J<sub>3',2'</sub> = 10.8, J<sub>3',4'</sub> = 6.1, J<sub>3',2'</sub> = 4.9 Hz, H-3'), 4.23 (dd, 1H, J<sub>GEM</sub> = 9.7, J<sub>1'a,2'</sub> = 6.8 Hz, H-1'a), 4.18 (dd, 1H, J<sub>GEM</sub> = 9.6, J<sub>1'b,2'</sub> = 5.4 Hz, H-1'b), 3.86 (dt, 1H, J<sub>4',3'</sub> = 6.2, J<sub>4',5'</sub> = 4.4 Hz, H-4'), 3.71 (dd, 1H, J<sub>GEM</sub> = 11.9, J<sub>5'a,4'</sub> = 4.5 Hz, H-5'a), 3.65 (dd, 1H, J<sub>GEM</sub> = 11.9, J<sub>5'b,4'</sub> = 4.3 Hz, H-5'b). <sup>13</sup>C NMR (101 MHz, DMSO-*d*<sub>6</sub>) δ 165.81 (CON), 152.46 (C-4), 151.63 (C-2), 150.37 (C-6), 143.51 (C-8), 133.63 (Bz-*i*), 128.68 (Bz-*o,m*), 125.61 (C-5), 84.81 (d, J<sub>4',P</sub> = 3.0 Hz, C-4'), 77.35 (d, J<sub>3',P</sub> = 4.4 Hz, C-3'), 69.31 (C-1'), 61.36 (d, J<sub>2',P</sub> = 5.5 Hz, C-2'), 61.30 (C-5'). <sup>31</sup>P NMR (162 MHz, DMSO) δ 3.56. ESI MS *m/z* (%): 420.2 (100) [M + H]; HRMS ESI (C<sub>17</sub>H<sub>18</sub>N<sub>6</sub>O<sub>6</sub>P) calculated: 420.1073; found: 420.1074.

**N-(9-((3R,4S,5R)-4-Hydroxy-5-(hydroxymethyl)tetrahydrofuran-3-yl)-9H-purin-6-yl)pent-4-enamide (8)**

Intermediate 6 (1 g, 4 mmol) was azeotroped with pyridine (2 × 10 mL), dissolved in pyridine (15 mL), and TMSCl (2.5 mL, 20 mmol) was added dropwise. After stirring the reaction mixture at ambient temperature for 1 h, pentenoic anhydride (2.9 mL, 16 mmol) was added dropwise, and stirring was continued for a further 12 h. TEA (1 mL) was added, and after cooling to 0 °C, water (4 mL) was added and stirring was continued for 5 min. Then, aqueous ammonia was added (25%, 4 mL) while still at 0 °C, and stirring was continued for another 30 min. The volatiles were quickly evaporated at 30 °C, and the residue was passed through a plug of silica in DCM-MeOH 19:1 affording product (1.2 g) of ca 80% purity, sufficient for the next reaction. ESI MS *m/z* (%): 334.2 (100) [M + H].

**N-(9-((3R,4S,5R)-5-(Bis(4-methoxyphenyl)(phenyl)methoxy)methyl)-4-hydroxytetrahydrofuran-3-yl)-9H-purin-6-yl)pent-4-enamide (10)**

The partially protected nucleoside 8 (1.2 g, 80% purity, 3.0 mmol of pure) was azeotroped with pyridine (2 × 10 mL), dissolved in pyridine (15 mL), and DMTrCl (1.12 g, 3.2 mmol) was added at 0 °C in five portions. The reaction mixture was stirred at ambient temperature for 12 h, after which all volatiles were evaporated. The residue was dissolved in a small volume of DCM and applied to a TEA-deactivated silica gel column. Flash chromatography (acetone in cyclohexane 10–60%) afforded 8 (1.6 g, 89%). <sup>1</sup>H NMR (400 MHz, DMSO-*d*<sub>6</sub>) δ 10.69 (s, 1H, NH), 8.64 (s, 1H, H-2), 8.47 (s, 1H, H-8), 7.42–7.36 (m, 2H, DMTr-*o*), 7.32–7.18 (m, 7H, DMTr-*m,p*, DMTr-2), 6.90–6.84 (m, 4H, DMTr-3), 5.88 (ddt, 1H, J<sub>3',4'a</sub> = 17.3, J<sub>3',4'b</sub> = 10.3, J<sub>3',2'</sub> = 6.4 Hz, H-3'), 5.79 (d, 1H, J<sub>OH,3'</sub> = 5.7 Hz, OH), 5.08 (dq, 1H, J<sub>4'a,3'</sub> = 17.3, J<sub>4'a,2'</sub> = J<sub>GEM</sub> = 1.7 Hz, H-4'a), 5.05–4.91 (m, 2H, H-2', H-4'b), 4.53 (dt, 1H, J<sub>3',4'</sub> = 6.8, J<sub>3',2'</sub> = 5.6 Hz, H-3'), 4.36 (dd, 1H, J<sub>GEM</sub> = 9.6, J<sub>1'a,2'</sub> = 5.9 Hz, H-1'a), 4.27 (dd, 1H, J<sub>GEM</sub> = 9.6, J<sub>1'b,2'</sub> = 7.1 Hz, H-1'b), 3.92 (dt, 1H, J<sub>4',3'</sub> = 6.7, J<sub>4',5'</sub> = 4.5 Hz, H-4'), 3.73 (s, 6H, DMTr-OCH<sub>3</sub>), 3.16 (d, 2H, J<sub>5',4'</sub> = 4.5 Hz, H-5'), 2.68 (t, 2H, J<sub>1',2'</sub> = 7.4 Hz, H-1'), 2.36 (dtt, 2H, J<sub>2',3'</sub> = 8.7, J<sub>2',1'</sub> = 7.3, J<sub>2',4'</sub> = 1.6 Hz, H-2'). <sup>13</sup>C NMR (101 MHz, DMSO-*d*<sub>6</sub>) δ 171.07 (CON), 158.23 (DMTr-4), 152.13 (C-4), 151.59 (C-2), 149.66 (C-6), 145.05 (DMTr-*i*), 142.94 (C-8), 137.68 (C-3'), 135.80 and 135.77 (DMTr-1), 129.89 (DMTr-2), 127.99 and 127.91 (DMTr-*o,m*), 126.83 (DMTr-*p*), 123.77 (C-5), 115.48 (C-4'), 113.35 (DMTr-3), 85.50 (DMTr-C), 83.59 (C-4'), 75.20 (C-3'), 68.70 (C-1'), 63.68 (C-5'), 62.34 (C-2'), 55.21 (DMTr-OCH<sub>3</sub>), 35.56 (C-1'), 28.83 (C-2'). ESI MS *m/z* (%): 636.3 (100) [M + H]; HRMS ESI (C<sub>36</sub>H<sub>37</sub>N<sub>6</sub>O<sub>8</sub>) calculated: 636.2822; found: 636.2825.

**(2R,3S,4R)-2-(Hydroxymethyl)-4-(6-(pent-4-enamido)-9H-purin-9-yl)tetrahydrofuran-3-yl hydrogen phosphonate (12)**

Partially protected nucleoside 10 (200 mg, 0.31 mmol) was azeotroped with pyridine (2 × 10 mL), dissolved in pyridine (10 mL), and diphenyl phosphite (85%, 860 μL, 3.82 mmol) was added in one portion. After stirring at ambient temperature for 20 min, TEA (1.5 mL) was added, followed by water (1.5 mL), and the reaction was stirred for a further 20 min. The resulting solution was diluted with DCM (80 mL) and washed with a saturated aqueous solution of NaHCO<sub>3</sub> (20 mL) and with water (20 mL). The organic layer was dried with sodium sulfate and evaporated. To a solution of obtained intermediate in DCM (15 mL), water (229 μL, 12.7 mmol) and a solution of DCA (0.94 mL, 11.4 mmol) in DCM (10 mL) were added, and the reaction mixture was stirred at ambient temperature for 30 min, after which it was quenched with pyridine (2 mL). Purification and separation of isomers on reverse phase FCC (ACN in water, 0-50%) afforded 24 (119 mg, 83%) as triethylammonium salt. <sup>1</sup>H NMR (400 MHz, DMSO-*d*<sub>6</sub>) δ 10.68 (s, 1H, NH), 8.64 (s, 1H, H-2), 8.61 (s, 1H, H-8), 6.45 (d, 1H, J<sub>1,2</sub> = 587.4 Hz, PH), 5.87 (ddt, 1H, J<sub>4',3'</sub> = 16.8, J<sub>4',5'</sub> = 10.2, J<sub>4',3'</sub> = 6.4 Hz, H-4'), 5.16 (m, 1H, H-2'), 5.08 (dq, 1H, J<sub>5'a,4'</sub> = 17.2, J<sub>5'a,3'</sub> = J<sub>5'a,5'</sub> = 1.7 Hz, H-5'a), 4.98 (ddt, 1H, J<sub>5'b,4'</sub> = 10.2, J<sub>5'b,5'</sub> = 2.3, J<sub>5'b,3'</sub> = 1.3 Hz, H-5'b), 4.88 (ddd, 1H, J<sub>3',2'</sub> = 11.1, J<sub>3',4'</sub> = 6.2, J<sub>3',2'</sub> = 5.1 Hz, H-3'), 4.23–4.12 (m, 2H, H-1'), 3.84 (dt, 1H, J<sub>4',3'</sub> = 6.3, J<sub>4',5'</sub> = 4.4 Hz, H-4'), 3.69 (dd, 1H, J<sub>GEM</sub> = 11.8, J<sub>5'a,4'</sub> = 4.7 Hz, H-5'a), 3.63 (dd, 1H, J<sub>GEM</sub> = 11.8, J<sub>5'b,4'</sub> = 4.3 Hz, H-5'b), 2.99 (q, 1.5H, J<sub>CH<sub>2</sub>,CH<sub>3</sub></sub> = 7.3 Hz, TEA-CH<sub>3</sub>), 2.71–2.65 (m, 2H, H-2'), 2.35 (dtd, 2H, J<sub>3',2'</sub> = 7.3, J<sub>3',4'</sub> = 6.4, J<sub>3',5'</sub> = 1.6 Hz, H-3'), 1.12 (t, 2.1H, J<sub>CH<sub>3</sub>,CH<sub>2</sub></sub> = 7.3 Hz, TEA-CH<sub>3</sub>). <sup>13</sup>C NMR (101 MHz, DMSO-*d*<sub>6</sub>) δ 171.09 (H-1'), 152.01 (C-4), 151.02 (C-2), 149.57 (C-6), 143.08 (C-8), 137.09 (C-4'), 123.50 (C-5), 115.48 (C-5'), 84.60 (d, J<sub>4',P</sub> = 2.9 Hz, C-4'), 77.31 (d, J<sub>3',P</sub> = 4.5 Hz, C-3'), 69.15 (C-1'), 61.38 (C-5'), 61.27



(d,  $J_{2',F} = 5.3$  Hz, C-2'), 45.55 (TEA-CH<sub>2</sub>), 35.54 (C-2''), 28.82 (C-3'), 8.62 (TEA-CH<sub>3</sub>). <sup>31</sup>P NMR (162 MHz, DMSO)  $\delta$  3.74. ESI MS  $m/z$  (%): 398.2 (100) [M + H]; HRMS ESI (C<sub>15</sub>H<sub>20</sub>N<sub>5</sub>O<sub>6</sub>P) calculated: 398.1229; found: 398.1229.

**Synthesis of PNT protected 2',2'-dA phosphoramidite (14) (Figure S2)**

**N-(9-((2,3,4,5R)-3-Fluoro-4-hydroxy-5-(hydroxymethyl)tetrahydrofuran-2-yl)-9H-purin-6-yl)pent-4-enamide (S2).** S1 (1 g, 3.7 mmol, CAS: 64,183-27-3, Chemgenes corp.) was azeotroped with pyridine (2 × 10 mL), dissolved in pyridine (15 mL), and TMSCl (2.36 mL, 18.6 mmol) was added dropwise. After stirring the reaction mixture at ambient temperature for 1 h, pentenoic anhydride (1.7 mL, 9.3 mmol) was added dropwise and stirring was continued for further 12 h. TEA (1 mL) was added, and, after cooling to 0 °C, water (4 mL) was added and stirring was continued for 5 min. Then aqueous ammonia was added (25%, 4 mL), while still at 0 °C and stirring was continued for another 30 min. Volatiles were quickly evaporated at 30 °C and the residue was passed through a plug of silica in DCM-MeOH 19:1 affording product (1.1 g) of ca 90% purity, suitable for next reaction. ESI MS  $m/z$  (%): 352.1 (100) [M + H].

**N-(9-((2,3,4,5R)-5-((Bis(4-methoxyphenyl)(phenyl)methoxy)methyl)-3-fluoro-4-hydroxytetrahydrofuran-2-yl)-9H-purin-6-yl)pent-4-enamide (S3).** Partially protected nucleoside S2 (1.09 g, 3.1 mmol) was azeotroped with pyridine (2 × 10 mL), dissolved in pyridine (15 mL) and DMTrCl (1.15 g, 3.4 mmol) was added at 0 °C in five portions. Reaction mixture was stirred at ambient temperature for 12 h, after which all volatiles were evaporated. Residue was dissolved in small volume of DCM and applied to a pre-conditioned silicagel column (10% acetone in cyclohexane, 1% TEA), and flash chromatography (10-80% acetone in cyclohexane) afforded 12 (1.7 g, 84%). <sup>1</sup>H NMR (400 MHz, DMSO-*d*<sub>6</sub>)  $\delta$  10.76 (s, 1H, NH), 8.64 (s, 1H, H-2), 8.60 (s, 1H, H-8), 7.32-7.28 (m, 2H, DMTr-o), 7.24-7.14 (m, 7H, DMTr-m,p, DMTr-2), 6.82-6.75 (m, 4H, DMTr-3), 6.40 (dd, 1H,  $J_{1',F} = 20.0$ ,  $J_{1',2'} = 1.5$  Hz, H-1'), 5.87 (ddt, 1H,  $J_{3',4'a} = 16.8$ ,  $J_{3',4'b} = 10.2$ ,  $J_{3',2'} = 6.4$  Hz, H-3'), 5.75 (d, 1H,  $J_{OH,3'} = 6.9$  Hz, OH), 5.65 (ddd, 1H,  $J_{2',F} = 52.7$ ,  $J_{2',3'} = 4.5$ ,  $J_{2',1'} = 1.4$  Hz, H-2'), 5.08 (dq, 1H,  $J_{4'a,3'} = 17.2$ ,  $J_{4'a,2'} = J_{GEM} = 1.7$  Hz, H-4'a), 4.98 (ddt, 1H,  $J_{4'b,3'} = 10.2$ ,  $J_{4'b,2'} = 2.2$ ,  $J_{4'b,F} = J_{GEM} = 1.4$  Hz, H-4'b), 4.84 (dddd, 1H,  $J_{3',F} = 23.2$ ,  $J_{3',4'} = 8.3$ ,  $J_{3',OH} = 6.9$ ,  $J_{3',2'} = 4.5$  Hz, H-3'), 4.12 (ddd, 1H,  $J_{4',3'} = 8.0$ ,  $J_{4',5'b} = 5.1$ ,  $J_{4',5'a} = 2.4$  Hz, H-4'), 3.71 (s, 6H, DMTr-OCH<sub>3</sub>), 3.28 (dd, 1H,  $J_{GEM} = 10.7$ ,  $J_{5'a,4'} = 2.5$  Hz, H-5'a), 3.22 (dd, 1H,  $J_{GEM} = 10.8$ ,  $J_{5'b,4'} = 5.3$  Hz, H-5'b), 2.68 (t, 2H,  $J_{1'',2''} = 7.4$  Hz, H-1''), 2.35 (dtt, 2H,  $J_{2'',3''} = 8.7$ ,  $J_{2'',1''} = 7.4$ ,  $J_{2'',4''} = 1.5$  Hz, H-2''). <sup>13</sup>C NMR (101 MHz, DMSO-*d*<sub>6</sub>)  $\delta$  171.05 (CON), 158.20 (DMTr-4), 151.99 (C-2), 151.29 (C-4), 149.90 (C-6), 144.91 (DMTr-1), 143.24 (C-8), 137.65 (C-3'), 135.63 and 135.60 (DMTr-1), 129.82 (DMTr-2), 127.90 and 127.81 (DMTr-o,m), 126.79 (DMTr-p), 123.83 (C-5), 115.47 (C-4'), 113.27 (DMTr-3), 93.48 (d,  $J_{2',F} = 184.6$  Hz, C-2'), 86.83 (d,  $J_{1',F} = 34.7$  Hz, C-1'), 85.55 (DMTr-C), 81.59 (C-4), 68.85 (d,  $J_{3',F} = 16.5$  Hz, C-3') 62.77 (C-5'), 55.17 (DMTr-OCH<sub>3</sub>), 35.56 (C-1''), 28.78 (C-2''). <sup>19</sup>F NMR (377 MHz, DMSO-*d*<sub>6</sub>)  $\delta$  -201.20 (ddd,  $J = 52.9$ , 23.2, 20.1 Hz). ESI MS  $m/z$  (%): 654.3 (100) [M + H]; HRMS ESI (C<sub>36</sub>H<sub>38</sub>N<sub>6</sub>O<sub>6</sub>F) calculated: 654.2728; found: 654.2723.

**(2R,3R,4R,5R)-2-((Bis(4-methoxyphenyl)(phenyl)methoxy)methyl)-4-fluoro-5-(6-(pent-4-enamido)-9H-purin-9-yl)tetrahydrofuran-3-yl (2-cyanoethyl) diisopropylphosphoramidite (14).** To a solution of S3 (688 mg, 1.05 mmol) in DCE (11 mL) under argon atmosphere was via syringe added 2-cyanoethyl *N,N,N,N'*-tetraisopropylphosphorodiamidite (0.67 mL, 2.1 mmol) followed by tetrazole (0.45M in ACN, 5.85 mL, 2.63 mmol). Reaction mixture was stirred at ambient temperature for 30 min, diluted with DCM (150 mL), washed with sat. aq. NaHCO<sub>3</sub> (50 mL), dried over sodium sulfate and evaporated. Crude product was dissolved in DCM (2 mL) and applied to a pre-conditioned (10% acetone in cyclohexane, 1% TEA) silicagel column and eluted with a gradient of acetone in cyclohexane 10-60%. Product was freeze-dried from benzene to afford 13 (700 mg, 78%) as a 3:2 mixture of diastereomers. <sup>31</sup>P NMR (162 MHz, Benzene-*d*<sub>6</sub>)  $\delta$  151.69, 151.66. <sup>19</sup>F NMR (377 MHz, Benzene-*d*<sub>6</sub>)  $\delta$  -198.55 (dt,  $J = 51.2$ , 17.7 Hz), -198.96 (ddd,  $J = 51.1$ , 21.6, 15.6 Hz).

**Synthesis of 5'-DMT-<sup>isonuc</sup>A(bz) phosphoramidite (S4) (Figure S3)**

**(2R,3S,4R)-4-(6-Benzamido-9H-purin-9-yl)-2-((bis(4-methoxyphenyl)(phenyl)methoxy)methyl) tetrahydrofuran-3-yl (2-cyanoethyl) diisopropylphosphoramidite (S4).** To a solution of 9 (460 mg, 0.7 mmol) in DCE (7 mL) under argon atmosphere was via syringe added 2-cyanoethyl *N,N,N,N'*-tetraisopropylphosphorodiamidite (0.44 mL, 1.4 mmol) followed by tetrazole (0.45M in ACN, 3.9 mL, 1.74 mmol). Reaction mixture was stirred at ambient temperature for 30 minutes, diluted with DCM (150 mL), washed with sat. aq. NaHCO<sub>3</sub> (50 mL), dried over sodium sulfate and evaporated. Crude product was dissolved in DCM (2 mL) and applied to a pre-conditioned (10% acetone in cyclohexane, 1% TEA) silicagel column and eluted with a gradient of acetone in cyclohexane 10-60%. Product was freeze-dried from benzene to afford S4 (370 mg, 62%) as a 2:1 mixture of diastereomers. <sup>31</sup>P NMR (162 MHz, Benzene-*d*<sub>6</sub>)  $\delta$  153.55, 153.16.

**Synthesis of protected <sup>isonuc</sup>G H-phosphonate monomer (S9) (Figure S4)**

**2-Amino-9-((3R,4S,5R)-4-hydroxy-5-(hydroxymethyl)tetrahydrofuran-3-yl)-1,9-dihydro-6H-purin-6-one (S6).** A mixture of 4 (1.5 g, 4 mmol), 2-amino-6-chloropurine (1 g, 6 mmol) and triphenylphosphine (2.1 g, 8 mmol) in THF (48 mL) was cooled to 0 °C and DIAD (1.6 mL, 8 mmol) was added dropwise during 10 min. After 30 min at ambient temperature was the reaction mixture heated to 60 °C for 20 h. Volatiles were evaporated and the residue was purified by flash chromatography on silica gel (ethyl acetate in cyclohexane, 0-45%). An inseparable mixture of S5 (ESI MS  $m/z$  (%): 528.2 (100) [M + H]) and its adduct with triphenylphosphine (ESI MS  $m/z$  (%): 788.3 (100) [M + H]) was obtained. This mixture was dissolved in aq. HCOOH (85 mL, 80%) and heated to 100 °C for 16 h. Reaction mixture was then taken down, co-evaporated with ethanol (3 × 100 mL) and re-dissolved in ethanol (40 mL). To this solution, aq. ammonia (20 mL, 25%) was added and the mixture was stirred at ambient temperature for 3 h, evaporated to dryness and co-evaporated with ethanol (2 × 100 mL). Product was isolated by FCC on silica (ethyl acetate to ethyl acetate:acetone:ethanol:water 4:1:1:1, 0-100%) to afford S6 (640 mg, 60%) of purity sufficient for the next reaction. <sup>1</sup>H NMR (400 MHz, DMSO-*d*<sub>6</sub>)  $\delta$  10.57 (s, 1H, NH), 7.77 (s, 1H, H-8), 6.43 (s, 2H, NH<sub>2</sub>), 5.69 (d,  $J_{OH,3'} = 5.5$ , 1H, 3'-OH), 4.90 (t,  $J_{OH,5'} = 5.7$ , 1H, 5'-OH), 4.68-4.62 (m, 1H, H-2'),

4.32–4.25 (m, 1H, H-3'), 4.28 (dd,  $J_{gem} = 9.7$ ,  $J_{1'a,2'} = 6.8$ , 1H, H-1'a), 3.93 (dd,  $J_{gem} = 9.7$ ,  $J_{1'b,2'} = 4.7$ , 1H, H-1'b), 3.67–3.60 (m, 2H, H-4', H-5'a), 3.60–3.52 (m, 1H, H-5'b).  $^{13}C$  NMR (101 MHz, DMSO- $d_6$ )  $\delta$  156.98 (C-6), 153.60 (C-2), 151.29 (C-4), 135.55 (C-8), 116.55 (C-5), 86.16 (C-4'), 76.15 (C-3'), 70.22 (C-1'), 61.60 (C-2'), 60.99 (C-5'). ESI MS  $m/z$ : 268.2 (M + H) $^+$ .  $^1H$  NMR spectrum matches literature data (Kakefuda et al., 1994).

**N-(9-((3R,4S,5R)-4-Hydroxy-5-(hydroxymethyl)tetrahydrofuran-3-yl)-6-oxo-6,9-dihydro-1H-purin-2-yl)isobutyramide (S7).** Nucleoside S6 (1.07 g, 4 mmol) was azeotroped with pyridine (3 x 40 mL), dissolved in pyridine (45 mL), cooled to 0°C and TMSCl (4.2 mL, 32.7 mmol) was added dropwise during 5 min. Reaction mixture was stirred at 0°C for 1 h and then at ambient temperature for another 1 h and cooled to 0°C. Isobutryl chloride (1.26 mL, 12 mmol) was slowly added at 0°C and the resulting solution was stirred overnight at ambient temperature. The reaction mixture was cooled to 0°C, quenched with water (17 mL, dropwise) and then stirred at ambient temperature for 30 min. Reaction mixture was re-cooled to 0°C and aq. ammonia (17 mL, 25%) was added dropwise. After further 15 min at 0°C and 20 min at ambient temperature were all volatiles evaporated and product was isolated by on reverse phase FCC (ACN in water, 0–50%) to afford S7 (722 mg, 54%) as white solid.  $^1H$  NMR (400 MHz, DMSO- $d_6$ )  $\delta$  12.06 and 11.64 (2 x bs, 2H, NHCO, NH), 8.08 (s, 1H, H-8), 5.74 (d,  $J_{OH,3'} = 5.3$ , 1H, 3'-OH), 4.94 (t,  $J_{OH,5'} = 5.4$ , 1H, 5'-OH), 4.79–4.73 (m, 1H, H-2'), 4.34–4.29 (m, 1H, H-3'), 4.14 (dd,  $J_{gem} = 9.8$ ,  $J_{1'a,2'} = 6.5$ , 1H, H-1'a), 4.01 (dd,  $J_{gem} = 9.8$ ,  $J_{1'b,2'} = 4.5$ , 1H, H-1'b), 3.69–3.63 (m, 2H, H-4', H-5'a), 3.62–3.55 (m, 1H, H-5'b), 2.84–2.75 (m, 1H, CH(CH $_3$ ) $_2$ ), 1.12 (d,  $J_{CH_3,CH} = 6.8$ , 3H, CH $_3$ ), 1.11 (d,  $J_{CH_3,CH} = 6.8$ , 3H, CH $_3$ ).  $^{13}C$  NMR (101 MHz, DMSO- $d_6$ )  $\delta$  180.30 (CON), 155.07 and 147.97 (C-2, C-6), 148.77 (C-4), 137.82 (C-8), 119.99 (C-5), 86.28 (C-4'), 76.41 (C-3'), 70.28 (C-1'), 62.10 (C-2'), 60.83 (C-5'), 34.88 (CH), 19.06 and 19.06 (2 x CH $_3$ ). ESI MS  $m/z$ : 338.2 (M + H) $^+$ .

**N-(9-((3R,4S,5R)-5-(Bis(4-methoxyphenyl)(phenyl)methoxy)methyl)-4-hydroxytetrahydrofuran-3-yl)-6-oxo-6,9-dihydro-1H-purin-2-yl)isobutyramide (S8).** Compound S7 (700 mg, 2.08 mmol) was azeotroped with pyridine (3 x 40 mL), dissolved in pyridine (25 mL) and DMTrCl (773 mg, 2.29 mmol) was added in one portion at 0°C. Reaction mixture was stirred at ambient temperature for 15 h. Second portion of DMTrCl (141 mg, 0.42 mmol) was added at 0°C and reaction mixture was allowed to stir for another 4 h, then quenched with satd. aq. NaHCO $_3$  (8 mL) and evaporated. Residue was dissolved in ethyl acetate (400 mL) and washed with saturated aqueous solution of NaHCO $_3$  (2 x 150 mL) and brine (150 mL). Organic phase was dried over sodium sulfate and evaporated. Product was purified by FCC on silica (acetone in dichloromethane, 50–70%) on a TEA-deactivated silica to afford S8 (1.2 g, 90%) as white foam.  $^1H$  NMR (400 MHz, DMSO- $d_6$ )  $\delta$  12.09 (s, 1H, NH), 11.65 (s, 1H, 2-NH), 8.03 (s, H-8), 7.41–7.36 (m, 2H, DMTr-o), 7.33–7.28 (m, 2H, DMTr-m), 7.27–7.19 (m, 5H, DMTr-p, DMTr-2), 6.92–6.85 (m, 4H, DMTr-3), 5.75 (d,  $J_{OH,3'} = 5.6$ , 1H, 3'-OH), 4.81–4.75 (m, 1H, H-2'), 4.28–4.21 (m, 2H, H-3', H-1'a), 4.16 (dd,  $J_{gem} = 9.8$ ,  $J_{1'b,2'} = 5.5$ , 1H, H-1'b), 3.93–3.87 (m, 1H, H-4'), 3.74 (s, 6H, DMTr-OCH $_3$ ), 3.23–3.14 (m, 2H, H-5'), 2.84–2.75 (m, 1H, CH(CH $_3$ ) $_2$ ), 1.13 (d,  $J_{CH_3,CH} = 6.8$ , 2H, two x CH $_3$ ).  $^{13}C$  NMR (101 MHz, DMSO- $d_6$ )  $\delta$  180.32 (CON), 158.22 (DMTr-4), 155.03 and 148.00 (C-6, C-2), 148.97 (C-4), 144.99 (DMTr-i), 137.48 (C-8), 135.73 and 135.67 (DMTr-1), 129.88 (DMTr-2), 127.97 and 127.89 (DMTr-o,m), 126.82 (DMTr-p), 120.22 (C-5), 113.33 (DMTr-3), 85.57 (DMTr-C), 83.96 (C-4'), 76.41 (C-3'), 69.66 (C-1'), 63.91 (C-5'), 61.50 (C-2'), 55.19 (DMTr-OMe), 34.86 (CH), 19.05 and 19.02 (2 x CH $_3$ ). ESI MS  $m/z$ : 640.3 (M + H) $^+$ .

**(2R,3S,4R)-2-(Hydroxymethyl)-4-(2-isobutyramido-6-oxo-1,6-dihydro-9H-purin-9-yl)tetrahydrofuran-3-yl hydrogen phosphonate (S9).** Compound S8 (600 mg, 0.94 mmol) was azeotroped with pyridine (2 x 15 mL), dissolved in pyridine (10 mL), and diphenyl phosphite (85%, 636  $\mu$ L, 2.8 mmol) was added in one portion. After stirring at ambient temperature for 40 min, TEA (1.4 mL) was added followed by water (1.4 mL), and the reaction mixture was stirred for further 20 min. Resulting solution was diluted with DCM (350 mL) and washed with saturated aqueous solution of NaHCO $_3$  (150 mL). Water phase was extracted with DCM (2 x 100 mL). Combined organic layers were dried over sodium sulfate and evaporated. Resulting intermediate was purified by FCC (1% Et $_3$ N-MeOH in DCM 0–25%). To a solution of obtained intermediate in DCM (14 mL) was added water (322  $\mu$ L, 17.9 mmol) followed by a solution of DCA (0.7 mL, 8.6 mmol) in DCM (7.7 mL). Reaction mixture was stirred at ambient temperature for 30 min, quenched with pyridine (5 mL) and volatiles were evaporated. Purification on reverse phase FCC (ACN in water, 0–40%) afforded S9 (332 mg, 84%, triethylammonium salt) as white foam.  $^1H$  NMR (400 MHz, DMSO- $d_6$ )  $\delta$  12.07 and 11.80 (bs, 1H, H-1', NH), 8.14 (s, 1H, H-8), 6.53 (d, 1H,  $J_{1',P} = 590.9$  Hz, PH), 4.95 (dt, 1H,  $J_{2',1'b} = 6.5$ ,  $J_{2',1'b} = J_{2',3'} = 4.5$  Hz, H-2'), 4.74 (ddd, 1H,  $J_{3',P} = 10.4$ ,  $J_{3',4'} = 6.0$ ,  $J_{3',2'} = 4.3$  Hz, H-3'), 4.13 (dd, 1H,  $J_{gem} = 9.7$ ,  $J_{1'a,2'} = 6.5$  Hz, H-1'a), 4.02 (dd, 1H,  $J_{gem} = 9.7$ ,  $J_{1'b,2'} = 4.8$  Hz, H-1'b), 3.81 (dt, 1H,  $J_{4',3'} = 6.0$ ,  $J_{4',5'} = 4.2$  Hz, H-4'), 3.71 (dd, 1H,  $J_{gem} = 11.9$ ,  $J_{5'a,4'} = 4.4$  Hz, H-5'a), 3.64 (dd, 1H,  $J_{gem} = 11.9$ ,  $J_{5'b,4'} = 4.2$  Hz, H-5'b), 3.00 (q, 2H,  $J_{CH_2,CH_3} = 7.3$  Hz, TEA-CH $_3$ ), 2.78 (hept, 1H,  $J_{CH,CH_3} = 6.8$  Hz, *i*Pr-CH), 1.12 (t, 3H,  $J_{CH_3,CH_2} = 7.3$  Hz, TEA-CH $_3$ ), 1.11 and 1.11 (d, 3H,  $J_{CH_3,CH_2} = 6.7$  Hz, *i*Pr-CH $_3$ ).  $^{13}C$  NMR (101 MHz, DMSO- $d_6$ )  $\delta$  180.40 (CON), 155.10 (C-6), 148.78 (C-2), 148.05 (C-2), 138.02 (C-8), 119.98 (C-5), 85.12 (d,  $J_{4',P} = 3.0$  Hz, C-4'), 78.12 (d,  $J_{3',P} = 4.6$  Hz, C-3'), 70.15 (C-1'), 61.14 (C-5'), 60.95 (d,  $J_{2',P} = 5.6$  Hz, C-2'), 45.57 (TEA-CH $_3$ ), 34.89 (*i*Pr-CH), 19.14 and 19.03 (*i*Pr-CH $_3$ ), 8.63 (TEA-CH $_3$ ).  $^{31}P$  NMR (162 MHz, DMSO)  $\delta$  3.60.

#### Preparation of CDNs with phosphate linkers

**3',3'-c-(2',2'-dAMP, isonucleic AMP) (19).** A mixture of 12 (36 mg, 0.077 mmol) and pyridinium trifluoroacetate (22 mg, 0.12 mmol) was codistilled with dry ACN (3 x 3 mL), suspended in dry ACN (1 mL), and stirred overnight in a sealed vessel over activated 3 Å molecular sieves. In a separate flask, 14 (75 mg, 0.10 mmol, CAS: 144,089-97-4, Sigma-Aldrich) was codistilled with dry ACN (3 x 3 mL), dissolved in dry ACN (1 mL), and stirred overnight in a sealed vessel over activated 3 Å molecular sieves. A solution of 14 was transferred via syringe to a flask with the suspension of 12 with py-TFA, and the resulting solution was stirred for 1 h at ambient temperature. TBHP (5.5M solution in decane, 42  $\mu$ L, 0.23 mmol) was added, and the reaction mixture was stirred for a further 30 min. The reaction mixture was quenched with NaHSO $_3$  (39% in water, 31  $\mu$ L, 0.27 mmol) and evaporated to afford crude tritylated linear dimer which was used in the next reaction without further purification. To a solution of this residue in DCM (3 mL) was added water (14  $\mu$ L, 0.77 mmol) and a solution of DCA (57  $\mu$ L, 0.7 mmol) in DCM (3 mL) dropwise. After stirring the reaction mixture for 30 min, TES



(1.2 mL) was added, and the reaction mixture was stirred for a further 90 min, after which it was quenched by the addition of pyridine (1.2 mL). All solids were removed by filtration and thoroughly washed with pyridine. Volatiles were evaporated, and 16 (29 mg) was isolated on RP FCC (ACN in 0.05M NH<sub>4</sub>COOH, 0-50%) as a mixture of diastereomers. 16 was azeotroped with pyridine (2 × 2 mL), dissolved in pyridine (2 mL), DMOCP (50 mg, 0.27 mmol) was added, and the reaction mixture was stirred at ambient temperature for 1 h. Water (46 μL, 2.54 mmol) followed by iodine (26 mg, 0.1 mmol) were added, and the reaction mixture was stirred at ambient temperature for 10 min, after which it was quenched with NaHSO<sub>3</sub> (39% in water, 31 μL, 0.27 mmol) and evaporated to afford crude cyclic dimer 18 which was used in the next reaction without further purification. CH<sub>3</sub>NH<sub>2</sub> (33% in ethanol, 1 mL) was added to the crude 18, and the reaction mixture was stirred at ambient temperature for 3 h. Volatiles were evaporated, and the product was purified on a preparative HPLC (ACN in 0.1M TEAB, 0-30%). Appropriate fractions were pooled, evaporated, codistilled with water (3 × 5 mL) and methanol (3 × 5 mL), dissolved in water (1 mL) and slowly passed through a 1 mL column of Dowex 50 (Na<sup>+</sup> cycle). Freeze-drying the eluent afforded the sodium salt of 19 (23 mg, 43%). <sup>1</sup>H NMR (501 MHz, D<sub>2</sub>O) δ 8.16 (s, 1H, B-8), 8.10 (s, 1H, A-2), 8.10 (s, 1H, A-8), 8.05 (s, 1H, B-2), 6.34 (d, 1H, J<sub>1',F</sub> = 16.5 Hz, A-1'), 5.53 (dd, 1H, J<sub>2',F</sub> = 51.4, J<sub>2',3'</sub> = 4.0 Hz, A-2'), 5.39 (dt, 1H, J<sub>2',1'a</sub> = 6.9, J<sub>2',1'b</sub> = 3.8 Hz, B-2'), 5.29 (td, 1H, J<sub>3',P</sub> = J<sub>3',A'</sub> = 7.1, J<sub>3',2'</sub> = 3.7 Hz, B-3'), 4.92 (dtd, 1H, J<sub>3',F</sub> = 21.1, J<sub>3',P</sub> = J<sub>3',A'</sub> = 9.6, J<sub>3',2'</sub> = 4.0 Hz, A-3'), 4.51 (ddd, 1H, J<sub>4',3'</sub> = 9.4, J<sub>4',5'a</sub> = 2.0, J<sub>4',5'b</sub> = 1.4 Hz, A-4'), 4.40 (dd, 1H, J<sub>GEM</sub> = 12.1, J<sub>5',A'</sub> = 2.0 Hz, A-5'a), 4.37 (dd, 1H, J<sub>GEM</sub> = 10.5, J<sub>1'a,2'</sub> = 6.9 Hz, B-1'a), 4.35 (dd, 1H, J<sub>GEM</sub> = 11.7, J<sub>5',A'</sub> = 2.3 Hz, B-5'a), 4.23 (dq, 1H, J<sub>4',3'</sub> = 7.1, J<sub>4',5'</sub> = J<sub>4',P</sub> = 2.3 Hz, B-4'), 4.20 (ddd, 1H, J<sub>GEM</sub> = 11.7, J<sub>5',P</sub> = 5.2, J<sub>5',A'</sub> = 2.0 Hz, B-5'b), 4.10 (ddd, 1H, J<sub>GEM</sub> = 12.1, J<sub>5',P</sub> = 4.2, J<sub>5',A'</sub> = 1.4 Hz, A-5'b), 4.10 (dd, 1H, J<sub>GEM</sub> = 10.5, J<sub>1'a,2'</sub> = 3.9 Hz, B-1'b). <sup>13</sup>C NMR (101 MHz, D<sub>2</sub>O) δ 157.97 (A-6), 157.97 (B<sub>6</sub>), 155.36 (B-2), 154.96 (A-2), 151.48 (B-4), 150.21 (A-4), 143.55 (B-8), 141.55 (A-8), 121.36 (A-5), 121.01 (B-5), 94.78 (d, J<sub>2',F</sub> = 189.2 Hz, A-2'), 90.27 (d, J<sub>1',F</sub> = 34.0 Hz, A-1'), 85.05 (t, J<sub>4',P</sub> = 10.2 Hz, B-4'), 82.44 (t, J<sub>4',F</sub> = J<sub>4',P</sub> = 11.3 Hz, A-4'), 80.39 (d, J<sub>3',P</sub> = 5.5 Hz, B-3'), 74.44 (B-1'), 72.03 (dd, J<sub>3',F</sub> = 16.4, J<sub>3',P</sub> = 5.5 Hz, A-3'), 65.67 (d, J<sub>5',P</sub> = 4.4 Hz, B-5'), 64.58 (d, J<sub>5',P</sub> = 4.7 Hz, A-5'), 64.31 (A-2'). <sup>31</sup>P NMR (202.4 MHz, D<sub>2</sub>O) δ 0.70, 0.36. <sup>19</sup>F NMR (470.4 MHz, D<sub>2</sub>O) δ -198.17. HPLC retention time (HILIC, min): 3.48.

**3',3'-c-(2'F,2'dGMP, isonucleic AMP) (21).** From 11 and a commercial phosphoramidite (CAS 144089-97-4, Sigma-Aldrich), yield 8 mg, 15%. <sup>1</sup>H NMR (400 MHz, D<sub>2</sub>O) δ 8.19 (s, 1H, A-8), 8.10 (s, 1H, A-2), 7.71 (s, 1H, G-8), 6.12 (d, J<sub>1',F</sub> = 18.1 Hz, 1H, G-1'), 5.57 (dd, J<sub>2',F</sub> = 51.6, J<sub>2',3'</sub> = 4.2 Hz, 1H, G-2'), 5.39 (dt, J<sub>2',1'a</sub> = 6.8, J<sub>2',1'b</sub> = J<sub>2',3'</sub> = 3.4 Hz, 1H, A-2'), 5.18 (td, J<sub>3',A'</sub> = J<sub>3',P</sub> = 7.1, J<sub>3',2'</sub> = 3.5 Hz, 1H, A-3'), 4.99 (m, 1H, G-3'), 4.45 (dm, J<sub>4',3'</sub> = 9.0 Hz, 1H, G-4'), 4.39 (dd, J<sub>GEM</sub> = 10.5, J<sub>1'a,2'</sub> = 6.8 Hz, 1H, A-1'a), 4.36 (bdd, J<sub>GEM</sub> = 12.0, J<sub>5'a,A'</sub> = 2.5 Hz, 1H, A-5'a), 4.35 (bdd, J<sub>GEM</sub> = 12.0, J<sub>5',A'</sub> = 1.7 Hz, 1H, G-5'a), 4.22 (dq, J<sub>4',3'</sub> = 7.0, J<sub>4',5'</sub> = J<sub>4',P</sub> = 2.3 Hz, 1H, A-4'), 4.20 (ddd, J<sub>GEM</sub> = 12.0, J<sub>5'b,P</sub> = 5.1, J<sub>5'b,A'</sub> = 2.1 Hz, 1H, A-5'b), 4.17 (bdd, J<sub>GEM</sub> = 10.5, J<sub>1'b,2'</sub> = 3.3 Hz, 1H, A-1'b), 4.07 (ddd, J<sub>GEM</sub> = 12.0, J<sub>5'b,P</sub> = 4.0, J<sub>5'b,A'</sub> = 1.5 Hz, 1H, G-5'b). <sup>13</sup>C NMR (101 MHz, D<sub>2</sub>O) δ 160.55 (G-6), 157.81 (A-6), 156.27 (G-2), 154.61 (A-2), 152.71 (G-4), 151.37 (A-4), 143.38 (A-8), 139.09 (G-8), 120.80 (A-5), 119.04 (G-5), 94.83 (d, J<sub>2',F</sub> = 188.5 Hz, G-2'), 90.60 (d, J<sub>1',F</sub> = 34.7 Hz, G-1'), 84.97 (t, J<sub>4',P</sub> = 10.1 Hz, A-4'), 82.57 (t, J<sub>4',F</sub> = 10.8 Hz, G-4'), 80.88 (A-3'), 74.56 (A-1'), 72.15 (dd, J<sub>3',F</sub> = 16.1, J<sub>3',P</sub> = 5.1 Hz, G-3'), 65.57 (d, J<sub>5',P</sub> = 4.8 Hz, A-5'), 64.64 (d, J<sub>5',P</sub> = 4.8 Hz, G-5'), 64.08 (A-2'). <sup>31</sup>P NMR (162 MHz, D<sub>2</sub>O) δ 1.00, 0.92. <sup>19</sup>F NMR (376 MHz, D<sub>2</sub>O) δ -200.97. HPLC retention time (HILIC, min): 3.40.

**3',3'-c-(2'F,2'dAMP, isonucleic GMP) (22).** From S9 and a commercial phosphoramidite (CAS 136834-22-5, Sigma-Aldrich), yield 14 mg, 28%. <sup>1</sup>H NMR (400 MHz, D<sub>2</sub>O) δ 8.25 (s, 1H, A-2), 8.16 (s, 1H, A-8), 7.72 (s, 1H, G-8), 6.42 (d, 1H, J<sub>1',F</sub> = 14.3 Hz, A-1'), 6.12 (dt, 1H, J<sub>3',A'</sub> = 7.2, J<sub>3',P</sub> = J<sub>3',2'</sub> = 5.8 Hz, G-3'), 5.46 (dd, 1H, J<sub>2',F</sub> = 51.5, J<sub>2',3'</sub> = 3.5 Hz, A-2'), 5.20 (dt, 1H, J<sub>2',1'a</sub> = 8.5, J<sub>2',1'b</sub> = J<sub>2',3'</sub> = 5.8 Hz, G-2'), 4.94-4.83 (m, 1H, A-3'), 4.54 (dm, 1H, J<sub>4',3'</sub> = 9.8 Hz, A-4'), 4.46 (dd, 1H, J<sub>GEM</sub> = 12.3, J<sub>5',P</sub> = 2.3 Hz, A-5'a), 4.35 (dd, 1H, J<sub>GEM</sub> = 9.9, J<sub>1'a,2'</sub> = 8.5 Hz, G-1'a), 4.29 (dd, 1H, J<sub>GEM</sub> = 11.5, J<sub>5'a,P</sub> = 2.6 Hz, G-5'a), 4.25-4.20 (m, 1H, G-4'), 4.16-4.06 (m, 2H, A-5'b, G-5'b), 3.98 (dd, 1H, J<sub>GEM</sub> = 9.8, J<sub>1'b,2'</sub> = 6.0 Hz, G-1'b). <sup>13</sup>C NMR (101 MHz, D<sub>2</sub>O) δ 159.65 (G-6), 156.24 (A-6), 153.49 (A-2), 152.93 (G-2), 151.87 (G-4), 148.25 (A-4), 141.69 (G-8), 139.02 (A-8), 119.28 (A-5), 117.57 (G-5), 92.91 (d, J<sub>2',F</sub> = 190.1 Hz, A-2'), 88.05 (d, J<sub>1',F</sub> = 32.8 Hz, A-1'), 82.76 (t, J<sub>4',P</sub> = 10.8 Hz, G-4'), 80.32 (t, J<sub>4',P</sub> = 11.1 Hz, A-4'), 74.62 (d, J<sub>3',P</sub> = 5.8 Hz, G-3'), 72.15 (G-1'), 69.71 (dd, J<sub>3',F</sub> = 16.2, J<sub>3',P</sub> = 5.1 Hz, A-3'), 64.14 (G-2'), 63.93 (d, J<sub>5',P</sub> = 5.6 Hz, G-5'), 62.43 (d, J<sub>5',P</sub> = 4.8 Hz, A-5'). <sup>31</sup>P NMR (162 MHz, D<sub>2</sub>O) δ 1.04, 0.81. <sup>19</sup>F NMR (376 MHz, D<sub>2</sub>O) δ -202.50 (ddd, J = 51.5, 23.9, 14.4 Hz). HPLC retention time (HILIC, min): 4.24.

**3',3'-c-(dAMP, isonucleic AMP) (23).** From 11 and a commercial phosphoramidite (CAS 98796-53-3, Sigma-Aldrich), yield 9 mg, 19%. <sup>1</sup>H NMR (400 MHz, D<sub>2</sub>O) δ 8.25 (s, 1H, B-8), 8.19 (s, 1H, A-8), 8.15 (s, 1H, B-2), 8.10 (s, 1H, A-2), 6.48 (dd, J<sub>1',2'a</sub> = 7.1, J<sub>1',2'b</sub> = 3.8 Hz, 1H, A-1'), 5.37 (dt, J<sub>2',1'a</sub> = 7.1, J<sub>2',1'b</sub> = J<sub>2',3'</sub> = 4.1 Hz, 1H, B-2'), 5.25 (td, J<sub>3',A'</sub> = J<sub>3',P</sub> = 7.2, J<sub>3',2'</sub> = 4.1 Hz, 1H, B-3'), 4.95 (p, J<sub>3',2'</sub> = J<sub>3',P</sub> = 7.0 Hz, 1H, A-3'), 4.40 (dd, J<sub>GEM</sub> = 10.3, J<sub>1',2'a</sub> = 7.1 Hz, 1H, B-1'a), 4.30 (ddd, J<sub>GEM</sub> = 11.8, J<sub>5'a,A'</sub> = 2.6, J<sub>5'a,P</sub> = 1.3 Hz, 1H, B-5'a), 4.27 (dtd, J<sub>4',3'</sub> = 6.6, J<sub>4',5'a</sub> = 4.3, J<sub>4',5'b</sub> = J<sub>4',P</sub> = 2.2 Hz, 1H, A-4'), 4.22 (dq, J<sub>4',3'</sub> = 7.0, J<sub>4',5'a</sub> = J<sub>4',5'b</sub> = J<sub>4',P</sub> = 2.4 Hz, 1H, B-4'), 4.39 (ddd, J<sub>GEM</sub> = 11.7, J<sub>5'a,P</sub> = 2.7, J<sub>5'a,A'</sub> = 2.0 Hz, 1H, B-5'a), 4.35 (dd, J<sub>GEM</sub> = 10.4, J<sub>1'a,2'</sub> = 6.4 Hz, 1H, B-1'a), 4.25 (dq, J<sub>4',3'</sub> = 6.6, J<sub>4',5'a</sub> = J<sub>4',5'b</sub> = J<sub>4',P</sub> = 2.3 Hz, 1H, B-4'), 4.17 (dd, J<sub>GEM</sub> = 10.3, J<sub>1',2'a</sub> = 4.1 Hz, 1H, B-1'b), 4.15 (ddd, J<sub>GEM</sub> = 11.8, J<sub>5'b,A'</sub> = 2.2, J<sub>5'b,P</sub> = 1.7 Hz, 1H, B-5'b), 4.11 (ddd, J<sub>GEM</sub> = 11.6, J<sub>5'a,A'</sub> = 4.3, J<sub>5'a,P</sub> = 2.5 Hz, 1H, A-5'a), 4.04 (ddd, J<sub>GEM</sub> = 11.6, J<sub>5'a,P</sub> = 4.2, J<sub>5'a,A'</sub> = 2.4 Hz, 1H, A-5'b), 2.95 (ddd, J<sub>GEM</sub> = 14.1, J<sub>2'b,3'</sub> = 7.3, J<sub>2'b,1'</sub> = 3.8 Hz, 1H, A-2'b), 2.78 (dt, J<sub>GEM</sub> = 14.1, J<sub>2'a,3'</sub> = J<sub>2'b,1'</sub> = 7.2 Hz, 1H, A-2'a). <sup>13</sup>C NMR (101 MHz, D<sub>2</sub>O) δ 158.16 (B<sub>6</sub>), 158.11 (A-6), 155.30 (A-2), 155.11 (B-2), 151.67 (B-4), 150.80 (A-4), 143.44 (B-8), 142.18 (A-8), 121.38 (A-5), 121.15 (B-5), 86.18 (A-1'), 85.34 (t, J<sub>4',P</sub> = 10.3 Hz, A-4'), 84.90 (t, J<sub>4',P</sub> = 10.2, 8.6 Hz, B-4'), 80.44 (d, J<sub>3',P</sub> = 5.6 Hz, B-3'), 74.16 (d, J<sub>3',P</sub> = 5.1 Hz, A-1'), 73.94 (B-1'), 65.37 (d, J<sub>5',P</sub> = 4.9 Hz, B-5'), 64.03 (d, J<sub>2',P</sub> = 1.9 Hz, B-2'), 64.01 (d, J<sub>5',P</sub> = 5.0 Hz, A-5'), 41.18 (A-2'). <sup>31</sup>P NMR (162 MHz, D<sub>2</sub>O) δ 1.63, 1.04. 50: HPLC retention time (HILIC, min): 3.57.

**3',3'-c-(dAMP, isonucleic GMP) (24).** From S9 and a commercial phosphoramidite (CAS 98796-53-3, Sigma-Aldrich), yield 12 mg, 24%. <sup>1</sup>H NMR (400 MHz, D<sub>2</sub>O) δ 8.21 (s, 1H, A-2), 8.19 (s, 1H, A-8), 7.74 (s, 1H, G-8), 6.41 (d, 1H, J<sub>1',2'b</sub> = 6.7 Hz, A-1'), 6.09 (q, 1H, J<sub>3',2'</sub> = J<sub>3',A'</sub> = J<sub>3',P</sub> = 6.7 Hz, G-3'), 5.20 (dt, 1H, J<sub>2',1'</sub> = 8.3, J<sub>2',3'</sub> = J<sub>2',1'</sub> = 5.8 Hz, G-2'), 4.98 (m, 1H, A-3'), 4.41-4.19 (m, 5H, A-4', A-5'a, G-1'a,

G-4', G-5'a), 4.13–3.99 (m, 3H, A-5'b, G-1'b, G-5'b), 2.91 (dd, 1H,  $J_{\text{GEM}} = 13.4$ ,  $J_{2'a,3'} = 6.8$  Hz, A-2'a), 2.78 (ddd, 1H,  $J_{\text{GEM}} = 13.3$ ,  $J_{2'b,3'} = 10.0$ ,  $J_{2'b,1'} = 6.9$  Hz, A-2'b).  $^{13}\text{C}$  NMR (101 MHz,  $\text{D}_2\text{O}$ )  $\delta$  159.72 (G-6), 156.17 (A-6), 153.12 (A-2), 153.07 (G-2), 152.00 (G-4), 148.12 (A-4), 141.57 (G-8), 139.45 (A-8), 119.29 (A-5), 117.40 (G-5), 85.13 (A-1'), 83.14 (d,  $J_{4',P} = 10.9$  Hz, A-4' or G-4'), 82.93 (d,  $J_{4',P} = 9.7$  Hz, A-4' or G-4'), 75.00 (d,  $J_{3',P} = 5.7$  Hz, G-3'), 72.02 (G-1'), 69.88 (d,  $J_{3',P} = 5.2$  Hz, A-3'), 63.99 (G-2'), 63.74 (d,  $J_{5',P} = 5.3$  Hz, A-5' or G-5'), 62.54 (d,  $J_{5',P} = 5.1$  Hz, A-5' or G-5'), 40.35 (A-2').  $^{31}\text{P}$  NMR (162 MHz,  $\text{D}_2\text{O}$ )  $\delta$  1.77, 1.02. HPLC retention time (HILIC, min): 3.62.

**3',3'-c-( $^{18}\text{O}$ AMP,  $^{18}\text{O}$ GMP) (25).** From S9 and phosphoramidite S4, yield 16 mg, 32%.  $^1\text{H}$  NMR (400 MHz,  $\text{D}_2\text{O}$ )  $\delta$  8.24 (s, 1H, A-2), 8.06 (s, 1H, A-8), 7.71 (s, 1H, G-8), 5.78 (m, 1H, G-3'), 5.38 (bd, 1H,  $J_{2',3'} = 5.2$  Hz, A-2'), 5.20–5.13 (m, 2H, G-2', A-3'), 4.40–4.32 (m, 3H, G-1'a, G-5'a, A-5'a), 4.26 (dd, 1H,  $J_{\text{GEM}} = 10.6$ ,  $J_{1'a,2'} = 5.1$  Hz, A-1'a), 4.23–4.13 (m, 3H, A-4', G-4', A-5'b), 4.06 (ddd, 1H,  $J_{\text{GEM}} = 11.1$ ,  $J_{5'b,4'} = 4.0$ ,  $J_{5'b,P} = 2.3$  Hz, G-5'b), 3.93 (bd, 1H,  $J_{\text{GEM}} = 10.4$  Hz, A-1'b), 3.89 (dd, 1H,  $J_{\text{GEM}} = 10.3$ ,  $J_{1'b,2'} = 5.3$  Hz, G-1'b).  $^{13}\text{C}$  NMR (101 MHz,  $\text{D}_2\text{O}$ )  $\delta$  159.61 (G-6), 156.19 (A-6), 153.30 (A-2), 153.02 (G-2), 152.03 (G-4), 149.50 (A-4), 141.43 (G-8), 140.54 (A-8), 118.56 (A-5), 117.08 (G-5), 84.54 (t,  $J_{4',P} = 9.9$  Hz, A-4'), 83.34 (t,  $J_{4',P} = 11.4$  Hz, G-4'), 79.56 (d,  $J_{3',P} = 5.6$  Hz, A-3'), 76.34 (d,  $J_{3',P} = 5.3$  Hz, G-3'), 73.53 (A-1'), 72.34 (G-1'), 64.70 (G-2'), 63.53 (d,  $J_{5',P} = 5.1$  Hz, A-5'), 63.13 (d,  $J_{5',P} = 5.1$  Hz, G-5'), 61.98 (A-2').  $^{31}\text{P}$  NMR (162 MHz,  $\text{D}_2\text{O}$ )  $\delta$  1.39, 1.14. HPLC retention time (HILIC, min): 3.64.

**Preparation of a CDN with thiophosphate linkers: 3',3'-c-(2F,2'dAMP(S),  $^{18}\text{O}$ AMP(S)) (20)**

A mixture of 11 (45 mg, 0.1 mmol) and pyridinium trifluoroacetate (29 mg, 0.15 mmol) was codistilled with dry MeCN (3  $\times$  3 mL), suspended in dry MeCN (1 mL), and stirred overnight in a sealed vessel over activated molecular sieves. In a separate flask, 13 (110 mg, 0.125 mmol, CAS # 136,834-22-5, Sigma-Aldrich) was codistilled with dry MeCN (3  $\times$  3 mL), dissolved in dry MeCN (1 mL) and stirred overnight in a sealed vessel over activated molecular sieves. A solution of the commercial phosphoramidite was transferred via syringe to the flask with the suspension of 11 with py-TFA, and the resulting solution was stirred for 1 h at ambient temperature. 3-((*N,N*-dimethylaminomethylidene)amino)-3*H*-1,2,4-dithiazole-5-thione (23 mg, 0.11 mmol) was added, and the reaction mixture was stirred for a further 30 min. Volatiles were evaporated, and the residue dissolved in DCM (3 mL). Water was then added (18  $\mu\text{L}$ , 1 mmol), followed by a solution of DCA (74  $\mu\text{L}$ , 0.9 mmol) in DCM (3 mL) added dropwise. After stirring the reaction mixture for 30 min, TES (1.5 mL) was added, and the reaction mixture was stirred for a further 90 min, after which it was quenched by the addition of pyridine (1.5 mL). Volatiles were evaporated, and the crude 15 was codistilled with dry pyridine (3  $\times$  3 mL) and used in the next reaction without further purification. To a solution of the crude 15 in pyridine (2 mL) was added DMOCF (65 mg, 0.35 mmol), and the reaction mixture was stirred at ambient temperature for 1 h. Water (18  $\mu\text{L}$ , 1 mmol) was added, followed by 3*H*-1,2-benzodithiol-3-one (25 mg, 0.15 mmol), and the reaction mixture was stirred for 10 min. Volatiles were evaporated and product was isolated on reverse phase FCC (MeCN in 50 mM aqueous  $\text{NH}_4\text{HCO}_3$  0-70%) to afford 17 as a mixture of diastereomers. A solution of 17 in  $\text{CH}_3\text{NH}_2$  (33% in ethanol, 1 mL) was stirred at ambient temperature for 3 h. Volatiles were evaporated, and the product was purified on a preparative HPLC (ACN in 0.1M TEAB, 0-60%). Appropriate fractions were pooled, evaporated, and then codistilled with water (3  $\times$  5 mL) and methanol (3  $\times$  5 mL). Freeze-drying the eluent afforded the TEA<sup>+</sup> salts of 20A and 20B (10 and 11 mg, respectively, total yield 29%). 20A:  $^1\text{H}$  NMR (600 MHz,  $\text{D}_2\text{O}$ )  $\delta$  8.21 (s, 1H, A-2), 8.20 (s, 1H, B-8), 8.11 (s, 1H, A-8), 8.07 (s, 1H, B-2), 6.42 (d,  $J_{1',F} = 15.8$  Hz, 1H, A-1'), 5.78 (dd,  $J_{2',F} = 51.0$ ,  $J_{2',3'} = 3.8$  Hz, 1H, A-2'), 5.34 (dt,  $J_{2',1'a} = 6.2$ ,  $J_{2',1'b} = J_{2',3'} = 3.0$  Hz, 1H, B-2'), 5.32 (m, 1H, B-3'), 4.90 (m, 1H, A-3'), 4.56 (m, 1H, A-4'), 4.50 (bd,  $J_{\text{GEM}} = 11.8$  Hz, 1H, A-5'a), 4.37 (dd,  $J_{\text{GEM}} = 10.5$ ,  $J_{1'a,2'} = 6.2$  Hz, 1H, B-1'a), 4.29 (m, 1H, B-5'a), 4.28 (m, 1H, B-4'), 4.17 (m, 1H, B-5'b), 4.13 (bdd,  $J_{\text{GEM}} = 10.5$ ,  $J_{1'b,2'} = 3.0$  Hz, 1H, B-1'b), 4.03 (bdd,  $J_{\text{GEM}} = 11.8$ ,  $J_{5'b,P} = 4.2$  Hz, 1H, A-5'b), 3.16 (q,  $J_{\text{CH}_2,\text{CH}_3} = 7.3$  Hz, 12H,  $\text{CH}_2$ -TEA), 1.24 (t,  $J_{\text{CH}_3,\text{CH}_2} = 7.4$  Hz, 18H,  $\text{CH}_3$ -TEA).  $^{13}\text{C}$  NMR (151 MHz,  $\text{D}_2\text{O}$ )  $\delta$  157.74 (A-6 and B<sub>6</sub>), 154.96 (A-2), 154.81 (B-2), 151.60 (B-4), 150.21 (A-4), 143.06 (B-8), 141.42 (A-8), 121.30 (B-5), 121.12 (A-5), 94.56 (d,  $J_{2',F} = 189.7$  Hz, A-2'), 89.74 (d,  $J_{1',F} = 33.7$  Hz, A-1'), 84.98 (t,  $J_{4',P} = 10.7$  Hz, B-4'), 81.85 (dd,  $J_{4',P} = 11.6$ ,  $J_{4',P} = 8.7$  Hz, A-4'), 80.94 (d,  $J_{3',P} = 8.3$  Hz, B-3'), 73.18 (dd,  $J_{3',F} = 26.0$ ,  $J_{3',P} = 4.7$  Hz, A-3'), 74.42 (B-1'), 65.66 (d,  $J_{5',P} = 4.7$  Hz, A-5'), 65.44 (d,  $J_{5',P} = 6.6$  Hz, B-5'), 64.47 (B-2'), 49.48 ( $\text{CH}_2$ -TEA), 10.95 ( $\text{CH}_3$ -TEA).  $^{31}\text{P}$  NMR (243 MHz,  $\text{D}_2\text{O}$ )  $\delta$  57.87, 55.36.  $^{19}\text{F}$  NMR (565 MHz,  $\text{D}_2\text{O}$ )  $\delta$  -202.97. HPLC retention time (C18, min): 2.52, 2.0B:  $^1\text{H}$  NMR (600 MHz,  $\text{D}_2\text{O}$ )  $\delta$  8.18 (s, 2H, A-8, B-8), 8.08 (s, 2H, A-2, B-2), 6.40 (d,  $J_{1',F} = 16.0$  Hz, 1H, A-1'), 5.48 (dd,  $J_{2',F} = 51.5$ ,  $J_{2',3'} = 3.9$  Hz, 1H, A-2'), 5.37 (dt,  $J_{2',1'a} = 6.4$ ,  $J_{2',1'b} = J_{2',3'} = 3.5$  Hz, 1H, B-2'), 5.35 (m, 1H, B-3'), 4.96 (m, 1H, A-3'), 4.52 (dm,  $J_{4',3'} = 9.0$  Hz, 1H, A-4'), 4.48 (dm,  $J_{\text{GEM}} = 12.2$  Hz, 1H, A-5'a), 4.39 (ddd,  $J_{\text{GEM}} = 11.7$ ,  $J_{5'a,P} = 2.7$ ,  $J_{5'a,4'} = 2.0$  Hz, 1H, B-5'a), 4.35 (dd,  $J_{\text{GEM}} = 10.4$ ,  $J_{1'a,2'} = 6.4$  Hz, 1H, B-1'a), 4.25 (dq,  $J_{4',3'} = 6.6$ ,  $J_{4',5'a} = J_{4',5'b} = J_{4',P} = 2.3$  Hz, 1H, B-4'), 4.15 (ddd,  $J_{\text{GEM}} = 11.7$ ,  $J_{5'b,P} = 6.2$ ,  $J_{5'b,4'} = 2.2$  Hz, 1H, B-5'b), 4.09 (bdd,  $J_{\text{GEM}} = 10.4$ ,  $J_{1'b,2'} = 3.5$  Hz, 1H, B-1'b), 4.03 (ddd,  $J_{\text{GEM}} = 12.2$ ,  $J_{5'b,P} = 4.8$ ,  $J_{5'b,4'} = 1.3$  Hz, 1H, A-5'b), 3.17 (q,  $J_{\text{CH}_2,\text{CH}_3} = 7.3$  Hz, 12H,  $\text{CH}_2$ -TEA), 1.26 (t,  $J_{\text{CH}_3,\text{CH}_2} = 7.3$  Hz, 18H,  $\text{CH}_3$ -TEA).  $^{13}\text{C}$  NMR (151 MHz,  $\text{D}_2\text{O}$ )  $\delta$  157.80 (A-6 and B<sub>6</sub>), 155.02 (B-2), 154.66 (A-2), 151.53 (A-4), 150.22 (B-4), 143.24 (A-8), 141.50 (B-8), 121.26 (A-5), 121.07 (B-5), 95.11 (d,  $J_{2',F} = 190.0$  Hz, A-2'), 89.97 (d,  $J_{1',F} = 33.9$  Hz, A-1'), 84.66 (dd,  $J_{4',P} = 11.3$ , 8.4 Hz, B-4'), 82.06 (dd,  $J_{4',P} = 11.4$ , 9.8 Hz, A-4'), 80.71 (d,  $J_{3',P} = 8.5$  Hz, B-3'), 74.39 (B-1'), 72.02 (dd,  $J_{3',F} = 16.4$ ,  $J_{3',P} = 8.5$  Hz, A-3'), 66.82 (d,  $J_{5',P} = 4.7$  Hz, B-5'), 65.11 (d,  $J_{5',P} = 4.4$  Hz, A-5'), 64.45 (B-2), 49.50 ( $\text{CH}_2$ -TEA), 10.96 ( $\text{CH}_3$ -TEA).  $^{31}\text{P}$  NMR (243 MHz,  $\text{D}_2\text{O}$ )  $\delta$  55.76, 53.81.  $^{19}\text{F}$  NMR (565 MHz,  $\text{D}_2\text{O}$ )  $\delta$  -201.15. HPLC retention time (C18, min): 2.59.

**Synthesis of alkylating reagents 27b-d**

**General procedure.** Sodium iodide (4.5 g, 30 mmol) was added to a solution of acyloxymethyl chloride (15 mmol) in acetonitrile (50 mL) and the suspension was allowed to stir at ambient overnight under an argon atmosphere. A mixture of DCM (250 mL) and water (250 mL) was added. The mixture was allowed to stir for 10 min, then separated into two layers. The aqueous layer was discarded and the organic layer was washed with sodium thiosulfate (2%, 100 mL). The organic layer was dried over anhydrous magnesium sulfate and concentrated under vacuum to give acyloxymethyl iodide (Maiti et al., 2013).

**Iodomethyl 2,2-dimethylbutanoate (27b).** Clear oil, 79% yield.  $^1\text{H NMR}$  (401 MHz,  $\text{CDCl}_3$ )  $\delta$  5.92 (s, 2H), 1.58 (q,  $J = 7.5$  Hz, 2H), 1.15 (s, 6H), 0.86 (t,  $J = 7.5$  Hz, 3H).  $^{13}\text{C NMR}$  (101 MHz,  $\text{CDCl}_3$ )  $\delta$  176.06, 42.94, 33.06, 31.40, 24.25, 24.25, 9.20. HRMS CI ( $\text{C}_7\text{H}_{14}\text{IO}_2$ ) calculated: 257.0039; found: 257.0040.

**Iodomethyl 1-methylcyclohexanoate (27c).** Clear oil, 86% yield.  $^1\text{H NMR}$  (401 MHz,  $\text{CDCl}_3$ )  $\delta$  5.94 (s, 2H), 2.06–1.98 (m, 2H), 1.62–1.49 (m, 3H), 1.43–1.31 (m, 2H), 1.30–1.18 (m, 3H), 1.13 (s, 3H).  $^{13}\text{C NMR}$  (101 MHz,  $\text{CDCl}_3$ )  $\delta$  175.81, 43.48, 35.35, 31.59, 25.83, 25.68, 23.15. HRMS CI ( $\text{C}_9\text{H}_{16}\text{IO}_2$ ) calculated: 283.0195; found: 283.0196.

**Iodomethyl octanoate (27d).** Clear oil, 88% yield.  $^1\text{H NMR}$  (401 MHz,  $\text{CDCl}_3$ )  $\delta$  5.90 (s, 2H), 2.32 (t,  $J = 7.5$  Hz, 2H), 1.68–1.57 (m, 2H), 1.36–1.22 (m, 8H), 0.91–0.83 (m, 3H).  $^{13}\text{C NMR}$  (101 MHz,  $\text{CDCl}_3$ )  $\delta$  172.00, 34.41, 31.72, 30.71, 29.01, 28.97, 24.62, 22.70, 14.19. HRMS CI ( $\text{C}_9\text{H}_{18}\text{IO}_2$ ) calculated: 285.0352; found: 285.0354.

#### Preparation of prodrugs

**Bis-POM prodrug of 3',3'-c-(2'F,2'dAMP, isonuc AMP) (28A-D).** Crude 18 (cyclization starting from 46 mg of 12) was treated with neat  $t\text{BuNH}_2$  (5 mL) at ambient temperature for 20 min. Volatiles were evaporated, and the nucleobase-protected CDN was purified on RP FCC (ACN in 50 mM TEAB, 0–100%) to afford a base-only protected cyclic dinucleotide (32 mg, TEA<sup>+</sup> salt). TEA<sup>+</sup> cation was exchanged for a tetrabutylammonium by slowly passing a methanolic solution through a 1 mL column of DOWEX 50 (TBA<sup>+</sup> cycle). All volatiles were evaporated afterwards. 26 (2  $\mu\text{mol}$ ) was azeotroped with dry toluene (1  $\times$  500  $\mu\text{L}$ ) and dry ACN (2  $\times$  500  $\mu\text{L}$ ), dissolved in dry ACN (700  $\mu\text{L}$ ), and treated with pivaloyloxymethyl iodide (4.8 mg, 20  $\mu\text{mol}$ ) under an argon atmosphere at ambient temperature for 1 h. The reaction mixture was quenched with 1 mL of 50%  $\text{H}_2\text{O}/\text{ACN}$ , further diluted with 3 mL of water, and purified on semi-preparative HPLC. Fractions containing products (all four diastereoisomers) were pooled, evaporated and azeotroped with dry ACN (3  $\times$  2 mL). NIS (2.2 mg, 10  $\mu\text{mol}$ ) was added to a solution of this intermediate in dry ACN (1 mL) under an argon atmosphere. The reaction mixture was stirred at ambient temperature for 1 h, after which water (100  $\mu\text{L}$ ) was added, followed by acetic acid (10  $\mu\text{L}$ ). After 30 min of further stirring, the reaction was quenched with a saturated aqueous solution of  $\text{Na}_2\text{S}_2\text{O}_3$  (until decolorization), the mixture was diluted with water (2 mL), and then purified on semi-preparative HPLC affording 28A-D (separate diastereoisomers) in approximately equimolar ratio. From 26 (2  $\mu\text{mol}$ ), yield 158 nmol (28A):  $^1\text{H NMR}$  (501 MHz,  $\text{CD}_3\text{CN}$ )  $\delta$  8.29 and 7.81 (s, 1H, A-2, B-2), 7.97 and 7.87 (s, 1H, A-8, B-8), 6.26 (bs, 2H,  $\text{NH}_2$ ), 6.18 (m, 1H, A-1'), 6.16 (bs, 2H,  $\text{NH}_2$ ), 5.60–5.76 (m, 4H, A-2', A-3', O- $\text{CH}_2$ -O), 5.52 (m, 1H, B-3'), 5.28 (td,  $J_{2',1'} = 6.9$ ,  $J_{2',3'} = 4.6$  Hz, 1H, B-2'), 4.82–4.91 (m, 2H, O- $\text{CH}_2$ -O), 4.27–4.45 (m, 8H, B-1', B-4', B-5', A-4', A-5'), 1.15 and 0.95 (s, 9H,  $\text{CH}_3$ ).  $^{31}\text{P NMR}$  (202.4 MHz,  $\text{CD}_3\text{CN}$ )  $\delta$  -4.78 (s), -5.18 (s).  $^{19}\text{F NMR}$  (470.4 MHz,  $\text{CD}_3\text{CN}$ )  $\delta$  -196.67 (dm,  $J_{F,2'} = 52.5$  Hz). HPLC retention time (C18, min): 3.42.

Yield 130 nmol (28B):  $^1\text{H NMR}$  (501 MHz,  $\text{CD}_3\text{CN}$ )  $\delta$  8.29 and 7.77 (s, 1H, A-2, B-2), 8.03 and 7.87 (s, 1H, A-8, B-8), 6.19 (dd, 1H,  $J_{1',F} = 21.7$ ,  $J_{1',2'} = 1.1$  Hz, A-1'), 6.18 and 6.12 (bs, 2H,  $\text{NH}_2$ ), 5.63–5.82 (m, 4H, A-2', A-3', O- $\text{CH}_2$ -O), 5.32–5.39 (m, 2H, B-2', B-3'), 5.15 (dd,  $J_{1',P} = 15.4$ ,  $J_{\text{GEM}} = 5.2$  Hz, 1H, O- $\text{CH}_2$ -O), 5.03 (dd,  $J_{1',P} = 12.6$ ,  $J_{\text{GEM}} = 5.2$  Hz, 1H, O- $\text{CH}_2$ -O), 4.27–4.44 (m, 8H, B-1', B-4', B-5', A-4', A-5'), 1.23 and 0.93 (s, 9H,  $\text{CH}_3$ ).  $^{31}\text{P NMR}$  (202.4 MHz,  $\text{CD}_3\text{CN}$ )  $\delta$  -2.38, -4.97.  $^{19}\text{F NMR}$  (470.4 MHz,  $\text{CD}_3\text{CN}$ )  $\delta$  -195.22 (dt,  $J_{F,2'} = 52.5$ ,  $J_{F,1'} = J_{F,3'} = 21.0$  Hz). HPLC retention time (C18, min): 3.61.

Yield 105 nmol (28C):  $^1\text{H NMR}$  (501 MHz,  $\text{CD}_3\text{CN}$ )  $\delta$  8.21 and 8.01 (s, 1H, A-2, B-2), 7.97 and 7.93 (s, 1H, A-8, B-8), 6.23 (dd, 1H,  $J_{1',F} = 18.8$ ,  $J_{1',2'} = 1.5$  Hz, A-1'), 6.04 (bs, 4H,  $\text{NH}_2$ ), 5.47–5.73 (m, 7H, A-2', A-3', B-3', O- $\text{CH}_2$ -O), 5.31 (m, 1H, B-2'), 4.27–4.49 (m, 8H, B-1', B-4', B-5', A-4', A-5'), 1.16 and 1.14 (s, 9H,  $\text{CH}_3$ ).  $^{31}\text{P NMR}$  (202.4 MHz,  $\text{CD}_3\text{CN}$ )  $\delta$  -2.82, -4.78.  $^{19}\text{F NMR}$  (470.4 MHz,  $\text{CD}_3\text{CN}$ )  $\delta$  -198.00 (dt,  $J_{F,2'} = 51.8$ ,  $J_{F,1'} = J_{F,3'} = 18.7$  Hz). HPLC retention time (C18, min): 3.62. 28D: Yield 142 nmol,  $^1\text{H NMR}$  (501 MHz,  $\text{CD}_3\text{CN}$ )  $\delta$  8.22 (s, 1H) and 8.02 (s, 2H) and 7.92 (s, 1H, A-2, B-2, A-8, B-8), 6.23 (dd,  $J_{1',F} = 20.3$ ,  $J_{1',2'} = 1.2$  Hz, 1H, A-1'), 6.05 and 6.04 (bs, 2H,  $\text{NH}_2$ ), 5.49–5.77 (m, 7H, A-2', A-3', B-3', O- $\text{CH}_2$ -O), 5.35 (m, 1H, B-2'), 4.17–4.49 (m, 8H, B-1', B-4', B-5', A-4', A-5'), 1.23 and 1.15 (s, 9H,  $\text{CH}_3$ ).  $^{31}\text{P NMR}$  (202.4 MHz,  $\text{CD}_3\text{CN}$ )  $\delta$  -2.15 (s), -2.42 (s).  $^{19}\text{F NMR}$  (470.4 MHz,  $\text{CD}_3\text{CN}$ )  $\delta$  -195.73 (dt,  $J_{F,2'} = 51.9$ ,  $J_{F,1'} = J_{F,3'} = 19.9$  Hz). HPLC retention time (C18, min): 3.84.

**Bis-(tert-pentanyloxymethyl) prodrug of 3',3'-c-(2'F,2'dAMP, isonuc AMP) (29).** From 26 (2  $\mu\text{mol}$ ), yield 189 nmol: 29A HPLC retention time (C18, min): 3.61. Yield 164 nmol 29B HPLC retention time (C18, min): 3.83. Yield 137 nmol 29C HPLC retention time (C18, min): 3.84. Yield 141 nmol 29D:  $^1\text{H NMR}$  (501 MHz,  $\text{CD}_3\text{CN}$ )  $\delta$  8.22 (s, 1H, B-2), 8.02 and 8.02 (s, 1H, A-2, B-8), 7.92 (s, 1H, A-8), 6.24 (dd, 1H,  $J_{1',F} = 20.2$ ,  $J_{1',2'} = 1.2$  Hz, A-1'), 6.05 and 6.03 (bs, 2H,  $\text{NH}_2$ ), 5.49–5.77 (m, 7H, A-2', A-3', B-3', O- $\text{CH}_2$ -O), 5.35 (m, 1H, B-2'), 4.17–4.49 (m, 8H, B-1', B-4', B-5', A-4', A-5'), 1.61 and 1.54 (q, 2H,  $J_{\text{CH}_2\text{CH}_3} = 7.5$  Hz,  $\text{CH}_2\text{CH}_3$ ), 1.18 (s, 6H,  $\text{C}(\text{CH}_3)_2$ ), 1.12 and 1.11 (s, 3H,  $\text{C}(\text{CH}_3)_2$ ), 0.86 and 0.79 (t, 3H,  $J_{\text{CH}_3\text{CH}_2} = 7.5$  Hz,  $\text{CH}_3\text{CH}_2$ ).  $^{31}\text{P NMR}$  (202.4 MHz,  $\text{CD}_3\text{CN}$ )  $\delta$  -2.16, -2.34.  $^{19}\text{F NMR}$  (470.4 MHz,  $\text{CD}_3\text{CN}$ )  $\delta$  -195.71 (dt,  $J_{F,2'} = 52.0$ ,  $J_{F,1'} = J_{F,3'} = 19.9$  Hz). HPLC retention time (C18, min): 4.08.

**Bis-(1-methyl-1-cyclohexanyloxymethyl) prodrug of 3',3'-c-(2'F,2'dAMP, isonuc AMP) (30).** From 26 (2  $\mu\text{mol}$ ), yield 236 nmol: 30A: HPLC retention time (C18, min): 3.88. Yield 199 nmol 30B: HPLC retention time (C18, min): 4.14. Yield 192 nmol 30C: HPLC retention time (C18, min): 4.14. Yield 159 nmol 30D:  $^1\text{H NMR}$  (501 MHz,  $\text{CD}_3\text{CN}$ )  $\delta$  8.22 (s, 1H, B-2), 8.05 (s, 2H, A-2, B-8), 7.91 (s, 1H, A-8), 6.26 (d, 1H,  $J_{1',F} = 16.4$  Hz, A-1'), 6.09 and 6.07 (bs, 2H,  $\text{NH}_2$ ), 5.51–5.78 (m, 7H, A-2', A-3', B-3', O- $\text{CH}_2$ -O), 5.35 (m, 1H, B-2'), 4.17–4.50 (m, 8H, B-1', B-4', B-5', A-4', A-5'), 1.98–2.05 (m, 4H, cyclohex), 1.19–1.62 (m, 16H, cyclohex), 1.19 and 1.11 (s, 3H,  $\text{CH}_3$ ).  $^{31}\text{P NMR}$  (202.4 MHz,  $\text{CD}_3\text{CN}$ )  $\delta$  -2.18, -2.27.  $^{19}\text{F NMR}$  (470.4 MHz,  $\text{CD}_3\text{CN}$ )  $\delta$  -195.70 (dt,  $J_{F,2'} = 52.0$ ,  $J_{F,1'} = J_{F,3'} = 19.9$  Hz). HPLC retention time (C18, min): 4.41.

#### Bis-(n-octanyloxymethyl) prodrug of 3',3'-c-(2'F,2'dAMP, isonuc AMP) (31)

From 26 (2  $\mu\text{mol}$ ), yield 127 nmol: 31A: HPLC retention time (C18, min): 4.38. Yield 73 nmol 31B: HPLC retention time (C18, min): 4.58. Yield 66 nmol 31C: HPLC retention time (C18, min): 4.58. Yield 56 nmol 31D:  $^1\text{H NMR}$  (501 MHz,  $\text{CD}_3\text{CN}$ )  $\delta$  8.22 (s, 1H, B-2),



8.05 and 8.02 (s, 1H, A-2, B-8), 7.93 (s, 1H, A-8), 6.24 (dd, 1H,  $J_{1',F} = 20.1$ ,  $J_{1',2'} = 1.3$  Hz, A-1'), 6.03 and 6.01 (bs, 2H, NH<sub>2</sub>), 5.48-5.75 (m, 7H, A-2', A-3', B-3', O-CH<sub>2</sub>-O), 5.34 (m, 1H, B-2'), 4.17-4.48 (m, 8H, B-1', B-4', B-5', A-4', A-5'), 2.41 (t, 2H,  $J_{1',2'} = 7.5$  Hz, A-1''), 2.33 (m, 2H, A-1''), 1.52-1.63 (m, 4H, 2''), 1.20-1.40 (m, 16H, 3''-6''), 0.87 and 0.86 (t, 3H,  $J_{7',8'} = 7.1$  Hz, 7''). <sup>31</sup>P NMR (202.4 MHz, CD<sub>3</sub>CN)  $\delta$  -2.15, -2.37. <sup>19</sup>F NMR (470.4 MHz, CD<sub>3</sub>CN)  $\delta$  -195.95 (dt,  $J_{F,2'} = 52.1$ ,  $J_{F,1'} = J_{F,3'} = 19.9$  Hz). HPLC retention time (C18, min): 4.81.

#### QUANTIFICATION AND STATISTICAL ANALYSIS

Quantification of biochemical and biological data was performed using Prism. Data are reported as the mean in triplicates with standard error mean. Crystallographic statistics of data collection, processing, structure solution and refinement are summarized in [Supplementary Tables 1 and 2](#).

Structure, Volume 30

**Supplemental Information**

**Discovery of isonucleotidic CDNs**

**as potent STING agonists**

**with immunomodulatory potential**

**Milan Dejmek, Michal Šála, Andrea Brazdova, Lenka Vanekova, Miroslav Smola, Martin Klíma, Petra Břehová, Miloš Buděšínský, Martin Dračínský, Eliška Procházková, Martin Zavřel, Ondřej Šimák, Ondřej Páv, Evzen Boura, Gabriel Birkuš, and Radim Nencka**

## Supporting information

### Discovery of Isonucleotidic CDNs as potent STING agonists with immunomodulatory potential

Milan Dejmek,<sup>1</sup> Michal Šála,<sup>1</sup> Andrea Brazdova,<sup>1</sup> Lenka Vanekova,<sup>1,2</sup> Miroslav Smola,<sup>1</sup> Martin Klíma,<sup>1</sup> Petra Břehová,<sup>1</sup> Miloš Buděšínský,<sup>1</sup> Martin Dračínský,<sup>1</sup> Eliška Procházková,<sup>1</sup> Martin Zavřel,<sup>1</sup> Ondřej Šimák,<sup>1</sup> Ondřej Páv,<sup>1</sup> Evzen Boura,<sup>1</sup> Gabriel Birkuš<sup>1</sup> and Radim Nencka<sup>1,\*</sup>

<sup>1</sup>Institute of Organic Chemistry and Biochemistry of the Czech Academy of Sciences, Prague 166 10, Czech Republic

<sup>2</sup>Faculty of Science, Charles University, Prague 128 00, Czech Republic

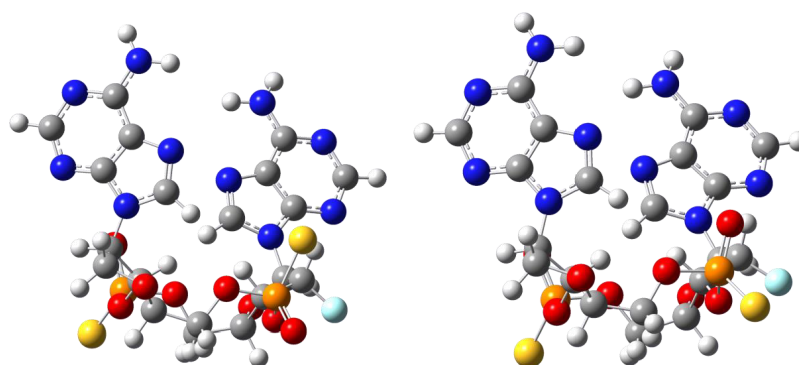
\*Author to whom all correspondence should be addressed: nencka@uochb.cas.cz

**Supplementary Table 1:** Statistics of data collection and processing for STING in complex with ligand 19. Numbers in parentheses refer to the highest resolution shell. Related to STAR Methods.

Diffraction source	Rigaku Micromax-007 HF
Detector	Dectris Pilatus 200K
Wavelength (Å)	1.54187
Temperature (K)	100
Crystal-to-detector distance (mm)	60
Rotation range per image (°)	0.25
Total rotation range (°)	125
Space group	P 41 21 2
Cell dimensions - a, b, c (Å)	110.7 110.7 35.7
Cell dimensions - $\alpha$ , $\beta$ , $\gamma$ (°)	90.0 90.0 90.0
Resolution range (Å)	34.02 - 2.56 (2.65 - 2.56)
No. of total reflections	64,342 (6,180)
No. of unique reflections	7,593 (716)
Completeness (%)	99.7 (98.5)
Multiplicity	8.5 (8.6)
Mean I/ $\sigma$ (I)	7.70 (1.97)
Wilson B factor (Å <sup>2</sup> )	38.0
R-merge (%)	22.18 (96.21)
R-meas (%)	23.67 (102.3)
CC1/2 (%)	99.0 (77.7)
CC* (%)	99.8 (93.5)

**Supplementary Table 2:** Statistics of structure solution and refinement of the crystal structure of the STING/ligand-19 complex. Numbers in parentheses refer to the highest resolution shell. R.m.s., root-mean-square. Related to STAR Methods.

R-work (%)	19.46 (25.69)
R-free (%)	23.17 (33.23)
CC-work (%)	95.3 (86.5)
CC-free (%)	90.1 (70.5)
R.m.s. deviations - bonds (Å)	0.007
R.m.s. deviations - angles (°)	1.09
Ramachandran favored (%)	97.7
Ramachandran allowed (%)	2.3
Ramachandran outliers (%)	0.0
Rotamer outliers (%)	0.0
Clashscore	0.0
Average <i>B</i> factors - overall (Å <sup>2</sup> )	39.50
Average <i>B</i> factors - protein (Å <sup>2</sup> )	40.01
Average <i>B</i> factors - ligand (Å <sup>2</sup> )	25.40
Average <i>B</i> factors - solvent (Å <sup>2</sup> )	36.93
PDB accession code	7Q3B



**Supplementary Figure 1.** Optimized structures of compound **20A** (*RpSp*, left) and **20B** (*RpRp*, right). Related to STAR Methods.

**Supplementary Table 3:** Experimental <sup>1</sup>H chemical shifts of compounds **20A** and **20B** and calculated nuclear shieldings of hydrogen atoms in four possible diastereomers of the compound. All values are in ppm. Related to STAR Methods.

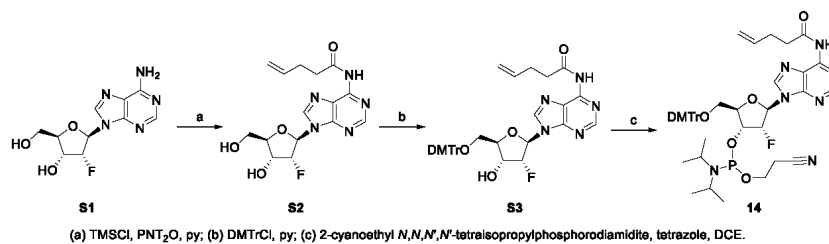
	Exp. <b>20A</b>	Exp. <b>20B</b>	<i>SpSp</i>	<i>SpRp</i>	<i>RpSp</i>	<i>RpRp</i>
2'-fluoro H1'	6.42	6.40	25.07	25.07	25.09	25.09

	H2'	5.78	5.48	26.03	26.48	26.05	26.46
	H3'	4.90	4.96	26.60	26.44	26.63	26.49
	H4'	4.56	4.52	27.26	27.31	27.25	27.30
	H5'a	4.03	4.03	27.54	27.56	27.71	27.72
	H5'b	4.50	4.48	27.11	27.14	27.17	27.20
iso-A	H1'a	4.13	4.09	27.90	27.90	27.85	27.87
	H1'b	4.37	4.35	27.36	27.36	27.28	27.29
	H2'	5.34	5.37	26.15	26.14	26.28	26.26
	H3'	5.32	5.35	26.30	26.31	26.28	26.28
	H4'	4.28	4.25	27.71	27.69	27.74	27.71
	H5'a	4.29	4.39	27.17	27.20	27.19	27.24
	H5'b	4.17	4.15	27.32	27.46	27.37	27.51

**Supplementary Table 4:** Experimental  $^{13}\text{C}$  chemical shifts of compounds **20A** and **20B** and calculated nuclear shieldings of hydrogen atoms in four possible diastereomers of the compound. All values are in ppm. Related to STAR Methods.

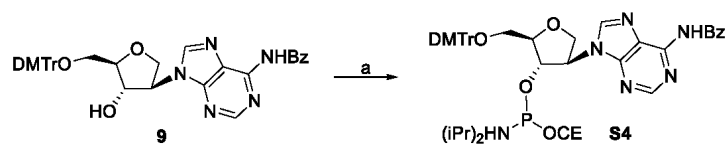
		Exp. <b>20A</b>	Exp. <b>20B</b>	<i>SpSp</i>	<i>SpRp</i>	<i>RpSp</i>	<i>RpRp</i>
2'-fluoro	C1'	89.74	89.97	102.11	102.00	102.14	101.95
	C2'	94.56	95.11	94.02	93.08	94.02	93.02
	C3'	73.18	72.02	120.11	121.01	119.75	120.57
	C4'	81.85	82.06	108.17	108.25	108.12	108.18
	C5'	65.66	65.81	128.67	128.59	126.56	126.57
iso-A	C1'	74.42	74.39	116.15	116.25	115.88	116.02
	C2'	64.47	64.45	127.12	127.21	126.57	126.69
	C3'	80.94	80.71	110.78	110.38	110.75	110.30
	C4'	84.98	84.66	104.25	104.20	104.76	104.62
	C5'	65.44	66.82	127.53	125.67	127.77	125.93

**Supplementary figure 2:** Related to STAR Methods.



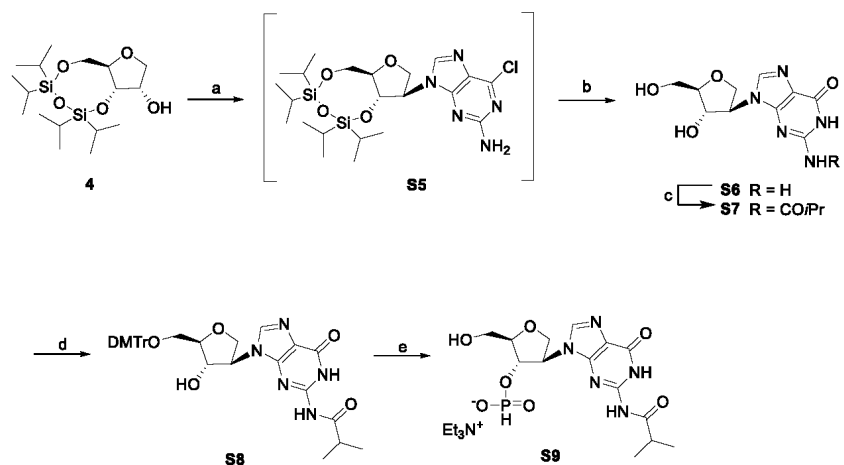


Supplementary figure 3: Related to STAR Methods.



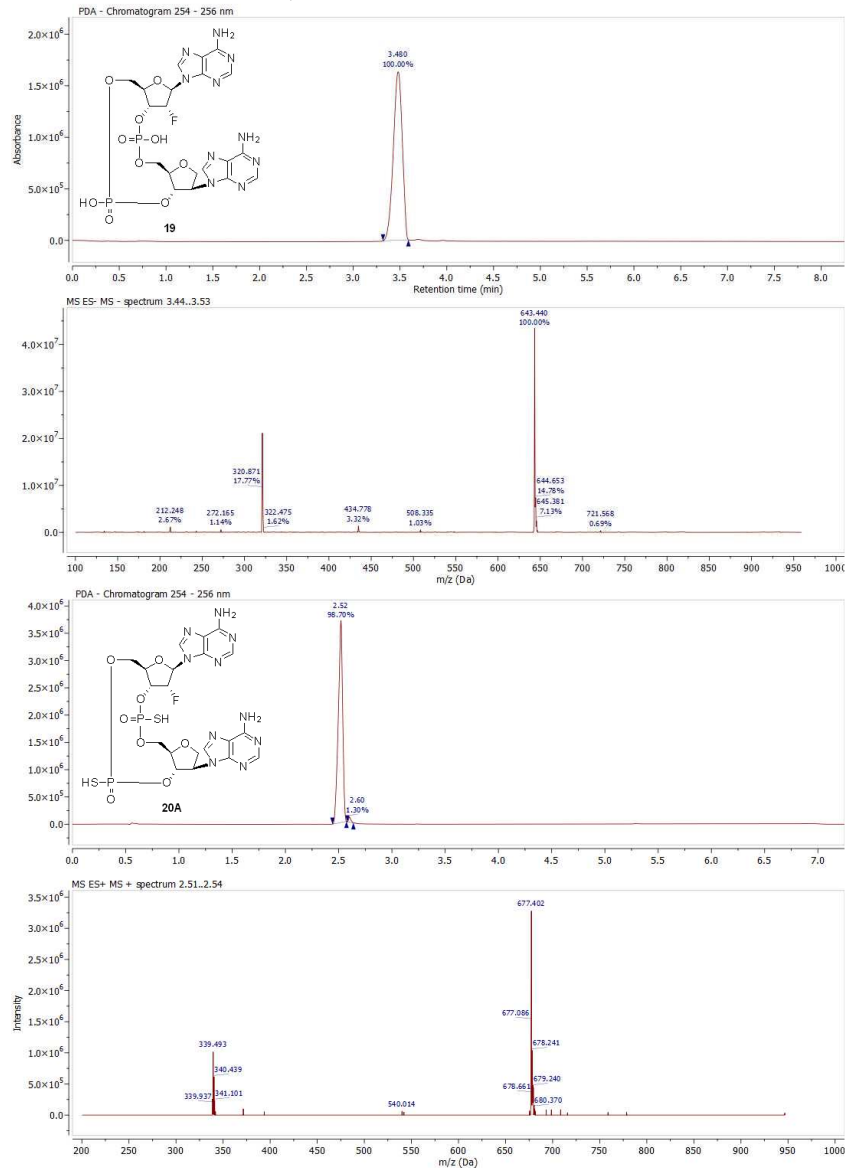
(a) 2-cyanoethyl *N,N,N',N'*-tetraisopropylphosphorodiamidite, tetrazole, DCE.

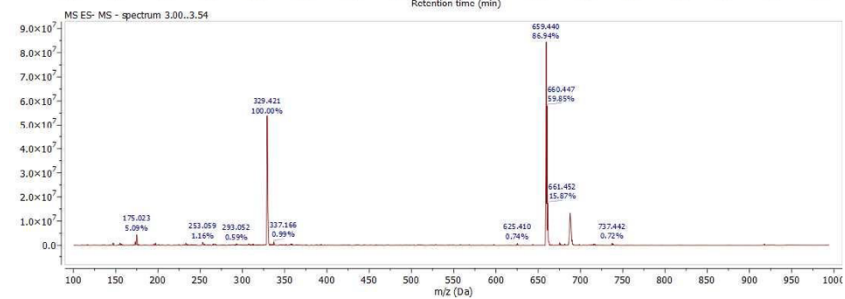
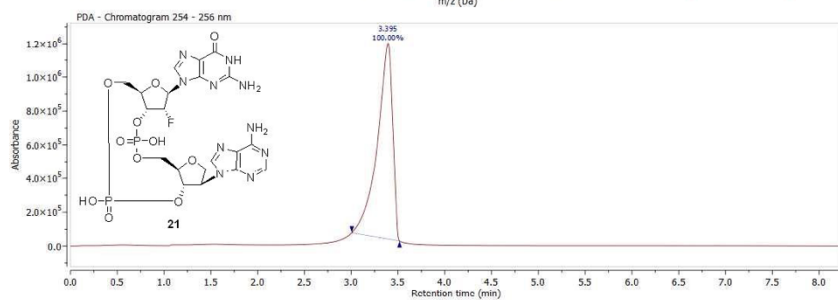
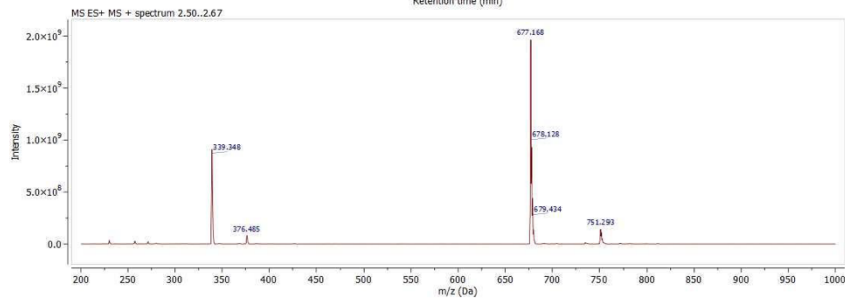
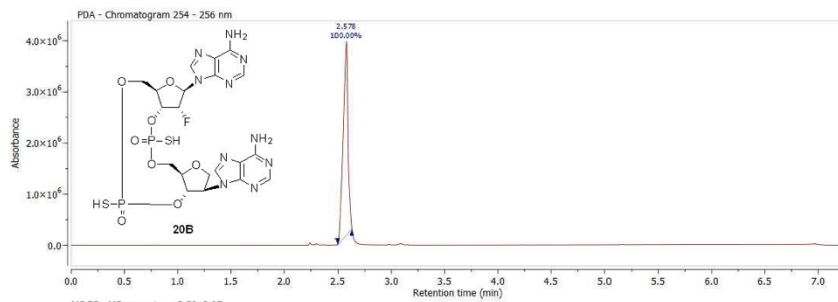
Supplementary figure 4: Related to STAR Methods.

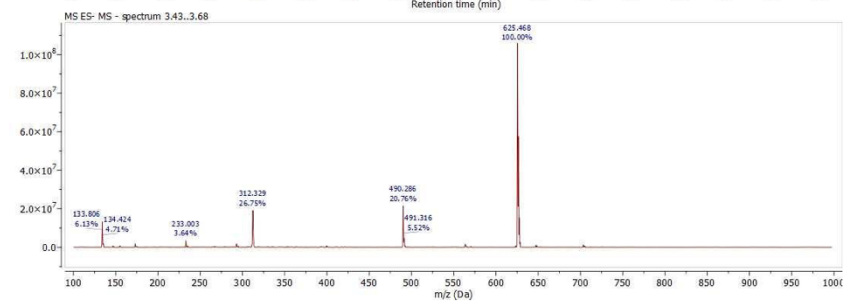
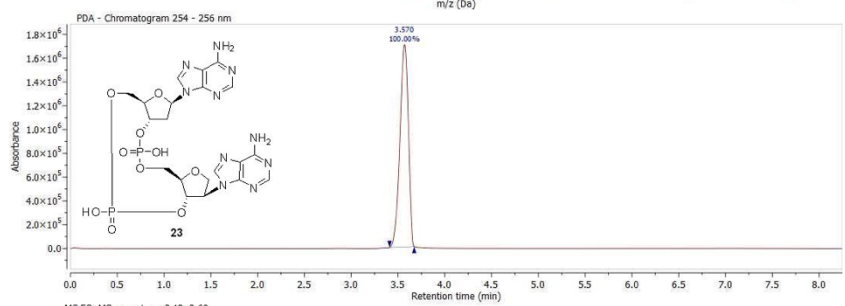
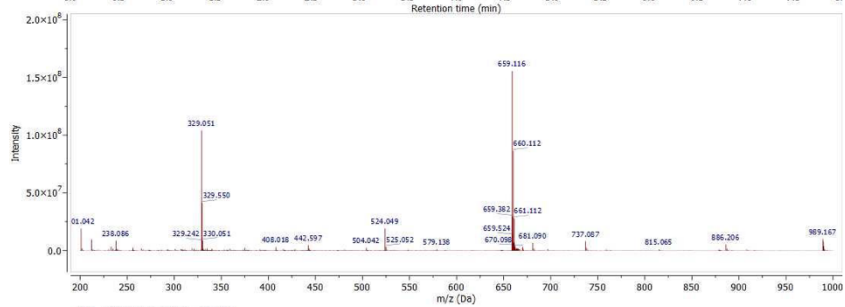
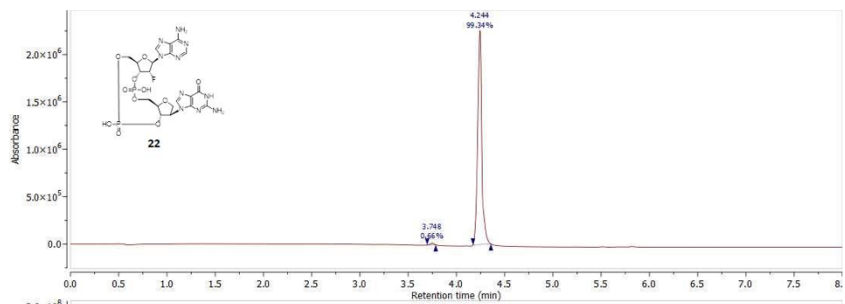


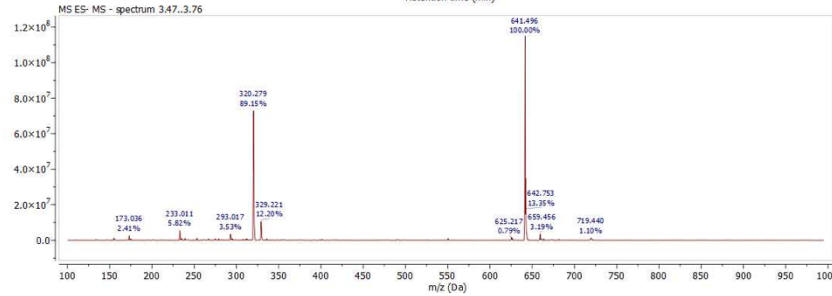
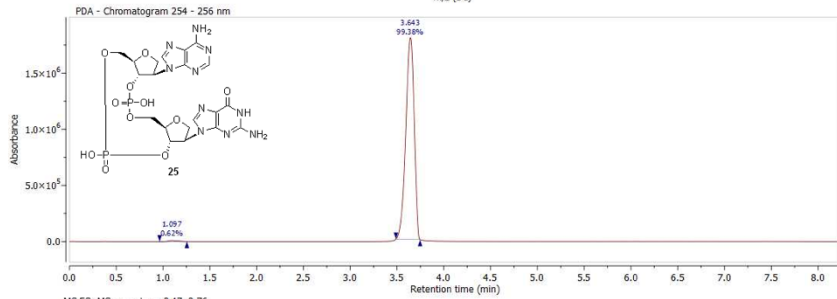
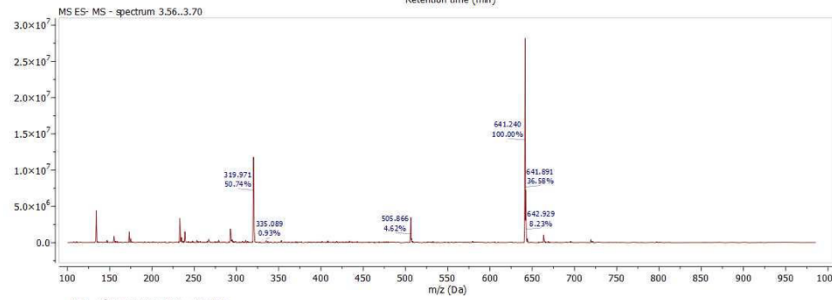
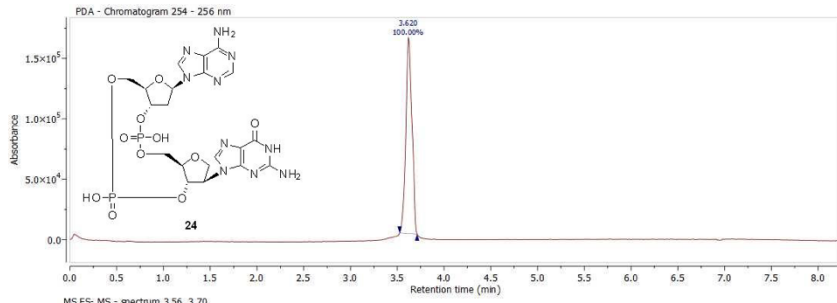
(a) 2-amino-6-chloropurine, PPh<sub>3</sub>, DIAD, THF, 0 °C to 60 °C; (b) 80 % FA, 65 °C, 18 h; (c) TMSCl, isobutyryl chloride, py; (d) DMTrCl, py; (e) 1. diphenyl phosphite, py, rt, 40 min, 2. DCA, DCM, rt, 30 min.

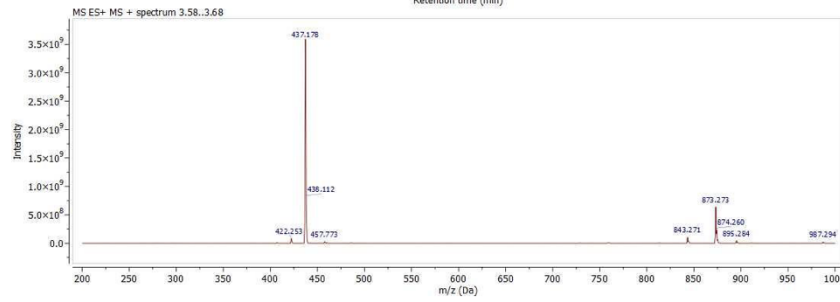
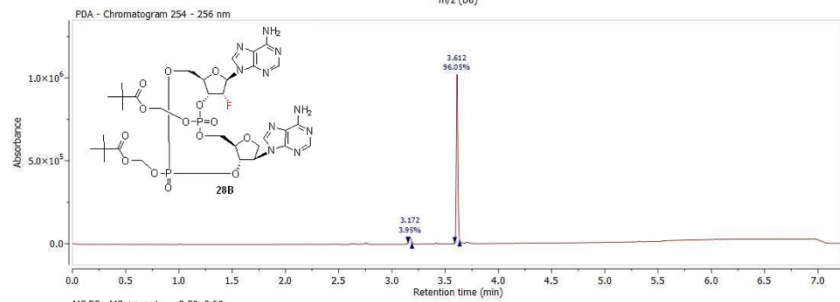
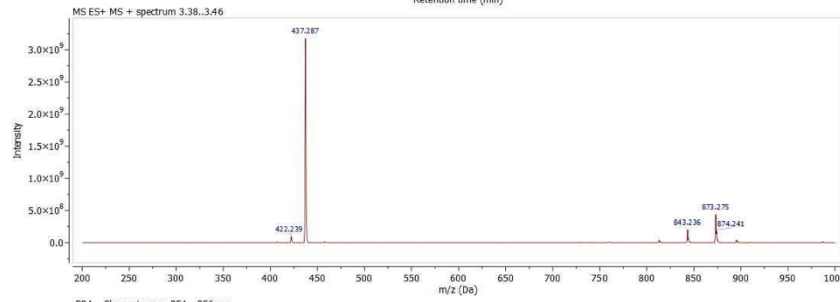
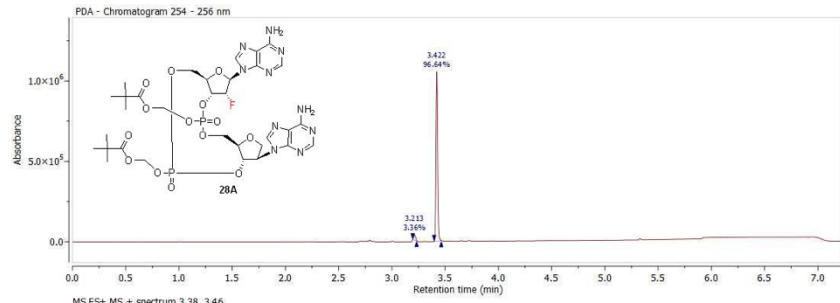
**Data S1. LCMS traces of final compounds. Related to STAR Methods.**

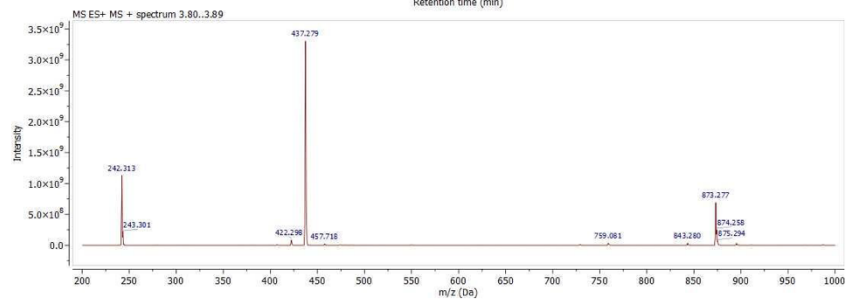
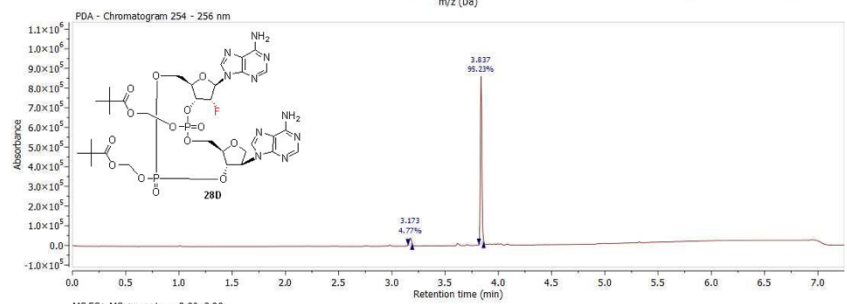
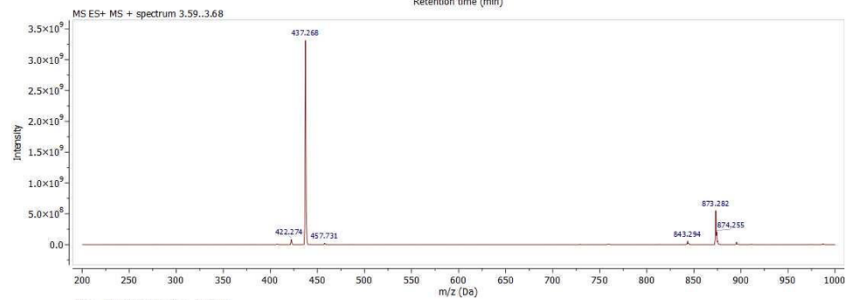
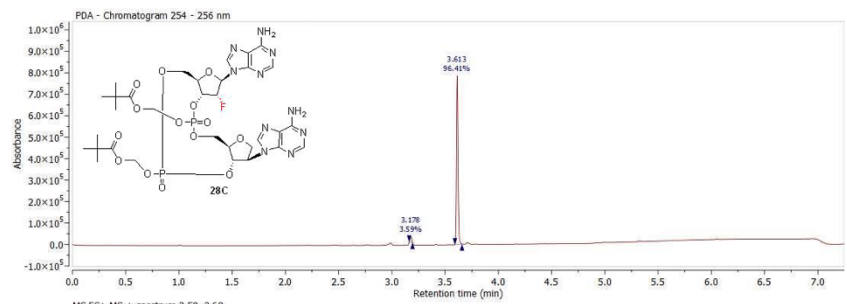


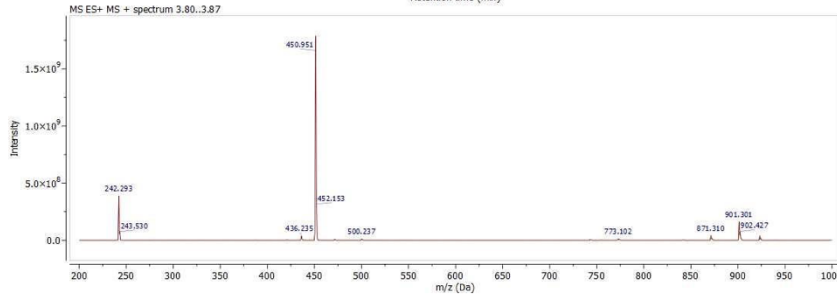
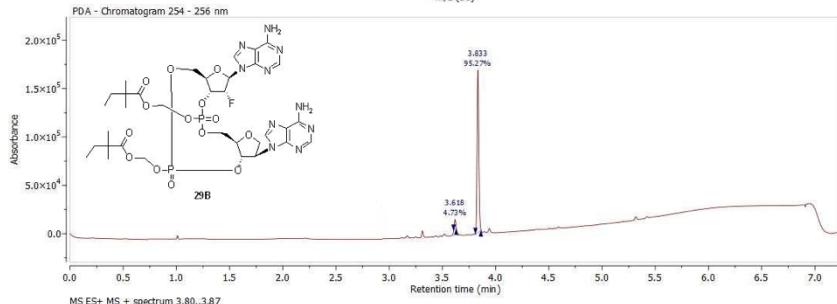
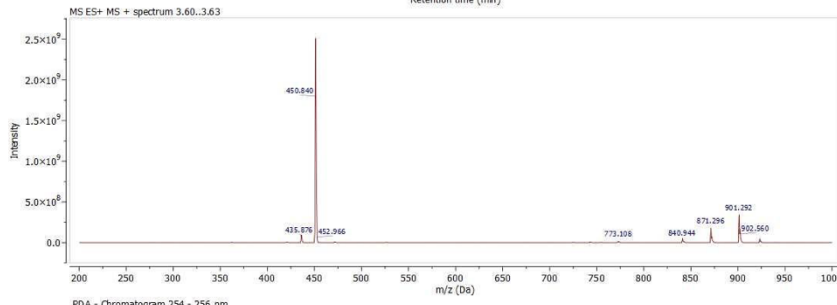
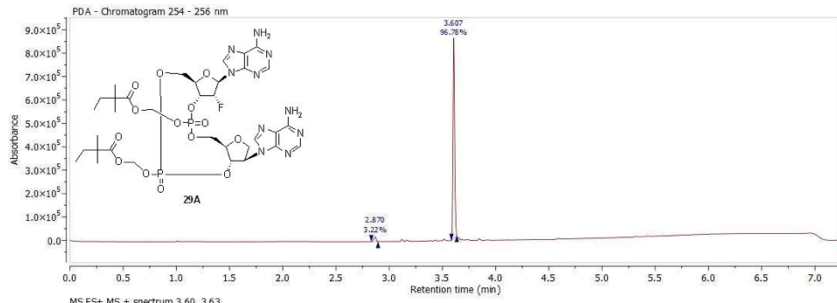




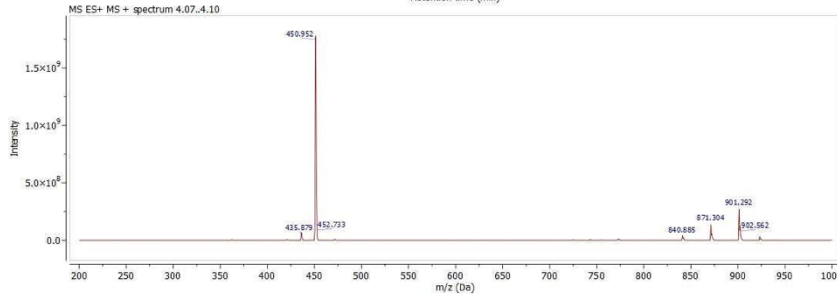
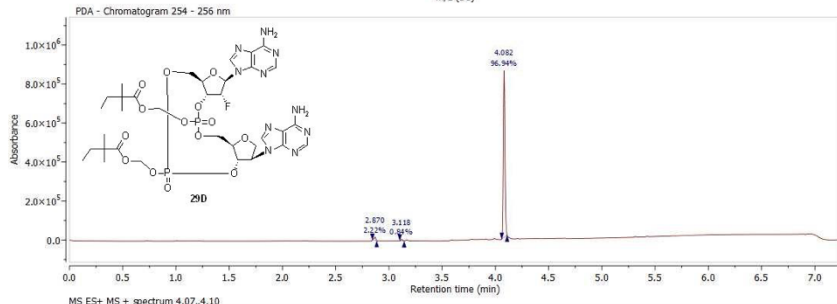
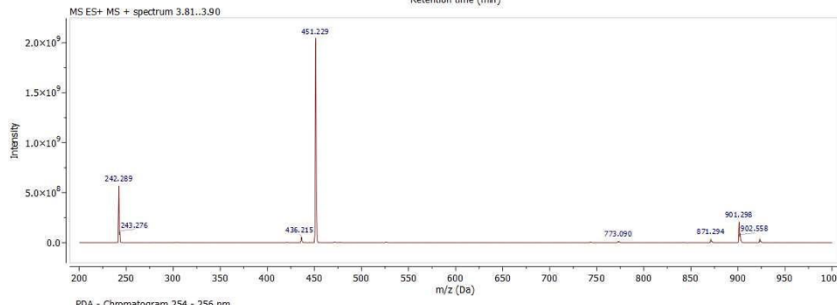
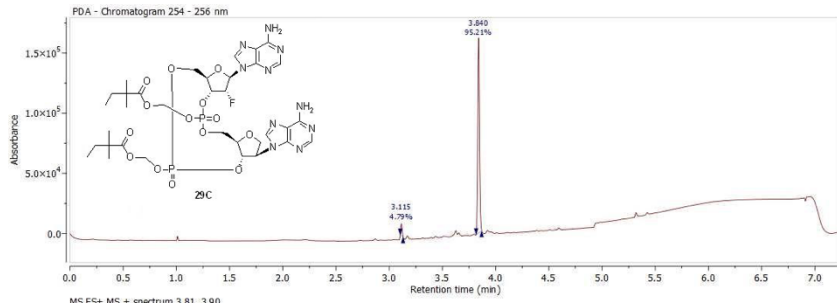


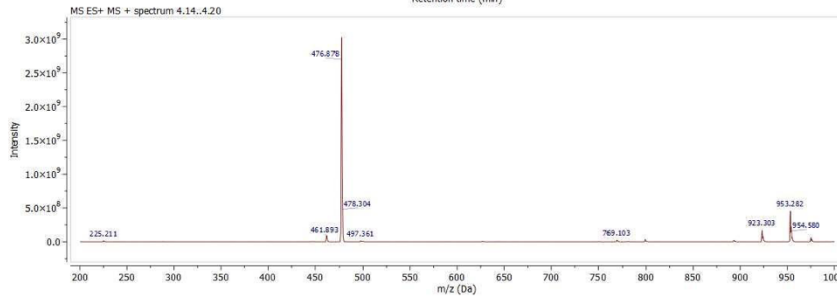
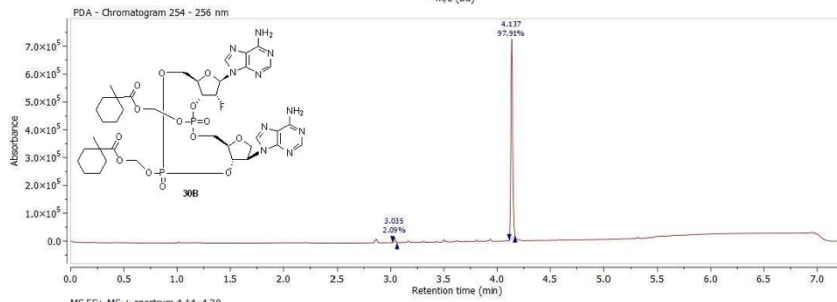
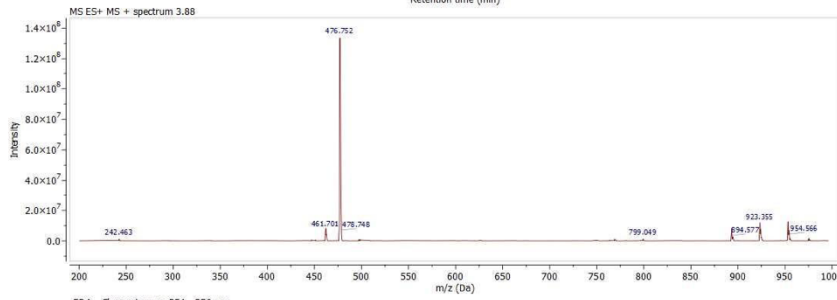
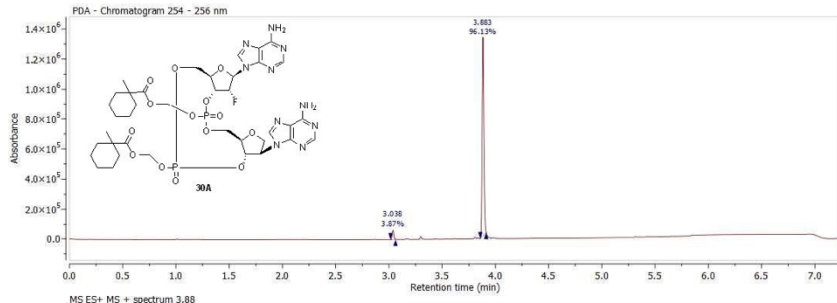


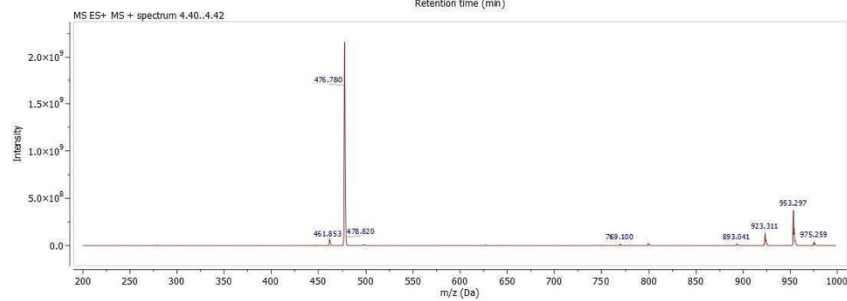
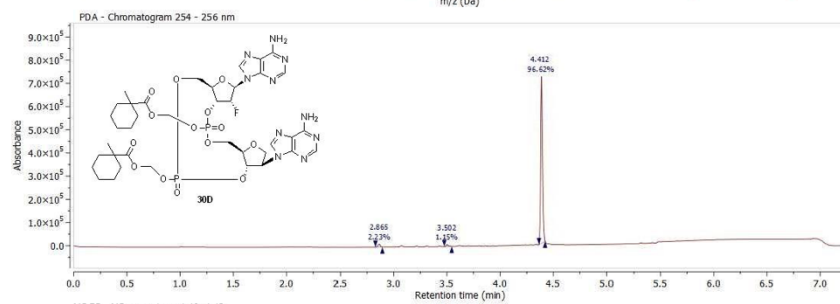
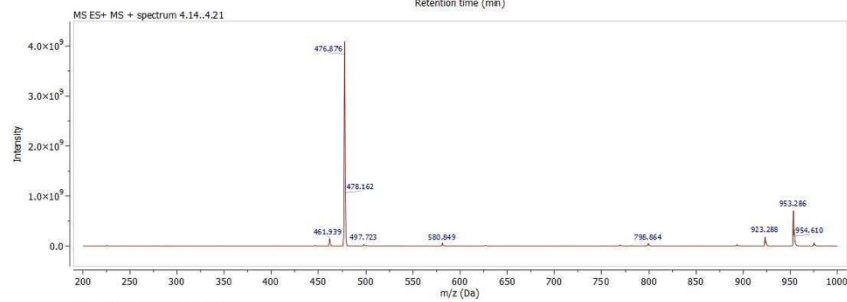
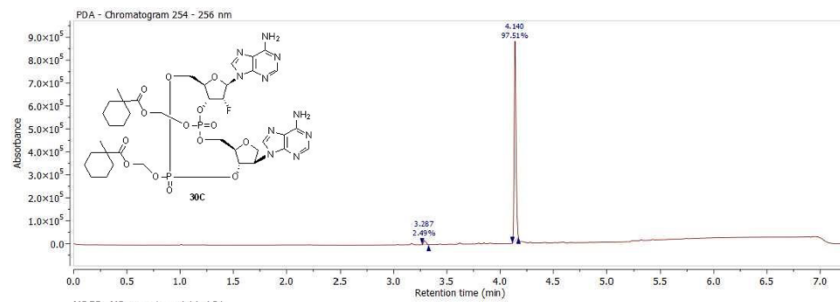


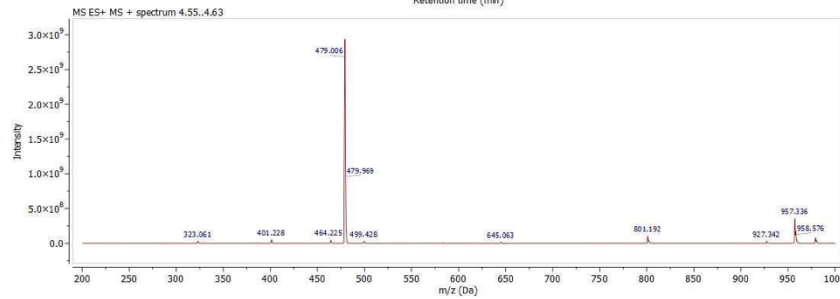
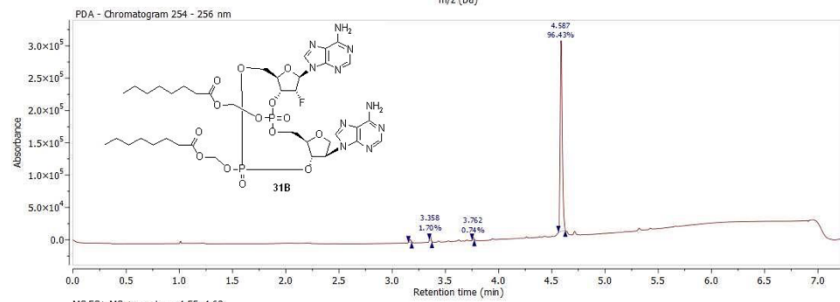
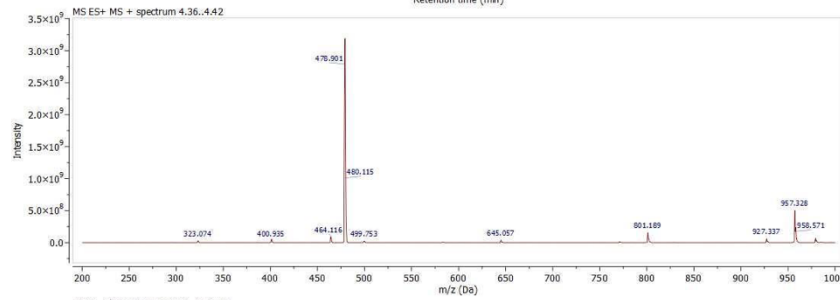
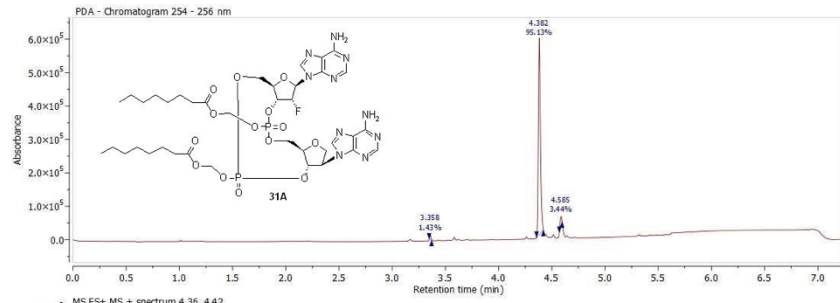


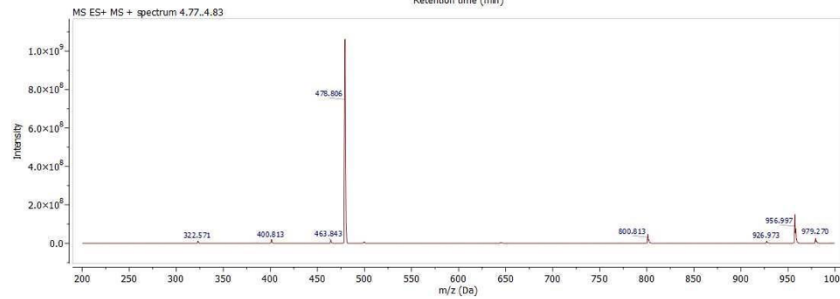
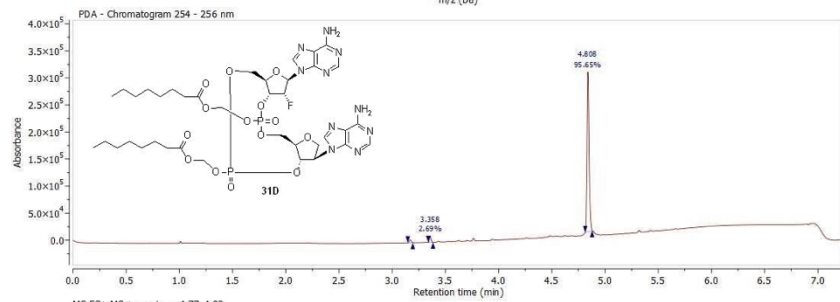
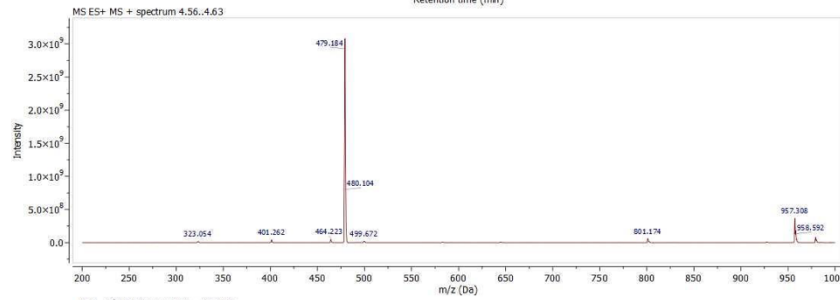
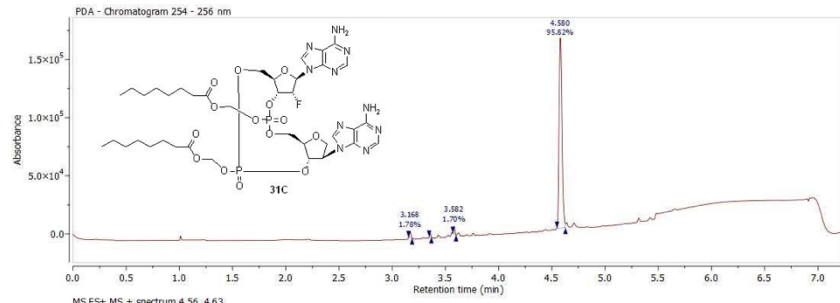




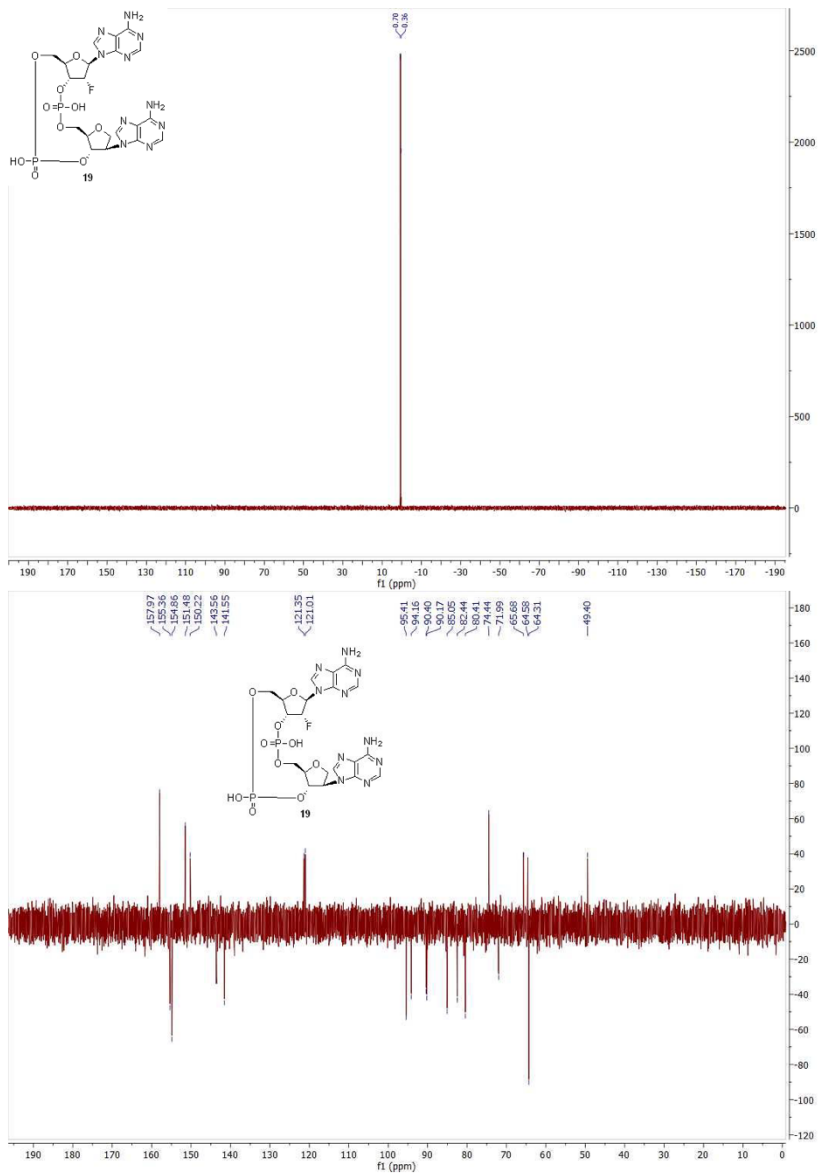


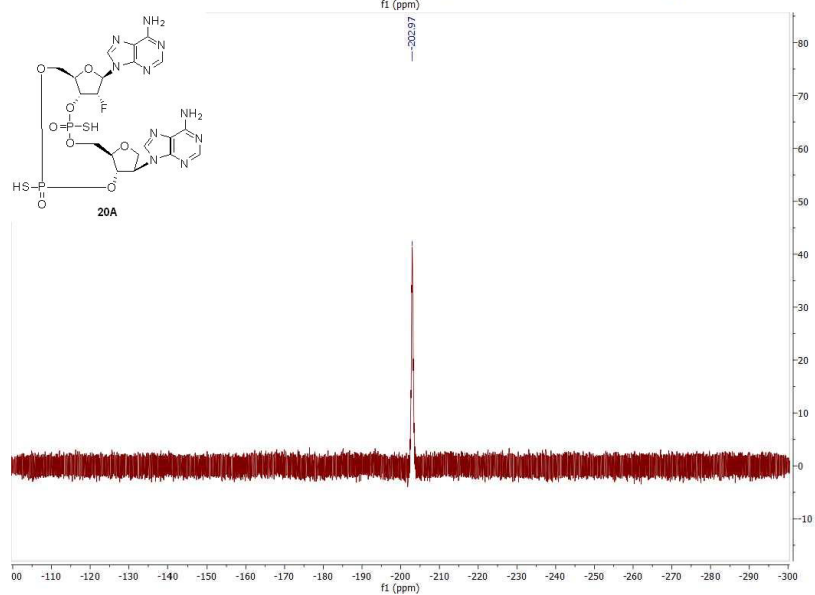
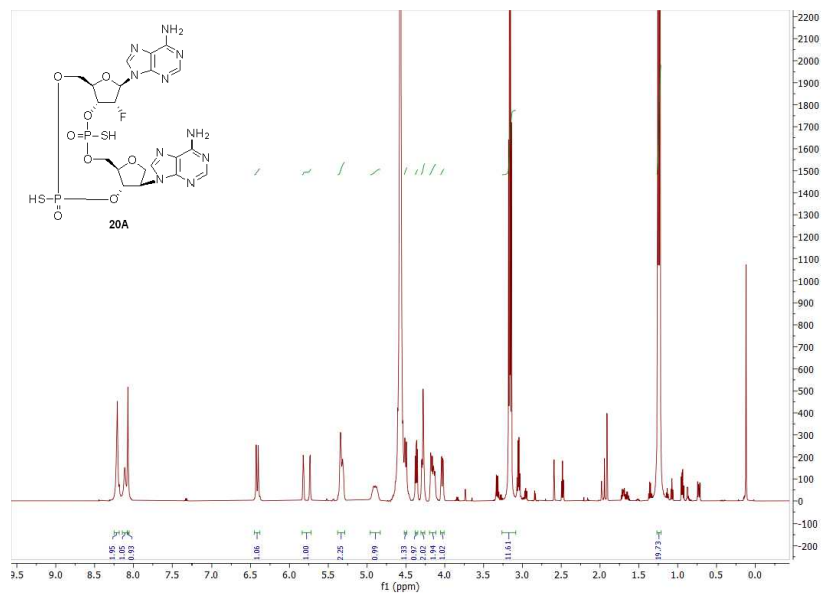




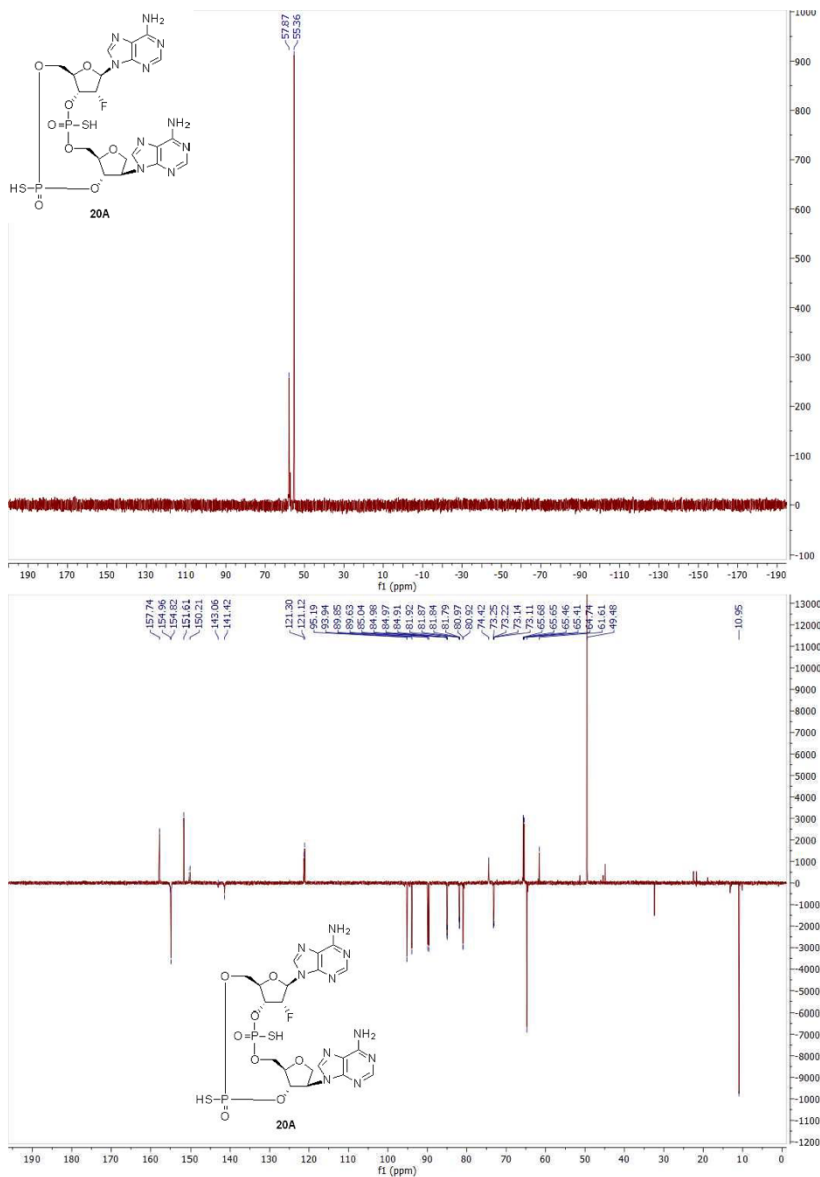




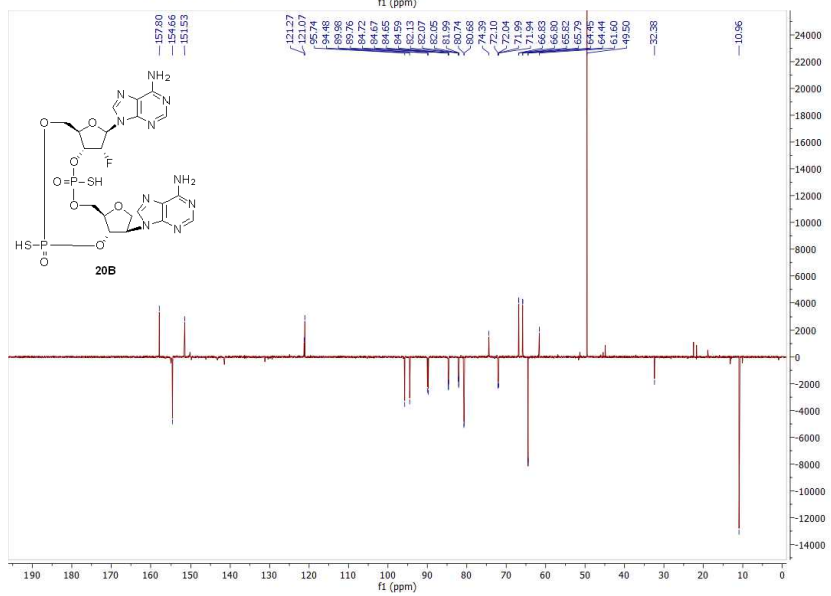
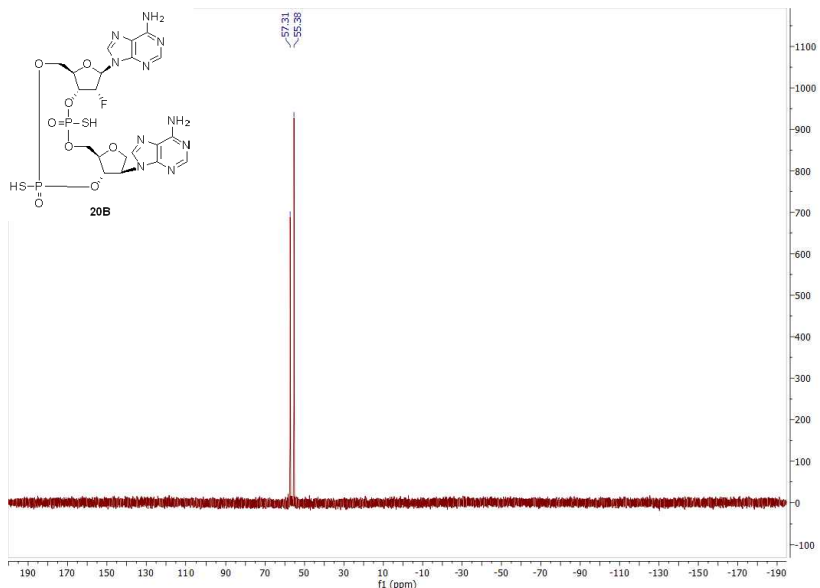


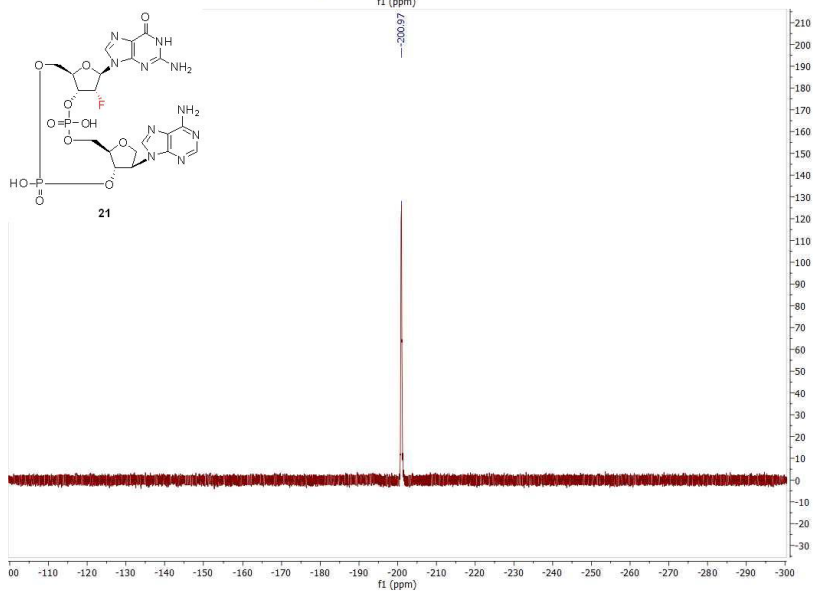
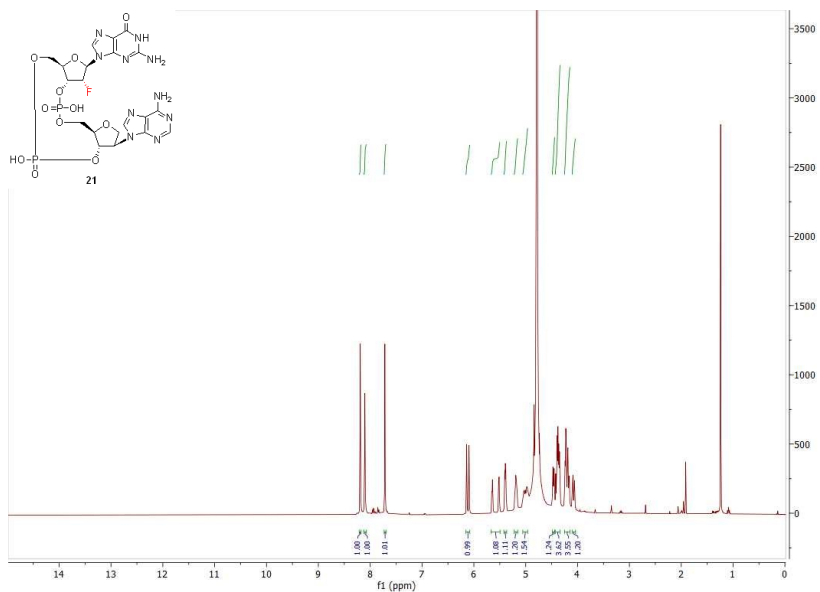


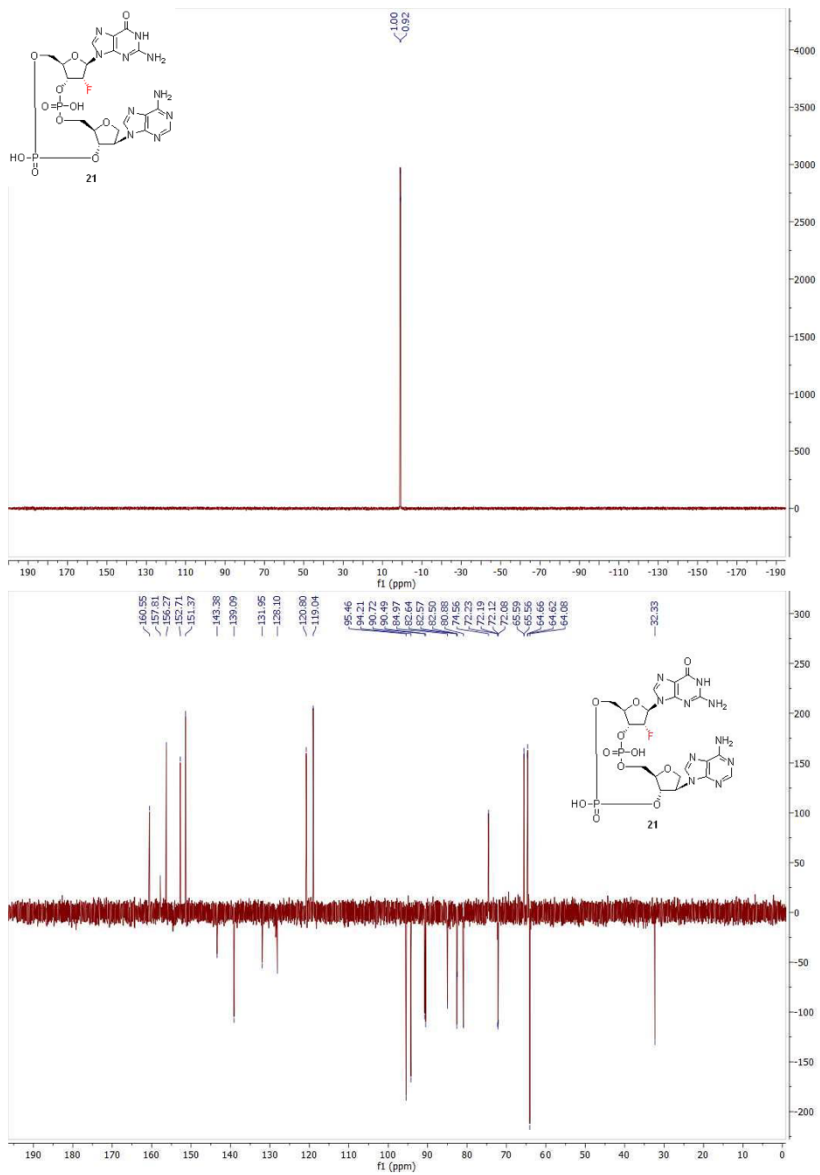


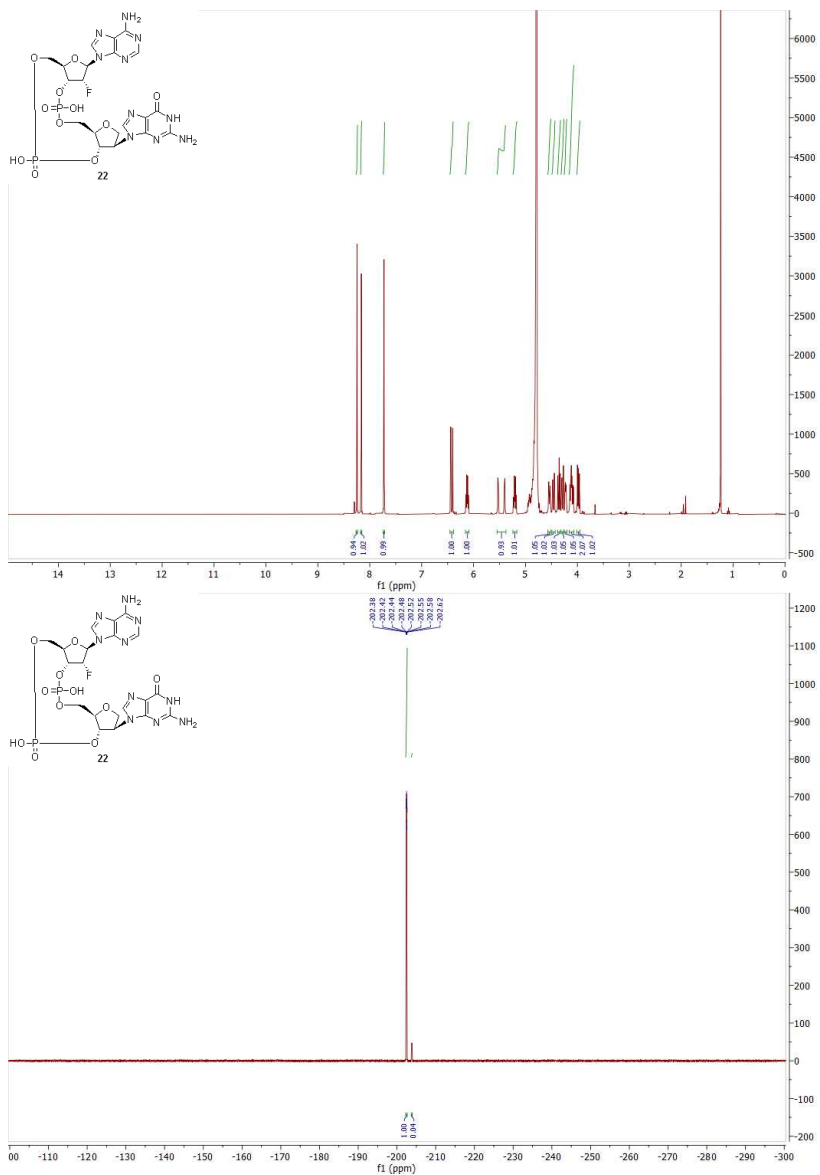


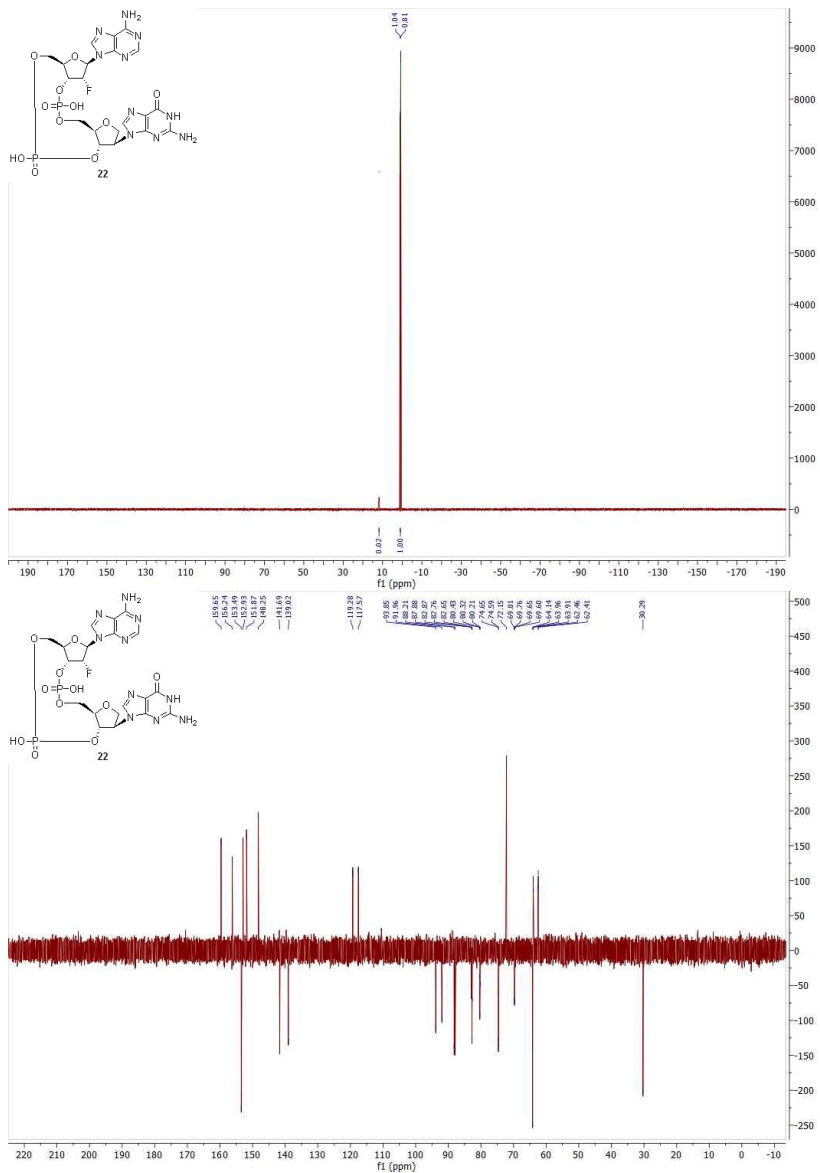


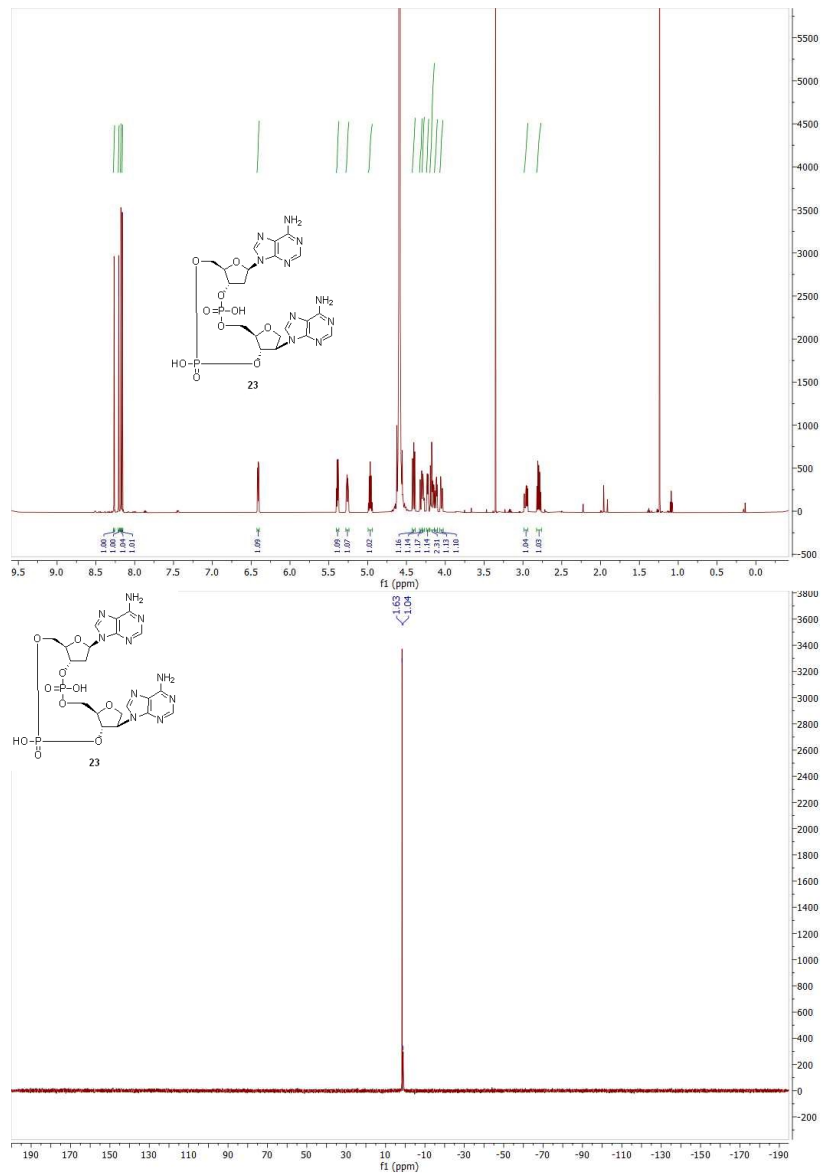




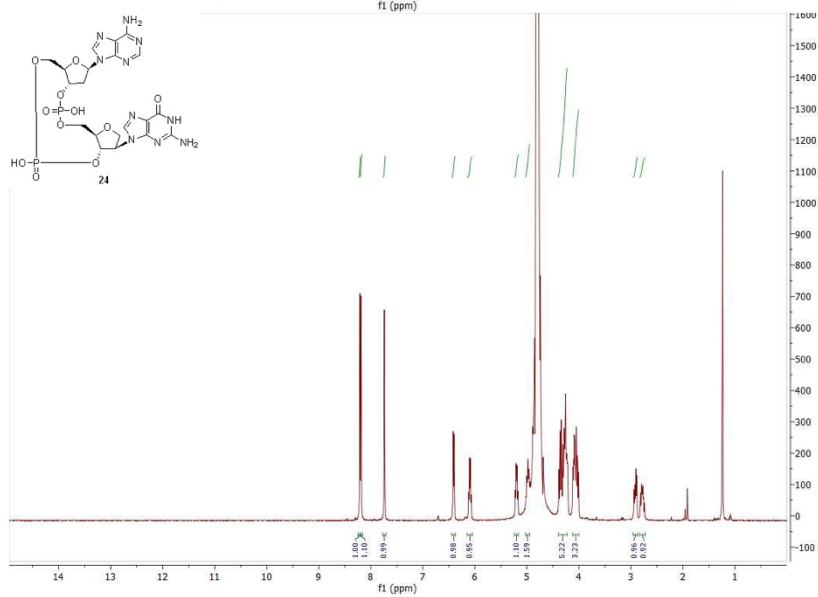
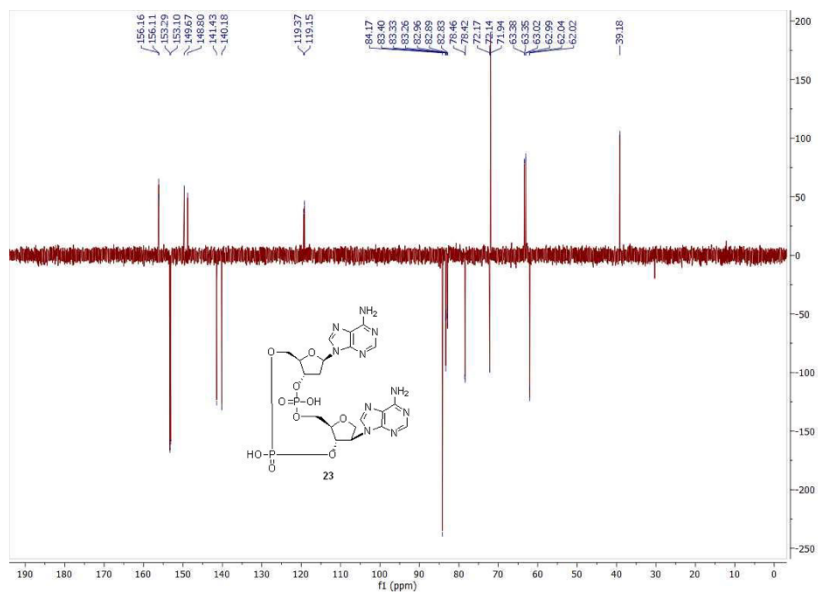


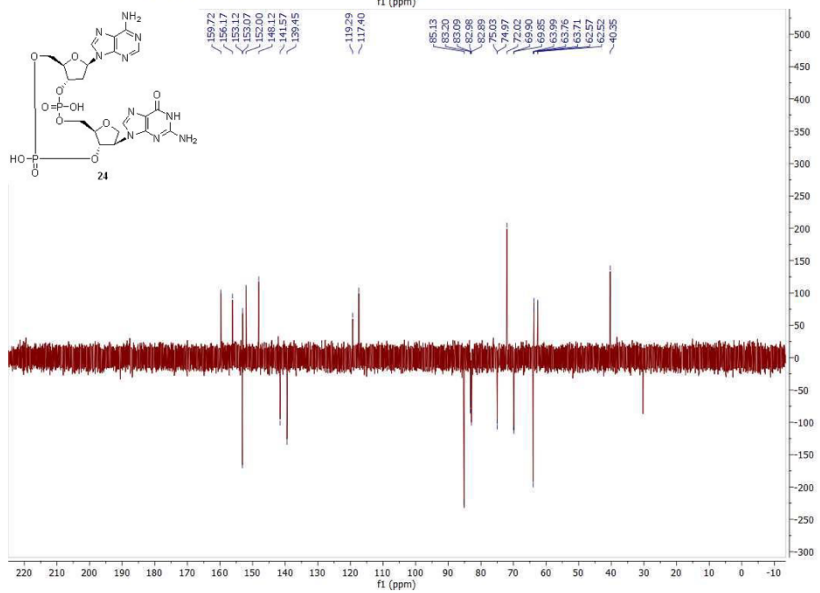
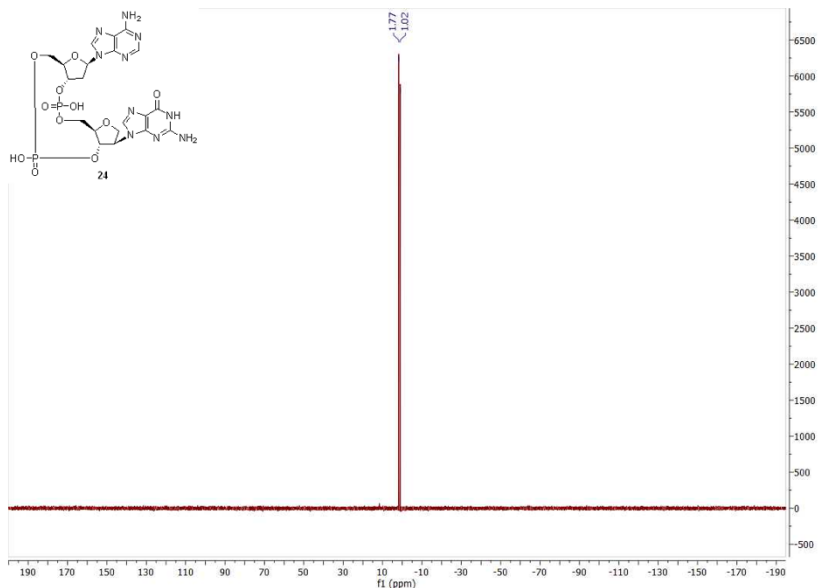


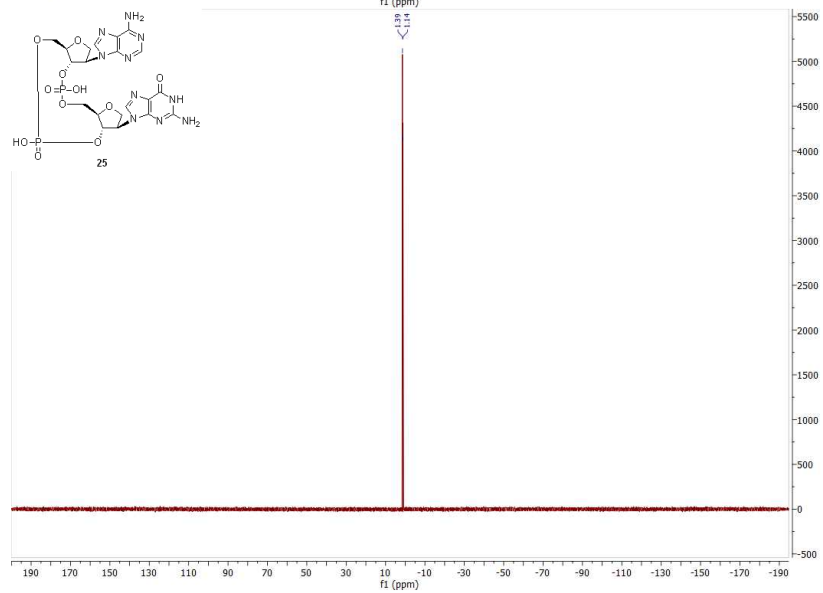
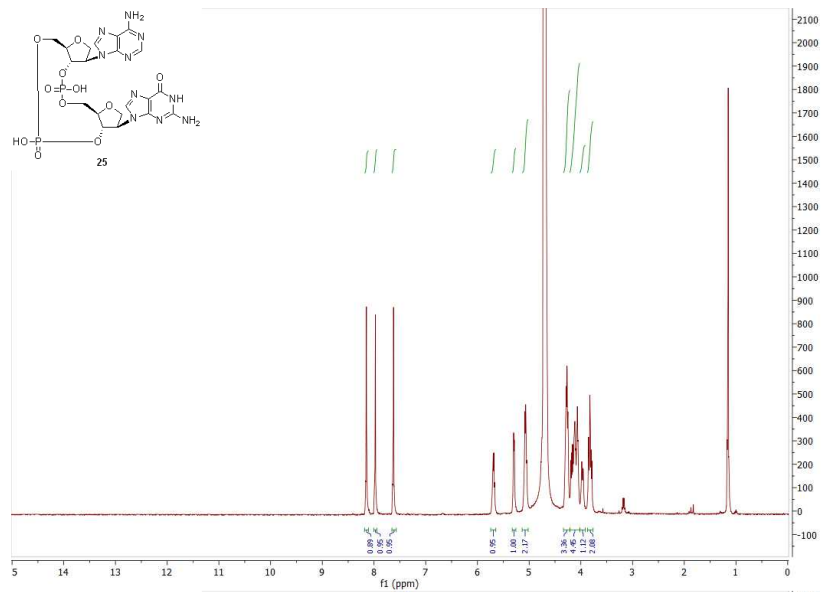


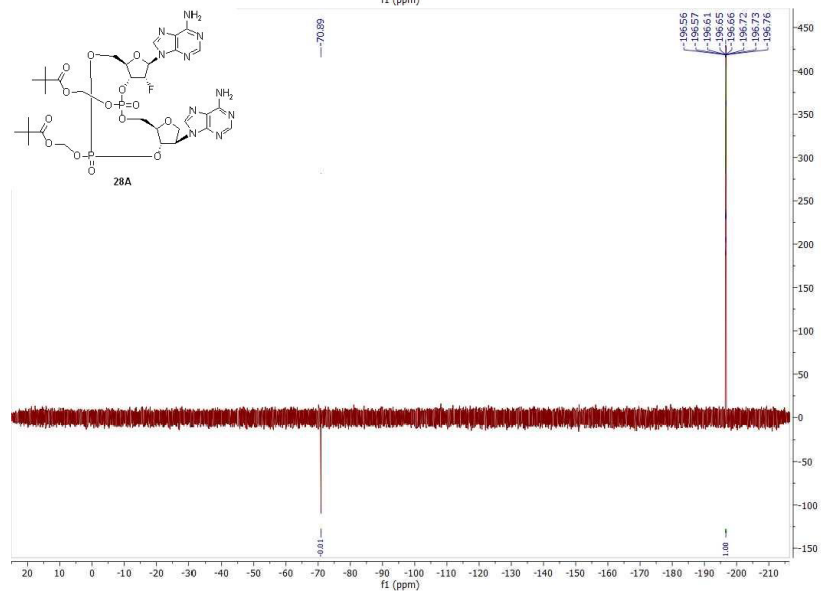
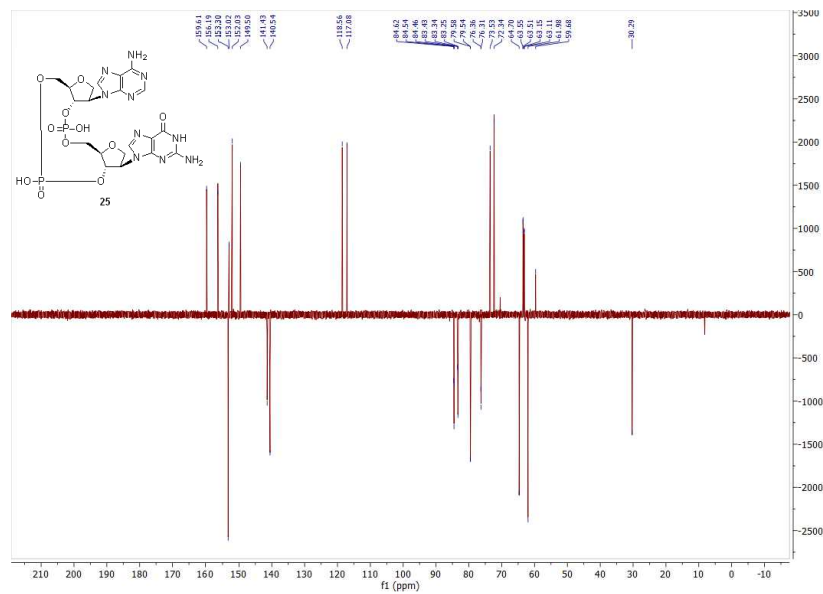


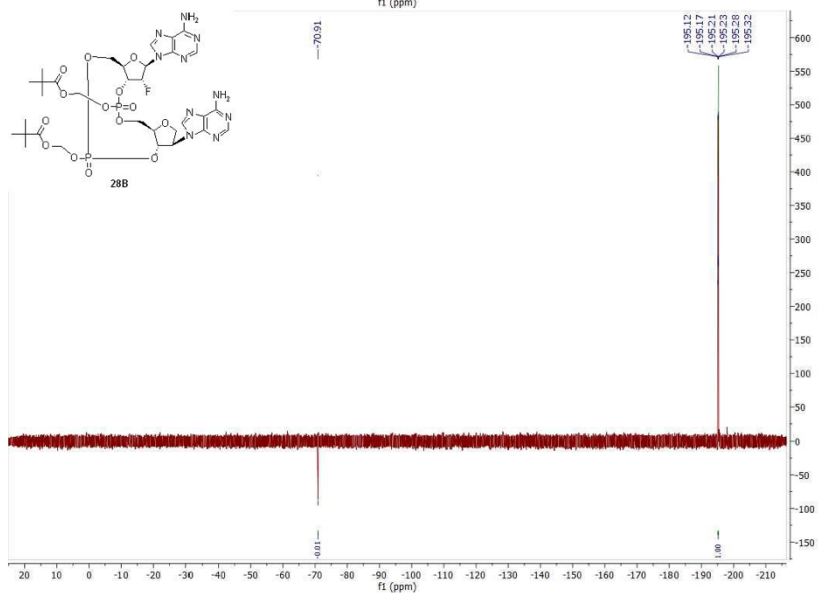
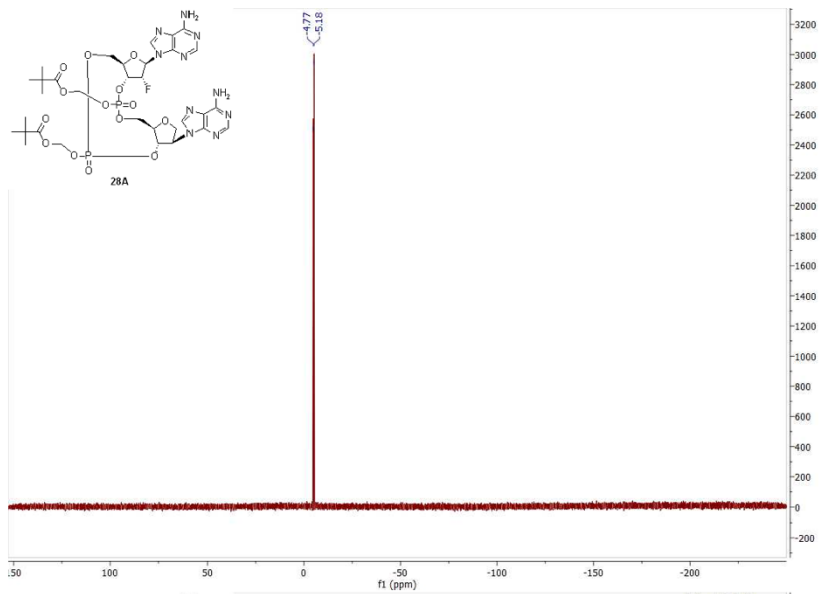


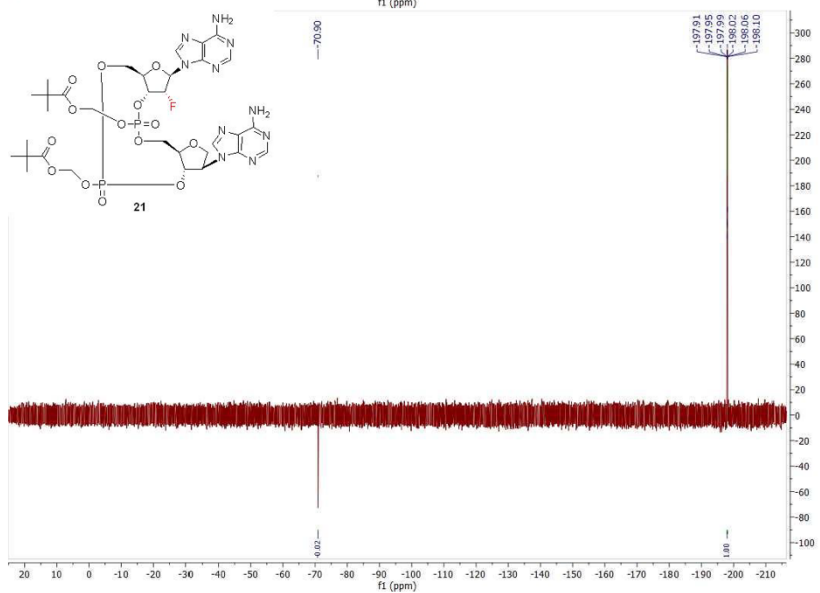
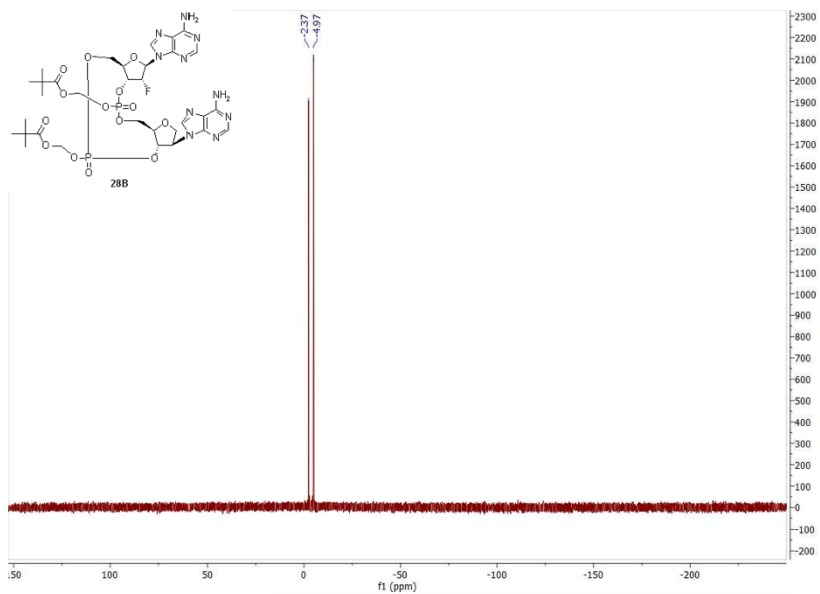


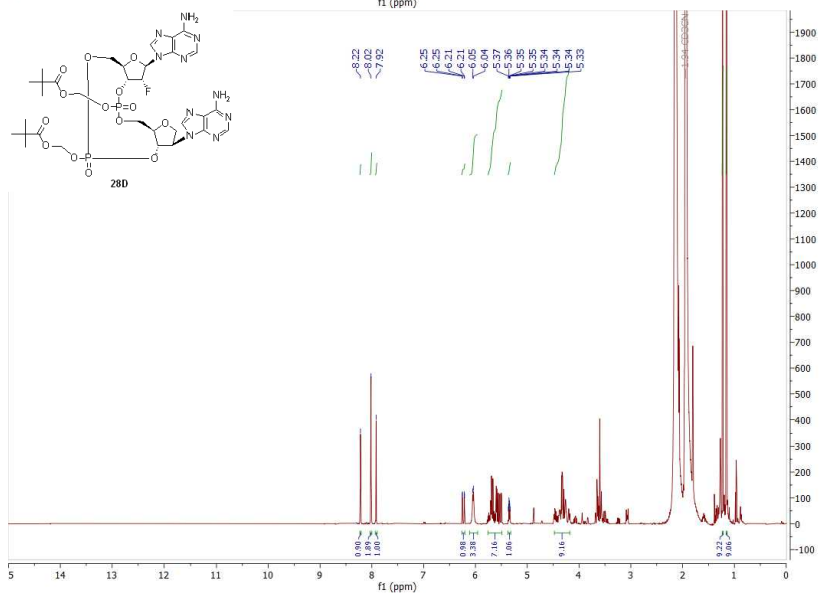
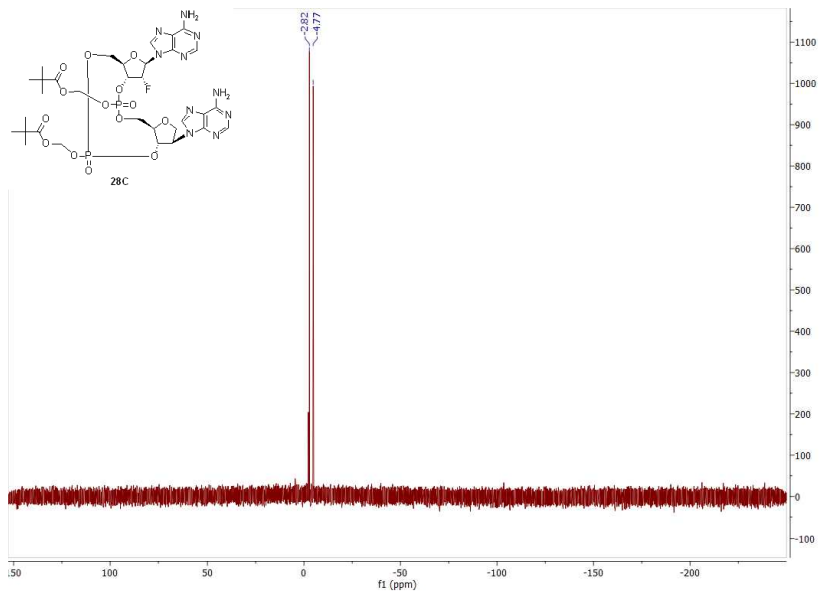


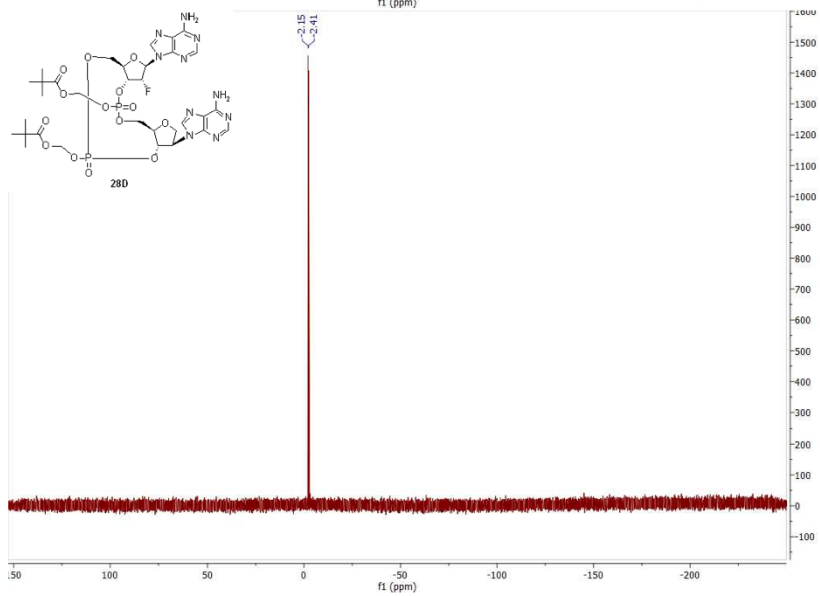
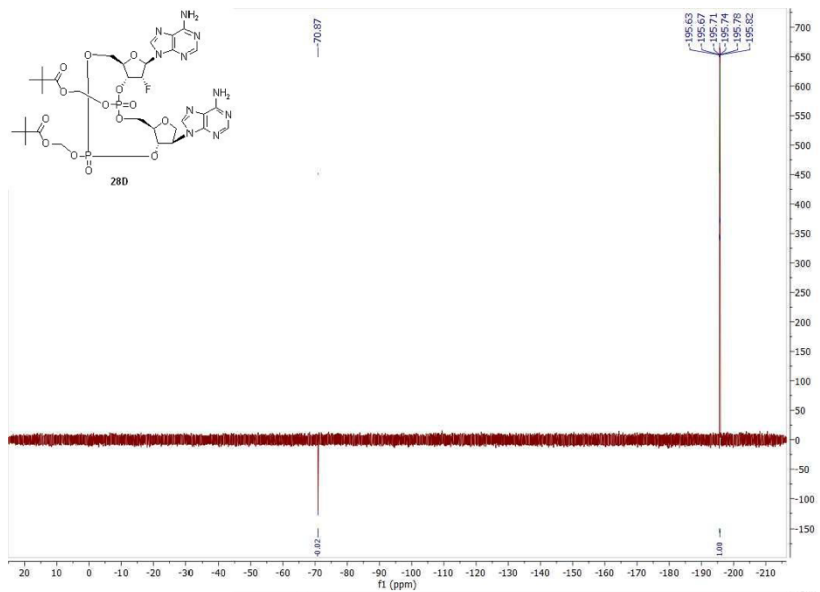




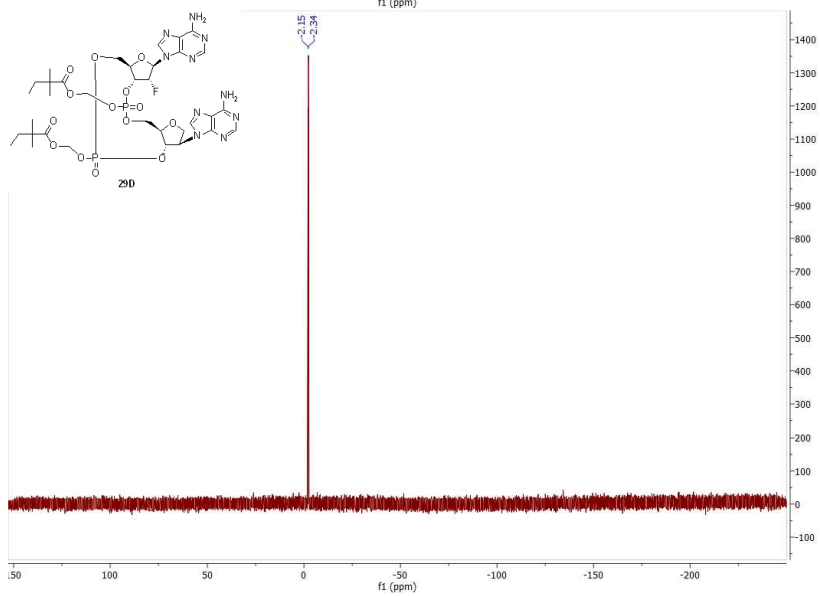
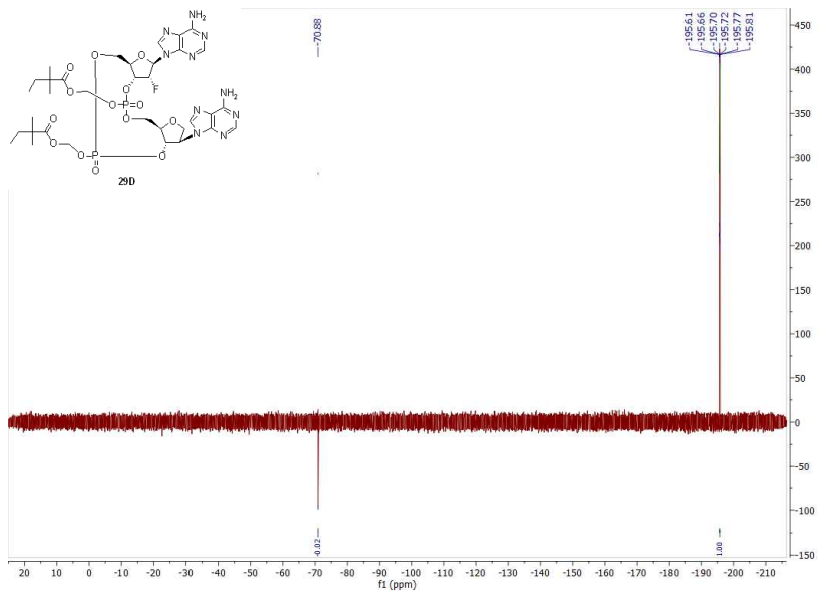


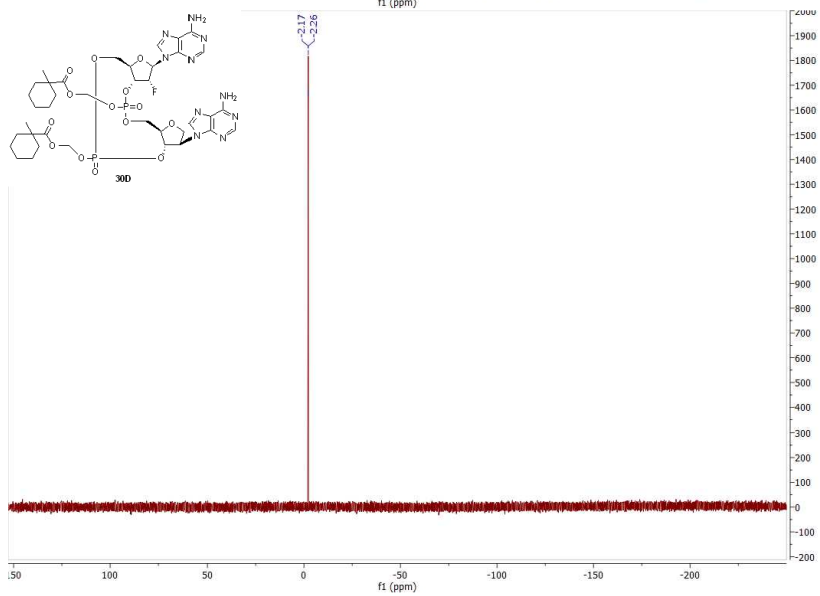
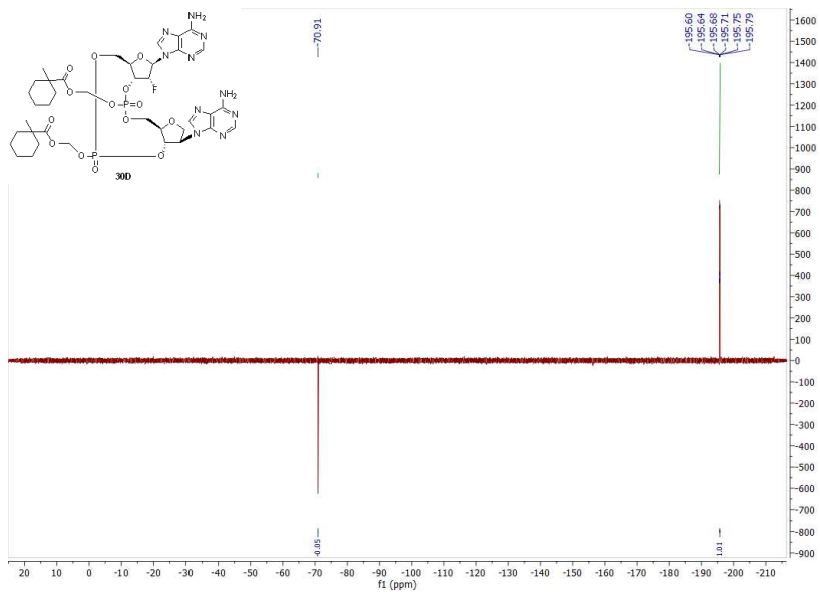


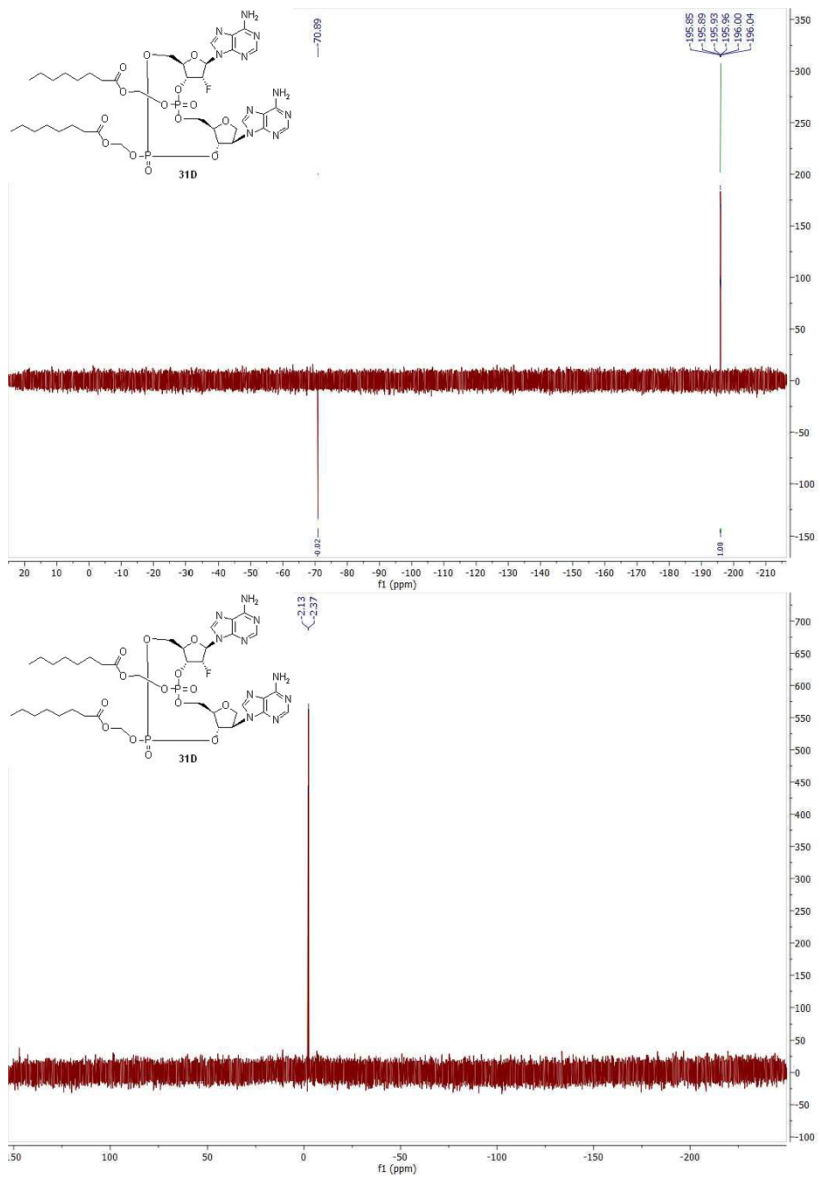












**8.3. Supplement S3: Design, Synthesis, and Biochemical and Biological Evaluation of Novel 7-Deazapurine Cyclic Dinucleotide Analogues as STING Receptor Agonists**

*Vavřina, Z., Perlíková, P., Milisavljević, N., Chevrier, F., Smola, M., Smith, J., Dejmek, M., Havlíček, V., Buděšínský, M., Liboska, R., Vaneková, L., Brynda, J., Boura, E., Řezáčová, P., Hocek, M., & Birkuš, G. (2022). Design, Synthesis, and Biochemical and Biological Evaluation of Novel 7-Deazapurine Cyclic Dinucleotide Analogues as STING Receptor Agonists. Journal of medicinal chemistry, 65(20), 14082–14103. <https://doi.org/10.1021/acs.jmedchem.2c01305>*

My contribution:

*In vitro* screening of tested CDNs using established DSF and cell-based *in vitro* assays, data evaluation and interpretation, participation in manuscript preparation.

## Design, Synthesis, and Biochemical and Biological Evaluation of Novel 7-Deazapurine Cyclic Dinucleotide Analogues as STING Receptor Agonists

Zdeněk Vavřina,<sup>¶</sup> Pavla Perlíková,<sup>\*,¶</sup> Nemanja Milisavljević, Florian Chevrier, Miroslav Smola, Joshua Smith, Milan Dejmek, Vojtěch Havlíček, Miloš Buděšínský, Radek Liboska, Lenka Vaneková, Jiří Brynda, Evzen Boura, Pavlína Rezáčová, Michal Hocek, and Gabriel Birkuš<sup>\*</sup> Cite This: *J. Med. Chem.* 2022, 65, 14082–14103

Read Online

ACCESS |

Metrics &amp; More

Article Recommendations

Supporting Information

**ABSTRACT:** Cyclic dinucleotides (CDNs) are second messengers that activate stimulator of interferon genes (STING). The cGAS-STING pathway plays a promising role in cancer immunotherapy. Here, we describe the synthesis of CDNs containing 7-substituted 7-deazapurine moiety. We used mouse cyclic GMP–AMP synthase and bacterial dinucleotide synthases for the enzymatic synthesis of CDNs. Alternatively, 7-(het)aryl 7-deazapurine CDNs were prepared by Suzuki–Miyaura cross-couplings. New CDNs were tested in biochemical and cell-based assays for their affinity to human STING. Eight CDNs showed better activity than 2′3′-cGAMP, the natural ligand of STING. The effect on cytokine and chemokine induction was also evaluated. The best activities were observed for CDNs bearing large aromatic substituents that point above the CDN molecule. We solved four X-ray structures of complexes of new CDNs with human STING. We observed  $\pi$ – $\pi$  stacking interactions between the aromatic substituents and Tyr240 that are involved in the stabilization of CDN–STING complexes.



## ■ INTRODUCTION

The cyclic GMP–AMP synthase (cGAS)–stimulator of interferon genes (STING) pathway is an important player in detecting damage-associated (DAMPs) and pathogen-associated molecular patterns (PAMPs).<sup>1–4</sup> Upon dsDNA detection in cytosol, cGAS synthesizes a STING ligand 2′3′-cGAMP (**1a**, cyclic [G(2′,5′)pA(3′,5′)p] with mixed 2′–5′ and 3′–5′ phosphodiester linkages).<sup>5,6</sup> Besides eukaryotic 2′3′-cGAMP, STING can be also activated by bacterial cyclic dinucleotides (CDNs) such as 3′3′-cGAMP (**1b**), *c*-di-GMP (**1c**), and *c*-di-AMP (**1d**), containing two 3′–5′ phosphodiester bonds (Scheme 1).<sup>7–10</sup> Binding of CDNs to STING triggers a downstream response that results in the expression of proinflammatory cytokines (TNF- $\alpha$ , IL-1 $\beta$ ) via a nuclear factor  $\kappa$ -light-chain enhancer of activated B-cells (NF- $\kappa$ B) and/or the expression of type I interferons (IFN- $\alpha$ , IFN- $\beta$ ) via an interferon regulatory factor 3 (IRF3).<sup>11–15</sup> When taking into consideration this response, STING plays a crucial role in defense against pathogen infections, immune surveillance of tumor cells, and maintenance of the normal immune functions of the body.<sup>16–19</sup>

Human STING agonists<sup>21,22</sup> can be divided into two major groups: (1) CDNs and their derivatives (ADU-S100,<sup>23</sup> MK-1454,<sup>24</sup> TAK-676,<sup>25</sup> etc.<sup>26</sup>) and (2) synthetic non-nucleotide

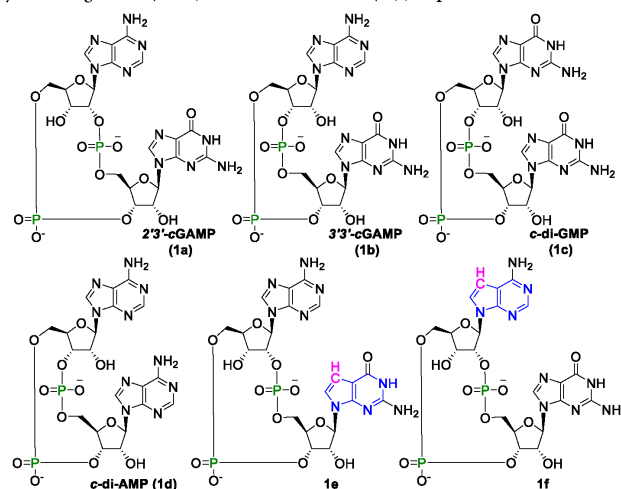
STING agonists (diABZI,<sup>27</sup> G10,<sup>28,29</sup> MSA-2,<sup>30</sup> etc.<sup>31,32</sup>). Due to the importance of the cGAS-STING pathway, there has been an increased interest in identifying new STING agonists with improved drug-like properties compared to the natural STING ligands. This attention is highlighted by the fact that seven different STING agonists are presently being investigated in different phases of clinical trials.<sup>22</sup>

Herein, we report the design, synthesis, and biochemical and biological evaluation of 7-substituted 7-deazapurine CDNs that activate STING signaling. As we reported in our previous study,<sup>20</sup> 7-deazapurine CDN (Scheme 1) can be tolerated when forming the STING–CDN complex. In an effort to further probe CDN–STING interactions, we decided to explore the effect of 7-substitutions on the activity of CDNs by preparing 24 new 7-substituted 7-deazapurine CDNs. Considering the results of the initial trials, we decided to focus mainly on 7-deazaadenine derivatives due to the fact that the

Received: August 9, 2022

Published: October 6, 2022



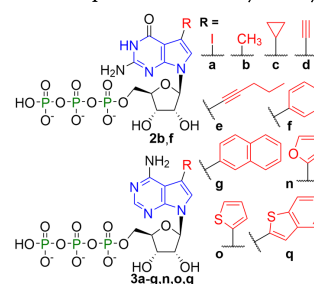
Scheme 1. Naturally Occurring CDNs (1a–d) and 7-Deaza Variants (1e,f) Reported in Our Previous Study<sup>20</sup>

presence of 7-deazaguanine in compound **1e** caused a substantial drop in affinity to wt hSTING.<sup>20</sup> When possible, compounds were prepared enzymatically by mouse cGAS (mcGAS) as previously shown or with bacterial dinucleotide cyclase from *Vibrio cholerae* (DncV) and diadenylate cyclase from *Bacillus thuringiensis* (DisA).<sup>20,33–35</sup> Otherwise, the compounds were prepared by chemical synthesis, either by arylation of an enzymatically prepared precursor or by total synthesis. All compounds were tested by differential scanning fluorimetry (DSF) and in cell-based assays. For four of the compounds, we determined their structures in complex with STING by X-ray crystallography to better understand their binding mode.

## RESULTS AND DISCUSSION

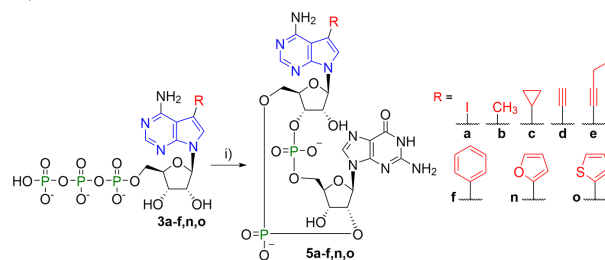
**Enzymatic Synthesis.** As shown in previous works, cGAS and bacterial dinucleotide cyclases DncV and DisA can be used for the synthesis of CDNs by employing various NTP analogues.<sup>20,33,34</sup> This allows for the substitution of a long and multi-step total synthesis of CDNs<sup>36</sup> with a one-step enzymatic reaction. Only the enzymatic synthesis of CDNs from nucleoside triphosphates (NTPs) bearing small nucleobase modifications has been studied so far.<sup>33</sup> Therefore, we decided to explore 7-substituted 7-deazaguanosine triphosphates **2** (G<sup>R</sup>TTPs) and 7-substituted 7-deazaadenosine triphosphates **3** (A<sup>R</sup>TTPs) as substrates for these enzymes (Scheme 2). Successful enzymatic synthesis of CDNs **4b** (2'3'-cG<sup>R</sup>AMP), **5a–f,n,o** (2'3'-cGA<sup>R</sup>MPs), and **6f** (2'3'-cG<sup>R</sup>A<sup>R</sup>MP) indicates that mcGAS tolerates small substituents in position 7 of 7-deazapurine NTPs including halogen, alkyl, cycloalkyl, alkynyl, small hetaryl, and phenyl groups (Schemes 3 and 4). Unfortunately, NTPs with aryls bigger than phenyl, that is, 2-naphthyl (**3g**) and 2-benzothieryl (**3q**),<sup>37</sup> caused a disruption of the enzymatic reaction, leaving triphosphates unreacted. In some cases, such as CDN **5a**, the conversions were quantitative; thus, we were able to enzymatically prepare

Scheme 2. 7-Deazapurine NTPs for Enzymatic Synthesis

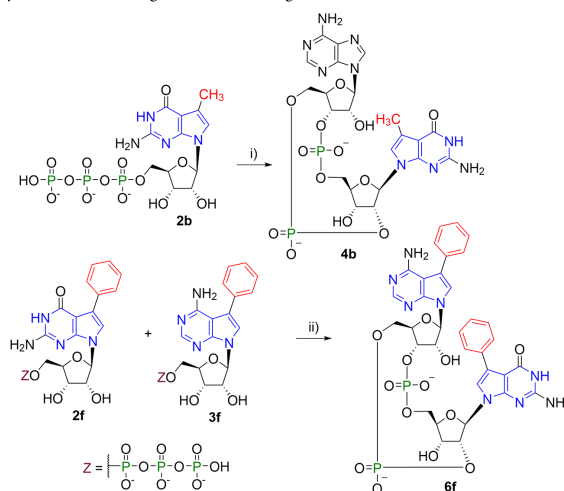


more than 70 mg of this CDN in one batch, which was further arylated as described below. For the synthesis of the 7-substituted 3'3'-CDNs **7a** and **8a**, we used the bacterial enzymes DncV and DisA (Scheme 5).

**Chemistry.** Chemical synthesis of 7-aryl-7-deazaadenine CDNs relied on a modular approach. The key intermediates, 7-iodo-7-deazaadenine CDNs **5a**, **7a**, and **8a**, were converted to the desired aryl-CDNs using Suzuki–Miyaura cross-coupling reactions. The iodinated CDNs can be prepared by chemical synthesis (i.e., **5a**) and/or enzymatic synthesis (i.e., **5a**, **7a**, and **8a**). The chemical synthesis of iodinated 7-deazaadenine CDN **5a** started from 7-iodo-7-deazaadenosine (**9**). First, H-phosphonate **12** had to be synthesized (Scheme 6). Iodinated nucleoside **9** was *N*-benzoylated using transient silyl protection.<sup>38</sup> The *N*-benzoylated intermediate was not isolated due to its poor solubility that complicated its chromatographic purification. The crude product was directly used in a tritylation step to obtain 5'-O-DMTr-protected nucleoside **10** (68% over two steps). Regioselective 2'-*O*-silylation using

Scheme 3. Enzymatic Synthesis of 2'-3'-cGA<sup>R</sup>MPs<sup>4f</sup>

<sup>4f</sup>Reagents and conditions: (i) GTP, Tris-HCl [pH 8.0], MgCl<sub>2</sub>, dsDNA, mcGAS, 37 °C 16 h.

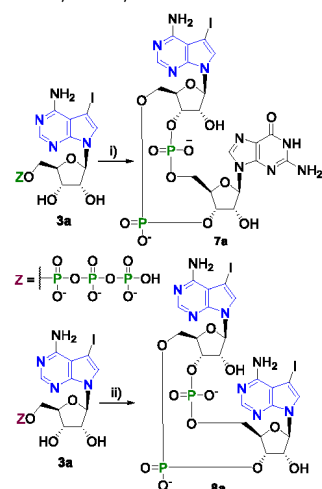
Scheme 4. Enzymatic Synthesis of 7-Deazaguanine Containing CDNs<sup>4f</sup>

<sup>4f</sup>Reagents and conditions: (i) ATP, Tris-HCl [pH 8.0], MgCl<sub>2</sub>, dsDNA, mcGAS, 37 °C 16 h; (ii) Tris-HCl [pH 8.0], MgCl<sub>2</sub>, dsDNA, mcGAS, 37 °C 16 h.

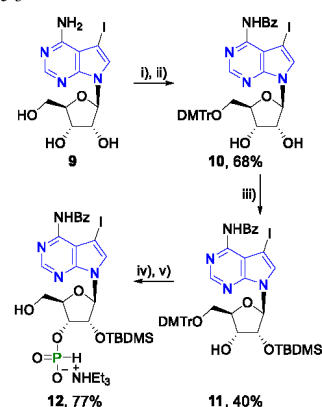
silver nitrate catalysis<sup>39</sup> provided nucleoside **11**. 3'-O-Silyl isomer was also formed during the reaction as a minor product, but it could not be efficiently separated from the 2'-O-silyl isomer **11**. However, the mixture of silylated products could be easily deprotected using TBAF in THF to regenerate the starting material **10**. 3'-H-Phosphonate moiety was installed by the reaction of **11** with diphenyl phosphite. The crude product was directly used for the next step in order to avoid a loss of the material during column chromatography. After the removal of the DMTr-group by DCA, H-phosphonate **12** was obtained as a triethylammonium salt (77% over two steps).

The reaction of H-phosphonate building blocks with phosphoramidites is typically performed in acetonitrile in the presence of a coupling activator,<sup>40</sup> such as py-TFA. However, due to the low solubility of **12** in acetonitrile, its reaction with guanosine phosphoramidite **13** proceeded poorly. Efforts to improve the reaction yield by increasing the amount of py-TFA

or by the use of other coupling activators, such as ethylthio-1*H*-tetrazole (ETT), failed. However, when **12** was treated with DCA in order to convert the triethylammonium salt to a standard H-phosphonate, the solubility in acetonitrile improved, and the reaction with guanosine phosphoramidite **13** proceeded even without any coupling activator. After detritylation, linear dinucleotide **14** was partially purified using reverse phase flash chromatography. The crude linear product **14** was cyclized using 2-chloro-5,5-dimethyl-1,3,2-dioxaphosphorinane 2-oxide (DMOCP).<sup>41</sup> After oxidation with iodine and a partial purification on a reverse phase C18 column, the protected CDN **15** was obtained as a crude material. Deprotection of nucleobases and the phosphate using CH<sub>3</sub>NH<sub>2</sub> and the removal of silyl groups by Et<sub>3</sub>N·3HF provided 7-iodinated 7-deazaadenine CDN **5a** in an overall yield of 18% (starting from H-phosphonate **12**, Scheme 7).

Scheme 5. Enzymatic Synthesis with Bacterial Enzymes<sup>42</sup>

<sup>42</sup>Reagents and conditions: (i) GTP, HEPES [pH 8.0], MgCl<sub>2</sub>, NaCl, DTT, DncV, 37 °C 16 h; (ii) HEPES [pH 8.0], MgCl<sub>2</sub>, NaCl, DTT, DisA, 50 °C 16 h.

Scheme 6<sup>42</sup>

<sup>42</sup>Reagents and conditions: (i) TMSCl, BzCl/py, 0 °C—rt, 16 h; (ii) DMTcCl/py, rt, 16 h; (iii) TBDMSCl, AgNO<sub>3</sub>, py/THF, rt, 16 h; (iv) (1) PO(OPh)<sub>2</sub>/py, rt, 1 h, (2) H<sub>2</sub>O, rt, 5 min; (v) (1) DCA/DCM, rt, 15 min, (2) TES, rt, 30 min.

The Suzuki–Miyaura cross-coupling reaction is a generally used method for the introduction of aryl and hetaryl groups into the position 7 of 7-deazapurine nucleotides.<sup>42</sup> Hydrolysis of the phosphodiester backbone was observed during the synthesis of 8-arylguanosine-containing CDNs using Suzuki–Miyaura cross-coupling.<sup>43</sup> Therefore, we decided to use

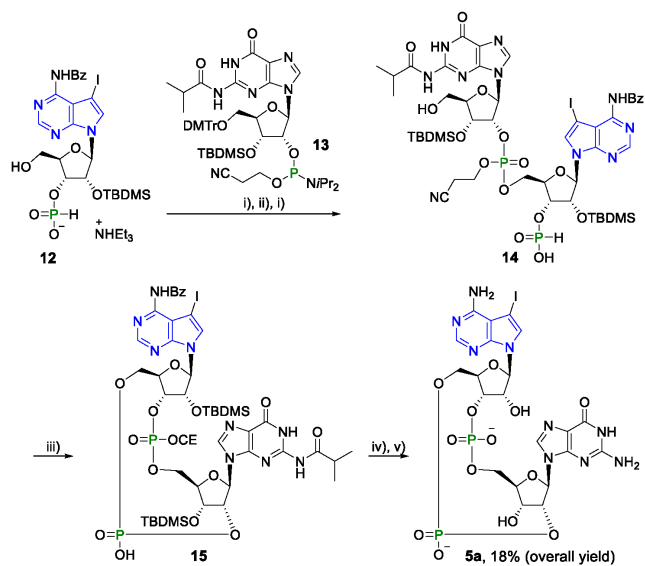
reaction conditions that were originally optimized for the synthesis of 7-deazapurine NTPs that also suffer from hydrolytic instability.<sup>44,45</sup> A short reaction time (30 min) was crucial in order to avoid excessive hydrolysis. The cross-coupling reactions were performed under Pd(OAc)<sub>2</sub> catalysis in the presence of a water-soluble ligand, triphenylphosphane-3,3',3''-trisulfonate (TPPTS), and Cs<sub>2</sub>CO<sub>3</sub> in water–acetonitrile mixture (2:1). The reaction of iodinated CDN 5a with 2 equiv of phenylboronic acid did not provide full conversion so that phenyl derivative 5f was obtained in low yield (18%, Scheme 8). With 5 equiv of arylboronic acids (or arylboronic acid pinacol esters), the cross-couplings proceeded smoothly. Nevertheless, the yields were affected by the hydrolysis. Arylated 2'3'-cGA<sup>R</sup>MPs 5f–m and p–r were prepared in 30–59% yield (Scheme 8). From the reaction with dibenzofuran-4-ylboronic acid, isomerized side product 16 (Figure 1) was obtained in 13% yield. Similar byproducts were observed in all cross-coupling reactions, but the byproducts were not isolated. Due to hindered rotation at room temperature, CDNs 5h–j were prepared as inseparable mixtures of diastereomers/atropoisomers. Hindered rotation of bulky aryl substituents has been reported among corresponding 7-aryl-7-deazaadenosines.<sup>46</sup>

The conditions for the Suzuki–Miyaura cross-coupling reaction were also applied for the synthesis of 3'3'-CDNs. Iodinated CDNs 7a and 8a were converted to corresponding phenyl derivatives 7f (66%) and 8f (78%), respectively (Scheme 9). In these reactions, higher yields were achieved because the hydrolysis rate of 3'3'-CDNs during the cross-coupling reaction was significantly lower compared to that of 2'3'-CDNs.

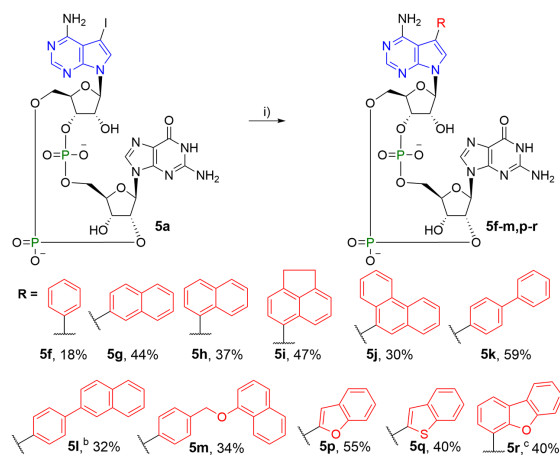
**Biochemistry and Biology.** In order to biochemically and biologically characterize prepared CDNs, all CDNs were tested using DSF and 293T cell-based reporter assays. The selected compounds that showed activity were further evaluated for the induction of cytokines using human peripheral blood mononuclear cells (PBMCs). DSF was performed using wild-type human STING protein (UniProt Q86WV6). This method provides a useful insight into the STING binding properties of CDNs by determining their ability to improve the thermal stability of the protein.<sup>47,48</sup> Digitonin 293T cell-based assays were performed using five major allelic variants (wild type, HAQ, AQ, Q, and REF)<sup>49</sup> in the presence of digitonin A that facilitates entry of CDNs into cells due to the permeabilization of cell membranes.<sup>20</sup> The standard format of the 293T cell assay was carried out only with cells expressing wild-type human STING and in the absence of the permeabilizing agent.<sup>20</sup>

Our initial experiments with 7-deaza substituted 2'3'-cGAMP showed that 7-methyl was much less tolerated on 7-deazaguanine (4b) than on 7-deazaadenine (5b) (Table 1). 7-Deazaguanine-modified 4b had  $\Delta T_m$  in a DSF assay of 3.3 °C while 7-deazaadenine-modified 5b of 11.5 °C. This suggests that the noncovalent interactions of the NH group at position 7 of the nucleobases have a bigger impact on the CDN binding to STING for guanine than for adenine. The results are in agreement with the data for the 7-deaza modification that we reported on earlier.<sup>20</sup> These findings were further confirmed by improved activity of 5b than of 4b in the 293T cell-based reporter assay (Table 1). This led to focusing our efforts on the synthesis of 2'3'-cGA<sup>R</sup>MP-derived CDNs. We prepared compounds 5c–r, each containing a substituent of different size at position 7 of 2'3'-cGA<sup>R</sup>MP. Surprisingly, STING turned



Scheme 7<sup>44</sup>

<sup>44</sup>Reagents and conditions: (i) DCA/DCM, rt, 10 min; (ii) (1) 13/MeCN, rt, 10 min, (2) *t*BuOOH, rt, 30 min; (iii) (1) DMOCOP/py, rt, 110 min, (2)  $\text{I}_2$ ,  $\text{H}_2\text{O}$ , rt, 10 min; (iv)  $\text{CH}_3\text{NH}_2/\text{EtOH}$ , rt, 3 h; (v)  $\text{Et}_3\text{N}\cdot 3\text{HF}/\text{py}$ ,  $\text{Et}_3\text{N}$ , 50 °C, 3.5 h.

Scheme 8<sup>44</sup>

<sup>44</sup>Reagents and conditions: (i)  $\text{RB}(\text{OH})_2$ ,  $\text{C}_5\text{CO}_3$ , TPPTS,  $\text{Pd}(\text{OAc})_2/\text{H}_2\text{O}-\text{MeCN}$  (2:1), 100 °C, 30 min. <sup>b</sup>RBpin was used instead of  $\text{RB}(\text{OH})_2$ . <sup>c</sup>Open isomer 16 (13%) was also isolated.

out to tolerate not only relatively small substituents, that is, iodine (5a), cyclopropyl (5c), and ethynyl (5d), but also small

aromatic substituents, that is, phenyl (5f), 2-furyl (5n), and 2-thienyl (5o) substituents, and even relatively large aromatic

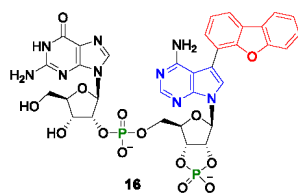


Figure 1. Open isomerized side product of a cross-coupling reaction.

groups such as 2-naphthyl (5g), 4-biphenyl (5k), 4-(2-naphthyl)phenyl (5l), 4-[(2-naphthoxy)methyl]phenyl (5m), 2-benzofuryl (5p), and 2-benzothieryl (5q).

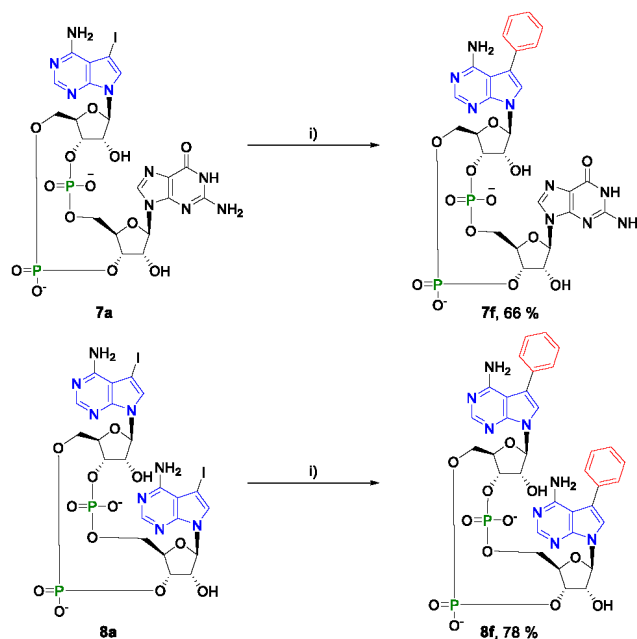
When considering  $\Delta T_m$  for 5c, it decreased by only 0.7 °C, whereas 5d showed a nearly 3 °C drop compared to 5b. This minor decrease suggests that in position 7 of 7-deazaadenine, there is a space for the introduction of larger modifications than just a methyl group. When tested in a digitonin cell-based reporter assay, modifications on both 5c and 5d were tolerated. However, for 5d, the  $EC_{50}$  value obtained from an assay in cells expressing the REF allelic form increased by nearly 6-fold, whereas at all other tested allelic forms, the increase was not higher than 3-fold. This suggests a disruption of interactions between 5d and STING when R232 is replaced by H232. In a

standard cell-based reporter assay for compounds 5c and 5d, we observed a deterioration of cellular activity, which was not present when tested with a membrane-permeabilizing agent.

After proving that there might be space for the introduction of larger substituents in the binding site of STING, we introduced phenyl (5f), small heterocycles (5n, 5o), and pent-1-ynyl (5e) into position 7 of 7-deazaadenine. Surprisingly, we found that  $\Delta T_m$  for 5f, 5n, and 5o decreased by less than 3 °C, and  $EC_{50}$  values in the digitonin assay for these compounds did not increase by more than 2-fold compared to 5c. Moreover, for compounds 5f, 5n, and 5o, we observed restored activity in the standard assay, which was deteriorated for 5c and 5d (Table 1). In fact,  $EC_{50}$  for 5o in the assay was even slightly lower than that for 2'3'-cGAMP. We also solved the crystallographic structure for 5f in complex with STING.

Considering the structure of 5f, we hypothesized that there exists a possibility of intramolecular stabilization through  $\pi$ - $\pi$  stacking between phenyl and guanine in 5f that might help to improve its activity. To prove this possibility, we prepared 2'3'-cG<sup>Phe</sup>A<sup>Phe</sup>MP (6f), 3'3'-cG<sup>Phe</sup>A<sup>Phe</sup>MP (7f), and 3'3'-diA<sup>Phe</sup>MP (8f). Unfortunately, substitutions with phenyl in these compounds did not show an improvement at STING in DSF or cell-based reporter assays compared to 5f. For 7f, we found a decrease in  $\Delta T_m$  by 3 °C, but in digitonin assay,  $EC_{50}$  values for allelic form HAQ and AQ remained nearly the same. For other tested allelic forms,  $EC_{50}$  did not increase more than

Scheme 9<sup>a</sup>



<sup>a</sup>Reagents and conditions: (i) PhB(OH)<sub>2</sub>, Cs<sub>2</sub>CO<sub>3</sub>, TPPTS, Pd(OAc)<sub>2</sub>/H<sub>2</sub>O–MeCN (2:1), 100 °C, 30 min.

14087

<https://doi.org/10.1021/acs.jmedchem.2c01305>  
J. Med. Chem. 2022, 65, 14082–14103

Table 1. Activities of Synthesized 7-Deazapurine CDNs in DSF and Cell-Based Assays

**4, 2'3'-cG<sup>R</sup>AMP: X = N, Y = CR**  
**5, 2'3'-cGA<sup>R</sup>MP: X = CR, Y = N**  
**6, 2'3'-cG<sup>R</sup>A<sup>R</sup>MP: X = CR, Y = CR**  
**7, 3'3'-cGA<sup>R</sup>MP**  
**8, 3'3'-c-dIA<sup>R</sup>MP**

compound	R	DSF $\Delta T_{50}$ ( $^{\circ}\text{C}$ ) <sup>a</sup>		digitonin assay $\text{EC}_{50}$ ( $\mu\text{M}$ ) <sup>b</sup>				standard assay $\text{EC}_{50}$ ( $\mu\text{M}$ )
		wt	wt	HAQ	REF	AQ	Q	
4b	methyl	3.3	3.01	1.38	13.34	1.37	2.54	>150
5a	I	8.3	0.066	0.127	2.48	0.097	2.30	>150
5b	methyl	11.5	0.009	0.082	0.189	0.080	0.275	31.30
5c	cyclopropyl	10.8	0.064	0.403	0.379	0.291	0.302	>150
5d	ethynyl	8.7	0.020	0.132	1.09	0.111	0.885	>150
5e	pent-1-ynyl	6.7	0.116	0.243	6.77	0.181	2.71	112.9
5f	phenyl	8.1	0.063	0.385	5.90	0.307	1.70	40.7
5g	2-naphthyl	14.4	0.048	0.695	1.40	0.550	0.700	7.63
5h	1-naphthyl	4.4	1.10	0.497	18.90	0.470	7.23	42.45
5i	5-acenaphthenyl	2.5	1.16	1.63	>45	1.53	35.85	>150
5j	9-phenanthrenyl	4.4	0.061	0.900	>45	1.40	>45	65.45
5k	4-biphenyl	12.3	0.013	0.173	0.346	0.092	0.235	2.95
5l	4-(2-naphthyl)phenyl	13.0	0.032	0.132	1.00	0.160	0.950	3.06
5m	4-[(2-naphthoxy)methyl]phenyl	13.1	0.043	0.113	1.75	0.095	1.29	2.58
5n	2-furyl	8.9	0.025	0.163	0.816	0.115	0.469	41.30
5o	2-thienyl	9.8	0.028	0.174	0.647	0.184	1.85	27.30
5p	2-benzofuryl	12.1	0.076	0.060	0.334	0.085	0.176	10.94
5q	2-benzothienyl	13.5	0.035	0.195	0.350	0.330	0.250	8.69
5r	4-dibenzofuryl	7.1	0.367	0.503	8.97	0.869	7.07	19.10
6f	phenyl	1.0	6.41 <sup>d</sup>	9.42 <sup>d</sup>	19.49 <sup>d</sup>	10.30 <sup>d</sup>	0.271 <sup>d</sup>	>150 <sup>d</sup>
7a	I	4.4	0.101	0.896	>45	0.780	12.85	>150
7f	phenyl	5.1	0.110	0.367	10.37	0.280	4.480	>150
8a	I	0.5	3.488	>45	>45	>45	>45	>150
8f	phenyl	-0.6	>45	>45	>45	>45	>45	>150
2'3'-cGAMP		15.3	0.020	0.021	0.074	0.041	0.048	28.37
3'3'-cGAMP		5.1	0.121	0.123	4.26	0.260	2.06	68.37
2'2'-cGAMP		2.5	0.260	0.189	59.54	0.173	7.09	>150
ADU-S100		9.3 <sup>e</sup>	0.08 <sup>e</sup>	0.26 <sup>e</sup>	1.64 <sup>e</sup>	0.23 <sup>e</sup>	1.01 <sup>e</sup>	3.32 <sup>e</sup>

<sup>a</sup>Values were obtained using DSF assay with wt hSTING as described in the Methods section. Measurements were performed as two independent experiments ( $n = 2$ ). <sup>b</sup>Results of digitonin assay in 293T reporter cells expressing hSTING allelic variants were obtained as described in the Methods section.  $\text{EC}_{50}$  values are the mean of three independent experiments ( $n = 3$ ) measured in triplicate with SD < 50% of  $\text{EC}_{50}$  values. <sup>c</sup>Results of standard assay in 293T reporter cells expressing wt hSTING were obtained as described in the Methods section.  $\text{EC}_{50}$  values are the mean of two independent experiments ( $n = 2$ ) measured in triplicate with SD < 50% of  $\text{EC}_{50}$  values. <sup>d</sup>Data from one experiment only ( $n = 1$ ). <sup>e</sup>Data from Dejinek et al.<sup>50</sup>

2-fold compared to 5f. However, we observed a deterioration of activity in the standard cell-based reporter assay similar to compounds 5c and 5d. According to data from both DSF and cell-based reporter assays, substitutions in 6f caused a significant drop of STING activity and led to the inactivity of 8f. Substitutions in these compounds might potentially lead

to the disruption of interactions with both R238 residues, which we have already reported to significantly affect the binding of CDNs.<sup>47</sup>

When we considered the fact that the results for 5n and 5o showed better activity than compounds with phenyl substituents 5–8f, we focused on larger heterocycles like

benzofuryl (**5p**), benzothienyl (**5q**), and dibenzofuryl (**5r**). For **5p** and **5q**, we observed an increase in  $\Delta T_m$  by more than 3 °C when compared to **5n** and **5o**, respectively. Higher  $\Delta T_m$  suggests increasing stabilization of complex STING–CDN.<sup>47,48</sup> We can only speculate that this stabilization could be related to the introduction of a benzofused heterocycle, which might be in a better position to form  $\pi$ – $\pi$  stacking with guanine. Consistent with DSF, we observed that **5p** showed lower  $EC_{50}$  values than **5n**, except for wild-type STING. Derivative **5q** showed lower  $EC_{50}$  for REF and Q than **5o**. Compound **5r** did not show any improvement in DSF or in digitonin assay when compared to **5n**, **5o**, **5p**, or **5q**. Nevertheless, all **5p**, **5q**, and **5r** compounds showed an improvement in a standard assay compared to **5n**, **5o**, and 2′3′-cGAMP. In the case of **5q**, it was 3-fold better than 2′3′-cGAMP.

We proved that there is a space for larger modifications without a reduction in activity in position 7 of 7-deazaadenine in 2′3′-cGAMP. When correlated with findings about improved activity in the standard assay for compounds with heterocyclic substituents, we designed compounds modified with large 2-naphthyl (**5g**), 1-naphthyl (**5h**), 5-acenaphthenyl (**5i**), and 9-phenanthrenyl (**5j**) substituents. Interestingly, derivatives **5h**, **5i**, and **5j** showed lower  $\Delta T_m$  and considerably higher  $EC_{50}$ s compared to **5n**, **5o**, **5p**, **5q**, and **5r**. On the other hand, **5g** showed a  $\Delta T_m$  of 14.4 °C and a nearly 4-fold lowered  $EC_{50}$  in a standard cell-based reporter assay when compared to 2′3′-cGAMP. Unfortunately, **5g** showed lower activation of HAQ, AQ, and REF allelic forms. These results show that interactions in the STING binding pocket are more likely to tolerate substitutions pointing above the adenine moiety rather than substitutions that need additional interactions and space around the cGAMP molecule.

We designed a 4-biphenyl-substituted 2′3′-cGAMP (**5k**) by applying our findings about the preference of the STING protein in the site above AMP in 2′3′-cGAMP and with the knowledge of the relative flexibility of the lid above the binding.<sup>81</sup> The biphenyl substituent brings additional lipophilicity to the compound, as in the case of **5g**, but with the substitution pointing above the cGAMP molecule, as in the case of **5f**. This substitution caused a decrease of only 3 °C in DSF, and  $EC_{50}$ s were comparable to those of 2′3′-cGAMP. Moreover, **5k** showed nearly 10 times better activity than 2′3′-cGAMP in the standard assay.

Considering the results for **5k**, we designed a substitution with 4-(2-naphthyl)phenyl (**5l**). This modification resulted in nearly the same  $\Delta T_m$  and  $EC_{50}$ s despite the change from phenyl to naphthyl, which might cause more significant collisions with the lid of the STING binding pocket.

Compound **5m** contained the largest modification we introduced, 4-[(2-naphthoxy)methyl]phenyl. Despite the introduction of such a large modification that was expected to largely clash with a lid of the STING binding pocket, we observed similar complex stability for **5m** and **5l** in DSF. Moreover, we observed comparable activities in cell-based reporter assays. When comparing the activities of derivatives **5k–m** with those of the clinical candidate ADU-S100,<sup>23,50</sup> similar or better activities were observed in digitonin assay. Moreover, in the standard 293T cell-based assay, compounds **5k–m** showed lower  $EC_{50}$  values than ADU-S100. To explain potent activities of compounds **5k–m**, we solved the X-ray crystallographic structure for the complex of STING and corresponding CDNs.

**Structural Studies.** To understand the interactions of large moieties in position 7 of 7-deazaadenine in 2′3′-cGAMPs, we crystallized human wild-type STING truncated to residues 140–379 in complexes with **5f**, **5k**, **5l**, and **5m** using our improved STING crystallization protocols.<sup>52</sup> Crystal structures were determined at resolution 2.69–1.89 Å, and the asymmetric unit consisted of two STING heterodimers (chain A/B) and one molecule of the ligand (Table S1). Protein residues were modeled into a well-defined electron density map, except for several regions belonging to flexible surface exposed loops that could not be resolved owing to their dynamic disorder (Table S2). All ligands were modeled into the binding site with full occupancy; however, some parts of the maps for substitutions of position 7 of 7-deazaadenine were not as well defined, suggesting some flexibility of this part of the molecule (Figure 2A).

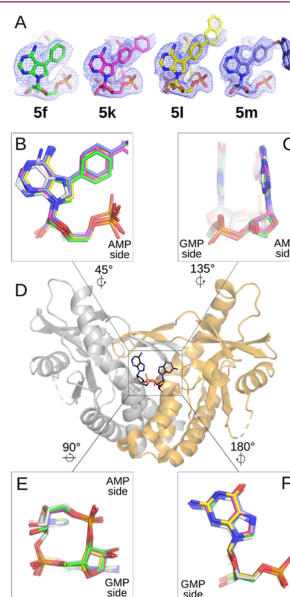


**Figure 2.** Crystal structures of human STING in complex with 2′3′-cGAMPs. (A) Binding poses of compounds are shown with  $2F_o - F_c$  maps contoured at  $1\sigma$ . Compounds are distinguished by carbon colors (**5f** in green, PDB 8A2H; **5k** in purple, PDB 8A2J; **5l** in yellow, PDB 8A2K; and **5m** in blue, PDB 8A2L), while nitrogen, oxygen, and phosphorus atoms are colored blue, red, and orange. (B) AMP side view of **5f**, **5k**, **5l**, and **5m** binding poses superposed with 2′3′-cGAMP (PDB 4KSY), showing the trend in positions of 7-deazaadenosine for all of our compounds, which differs from the position of adenosine in 2′3′-cGAMP (in white). (C) Side view superposition of ligands showing similarity of localization of nucleobases in this orientation. (D) Human STING dimer shown as a biological unit with differently colored monomers with 2′3′-cGAMP located in the binding site (PDB 4KSY). (E) Bottom view and (F) GMP side view of superposed ligands.

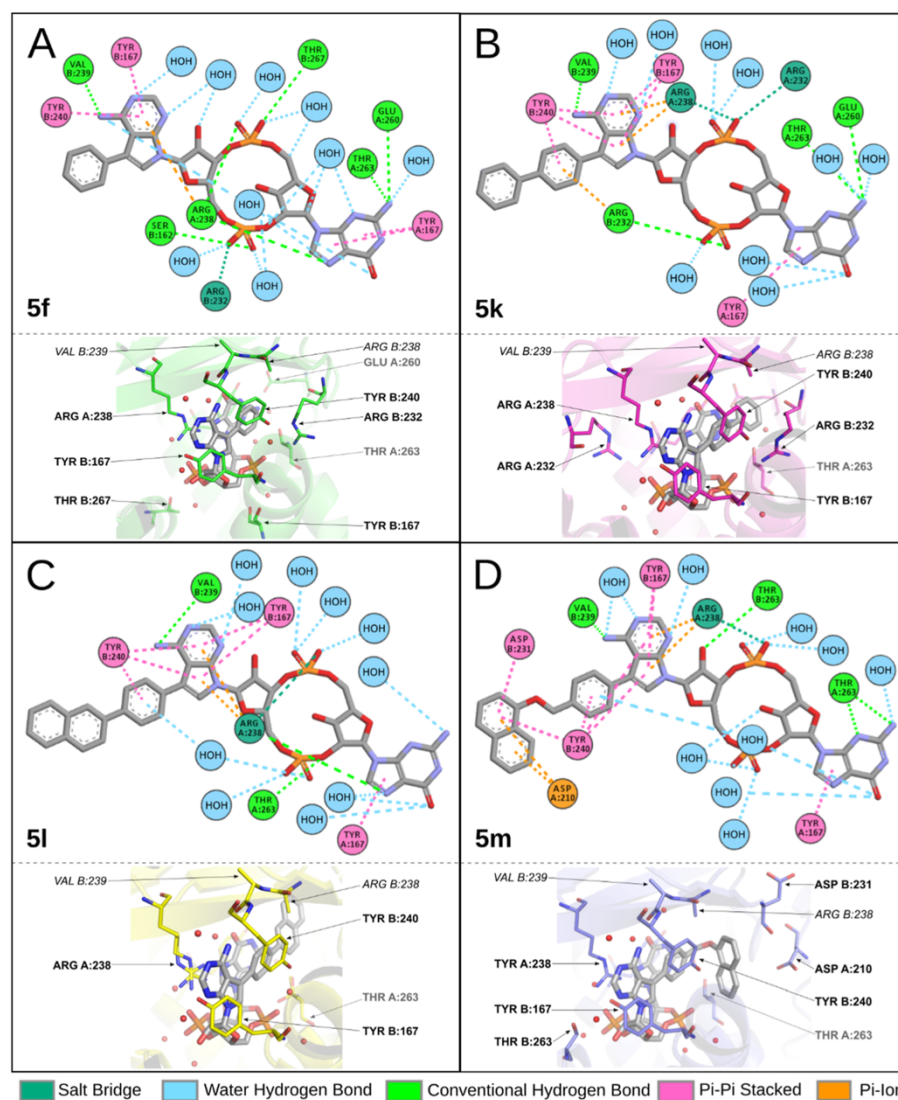


**Figure 3.** Interaction scheme of 5f (A; PDB 8A2H), 5k (B; PDB 8A2J), 5l (C; PDB 8A2I), and 5m (D; PDB 8A2K) in STING ligand-binding site, as seen in our structures.

The binding site is formed at the interface of two STING monomers and is covered by two “lids” (residues 227–241). The electron density for the lid region was mostly well defined, with some exceptions pointing to residues disordered by the

binding of a voluminous ligand (residue Ile235 in **5l** complex; Arg232 in **5m** complex; and Tyr240 in **5k**, **5l**, and **5m**, Figure S1). Ligands are deeply buried in the binding site (Figure 3), with basic orientation resembling that of natural ligand 2’3’-

cGAMP (PDB 4KSY).<sup>5</sup> Most of the interactions observed in the binding site were similar to those described for a natural ligand (Figure S2): Tyr167  $\pi$ - $\pi$  stacking with nucleobases, Arg232 forming a salt bridge with phosphates, a side chain of Thr263 forming a hydrogen bond with NH<sub>2</sub> of guanine, Arg238 interacting through a hydrogen bond with phosphates, and Arg238 cation- $\pi$  stacking with nucleobases on the opposite of the binding site. Ribose moiety and the central part are linked to the protein residues through a network of water-mediated hydrogen bonds. In all our structures, we also observed Val239 carbonyl forming a hydrogen bond with NH<sub>2</sub> at 7-deazaadenosine and Tyr240  $\pi$ - $\pi$  stacking with introduced aromatic substituents (Figure 3).

When comparing the binding pose of the natural ligand with our compounds, the GMP side for all of the compounds shows only an insignificant shift in position (Figure 2C,E,F). For the AMP side, the ribose and nucleobase are slightly shifted upward, potentially because of our large substitutions at 7-deazaadenine. The substitutions in all of our structures displace the side chain of Arg238 from chain B and thus prevent interaction with guanosine (Figure 2B,C). This shift enables direct interaction with Tyr240 from chain B that was not observed for the natural ligand binding. This residue interacts with 7-deazaadenine through parallel displaced  $\pi$ - $\pi$  stacking. This interaction is enabled by a change of AMP positioning, and the extent of its interaction with Tyr240 differs in our structures due to the different sizes of substituents. Additionally, for the bulky substituent **5m**, we observed unique interactions with Asp234 and Asp210, respectively (Figure 3D).

The main difference between the binding of the **5f** molecule and the binding of the natural ligand 2'3'-cGAMP that we observed is the interaction of **5f** with Tyr240, as described earlier (Figure 3A). By modifying 7-deazaadenine with phenyl, we displaced Arg238 from chain B; we also brought additional intramolecular stabilization of the ligand conformation through cation- $\pi$  stacking of the phenyl moiety with guanosine on the opposite side of the molecule. However, this interaction was not sufficient and resulted in lower stability of STING-**5f** in DSF compared to 2'3'-cGAMP and **5b**.

Intramolecular interactions were further strengthened in compound **5k**, where the phenyl ring was replaced by biphenyl. Similar to **5f**, this led to a stacking interaction between Tyr240 and nucleobase. Additionally, Tyr240 was involved in a stacking interaction with the phenyl closer to the nucleobase in biphenyl substituent (Figure 3B), which resulted in a 1.5-fold higher stability of STING-**5k** complex in DSF when compared to **5f**.

For **5l** with a 4-(2-naphthyl)phenyl substitution, we preserved the interactions that were observed for **5k** (Figure 3C); however, naphthyl substitution clashed with Ile235 of the lid, making this residue disordered (Figure S1). Despite this clash, **5l** exhibited a slightly better stabilization of complex in DSF when compared to **5k** (Table 1).

Compound **5m** showed additional  $\pi$ -stacking interactions with Tyr240 and an unexpected change in the binding mode of the substituent. The structural reason for this is a change in the position of the naphthyl group, that is, in **5m**, observed in the position regularly occupied by the Arg232 side chain. This position change is allowed due to the flexibility of the longer methoxy linker connecting the naphthyl group that enables the formation of a T-shaped  $\pi$ -stacking between the naphthyl of **5m** and Tyr240,  $\pi$ -amide interaction with the backbone of

Asp231 and  $\pi$ -anion interaction with Asp210 (Figure 3D). A substitution at **5m** resulted in just a slightly lower stabilization in DSF when compared to 2'3'-cGAMP.

**PBMC Assay.** Selected compounds were further tested for induction of IFN $\gamma$ , TNF $\alpha$ , and IFN $\alpha$  secretion using PBMCs (Table 2). None of the tested compounds showed any

**Table 2. Cytokine Level Determination in PBMCs upon Treatment with Synthesized Compounds**

compound	EC <sub>50</sub> ( $\mu$ M) <sup>a</sup>		
	IFN $\gamma$	TNF $\alpha$	IFN $\alpha$
<b>5b</b>	7.8	50.60	30.60
<b>5c</b>	1.29	37.59	4.95
<b>5f</b>	6.84	52.45	7.36
<b>5g</b>	7.54	98.80	11.71
<b>5h</b>	34.51	>200	28.78
<b>5i</b>	85.20	>200	74.73
<b>5j</b>	47.54	>200	>200
<b>5k</b>	2.05	13.64	7.43
<b>5l</b>	1.77	53.86	5.09
<b>5m</b>	1.16	43.38	4.27
<b>5n</b>	2.24	6.72	2.80
<b>5o</b>	2.60	2.66	2.88
<b>5p</b>	8.33	24.56	12.84
<b>5q</b>	0.87	1.43	4.04
<b>5r</b>	5.63	99.70	26.98
<b>7f</b>	12.56	65.77	6.92
2'3'-cGAMP	7.10	36.03	8.46
3'3'-cGAMP	17.25	18.72	7.65
2'2'-cGAMP	11.75	44.54	7.21

<sup>a</sup>EC<sub>50</sub> values are the mean of three independent experiments ( $n = 3$ ), each of them performed on PBMCs from a different donor, measured in triplicate with SD < 50% of EC<sub>50</sub> values.

cytotoxicity (Table S4). Most of the tested compounds induced higher levels of IFN $\gamma$ , TNF $\alpha$ , and IFN $\alpha$  secretion when compared to 2'3'-cGAMP. EC<sub>50</sub> obtained from testing at PBMCs correlated with data from a standard 293T cell-based reporter assay for most of the tested compounds.

## CONCLUSIONS

Here, we report the design, synthesis, and biochemical and biological evaluation of a novel class of 7-substituted 7-deazaadenine containing CDNs capable of STING activation. During the preparation of this class of compounds, we demonstrated a mixed enzymatic-chemical synthetic approach for the preparation of CDNs. This approach allowed us to efficiently overcome the total synthesis of the whole CDN, a multistep and time-consuming process.<sup>53</sup> In the optimization process of biochemical binding potency of our compounds, SAR revealed an unexpected potential for modifications with large aromatic groups. This potential is applicable for 2'3'-cGAMP analogues with a preference for modifications that point above the CDN molecule. We observed  $\pi$ - $\pi$  stacking interactions between the aromatic substituents and Tyr240 that are involved in stabilization of CDN-STING complexes. In the case of 3'3'-cGAMP and  $\epsilon$ -di-AMP, our modifications did not lead to increased binding potency. Substitutions with large aromatic moieties increased lipophilicity and thus potentially permeability into cells. They might also be more efficiently transported by an SLC19A1 receptor or an LRRc8A transporter, which would result in improved cellular activity.<sup>54</sup>



## ■ EXPERIMENTAL SECTION

**General Synthetic and Enzymatic Methods.** Unless otherwise noted, all starting materials, solvents, and reagents were purchased from commercial suppliers and used as received. 7-Iodo-7-adenosine **9** and 7-deazapurine NTPs **2b-f**, **3a-d**, **6n**, and **o** were prepared according to the literature.<sup>37,44,45,55</sup> The synthesis of **3e** is described in the Supporting Information (Scheme S1). All chemical reactions were performed under an argon atmosphere. Reactions were monitored by thin layer chromatography (TLC) on TLC Silica gel 60 F<sub>254</sub> (Merck) and detected by UV (254 nm). NMR spectra were measured on a Bruker AVANCE 500 MHz spectrometer (499.8 MHz for <sup>1</sup>H, 125.7 MHz for <sup>13</sup>C, and <sup>31</sup>P at 202.4 MHz) or on a Bruker 600 AVANCE III HD instrument (<sup>1</sup>H at 600 MHz, <sup>13</sup>C at 150.9 MHz) equipped with 5 mm cryo-probe at 25 °C in D<sub>2</sub>O (dioxane used as external standard, [ $\delta$ (<sup>1</sup>H) = 3.75 ppm,  $\delta$ (<sup>13</sup>C) = 67.19 ppm]) or in CD<sub>3</sub>OD (referenced to the residual solvent signal, [ $\delta$ (<sup>1</sup>H) = 3.31 ppm,  $\delta$ (<sup>13</sup>C) = 49.0 ppm]). <sup>31</sup>P NMR spectra were referenced externally to the signal of H<sub>3</sub>PO<sub>4</sub>. Chemical shifts are given in ppm ( $\delta$ -scale), and coupling constants (*J*) are given in Hz. The complete assignment of all NMR signals was performed using a combination of H,H-COSY, H,H-ROESY, H,C-HSQC, and H,C-HMBC experiments. Low resolution mass spectra were measured using electrospray ionization (ESI). High resolution mass spectra were measured on LTQ Orbitrap XL (Thermo Fisher Scientific) using ESI. High performance flash chromatography (HPFC) was performed with ISCO Combiflash Rf system on RediSep Rf Gold Silica Gel columns or Reverse Phase (C18) RediSep Rf Gold columns. Purification of CDNs was performed using HPLC (Waters modular HPLC system) on a column packed with 5  $\mu$ m polar C18 reversed phase (Luna Omega 5  $\mu$ m Polar C18 column, Phenomenex). The purity of all final compounds was determined by clean NMR spectra and by UPLC. The identification of CDNs was performed on ACQUITY UPLC H-Class PLUS chromatographic system with MS SQ Detector 2 (Waters, Milford, USA) using Acuity UPLC BEH C18 column 50 mm  $\times$  2.1 mm, 1.7  $\mu$ m (Waters, Milford, MA, USA), and 20 mM ammonium acetate buffer, pH 6.8, with a linear gradient of acetonitrile (0 to 50% in 4 min, additional 2 min at 50% acetonitrile; flow rate 0.5 mL/min). Column temperature was kept at 40 °C. Negative ESI method was used for ionization. UPLC purity (>95% with exception of enzymatically synthesized CDNs **4b**, **5b**, and **5e**) is shown in Table S3.

**Enzymatic Synthesis.** Enzymatically prepared 2'3'-CDNs (Schemes 3 and 4) were synthesized using mcGAS as described previously.<sup>20</sup> Briefly, the appropriate NTPs were mixed to the final 2 mM concentration with 5  $\mu$ M of mcGAS and 0.1 mg/mL herring testes DNA in 1 mL buffer containing 20 mM Tris-HCl [pH 8.0] and 20 mM MgCl<sub>2</sub>, and incubated for 16 h at 37 °C in a heating shaker. The synthesis of **7a** was performed by using 2 mM **3a**, 2 mM GTP, and 2  $\mu$ M DncV in 1 mL of 50 mM HEPES buffer [pH 8.0] supplemented with 100 mM NaCl, 10 mM MgCl<sub>2</sub>, and 1 mM DTT. The whole mixture was incubated overnight at 37 °C in a heating shaker. The synthesis of **8a** was done overnight at 50 °C in a 1 mL reaction mixture containing 4 mM **3a**, 20  $\mu$ M DisA, and 50 mM HEPES buffer [pH 8.0] supplemented with 100 mM NaCl, 10 mM MgCl<sub>2</sub>, and 1 mM DTT. The next morning, the reactions were spun at 25,000g for 15 min and supernatants were passed through Nanosep 3K Omega (Pall Corporation, USA). The purification of CDNs was continued by adding 3 mL of ddH<sub>2</sub>O to the flow-through fractions, and CDNs were purified on a semipreparative C18 column (Luna 5  $\mu$ m C18 250 mm  $\times$  10 mm) using a 60 min gradient at a flow rate of 3 mL/min of 0–20% acetonitrile in 0.1 M TEAB buffer [pH 8.5]. TEAB was removed from the collected fractions by 3 cycles of evaporation/dissolution in 50% methanol.

**Cyclo-adenosine 5'-O-Phosphate (3'  $\rightarrow$  5') 2-Amino-5-methyl-7- $\beta$ -D-ribofuranosyl-7H-pyrrolo[2,3-d]pyrimidin-4(3H)-one 5'-O-Phosphate (2'  $\rightarrow$  5') Sodium Salt (**4b**).** NTP **2b** (2  $\mu$ mol) and ATP (2  $\mu$ mol) were enzymatically cyclized using mcGAS. The final product was purified by HPLC (5–30% MeCN in 0.1 M TEAB). The conversion to a sodium salt form on a Dowex 50WX8 (in a Na<sup>+</sup> cycle) provided CDN **4b** (73 nmol, 4%). <sup>1</sup>H NMR (600 MHz, D<sub>2</sub>O): 1.81

(bs, 3H, CH<sub>3</sub>); 4.14 (ddd, 1H, *J*<sub>5',6',4'</sub> = 1.7, *J*<sub>5',6',5''</sub> = 11.8, *J*<sub>5',6'</sub> = 3.4, HS'b-G); 4.23 (ddd, 1H, *J*<sub>5',6',4'</sub> = 2.3, *J*<sub>5',6',5''</sub> = 11.8, *J*<sub>5',6'</sub> = 2.7, HS'a-G); 4.23 (ddd, 1H, *J*<sub>5',6',4'</sub> = 1.4, *J*<sub>5',6',5''</sub> = 12.1, *J*<sub>5',6'</sub> = 3.6, HS'b-A); 4.37 (ddd, 1H, *J*<sub>4',5',4'</sub> = 2.3, *J*<sub>4',5',6'</sub> = 1.7, *J*<sub>4',5'</sub> = 3.8, H4'-G); 4.47 (m, 1H, HS'a-A); 4.49 (dm, 1H, *J*<sub>4',5',6'</sub> = 8.7, H4'-A); 4.62 (d, 1H, *J*<sub>5',4'</sub> = 4.1, H3'-G); 4.75 (dd, *J*<sub>5',1'</sub> = 1.1, *J*<sub>5',3'</sub> = 4.3, H2'-A); 4.99 (ddd, 1H, *J*<sub>5',2'</sub> = 4.3, *J*<sub>5',4'</sub> = 8.7, *J*<sub>5',6'</sub> = 6.9, H3'-A); 5.33 (um, 1H, H2'-G); 6.01 (d, 1H, *J*<sub>1',2'</sub> = 8.3, H1'-G); 6.19 (d, 1H, *J*<sub>1',2'</sub> = 1.1, H1'-A); 6.83 (q, 1H, *J*<sub>8,CH3</sub> = 1.3, H8-G); 8.23 (s, 1H, H8-A); 8.27 (s, 1H, H2-A). <sup>13</sup>C NMR (150.9 MHz, D<sub>2</sub>O): 12.90 (5-CH<sub>3</sub>); 65.61 (C5'-A); 68.75 (C5'-G); 73.55 (C3'-A); 74.20 (C3'-G); 76.54 (C2'-A); 79.46 (C2'-G); 83.02 (C4'-A); 85.95 (C4'-G); 87.70 (C1'-G); 92.47 (C1'-A); 103.55 (C5-G); 118.24 (C4a-G); 119.52 (C6-G); 121.67 (C5-A); 141.42 (C8-A); 150.64 (C4-A); 154.81 (C7a-G); 155.07 (C2-G); 155.40 (C2-A); 158.26 (C6-A). <sup>31</sup>P NMR (<sup>1</sup>H-dsc, 202.4 MHz, D<sub>2</sub>O): -0.20 and -1.02. ESI MS *m/z* (rel. %): 342 (100) [M-2H]<sup>2-</sup>, 686 (37) [M-H]<sup>-</sup>, 708 (8) [M-2H+Na]<sup>-</sup>. HR MS (ESI): for C<sub>22</sub>H<sub>32</sub>N<sub>6</sub>O<sub>13</sub>P<sub>3</sub> [M-H]<sup>-</sup>, calcd 686.11308; found, 686.11212.

**Cyclo-4-amino-5-iodo-7- $\beta$ -D-ribofuranosyl-7H-pyrrolo[2,3-d]pyrimidine 5'-O-Phosphate (3'  $\rightarrow$  5') Guanosine 5'-O-Phosphate (2'  $\rightarrow$  5') Sodium Salt (**5a**).** Enzymatic synthesis: NTP **3a** (75  $\mu$ mol, 107  $\mu$ mol) and GTP (107  $\mu$ mol) were enzymatically cyclized using mcGAS. The final product was purified by HPLC (5–30% MeCN in 0.1 M TEAB). The conversion to a sodium salt form on a Dowex 50WX8 (in a Na<sup>+</sup> cycle) provided CDN **5a** (56 mg, 61%) as a white lyophilizate (water).

**Chemical synthesis:** Phosphonate **12** (161 mg, 0.21 mmol) was dissolved in DCM (2.5 mL). Water (38  $\mu$ L, 2.11 mmol) and dichloroacetic acid in DCM (6%, 2.5 mL, 1.81 mmol) were added, and the solution was stirred for 10 min. Then, pyridine (298  $\mu$ L, 3.70 mmol) was added, and the mixture was evaporated under reduced pressure and co-evaporated with anhydrous acetonitrile (3 $\times$ ). The residue was dissolved in anhydrous acetonitrile (480  $\mu$ L), and a solution of phosphoramidite **13** (262 mg, 0.268 mmol) in anhydrous acetonitrile (1.45 mL) was added. The mixture was stirred at rt for 10 min, then *t*-butylhydroperoxide (5.5 mL solution in decane, 113  $\mu$ L, 0.621 mmol) was added, and the stirring continued for another 30 min. Then, the solution was cooled to 0 °C, and a solution of NaHSO<sub>3</sub> (33% wt, 627  $\mu$ L, 2.46 mmol) was added. The mixture was stirred for 10 min at 0 °C and then for 5 min at rt. Then, solvent was removed in vacuo, and the residue was dissolved in DCM (3.22 mL). Water (38  $\mu$ L, 2.11 mmol) and dichloroacetic acid in DCM (6%, 3.22 mL, 2.33 mmol) were added. The mixture was stirred for 10 min, then pyridine (670  $\mu$ L, 8.32 mmol) was added, and the mixture was evaporated under reduced pressure and co-evaporated with water. Product **14** was partially purified by flash chromatography (C18 column, gradient 5–100% MeCN in 0.1 M TEAB).

Crude **14** was co-evaporated with anhydrous pyridine (3  $\times$  2 mL) and dissolved in anhydrous pyridine (2.6 mL). DMOCOP was added (85 mg, 0.46 mmol), and the mixture was stirred for 110 min at rt. Then, water (77  $\mu$ L, 0.46 mmol) and iodine (44 mg, 0.46 mmol) were added, and the stirring continued for another 10 min at rt. The mixture was cooled to 0 °C, and an aqueous solution of NaHSO<sub>3</sub> (40% wt, 64  $\mu$ L) was added. After stirring for 5 min at 0 °C, another portion of NaHSO<sub>3</sub> solution (40% wt, 40  $\mu$ L) was added. The clear solution was evaporated under reduced pressure and co-evaporated with water. Crude **15** was partially purified by flash chromatography (C18 column, gradient 5–100% MeCN in 0.1 M TEAB).

Crude **15** was dissolved in ethanolic solution of CH<sub>3</sub>NH<sub>2</sub> (33% wt, 4 mL, 32.1 mmol), and the solution was stirred for 3 h at rt. Then, the mixture was evaporated under reduced pressure, and the residue was co-evaporated with anhydrous pyridine (3  $\times$  2 mL). A mixture of anhydrous pyridine, Et<sub>3</sub>N (1:1 v/v, 4 mL), and Et<sub>3</sub>N-3HF (640  $\mu$ L, 3.93 mmol) was added, and the mixture was stirred at 50 °C for 3.5 h. Then, aqueous ammonium acetate (1 M, 6 mL) was added, and the solvents were removed in vacuo. The residue was co-evaporated with water. After HPLC purification (0–15% MeCN in 0.1 M TEAB) and conversion to a sodium salt form on a Dowex 50WX8 (in a Na<sup>+</sup> cycle), CDN **5a** (32 mg, 18% overall yield) was obtained as a white lyophilizate (water). <sup>1</sup>H NMR (600 MHz, D<sub>2</sub>O): 4.14 (ddd, 1H, *J*<sub>5',6',4'</sub>

= 1.8,  $J_{5b,5a} = 11.7$ ,  $J_{5b,p} = 2.1$ , HS'b-G); 4.22 (ddd, 1H,  $J_{5a,4'} = 3.1$ ,  $J_{5a,5b} = 11.7$ ,  $J_{5a,p} = 4.6$ , HS'a-G); 4.23 (ddd, 1H,  $J_{5b,5a} = 12.0$ ,  $J_{5b,4'} = 1.3$ ,  $J_{5b,p} = 2.2$ , HS'b-A); 4.41 (ddd, 1H,  $J_{4',5a} = 3.1$ ,  $J_{4',5b} = 1.8$ ,  $J_{4',p} = 3.6$ , H4'-G); 4.44 (dm, 1H,  $J_{4',5'} = 9.3$ , H4'-A); 4.52 (dm, 1H,  $J_{5a,5b} = 12.0$ , HS'a-A); 4.61 (d, 1H,  $J_{5',2'} = 4.0$ , H3'-G); 4.67 (bd, 1H,  $J_{5',2'} = 4.0$ , H2'-A); 4.92 (ddd, 1H,  $J_{5',2'} = 4.0$ ,  $J_{5',4'} = 9.3$ ,  $J_{5',p} = 6.6$ , H3'-A); 5.62 (ddd, 1H,  $J_{1',2'} = 8.6$ ,  $J_{2',3'} = 4.0$ ,  $J_{2',p} = 4.4$ , H2'-G); 5.94 (d, 1H,  $J_{1',2'} = 8.6$ , H1'-G); 6.10 (s, 1H, H1'-A); 7.71 (s, 1H, H6-A); 7.88 (s, 1H, H8-G); 8.09 (s, 1H, H2-A).  $^{13}\text{C}$  NMR (150.9 MHz, D<sub>2</sub>O): 51.15 (C5-A); 65.23 (d,  $J_{C,p} = 4.5$ , C5'-A); 68.48 (d,  $J_{C,p} = 5.2$ , C5'-G); 72.88 (d,  $J_{C,p} = 5.6$ , C3'-A); 73.75 (C3'-G); 76.68 (C2'-A); 77.43 (d,  $J_{C,p} = 5.4$ , C2'-G); 82.55 (t,  $J_{C,p1} = J_{C,p2} = 11.3$ , C4'-A); 85.14 (d,  $J_{C,p} = 10.1$ , C4'-G); 89.10 (d,  $J_{C,p} = 12.0$ , C1'-G); 92.50 (C1'-A); 106.80 (C4a-A); 120.60 (C5-G); 129.42 (C6-A); 143.38 (C8-G); 150.09 (C7a-A); 153.95 (C2-A); 154.71 (C4-G); 155.84 (C2-G); 159.59 (C4-A); 161.74 (C6-G).  $^{31}\text{P}$  NMR ( $^1\text{H}$ -dec, 202.4 MHz, D<sub>2</sub>O): -0.32 and -1.41. ESI MS  $m/z$  (rel. %): 398 (100) [M-2H] $^{2-}$ , 798 (97) [M-H] $^{-}$ , 820 (30) [M-2H + Na] $^{-}$ . HR MS (ESI): for C<sub>22</sub>H<sub>33</sub>O<sub>13</sub>N<sub>5</sub>P<sub>2</sub>, [M-H] $^{-}$ , calcd 797.99407; found, 797.99335.

**Cyclo-4-amino-5-methyl-7-β-D-ribofuranosyl-7H-pyrrolo[2,3-dj-pyrimidine 5'-O-Phosphate (3' → 5') Guanosine 5'-O-Phosphate (2' → 5') Sodium Salt (5b).** NTP 3b (2 μmol) and GTP (2 μmol) were enzymatically cyclized using mcGAS. The final product was purified by HPLC (5–30% MeCN in 0.1 M TEAB). The conversion to a sodium salt form on a Dowex 50WX8 (in a Na<sup>+</sup> cycle) provided CDN 5b (354 nmol, 18%).  $^1\text{H}$  NMR (600 MHz, D<sub>2</sub>O): 1.98 (d, 3H,  $J_{CH3,p} = 1.1$ , CH<sub>3</sub>); 4.17 (m, 1H, HS'b-G); 4.18 (ddd, 1H,  $J_{5b,5a} = 11.7$ ,  $J_{5b,4'} = 2.4$ ,  $J_{5b,p} = 1.8$ , HS'b-A); 4.26 (ddd, 1H,  $J_{5a,5b} = 11.7$ ,  $J_{5a,4'} = 3.2$ ,  $J_{5a,p} = 4.7$ , HS'a-A); 4.43 (m, 2H, H4'-A and H4'-G); 4.44 (m, 1H, HS'a-G); 4.63 (d, 1H,  $J_{5',2'} = 4.1$ , H3'-G); 4.71 (bd, 1H,  $J_{5',2'} = 4.3$ , H2'-A); 5.06 (ddd, 1H,  $J_{5',2'} = 4.3$ ,  $J_{5',4'} = 9.0$ ,  $J_{5',p} = 6.7$ , H3'-A); 5.62 (ddd, 1H,  $J_{1',2'} = 8.5$ ,  $J_{2',3'} = 4.1$ ,  $J_{2',p} = 6.6$ , H2'-G); 5.96 (d, 1H,  $J_{1',2'} = 8.5$ , H1'-G); 6.23 (s, 1H, H1'-A); 7.36 (q, 1H,  $J_{6,CH3} = 1.1$ , H6-A); 7.92 (s, 1H, H8-G); 8.19 (bs, 1H, H2-A).  $^{13}\text{C}$  NMR (150.9 MHz, D<sub>2</sub>O); chemical shifts obtained from 2D-HSQC and 2D-HMBC spectra;  $J(C,P)$  and shifts of C4-A, C2-G, and C6-G were not determined): 13.29 (CH<sub>3</sub>); 64.98 (C5'-A); 68.33 (C5'-G); 73.32 (C3'-A); 73.85 (C3'-G); 77.08 (C2'-A); 77.49 (C2'-G); 82.64 (C4'-A); 86.11 (C4'-G); 88.85 (C1'-G); 92.20 (C1'-A); 105.17 (C4a-A); 114.97 (C5-A); 119.83 (C5-G); 123.61 (C6-A); 143.19 (C8-G); 147.84 (C2-A); 149.48 (C7a-A); 154.89 (C4-G).  $^{31}\text{P}$  NMR ( $^1\text{H}$ -dec, 202.4 MHz, D<sub>2</sub>O): -0.27 and -1.18. ESI MS  $m/z$  (rel. %): 342 (100) [M-2H] $^{2-}$ , 353 (3) [M-3H + Na] $^{2-}$ , 686 (36) [M-H] $^{-}$ , 708 (8) [M-2H + Na] $^{-}$ . HR MS (ESI): for C<sub>22</sub>H<sub>37</sub>N<sub>5</sub>O<sub>13</sub>P<sub>2</sub>, calcd 686.11308; found, 686.11212.

**Cyclo-4-amino-5-cyclopropyl-7-β-D-ribofuranosyl-7H-pyrrolo[2,3-dj-pyrimidine 5'-O-Phosphate (3' → 5') Guanosine 5'-O-Phosphate (2' → 5') Sodium Salt (5c).** NTP 3c (2 μmol) and GTP (2 μmol) were enzymatically cyclized using mcGAS. The final product was purified by HPLC (5–30% MeCN in 0.1 M TEAB). The conversion to a sodium salt form on a Dowex 50WX8 (in a Na<sup>+</sup> cycle) provided CDN 5c (387 nmol, 19%).  $^1\text{H}$  NMR (600 MHz, D<sub>2</sub>O): 0.16 m and 0.74 m (2H, H3-cyclopropyl); 0.31 m and 0.47 m (2H, H2-cyclopropyl); 1.52 (m, 1H, H1-cyclopropyl); 4.18 (dt, 1H,  $J_{5b,4'} = 1.8$ ,  $J_{5b,5a} = 11.7$ ,  $J_{5b,p} = 1.8$ , HS'b-G); 4.24 (ddd, 1H,  $J_{5b,5a} = 11.8$ ,  $J_{5b,4'} = 2.6$ ,  $J_{5b,p} \sim 1.0$ , HS'b-A); 4.26 (ddd, 1H,  $J_{5a,4'} = 3.2$ ,  $J_{5a,5b} = 11.7$ ,  $J_{5a,p} = 4.3$ , HS'a-G); 4.41 (dm, 1H,  $J_{4',5'} = 9.2$ , H4'-A); 4.44 (m, 1H,  $J_{5a,5b} = 11.8$ , HS'a-A); 4.45 (m, 1H, H4'-G); 4.66 (d, 1H,  $J_{5',2'} = 4.0$ , H3'-G); 4.70 (d, 1H,  $J_{5',2'} = 4.2$ , H2'-A); 5.05 (ddd, 1H,  $J_{5',2'} = 4.2$ ,  $J_{5',4'} = 9.2$ ,  $J_{5',p} = 6.7$ , H3'-A); 5.65 (ddd, 1H,  $J_{1',2'} = 8.6$ ,  $J_{2',3'} = 4.0$ ,  $J_{2',p} = 4.8$ , H2'-G); 5.98 (d, 1H,  $J_{1',2'} = 8.6$ , H1'-G); 6.22 (s, 1H, H1'-A); 7.10 (s, 1H, H6-A); 7.96 (bs, 1H, H8-G); 8.18 (bs, 1H, H2-A).  $^{13}\text{C}$  NMR (150.9 MHz, D<sub>2</sub>O, chemical shifts of quaternary carbons C2-G, C4-G, C5-G, C6-G, and C2-A were not determined): 6.49 (C2-cyclopropyl); 8.97 (C1-cyclopropyl); 10.80 (C3-cyclopropyl); 65.31 (d,  $J_{C,p} = 5.0$ , C5'-A); 68.48 (d,  $J_{C,p} = 4.7$ , C5'-G); 73.09 (d,  $J_{C,p} = 5.6$ , C3'-A); 73.66 (C3'-G); 76.99 (C2'-A); 77.63 (d,  $J_{C,p} = 5.7$ , C2'-G); 82.42 (dd,  $J_{C,p1} = 11.3$ ,  $J_{C,p2} = 10.5$ , C4'-A); 86.08 (d,  $J_{C,p} = 10.2$ , C4'-G); 89.02 (d,  $J_{C,p} = 12.7$ , C1'-G); 91.94 (C1'-A); 105.76 (C5-A); 121.01 (C6-A); 121.77 (C4a-A); 143.31 (C8-G); 149.79

(C7a-A); 161.15 (C4-A).  $^{31}\text{P}$  NMR ( $^1\text{H}$ -dec, 202.4 MHz, D<sub>2</sub>O): -0.26 and -1.09. ESI MS  $m/z$  (rel. %): 356 (100) [M-2H] $^{2-}$ , 367 (6) [M-3H + Na] $^{2-}$ , 712 (7) [M-H] $^{-}$ , 734 (8) [M-2H + Na] $^{-}$ . HR MS (ESI): for C<sub>24</sub>H<sub>36</sub>O<sub>13</sub>N<sub>5</sub>P<sub>2</sub>, calcd 712.12873; found, 712.12814.

**Cyclo-4-amino-5-ethynyl-7-β-D-ribofuranosyl-7H-pyrrolo[2,3-dj-pyrimidine 5'-O-Phosphate (3' → 5') Guanosine 5'-O-Phosphate (2' → 5') Sodium Salt (5d).** NTP 3d (2 μmol) and GTP (2 μmol) were enzymatically cyclized using mcGAS. The final product was purified by HPLC (5–30% MeCN in 0.1 M TEAB). The conversion to a sodium salt form on a Dowex 50WX8 (in a Na<sup>+</sup> cycle) provided CDN 5d (196 nmol, 10%).  $^1\text{H}$  NMR (600 MHz, D<sub>2</sub>O): 3.41 (s, 1H, -C≡CH); 4.17 (dt, 1H,  $J_{5b,4'} = 2.0$ ,  $J_{5b,5a} = 11.8$ ,  $J_{5b,p} = 2.2$ , HS'b-G); 4.22 (bdd, 1H,  $J_{5b,4'} = 2.5$ ,  $J_{5b,5a} = 12.0$ , HS'b-A); 4.24 (ddd, 1H,  $J_{5a,4'} = 3.1$ ,  $J_{5a,5b} = 11.8$ ,  $J_{5a,p} = 4.6$ , HS'a-G); 4.42 (dt, 1H,  $J_{4',5a} = 3.1$ ,  $J_{4',5b} = 2.0$ ,  $J_{4',p} = 3.1$ , H4'-G); 4.46 (bd, 1H,  $J_{4',2'} = 9.4$ ,  $J_{4',5a} = 2.5$ ,  $J_{4',5b} = 2.5$ , H4'-A); 4.50 (dm, 1H,  $J_{5a,5b} = 12.0$ , HS'a-A); 4.63 (d, 1H,  $J_{5',4'} = 4.1$ , H3'-G); 4.66 (bd, 1H,  $J_{5',2'} = 4.0$ , H2'-A); 4.99 (ddd, 1H,  $J_{5',2'} = 4.0$ ,  $J_{5',4'} = 9.4$ ,  $J_{5',p} = 6.6$ , H3'-A); 5.69 (ddd, 1H,  $J_{1',2'} = 8.5$ ,  $J_{2',3'} = 4.1$ ,  $J_{2',p} = 5.7$ , H2'-G); 5.96 (d, 1H,  $J_{1',2'} = 8.5$ , H1'-G); 6.26 (s, 1H, H1'-A); 7.86 (s, 1H, H6-A); 7.91 (s, 1H, H8-G); 8.23 (s, 1H, H2-A).  $^{13}\text{C}$  NMR (150.9 MHz, D<sub>2</sub>O); chemical shifts obtained from 2D-HSQC and 2D-HMBC spectra;  $J(C,P)$  and shifts of C2-G and C6-G not determined): 61.36 (-C≡CH); 65.02 (C5'-A); 68.40 (C5'-G); 72.82 (C3'-A); 73.82 (C3'-G); 76.91 (C2'-A); 77.38 (C2'-G); 82.47 (C4'-A); 84.18 (-C≡CH); 85.94 (C4'-G); 88.89 (C1'-G); 92.31 (C1'-A); 97.30 (C5-A); 105.67 (C4a-A); 120.22 (C5-G); 130.16 (C6-A); 143.10 (C8-G); 149.06 (C7a-A); 154.62 (C4-G); 151.83 (C2-A); 157.90 (C4-A).  $^{31}\text{P}$  NMR ( $^1\text{H}$ -dec, 202.4 MHz, D<sub>2</sub>O): -0.18 and -1.14. ESI MS  $m/z$  (rel. %): 348 (100) [M-2H] $^{2-}$ , 696 (21) [M-H] $^{-}$ , 718 (16) [M-2H + Na] $^{-}$ . HR MS (ESI): for C<sub>23</sub>H<sub>33</sub>O<sub>13</sub>N<sub>5</sub>P<sub>2</sub>, calcd 696.09743; found, 696.09637.

**Cyclo-4-amino-5-(pent-1-yn-1-yl)-7-β-D-ribofuranosyl-7H-pyrrolo[2,3-dj-pyrimidine 5'-O-Phosphate (3' → 5') Guanosine 5'-O-Phosphate (2' → 5') Sodium Salt (5e).** NTP 3e (2 μmol) and GTP (2 μmol) were enzymatically cyclized using mcGAS. The final product was purified by HPLC (5–30% MeCN in 0.1 M TEAB). The conversion to a sodium salt form on a Dowex 50WX8 (in a Na<sup>+</sup> cycle) provided CDN 5e (84 nmol, 4%).  $^1\text{H}$  NMR (600 MHz, D<sub>2</sub>O): 0.91 (t, 3H, H5-pentynyl); 1.47 (m, 2H, H4-pentynyl); 2.29 (m, 2H, H3-pentynyl); 4.15 (ddd, 1H,  $J_{5b,4'} = 2.0$ ,  $J_{5b,5a} = 11.9$ ,  $J_{5b,p} = 2.0$ , HS'b-G); 4.23 (ddd, 1H,  $J_{5a,4'} = 3.0$ ,  $J_{5a,5b} = 11.9$ ,  $J_{5a,p} = 4.7$ , HS'a-G); 4.25 (dm, 1H,  $J_{5b,5a} = 12.0$ , HS'b-A); 4.41 (dt, 1H,  $J_{4',5a} = 3.0$ ,  $J_{4',5b} = 2.0$ ,  $J_{4',p} = 3.2$ , H4'-G); 4.45 (dm, 1H,  $J_{4',2'} = 9.5$ , H4'-A); 4.51 (dm, 1H,  $J_{5a,5b} = 12.0$ , HS'a-A); 4.62 (d, 1H,  $J_{5',4'} = 4.3$ , H3'-G); 4.63 (d, 1H,  $J_{5',2'} = 4.1$ , H2'-A); 4.98 (ddd, 1H,  $J_{5',4'} = 4.1$ ,  $J_{5',4'} = 9.5$ ,  $J_{5',p} = 6.6$ , H3'-A); 5.75 (dt, 1H,  $J_{5',2'} = 8.6$ ,  $J_{2',3'} = 4.3$ ,  $J_{2',p} = 4.3$ , H2'-G); 5.95 (d, 1H,  $J_{1',2'} = 8.6$ , H1'-G); 6.22 (s, 1H, H1'-A); 7.67 (s, 1H, H6-A); 7.88 (bs, 1H, H8-G); 8.18 (bs, 1H, H2-A).  $^{13}\text{C}$  NMR (150.9 MHz, D<sub>2</sub>O); chemical shifts obtained from 2D-HSQC and 2D-HMBC spectra;  $J(C,P)$  and shifts of C2-G, C4-G, C5-G, and C6-G not determined): 15.55 (C5-pentynyl); 23.44 (C3-pentynyl); 24.04 (C4-pentynyl); 65.09 (C5'-A); 68.48 (C5'-G); 72.73 (C3'-A); 73.80 (C3'-G); 74.50 (C1-pentynyl); 76.83 (C2'-A); 77.11 (C2'-G); 82.28 (C4'-A); 85.73 (C4'-G); 89.00 (C1'-G); 92.02 (C1'-A); 96.60 (C2-pentynyl); 98.09 (C5-A); 105.93 (C4a-A); 127.64 (C6-A); 143.12 (C8-G); 149.52 (C7a-A); 154.41 (C2-A); 159.83 (C4-A).  $^{31}\text{P}$  NMR ( $^1\text{H}$ -dec, 202.4 MHz, D<sub>2</sub>O): -0.15 and -0.83. ESI MS  $m/z$  (rel. %): 368 (100) [M-2H] $^{2-}$ , 738 (15) [M-H] $^{-}$ , 760 (9) [M-2H + Na] $^{-}$ . HR MS (ESI): for C<sub>28</sub>H<sub>36</sub>O<sub>13</sub>N<sub>5</sub>P<sub>2</sub>, calcd 738.14438; found, 738.14313.

**Cyclo-4-amino-5-phenyl-7-β-D-ribofuranosyl-7H-pyrrolo[2,3-dj-pyrimidine 5'-O-Phosphate (3' → 5') Guanosine 5'-O-Phosphate (2' → 5') Sodium Salt (5f).** Enzymatic synthesis: NTP 3f (2 μmol) and GTP (2 μmol) were enzymatically cyclized using mcGAS. The final product was purified by HPLC (5–30% MeCN in 0.1 M TEAB). The conversion to a sodium salt form on a Dowex 50WX8 (in a Na<sup>+</sup> cycle) provided CDN 5f (100 nmol, 5%).

Chemical synthesis: CDN 5a (15 mg, 17.8 μmol), phenylboronic acid (4.3 mg, 35.6 μmol), and cesium carbonate (17.4 mg, 53.4 μmol)



were mixed with MeCN–H<sub>2</sub>O (1:2 v/v, 600  $\mu$ L) in an argon purged vial. In a separate vial, Pd(OAc)<sub>2</sub> (1.0 mg, 4.45  $\mu$ mol) and TPPTS (12.6 mg, 22.2  $\mu$ mol) were dissolved in MeCN–H<sub>2</sub>O (1:2 v/v, 1.0 mL), and the solution was sonicated under an argon atmosphere for 30 s. Then, 200  $\mu$ mol (i.e., 1/5) of this solution was transferred into the mixture containing the CDN 5a, and the reaction was stirred at 100 °C for 30 min. Then, the reaction mixture was cooled to rt, diluted with water to approx. 3 mL, and filtered through a 5  $\mu$ m nylon syringe filter. The filtrate was directly applied on HPLC for purification. After two HPLC separations (0–15% MeCN in 0.1 M TEAB) and conversion to a sodium salt form on a Dowex 50WX8 (in a Na<sup>+</sup> cycle), CDN 5f (2.5 mg, 18%) was obtained as a white lyophilizate (water). <sup>1</sup>H NMR (600 MHz, D<sub>2</sub>O): 4.15 (ddd, 1H, J<sub>5b,5a</sub> = 1.8, J<sub>5b,5c</sub> = 11.8, J<sub>5b,5d</sub> = 2.5, HS<sup>b</sup>-G); 4.25 (ddd, 1H, J<sub>5c,4a</sub> = 2.8, J<sub>5c,5b</sub> = 11.8, J<sub>5c,5d</sub> = 5.0, HS<sup>a</sup>-A); 4.29 (m, 1H, HS<sup>b</sup>-A); 4.43 (ddd, 1H, J<sub>4c,5a</sub> = 2.8, J<sub>4c,5b</sub> = 1.8, J<sub>4c,5d</sub> = 3.6, H4<sup>c</sup>-G); 4.49 (dm, 1H, J<sub>4c,5c</sub> = 9.1, H4<sup>a</sup>-A); 4.51 (m, 1H, HS<sup>a</sup>-A); 4.66 (d, 1H, J<sub>5c,2c</sub> = 4.1, H3<sup>c</sup>-G); 4.79 (bd, 1H, J<sub>5c,3c</sub> = 4.1, H2<sup>a</sup>-A); 5.02 (ddd, 1H, J<sub>5c,2c</sub> = 4.1, J<sub>5c,4c</sub> = 9.1, J<sub>5c,5d</sub> = 6.9, H3<sup>a</sup>-A); 5.73 (dt, 1H, J<sub>5c,1c</sub> = 8.6, J<sub>5c,2c</sub> = 4.1, J<sub>5c,5d</sub> = 4.1, H2<sup>c</sup>-G); 6.01 (d, 1H, J<sub>5c,2c</sub> = 8.6, H1<sup>c</sup>-G); 6.29 (s, 1H, H1<sup>a</sup>-A); 7.09 (m, 2H, o-Ph-A); 7.24 (m, 2H, m-Ph-A); 7.25 (m, 1H, p-Ph); 7.63 (s, 1H, H6-A); 7.89 (s, 1H, H8-G); 8.22 (s, 1H, H2-A). <sup>13</sup>C NMR (150.9 MHz, D<sub>2</sub>O): 65.53 (d, J<sub>C,P</sub> = 4.6, CS<sup>a</sup>-A); 68.66 (d, J<sub>C,P</sub> = 5.4, CS<sup>c</sup>-G); 73.07 (d, J<sub>C,P</sub> = 5.5, C3<sup>a</sup>-A); 73.93 (C3<sup>c</sup>-G); 76.96 (C2<sup>a</sup>-A); 77.87 (d, J<sub>C,P</sub> = 4.6, C2<sup>c</sup>-G); 82.61 (t, J<sub>C,P</sub> = 11.3, C4<sup>a</sup>-A); 86.04 (d, J<sub>C,P</sub> = 9.7, C4<sup>c</sup>-G); 88.70 (d, J<sub>C,P</sub> = 12.5, C1<sup>a</sup>-G); 92.27 (C1<sup>c</sup>-A); 103.79 (C4a-A); 119.40 (C5-A); 119.88 (C5-G); 122.74 (C6-A); 129.47 (p-Ph-A); 130.27 (o-Ph-A); 131.61 (m-Ph-A); 135.65 (i-Ph-A); 142.42 (C8-G); 151.35 (C7a-A); 153.88 (C2-A); 154.58 (C4-G); 155.99 (C2-G); 160.08 (C4-A); 161.17 (C6-G). <sup>31</sup>P NMR (<sup>1</sup>H-dec, 202.4 MHz, D<sub>2</sub>O): -0.19 and -0.90. ESI MS m/z (rel. %): 373 (100) [M–2H]<sup>2-</sup>, 385 (5) [M–3H + Na]<sup>2-</sup>, 748 (2) [M–H]<sup>-</sup>, 770 (6) [M–2H + Na]<sup>-</sup>. HR MS (ESI): for C<sub>27</sub>H<sub>23</sub>O<sub>13</sub>N<sub>9</sub>P<sub>2</sub> [M–H]<sup>-</sup>, calcd 748.12873; found, 748.12862.

**Cyclo-4-amino-5-(naphthalen-2-yl)-7- $\beta$ -D-ribofuranosyl-7H-pyrrolo[2,3-d]pyrimidine 5'-O-phosphate (3'  $\rightarrow$  5') Guanosine 5'-O-phosphate (2'  $\rightarrow$  5') Sodium Salt (5g).** CDN 5a (13 mg, 15.4  $\mu$ mol), naphthalene-2-boric acid (13.3 mg, 77.1  $\mu$ mol), and cesium carbonate (15 mg, 46.2  $\mu$ mol) were mixed with MeCN–H<sub>2</sub>O (1:2 v/v, 520  $\mu$ L) in an argon purged vial. In a separate vial, Pd(OAc)<sub>2</sub> (1.0 mg, 4.45  $\mu$ mol) and TPPTS (12.6 mg, 22.2  $\mu$ mol) were dissolved in MeCN–H<sub>2</sub>O (1:2 v/v, 1.0 mL), and the solution was sonicated under argon atmosphere for 30 s. Then, 173  $\mu$ mol of this solution was transferred into the mixture containing the CDN 5a, and the reaction mixture was stirred at 100 °C for 30 min. Then, the reaction mixture was cooled to rt, diluted with water to approx. 3 mL, and filtered through a 5  $\mu$ m nylon syringe filter. The filtrate was directly applied on HPLC for purification (5–25% MeCN in 0.1 M TEAB). After HPLC repurification (9–24% MeCN in 0.1 M TEAB) and conversion to a sodium salt form on a Dowex 50WX8 (in a Na<sup>+</sup> cycle), CDN 5g (5.7 mg, 44%) was obtained as a white lyophilizate (water). <sup>1</sup>H NMR (600 MHz, D<sub>2</sub>O): 4.13 (ddd, 1H, J<sub>5b,5a</sub> = 1.6, J<sub>5b,5c</sub> = 11.8, J<sub>5b,5d</sub> = 2.6, HS<sup>b</sup>-G); 4.26 (ddd, 1H, J<sub>5c,4a</sub> = 2.7, J<sub>5c,5b</sub> = 11.8, J<sub>5c,5d</sub> = 4.5, HS<sup>a</sup>-A); 4.36 (ddd, 1H, J<sub>5b,5a</sub> = 1.3, J<sub>5b,5c</sub> = 12.1, J<sub>5b,5d</sub> = 2.9, HS<sup>b</sup>-A); 4.45 (ddd, 1H, J<sub>4c,5a</sub> = 2.7, J<sub>4c,5b</sub> = 1.6, J<sub>4c,5d</sub> = 3.8, H4<sup>c</sup>-G); 4.53 (dm, 1H, J<sub>4c,5c</sub> = 9.6, H4<sup>a</sup>-A); 4.57 (ddd, 1H, J<sub>5c,4a</sub> = 2.3, J<sub>5c,5b</sub> = 12.1, J<sub>5c,5d</sub> = 1.1, HS<sup>a</sup>-A); 4.73 (d, 1H, J<sub>5c,2c</sub> = 4.0, H3<sup>c</sup>-G); 4.81 (d, J<sub>5c,2c</sub> = 3.9, H2<sup>a</sup>-A); 5.03 (ddd, 1H, J<sub>5c,2c</sub> = 3.9, J<sub>5c,4c</sub> = 9.6, J<sub>5c,5d</sub> = 6.6, H3<sup>a</sup>-A); 5.67 (um, 1H, H2<sup>c</sup>-G); 6.07 (d, 1H, J<sub>5c,1c</sub> = 8.6, H1<sup>c</sup>-G); 6.34 (s, 1H, H1<sup>a</sup>-A); 7.32 (dd, 1H, J<sub>5c,2c</sub> = 1.8, J<sub>5c,4c</sub> = 8.3, H3-naphth); 7.53 (m, 1H, H7-naphth); 7.545 (m, 1H, H6-naphth); 7.64 (dm, 1H, J<sub>1,3</sub> = 1.8, H1-naphth); 7.74 (s, 1H, H8-G); 7.75 (s, 1H, H6-A); 7.77 (dm, 1H, J<sub>6,3</sub> = 8.3, H4-naphth); 7.82 (m, 1H, HS-naphth); 7.90 (m, 1H, H8-naphth); 8.25 (s, 1H, H2-A). <sup>13</sup>C NMR (150.9 MHz, D<sub>2</sub>O): 65.66 (d, J<sub>C,P</sub> = 4.7, CS<sup>a</sup>-A); 68.76 (d, J<sub>C,P</sub> = 5.2, CS<sup>c</sup>-G); 73.16 (d, J<sub>C,P</sub> = 5.4, C3<sup>a</sup>-A); 73.91 (C3<sup>c</sup>-G); 76.98 (C2<sup>a</sup>-A); 79.00 (C2<sup>c</sup>-G); 82.58 (t, J<sub>C,P</sub> = 11.6, C4<sup>a</sup>-A); 86.13 (d, J<sub>C,P</sub> = 9.6, C4<sup>c</sup>-G); 87.80 (C1<sup>c</sup>-G); 92.32 (C1<sup>a</sup>-A); 103.93 (CS-A); 119.40 (C4a-A); 119.61 (C5-G); 123.09 (C6-A); 128.19 (C1-naphth); 128.51 (C3-naphth); 128.70 (C7-naphth); 129.24 (C6-naphth); 130.26 (C8-

naphth); 130.89 (C5-naphth); 131.18 (C4-naphth); 133.19 (C2-naphth); 134.43 (C4a-naphth); 135.96 (C8a-naphth); 141.25 (C8-G); 151.60 (C7a-A); 153.89 (C2-A); 154.34 (C4-G); 155.90 (C2-G); 160.32 (C4-A); 160.72 (C6-G). <sup>31</sup>P NMR (<sup>1</sup>H-dec, 202.4 MHz, D<sub>2</sub>O): -0.12 and -0.96. ESI MS m/z (rel. %): 398 (100) [M–2H]<sup>2-</sup>, 798 (47) [M–H]<sup>-</sup>, 820 (35) [M–2H + Na]<sup>-</sup>. HR MS (ESI): for C<sub>31</sub>H<sub>23</sub>O<sub>13</sub>N<sub>9</sub>P<sub>2</sub> [M–2H]<sup>2-</sup>, calcd 398.56855; found, 398.56823.

**Cyclo-4-amino-5-(naphthalen-1-yl)-7- $\beta$ -D-ribofuranosyl-7H-pyrrolo[2,3-d]pyrimidine 5'-O-phosphate (3'  $\rightarrow$  5') Guanosine 5'-O-phosphate (2'  $\rightarrow$  5') Sodium Salt (5h).** CDN 5h was prepared as described for 5g from iodinated CDN 5a (15 mg, 17.8  $\mu$ mol) and naphthalene-1-boric acid (17.6 mg, 88.9  $\mu$ mol). The final product was purified by HPLC (5–30% MeCN in 0.1 M TEAB). After HPLC repurification (5–50% MeOH in 0.1 M TEAB) and conversion to a sodium salt form on a Dowex 50WX8 (in a Na<sup>+</sup> cycle), CDN 5h (5.6 mg, 37%) was obtained as a white lyophilizate (water). The final product was a mixture of two diastereomers (63:37) due to hindered rotation (at 298 K). Chemical shifts of the resolved signals of minor isomer are given in italics. <sup>1</sup>H NMR (600 MHz, D<sub>2</sub>O): 4.125 (dt, 1H, J<sub>5b,5a</sub> = 2.1, J<sub>5b,5c</sub> = 11.8, J<sub>5b,5d</sub> = 2.2, HS<sup>b</sup>-G); 4.13 (ddd, 1H, J<sub>5b,5a</sub> = 2.3, J<sub>5b,5c</sub> = 11.9, J<sub>5b,5d</sub> = 3.5, HS<sup>b</sup>-G); 4.23 (dd, 1H, J<sub>5c,4a</sub> = 2.6, J<sub>5c,5b</sub> = 11.8, HS<sup>a</sup>-A); 4.24 (dd, 1H, J<sub>5c,4a</sub> = 2.6, J<sub>5c,5b</sub> = 11.9, HS<sup>a</sup>-G); 4.25 (m, 1H, HS<sup>b</sup>-A); 4.28 (ddd, 1H, J<sub>5b,5a</sub> = 1.5, J<sub>5b,5c</sub> = 12.1, J<sub>5b,5d</sub> = 2.8, HS<sup>b</sup>-A); 4.385 (m, 1H, H4<sup>c</sup>-G); 4.39 (m, 1H, H4<sup>c</sup>-G); 4.44 (dm, 1H, J<sub>4c,5b</sub> = 12.1, HS<sup>a</sup>-A); 4.47 (dm, 1H, J<sub>4c,5c</sub> = 8.4, H4<sup>a</sup>-A); 4.50 (dm, 1H, J<sub>4c,5c</sub> = 9.0, H4<sup>a</sup>-A); 4.615 (d, 1H, J<sub>5c,2c</sub> = 4.1, H3<sup>c</sup>-G); 4.64 (d, 1H, J<sub>5c,2c</sub> = 4.1, H3<sup>c</sup>-G); 5.025 (d, 1H, J<sub>5c,2c</sub> = 4.3, H2<sup>a</sup>-A); 5.04 (dd, 1H, J<sub>5c,2c</sub> = 4.4, J<sub>5c,4c</sub> = 1.1, H2<sup>a</sup>-A); 5.09 (ddd, 1H, J<sub>5c,2c</sub> = 4.3, J<sub>5c,4c</sub> = 9.0, J<sub>5c,5d</sub> = 6.2, H3<sup>a</sup>-A); 5.34 (ddd, 1H, J<sub>5c,2c</sub> = 4.4, J<sub>5c,4c</sub> = 8.4, J<sub>5c,5d</sub> = 6.6, H3<sup>a</sup>-A); 5.79 (ddd, 1H, J<sub>5c,1c</sub> = 8.6, J<sub>5c,2c</sub> = 4.1, J<sub>5c,5d</sub> = 3.7, H2<sup>c</sup>-G); 5.87 (dt, 1H, J<sub>5c,1c</sub> = 8.6, J<sub>5c,2c</sub> = 4.1, J<sub>5c,5d</sub> = 3.9, H2<sup>c</sup>-G); 5.97 (d, 1H, J<sub>5c,2c</sub> = 8.6, H1<sup>c</sup>-G); 5.98 (d, 1H, J<sub>5c,2c</sub> = 8.6, H1<sup>c</sup>-G); 6.38 (s, 1H, H1<sup>a</sup>-A); 6.55 (d, 1H, J<sub>5c,2c</sub> = 1.1, H1<sup>a</sup>-A); 6.895 (dd, 1H, J<sub>5c,3c</sub> = 7.0, J<sub>5c,4c</sub> = 1.3, H8-naphth); 7.18 (dd, 1H, J<sub>5c,3c</sub> = 8.3, J<sub>5c,4c</sub> = 7.0, H3-naphth); 7.21 (s, 1H, H6-A); 7.36 (dd, 1H, J<sub>5c,3c</sub> = 8.4, J<sub>5c,4c</sub> = 7.0, H3-naphth); 7.38 (ddd, 1H, J<sub>6,7</sub> = 8.2, J<sub>6,8</sub> = 6.8, J<sub>6,9</sub> = 1.5, H6-naphth); 7.38 (dd, 1H, J<sub>2,3</sub> = 7.0, J<sub>2,4</sub> = 1.5, H8-naphth); 7.41 (ddd, 1H, J<sub>7,8</sub> = 6.8, J<sub>7,9</sub> = 8.2, J<sub>7,5</sub> = 1.4, H7-naphth); 7.485 (ddd, 1H, J<sub>6,7</sub> = 8.5, J<sub>6,8</sub> = 6.8, J<sub>6,9</sub> = 1.3, H6-naphth); 7.52 (s, 1H, H6-A); 7.59 (ddd, 1H, J<sub>7,8</sub> = 6.8, J<sub>7,9</sub> = 8.5, J<sub>7,5</sub> = 1.3, H7-naphth); 7.64 (dd, 1H, J<sub>5c,6</sub> = 6.8, J<sub>5c,7</sub> = 1.3, H5-naphth); 7.70 (dd, 1H, J<sub>5c,6</sub> = 6.8, J<sub>5c,7</sub> = 1.4, H5-naphth); 7.86 (dd, 1H, J<sub>4,5</sub> = 8.3, J<sub>4,3</sub> = 1.5, H4-naphth); 7.90 (dd, 1H, J<sub>5c,7</sub> = 6.8, J<sub>5c,6</sub> = 1.5, H8-naphth); 7.905 (dd, 1H, J<sub>4,5</sub> = 8.4, J<sub>4,3</sub> = 1.3, H4-naphth); 7.91 (s, 1H, H8-G); 7.995 (dd, 1H, J<sub>6,7</sub> = 6.8, J<sub>6,8</sub> = 1.3, H8-naphth); 8.20 (s, 1H, H2-A); 8.235 (s, 1H, H2-A). <sup>13</sup>C NMR (150.9 MHz, D<sub>2</sub>O): 65.48 (d, J<sub>C,P</sub> = 4.5, CS<sup>a</sup>-A); 68.92 (d, J<sub>C,P</sub> = 5.5, CS<sup>c</sup>-G); 65.98 (d, J<sub>C,P</sub> = 5.0, CS<sup>a</sup>-A); 68.79 (d, J<sub>C,P</sub> = 5.1, CS<sup>c</sup>-G); 73.59 (d, J<sub>C,P</sub> = 5.4, C3<sup>a</sup>-A); 73.71 (d, J<sub>C,P</sub> = 5.3, C3<sup>a</sup>-A); 74.19 (C3<sup>c</sup>-G); 74.32 (C3<sup>c</sup>-G); 76.70 (C2<sup>a</sup>-A); 76.84 (C2<sup>a</sup>-A); 77.34 (d, J<sub>C,P</sub> = 5.2, C2<sup>c</sup>-G); 77.50 (d, J<sub>C,P</sub> = 5.5, C2<sup>c</sup>-G); 82.55 (t, J<sub>C,P</sub> = 11.3, C4<sup>a</sup>-A); 82.83 (t, J<sub>C,P</sub> = 11.2, C4<sup>a</sup>-A); 85.72 (d, J<sub>C,P</sub> = 9.1, C4<sup>c</sup>-G); 85.75 (d, J<sub>C,P</sub> = 9.4, C4<sup>c</sup>-G); 88.63 (d, J<sub>C,P</sub> = 12.5, C1<sup>a</sup>-G); 89.02 (d, J<sub>C,P</sub> = 13.0, C1<sup>a</sup>-G); 90.32 (C1<sup>a</sup>-A); 91.67 (C1<sup>a</sup>-A); 105.81 (C4a-A); 106.86 (C4a-A); 117.04 (C5-A); 118.96 (C5-A); 119.75 (C5-G); 119.79 (C5-G); 123.68 (C6-A); 123.73 (C6-A); 127.65 (CS-naphth); 127.82 (CS-naphth); 128.11 (C3-naphth); 128.24 (C3-naphth); 128.92 (C7-naphth); 129.03 (C7-naphth); 129.64 (C6-naphth); 129.69 (C6-naphth); 130.82 (C2-naphth); 130.97 (C4-naphth); 131.06 (C8-naphth); 131.26 (C4-naphth); 131.45 (C2-naphth); 131.48 (C8-naphth); 132.48 (C4a-naphth); 132.73 (C4a-naphth); 134.11 (C8a-naphth); 134.28 (C8a-naphth); 136.12 (C1-naphth); 136.20 (C1-naphth); 142.91 (C8-G); 142.91 (C8-G); 151.38 (C7a-A); 152.67 (C7a-A); 154.21 (C2-A); 154.40 (C4-G); 154.40 (C4-G); 154.59 (C2-A); 156.04 (C2-G); 156.89 (C2-G); 159.90 (C4-A); 160.06 (C4-A); 160.28 (C6-G); 160.94 (C6-G). <sup>31</sup>P NMR (<sup>1</sup>H-dec, 202.4 MHz, D<sub>2</sub>O): -0.08; -0.25; -0.32; -0.61. ESI MS m/z (rel. %): 398 (100) [M–2H]<sup>2-</sup>, 798 (25) [M–H]<sup>-</sup>. HR MS (ESI): for C<sub>31</sub>H<sub>23</sub>O<sub>13</sub>N<sub>9</sub>P<sub>2</sub> [M–H]<sup>-</sup>, calcd 798.114438; found, 798.114472.

**Cyclo-4-amino-5-(1,2-dihydroacacenaphthylen-5-yl)-7- $\beta$ -D-ribofuranosyl-7H-pyrrolo[2,3-d]pyrimidine 5'-O-phosphate (3'  $\rightarrow$  5')**

**Guanosine 5'-O-phosphate (2' → 5') Sodium Salt (5i).** CDN 5i was prepared as described for **5g** from iodinated CDN **5a** (15 mg, 17.8 μmol) and acenaphthene-5-boronic acid (17.6 mg, 88.9 μmol). The final product was purified by HPLC (5–30% MeCN in 0.1 M TEAB). The conversion to a sodium salt form on a Dowex 50WX8 (in a Na<sup>+</sup> cycle) provided CDN **5i** (7.3 mg, 47%) as a white lyophilizate (water). The final product was a mixture of two diastereomers (78:22) due to hindered rotation (at 298 K). The hindered rotation resulted in the line broadening of most NMR signals. Only a few resolved proton signals of minor isomer could be detected, and their chemical shifts are given in italics. <sup>1</sup>H NMR (600 MHz, D<sub>2</sub>O): 3.38 (um, 2H, 2 × H1-acenaphthylene); 3.46 (um, 2H, 2 × H2-acenaphthylene); 4.11 (dm, 1H, J<sub>5,5'</sub> = 11.9, H5'<sup>b</sup>-G); 4.23 (ddd, 1H, J<sub>5,5'</sub> = 2.4, J<sub>5,5''</sub> = 11.9, J<sub>5,5''</sub> = 6.0, H5'<sup>b</sup>-G); 4.30 (dm, 1H, J<sub>5,5'</sub> ≈ 12.0, H5'<sup>b</sup>-A); 4.38 (dt, 1H, J<sub>4,5'</sub> = 2.4, J<sub>4,5''</sub> = 2.2, J<sub>4,5''</sub> = 3.4, H4'-G); 4.43 (dm, 1H, J<sub>4,5'</sub> ≈ 12.0, H5'<sup>a</sup>-A); 4.48 (dm, 1H, J<sub>4,5'</sub> ≈ 9.0, H4'-A); 4.62 (bd, 1H, J<sub>5,5'</sub> = 3.9, H3'-G); 4.99 (br, 1H, H2'-A); 5.13, 5.30 (um, 1H, H3'-A); 5.85 (um, 1H, H2'-G); 5.96, 5.90 (bd, 1H, J<sub>1,2'</sub> ≈ 8.0, H1'-G); 6.44, 6.52 (s, 1H, H1'-A); 7.03, 6.96 (bd, 1H, J<sub>3,4</sub> = 6.9, H3-acenaphthylene); 7.15 (bd, 1H, J<sub>6,7</sub> = 6.8, H6-acenaphthylene); 7.24 (bd, 1H, J<sub>4,3</sub> = 6.9, H4-acenaphthylene); 7.26 (bd, 1H, J<sub>8,7</sub> = 8.0, H8-acenaphthylene); 7.29 (bt, 1H, J<sub>7,8</sub> = 8.0, J<sub>7,6</sub> = 6.8, H7-acenaphthylene); 7.44 (bs, 1H, H6-A); 7.85 (s, 1H, H8-G); 8.21 (s, 1H, H2-A). <sup>13</sup>C NMR (150.9 MHz, D<sub>2</sub>O): 32.48 (C1-acenaphthylene); 32.83 (C2-acenaphthylene); 65.48 (C5'-A); 68.89 (d, J<sub>CP</sub> = 5.3, C5'-G); 73.69 (C3'-A); 74.29 (C3'-G); 76.93 (C2'-A); 77.37 (d, J<sub>CP</sub> = 4.8, C2'-G); 82.27 (C4'-A); 85.62 (d, J<sub>CP</sub> = 9.3, C4'-G); 88.92 (d, J<sub>CP</sub> = 13.9, C1'-G); 91.06 (C1'-A); 105.17 (C4-A); 117.20 (C5-A); 119.55 (C5-G); 121.73 (C4-acenaphthylene); 122.41 (C6-acenaphthylene); 122.58 (C8-acenaphthylene); 123.48 (C6-A); 127.73 (C5a-acenaphthylene); 131.66 (C7-acenaphthylene); 132.01 (C3-acenaphthylene); 132.25 (C5-acenaphthylene); 141.70 (C8b-acenaphthylene); 142.56 (C8-G); 148.94 (C8a-acenaphthylene); 149.81 (C2a-acenaphthylene); 151.60 (C7a-A); 154.28 (C2-A); 154.24 (C4-G); 155.89 (C2-G); 160.11 (C4-A); 160.68 (C6-G); <sup>31</sup>P NMR (<sup>1</sup>H-dec, 202.4 MHz, D<sub>2</sub>O): -0.22 and -0.45. ESI MS *m/z* (rel. %): 411 (100) [M-2H]<sup>2-</sup>, 824 (22) [M-H]<sup>-</sup>, 846 (26) [M-2H + Na]<sup>-</sup>. HR MS (ESI): for C<sub>25</sub>H<sub>32</sub>O<sub>13</sub>N<sub>5</sub>P<sub>2</sub> [M-H]<sup>-</sup>, calcd 824.16003; found, 824.15900.

**Cyclo-4-amino-5-(phenanthren-9-yl)-7-β-D-ribofuranosyl-7H-pyrrolo[2,3-d]pyrimidine 5'-O-phosphate (3' → 5') Guanosine 5'-O-phosphate (2' → 5') Sodium Salt (5j).** CDN 5j was prepared as described for **5g** from iodinated CDN **5a** (15 mg, 17.8 μmol) and phenanthrene-9-boronic acid (19.4 mg, 88.9 μmol). The final product was purified by HPLC (5–30% MeCN in 0.1 M TEAB). The conversion to a sodium salt form on a Dowex 50WX8 (in a Na<sup>+</sup> cycle) provided CDN **5j** (4.7 mg, 30%) as a white lyophilizate (water). The final product was a mixture of two diastereomers (63:37) due to hindered rotation (at 298 K). Chemical shifts of the resolved signals of minor isomer are given in italics. <sup>1</sup>H NMR (600 MHz, D<sub>2</sub>O): 4.07 (dt, 1H, J<sub>5,5'</sub> = 2.1, J<sub>5,5''</sub> = 11.8, J<sub>5,5''</sub> = 2.1, H5'<sup>b</sup>-G); 4.125 (dt, 1H, J<sub>5,5'</sub> = 2.1, J<sub>5,5''</sub> = 11.8, J<sub>5,5''</sub> = 2.1, H5'<sup>b</sup>-G); 4.22 (ddd, 1H, J<sub>5,5'</sub> = 2.4, J<sub>5,5''</sub> = 11.8, J<sub>5,5''</sub> = 5.1, H5'<sup>a</sup>-G); 4.25 (ddd, 1H, J<sub>5,5'</sub> = 2.6, J<sub>5,5''</sub> = 11.8, J<sub>5,5''</sub> = 5.5, H5'<sup>a</sup>-G); 4.30 (ddd, 1H, J<sub>5,5'</sub> = 1.6, J<sub>5,5''</sub> = 11.8, J<sub>5,5''</sub> = 2.8, H5'<sup>b</sup>-A); 4.33 (m, 2H, H5'<sup>a</sup>-A and H5'<sup>b</sup>-A); 4.35 (dt, 1H, J<sub>4,5'</sub> = 2.4, J<sub>4,5''</sub> = 2.1, J<sub>4,5''</sub> = 3.6, H4'-G); 4.415 (dt, 1H, J<sub>4,5'</sub> = 2.6, J<sub>4,5''</sub> = 2.1, J<sub>4,5''</sub> = 3.4, H4'-G); 4.47 (dm, 1H, J<sub>5,5'</sub> = 11.8, H5'<sup>a</sup>-A); 4.49 (dm, 1H, J<sub>4,5'</sub> = 8.6, H4'-A); 4.53 (dm, 1H, J<sub>4,5'</sub> = 9.0, H4'-A); 4.66 (d, 1H, J<sub>5,5'</sub> = 4.0, H3'-G); 4.67 (d, 1H, J<sub>5,5'</sub> = 3.9, H3'-G); 5.09 (ddd, 1H, J<sub>5,5'</sub> = 4.3, J<sub>5,5''</sub> = 9.0, J<sub>5,5''</sub> = 6.3, H3'-A); 5.10 (d, 1H, J<sub>2,3'</sub> = 4.5, H2'-A); 5.12 (d, 1H, J<sub>2,3'</sub> = 4.3, H2'-A); 5.47 (ddd, 1H, J<sub>2,3'</sub> = 4.5, J<sub>5,5'</sub> = 8.6, J<sub>5,5''</sub> = 6.8, H3'-A); 5.80 (ddd, 1H, J<sub>5,5'</sub> = 8.6, J<sub>5,5''</sub> = 4.0, J<sub>5,5''</sub> = 3.5, H2'-G); 5.86 (d, 1H, J<sub>1,2'</sub> = 8.6, H1'-G); 5.92 (um, 1H, H2'-G); 6.06 (d, 1H, J<sub>1,2'</sub> = 8.6, H1'-G); 6.35 (s, 1H, H1'-A); 6.62 (s, 1H, H1'-A); 7.305 (s, 1H, H10-phen); 7.32 (s, 1H, H6-A); 7.34 (br, 1H, H8-G); 7.515 (ddd, 1H, J<sub>3,1</sub> = 8.3, J<sub>3,2</sub> = 6.9, J<sub>2,4</sub> = 1.2, H2-phen); 7.61 (m, 1H, H2-phen); 7.63 (m, 1H, H6-phen); 7.635 (m, 1H, H7-phen); 7.65 (s, 1H, H6-A); 7.725 (m, 2H, H6 and H8-phen); 7.75 (m, 1H, H1-phen); 7.765 (m, 1H, H3-phen); 7.77 (m, 1H, H7-phen); 7.785 (s, 1H, H10-phen); 7.79 (m, 1H, H3-

phen); 7.805 (m, 1H, H1-phen); 7.90 (br, 1H, H8-G); 8.21 (s, 1H, H2-A); 8.25 (s, 1H, H2-A); 8.76 (dm, 1H, J<sub>4,3</sub> = 8.5, H4-phen); 8.79 (dm, 1H, J<sub>5,6</sub> = 8.5, H5-phen); 8.795 (dm, 1H, J<sub>4,3</sub> = 8.5, H4-phen); 8.84 (dm, 1H, J<sub>5,6</sub> = 8.5, H5-phen). <sup>13</sup>C NMR (150.9 MHz, D<sub>2</sub>O): 65.52 (C5'-A); 66.17 (C5'-A); 68.79 (C5'-G); 69.00 (C5'-G); 73.73 (C3'-A); 74.17 (C3'-G); 74.29 (C3'-G); 74.66 (C3'-A); 76.43 (C2'-A); 76.89 (C2'-A); 77.91 (C2'-G); 77.91 (C2'-G); 82.66 (C4'-A); 82.73 (C4'-A); 85.34 (C4'-G); 85.88 (C4'-G); 88.17 (C1'-G); 88.67 (C1'-G); 90.19 (C1'-A); 91.83 (C1'-A); 105.86 (C4a-A); 106.05 (C4a-A); 116.93 (C5-A); 118.78 (C5-G); 119.24 (C5-A); 119.48 (C5-G); 123.85 (C6-A); 124.16 (C6-A); 125.23 (C4-phen); 125.34 (C4-phen); 125.60 (C5-phen); 126.24 (C5-phen); 128.53 (C8-phen); 128.79 (C8-phen); 129.70 (C7-phen); 129.76 (C7-phen); 129.84 (C3-phen); 129.84 (C6-phen); 130.00 (C2-phen); 130.03 (C2-phen); 130.88 (C8a-phen); 131.18 (C10-phen); 131.48 (C10-phen); 131.49 (C8a-phen); 131.74 (C1-phen); 132.33 (C4a-phen); 132.35 (C1-phen); 132.45 (C4a-phen); 132.84 (C4b-phen); 133.02 (C9-phen); 133.09 (C4b-phen); 133.18 (C9-phen); 141.58 (C8-G); 142.58 (C8-G); 151.23 (C7a-A); 152.86 (C7a-A); 153.68 (C4-G); 154.05 (C2-A); 154.37 (C4-G); 154.57 (C2-A); 155.96 (C2-G); 155.98 (C2-G); 159.90 (C4-A); 159.68 (C6-G); 159.74 (C6-G); 160.72 (C4-A). <sup>31</sup>P NMR (<sup>1</sup>H-dec, 202.4 MHz, D<sub>2</sub>O): -0.07; -0.23; -0.44; -0.68. ESI MS *m/z* (rel. %): 423 (100) [M-2H]<sup>2-</sup>, 856 (9) [M-2H + Na]<sup>-</sup>. HR MS (ESI): for C<sub>35</sub>H<sub>35</sub>O<sub>13</sub>N<sub>5</sub>P<sub>2</sub> [M-H]<sup>-</sup>, calcd 848.16003; found, 848.15924.

**Cyclo-4-amino-5-(biphenyl-4-yl)-7-β-D-ribofuranosyl-7H-pyrrolo[2,3-d]pyrimidine 5'-O-phosphate (3' → 5') Guanosine 5'-O-phosphate (2' → 5') Sodium Salt (5k).** CDN 5k was prepared as described for **5g** from iodinated CDN **5a** (15 mg, 17.8 μmol) and 4-biphenylboronic acid (17.6 mg, 88.9 μmol). The final product was purified by HPLC (5–25% MeCN in 0.1 M TEAB). The conversion to a sodium salt form on a Dowex 50WX8 (in a Na<sup>+</sup> cycle) provided CDN **5k** (9.1 mg, 59%) as a white lyophilizate (water). <sup>1</sup>H NMR (600 MHz, D<sub>2</sub>O): 4.13 (ddd, 1H, J<sub>5,5'</sub> = 1.7, J<sub>5,5''</sub> = 11.7, J<sub>5,5''</sub> = 2.5, H5'<sup>b</sup>-G); 4.24 (ddd, 1H, J<sub>5,5'</sub> = 2.7, J<sub>5,5''</sub> = 11.7, J<sub>5,5''</sub> = 4.7, H5'<sup>a</sup>-G); 4.32 (ddd, 1H, J<sub>5,5'</sub> = 2.9, J<sub>5,5''</sub> = 11.8, J<sub>5,5''</sub> = 1.2, H5'<sup>b</sup>-A); 4.42 (ddd, 1H, J<sub>4,5'</sub> = 2.7, J<sub>4,5''</sub> = 1.7, J<sub>4,5''</sub> = 3.7, H4'-G); 4.50 (dm, 1H, J<sub>4,5'</sub> = 9.3, H4'-A); 4.56 (bdd, 1H, J<sub>4,5'</sub> = 2.1, J<sub>5,5''</sub> = 11.8, J<sub>5,5''</sub> = <1, H5'<sup>a</sup>-A); 4.68 (d, 1H, J<sub>5,5'</sub> = 4.1, H3'-G); 4.74 (d, 1H, J<sub>5,5'</sub> = 4.0, H2'-A); 4.97 (ddd, 1H, J<sub>5,5'</sub> = 4.0, J<sub>5,5''</sub> = 9.3, J<sub>5,5''</sub> = 6.5, H3'-A); 5.64 (um, 1H, H2'-G); 6.02 (d, 1H, J<sub>1,2'</sub> = 8.5, H1'-G); 6.25 (s, 1H, H1'-A); 7.11 (m, 2H, H3-phenylene + H5-phenylene); 7.41 (m, 1H, H4'-Ph); 7.48 (m, 2H, H2-phenylene + H6-phenylene); 7.51 (m, 2H, H3'-Ph + H5'-Ph); 7.66 (s, 1H, H6-A); 7.71 (m, 2H, H2'-Ph + H6'-Ph); 7.82 (s, 1H, H8-G); 8.18 (s, 1H, H2-A). <sup>13</sup>C NMR (150.9 MHz, D<sub>2</sub>O): 65.54 (d, J<sub>CP</sub> = 4.8, C5'-A); 68.72 (d, J<sub>CP</sub> = 5.2, C5'-G); 73.09 (d, J<sub>CP</sub> = 6.5, C3'-A); 73.80 (C3'-G); 76.97 (C2'-A); 78.50 (C2'-G); 82.55 (t, J<sub>CP1</sub> = J<sub>CP2</sub> = 11.3, C4'-A); 86.10 (d, J<sub>CP</sub> = 9.2, C4'-G); 88.07 (C1'-G); 92.24 (C1'-A); 103.65 (C4a-A); 119.08 (C5-A); 119.67 (C5-G); 122.79 (C6-A); 129.37 (C2'-Ph + C6'-Ph); 129.67 (C2-phenylene + C6-phenylene); 130.31 (C4'-Ph); 130.49 (C3-phenylene + C5-phenylene); 131.82 (C3'-Ph + C5'-Ph); 134.81 (C4-phenylene); 140.79 (C1-phenylene); 141.33 (C8-G); 142.49 (C1'-Ph); 151.25 (C7a-A); 153.39 (C2-A); 154.49 (C4-G); 155.98 (C2-G); 159.95 (C4-A); 160.98 (C6-G). <sup>31</sup>P NMR (<sup>1</sup>H-dec, 202.4 MHz, D<sub>2</sub>O): -0.14 and -0.93. ESI MS *m/z* (rel. %): 411 (100) [M-2H]<sup>2-</sup>, 824 (43) [M-H]<sup>-</sup>, 846 (17) [M-2H + Na]<sup>-</sup>. HR MS (ESI): for C<sub>35</sub>H<sub>35</sub>O<sub>13</sub>N<sub>5</sub>P<sub>2</sub> [M-H]<sup>-</sup>, calcd 824.16003; found, 824.16012.

**Cyclo-4-amino-5-(4-(naphthalen-2-yl)phenyl)-7-β-D-ribofuranosyl-7H-pyrrolo[2,3-d]pyrimidine 5'-O-phosphate (3' → 5') Guanosine 5'-O-phosphate (2' → 5') Sodium Salt (5l).** CDN 5l was prepared as described for **5g** from iodinated CDN **5a** (15 mg, 17.8 μmol) and 4-(naphthalen-2-yl)phenylboronic acid pinacol ester (29.4 mg, 88.9 μmol). The final product was purified by HPLC (5–30% MeCN in 0.1 M TEAB). The conversion to a sodium salt form on a Dowex 50WX8 (in a Na<sup>+</sup> cycle) provided CDN **5l** (5.3 mg, 32%) as a white lyophilizate (water). <sup>1</sup>H NMR (600 MHz, D<sub>2</sub>O): 4.14 (ddd, 1H, J<sub>5,5'</sub> = 1.8, J<sub>5,5''</sub> = 11.7, J<sub>5,5''</sub> = 2.4, H5'<sup>b</sup>-G); 4.22 (ddd, 1H, J<sub>5,5'</sub> = 2.5, J<sub>5,5''</sub> = 11.7, J<sub>5,5''</sub> = 4.8, H5'<sup>a</sup>-G); 4.35 (ddd, 1H, J<sub>5,5'</sub> = 11.9, J<sub>5,5''</sub> = 1.1, J<sub>5,5''</sub> = 2.7, H5'<sup>b</sup>-A); 4.44 (ddd, 1H, J<sub>4,5'</sub> =

2.5,  $J_{4',5'} = 1.8$ ,  $J_{4',P} = 3.7$ , H4'-G); 4.52 (dm, 1H,  $J_{4',5'} = 9.3$ , H4'-A); 4.58 (ddd, 1H,  $J_{3',4'} = 11.9$ ,  $J_{3',5'} = 2.0$ ,  $J_{3',P} = <1$ , H5'-a-A); 4.70 (d, 1H,  $J_{3',2'} = 4.0$ , H3'-G); 4.76 (overlap, H2'-A); 4.98 (ddd, 1H,  $J_{3',2'} = 4.0$ ,  $J_{3',4'} = 9.3$ ,  $J_{3',P} = 6.6$ , H3'-A); 5.61 (um, 1H, H2'-G); 6.03 (d, 1H,  $J_{3',2'} = 8.5$ , H1'-G); 6.30 (s, 1H, H1'-A); 7.16 (m, 2H, H2 + H6-phenylene); 7.53 (m, 1H, H7-naphth); 7.54 (m, 1H, H6-naphth); 7.57 (m, 2H, H3 + H5-phenylene); 7.65 (s, 1H, H6-A); 7.81 (s, 1H, H8-G); 7.84 (dd, 1H,  $J_{3,1} = 1.9$ ,  $J_{3,4} = 8.6$ , H3-naphth); 7.90 (m, 1H, H8-naphth); 7.91 (m, 1H, H5-naphth); 7.94 (d, 1H,  $J_{4,3} = 8.6$ , H4-naphth); 8.12 (bd, 1H,  $J_{1,3} = 1.9$ , H1-naphth); 8.12 (s, 1H, H2-A).  $^{13}\text{C}$  NMR (150.9 MHz, D<sub>2</sub>O): 65.71 (d,  $J_{C,P} = 3.2$ , C5'-A); 68.78 (d,  $J_{C,P} = 4.8$ , C5'-G); 73.19 (d,  $J_{C,P} = 6.5$ , C3'-A); 73.96 (C3'-G); 76.98 (C2'-A); 78.87 (C2'-G); 82.58 (t,  $J_{C,P1} = J_{C,P2} = 11.4$ , C4'-A); 86.12 (d,  $J_{C,P} = 9.5$ , C4'-G); 87.90 (d,  $J_{C,P} = 13.9$ , C1'-G); 92.18 (C1'-A); 103.64 (C4-A); 119.16 (C5-A); 119.61 (C5-G); 122.71 (C6-A); 127.76 (C1-naphth); 127.81 (C3-naphth); 128.93 (C7-naphth); 129.24 (C6-naphth); 129.89 (C3 and C5-phenylene); 130.24 (C8-naphth); 130.57 (C2 and C6-phenylene); 130.82 (C5-naphth); 131.15 (C4-naphth); 134.88 (C1-phenylene); 134.99 (C4a-naphth); 136.05 (C8a-naphth); 139.85 (C2-naphth); 140.55 (C4-phenylene); 141.08 (C8-b-G); 151.23 (C7a-A); 153.51 (C2-A); 154.49 (C4-G); 156.00 (C2-G); 159.89 (C4-A); 160.98 (C6-G).  $^{31}\text{P}$  NMR (H<sub>2</sub>O, 202.4 MHz, D<sub>2</sub>O): -0.14 and -0.93. ESI MS  $m/z$  (rel. %): 436 (100) [M-2H]<sup>2-</sup>, 874 (17) [M-H]<sup>-</sup>, 896 (14) [M-2H + Na]<sup>-</sup>. HR MS (ESI): for C<sub>37</sub>H<sub>34</sub>O<sub>13</sub>N<sub>4</sub>P<sub>2</sub> [M-H]<sup>-</sup>, calcd 874.17568; found, 874.17462.

**Cyclo-4-amino-5-[4-(naphthalen-1-yloxy)methyl]phenyl]-7-β-D-ribofuranosyl-7H-pyrrolo[2,3-d]pyrimidine 5'-O-phosphate (3' → 5') Guanosine 5'-O-phosphate (2' → 5') Sodium Salt (5m).** CDN 5m was prepared as described for 5g from iodinated CDN 5a (15 mg, 17.8 μmol) and [(1-naphthylthio)methyl]phenylboronic acid (24.7 mg, 88.9 μmol). The final product was purified by HPLC (5–32.5% MeCN in 0.1 M TEAB). The conversion to a sodium salt form on a Dowex 50WX8 (in a Na<sup>+</sup> cycle) provided CDN 5m (5.7 mg, 34%) as a white lyophilizate (water).  $^1\text{H}$  NMR (600 MHz, D<sub>2</sub>O): 4.13 (dt, 1H,  $J_{3',4'} = 1.8$ ,  $J_{3',5'} = 11.8$ ,  $J_{3',P} = 1.8$ , H5'-b-G); 4.24 (ddd, 1H,  $J_{3',4'} = 2.7$ ,  $J_{3',5'} = 11.8$ ,  $J_{3',P} = 4.8$ , H5'-a-G); 4.30 (dm, 1H,  $J_{3',5'} = 11.7$ , H5'-b-A); 4.42 (m, 1H, H4'-G); 4.49 (dm, 1H,  $J_{4',5'} = 9.5$ , H4'-A); 4.53 (dm, 1H,  $J_{3',5'} = 11.7$ , H5'-a-A); 4.66 (d, 1H,  $J_{3',4'} = 4.0$ , H3'-G); 4.72 (bd, 1H,  $J_{3',2'} = 4.0$ , H2'-A); 4.97 (ddd, 1H,  $J_{3',2'} = 4.0$ ,  $J_{3',4'} = 9.5$ ,  $J_{3',P} = 6.5$ , H3'-A); 5.26 (d, 1H,  $J_{3',2'} = 11.5$ , O-CHaHb); 5.30 (d, 1H,  $J_{3',2'} = 11.5$ , O-CHaHb); 5.68 (dt, 1H,  $J_{3',2'} = 8.5$ ,  $J_{3',5'} = 4.0$ ,  $J_{3',P} = 4.0$ , H2'-G); 5.97 (d, 1H,  $J_{3',2'} = 8.5$ , H1'-G); 6.11 (s, 1H, H1'-A); 7.09 (bd, 1H,  $J_{3,3} = 7.6$ , H2-naphth-A); 7.12 (m, 2H, H2 and H6-phenylene); 7.34 (m, 2H, H3 and H5-phenylene); 7.47 (m, 2H, H3 and H7-naphth-A); 7.54 (s, 1H, H6-A); 7.54 (m, 2H, H4 and H6-naphth-A); 7.76 (s, 1H, H8-G); 7.87 (bd, 1H,  $J_{5,6} = 8.3$ , H5-naphth-A); 8.03 (s, 1H, H2-A); 8.17 (bd, 1H,  $J_{8,7} = 8.5$ , H8-naphth-A).  $^{13}\text{C}$  NMR (150.9 MHz, D<sub>2</sub>O): 65.51 (d,  $J_{C,P} = 4.0$ , C5'-A); 68.67 (d,  $J_{C,P} = 5.1$ , C5'-G); 73.02 (CH<sub>2</sub>O); 73.15 (d,  $J_{C,P} = 5.6$ , C3'-A); 73.91 (C3'-G); 76.88 (C2'-A); 78.06 (d,  $J_{C,P} = 5.8$ , C2'-G); 82.56 (t,  $J_{C,P1} = J_{C,P2} = 11.2$ , C4'-A); 85.95 (d,  $J_{C,P} = 9.4$ , C4'-G); 88.51 (d,  $J_{C,P} = 12.2$ , C1'-G); 92.09 (C1'-A); 103.57 (C4a-A); 109.29 (C2-naphth); 118.94 (C5-A); 119.81 (C5-G); 122.80 (C6-A); 123.49 (C4-naphth); 124.15 (C8-naphth); 127.72 (C4a-naphth); 128.35 (C7-naphth); 129.04 (C3-naphth); 129.41 (C6-naphth); 130.23 (C5-naphth); 130.46 (C2 and C6-phenylene); 130.98 (C3 and C5-phenylene); 136.61 (C1-phenylene); 136.86 (C8a-naphth-A); 137.84 (C4-phenylene); 142.06 (C8-G); 150.92 (C7a-A); 153.37 (C2-A); 154.50 (C4-G); 155.92 (C2-G); 156.43 (C1-naphth-A); 159.61 (C4-A); 161.05 (C6-G).  $^{31}\text{P}$  NMR (H<sub>2</sub>O, 202.4 MHz, D<sub>2</sub>O): -0.21 and -0.96. ESI MS  $m/z$  (rel. %): 451 (100) [M-2H]<sup>2-</sup>, 462 (5) [M-3H + Na]<sup>2-</sup>, 904 (6) [M-H]<sup>-</sup>. HR MS (ESI): for C<sub>38</sub>H<sub>36</sub>O<sub>14</sub>N<sub>4</sub>P<sub>2</sub> [M-H]<sup>-</sup>, calcd 904.18624; found, 904.18469.

**Cyclo-4-amino-5-(furan-2-yl)-7-β-D-ribofuranosyl-7H-pyrrolo[2,3-d]pyrimidine 5'-O-phosphate (3' → 5') Guanosine 5'-O-phosphate (2' → 5') Sodium Salt (5n).** NTP 3n (2 μmol) and GTP (2 μmol) were enzymatically cyclized using mcGAS. The final product was purified by HPLC (5–30% MeCN in 0.1 M TEAB). The conversion to a sodium salt form on a Dowex 50WX8 (in a Na<sup>+</sup> cycle)

provided CDN 5n (299 nmol, 15%).  $^1\text{H}$  NMR (600 MHz, D<sub>2</sub>O): 4.13 (ddd, 1H,  $J_{3',4'} = 1.9$ ,  $J_{3',5'} = 11.8$ ,  $J_{3',P} = 2.0$ , H5'-b-G); 4.23 (ddd, 1H,  $J_{3',4'} = 3.1$ ,  $J_{3',5'} = 11.8$ ,  $J_{3',P} = 4.5$ , H5'-a-G); 4.34 (ddd, 1H,  $J_{3',5'} = 12.0$ ,  $J_{3',6'} = 2.7$ ,  $J_{3',P} = 1.1$ , H5'-b-A); 4.42 (ddd, 1H,  $J_{4',5'} = 3.1$ ,  $J_{4',6'} = 1.9$ ,  $J_{4',P} = 3.6$ , H4'-G); 4.50 (dm, 1H,  $J_{4',5'} = 9.7$ , H4'-A); 4.61 (ddd, 1H,  $J_{3',4'} = 12.0$ ,  $J_{3',5'} = 2.2$ ,  $J_{3',P} < 1.0$ , H5'-a-A); 4.66 (d, 1H,  $J_{3',4'} = 4.0$ , H3'-G); 4.66 (d, 1H,  $J_{3',2'} = 4.0$ , H2'-A); 5.01 (ddd, 1H,  $J_{3',2'} = 4.0$ ,  $J_{3',4'} = 9.7$ ,  $J_{3',P} = 6.6$ , H3'-A); 5.74 (ddd, 1H,  $J_{3',2'} = 8.7$ ,  $J_{3',4'} = 4.0$ ,  $J_{3',P} = 3.8$ , H2'-G); 5.93 (d, 1H,  $J_{3',2'} = 8.7$ , H1'-G); 6.27 (s, 1H, H1'-A); 6.26 (dd, 1H,  $J_{4,3} = 3.5$ ,  $J_{4,5} = 1.8$ , H4-furyl); 6.28 (dd, 1H,  $J_{3,4} = 3.5$ ,  $J_{3,5} = 0.8$ , H3-furyl); 7.42 (dd, 1H,  $J_{5,4} = 1.8$ ,  $J_{5,3} = 0.8$ , H5-furyl); 7.75 (s, 1H, H8-G); 8.00 (s, 1H, H6-A); 8.19 (s, 1H, H2-A).  $^{13}\text{C}$  NMR (150.9 MHz, D<sub>2</sub>O): 65.48 (d,  $J_{C,P} = 4.0$ , C5'-A); 68.56 (d,  $J_{C,P} = 5.2$ , C5'-G); 72.66 (d,  $J_{C,P} = 5.3$ , C3'-A); 73.70 (C3'-G); 76.92 (C2'-A); 77.59 (br, C2'-G); 82.34 (t,  $J_{C,P1} = J_{C,P2} = 11.5$ , C4'-A); 85.82 (d,  $J_{C,P} = 10.2$ , C4'-G); 88.84 (d,  $J_{C,P} = 15.0$ , C1'-G); 92.50 (C1'-A); 102.40 (C5-A); 106.58 (C3-furyl); 109.14 (C4a-A); 114.75 (C4-furyl); 119.79 (C5-G); 120.95 (C6-A); 142.52 (C8-G); 143.61 (C5-furyl); 150.48 (C2-furyl); 150.75 (C7a-A); 154.03 (C2-A); 154.47 (C4-G); 155.82 (C2-G); 159.59 (C4-A); 161.11 (C6-G).  $^{31}\text{P}$  NMR (H<sub>2</sub>O, 202.4 MHz, D<sub>2</sub>O): -0.16 and -1.18. ESI MS  $m/z$  (rel. %): 368 (100) [M-2H]<sup>2-</sup>, 379 (6) [M-3H + Na]<sup>2-</sup>, 738 (14) [M-H]<sup>-</sup>, 760 (14) [M-2H + Na]<sup>-</sup>. HR MS (ESI): for C<sub>24</sub>H<sub>26</sub>O<sub>14</sub>N<sub>4</sub>P<sub>2</sub> [M-H]<sup>-</sup>, calcd 738.10799; found, 738.10760.

**Cyclo-4-amino-7-β-D-ribofuranosyl-5-(thiophen-2-yl)-7H-pyrrolo[2,3-d]pyrimidine 5'-O-phosphate (3' → 5') Guanosine 5'-O-phosphate (2' → 5') Sodium Salt (5o).** NTP 3c (2 μmol) and GTP (2 μmol) were enzymatically cyclized using mcGAS. The final product was purified by HPLC (5–30% MeCN in 0.1 M TEAB). The conversion to a sodium salt form on a Dowex 50WX8 (in a Na<sup>+</sup> cycle) provided CDN 5o (266 nmol, 13%).  $^1\text{H}$  NMR (600 MHz, D<sub>2</sub>O): 4.15 (ddd, 1H,  $J_{3',4'} = 1.8$ ,  $J_{3',5'} = 11.8$ ,  $J_{3',P} = 2.2$ , H5'-b-G); 4.29 (ddd, 1H,  $J_{3',4'} = 2.8$ ,  $J_{3',5'} = 11.8$ ,  $J_{3',P} = 4.9$ , H5'-a-G); 4.31 (ddd, 1H,  $J_{3',5'} = 12.0$ ,  $J_{3',6'} = 3.1$ ,  $J_{3',P} = 1.2$ , H5'-b-A); 4.44 (ddd, 1H,  $J_{4',5'} = 2.8$ ,  $J_{4',6'} = 1.8$ ,  $J_{4',P} = 3.6$ , H4'-G); 4.49 (dm, 1H,  $J_{4',5'} = 9.2$ , H4'-A); 4.52 (dm, 1H,  $J_{3',4'} = 12.0$ , H5'-a-A); 4.66 (d, 1H,  $J_{3',4'} = 4.0$ , H3'-G); 4.79 (overlap, H2'-A); 5.00 (ddd, 1H,  $J_{3',2'} = 4.0$ , H2'-G);  $J_{3',P} = 6.5$ , H3'-A); 5.70 (dt, 1H,  $J_{3',2'} = 8.7$ ,  $J_{3',5'} = 4.0$ ,  $J_{3',P} = 4.0$ , H2'-G); 5.99 (d, 1H,  $J_{3',2'} = 8.7$ , H1'-G); 6.28 (s, 1H, H1'-A); 6.82 (dd, 1H,  $J_{5,4} = 3.5$ ,  $J_{5,3} = 1.2$ , H5-thienyl); 6.98 (dd, 1H,  $J_{4,3} = 5.2$ ,  $J_{4,5} = 3.5$ , H4-thienyl); 7.24 (dd, 1H,  $J_{3,4} = 5.2$ ,  $J_{3,5} = 1.2$ , H3-thienyl); 7.65 (s, 1H, H6-A); 7.87 (s, 1H, H8-G); 8.24 (s, 1H, H2-A).  $^{13}\text{C}$  NMR (150.9 MHz, D<sub>2</sub>O): 65.53 (d,  $J_{C,P} = 4.2$ , C5'-A); 68.66 (d,  $J_{C,P} = 5.2$ , C5'-G); 73.03 (d,  $J_{C,P} = 5.6$ , C3'-A); 73.86 (C3'-G); 76.84 (C2'-A); 77.74 (C2'-G); 82.62 (t,  $J_{C,P1} = 11.1$ , C4'-A); 85.96 (d,  $J_{C,P} = 9.8$ , C4'-G); 88.78 (d,  $J_{C,P} = 9.8$ , C1'-G); 92.20 (C1'-A); 103.70 (C5-A); 112.08 (C4a-A); 120.00 (C5-G); 123.16 (C6-A); 128.07 (C3-thienyl); 128.26 (C5-thienyl); 130.70 (C4-thienyl); 137.46 (C2-thienyl); 142.56 (C8-G); 151.16 (C7a-A); 154.12 (C2-A); 154.69 (C4-G); 155.97 (C2-G); 160.00 (C4-A); 161.29 (C6-G).  $^{31}\text{P}$  NMR (H<sub>2</sub>O, 202.4 MHz, D<sub>2</sub>O): -0.24 and -0.93. ESI MS  $m/z$  (rel. %): 376 (100) [M-2H]<sup>2-</sup>, 387 (4) [M-H + Na]<sup>2-</sup>, 754 (4) [M-H]<sup>-</sup>, 776 (10) [M-2H + Na]<sup>-</sup>. HR MS (ESI): for C<sub>22</sub>H<sub>26</sub>O<sub>13</sub>N<sub>4</sub>P<sub>2</sub> [M-H]<sup>-</sup>, calcd 754.08515; found, 754.08502.

**Cyclo-4-amino-5-(benzofuran-2-yl)-7-β-D-ribofuranosyl-7H-pyrrolo[2,3-d]pyrimidine 5'-O-phosphate (3' → 5') Guanosine 5'-O-phosphate (2' → 5') Sodium Salt (5p).** CDN 5p was prepared as described for 5g from iodinated CDN 5a (15 mg, 17.8 μmol) and benzofuran-2-ylboronic acid (14.4 mg, 88.9 μmol). After two HPLC purifications (5–25% MeCN in 0.1 M TEAB and 5–50% MeOH in 0.1 M TEAB) and conversion to a sodium salt form on a Dowex 50WX8 (in a Na<sup>+</sup> cycle), CDN 5p (8.1 mg, 55%) was obtained as a white lyophilizate (water).  $^1\text{H}$  NMR (600 MHz, D<sub>2</sub>O): 4.07 (ddd, 1H,  $J_{3',4'} = 1.8$ ,  $J_{3',5'} = 11.8$ ,  $J_{3',P} = 2.4$ , H5'-b-G); 4.20 (ddd, 1H,  $J_{3',4'} = 2.9$ ,  $J_{3',5'} = 11.8$ ,  $J_{3',P} = 4.2$ , H5'-a-G); 4.35 (ddd, 1H,  $J_{3',4'} = 1.0$ ,  $J_{3',5'} = 11.8$ ,  $J_{3',P} = 2.6$ , H5'-b-A); 4.38 (ddd, 1H,  $J_{4',5'} = 2.9$ ,  $J_{4',6'} = 1.8$ ,  $J_{4',P} = 3.6$ , H4'-G); 4.51 (dm, 1H,  $J_{4',5'} = 9.5$ , H4'-A); 4.59 (d, 1H,  $J_{3',2'} = 3.8$ , H2'-A); 4.65 (ddd, 1H,  $J_{3',4'} = 2.0$ ,  $J_{3',5'} = 11.8$ ,  $J_{3',P} < 1$ , H5'-a-A); 4.67 (d, 1H,  $J_{3',4'} = 3.8$ , H3'-G); 4.93 (ddd, 1H,  $J_{3',2'} = 3.8$ ,  $J_{3',4'} = 9.5$ ,  $J_{3',P} = 6.5$ , H3'-A); 5.62 (um, H2'-G); 5.90 (d,

<sup>1</sup>H,  $J_{1,2} = 8.5$ , H1'-G); 6.18 (s, 1H, H1'-A); 6.65 (d, 1H,  $J_{3,4} = 3.8$ , H3-benzofuryl); 7.22 (td, 1H,  $J_{5,6} = 6.8$ ,  $J_{5,4} = 6.8$ ,  $J_{5,7} = 1.3$ , H5-benzofuryl); 7.24 (ddd, 1H,  $J_{6,5} = 6.8$ ,  $J_{6,7} = 7.1$ ,  $J_{6,4} = 1.6$ , H6-benzofuryl); 7.42 (m, 2H, H4-benzofuryl + H7-benzofuryl); 7.47 (s, 1H, H8-G); 8.09 (s, 1H, H2-A); 8.10 (s, 1H, H6-A). <sup>13</sup>C NMR (150.9 MHz, D<sub>2</sub>O): 65.53 (C5'-A); 68.59 (d,  $J_{C,P} = 3.7$ , C5'-G); 72.68 (d,  $J_{C,P} = 4.3$ , C3'-A); 82.33 (t,  $J_{C,P1} = J_{C,P2} = 10.6$ , C4'-A); 85.83 (d,  $J_{C,P} = 6.3$ , C4'-G); 88.02 (d,  $J_{C,P} = 12.0$ , C1'-G); 92.25 (C1'-A); 102.44 (C4a-A); 102.51 (C3-benzofuryl); 108.58 (C5-A); 113.48 (C7-benzofuryl); 119.31 (C5-G); 122.77 (C6-A); 123.46 (C4-benzofuryl); 125.99 (C5-benzofuryl); 126.32 (C6-benzofuryl); 131.49 (C3a-benzofuryl); 141.30 (C8-G); 150.77 (C7a-A); 152.57 (C2-benzofuryl); 153.71 (C2-A); 154.26 (C4-G); 155.77 (C2-G); 156.02 (C7a-benzofuryl); 159.60 (C4-A); 160.54 (C6-G). <sup>31</sup>P NMR (<sup>1</sup>H-dec, 202.4 MHz, D<sub>2</sub>O): -0.10 and -1.10. ESI MS  $m/z$  (rel. %): 393 (100) [M-2H]<sup>2-</sup>, 788 (44) [M-H]<sup>-</sup>, 810 (21) [M-2H + Na]<sup>-</sup>. HR MS (ESI): for C<sub>23</sub>H<sub>18</sub>O<sub>14</sub>N<sub>2</sub>P<sub>2</sub> [M-H]<sup>-</sup>, calcd 788.12364; found, 788.12413.

**Cyclo-4-amino-5-(benzothiophen-2-yl)-7-β-D-ribofuranosyl-7H-pyrrolo[2,3-d]pyrimidine 5'-O-phosphate (3' → 5') Guanosine 5'-O-phosphate (2' → 5') Sodium Salt (5q).** CDN 5q was prepared as described for 5g from iodinated CDN 5a (12 mg, 14.2 μmol) and benzothiophen-2-ylboronic acid (12.6 mg, 71.1 μmol). After two HPLC purifications (5–25% MeCN in 0.1 M TEAB and 9–24% MeCN in 0.1 M TEAB) and conversion to a sodium salt form on a Dowex 50WX8 (in a Na<sup>+</sup> cycle), CDN 5q (4.8 mg, 40%) was obtained as a white lyophilizate (water). <sup>1</sup>H NMR (600 MHz, D<sub>2</sub>O): 4.12 (ddd, 1H,  $J_{5'b,4'} = 1.6$ ,  $J_{5'b,5'a} = 11.8$ ,  $J_{5'b,P} = 2.5$ , H5'-b-G); 4.25 (ddd, 1H,  $J_{5'a,4'} = 2.6$ ,  $J_{5'a,5'b} = 11.8$ ,  $J_{5'a,P} = 4.4$ , H5'-a-G); 4.35 (ddd, 1H,  $J_{5'b,4'} \sim 1.0$ ,  $J_{5'b,5'a} = 12.0$ ,  $J_{5'b,P} = 2.5$ , H5'-b-A); 4.44 (ddd, 1H,  $J_{4',5'a} = 2.6$ ,  $J_{4',5'b} = 1.6$ ,  $J_{4',P} = 3.8$ , H4'-G); 4.52 (dm, 1H,  $J_{4',3'} = 9.3$ , H4'-A); 4.57 (dm, 1H,  $J_{5'a,5'b} = 12.0$ , H5'-a-A); 4.71 (d, 1H,  $J_{5',4'} = 4.0$ , H3'-G); 4.77 (overlap, H2'-A); 4.95 (ddd, 1H,  $J_{2',3'} = 4.0$ ,  $J_{5',4'} = 9.3$ ,  $J_{5',P} = 6.7$ , H3'-A); 5.60 (unm, 1H, H2'-G); 6.03 (d, 1H,  $J_{1',2'} = 8.7$ , H1'-G); 6.30 (s, 1H, H1'-A); 7.10 (s, 1H, H3-benzothiophenyl); 7.36 (ddd, 1H,  $J_{6,5} = 1.3$ ,  $J_{6,7} = 7.0$ ,  $J_{6,7} = 8.0$ , H6-benzothiophenyl); 7.41 (ddd, 1H,  $J_{5,4} = 8.0$ ,  $J_{5,6} = 7.0$ ,  $J_{5,7} = 1.2$ , H5-benzothiophenyl); 7.72 (dd, 1H,  $J_{4,5} = 8.0$ ,  $J_{4,6} = 1.3$ , H4-benzothiophenyl); 7.75 (s, 1H, H6-A); 7.78 (s, 1H, H8-G); 7.82 (dd, 1H,  $J_{7,8} = 8.0$ ,  $J_{7,5} = 1.2$ , H7-benzothiophenyl); 8.23 (s, 1H, H2-A); 8.37 (dd, 1H,  $J_{3',4'} = 3.8$ ,  $J_{3',5'} = 10.6$ , C3'-A); 65.61 (b, C5'-A); 68.75 (d,  $J_{C,P} = 4.3$ , C5'-G); 72.96 (d,  $J_{C,P} = 5.4$ , C3'-A); 73.90 (C3'-G); 76.89 (C2'-A); 78.91 (C2'-G); 82.52 (t,  $J_{C,P} = 11.3$ , C4'-A); 86.08 (d,  $J_{C,P} = 9.6$ , C4'-G); 87.84 (C1'-G); 92.23 (C1'-A); 103.70 (C5-A); 112.55 (C4a-A); 119.66 (C5-G); 123.70 (C6-A); 124.04 (C3-benzothiophenyl); 124.89 (C7-benzothiophenyl); 126.22 (C4-benzothiophenyl); 126.99 (C6-benzothiophenyl); 127.37 (C6-benzothiophenyl); 141.14 (C8-G); 138.36 (C2-benzothiophenyl); 141.78 (C7a-benzothiophenyl); 142.94 (C3a-benzothiophenyl); 151.46 (C7a-A); 154.26 (C2-A); 154.59 (C4-G); 156.00 (C2-G); 160.18 (C4-A); 160.87 (C6-G). <sup>31</sup>P NMR (<sup>1</sup>H-dec, 202.4 MHz, D<sub>2</sub>O): -0.16 and -0.88. ESI MS  $m/z$  (rel. %): 436 (100) [M-2H]<sup>2-</sup>, 874 (16) [M-H]<sup>-</sup>, 896 (14) [M-2H + Na]<sup>-</sup>. HR MS (ESI): for C<sub>23</sub>H<sub>18</sub>O<sub>14</sub>N<sub>2</sub>P<sub>2</sub> [M-H]<sup>-</sup>, calcd 874.17568; found, 874.17462.

**Cyclo-4-amino-5-(dibenzo[b,d]furan-4-yl)-7-β-D-ribofuranosyl-7H-pyrrolo[2,3-d]pyrimidine 5'-O-phosphate (3' → 5') Guanosine 5'-O-phosphate (2' → 5') Sodium Salt (5r) and Open Isomer 16.** CDN 5r was prepared as described for 5g from iodinated CDN 5a (15 mg, 17.8 μmol) and dibenzofuran-4-ylboronic acid (19 mg, 89.6 μmol). After two purifications (5–25% MeCN in 0.1 M TEAB) and conversion to a sodium salt form on a Dowex 50WX8 (in a Na<sup>+</sup> cycle), CDN 5r (6.3 mg, 40%) was obtained as a white lyophilizate (water). As a byproduct, compound 16 was isolated and converted to a sodium salt form on a Dowex 50WX8 (in a Na<sup>+</sup> cycle). Open isomer 16 (2.0 mg, 13%) was obtained as a white lyophilizate (water). CDN 5r: <sup>1</sup>H NMR (600 MHz, D<sub>2</sub>O): 4.10 (ddd, 1H,  $J_{5'b,4'} = 2.1$ ,  $J_{5'b,5'a} = 11.9$ ,  $J_{5'b,P} = 2.4$ , H5'-b-G); 4.22 (ddd, 1H,  $J_{5'a,4'} = 2.5$ ,  $J_{5'a,5'b} = 11.9$ ,  $J_{5'a,P} = 5.8$ , H5'-a-G); 4.33 (m, 1H, H5'-b-A); 4.38 (ddd, 1H,  $J_{4',5'a} = 2.5$ ,  $J_{4',5'b} = 2.1$ ,  $J_{4',P} = 3.4$ , H4'-G); 4.48 (m, 1H, H5'-a-A); 4.49 (dm, 1H,  $J_{4',3'} = 9.0$ , H4'-A); 4.64 (d, 1H,  $J_{5',4'} = 3.5$ , H3'-G); 4.85 (d, 1H,

$J_{2',3'} = 4.6$ , H2'-A); 5.10 (ddd, 1H,  $J_{5',4'} = 4.6$ ,  $J_{5',5'a} = 9.0$ ,  $J_{5',P} = 6.2$ , H3'-A); 5.84 (ddd, 1H,  $J_{1',2'} = 8.6$ ,  $J_{1',3'} = 3.5$ ,  $J_{1',P} = 3.7$ , H2'-G); 5.92 (d, 1H,  $J_{1',2'} = 8.6$ , H1'-G); 6.40 (s, 1H, H1'-A); 7.04 (dd, 1H,  $J_{3,2} = 7.5$ ,  $J_{3,1} = 1.3$ , H3-dibenzofuryl); 7.14 (dd, 1H,  $J_{2,3} = 7.5$ ,  $J_{2,1} = 7.8$ , H2-dibenzofuryl); 7.40 (td, 1H,  $J_{6,5} = 7.4$ ,  $J_{6,7} = 7.4$ ,  $J_{6,6} = 1.2$ , H8-dibenzofuryl); 7.44 (ddd, 1H,  $J_{7,6} = 8.2$ ,  $J_{7,8} = 7.4$ ,  $J_{7,9} = 1.5$ , H7-dibenzofuryl); 7.49 (s, 1H, H6-A); 7.59 (ddd, 1H,  $J_{6,7} = 8.2$ ,  $J_{6,8} = 1.2$ ,  $J_{6,9} = 0.7$ , H6-dibenzofuryl-A); 7.68 (s, 1H, H8-G); 7.76 (dd, 1H,  $J_{1,2} = 7.8$ ,  $J_{1,3} = 1.3$ , H1-dibenzofuryl); 8.00 (ddd, 1H,  $J_{3,4} = 7.4$ ,  $J_{3,5} = 1.5$ ,  $J_{3,6} = 0.7$ , H9-dibenzofuryl); 8.19 (s, 1H, H2-A). <sup>13</sup>C NMR (150.9 MHz, D<sub>2</sub>O): 65.59 (d,  $J_{C,P} = 4.9$ , C5'-A); 68.80 (d,  $J_{C,P} = 4.9$ , C5'-G); 73.79 (d,  $J_{C,P} = 5.5$ , C3'-A); 74.22 (C3'-G); 77.14 (C2'-A); 77.50 (d,  $J_{C,P} = 4.5$ , C2'-G); 82.84 (t,  $J_{C,P1} = J_{C,P2} = 11.2$ , C4'-A); 85.76 (d,  $J_{C,P} = 9.5$ , C4'-G); 88.79 (d,  $J_{C,P} = 12.3$ , C1'-G); 91.31 (C1'-A); 104.21 (C4a-A); 113.84 (C5-A); 114.61 (C6-dibenzofuryl); 119.57 (C4-dibenzofuryl); 119.60 (C5-G); 122.52 (C1-dibenzofuryl); 123.72 (C9-dibenzofuryl); 124.05 (C6-A); 125.81 (C8-dibenzofuryl); 126.08 (C2-dibenzofuryl); 126.44 (C9a-dibenzofuryl); 127.01 (C9b-dibenzofuryl); 130.15 (C7-dibenzofuryl); 130.40 (C3-dibenzofuryl); 142.45 (C8-G); 151.79 (C7a-A); 154.22 (C4-G); 154.27 (C2-A); 155.08 (C4a-dibenzofuryl); 155.88 (C2-G); 158.29 (C5a-dibenzofuryl); 160.13 (C4-A); 160.59 (C6-G). <sup>31</sup>P NMR (<sup>1</sup>H-dec, 202.4 MHz, D<sub>2</sub>O): -0.19 and -0.44. ESI MS  $m/z$  (rel. %): 418 (100) [M-2H]<sup>2-</sup>, 838 (28) [M-H]<sup>-</sup>, 860 (13) [M-2H + Na]<sup>-</sup>. HR MS (ESI): for C<sub>33</sub>H<sub>30</sub>O<sub>14</sub>N<sub>2</sub>P<sub>2</sub> [M-H]<sup>-</sup>, calcd 838.13929; found, 838.13778. Open isomer 16: <sup>1</sup>H NMR (600 MHz, D<sub>2</sub>O): 3.34 (dd, 1H,  $J_{5'b,4'} = 4.5$ ,  $J_{5'b,5'a} = 12.8$ , H5'-b-G); 3.46 (dd, 1H,  $J_{5'a,4'} = 2.5$ ,  $J_{5'a,5'b} = 12.8$ , H5'-a-G); 3.50 (dd, 1H,  $J_{5',2'} = 4.6$ ,  $J_{5',4'} = 7.8$ , H3'-G); 3.76 (ddd, 1H,  $J_{4',3'} = 7.8$ ,  $J_{4',5'a} = 2.5$ ,  $J_{4',5'b} = 4.5$ , H4'-G); 4.12 (ddd, 1H,  $J_{5'b,4'} = 2.6$ ,  $J_{5'b,5'a} = 11.7$ ,  $J_{5'b,P} = 4.2$ , H5'-b-A); 4.19 (ddd, 1H,  $J_{5'a,4'} = 2.8$ ,  $J_{5'a,5'b} = 11.7$ ,  $J_{5'a,P} = 5.1$ , H5'-a-A); 4.42 (ddd, 1H,  $J_{1',2'} = 2.1$ ,  $J_{1',3'} = 4.6$ ,  $J_{1',P} = 7.4$ , H2'-G); 4.58 (m, 1H,  $J_{4',3'} = 3.2$ ,  $J_{4',5'a} = 2.8$ ,  $J_{4',5'b} = 2.6$ ,  $J_{4',P} = 2.5$ , H4'-A); 5.19 (td, 1H,  $J_{5',2'} = 6.6$ ,  $J_{5',4'} = 3.2$ ,  $J_{5',P} = 6.6$ , H3'-A); 5.42 (ddd, 1H,  $J_{2',1'} = 4.3$ ,  $J_{2',3'} = 6.6$ ,  $J_{2',P} = 11.6$ , H2'-A); 5.60 (d, 1H,  $J_{1',2'} = 2.1$ , H1'-G); 6.34 (d, 1H,  $J_{1',2'} = 4.3$ , H1'-A); 7.00 (dd, 1H,  $J_{3,2} = 7.4$ ,  $J_{3,1} = 1.3$ , H3-dibenzofuryl); 7.25 (dd, 1H,  $J_{2,3} = 7.4$ ,  $J_{2,1} = 7.7$ , H2-dibenzofuryl); 7.39 (ddd, 1H,  $J_{6,5} = 7.7$ ,  $J_{6,7} = 7.2$ ,  $J_{6,6} = 1.0$ , H8-dibenzofuryl); 7.47 (s, 1H, H8-G); 7.49 (s, 1H, H6-A); 7.50 (ddd, 1H,  $J_{7,6} = 8.2$ ,  $J_{7,8} = 7.2$ ,  $J_{7,9} = 1.3$ , H7-dibenzofuryl); 7.56 (ddd, 1H,  $J_{5,7} = 8.2$ ,  $J_{5,8} = 1.0$ ,  $J_{5,9} = 0.7$ , H6-dibenzofuryl-A); 7.74 (dd, 1H,  $J_{1,2} = 7.7$ ,  $J_{1,3} = 1.3$ , H1-dibenzofuryl); 7.92 (ddd, 1H,  $J_{3,4} = 7.7$ ,  $J_{3,5} = 1.3$ ,  $J_{3,6} = 0.7$ , H9-dibenzofuryl); 8.01 (s, 1H, H2-A). <sup>13</sup>C NMR (150.9 MHz, D<sub>2</sub>O): 62.76 (C5'-G); 67.72 (d,  $J_{C,P} = 4.1$ , C5'-A); 71.28 (C3'-G); 79.98 (d,  $J_{C,P} = 5.4$ , C2'-G); 80.78 (d,  $J_{C,P} = 1.5$ , C3'-A); 84.00 (d,  $J_{C,P} = 1.1$ , C2'-A); 85.52 (C4'-G); 86.02 (d,  $J_{C,P} = 13.6$ , C4'-A); 89.95 (d,  $J_{C,P} = 6.7$ , C1'-G); 90.99 (d,  $J_{C,P} = 12.8$ , C1'-A); 103.36 (C4a-A); 114.12 (C5-A); 114.35 (C6-dibenzofuryl); 118.64 (C5-G); 119.57 (C4-dibenzofuryl); 122.29 (C1-dibenzofuryl); 123.51 (C9-dibenzofuryl); 124.43 (C6-A); 125.85 (C8-dibenzofuryl); 126.16 (C2-dibenzofuryl); 126.20 (C9a-dibenzofuryl); 127.03 (C9b-dibenzofuryl); 129.87 (C3-dibenzofuryl); 130.34 (C7-dibenzofuryl); 139.26 (C8-G); 152.46 (C7a-A); 152.86 (C4-G); 154.06 (C2-A); 154.96 (C4a-dibenzofuryl); 155.58 (C2-G); 158.12 (C5a-dibenzofuryl); 159.44 (C4-A); 160.77 (C6-G). <sup>31</sup>P NMR (<sup>1</sup>H-dec, 202.4 MHz, D<sub>2</sub>O): 0.66 and 20.92. ESI MS  $m/z$  (rel. %): 418 (100) [M-2H]<sup>2-</sup>, 838 (12) [M-H]<sup>-</sup>, 860 (17) [M-2H + Na]<sup>-</sup>, 882 (4) [M-3H+2Na]<sup>-</sup>. HR MS (ESI): for C<sub>33</sub>H<sub>30</sub>O<sub>14</sub>N<sub>2</sub>P<sub>2</sub> [M-H]<sup>-</sup>, calcd 838.13929; found, 838.13853.

**Cyclo-4-amino-5-phenyl-7-β-D-ribofuranosyl-7H-pyrrolo[2,3-d]pyrimidine 5'-O-phosphate (3' → 5') 2-Amino-5-phenyl-7-β-D-ribofuranosyl-7H-pyrrolo[2,3-d]pyrimidin-4(3H)-one 5'-O-phosphate (2' → 5') Sodium Salt (6f).** NTPs 2f (2 μmol) and 3f (2 μmol) were enzymatically cyclized using mcGAS. The final product was purified by HPLC (5–30% MeCN in 0.1 M TEAB). The conversion to a sodium salt form on a Dowex 50WX8 (in a Na<sup>+</sup> cycle) provided CDN 6f (128 nmol, 6%). <sup>1</sup>H NMR (600 MHz, D<sub>2</sub>O): 4.14 (ddd, 1H,  $J_{5'b,4'} = 1.2$ ,  $J_{5'b,5'a} = 11.6$ ,  $J_{5'b,P} = 3.0$ , H5'-b-G); 4.26 (ddd, 1H,  $J_{5'a,4'} = 2.1$ ,  $J_{5'a,5'b} = 11.6$ ,  $J_{5'a,P} = 2.7$ , H5'-a-G); 4.36 (ddd, 1H,  $J_{5'b,4'} = 1.2$ ,  $J_{5'b,5'a} = 12.2$ ,  $J_{5'b,P} = 3.2$ , H5'-b-A); 4.46 (m, 1H, H4'-G); 4.475 (dm, 1H,  $J_{4',3'} = 9.4$ , H4'-A); 4.52 (d,  $J_{2',3'} = 4.2$ , H2'-A); 4.53



(m, 1H, H5'-A); 4.76 (d, 1H,  $J_{5',4'} = 3.8$ , H3'-G); 4.99 (ddd, 1H,  $J_{3',2'} = 4.2$ ,  $J_{5',4'} = 9.4$ ,  $J_{3',P} = 7.2$ , H3'-A); 5.28 (um, 1H, H2'-G); 6.22 (s, 1H, H1'-A); 6.34 (d, 1H,  $J_{1',2'} = 8.4$ , H1'-G); 6.98 (m, 3H, *m*- and *p*-Ph-G); 7.11 (m, 2H, *o*-Ph-A); 7.26 (m, 3H, *m*- and *p*-Ph-A); 7.31 (m, 2H, *o*-Ph-G); 7.37 (s, 1H, H6-G); 7.54 (s, 1H, H6-A); 7.98 (s, 1H, H2-A).  $^{13}\text{C}$  NMR (150.9 MHz, D<sub>2</sub>O): 66.04 (C5'-A); 69.04 (C5'-G); 73.11 (C3'-A); 74.29 (C3'-G); 77.29 (C2'-A); 81.50 (C2'-G); 82.55 (C4'-A); 85.90 (C1'-G); 86.40 (C4'-G); 92.42 (C1'-A); 104.12 (C5-A); 117.34 (C6-G); 119.53 (C4-A); 122.67 (C6-A); 123.20 (*p*-Ph-G); 124.93 (C4-A-G); 129.29 (*o*-Ph-G); 129.85 (*o*-Ph-A); 130.10 (*m*-Ph-G); 131.27 (*m*-Ph and *p*-Ph-A); 151.02 (C7-A); 153.39 (C2-A); 155.51 (C7-A-G); 160.00 (C4-A); 163.10 (C4-G).  $^{31}\text{P}$  NMR (H<sub>2</sub>O, 202.4 MHz, D<sub>2</sub>O): 0.28 and -1.33. ESI MS *m/z* (rel. %): 411 (100) [M-2H]<sup>2-</sup>, 422 (13) [M-3H + Na]<sup>2-</sup>, 823 (11) [M-H]<sup>-</sup>, 845 (19) [M-2H + Na]<sup>-</sup>. HR MS (ESI): for C<sub>24</sub>H<sub>33</sub>N<sub>8</sub>O<sub>13</sub>P<sub>2</sub> [M-H]<sup>-</sup>, calcd 823.16478; found, 823.16454.

**Cyclo-4-amino-5-iodo-7-β-D-ribofuranosyl-7H-pyrrolo[2,3-d]pyrimidine 5'-O-phosphate (3' → 5') Guanosine 5'-O-phosphate (3' → 5') Sodium Salt (7a).** NTP 3a (13 μmol) and GTP (13 μmol) were enzymatically cyclized using DncV. The final product was purified by HPLC (5–30% MeCN in 0.1 M TEAB). The conversion to a sodium salt form on a Dowex 50WX8 (in a Na<sup>+</sup> cycle) provided CDN 7a (5.3 mg, 48%) as a white lyophilizate (water).  $^1\text{H}$  NMR (600 MHz, D<sub>2</sub>O): 4.11 (m, H5'-b-A); 4.12 (m, 1H, H5'-b-G); 4.36 (m, 1H, H5'-a-A); 4.39 (m, 1H, H4'-A); 4.42 (m, 2H, H4'-G + H5'-A-G); 4.55 (dd, 1H,  $J_{5',4'} = 1.0$ ,  $J_{5',P} = 4.6$ , H2'-A); 4.73 (overlap water, H3'-A); 4.79 (overlap water, H2'-G); 4.85 (m, 1H, H3'-G); 6.01 (d, 1H,  $J_{1',2'} = 1.0$ , H1'-G); 6.24 (d, 1H,  $J_{1',2'} = 1.0$ , H1'-A); 7.75 (s, 1H, H6-A); 8.05 (s, 1H, H8-G); 8.10 (s, 1H, H2-A).  $^{13}\text{C}$  NMR (150.9 MHz, D<sub>2</sub>O): 53.44 (C5-A); 64.77 (d,  $J_{C,P} = 5.0$ , C5'-A); 64.92 (d,  $J_{C,P} = 4.9$ , C5'-G); 73.32 (d,  $J_{C,P} = 4.8$ , C3'-A); 73.34 (d,  $J_{C,P} = 4.8$ , C3'-G); 76.57 (C2'-A); 76.74 (C2'-G); 81.85 (t,  $J_{C,P1} = J_{C,P2} = 10.4$ , C4'-A); 82.43 (t,  $J_{C,P1} = J_{C,P2} = 10.8$ , C4'-G); 91.90 (C1'-A); 92.86 (d,  $J_{C,P} = 12.0$ , C1'-G); 106.75 (C4-A); 119.66 (C5-G); 129.22 (C6-A); 139.65 (C8-G); 151.10 (C7-A); 153.43 (C4-G); 154.33 (C2-A); 158.62 (C2-G); 159.91 (C4-A); 161.62 (C6-G).  $^{31}\text{P}$  NMR (H<sub>2</sub>O, 202.4 MHz, D<sub>2</sub>O): -0.56 and -0.89. ESI MS *m/z* (rel. %): 398 (100) [M-2H]<sup>2-</sup>, 798 (45) [M-H]<sup>-</sup>, 820 (27) [M-2H + Na]<sup>-</sup>. HR MS (ESI): for C<sub>24</sub>H<sub>32</sub>O<sub>13</sub>N<sub>8</sub>P<sub>2</sub> [M-2H]<sup>2-</sup>, calcd 398.49340; found, 398.49324.

**Cyclo-4-amino-5-phenyl-7-β-D-ribofuranosyl-7H-pyrrolo[2,3-d]pyrimidine 5'-O-phosphate (3' → 5') Guanosine 5'-O-phosphate (3' → 5') Sodium Salt (7b).** CDN 7f was prepared as described for 5g from iodinated CDN 7a (13 mg, 15.4 μmol) and phenylboronic acid (9.4 mg, 77.1 μmol). The final product was purified using HPLC (0–15% MeCN in 0.1 M TEAB). The conversion to a sodium salt form on a Dowex 50WX8 (in a Na<sup>+</sup> cycle) provided CDN 7f (8.1 mg, 66%) as a white lyophilizate (water).  $^1\text{H}$  NMR (600 MHz, D<sub>2</sub>O): 4.10 (ddd, 1H,  $J_{5',4'} = 0.9$ ,  $J_{5',5b} = 12.0$ ,  $J_{5',P} = 4.4$ , H5'-b-A); 4.13 (dd, 1H,  $J_{5',5a} = 11.0$ ,  $J_{5',P} = 4.3$ , H5'-b-G); 4.37 (bdd, 1H,  $J_{5',4'} = 2.5$ ,  $J_{5',5b} = 12.0$ ,  $J_{5',P} < 1$ , H5'-a-A); 4.41 (m, 1H, H4'-A); 4.43 (m, 1H, H4'-G); 4.44 (dd, 1H,  $J_{5',4'} = 11.0$ ,  $J_{5',P} = 2.8$ , H5'-a-G); 4.52 (d, 1H,  $J_{2',3'} = 4.4$ , H2'-G); 4.61 (d, 1H,  $J_{2',3'} = 4.4$ , H2'-A); 4.78 (overlap, H3'-A); 4.80 (overlap, 1H, H3'-G); 5.98 (s, 1H, H1'-G); 6.42 (s, 1H, H1'-A); 7.18 (m, 3H, 2× *m*-Ph + *p*-Ph); 7.28 (m, 2H, 2× *o*-Ph); 7.47 (s, 1H, H6-A); 8.03 (s, 1H, H8-G); 8.18 (s, 1H, H2-A).  $^{13}\text{C}$  NMR (150.9 MHz, D<sub>2</sub>O): 64.73 (d,  $J_{C,P} = 5.9$ , C5'-A); 64.77 (d,  $J_{C,P} = 4.7$ , C5'-G); 72.94 (d,  $J_{C,P} = 4.8$ , C3'-A); 73.55 (d,  $J_{C,P} = 5.0$ , C3'-G); 76.74 (C2'-A); 76.86 (C2'-G); 81.62 (t,  $J_{C,P1} = J_{C,P2} = 10.8$ , C4'-A); 82.11 (t,  $J_{C,P} = 11.5$ , C4'-G); 91.51 (C1'-A); 92.46 (C1'-G); 103.77 (C4-A); 119.48 (C5-G); 120.80 (C5-A); 122.27 (C6-A); 129.37 (*p*-Ph); 130.68 (2× *o*-Ph); 131.16 (2× *m*-Ph); 135.81 (*i*-Ph); 138.74 (C8-G); 152.17 (C7-A); 152.78 (C4-G); 154.17 (C2-A); 156.67 (C2-G); 160.35 (C4-A); 161.40 (C6-G).  $^{31}\text{P}$  NMR (H<sub>2</sub>O, 202.4 MHz, D<sub>2</sub>O): -0.36 and -0.75. ESI MS *m/z* (rel. %): 373 (100) [M-2H]<sup>2-</sup>, 748 (6) [M-H]<sup>-</sup>, 770 (5) [M-2H + Na]<sup>-</sup>. HR MS (ESI): for C<sub>27</sub>H<sub>30</sub>O<sub>13</sub>N<sub>8</sub>P<sub>2</sub> [M-H]<sup>-</sup>, calcd 748.12873; found, 748.12726.

**Cyclic-di-4-amino-5-iodo-7-β-D-ribofuranosyl-7H-pyrrolo[2,3-d]pyrimidine 5'-O-phosphate (3' → 5') Sodium Salt (8a).** NTP 3a (26 μmol) was enzymatically cyclized using DisA. The final product

was purified by HPLC (5–30% MeCN in 0.1 M TEAB). The conversion to a sodium salt form on a Dowex 50WX8 (in a Na<sup>+</sup> cycle) provided CDN 8a (7.0 mg, 57%) as a white lyophilizate (water).  $^1\text{H}$  NMR (600 MHz, D<sub>2</sub>O): 4.15 (dd, 1H,  $J_{5',5a} = 11.7$ ,  $J_{5',P} = 5.1$ , H5'-b-A); 4.42 (dt, 1H,  $J_{4',3'} = 9.8$ ,  $J_{4',5a} = 2.7$ ,  $J_{5',P} = 2.8$ , H4'-A); 4.47 (bdd, 1H,  $J_{5',4'} = 2.7$ ,  $J_{5',5b} = 11.7$ ,  $J_{5',P} < 1$ , H5'-a-A); 4.60 (ddd, 1H,  $J_{2',3'} = 4.0$ ,  $J_{5',4'} = 9.8$ ,  $J_{5',P} = 6.2$ , H3'-A); 4.69 (d, 1H,  $J_{2',3'} = 4.0$ , H2'-A); 6.28 (s, 1H, H1'-A); 7.91 (s, 1H, H6-A); 8.12 (s, 1H, H2-A).  $^{13}\text{C}$  NMR (150.9 MHz, D<sub>2</sub>O): 52.38 (C5-A); 64.69 (d,  $J_{C,P} = 5.1$ , C5'-A); 73.45 (d,  $J_{C,P} = 5.3$ , C3'-A); 77.15 (C2'-A); 81.80 (t,  $J_{C,P1} = J_{C,P2} = 10.9$ , C4'-A); 92.67 (C1'-A); 107.78 (C4-A); 128.45 (C6-A); 150.57 (C7-A); 154.11 (C2-A); 160.03 (C4-A).  $^{31}\text{P}$  NMR (H<sub>2</sub>O, 202.4 MHz, D<sub>2</sub>O): -2.00. ESI MS *m/z* (rel. %): 452 (100) [M-2H]<sup>2-</sup>, 906 (28) [M-H]<sup>-</sup>, 928 (35) [M-2H + Na]<sup>-</sup>. HR MS (ESI): for C<sub>27</sub>H<sub>32</sub>O<sub>13</sub>N<sub>8</sub>P<sub>2</sub> [M-H]<sup>-</sup>, calcd 906.90055; found, 906.90021.

**Cyclic-di-4-amino-5-phenyl-7-β-D-ribofuranosyl-7H-pyrrolo[2,3-d]pyrimidine 5'-O-phosphate (3' → 5') Sodium Salt (8f).** CDN 8a (15 mg, 15.8 μmol), phenylboronic acid (19.2 mg, 157.5 μmol), and cesium carbonate (30.8 mg, 94.5 μmol) were mixed with MeCN-H<sub>2</sub>O (1:2 v/v, 1.065 mL) in an argon-purged vial. In a separate vial, Pd(OAc)<sub>2</sub> (1.0 mg, 4.45 μmol) and TPPS (12.6 mg, 22.2 μmol) were dissolved in MeCN-H<sub>2</sub>O (1:2 v/v, 1.0 mL), and the solution was sonicated under argon atmosphere for 30 s. Then, 353 μmol of this solution was transferred into the mixture containing CDN 8a, and the reaction was stirred at 100 °C for 30 min. Then, the reaction mixture was cooled to rt, diluted with water to approx. 3 mL, and filtered through a 5 μm nylon syringe filter. The filtrate was directly applied on HPLC for purification (0–17.5% MeCN in 0.1 M TEAB). The conversion to a sodium salt form on a Dowex 50WX8 (in a Na<sup>+</sup> cycle) provided CDN 8f (10.5 mg, 78%) as a white lyophilizate (water).  $^1\text{H}$  NMR (600 MHz, D<sub>2</sub>O): 4.18 (ddd, 1H,  $J_{5',5a} = 11.3$ ,  $J_{5',5b} = 1.5$ ,  $J_{5',P} = 4.8$ , H5'-b-A); 4.28 (d, 1H,  $J_{2',3'} = 3.9$ , H2'-A); 4.45 (m, 2H, H4'-A + H5'-A); 4.79 (overlap, H3'-A); 6.37 (s, 1H, H1'-A); 6.90 (m, 4H, *o*-Ph + *m*-Ph); 7.04 (m, 1H, *p*-Ph); 7.61 (s, 1H, H6-A); 8.16 (s, 1H, H2-A).  $^{13}\text{C}$  NMR (150.9 MHz, D<sub>2</sub>O): 64.78 (d,  $J_{C,P} = 5.0$ , C5'-A); 73.41 (d,  $J_{C,P} = 5.1$ , C3'-A); 77.32 (C2'-A); 81.62 (t,  $J_{C,P} = 10.9$ , C4'-A); 91.84 (C1'-A); 103.96 (C4-A); 120.61 (C5-A); 121.74 (C6-A); 129.62 (*p*-Ph); 130.32 (*o*-Ph); 130.85 (*m*-Ph); 135.28 (*i*-Ph); 151.20 (C7-A); 153.87 (C2-A); 159.85 (C4-A).  $^{31}\text{P}$  NMR (H<sub>2</sub>O, 202.4 MHz, D<sub>2</sub>O): -0.84. ESI MS *m/z* (rel. %): 403 (100) [M-2H]<sup>2-</sup>, 807 (3) [M-H]<sup>-</sup>, 829 (4) [M-2H + Na]<sup>-</sup>. HR MS (ESI): for C<sub>34</sub>H<sub>33</sub>O<sub>13</sub>N<sub>8</sub>P<sub>2</sub> [M-H]<sup>-</sup>, calcd 807.16986; found, 807.16888.

**4-Benzamido-5-iodo-7-[5-O-(4,4'-dimethoxytrityl)]-β-D-ribofuranosyl-7H-pyrrolo[2,3-d]pyrimidine (10).** 7-Iodo-7-deazaadenosine (9, ref 55, 500 mg, 1.28 mmol) was co-evaporated with anhydrous pyridine (2 × 3 mL) and suspended in anhydrous pyridine (5 mL). The suspension was cooled to 0 °C, and trimethylsilyl chloride (728 μL, 5.74 mmol) was added dropwise over a period of 30 min. Then, benzoyl chloride (222 μL, 1.91 mmol) was added, and the mixture was stirred at rt overnight. The reaction mixture was then cooled to 0 °C, and water (1.25 mL) was added. After stirring for 15 min, aqueous ammonia (25%, 2.5 mL) was added, and the stirring was continued for another 30 min. Solvents were then evaporated, and the residue was co-evaporated with anhydrous pyridine (2 × 3 mL) and dissolved in anhydrous pyridine (5 mL). DMTrCl (432 mg, 1.25 mmol) was added in two portions over 1 h, and the reaction mixture was stirred overnight. Then, DMTrCl (432 mg, 1.25 mmol) was added again in two portions over 1 h, and the reaction mixture was stirred for another 1.5 h. The solvent was removed in vacuo, the residue was suspended in DCM (35 mL), and the solid phase was filtered off through a pad of Celite. The filtrate was washed with saturated aqueous NaHCO<sub>3</sub>, dried over magnesium sulfate, and evaporated. Flash chromatography on silica (0–10% MeOH in DCM + 1% Et<sub>3</sub>N) provided nucleoside 10 (689 mg, 68%) as a white amorphous solid.  $^1\text{H}$  NMR (500.0 MHz, CD<sub>3</sub>OD): 3.39 (dd, 1H,  $J_{5',4'} = 10.7$ ,  $J_{5',5a} = 2.9$ , H5'-b); 3.42 (dd, 1H,  $J_{5',5a} = 10.7$ ,  $J_{5',4'} = 3.7$ , H5'-a); 3.757, 3.760 (2 × s, 2 × 3H, CH<sub>3</sub>O-DMTr); 4.19 (ddd, 1H,  $J_{4',3'} = 4.1$ ,  $J_{4',5a} = 3.7$ ,  $J_{4',5b} = 2.9$ , H4'-A); 4.46 (dd, 1H,  $J_{2',3'} = 5.0$ ,  $J_{2',3'} = 4.1$ , H3'-G); 4.72 (dd, 1H,  $J_{2',3'} = 5.4$ ,  $J_{2',3'} = 5.0$ , H2'-G); 6.37 (d, 1H,

$J_{1,2'} = 5.4$ , H-1'); 6.81–6.88 (m, 4H, H-m-C<sub>6</sub>H<sub>4</sub>-DMTr); 7.21 (m, 1H, H-p-C<sub>6</sub>H<sub>4</sub>-DMTr); 7.25–7.32 (m, 2H, H-m-C<sub>6</sub>H<sub>4</sub>-DMTr); 7.30–7.37 (m, 8H, H-o-C<sub>6</sub>H<sub>4</sub>-DMTr); 7.42–7.48 (m, 2H, H-o-C<sub>6</sub>H<sub>4</sub>-DMTr); 7.54–7.59 (m, 2H, H-m-Bz); 7.64 (m, 1H, H-p-Bz); 7.86 (s, 1H, H-6); 8.08–8.12 (m, 2H, H-o-Bz); 8.65 (s, 1H, H-2). <sup>13</sup>C NMR (125.7 MHz, CD<sub>3</sub>OD): 52.84 (C-5); 55.75, 55.76 (CH<sub>2</sub>O-DMTr); 64.74 (CH<sub>2</sub>-5'); 72.42 (CH-3'); 76.35 (CH-2'); 85.43 (CH-4'); 88.01 (C-DMTr); 89.41 (CH-1'); 114.23 (CH-m-C<sub>6</sub>H<sub>4</sub>-DMTr); 114.68 (C-4a); 127.99 (CH-p-C<sub>6</sub>H<sub>4</sub>-DMTr); 128.96 (CH-m-C<sub>6</sub>H<sub>4</sub>-DMTr); 129.23 (CH-o-Bz); 129.41 (CH-o-C<sub>6</sub>H<sub>4</sub>-DMTr); 129.90 (CH-m-Bz); 131.29, 131.40 (CH-o-C<sub>6</sub>H<sub>4</sub>-DMTr); 133.30 (CH-6); 133.78 (CH-p-Bz); 134.94 (C-i-Bz); 136.87, 137.15 (C-i-C<sub>6</sub>H<sub>4</sub>-DMTr); 146.04 (C-i-C<sub>6</sub>H<sub>4</sub>-DMTr); 152.24 (CH-2); 152.41 (C-4); 153.87 (C-7a); 160.17, 160.19 (C-p-C<sub>6</sub>H<sub>4</sub>-DMTr); 169.21 (C-i-Bz). ESI MS *m/z* (rel. %): 799 (23) [M + H]<sup>+</sup>, 821 (100) [M + Na]<sup>+</sup>, 837 (9) [M + K]<sup>+</sup>. HR MS (ESI): for C<sub>39</sub>H<sub>30</sub>O<sub>7</sub>N<sub>4</sub>I [M + H]<sup>+</sup>, calcd 799.16232; found, 799.16154.

**4-Benzamido-5-iodo-7-[2-O-tert-butylidimethylsilyl-5-O-(4,4'-dimethoxytrityl)-β-D-ribofuranosyl]-7H-pyrrolo[2,3-d]pyrimidine (11).** Nucleoside 10 (555 mg, 0.70 mmol) was co-evaporated with anhydrous pyridine (2 × 5 mL) and dissolved in anhydrous THF (10 mL). Anhydrous pyridine (485 μL) and silver nitrate (195 mg, 1.15 mmol) were added. The reaction flask was covered with aluminum foil, and the mixture was stirred at rt for 15 min. Then, TBDMSCl (183 mg, 1.21 mmol) was added, and the mixture was stirred overnight in the dark. The reaction mixture was then filtered through a pad of Celite. The filtration pad was washed with DCM, and the filtrate was evaporated. Flash chromatography on silica (5–50% EtOAc + 1% Et<sub>3</sub>N in cyclohexane) provided nucleoside 11 (251 mg, 40%) as a white foam. <sup>1</sup>H NMR (500.0 MHz, CD<sub>3</sub>OD): -0.13, 0.01 (2 × s, 2 × 3H, CH<sub>3</sub>Si); 0.81 (s, 9H, (CH<sub>3</sub>)<sub>3</sub>C); 3.43 (dd, 1H,  $J_{gem} = 10.7$ ,  $J_{3,4'} = 3.0$ , H-5'b); 3.46 (dd, 1H,  $J_{gem} = 10.7$ ,  $J_{3,4'} = 2.7$ , H-5'a); 3.779, 3.782 (2 × s, 2 × 3H, CH<sub>2</sub>O-DMTr); 4.29 (ddd, 1H,  $J_{1,2'} = 3.1$ ,  $J_{2,3'} = 2.7$ ,  $J_{2,3''} = 3.0$ , H-4'); 4.38 (dd, 1H,  $J_{2,3'} = 5.0$ ,  $J_{2,3''} = 3.1$ , H-3'); 4.80 (dd, 1H,  $J_{2,3'} = 5.9$ ,  $J_{2,3''} = 5.0$ , H-2'); 6.39 (d, 1H,  $J_{1,2'} = 5.9$ , H-1'); 6.85–6.90 (m, 4H, H-m-C<sub>6</sub>H<sub>4</sub>-DMTr); 7.24 (m, 1H, H-p-C<sub>6</sub>H<sub>4</sub>-DMTr); 7.28–7.33 (m, 2H, H-m-C<sub>6</sub>H<sub>4</sub>-DMTr); 7.34–7.39 (m, 8H, H-o-C<sub>6</sub>H<sub>4</sub>-DMTr); 7.45–7.49 (m, 2H, H-o-C<sub>6</sub>H<sub>4</sub>-DMTr); 7.55–7.60 (m, 2H, H-m-Bz); 7.66 (m, 1H, H-p-Bz); 7.91 (s, 1H, H-6); 8.09–8.13 (m, 2H, H-o-Bz); 8.65 (s, 1H, H-2). <sup>13</sup>C NMR (125.7 MHz, CD<sub>3</sub>OD): -4.94, -4.68 (CH<sub>3</sub>Si); 18.99 ((CH<sub>3</sub>)<sub>3</sub>C); 26.15 ((CH<sub>2</sub>)<sub>2</sub>C); 53.05 (C-5); 55.80 (CH<sub>2</sub>O-DMTr); 64.80 (CH<sub>2</sub>-5'); 72.98 (CH-3'); 78.48 (CH-2'); 86.02 (CH-4'); 88.27 (C-DMTr); 89.24 (CH-1'); 114.32 (CH-m-C<sub>6</sub>H<sub>4</sub>-DMTr); 114.57 (C-4a); 128.11 (CH-p-C<sub>6</sub>H<sub>4</sub>-DMTr); 129.05 (CH-m-C<sub>6</sub>H<sub>4</sub>-DMTr); 129.23 (CH-o-Bz); 129.35 (CH-o-C<sub>6</sub>H<sub>4</sub>-DMTr); 129.93 (CH-m-Bz); 131.33, 131.43 (CH-o-C<sub>6</sub>H<sub>4</sub>-DMTr); 133.16 (CH-6); 133.82 (CH-p-Bz); 134.94 (C-i-Bz); 136.74, 136.99 (C-i-C<sub>6</sub>H<sub>4</sub>-DMTr); 145.99 (C-i-C<sub>6</sub>H<sub>4</sub>-DMTr); 152.29 (CH-2); 152.55 (C-4); 153.92 (C-7a); 160.25, 160.26 (C-p-C<sub>6</sub>H<sub>4</sub>-DMTr); 169.22 (C-i-Bz). ESI MS *m/z* (rel. %): 913 (100) [M + H]<sup>+</sup>. HR MS (ESI): for C<sub>42</sub>H<sub>30</sub>O<sub>7</sub>N<sub>4</sub>ISI [M + H]<sup>+</sup>, calcd 913.24880; found, 913.24853.

**4-Benzamido-5-iodo-7-[2-O-tert-butylidimethylsilyl-β-D-ribofuranosyl]-7H-pyrrolo[2,3-d]pyrimidine 3'-O-Phosphonate Triethylammonium Salt (12).** Nucleoside 11 (525 mg, 0.58 mmol) was co-evaporated with anhydrous pyridine (2 × 5 mL) and dissolved in anhydrous pyridine (5 mL), and diphenyl phosphite (216 μL, 1.44 mmol) was added. The reaction mixture was stirred for 1 h, and then, water (8 mL) was added. The reaction mixture was stirred for 5 min, and it was then diluted with EtOAc and washed with brine. Aqueous phase was extracted twice with EtOAc. Combined organic phases were dried over MgSO<sub>4</sub> and evaporated. The residue was dissolved in DCM (7 mL), and then, water (104 μL) and a solution of dichloroacetic acid in DCM (6%, 6.58 mL, 5.0 mmol) were added. The solution was stirred at rt for 15 min, and then, triethylsilane (919 μL, 5.75 mmol) was added. The reaction mixture was stirred for another 30 min. The reaction was quenched with pyridine (823 μL), and solvents were removed in vacuo. Flash chromatography on C18 column (gradient 5–100% MeCN in 0.1 M TEAB) provided phosphonate 12 (354 mg, 77%) as a white foam. <sup>1</sup>H NMR (500.0

MHz, CD<sub>3</sub>OD): -0.24, 0.01 (2 × s, 2 × 3H, CH<sub>3</sub>Si); 0.77 (s, 9H, (CH<sub>3</sub>)<sub>3</sub>C); 1.31 (t, 9H,  $J_{ac} = 7.3$ , CH<sub>3</sub>CH<sub>2</sub>N); 3.20 (q, 6H,  $J_{ac} = 7.3$ , CH<sub>3</sub>CH<sub>2</sub>N); 3.87 (d, 2H,  $J_{2,3'} = 2.6$ , H-5'); 4.33 (q, 1H,  $J_{1,2'} = J_{4,5'} = 2.6$ , H-4'); 4.73–4.79 (m, 2H, H-2',3'); 6.33 (d, 1H,  $J_{1,2'} = 6.1$ , H-1'); 6.96 (d, 1H,  $J_{HP} = 630.1$ , HP); 7.54–7.59 (m, 2H, H-m-Bz); 7.65 (m, 1H, H-p-Bz); 8.07 (s, 1H, H-6); 8.10–8.15 (m, 2H, H-o-Bz); 8.67 (s, 1H, H-2). <sup>13</sup>C NMR (125.7 MHz, CD<sub>3</sub>OD): -5.22, -4.60 (CH<sub>3</sub>Si); 9.22 (CH, CH<sub>2</sub>N); 18.84 ((CH<sub>3</sub>)<sub>3</sub>C); 26.13 ((CH<sub>2</sub>)<sub>2</sub>C); 47.86 (CH<sub>3</sub>CH<sub>2</sub>N); 52.61 (C-5); 62.66 (CH<sub>2</sub>-5'); 75.43 (d,  $J_{CP} = 5.1$ , CH-3'); 77.09 (d,  $J_{CP} = 3.0$ , CH-2'); 87.07 (d,  $J_{CP} = 3.4$ , CH-4'); 89.77 (CH-1'); 114.84 (C-4a); 129.24 (CH-o-Bz); 129.89 (CH-m-Bz); 133.74 (CH-p-Bz); 133.93 (CH-6); 135.03 (C-i-Bz); 152.05 (CH-2); 152.68 (C-4); 153.65 (C-7a); 169.10 (C-i-Bz). <sup>31</sup>P{<sup>1</sup>H} NMR (202.4 MHz, CD<sub>3</sub>OD): 5.24. ESI MS *m/z* (rel. %): 673 (100) [M-H]<sup>-</sup>. HR MS (ESI): for C<sub>32</sub>H<sub>30</sub>O<sub>7</sub>N<sub>4</sub>IPSI [M-H]<sup>-</sup>, calcd 673.07498; found, 673.07515.

**Differential Scanning Fluorimetry.** Measurements were performed with wt hSTING as described earlier.<sup>27</sup> Briefly, thermal denaturation was performed in a 20 μL mixture consisting of 0.1 mg/mL wt hSTING, 150 μM CDN, 100 mM Tris-HCl [pH 7.4], 150 mM NaCl, and 1:500 (v/v) SYPRO Orange (Thermo Fisher Scientific, USA). Measurements were taken in a 96-well format on a LightCycler480 Instrument II (Roche, Switzerland). Thermal shift ( $\Delta T_m$ ) for each CDN was determined by subtracting the melting temperature ( $T_m$ ) of the reference sample (ligand-free STING) from the melting temperature of the STING-CDN complex.

**Standard 293T Cell-Based Reporter Assay.** The generation of 293T reporter cells expressing different full-length STING protein allelic variants and the assay procedure itself was described previously.<sup>20</sup> Briefly, the day before testing, the cells were seeded into 96-well transparent plates in a DMEM High glucose medium containing 10% (v/v) heat inactivated fetal bovine albumin (FBS). The medium was removed the next day, and the cells were incubated for 7 h (37 °C, 5% CO<sub>2</sub>) with serially diluted compounds. After incubation, the collected cell culture medium was mixed with Bright-Glo Luciferase Assay System reagent (Promega, USA) in white 96-well plates (Corning, USA). Luminescence readout was performed on a SPARK instrument (Tecan, Austria), and the values were used to calculate EC<sub>50</sub> values using nonlinear regression and software Prism (GraphPad, USA).

**Digitonin 293T Cell-Based Reporter Assay.** Cells were plated as described above for a standard 293T cell-based reporter assay. The following day, the medium was removed, and serially diluted compounds were incubated with cells for 30 min at 37 °C, 5% CO<sub>2</sub> in buffer containing 50 mM HEPES [pH 7.0], 100 mM KCl, 3 mM MgCl<sub>2</sub>, 0.1 mM DTT, 85 mM sucrose, 0.2% (w/w) BSA, 1 mM ATP, 0.1 mM GTP, and 10 μg/mL digitonin A. Next, the buffer was removed, and the cells were washed with a cell culture medium twice and then incubated for 5 h (37 °C, 5% CO<sub>2</sub>) with fresh medium. Finally, the levels of Lucia Luciferase in medium were determined using Bright Glo (Promega, USA), and EC<sub>50</sub>s were calculated as described above.

**PBMC Assay.** Buffy coats from healthy individuals were obtained from the Institute of Hematology and Blood Transfusion (IHBT, Prague, Czech Republic). An informed written consent was obtained from each individual enrolled. The study was approved by the Institutional Review Board of IHBT (ev. nb. 13/06/2012). The assay was performed as previously described.<sup>54</sup> Briefly, the isolation of PBMCs was performed using Ficoll density gradient centrifugation (Ficoll Paque Plus, GE Healthcare) in SepMate tubes (SepMate PBMC Isolation Tubes, Stemcell Technologies). Next, isolated PBMCs were seeded into a 96-well U-shape plate in RPMI 1640 media containing 10% (v/v) heat inactivated fetal bovine serum (Capricorn Scientific, Germany). Serially diluted CDNs were added, and the plates were incubated for a predetermined 16 h (37 °C, 5% CO<sub>2</sub>). Finally, secreted IFN $\alpha$ , IFN $\gamma$ , and TNF $\alpha$  were determined in the collected medium using ProcartaPlex Assays using a MAGPIX System (Merck, Germany) according to manufacturer's instruction. The cytotoxic effect of CDNs on PBMCs was determined using

CellTiter-Glo Luminescent Cell Viability Assay (Promega Corporation, USA) according to manufacturer's instruction.

**Protein Expression and Purification.** The expression and purification of mouse cGAS were performed as previously described<sup>49</sup> with minor changes. The recombinant plasmid was transformed in *Escherichia coli* BL21 (DE3) cells (Thermo Fisher, USA). The bacteria were grown at 37 °C until OD<sub>600nm</sub> of 0.6–0.8 units and cooled down to 20 °C, and then, cGAS expression was induced with 0.4 mM IPTG for 16 h in an orbital shaker. After cell collection, the pellet was resuspended in ice-cold lysis/wash buffer (50 mM Tris–HCl [pH 8], 300 mM NaCl, 20 mM imidazole, 10% (v/v) glycerol, 3 mM β-mercaptoethanol). The cells were lysed by sonication, and cell debris was removed by centrifugation. The supernatant was incubated with equilibrated Ni-NTA beads (Macherey-Nagel, Germany). The beads were loaded into a gravity flow column and washed with lysis/wash buffer. Next, the resin was washed with lysis/wash buffer supplemented with NaCl to 1 M concentration, then washed with lysis/wash buffer. The mcGAS was eluted with lysis/wash buffer supplemented with imidazole to a 300 mM concentration. The collected protein was further purified on a size-exclusion chromatography column HiLoad 26/60 Superdex 200 pg in buffer containing 50 mM Tris–HCl [pH 7.4] and 150 mM NaCl. The eluate was concentrated to about 5 mg/mL and stored in 20% glycerol at –80 °C.

Expression and purification of DncV and DisA proteins were performed as described previously.<sup>33</sup> Briefly, proteins were overexpressed in *E. coli* BL21 (DE3) cells (ThermoFisher, USA). Purification steps consisted of cell disintegration, Ni-NTA chromatography, and SEC chromatography using HiLoad 26/60 Superdex 200 pg. The DncV and DisA proteins were concentrated using an Amicon Ultra-15 10K device (Merck Millipore Ltd), and enzymes were flash-frozen in liquid nitrogen.

The expression and purification of wt hSTING were performed as described previously.<sup>47</sup> Briefly, the expression, lysis, and purification using Ni-NTA resin were done following mcGAS protocol. Eluate from the Ni-NTA resin was supplied with Ulp1 protease and incubated for 2 h at 4 °C. Digested wt hSTING protein was further purified by size exclusion with HiLoad 26/60 Superdex 200 pg (GE Healthcare, USA) equilibrated in buffer containing 50 mM Tris–HCl [pH 7.4] and 150 mM NaCl. Finally, the purified protein was concentrated to about 5 mg/mL and stored in 20% glycerol at –80 °C, for usage in DSE. For the crystallography experiments, wt hSTING was further purified on HiTrap Capto S (GE Healthcare, USA), equilibrated in 50 mM Tris–HCl [pH 8] buffer, and eluted with a gradient of 50–1000 mM NaCl in the same buffer. Fractions corresponding to wt hSTING were concentrated to about 20 mg/mL and stored at –80 °C without glycerol supplement.

**Crystallization and Structure Determination.** Crystallizations were done using our previously optimized protocol.<sup>52</sup> wt hSTING-5f was co-crystallized at 18 °C using sitting drop vapor diffusion in a condition composed of 200 mM ammonium nitrate, 20% (w/v) PEG 3350, with additive 10 mM EDTA. Crystals were cryoprotected in mother liquor supplemented with 20% (v/v) glycerol. A complete diffraction data set was collected for a single crystal to 2.69 Å. wt hSTING-5k was co-crystallized at 18 °C using sitting drop vapor diffusion in a condition composed of 100 mM tri-sodium citrate [pH 5.0] and 20% (w/v) PEG 6000, with additives of 10 mM EDTA and 100 mM tri-sodium citrate. Crystals were cryoprotected in mother liquor supplemented with 20% (v/v) ethylene glycol. A complete diffraction data set was collected for a single crystal to 2.32 Å. wt hSTING-5l was co-crystallized at 18 °C using sitting drop vapor diffusion in a condition composed of 100 mM citric acid, 20% (w/v) PEG 6000, with additive 10 mM EDTA. Crystals were cryoprotected in mother liquor supplemented with 20% (v/v) ethylene glycol. A complete diffraction data set was collected for a single crystal to 2.16 Å. wt hSTING-5m was co-crystallized at 18 °C using sitting drop vapor diffusion in a condition composed of 100 mM PIPES [pH 7.0], 100 mM magnesium formate dihydrate, 100 mM rubidium chloride, 25% (w/v) PEG smear high, with additives 10 mM EDTA and 100 mM tri-sodium citrate. Crystals were cryoprotected in mother liquor

supplemented with 20% (v/v) ethylene glycol. A complete diffraction data set was collected for a single crystal to 1.89 Å. Measurements for hSTING-5f and hSTING-5k were carried out at an in-house diffractometer (Rigaku, Japan) at 100 K. Measurements for hSTING-5l and hSTING-5m were carried out at MX14.1 operated by the Helmholtz-Zentrum Berlin (HZB) at the BESSY II electron storage ring (Berlin-Adlershof, Germany) at 100 K.<sup>56</sup> Data were reduced and processed by XDS.<sup>57</sup> The structures were solved by the molecular replacement method with MOLREP<sup>58</sup> using the structure of human STING (PDB entry 4KSY) as the search model. Model refinement was done using REFMAC from CCP4 suite,<sup>59</sup> PHENIX,<sup>60</sup> and Coot.<sup>61</sup> Parameters for structures and their geometry are summarized in Table S1.

## ■ ASSOCIATED CONTENT

### Supporting Information

The Supporting Information is available free of charge at <https://pubs.acs.org/doi/10.1021/acs.jmedchem.2c01305>.

Synthesis of compound 3e, crystal data and diffraction data collection and refinement statistics, UPLC purity of CDNs including UPLC traces, top signals and CC<sub>50</sub>s for compounds tested on PBMCs, 2Fo–Fc map of loops over ligand-binding sites, and interaction scheme of 2'3'-cGAMP in STING ligand-binding sites (PDF)  
Molecular formula strings (CSV)

### Accession Codes

PDB codes for human STING with bound 5f (8A2H), 5k (8A2J), 5l (8A2I), and 5m (8A2K). Authors will release the atomic coordinates upon article publication.

## ■ AUTHOR INFORMATION

### Corresponding Authors

**Pavla Perliková** – Institute of Organic Chemistry and Biochemistry, Czech Academy of Sciences, Prague 166 10, Czech Republic; Department of Organic Chemistry, Faculty of Chemical Technology, University of Chemistry and Technology, Prague 166 28, Czech Republic; [orcid.org/0000-0002-8500-0493](https://orcid.org/0000-0002-8500-0493); Phone: +420 220442039; Email: [Pavla.perlikova@vscht.cz](mailto:Pavla.perlikova@vscht.cz)

**Gabriel Birkus** – Institute of Organic Chemistry and Biochemistry, Czech Academy of Sciences, Prague 166 10, Czech Republic; [orcid.org/0000-0002-9850-2150](https://orcid.org/0000-0002-9850-2150); Phone: +420 770125014; Email: [Gabriel.birkus@uochb.cas.cz](mailto:Gabriel.birkus@uochb.cas.cz)

### Authors

**Zdeněk Vavřina** – Institute of Organic Chemistry and Biochemistry, Czech Academy of Sciences, Prague 166 10, Czech Republic; Department of Biochemistry, Faculty of Science, Charles University, Prague 128 00, Czech Republic; [orcid.org/0000-0002-6022-8918](https://orcid.org/0000-0002-6022-8918)

**Nemanja Milisavljević** – Institute of Organic Chemistry and Biochemistry, Czech Academy of Sciences, Prague 166 10, Czech Republic; Department of Organic Chemistry, Faculty of Science, Charles University, Prague 128 00, Czech Republic

**Florian Chevrier** – Institute of Organic Chemistry and Biochemistry, Czech Academy of Sciences, Prague 166 10, Czech Republic

**Miroslav Smola** – Institute of Organic Chemistry and Biochemistry, Czech Academy of Sciences, Prague 166 10, Czech Republic

**Joshua Smith** – Institute of Organic Chemistry and Biochemistry, Czech Academy of Sciences, Prague 166 10,

Czech Republic; First Faculty of Medicine, Charles University, Prague 121 08, Czech Republic

**Milan Dejmek** – Institute of Organic Chemistry and Biochemistry, Czech Academy of Sciences, Prague 166 10, Czech Republic; [orcid.org/0000-0002-8195-971X](https://orcid.org/0000-0002-8195-971X)

**Vojtěch Havlíček** – Institute of Organic Chemistry and Biochemistry, Czech Academy of Sciences, Prague 166 10, Czech Republic; Department of Organic Chemistry, Faculty of Science, Charles University, Prague 128 00, Czech Republic

**Miloš Buděšínský** – Institute of Organic Chemistry and Biochemistry, Czech Academy of Sciences, Prague 166 10, Czech Republic

**Radek Liboska** – Institute of Organic Chemistry and Biochemistry, Czech Academy of Sciences, Prague 166 10, Czech Republic

**Lenka Vaneková** – Institute of Organic Chemistry and Biochemistry, Czech Academy of Sciences, Prague 166 10, Czech Republic; Department of Cell Biology, Faculty of Science, Charles University, Prague 128 43, Czech Republic; [orcid.org/0000-0002-2572-1336](https://orcid.org/0000-0002-2572-1336)

**Jiří Brynda** – Institute of Organic Chemistry and Biochemistry, Czech Academy of Sciences, Prague 166 10, Czech Republic

**Evzen Boura** – Institute of Organic Chemistry and Biochemistry, Czech Academy of Sciences, Prague 166 10, Czech Republic; [orcid.org/0000-0002-9652-4065](https://orcid.org/0000-0002-9652-4065)

**Pavlna Rezáčová** – Institute of Organic Chemistry and Biochemistry, Czech Academy of Sciences, Prague 166 10, Czech Republic

**Michal Hocek** – Institute of Organic Chemistry and Biochemistry, Czech Academy of Sciences, Prague 166 10, Czech Republic; [orcid.org/0000-0002-1113-2047](https://orcid.org/0000-0002-1113-2047)

Complete contact information is available at:

<https://pubs.acs.org/10.1021/acs.jmedchem.2c01305>

#### Author Contributions

<sup>†</sup>Z.V. and P.P. contributed equally to this work.

#### Notes

The authors declare no competing financial interest.

#### ACKNOWLEDGMENTS

The work was supported by the National Institute for Cancer Research (Programme EXCELES, ID Project no. LX22NPO5102 to M.H., funded by the European Union—Next Generation EU) and the European Regional Development Fund; OP RDE (project “Chemical biology for drugging undruggable targets”, ChemBioDrug no. CZ.02.1.01/0.0/0.0/16\_019/0000729). Our special thanks go to Dr. Radek Pohl for his assistance with measurements of NMR spectra of intermediates and Tamara Jenkins for proofreading. We thank HZB for the allocation of synchrotron radiation beamtime.

#### ABBREVIATIONS

CDN, cyclic dinucleotide; cGAS, cyclic GMP–AMP synthase; DAMP, damage-associated molecular pattern; DisA, diadenylate cyclase from *Bacillus thuringiensis*; DMOCP, 2-chloro-5,5-dimethyl-1,3,2-dioxaphosphorinane 2-oxide; DMTr, 4,4'-dimethoxytrityl; DncV, dinucleotide cyclase from *Vibrio cholerae*; DSF, differential scanning fluorimetry; ETT, ethylthio-1H-tetrazole; FBS, fetal bovine albumin; IRF, interferon regulatory factor; *J*, coupling constant in Hz; mcGAS, mouse variant of cyclic GMP–AMP synthase; NF- $\kappa$ B, nuclear factor  $\kappa$ -light

chain enhancer of activated B-cells; NMR, nuclear magnetic resonance; NTP, nucleoside triphosphate; PAMP, pathogen-associated molecular pattern; rt, room temperature; SAR, structure–activity relationship; STING, stimulator of interferon genes; TBAF, tetrabutylammonium fluoride; TFA, trifluoroacetic acid; TLC, thin layer chromatography; TPPTS, triphenylphosphane-3,3',3''-trisulfonate; UV, ultraviolet; wt hSTING, wild type variant of human stimulator of interferon genes

#### REFERENCES

- (1) Ishikawa, H.; Barber, G. N. STING is an endoplasmic reticulum adaptor that facilitates innate immune signalling. *Nature* **2008**, *455*, 674–678.
- (2) Zhong, B.; Yang, Y.; Li, S.; Wang, Y.-Y.; Li, Y.; Diao, F.; Lei, C.; He, X.; Zhang, L.; Tien, P.; Shu, H.-B. The adaptor protein MITA links virus-sensing receptors to IRF3 transcription factor activation. *Immunity* **2008**, *29*, 538–550.
- (3) Sun, L.; Wu, J.; Du, F.; Chen, X.; Chen, Z. J. Cyclic GMP-AMP synthase is a cytosolic DNA sensor that activates the type I interferon pathway. *Science* **2013**, *339*, 786–791.
- (4) Wu, J.; Sun, L.; Chen, X.; Du, F.; Shi, H.; Chen, C.; Chen, Z. J. Cyclic GMP-AMP is an endogenous second messenger in innate immune signaling by cytosolic DNA. *Science* **2013**, *339*, 826–830.
- (5) Zhang, X.; Shi, H.; Wu, J.; Zhang, X.; Sun, L.; Chen, C.; Chen, Z. J. Cyclic GMP-AMP containing mixed phosphodiester linkages is an endogenous high-affinity ligand for STING. *Mol. Cell* **2013**, *51*, 226–235.
- (6) Ablasser, A.; Goldeck, M.; Cavlar, T.; Deimling, T.; Witte, G.; Röhl, I.; Hopfner, K.-P.; Ludwig, J.; Hornung, V. cGAS produces a 2'-5'-linked cyclic dinucleotide second messenger that activates STING. *Nature* **2013**, *498*, 380–384.
- (7) Ouyang, S.; Song, X.; Wang, Y.; Ru, H.; Shaw, N.; Jiang, Y.; Niu, F.; Zhu, Y.; Qiu, W.; Parvatiyar, K.; Li, Y.; Zhang, R.; Cheng, G.; Liu, Z.-J. Structural analysis of the STING adaptor protein reveals a hydrophobic dimer interface and mode of cyclic di-GMP binding. *Immunity* **2012**, *36*, 1073–1086.
- (8) Krasteva, P. V.; Sondermann, H. Versatile modes of cellular regulation via cyclic dinucleotides. *Nat. Chem. Biol.* **2017**, *13*, 350–359.
- (9) Burdette, D. L.; Monroe, K. M.; Sotelo-Troha, K.; Iwig, J. S.; Eckert, B.; Hyodo, M.; Hayakawa, Y.; Vance, R. E. STING is a direct innate immune sensor of cyclic di-GMP. *Nature* **2011**, *478*, 515–518.
- (10) Barker, J. R.; Koestler, B. J.; Carpenter, V. K.; Burdette, D. L.; Waters, C. M.; Vance, R. E.; Valdivia, R. H. STING-dependent recognition of cyclic di-AMP mediates type I interferon responses during *Chlamydia trachomatis* infection. *mBio* **2013**, *4*, No. e00018.
- (11) Keating, S. E.; Baran, M.; Bowie, A. G. Cytosolic DNA sensors regulating type I interferon induction. *Trends Immunol.* **2011**, *32*, 574–581.
- (12) Liu, S.; Cai, X.; Wu, J.; Cong, Q.; Chen, X.; Li, T.; Du, F.; Ren, J.; Wu, Y.-T.; Grishin, N. V.; Chen, Z. J. Phosphorylation of innate immune adaptor proteins MAVS, STING, and TRIF induces IRF3 activation. *Science* **2015**, *347*, aaa2630.
- (13) Shang, G.; Zhang, C.; Chen, Z. J.; Bai, X.-c.; Zhang, X. Cryo-EM structures of STING reveal its mechanism of activation by cyclic GMP-AMP. *Nature* **2019**, *567*, 389–393.
- (14) Zhang, C.; Shang, G.; Gui, X.; Zhang, X.; Bai, X.-c.; Chen, Z. J. Structural basis of STING binding with and phosphorylation by TBK1. *Nature* **2019**, *567*, 394–398.
- (15) Zhao, B.; Du, F.; Xu, P.; Shu, C.; Sankaran, B.; Bell, S. L.; Liu, M.; Lei, Y.; Gao, X.; Fu, X.; Zhu, F.; Liu, Y.; Laganowsky, A.; Zheng, X.; Ji, J.-Y.; West, A. P.; Watson, R. O.; Li, P. A conserved PLPLRT/SD motif of STING mediates the recruitment and activation of TBK1. *Nature* **2019**, *569*, 718–722.
- (16) Musella, M.; Manic, G.; De Maria, R.; Vitale, I.; Sistigu, A. Type-I-interferons in infection and cancer: Unanticipated dynamics



- with therapeutic implications. *OncoImmunology* 2017, 6, No. e1314424.
- (17) Barber, G. N. STING: infection, inflammation and cancer. *Nat. Rev. Immunol.* 2015, 15, 760–770.
- (18) Kumar, V. A. A STING to inflammation and autoimmunity. *J. Leukocyte Biol.* 2019, 106, 171–185.
- (19) Gao, D.; Li, T.; Li, X.-D.; Chen, X.; Li, Q.-Z.; Wight-Carter, M.; Chen, Z. J. Activation of cyclic GMP-AMP synthase by self-DNA causes autoimmune diseases. *Proc. Natl. Acad. Sci. U.S.A.* 2015, 112, No. E5699.
- (20) Novotná, B.; Vaneková, L.; Závřel, M.; Budešínský, M.; Dejmeek, M.; Smola, M.; Gutten, O.; Tehrani, Z. A.; Pimková Polidarová, M.; Brázdová, A.; Liboska, R.; Štěpánek, I.; Vavřina, Z.; Jandůšek, T.; Nencka, R.; Rulíšek, L.; Bouřa, E.; Brynda, J.; Páv, O.; Birkuš, G. Enzymatic preparation of 2'-5',3'-5'-cyclic dinucleotides, their binding properties to stimulator of interferon genes adaptor protein, and structure/activity correlations. *J. Med. Chem.* 2019, 62, 10676–10690.
- (21) Zhang, H.; You, Q.-D.; Xu, X.-L. Targeting stimulator of interferon genes (STING): A medicinal chemistry perspective. *J. Med. Chem.* 2020, 63, 3785–3816.
- (22) Le Naour, J.; Zitvogel, L.; Galluzzi, L.; Vacchelli, E.; Kroemer, G. Trial watch: STING agonists in cancer therapy. *OncoImmunology* 2020, 9, 1777624.
- (23) Fu, J.; Kanne, D. B.; Leong, M.; Glickman, L. H.; McWhirter, S. M.; Lemmens, E.; Mechette, K.; Leong, J. J.; Lauer, P.; Liu, W.; Sivick, K. E.; Zeng, Q.; Soares, K. C.; Zheng, L.; Portnoy, D. A.; Woodward, J. J.; Pardoll, D. M.; Dubensky, T. W.; Kim, Y. STING agonist formulated cancer vaccines can cure established tumors resistant to PD-1 blockade. *Sci. Transl. Med.* 2015, 7, 283ra52.
- (24) Chang, W.; Altman, M. D.; Lesburg, C. A.; Perera, S. A.; Piesvaux, J. A.; Schroeder, G. K.; Wyss, D. F.; Cemerski, S.; Chen, Y.; DiNunzio, E.; Haidle, A. M.; Ho, T.; Kariv, I.; Knemeyer, I.; Kopinja, J. E.; Lacey, B. M.; Laskey, J.; Lim, J.; Long, B. J.; Ma, Y.; Maddess, M. L.; Pan, B. S.; Presland, J. P.; Spooner, E.; Steinhuebel, D.; Truong, Q.; Zhang, Z.; Fu, J.; Addona, G. H.; Northrup, A. B.; Parmee, E.; Tata, J. R.; Bennett, D. J.; Cumming, J. N.; Siu, T.; Trotter, B. W. Discovery of MK-1454: A potent cyclic dinucleotide stimulator of interferon genes agonist for the treatment of cancer. *J. Med. Chem.* 2022, 65, 5675–5689.
- (25) Carideo Cunniff, E.; Sato, Y.; Mai, D.; Appleman, V. A.; Iwasaki, S.; Kolev, V.; Matsuda, A.; Shi, J.; Mochizuki, M.; Yoshikawa, M.; Huang, J.; Shen, L.; Haridas, S.; Shinde, V.; Gemski, C.; Roberts, E. R.; Ghasemi, O.; Bazzazi, H.; Menon, S.; Traore, T.; Shi, P.; Thelen, T. D.; Conlon, J.; Abu-Yousif, A. O.; Arendt, C.; Shaw, M. H.; Okaniwa, M. TAK-676: A novel stimulator of interferon genes (STING) agonist promoting durable IFN-dependent antitumor immunity in preclinical studies. *Cancer Res. Commun.* 2022, 2, 489–502.
- (26) Vyskocil, S.; Cardin, D.; Ciavarrì, J.; Conlon, J.; Cullis, C.; England, D.; Gershman, R.; Gigstad, K.; Gipsen, K.; Gould, A.; Greenspan, P.; Griffin, R.; Gulavita, N.; Harrison, S.; Hu, Z.; Hu, Y.; Hata, A.; Huang, J.; Huang, S.-C.; Janowick, D.; Jones, M.; Kolev, V.; Langston, S. P.; Lee, H. M.; Li, G.; Lok, D.; Ma, L.; Mai, D.; Malley, J.; Matsuda, A.; Mizutani, H.; Mizutani, M.; Molchanova, N.; Nunes, E.; Puskalkar, S.; Renou, C.; Rowland, S.; Sato, Y.; Shaw, M.; Shen, L.; Shi, Z.; Skene, R.; Soucy, F.; Stroud, S.; Xu, H.; Xu, T.; Abu-Yousif, A. O.; Zhang, J. Identification of novel carbocyclic pyrimidine cyclic dinucleotide STING agonists for antitumor immunotherapy using systemic intravenous route. *J. Med. Chem.* 2021, 64, 6902–6923.
- (27) Ramanjulu, J. M.; Pesiridis, G. S.; Yang, J.; Concha, N.; Singhaus, R.; Zhang, S.-Y.; Tran, J.-L.; Moore, P.; Lehmann, S.; Eberl, H. C.; Muelbaier, M.; Schneck, J. L.; Clemens, J.; Adam, M.; Mehlmann, J.; Romano, J.; Morales, A.; Kang, J.; Leister, L.; Graybill, T. L.; Charnley, A. K.; Ye, G.; Nevins, N.; Behnia, K.; Wolf, A. I.; Kasparcova, V.; Nurse, K.; Wang, L.; Puhl, Y.; Li, M.; Klein, C. B.; Hopson, J.; Guss, M.; Bantscheff, G.; Bergamini, M. A.; Reilly, Y.; Lian, K. J.; Duffy, J.; Adams, K. P.; Foley, P. J.; Gough, R. W.; Marquis, J.; Smothers, A.; Hoos, J.; Bertin, J. Design of amidobenzimidazole STING receptor agonists with systemic activity. *Nature* 2018, 564, 439–443.
- (28) Banerjee, M.; Mridha, S.; Shrivastava, R.; Basu, S.; Ghosh, R.; Pryde, D. C.; Yadav, D. B.; Surya, A. G10 is a direct activator of human STING. *PLoS One* 2020, 15, No. e0237743.
- (29) Sali, T. M.; Pryke, K. M.; Abraham, J.; Liu, A.; Archer, I.; Broeckel, R.; Staverosky, J. A.; Smith, J. L.; Al-Shammari, A.; Amisler, L.; Sheridan, K.; Nilsen, A.; Streblov, D. N.; DeFilippis, V. R. Characterization of a novel human-specific STING agonist that elicits antiviral activity against emerging alphaviruses. *PLoS Pathog.* 2015, 11, No. e1005324.
- (30) Pan, B.-S.; Perera, S. A.; Piesvaux, J. A.; Presland, J. P.; Schroeder, G. K.; Cumming, J. N.; Trotter, B. W.; Altman, M. D.; Buevich, A. V.; Cash, B.; Cemerski, S.; Chang, W.; Chen, Y.; Dandliker, P. J.; Feng, G.; Haidle, A.; Henderson, T.; Jewell, J.; Kariv, I.; Knemeyer, I.; Kopinja, J.; Lacey, B. M.; Laskey, J.; Lesburg, C. A.; Liang, R.; Long, B. J.; Lu, M.; Ma, Y.; Minnihan, E. C.; O'Donnell, G.; Otte, R.; Price, L.; Rakhilina, L.; Sauvagnat, B.; Sharma, S.; Tyagarajan, S.; Woo, H.; Wyss, D. F.; Xu, S.; Bennett, D. J.; Addona, G. H. An orally available non-nucleotide STING agonist with antitumor activity. *Science* 2020, 369, No. eaba6098.
- (31) Cherney, E. C.; Zhang, L.; Lo, J.; Huynh, T.; Wei, D.; Ahuja, V.; Quesnelle, C.; Schieven, G. L.; Futran, A.; Locke, G. A.; Lin, Z.; Monereau, L.; Chaudhry, C.; Blum, J.; Li, S.; Fereshteh, M.; Li-Wang, B.; Gangwar, S.; Pan, C.; Chong, C.; Zhu, X.; Posy, S. L.; Sack, J. S.; Zhang, P.; Ruzanov, M.; Harner, M.; Akhtar, F.; Schroeder, G. M.; Vite, G.; Fink, B. Discovery of non-nucleotide small-molecule STING agonists via chemotype hybridization. *J. Med. Chem.* 2022, 65, 3518–3538.
- (32) Jeon, M. J.; Lee, H.; Lee, J.; Baek, S. Y.; Lee, D.; Jo, S.; Lee, J.-Y.; Kang, M.; Jung, H. R.; Han, S. B.; Kim, N.-J.; Lee, S.; Kim, H. Development of potent immune modulators targeting stimulator of interferon genes receptor. *J. Med. Chem.* 2022, 65, 5407–5432.
- (33) Novotná, B.; Holá, L.; Staš, M.; Gutten, O.; Smola, M.; Závřel, M.; Vavřina, Z.; Budešínský, M.; Liboska, R.; Chevriér, F.; Dobiáš, J.; Bouřa, E.; Rulíšek, L.; Birkuš, G. Enzymatic synthesis of 3'-5', 3'-5' cyclic dinucleotides, their binding properties to the stimulator of interferon genes adaptor protein, and structure/activity correlations. *Biochemistry* 2021, 60, 3714–3727.
- (34) Rosenthal, K.; Becker, M.; Rolf, J.; Siedentop, R.; Hillen, M.; Nett, M.; Lütz, S. Catalytic Promiscuity of cGAS: A Facile Enzymatic Synthesis of 2'-3'-Linked Cyclic Dinucleotides. *ChemBioChem* 2020, 21, 3225–3228.
- (35) Bartsch, T.; Becker, M.; Rolf, J.; Rosenthal, K.; Lütz, S. Biotechnological production of cyclic dinucleotides—Challenges and opportunities. *Biotechnol. Bioeng.* 2022, 119, 677–684.
- (36) Schwede, F.; Genieser, H.-G.; Rentsch, A. The chemistry of the noncanonical cyclic dinucleotide 2'3'-cGAMP and its analogs. In *Non-canonical Cyclic Nucleotides*; Seifert, R., Ed.; Springer International Publishing: Cham, 2017; pp 359–384.
- (37) Milisavljević, N.; Konkolová, E.; Kozák, J.; Hodek, J.; Veselovská, L.; Šýkorová, V.; Čížek, K.; Pohl, R.; Eyer, L.; Svoboda, P.; Růžek, D.; Weber, J.; Nencka, R.; Bouřa, E.; Hocek, M. Antiviral activity of 7-substituted 7-deazapurine ribonucleosides, monophosphate prodrugs, and triphosphates against emerging RNA viruses. *ACS Infect. Dis.* 2021, 7, 471–478.
- (38) Zhu, X.-F.; Williams, H. J.; Ian Scott, A. An Improved Transient Method for the Synthesis of N-Benzoylated Nucleosides. *Synth. Commun.* 2003, 33, 1233–1243.
- (39) Hakimelahi, G. H.; Proba, Z. A.; Ogilvie, K. K. New catalysts and procedures for the dimethoxytritylation and selective silylation of ribonucleosides. *Can. J. Chem.* 1982, 60, 1106–1113.
- (40) Wei, X. Coupling activators for the oligonucleotide synthesis via phosphoramidite approach. *Tetrahedron* 2013, 69, 3615–3637.
- (41) Gaffney, B. L.; Veliath, E.; Zhao, J.; Jones, R. A. One-flask syntheses of c-di-GMP and the [Rp,Rp] and [Rp,Sp] thiophosphate analogues. *Org. Lett.* 2010, 12, 3269–3271.
- (42) Hocek, M. Synthesis of base-modified 2'-deoxyribonucleoside triphosphates and their use in enzymatic synthesis of modified DNA

for applications in bioanalysis and chemical biology. *J. Org. Chem.* **2014**, *79*, 9914–9921.

(43) Velith, E.; Kim, S.; Gaffney, B. L.; Jones, R. A. Synthesis and characterization of C8 analogs of c-di-GMP. *Nucleosides, Nucleotides Nucleic Acids* **2011**, *30*, 961–978.

(44) Bourderieux, A.; Naus, P.; Perlíková, P.; Pohl, R.; Pichová, I.; Votruba, I.; Džubák, P.; Konečný, P.; Hajdúch, M.; Stray, K. M.; Wang, T.; Ray, A. S.; Feng, J. Y.; Birkus, G.; Čihlar, T.; Hocek, M. Synthesis and significant cytostatic activity of 7-hetaryl-7-deazaadenosines. *J. Med. Chem.* **2011**, *54*, 5498–5507.

(45) Milisavljević, N.; Perlíková, P.; Pohl, R.; Hocek, M. Enzymatic synthesis of base-modified RNA by T7 RNA polymerase. A systematic study and comparison of 5-substituted pyrimidine and 7-substituted 7-deazapurine nucleoside triphosphates as substrates. *Org. Biomol. Chem.* **2018**, *16*, 5800–5807.

(46) Šnášel, J.; Naus, P.; Dostál, J.; Hnízda, A.; Fanfrlík, J.; Brynda, J.; Bourderieux, A.; Dušek, M.; Dvořáková, H.; Stolaříková, J.; Záborská, H.; Pohl, R.; Konečný, P.; Džubák, P.; Votruba, I.; Hajdúch, M.; Rezáčová, P.; Veverka, V.; Hocek, M.; Pichová, I. Structural basis for inhibition of mycobacterial and human adenosine kinase by 7-substituted 7-(het)aryl-7-deazaadenine ribonucleosides. *J. Med. Chem.* **2014**, *57*, 8268–8279.

(47) Vavřina, Z.; Gutten, O.; Smola, M.; Závřel, M.; Aliakbar Tehrani, Z.; Charvát, V.; Kožisek, M.; Boura, E.; Birkus, G.; Rulíšek, L. Protein-Ligand Interactions in the STING Binding Site Probed by Rationally Designed Single-Point Mutations: Experiment and Theory. *Biochemistry* **2021**, *60*, 607–620.

(48) Smola, M.; Gutten, O.; Dejmek, M.; Kožisek, M.; Evangelidis, T.; Tehrani, Z. A.; Novotná, B.; Nencka, R.; Birkus, G.; Rulíšek, L.; Boura, E. Ligand strain and its conformational complexity is a major factor in the binding of cyclic dinucleotides to STING protein. *Angew. Chem., Int. Ed. Engl.* **2021**, *60*, 10172–10178.

(49) Yi, G.; Brendel, V. P.; Shu, C.; Li, P.; Palanathan, S.; Cheng Kao, C. Single nucleotide polymorphisms of human STING can affect innate immune response to cyclic dinucleotides. *PLoS One* **2013**, *8*, No. e77846.

(50) Dejmek, M.; Šála, M.; Brazdova, A.; Vanekova, L.; Smola, M.; Klíma, M.; Břehová, P.; Buděšinský, M.; Dračínský, M.; Procházková, E.; Závřel, M.; Šimák, O.; Páv, O.; Boura, E.; Birkus, G.; Nencka, R. Discovery of isonucleotidic CDNs as potent STING agonists with immunomodulatory potential. *Structure* **2022**, *30*, 1146–1156.

(51) Shih, A. Y.; Damm-Ganamet, K. L.; Mirzadegan, T. Dynamic Structural Differences between Human and Mouse STING Lead to Differing Sensitivity to DMXAA. *Biophys. J.* **2018**, *114*, 32–39.

(52) Smola, M.; Birkus, G.; Boura, E. No magnesium is needed for binding of the stimulator of interferon genes to cyclic dinucleotides. *Acta Crystallogr., Sect. F: Struct. Biol. Commun.* **2019**, *75*, 593–598.

(53) Lioux, T.; Mauny, M.-A.; Lamoureux, A.; Bascoul, N.; Hays, M.; Vernejoul, F.; Baudru, A.-S.; Boularan, C.; Lopes-Vicente, J.; Qushair, G.; Tiraby, G. Design, Synthesis, and Biological Evaluation of Novel Cyclic Adenosine-Inosine Monophosphate (cAIMP) Analogs That Activate Stimulator of Interferon Genes (STING). *J. Med. Chem.* **2016**, *59*, 10253–10267.

(54) Pinková Polidarová, M.; Břehová, P.; Kaiser, M. M.; Smola, M.; Dračínský, M.; Smith, J.; Marek, A.; Dejmek, M.; Šála, M.; Gutten, O.; Rulíšek, L.; Novotná, B.; Brázdová, A.; Janeba, Z.; Nencka, R.; Boura, E.; Páv, O.; Birkus, G. Synthesis and biological evaluation of phosphoester and phosphorothioate prodrugs of STING agonist 3',3'-c-Di(2',2'-dAMP). *J. Med. Chem.* **2021**, *64*, 7596–7616.

(55) Seela, F.; Ming, X. 7-Functionalized 7-deazapurine  $\beta$ -d and  $\beta$ -l-ribonucleosides related to tubercidin and 7-deazainosine: glycosylation of pyrrolo[2,3-d]pyrimidines with 1-O-acetyl-2,3,5-tri-O-benzoyl- $\beta$ -d or  $\beta$ -l-ribofuranose. *Tetrahedron* **2007**, *63*, 9850–9861.

(56) Mueller, U.; Förster, R.; Hellmig, M.; Huschmann, F. U.; Kastner, A.; Malecki, P.; Pühringer, S.; Röwer, M.; Sparta, K.; Steffien, M.; Ühlein, M.; Wilk, P.; Weiss, M. S. The macromolecular crystallography beamlines at BESSY II of the Helmholtz-Zentrum Berlin: Current status and perspectives. *Eur. Phys. J. Plus* **2015**, *130*, 141.

(57) Kabsch, W. XDS. *Acta Crystallogr., Sect. D: Biol. Crystallogr.* **2010**, *66*, 125–132.

(58) Vagin, A.; Teplyakov, A. Molecular replacement with MOLREP. *Acta Crystallogr., Sect. D: Biol. Crystallogr.* **2010**, *66*, 22–25.

(59) Winn, M. D.; Ballard, C. C.; Cowtan, K. D.; Dodson, E. J.; Emsley, P.; Evans, P. R.; Keegan, R. M.; Krissinel, E. B.; Leslie, A. G. W.; McCoy, A.; McNicholas, S. J.; Murshudov, G. N.; Pannu, N. S.; Potterton, E. A.; Powell, H. R.; Read, R. J.; Vagin, A.; Wilson, K. S. Overview of the CCP4 suite and current developments. *Acta Crystallogr., Sect. D: Biol. Crystallogr.* **2011**, *67*, 235–242.

(60) Adams, P. D.; Afonine, P. V.; Bunkóczi, G.; Chen, V. B.; Davis, I. W.; Echols, N.; Headd, J. J.; Hung, L.-W.; Kapral, G. J.; Grosse-Kunstleve, R. W.; McCoy, A. J.; Moriarty, N. W.; Oeffner, R.; Read, R. J.; Richardson, D. C.; Richardson, J. S.; Terwilliger, T. C.; Zwart, P. H. PHENIX: a comprehensive Python-based system for macromolecular structure solution. *Acta Crystallogr., Sect. D: Biol. Crystallogr.* **2010**, *66*, 213–221.

(61) Debreczeni, J. E.; Emsley, P. Handling ligands with Coot. *Acta Crystallogr., Sect. D: Biol. Crystallogr.* **2012**, *68*, 425–430.

## ***Supporting Information***

### **Design, Synthesis, and Biochemical and Biological Evaluation of Novel 7-Deazapurine Cyclic Dinucleotide Analogues as STING Receptor Agonists**

*Zdeněk Vavřina<sup>a,b</sup>, Pavla Perliková<sup>a,c,\*</sup>, Nemanja Milisavljević<sup>a,d</sup>, Florian Chevrier<sup>a</sup>, Miroslav Smola<sup>a</sup>, Joshua Smith<sup>a,e</sup>, Milan Dejmek<sup>a</sup>, Vojtěch Havlíček<sup>a,d</sup>, Miloš Buděšínský<sup>a</sup>, Radek Liboska<sup>a</sup>, Lenka Vaneková<sup>a,f</sup>, Jiří Brynda<sup>a</sup>, Evžen Boura<sup>a</sup>, Pavlína Řezáčová<sup>a</sup>, Michal Hocek<sup>a</sup> and Gabriel Birkus<sup>a,\*</sup>*

<sup>a</sup> Institute of Organic Chemistry and Biochemistry, Czech Academy of Sciences, Flemingovo náměstí 542, Prague 166 10, Czech Republic; <sup>b</sup> Department of Biochemistry, Faculty of Science, Charles University, Hlavova 2030/8, Prague 128 00, Czech Republic; <sup>c</sup> Department of Organic Chemistry, Faculty of Chemical Technology, University of Chemistry and Technology, Technická 5, Prague 166 28, Czech Republic; <sup>d</sup> Department of Organic Chemistry, Faculty of Science, Charles University, Hlavova 2030/8, Prague 128 00, Czech Republic; <sup>e</sup> First Faculty of Medicine, Charles University, Katerinska 1660, Prague 121 08, Czech Republic; <sup>f</sup> Department of Cell Biology, Faculty of Science, Charles University, Vinicna 1594/7, Prague 128 43, Czech Republic.

Corresponding author's email:

P.P.: Pavla.Perlikova@vscht.cz

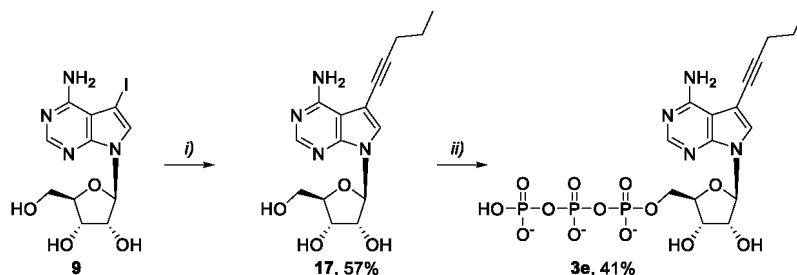
G.B.: Gabriel.Birkus@uochb.cas.cz

S1

**Table of Contents:**

Synthesis of <b>3e</b> .....	S3
Table S1: Crystal data and diffraction data collection and refinement statistics .....	S5
Table S2: Residues missing in the crystallographic models due to disordered maps. ....	S7
Table S3: UPLC purity of CDNs. ....	S7
UPLC traces of CDNs.....	S8
Table S4: Top signals and CC <sub>50s</sub> for compounds tested on PBMCs .....	S21
Figure S1: Interaction scheme of 2'3'-cGAMP in STING ligand-binding site. ....	S22
Figure S2: 2Fo-Fc map of loops over ligand-binding site depicted at 1 $\sigma$ . ....	S22

Synthesis of **3e**



Scheme S1: Reagents and conditions: *i*) pentyne, CuI, Et<sub>3</sub>N, Pd(PPh<sub>3</sub>)<sub>4</sub>, DMF *ii*) 1. POCl<sub>3</sub>, PO(OMe)<sub>3</sub>, 0 °C, 1.5 h; 2. (NHBu<sub>3</sub>)<sub>2</sub>H<sub>2</sub>P<sub>2</sub>O<sub>7</sub>, Bu<sub>3</sub>N, DMF, 0 °C, 2 h; 3. TEAB

**7-(Pent-1-yn-1-yl)-7-deazaadenosine (17)**

A suspension of 7-iodo-7-deazaadenosine (**9**, 200 mg, 0.51 mmol) and CuI (6 mg, 0.03 mmol) in anhydrous DMF (4 mL) was treated with pentyne (869 mg, 12.75 mmol), anhydrous Et<sub>3</sub>N (77 mg, 0.77 mmol), and Pd(PPh<sub>3</sub>)<sub>4</sub> (30 mg, 0.03 mmol). This mixture was stirred under argon atmosphere at 70 °C for 48 h to form a clear solution. The resulting suspension was evaporated in vacuo, resuspended in methanol, coevaporated with silica gel, and purified by phase flash chromatography (C18 column, 0 to 100% MeOH in water). Product **17** (97 mg, 57%) was isolated as a white solid. *R<sub>f</sub>* = 0.6 (SiO<sub>2</sub>; CHCl<sub>3</sub>/MeOH 5:1). <sup>1</sup>H NMR (500.0 MHz, DMSO-*d*<sub>6</sub>): 1.00 (t, 3H, *J*<sub>vic</sub> = 7.4, CH<sub>3</sub>CH<sub>2</sub>CH<sub>2</sub>); 1.57 (qt, 2H, *J*<sub>vic</sub> = 7.4, 7.0, CH<sub>3</sub>CH<sub>2</sub>CH<sub>2</sub>); 2.45 (t, 2H, *J*<sub>vic</sub> = 7.0, CH<sub>3</sub>CH<sub>2</sub>CH<sub>2</sub>); 3.53 (ddd, 1H, *J*<sub>gem</sub> = 11.9, *J*<sub>5'b,OH</sub> = 6.2, *J*<sub>5'b,4'</sub> = 3.8, H-5'b); 3.62 (ddd, 1H, *J*<sub>gem</sub> = 11.9, *J*<sub>5'a,OH</sub> = 5.0, *J*<sub>5'a,4'</sub> = 3.8, H-5'a); 3.88 (td, 1H, *J*<sub>4',5a'</sub> = *J*<sub>4',5b'</sub> = 3.8, *J*<sub>4',3'</sub> = 3.2, H-4'); 4.07 (ddd, 1H, *J*<sub>3',2'</sub> = 5.0, *J*<sub>3',OH</sub> = 4.7, *J*<sub>3',4'</sub> = 3.2, H-3'); 4.36 (td, 1H, *J*<sub>2',1'</sub> = *J*<sub>2',OH</sub> = 6.2, *J*<sub>2',3'</sub> = 5.0, H-2'); 5.12 (d, 1H, *J*<sub>OH,3'</sub> = 4.7, OH-3'); 5.20 (dd, 1H, *J*<sub>OH,5a'</sub> = 5.0, *J*<sub>OH,5b'</sub> = 6.2, OH-5'); 5.32 (d, 1H, *J*<sub>OH,2'</sub> = 6.2, OH-2'); 6.00 (d, 1H, *J*<sub>1',2'</sub> = 6.2, H-1'); 7.66 (s, 1H, H-6); 8.10 (s, 1H, H-2). <sup>13</sup>C NMR (125.7 MHz, DMSO-*d*<sub>6</sub>): 15.63 (CH<sub>3</sub>CH<sub>2</sub>CH<sub>2</sub>); 21.05 (CH<sub>3</sub>CH<sub>2</sub>CH<sub>2</sub>); 21.90 (CH<sub>3</sub>CH<sub>2</sub>CH<sub>2</sub>); 61.74 (CH<sub>2</sub>-5'); 70.73 (CH-3'); 73.94 (deazaA-C≡C-*n*Pr); 74.12 (CH-2'); 85.39 (CH-4'); 87.26 (CH-1'); 92.62 (deazaA-C≡C-*n*Pr); 95.65 (C-5); 102.60 (C-4a); 126.06 (CH-6); 149.60 (C-7a); 152.75 (CH-2); 157.79 (C-4). ESI MS *m/z* (rel. %) : 333 (100) [M+H]<sup>+</sup>, 355 (18) [M-H+Na]<sup>+</sup>. HR MS (ESI) for C<sub>16</sub>H<sub>21</sub>O<sub>4</sub>N<sub>4</sub> [M + H]<sup>+</sup>: calcd 333.15573; found 333.15569.

### 7-(Pent-1-yn-1-yl)-7-deazaadenosine 5'-O-triphosphate sodium salt (3e)

Nucleoside 17 (30 mg, 0.11 mmol) was dissolved in PO(OMe)<sub>3</sub> (300  $\mu$ L). POCl<sub>3</sub> (14  $\mu$ L, 0.14 mmol) was added, and the reaction mixture was stirred for 1.5h. Then, a solution of (NHBu<sub>3</sub>)<sub>2</sub>H<sub>2</sub>P<sub>2</sub>O<sub>7</sub> (293 mg, 0.54 mmol) and tributyl amine (110  $\mu$ L, 0.48 mmol) in anhydrous MeCN (1 mL) was added, and stirring continued for another 2 hours. Then, aqueous solution of TEAB (2M, 2 mL, 4 mmol) was added, and the mixture was evaporated under a reduced pressure. The residue was coevaporated with water several times. The product was purified by chromatography on HPLC (C18 column, 0.1M TEAB in water to 0.1M TEAB in 50% aq. MeOH), was coevaporated several times with water, and converted to a sodium salt form (Dowex 50WX8 in a Na<sup>+</sup> cycle). Triphosphate 3e (21 mg, 41 %) was obtained as a white lyophilizate (water). <sup>1</sup>H NMR (500.0 MHz, D<sub>2</sub>O, ref(*t*BuOH) = 1.24 ppm): 1.03 (t, 3H, *J*<sub>vic</sub> = 7.4, CH<sub>3</sub>CH<sub>2</sub>CH<sub>2</sub>); 1.64 (qt, 2H, *J*<sub>vic</sub> = 7.4, 7.1, CH<sub>3</sub>CH<sub>2</sub>CH<sub>2</sub>); 2.46 (t, 2H, *J*<sub>vic</sub> = 7.1, CH<sub>3</sub>CH<sub>2</sub>CH<sub>2</sub>); 4.12 (ddd, 1H, *J*<sub>gem</sub> = 11.7, *J*<sub>H,P</sub> = 4.7, *J*<sub>5'b,4'</sub> = 3.2, H-5'b); 4.27 (ddd, 1H, *J*<sub>gem</sub> = 11.7, *J*<sub>H,P</sub> = 6.8, *J*<sub>5'a,4'</sub> = 3.0, H-5'a); 4.34 (dddd, 1H, *J*<sub>4',5'</sub> = 3.2, 3.0, *J*<sub>4',3'</sub> = 2.7, *J*<sub>H,P</sub> = 1.7, H-4'); 4.58 (dd, 1H, *J*<sub>3',2'</sub> = 5.4, *J*<sub>3',4'</sub> = 2.7, H-3'); 4.68 (dd, 1H, *J*<sub>2',1'</sub> = 7.0, *J*<sub>2',3'</sub> = 5.4, H-2'); 6.22 (d, 1H, *J*<sub>1,2'</sub> = 7.0, H-1'); 7.68 (s, 1H, H-6); 8.16 (s, 1H, H-2). <sup>13</sup>C NMR (125.7 MHz, D<sub>2</sub>O, ref(*t*BuOH) = 32.43 ppm): 15.78 (CH<sub>3</sub>CH<sub>2</sub>CH<sub>2</sub>); 23.67 (CH<sub>3</sub>CH<sub>2</sub>CH<sub>2</sub>); 24.38 (CH<sub>3</sub>CH<sub>2</sub>CH<sub>2</sub>); 68.21 (d, *J*<sub>C,P</sub> = 5.6, CH<sub>2</sub>-5'); 73.29 (CH-3'); 75.48 (deazaA-C≡C-*n*Pr); 76.43 (CH-2'); 86.70 (d, *J*<sub>C,P</sub> = 8.8, CH-4'); 88.36 (CH-1'); 97.65 (deazaA-C≡C-*n*Pr); 100.57 (C-5); 106.08 (C-4a); 128.00 (CH-6); 152.21 (C-7a); 155.35 (CH-2); 160.65 (C-4). <sup>31</sup>P{<sup>1</sup>H} NMR (202.3 MHz, D<sub>2</sub>O): -20.45 (dd, *J* = 19.9, 19.4, P<sub>-</sub>); -9.68 (d, *J* = 19.4, P<sub>1</sub>); -4.56 (d, *J* = 19.9, P<sub>2</sub>). ESI MS *m/z* (rel. %): 491 (100) [M-H<sub>2</sub>PO<sub>3</sub>-H]<sup>-</sup>, 513 (50) [M-H<sub>2</sub>PO<sub>3</sub>-2H+Na]<sup>-</sup>, 571 (18) [M-H]<sup>-</sup>, 593 (29) [M-2H+Na]<sup>-</sup>, 615 (34) [M-3H+2Na]<sup>-</sup>. HR MS (ESI) for C<sub>16</sub>H<sub>22</sub>O<sub>13</sub>N<sub>4</sub>P<sub>3</sub> [M-H]<sup>-</sup> calcd 571.04017; found 571.03961.

Table S1: Crystal data and diffraction data collection and refinement statistics

	STING-5f	STING-5k	STING-5l	STING-5m
PDB code	8A2H	8A2J	8A2I	8A2K
<b>Data collection statistics</b>				
Space group	<i>P</i> 2 <sub>1</sub> 2 <sub>1</sub> 2	<i>P</i> 2 <sub>1</sub> 2 <sub>1</sub> 2	<i>P</i> 2 <sub>1</sub> 2 <sub>1</sub> 2	<i>P</i> 2 <sub>1</sub> 2 <sub>1</sub> 2
Cell parameters (Å; °)	95.187 117.98 36.48 90.00 90.00 90.00	94.29 116.91 35.98 90.00 90.00 90.00	94.12 117.28 35.93 90.00 90.00 90.00	93.90 117.26 35.88 90.00 90.00 90.00
Wavelength (Å)	1.5418	1.5418	0.9184	0.9184
Resolution (Å)	36.35 - 2.7 (2.8 - 2.7)	36.0 - 2.3 (2.4 - 2.3)	47.06 - 2.16 (2.26-2.16)	49.7-1.9 (2.0 - 1.9)
Number of unique reflections	21745 (3435)	32835 (3194)	21423 (2860)	32622 (3180)
Multiplicity	3.3 (3.4)	4.6 (2.6)	6.5 (4.0)	7.9 (7.7)
Completeness (%)	99.2 (95.5)	98.6 (97.1)	96.4 (81.1)	99.9 (99.8)
R <sub>merge</sub> <sup>a</sup>	7.0 (40.9)	14.8 (38.0)	16.1 (133.1)	14.5 (183.6)
Average I/σ(I)	9.0 (1.6)	7.6 (2.4)	9.1 (1.1)	11.0 (1.0)
CC1/2	99.1 (70.9)	98 (72.9)	99.7 (51.0)	99.9 (42.1)
Wilson B (Å <sup>2</sup> )	47.160	39.391	42.118	36.485
<b>Refinement statistics</b>				
Resolution range (Å)	36.35 - 2.7 (2.8 - 2.7)	36.0 - 2.3 (2.4 - 2.3)	47.06 - 2.16 (2.26 - 2.16)	49.7 - 1.9 (1.957 - 1.890)
No. of reflections in working set	11928 (1122)	17820 (1745)	20347 (1616)	32622 (3021)
No. of reflections in test set	598 (57)	888 (88)	1071 (85)	1632 (159)
R value (%) <sup>b</sup>	0.21 (0.32)	0.22 (0.23)	0.21 (0.32)	0.22 (0.34)

S5

R <sub>free</sub> value (%) <sup>c</sup>	0.28 (0.37)	0.26 (0.29)	0.25 (0.43)	0.26 (0.37)				
RMSD bond length (Å)	0.008	0.014	0.013	0.005				
RMSD angle (°)	1.5	1.7	1.6	0.9				
Number of atoms in AU (protein/ligand/water molecules)	Total Protein Ligand Water	2953 2800 51 102	Total Protein Ligand Water	2933 784 57 92	Total Protein Ligand Water	3047 2871 61 115	Total Protein Ligand Water	2969 2740 63 149
Mean B value (Å <sup>2</sup> )	31.17	54.45	41.89	33.62				
<b>Ramachandran plot statistics<sup>d</sup></b>								
Residues in favored regions (%)	96.00	97.46	96.11	97.42				
Residues in allowed regions (%)	4.00	2.54	3.89	2.58				

The data in parentheses refer to the highest-resolution shell.

<sup>a</sup> R<sub>merge</sub> =  $\sum_{hkl} \sum_i |I_i(hkl) - \langle I(hkl) \rangle| / \sum_{hkl} \sum_i I_i(hkl)$ , where the  $I_i(hkl)$  is an individual intensity of the  $i$ th observation of reflection  $hkl$  and  $\langle I(hkl) \rangle$  is the average intensity of reflection  $hkl$  with summation over all data.<sup>b</sup> R-value =  $\|F_o - |F_c|/|F_o|\|$ , where  $F_o$  and  $F_c$  are the observed and calculated structure factors, respectively.<sup>c</sup> R<sub>free</sub> is equivalent to R value but is calculated for 5 % of the reflections chosen at random and omitted from the refinement process (Brunger, 1992).<sup>d</sup> as determined by Molprobit

S6

Table S2: Residues missing in the crystallographic models due to disordered maps.

Complex	Chain	N-term	$\alpha$ 1- $\beta$ 1 loop	$\alpha$ 4- $\beta$ 7 loop	$\beta$ 7- $\alpha$ 5 loop	C-term
<b>5f</b>	A	140-152			317-318	336-379
	B	140-154	186-192		318	340-379
<b>5k</b>	A	140-150			317-318	337-379
	B	140-153	188-192		317	336-379
<b>5l</b>	A	140-147			317-320	338-379
	B	140-153	188-192		318	336-379
<b>5m</b>	A	140-147			318-319	338-379
	B	140-153	184-195	306	317-318	336-379

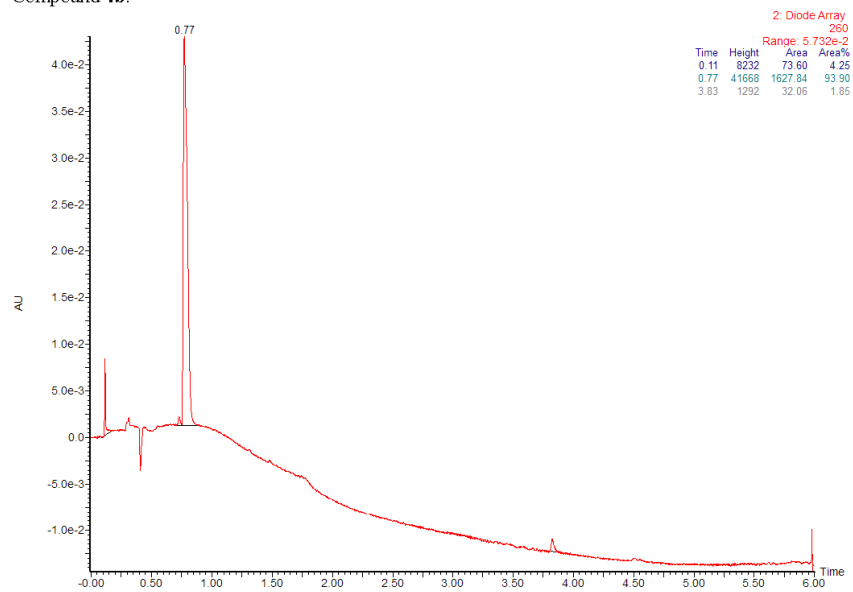
Table S3: UPLC purity of CDNs.

Compound	Retention time [min]	Purity [%]	Compound	Retention time [min]	Purity [%]
<b>4b</b>	0.77	93.9	<b>5l</b>	3.12	100
<b>5a</b>	0.89	98.67	<b>5m</b>	3.34	100
<b>5b</b>	1.93	92.24	<b>5n</b>	2.22	100
<b>5c</b>	1.58	97.18	<b>5o</b>	1.98	99.98
<b>5d</b>	1.58	97.2	<b>5p</b>	1.76	100
<b>5e</b>	0.87	87.79	<b>5q</b>	1.78	100
<b>5f</b>	1.36	98.67	<b>5r</b>	2.32	100
<b>5g</b>	1.87	100	<b>6f</b>	1.31	97
<b>5h</b>	1.91	99.53	<b>7a</b>	1.35	98.57
<b>5i</b>	2.23	100	<b>7f</b>	1.53	99.79
<b>5j</b>	2.51	99.47	<b>8a</b>	1.43	100
<b>5k</b>	2.38	99.71	<b>8f</b>	1.89	100



UPLC traces of CDNs.

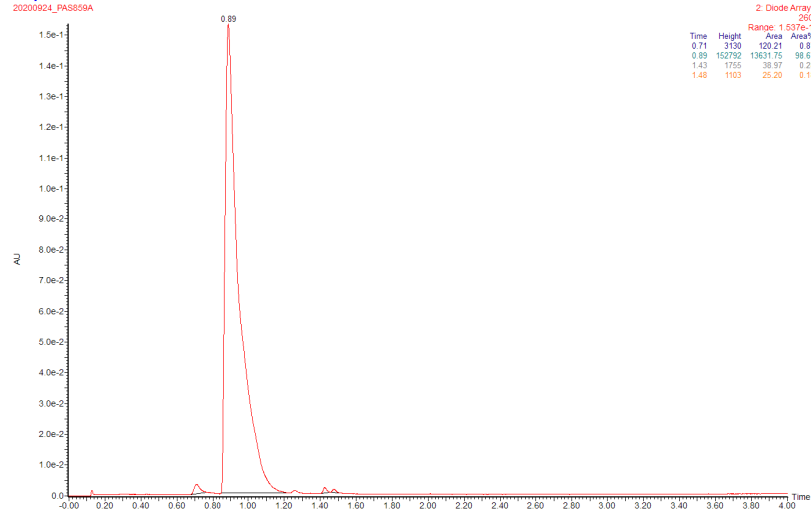
Compound **4b**:



S8

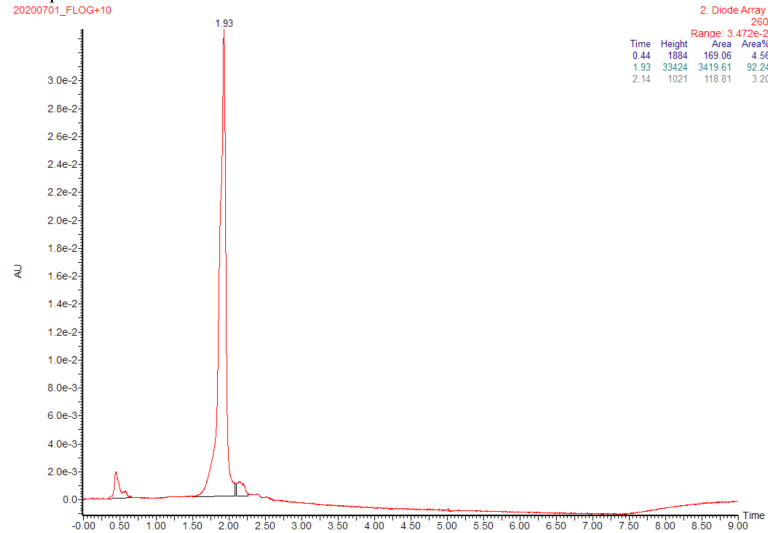
**Compound 5a:**

Purity PAS859  
20200924\_PAS859A



**Compound 5b:**

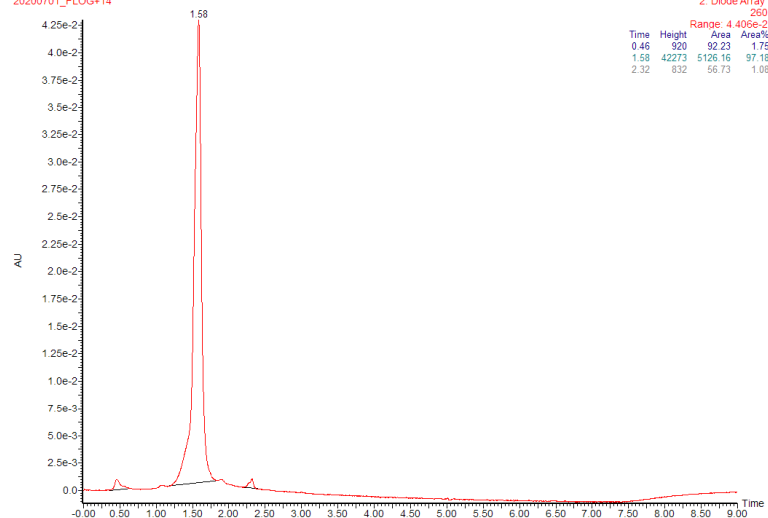
20200701\_FLOG+10



S9

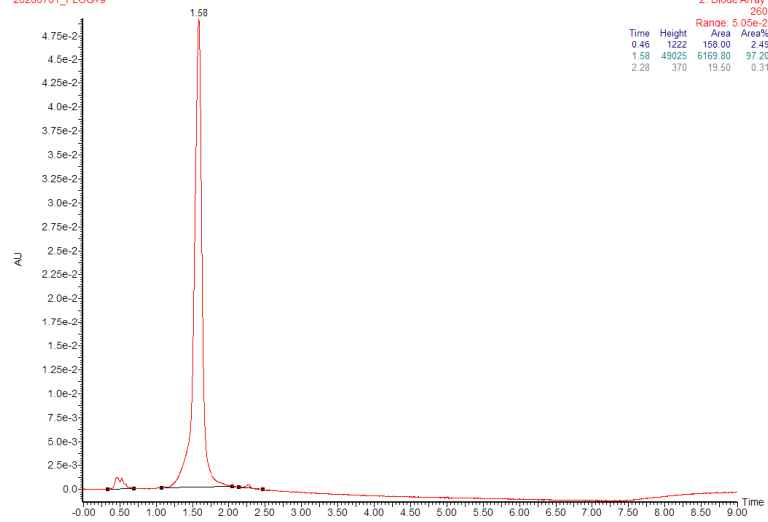
Compound 5c:

20200701\_FLOG+14



Compound 5d:

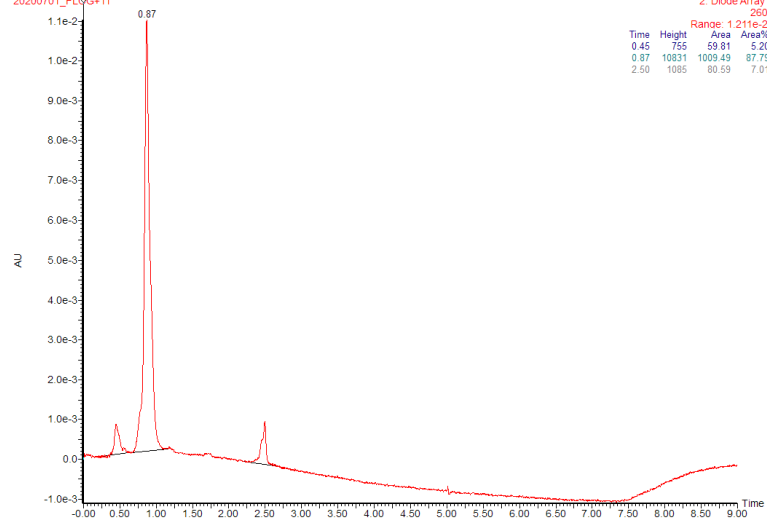
20200701\_FLOG+9



S10

Compound 5e:

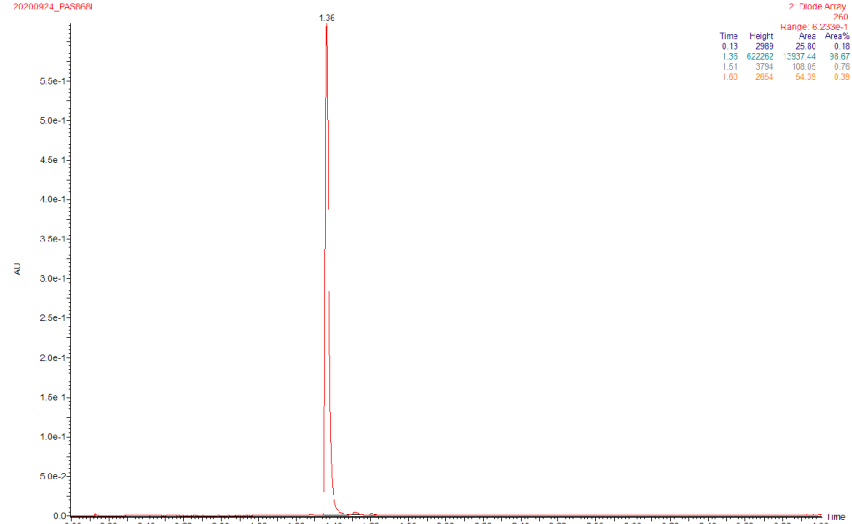
20200701\_FL155+11



Compound 5f:

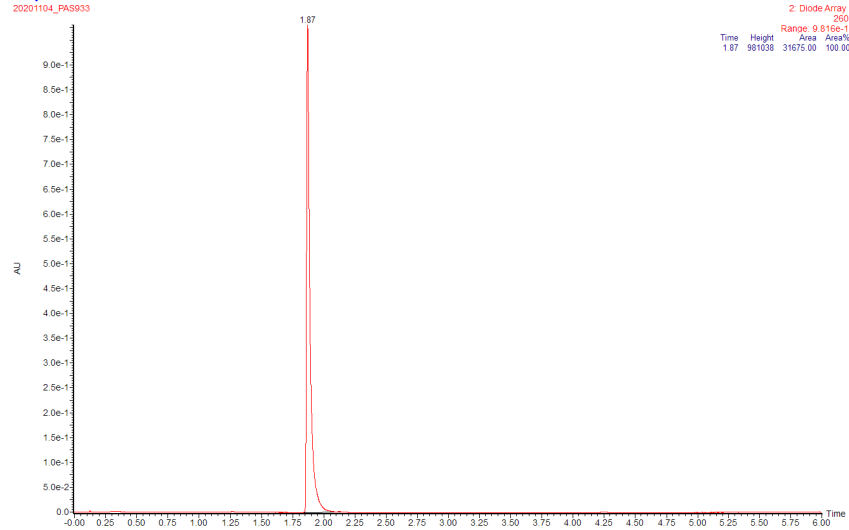
Purity PA5968

20200924\_PA5968

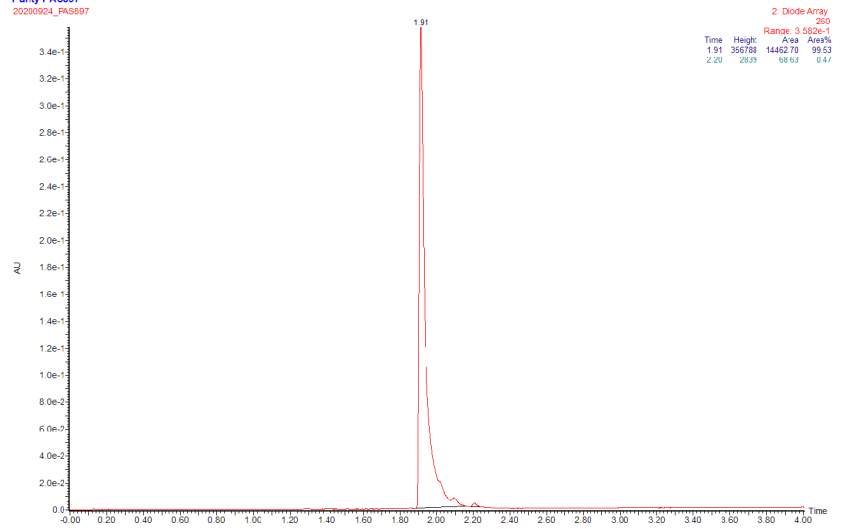


S11

Compound 5g:  
Purity PAS933  
20201104\_PAS933

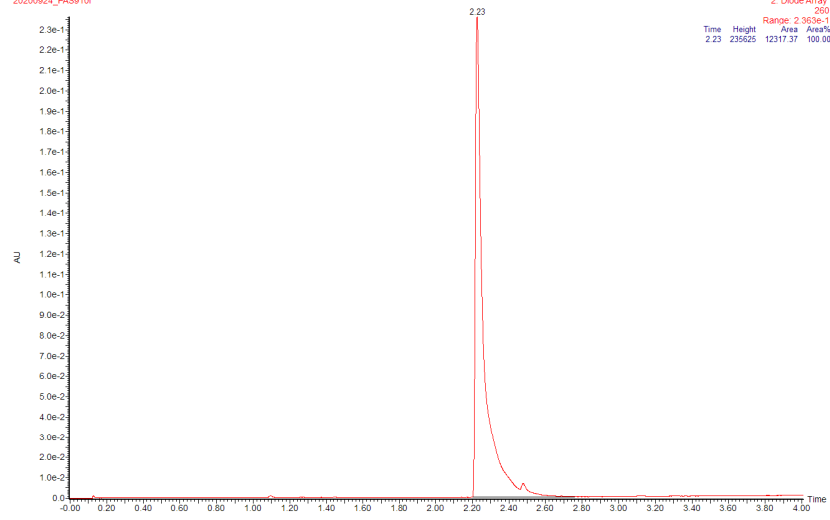


Compound 5h:  
Purity PAS897  
20200924\_PAS897

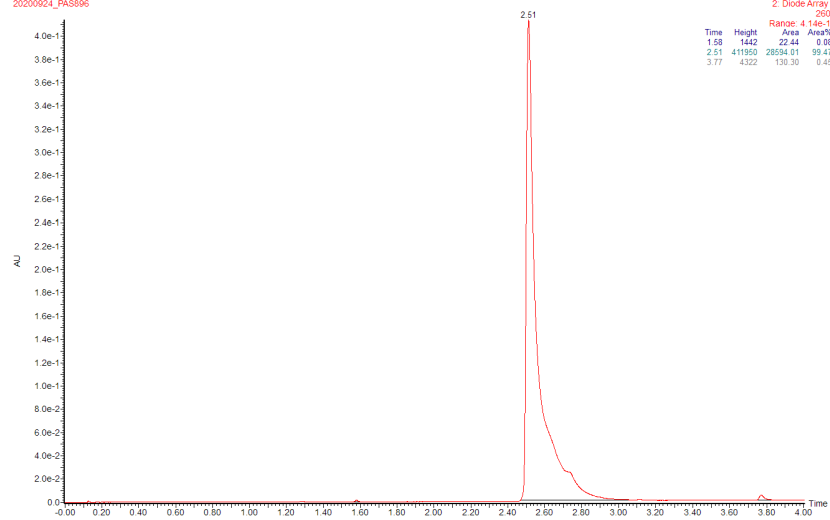


S12

Compound 5i:  
Purity PAS910  
20200924\_PAS910i

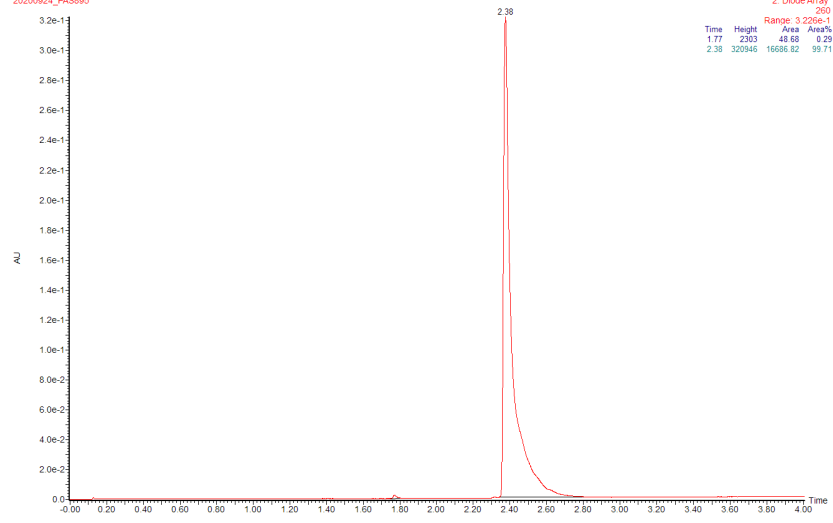


Compound 5j:  
Purity PAS896  
20200924\_PAS896

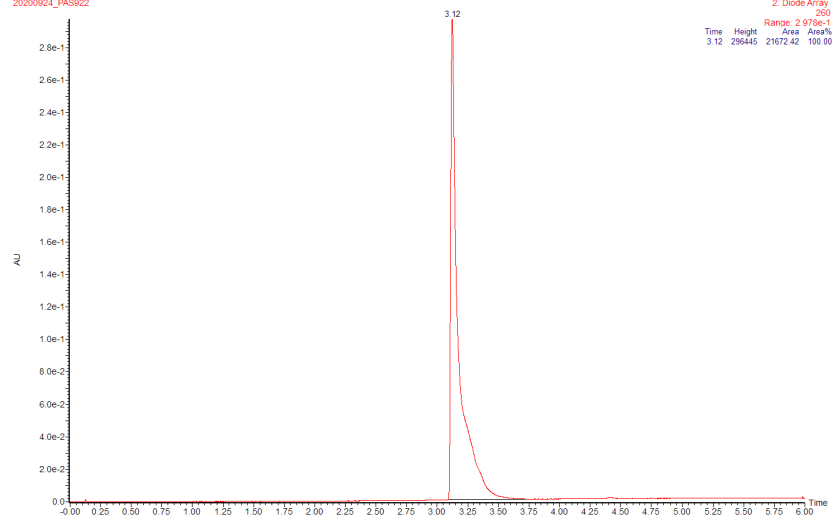


S13

Compound 5k:  
Purity PAS895  
20200924\_PAS895



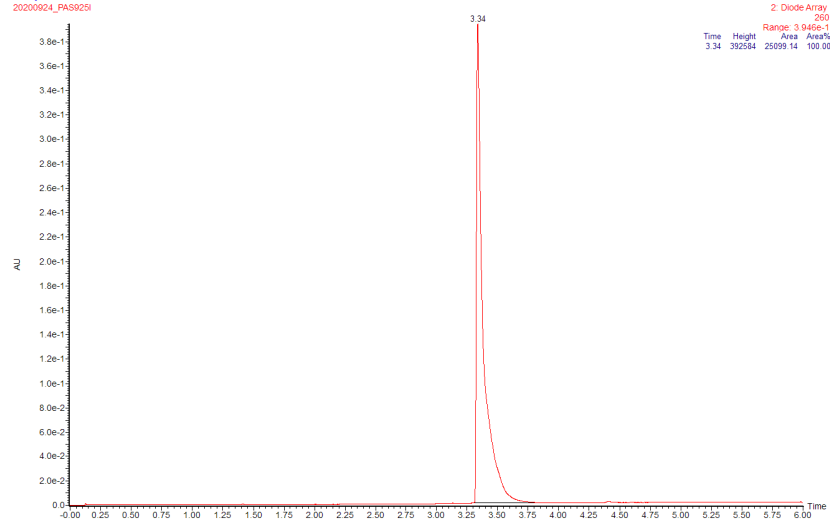
Compound 5l:  
Purity PAS922  
20200924\_PAS922



S14

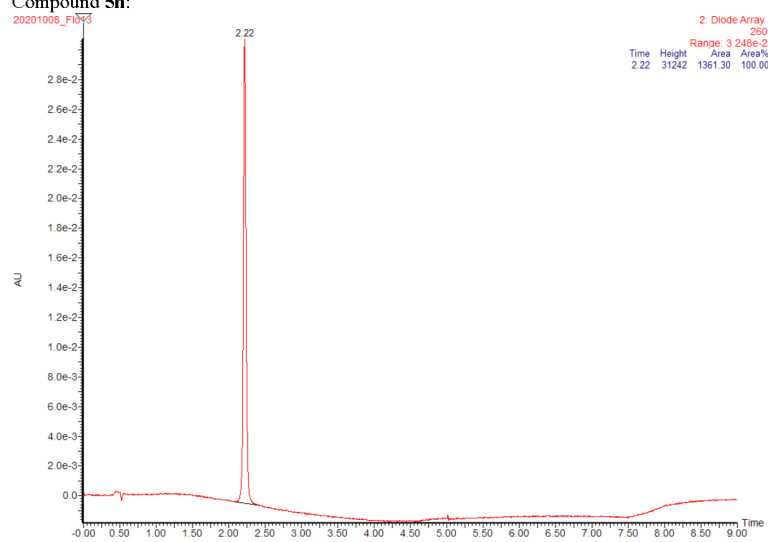
Compound 5m:

Purity PAS925  
20200924\_PAS925



Compound 5n:

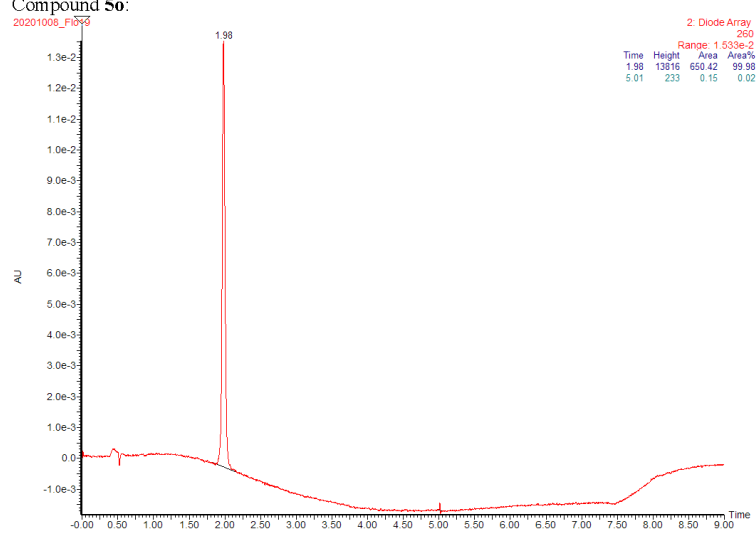
20201008\_F1073



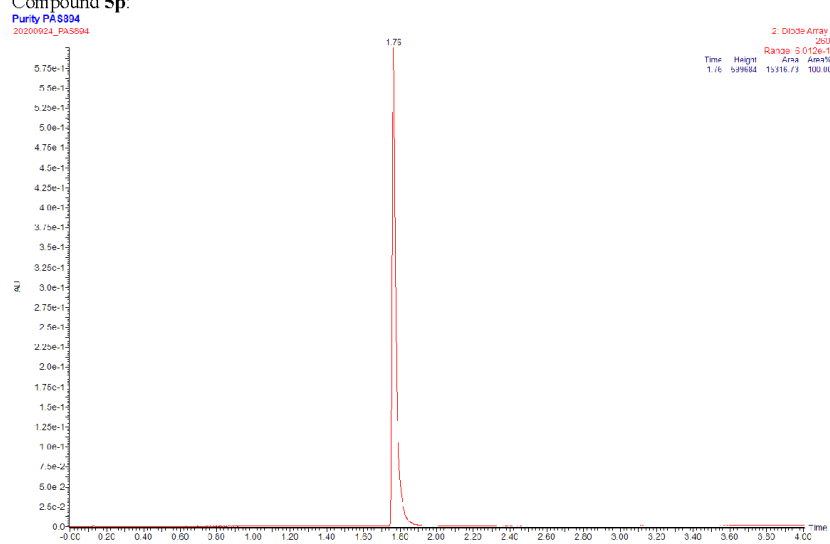
S15



Compound 5o:



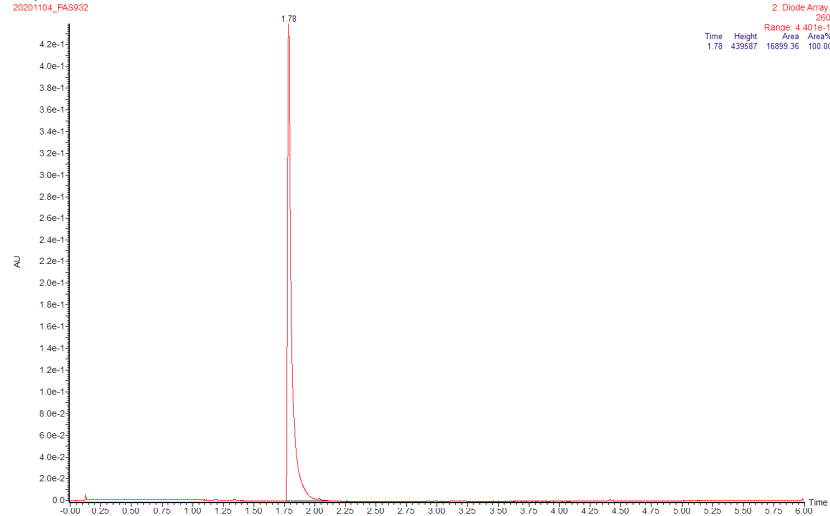
Compound 5p:



S16

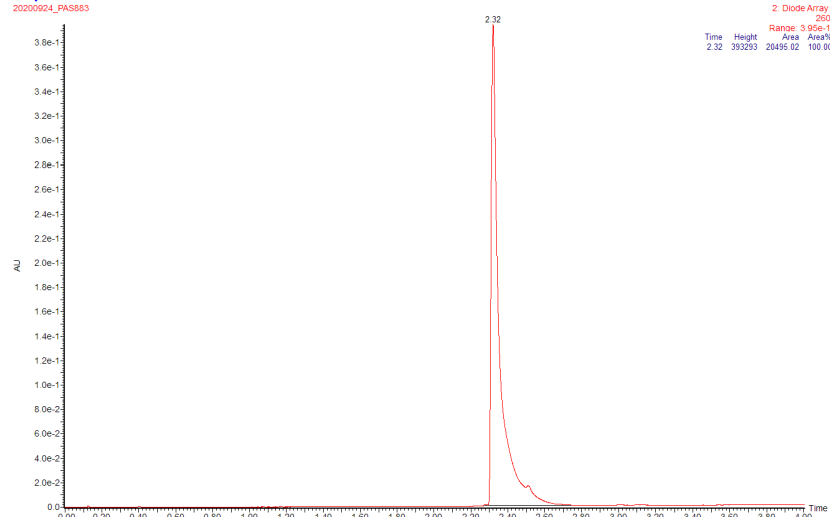
**Compound 5q:**

Purity PA8932  
20201104\_PA8932



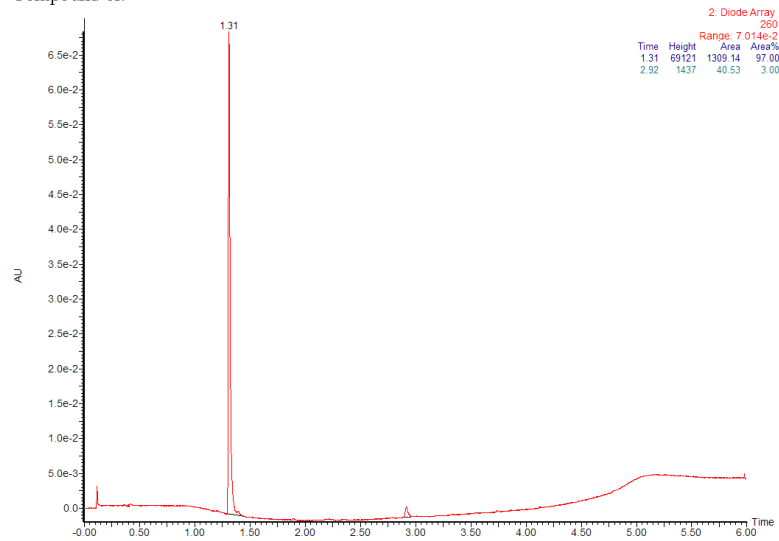
**Compound 5r:**

Purity PA883  
20200924\_PA883



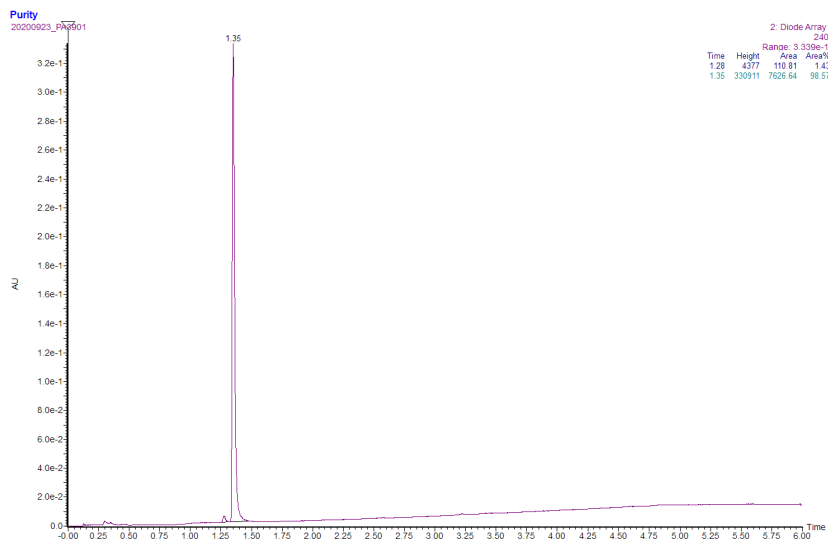
S17

Compound **6f**:

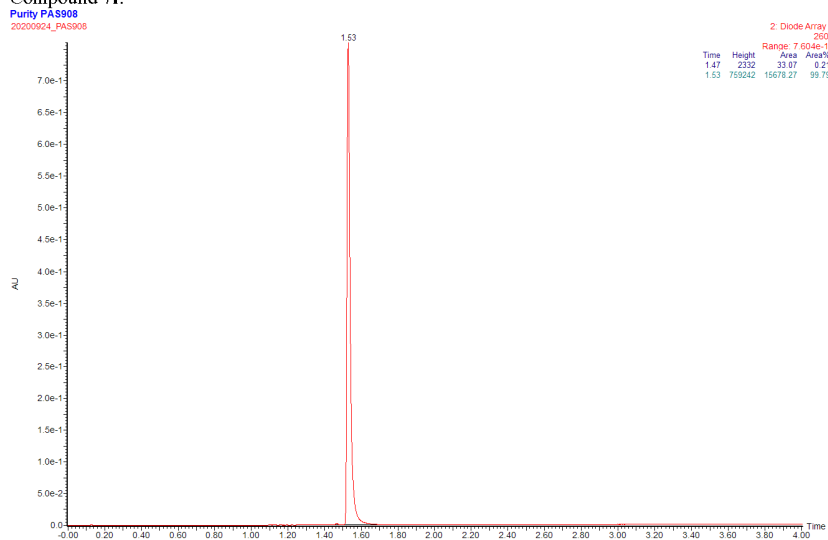


Compound **7a**:

S18

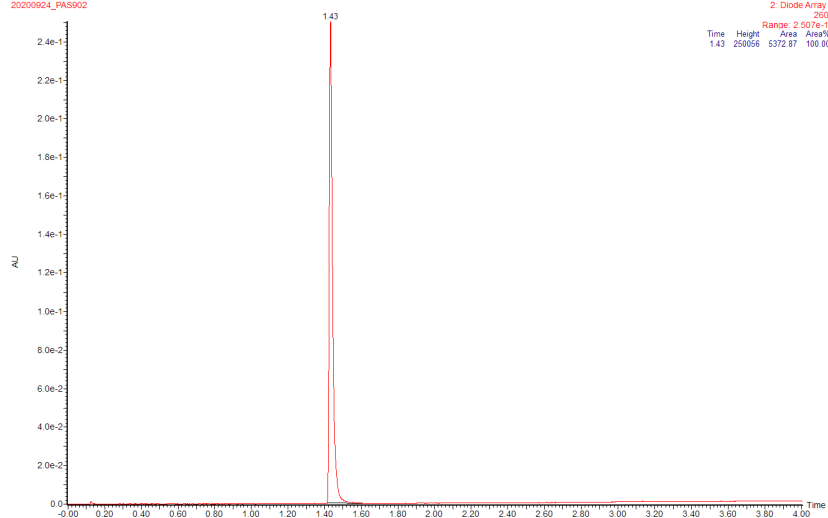


Compound 7f:



Compound 8a:

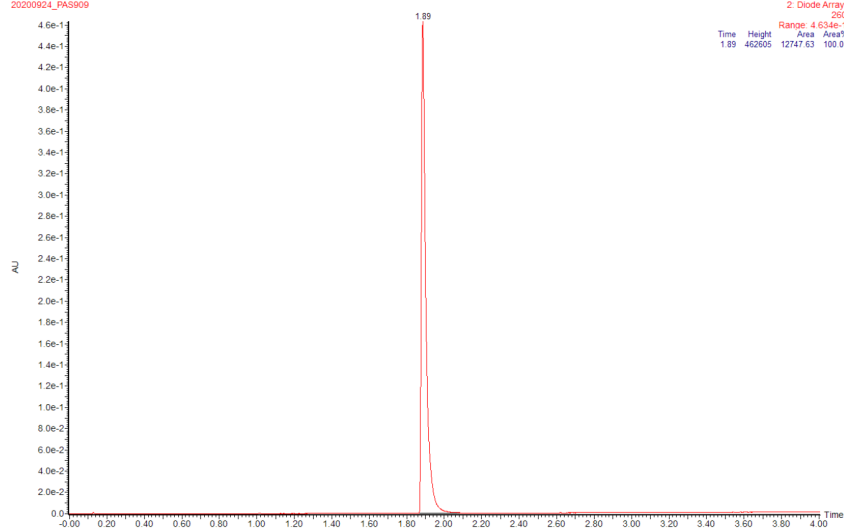
Purity PAS902  
20200924\_PAS902



2: Diode Array  
260  
Range: 2.507e-1  
Time Height Area Area%

Compound 8f:  
Purity PAS909

20200924\_PAS909



2: Diode Array  
260  
Range: 4.634e-1  
Time Height Area Area%

S20

Table S4: Top signals and CC<sub>50</sub>s for compounds tested on PBMCs.

Compound	Top <sup>a</sup>			CC <sub>50</sub> ( $\mu$ M)
	IFN $\gamma$	TNF $\alpha$	IFN $\alpha$	
<b>5b</b>	2.6	3.9	1.0	>200
<b>5c</b>	0.6	1.5	0.2	>200
<b>5f</b>	1.7	4.0	3.1	>200
<b>5g</b>	1.3	2.9	2.8	>200
<b>5h</b>	1.9	4.2	5.6	>200
<b>5i</b>	1.8	4.2	2.9	>200
<b>5j</b>	2.9	6.5	3.2	>200
<b>5k</b>	0.8	1.6	1.0	>200
<b>5l</b>	0.8	2.1	1.7	>200
<b>5m</b>	1.2	3.5	1.8	>200
<b>5n</b>	1.8	2.2	0.6	>200
<b>5o</b>	2.1	0.9	0.3	>200
<b>5p</b>	1.2	2.6	2.2	>200
<b>5q</b>	0.3	1.0	0.6	>200
<b>5r</b>	1.6	4.8	5.0	>200
<b>7f</b>	0.9	2.1	2.3	>200
2'3'-cGAMP	1.0	1.0	1.0	>200
3'3'-cGAMP	1.8	1.6	5.4	>200
2'2'-cGAMP	1.3	1.8	1.9	>200

<sup>a</sup>Maximal measured concentration of IFN $\alpha$ , TNF $\alpha$  and IFN $\gamma$ , relative to folds of concentration measured for 2'3'-cGAMP. The amount of cytokines induced by 2'3'-cGAMP treatment: INF  $\gamma$ , 10482 pg/mL; TNF $\alpha$ , 1878 pg/mL; INF  $\alpha$ , 710 pg/mL. Values are the mean of three independent experiment (n=3), each of them performed on PBMCs from different donor, measured in triplicates

S21

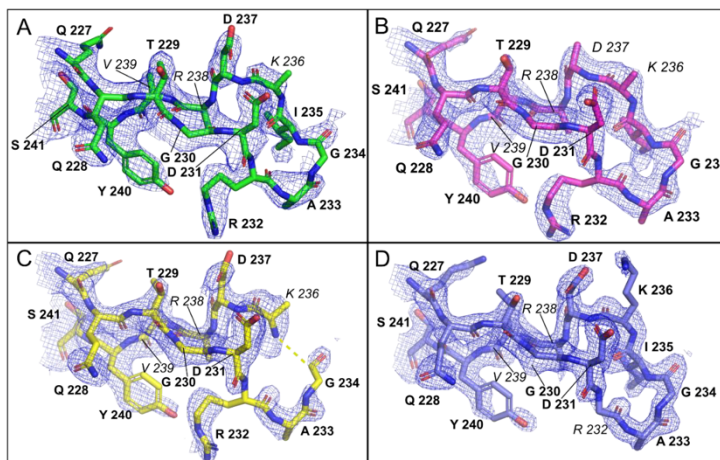


Figure S1:  $2F_o-F_c$  map of loops over ligand-binding site depicted at  $1\sigma$ . (A) **5f**, (B) **5k**, (C) **5l** and (D) **5m**.

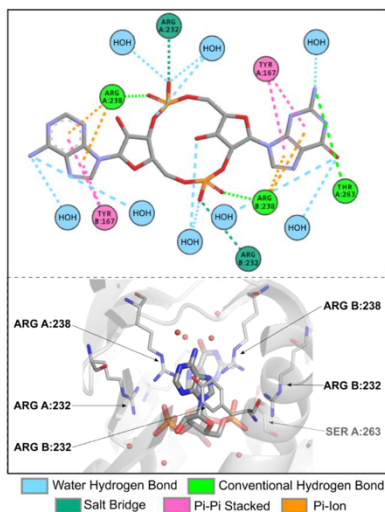


Figure S2: Interaction scheme of 2'3'-cGAMP in STING ligand-binding site.

S22

#### **8.4. Supplement S4: Development and characterisation of a chronic hepatitis B murine model with a mutation in the START codon of an HBV polymerase**

This paper was accepted 9.11.2022 for publication in Physiological research.

*Vanekova L, Polidarova M, Charvat V, Vavrina Z, Veverka V, Birkus G, Brazdova A. (2022) Development and characterisation of a chronic hepatitis B murine model with a mutation in the START codon of an HBV polymerase. Physiological research, doi:10.33549/physiolres.934979*

My contribution:

Development, establishment, and characterisation of HDI induced mouse model, data evaluation and interpretation, manuscript preparation and revision.



**Development and characterisation of a chronic hepatitis B murine model with a mutation in the START codon of an HBV polymerase**

Lenka Vanekova<sup>1,2</sup>, Marketa Polidarova<sup>1</sup>, Vilem Charvat<sup>1,3</sup>, Zdenek Vavrina<sup>1,2</sup>, Vaclav Veverka<sup>1,2</sup>, Gabriel Birkus<sup>1</sup>, and Andrea Brazdova<sup>1,\*</sup>

<sup>1</sup>Institute of Organic Chemistry and Biochemistry of the Czech Academy of Sciences, Prague, Czech Republic

<sup>2</sup>Faculty of Science, Charles University, Prague, Czech Republic

<sup>3</sup>First Faculty of Medicine, Charles University, Prague, Czech Republic

**\*Corresponding Author:**

Andrea Brazdova, Ph.D., Institute of Organic Chemistry and Biochemistry of the Czech Academy of Sciences, Flemingovo namesti 542/2, 160 00 Prague 6, Czech Republic; [andrea.brazdova@uochb.cas.cz](mailto:andrea.brazdova@uochb.cas.cz)

**Short title**

Development of murine model reflecting chronic hepatitis B

**Summary**

Chronic hepatitis B (CHB) is caused by the Hepatitis B virus (HBV) and affects millions of people worldwide. Developing an effective CHB therapy requires using *in vivo* screening methods, such as mouse models reflecting CHB based on hydrodynamic delivery of plasmid vectors containing a replication-competent HBV genome. However, long-term expression of HBV proteins is accompanied by production of progeny virions, thereby requiring a Biosafety Level (BSL) 3 animal facility. In the present study, we introduced a point mutation in the START codon of the HBV polymerase to develop a mouse model reflecting chronic hepatitis B infection without formation of viral progeny. We induced the mouse model by hydrodynamic injection of adeno-associated virus plasmid vector (pAAV) and minicircle plasmid (pMC) constructs into C57Bl/6 and C3H/HeN mouse strains, monitoring HBV

antigens and antibodies in blood by enzyme-linked immunosorbent assay and analysing liver expression of HBV core antigen by immunohistology. Persisting expression of viral antigens over 140 days (study endpoint) was observed only in the C3H/HeN mouse strain when using pAAV/1.2HBV-A and pMC/1.0HBV-D with pre-C and pre-S recombination sites. In addition, pAAV/1.2HBV-A in C3H/HeN sustained HBV core antigen positivity up to the study endpoint in C3H/HeN mice. Moreover, introducing the point mutation in the START codon of polymerase effectively prevented the formation of viral progeny. Our study establishes an accessible and affordable experimental paradigm for developing a robust mouse model reflecting CHB suitable for preclinical testing of anti-HBV therapeutics in a BSL2 animal facility.

#### **Keywords**

chronic hepatitis B murine model, HBsAg, HBeAg, pAAV system, minicircle HBV

#### **Introduction**

Hepatitis B is a viral infection caused by the hepatitis B virus (HBV), small, enveloped DNA virus classified into ten genotypes (A-J) [1] that specifically target liver tissue. Approximately 95% of adults suffering from acute HBV infection recover within 6 months by developing anti-HBV immunity. Those who do not develop immunity suffer from chronic hepatitis B (CHB), defined as the continuous blood circulation of a hepatitis B surface antigen (HBsAg) for more than six months. Moreover, up to 30% of HBV-infected children under 5 years and up to 95% of neonates develop CHB [2]. CHB may result in liver cirrhosis, steatosis, hepatocellular carcinoma, or adenoma [3–6].

The two available CHB therapies, interferon  $\alpha$ -based therapy and nucleos(t)ide analogues, rarely result in the complete cure and often require life-long application [7], causing side effects [8]. Additionally, the long-term application of the first generation of nucleos(t)ide analogues (lamivudine and adefovir, among others) most likely lead to viral resistance [9]. For these reasons, research and development of novel CHB therapeutics requires preclinical safety and efficacy validation.

Preclinical safety and efficacy research relies on animal models. However, the human HBV virus can only chronically infect humans and chimpanzees [10]. Alternatively, the human HBV-like family of viruses, which includes the woodchuck [11], domestic duck [12] and Beechey ground squirrel [13] subtypes, could be used as *in vivo* CHB models, but they require complying with stringent ethical, handling, and administrative procedures. Another difficulty with using these models is the lack of research tools for monitoring host-virus immune responses.

Murine CHB models, by contrast, are well established and much simpler to use. For example, transgenic HBV [14] and chimeric [15] mouse models are based on tail vein delivery of adeno-associated virus (AAV), whereas other models are induced by hydrodynamic injection (HDI [16]) of plasmid vectors carrying replication-competent DNA genome [17]. For these purposes, researchers usually resort to adeno-associated virus plasmid vector (pAAV) and covalently closed circular DNA plasmid produced by minicircle technology (pMC), which was primarily invented to address HBV cccDNA *in vivo* [17]. However, long-term HBV protein expression yields progeny virions, thereby requiring a Biosafety Level (BSL) 3 animal facility. Furthermore, sustained expression of viral markers in HDI-induced mouse models of CHB [18] depends on the selected mouse strain. In particular, major histocompatibility complex (MHC)-associated immune response to HBsAg affects model sustainability [19]. In terms of response to HBsAg, three different MHC genotypes are defined [19]: high (alleles H-2<sup>d,q</sup>), intermediate (alleles H-2<sup>a</sup>>H-2<sup>b</sup>>H-2<sup>k</sup>), and low/non-responders (alleles H-2<sup>s,f</sup>).

To overcome these limitations, in this study, we aimed to develop and characterise a mouse model reflecting CHB induced by HDI delivery of HBV genome-encoding plasmids with a mutation in the START codon of the polymerase, which prevents the secretion of progeny virions by hepatocytes [17,20], in two different immunocompetent mouse strains, C57Bl/6 and C3H/HeN. In addition, we compared two different plasmid systems that encode HBV genomes of genotypes A and D, more specifically pAAV/1.2HBV genotype A (pAAV/1.2HBV-A) and D (pAAV/1.2HBV-D), pMC/1.0HBV genotype D with pre-C (pMC/1.0HBV-D-pre-C; encoding HBeAg [21]) and pre-S (pMC/1.0HBV-D-pre-S; encoding envelope proteins [21]) residual recombination sites. Ultimately, the main purpose of this

study was to create a mouse model that stably expresses HBsAg and HBeAg and is therefore suitable for robust preclinical testing of novel CHB therapeutics in a BSL2 animal facility.

## **Methods**

### **Plasmids and mutagenesis**

Two different types of plasmid constructs, a pAAV and minicircle, were used for mutated HBV genome delivery to establish a mouse model reflecting CHB. Plasmids carrying 1.2mer of HBV genome, genotype A (GenBank: AF305422.1, kindly provided [22]) or D (GenBank: MN645906.1, prepared in house) were inserted between inverted terminal repeats from AAV2 [23] (Fig.1). Minicircle constructs [17,24] of 1.0mer of HBV genotype D genome with a residual recombination site in the pre-S or pre-C region were prepared according to Yan Z., et al. [17] and to Wang L., et al. [25]. A point mutation T2308C [17] of the polymerase START codon was introduced to prevent the formation of HBV virions. The pAAV plasmids were isolated using the Nucleobond Xtra Midi EF kit (Macherey Nagel) according to the manufacturer's instructions. The minicircles were prepared from pre-MC plasmids, also according to the manufacturer's instructions (MC-Easy Minicircle DNA Production Kit, BioCat), and isolated using the Nucleobond Xtra Maxi EF kit (Macherey Nagel). The endotoxin level in DNA was quantified using HEK-Blue™ LPS Detection Kit 2 (InvivoGen) in HEK-Blue™hTLR4 cells (InvivoGen), according to the manufacturer's instructions. Plasmid integrity, quality and functionality were tested (data not shown, plasmids were tested *in vitro* using HepG2-NTCP transfection system and the levels of HB-Ag secreted into media were tested; *in vivo* viral progeny absence was verified using qPCR).

### ***In vivo* mouse model reflecting CHB**

All animal procedures were approved by institutional and national committees for the care and use of laboratory animals (CAS 77/2018, MSMT 29416/2020-7, Czech Republic). All animal experiments were performed in accordance with European Guidelines on Laboratory Animal Care. The HDI model was induced in male C3H/HeN and C57Bl/6 mice (aged 4-6 weeks [26], purchased from the Charles River Laboratories) by tail vein injection of 10 µg of endotoxin free pAAV/1.2HBV plasmid DNA [27] or 5 µg

of endotoxin free pMC/1.0HBV DNA [17] in a tempered saline solution within 5-8 s in a volume equal to 10% of the mouse body weight [28]. Blood samples were collected into lithium-heparin tubes (Microvette CB 300, Sarstedt) every 1-3 weeks for up to 20 weeks. The mice were housed in specific, pathogen-free conditions in an individually ventilated cage-system with food and water ad libitum under controlled temperature and light settings and monitored weekly for general appearance (weight, fur ruffling, and mobility/activity).

#### **HBV antigen secretion analysis**

The blood levels of the HBV surface, the HBV envelope-relevant antigens (HBsAg and HBeAg), and the antibody against HBsAg (HBsAb) were determined using an ELISA kit (Bioneovan Co., Ltd.) according to the adapted manufacturer's recommendations. The absorbance was measured on a Spark reader (Tecan). The internally established positivity threshold was determined as 5x the mean of HDI controls for HB-Ag markers and as 3x the mean of HDI controls for the HBsAb marker.

#### **HBcAg immunohistochemistry**

The liver was preserved in 4% paraformaldehyde (Sigma-Aldrich) for 24-48 h and kept in 70% ethanol (Penta s.r.o.) until analysis. Liver tissue was stained with polyclonal rabbit anti-HBcAg antibody (DAKO-Agilent). HBcAg positivity was defined as a percentage of positive cells in the entire sample.

#### **Statistical analysis**

All statistical tests of experimental data were performed in GraphPad Prism software (La Jolla, CA, version 8.0.1). Data were presented as Kaplan-Meier curves or mean  $\pm$  standard error of mean (SEM). HB-Ag positivity was analysed using the Log-rank comparison test. The normality of distributions was tested using the Shapiro-Wilk test. The trend of HB-Ag levels over time was assessed according to the Spearman's rank correlation test, and the HB-Ag terminal levels was analysed using the Mann-Whitney U-test.

#### **Results**

**T2308C mutation of the polymerase START codon does not affect *in vitro* plasmid functionality.**

Both pAAV [22] and pMC [17,24] plasmids carrying the replication-competent HBV DNA genome (henceforth referred to as wild type, wt) or the HBV DNA genome with a mutation of the START codon of the polymerase (T2308C [17], Fig.1) were produced. The *in vitro/in vivo* quality, purity, and functionality were tested (data not shown). The T2308C point mutation was effectively introduced and had a non-significant effect on the *in vitro* expression of HB-Ag when compared to the wt plasmid using an *in vitro* HepG2-NTCP infection system [29]. The absence of HBV virions using plasmids with a point mutation in the START codon of polymerase was verified in mouse plasma by quantitative polymerase chain reaction (qPCR), showing that HBV DNA was below the limit of detection.

The *in vivo* mouse model was hydrodynamically induced via tail vein (Fig.2a). We compared PBS to a physiologic solution. The physiologic solution increased the HDI survival rate up to 100% (data not shown) in contrast to 20% using commercially available PBS (without calcium and magnesium chloride, Sigma Aldrich, cat.no. D8537).

C57Bl/6 and C3H/HeN male mice were hydrodynamically injected with either 10 µg of pAAV/1.2HBV or 5 µg of pMC/1.0HBV plasmids with the point mutation T2308C (Fig.2a). These doses were previously described as optimal when using nonmutated wild type (wt) plasmids for long-term HBV persistence without HBsAg seroconversion [17,27]. The models were evaluated based on the HB-Ag levels, and sustainability was determined by seroconversion in the presence of anti-HBsAg antibodies (HBsAb) in blood (Fig.2, Fig.3, Fig.4) and further confirmed by HBcAg expression in the liver (Fig.5).

**Hydrodynamic injection of pAAV/1.2HBV and pMC/1.0HBV with a START codon mutation of the polymerase into C57Bl/6 mice results only in transient expression of viral proteins.**

In C57Bl/6 mice, the blood levels of HBsAg and HBeAg started decreasing within the first week post HDI. Mice injected with pAAV/1.2HBV-D showed a rapid loss of HBsAg (no animal was positive by D35, Fig.2b). In addition, 80% of animals had cleared HBeAg within D21 post HDI (Fig.2c), and 80% of mice were positive for HBsAb (Fig.2d) by D35.

Due to this rapid clearance of HB-Ag (Fig.2b,c) and to the very low HBV persistence rate observed when using pAAV/1.2HBV-D, the minicircle construct [17] of genotype D was prepared. pMC/1.0HBV-D-pre-C injection into C57Bl/6 mice resulted in a relatively fast clearance of HBsAg (only 10% positive mice by D35, Fig.2b) and in lower HBsAg levels (Fig.3a) than when injecting the pAAV/1.2HBV-D (Fig.3a), albeit with 10% positivity up to D105 (Fig.2b). HBeAg positivity decreased from 70% (D7) to 30% (D49) and finally up to 10% (D77) and sustained to the terminal point of experiment (D105, Fig.2c), with more than 10x higher HBeAg levels than those observed in animals injected with pAAV/1.2HBV-D (Fig.3b). HBsAb were detected within 4 weeks post HDI, and by the end of the study, up to 40% animals had seroconverted (D105, Fig.2d).

By D21, mice injected with pMC/1.0HBV-D-pre-S showed a mild decrease of HBsAg-related positivity (10-20% loss every week, Fig.2b) with mean plasma HBsAg values >100 ng/ml (Fig.3a). However, HBsAg-related positivity rapidly dropped to 10% until D35 (Fig.2b), while HBeAg positivity decreased gradually to 20% until D49 (Fig.2c), with HBeAg plasma levels similar to but less consistent than those measured when injecting pMC/1.0HBV-D-pre-C (Fig.3b). HBsAb related positivity increased up to 50% until D28 (Fig.2d).

Even though C57Bl/6 mice injected with pAAV/1.2HBV-A showed the most promising results (with a mean peak HBsAg concentration of 4500 ng/ml, which was considerably higher than those of other induction systems, Fig.3a), all animals showed total loss of HBsAg and HBeAg by D49 (Fig.2b, Fig.2c, Fig.3a, Fig.3b), while HBsAg seroconversion rapidly increased from 10% (D21, Fig.2d) to 90% within 2-3 weeks post HDI (Fig.2d). Based on our results, when using pAAV/1.2HBV-A, we also tested pMC/1.0HBV-A-pre-C in CB7Bl/6 mice. However, we observed only acute expression of HB-Ag (total loss of HB-Ag by D28), as in pAAV/1.2HBV-D (data not shown).

**Hydrodynamic injection of pAAV/1.2HBV-A with a mutated polymerase START codon into C3H/HeN mice leads to a persistent expression of viral proteins.**

HDI injection of the plasmids into the C3H/HeN mouse strain led to a much more consistent and sustainable expression of viral proteins. More than 80% of animals remained HB-Ag-positive up to the end of the study (D140, the study endpoint) when using pMC/1.0HBV-D-pre-C, pMC/1.0HBV-D-pre-S, and pAAV/1.2HBV-A (Fig.2b,c, Fig.4a,b). However, pAAV/1.2HBV-D induced only a transient expression of viral proteins, albeit for a longer period time in C3H/HeN mouse strain than in C57Bl/6 mice (Fig.2b,c). On D7 after HDI, 70-80% of animals were HB-Ag-positive, but this positivity had dropped to 10% by D62 (Fig.2b,c). Furthermore, only 10% of the mice injected with pAAV/1.2HBV-D developed HBsAb (Fig.2d). In contrast to pAAV/1.2HBV-D, pAAV/1.2HBV-A, pMC/1.0HBV-D-pre-C and pMC/1.0HBV-D-pre-S showed a similar chronic expression of viral antigens (nonsignificant, Fig.2b,c). Interestingly, pMC/1.0HBV-A-pre-C showed only a transient expression of viral proteins (total loss of HB-Ag by D49, data not shown) similar to that of pAAV/1.2HBV-D.

We also observed differences in the average values of detected HB-Ag between all constructs. The minicircle constructs using genotype D had low HBsAg levels (pMC/1.0HBV-D-pre-C <200 ng/ml, pMC/1.0HBV-D-pre-S <500 ng/ml, Fig.4a), while pAAV/1.2HBV-A had >40x higher average values of HBsAg (<20000 ng/ml, Fig.4a). The endpoint HBsAg values were significantly different between pAAV/1.2HBV-A and pMC/1.0HBV-D-pre-S and pre-C, but the plasma endpoint levels of HBeAg were significantly higher when using the minicircle constructs (120-200 ng/ml, Fig.4b) than when using pAAV/1.2HBV-A (<30 ng/ml, Fig.4b).

**HBcAg was detected only in C3H/HeN mice hydrodynamically injected with both pAAV/1.2HBV and pMC/1.0HBV with a mutation of polymerase at the terminal point of the experiment.**

The expression of HBcAg in mouse hepatocytes was determined by immunohistochemical analysis of liver tissue on D7 [27] post HDI and at the terminal point of the experiment. In C57Bl/6 mice, IHC confirmed the presence of HBcAg positive cells on D7 post HDI regardless of HBV construct, with pAAV/1.2HBV-A resulting in 20-25% HBcAg-positive cells; pAAV/1.2HBV-D, 10-25% HBcAg-positive cells; and both pMC/1.0HBV-D-pre-C and pre-S, <10% HBcAg-positive cells (Fig.5). However, not a



single liver tissue showed the HBcAg positivity at the end of the study (Fig.5). C3H/HeN mice showed 20-25% HBcAg-positive hepatocytes for pAAV/1.2HBV-A and 10-15% HBcAg-positive hepatocytes for genotype D on D7 post HDI regardless of plasmid induction system. The HBcAg positivity of the genotype D of both systems, pAAV and pMC, decreased to <10% of positive cells at the terminal point of the experiment. Conversely, HBcAg positivity remained unchanged when using pAAV/1.2HBV-A in C3H/HeN mice. The positive hepatocytes were unevenly distributed in most samples. Mice injected only with physiologic solution (HDI control, Fig.5) were HBcAg-negative throughout the experiment regardless of induction construct.

Regardless of mouse strain or HBV genotype, HBV transduction was latent. In both mouse strains, none of the induction systems affected physiology, as confirmed by the absence of weight changes (Fig.2e). The mice were also monitored weekly for general appearance (fur ruffling, mobility, and activity), showing no pathologic changes.

#### **Discussion**

Our immunocompetent CHB mouse model induced by HDI delivery of plasmid vector [18] stably expresses the viral markers HBsAg and HBeAg for 20 weeks without viral progeny. As such, this model is suitable for robust preclinical safety and efficacy testing of novel CHB therapeutics. Although research on CHB mouse models has recently led to the development of several other murine models [18], such as transgenic [14] and chimeric [15] mouse models, as well as models based on tail vein delivery of viral vectors carrying HBV DNA genome [16], they all have some limitations, including requiring BSL3 animal facilities [30]. To overcome these limitations, we first compared two most commonly used vehicles for HDI injection, physiologic solution [27] and PBS [22] particularly regarding their formulation in terms of acid-base balance disruption (e.g., calcium, magnesium and/or potassium chloride). Despite the broad use of PBS as a vehicle for *in vivo* transfection (e.g., targeted [31] and pressurised [22]), the physiologic solution dramatically positively affected HDI survival. We also used pAAV [22,27] and pMC [17] plasmid vectors carrying 1.2mer and 1.0mer HBV DNA genome respectively

(genotype A and D) dosed as previously described [17,27] with a T2308C [17] point mutation of the START codon of the polymerase to prevent the production of infectious HBV progeny [17], as confirmed using all induction systems, without affecting HBV transcription and antigen expression. Therefore, this point mutation allows us to operate in a BSL2 animal facility.

We chose two mouse strains of different MHC classes with different immune responses to HBsAg that prevent spontaneous healing [19] namely C57Bl/6 and C3H/HeN, to comparatively assess HB-Ag persistence. HBsAg is considered a general marker of HBV in both mouse and human plasma [32], regardless of acute or chronic infection. Unlike HBsAg, HBsAb indicates the generation of specific immunity leading to host recovery. Since HBsAb production is affected by S region-encoding MHC class III complement components, including C<sup>6</sup> and C<sup>2</sup> [19], we tested mouse strains from an intermediate MHC genotype group with different haplotypes, i.e., C57Bl/6 (haplotype b) and C3H/HeN (haplotype k).

In line with Peng, et al. [20], we demonstrated that the C57Bl/6 mouse strain bearing the S<sup>b</sup> region with a sufficient response to HBsAg leads to HB-Ag clearance (Fig.2b, Fig.3), as observed across all induction systems, resulting in only an acute HBV model, unlike other studies [22,27], where HB-Ag expression persisted for more than 6 months when using replication-competent HBV genome in C57Bl/6 mice. This result could be explained by differences in positivity threshold setting and in animals from different vendors. Moreover, the introduced point mutation may also partly account for this discrepancy between studies.

The C3H/HeN mouse strain markedly increased and sustained viral antigen expression, as also demonstrated by Peng, et al. and Yan, et al. [17,20] using non-mutated pAAV/1.2HBV and pMC/1.0HBV. Based on humoral immunity in C3H/HeN mice (S<sup>k</sup> region), we assume that the insufficient HBsAg response reflects its persisting levels and the low levels of seroconversion (Fig.2b,d, Fig.4a).

We confirmed the persistence and clearance of viral markers by immunohistochemical analysis of HBcAg in liver tissue, showing HBV clearance through the decreased HBsAg and HBeAg positivity in C57Bl/6 mice over time (Fig.2b,c, Fig.3a,b) along with increased HBsAb levels (Fig.2d) matching the decreased HBcAg positivity. These results also corroborate Li L, et al. [27], who quantified HBcAg-levels in C57Bl/6 mice after using pAAV/1.2HBV. Unlike them [27], nevertheless, we detected lower HBcAg positivity on D7 after HDI and no HBcAg positivity at the terminal point of the experiment (D49). A possible reason for this difference may be the point mutation of the polymerase START codon. HBcAg positivity was sustained at a max. of 25% using pAAV/1.2HBV-A in C3H/HeN mice, matching the persisting levels of HBsAg expression (Fig. 2b, Fig. 4a). Our results using both mouse strains correlate with the findings of Peng, et al. [20] who reported that C3H/HeN mice were superior to C57Bl/6 mice in HBcAg positivity when using a non-mutated pAAV/1.2HBV induction system.

Considering the plasma levels of the viral markers, the efficacy of the induction systems in both C57Bl/6 and C3H/HeN mice was reflected as a trend of pAAV/1.2HBV-A  $\geq$  pMC/1.0HBV-D-pre-S > pMC/1.0HBV-D-pre-C >> pAAV/1.2HBV-D. Unlike all induction plasmids in C57Bl/6 mice and pAAV/1.2HBV-D in C3H/HeN mice, HB-Ag positivity persisted until the terminal point of the experiment (D140) using pAAV/1.2HBV-A and both minicircle constructs in C3H/HeN mice. In contrast to genotype A, genotype D has a 33-nucleotide deletion in the N terminus of the PreS1 region [33]. This deletion changes the ratio of the three S antigen forms and affects their secretion [34], which may thus explain why the HBsAg-levels were significantly lower in mice induced with genotype D.

The differences in HBeAg-levels among plasmids in both mouse strains might be associated with the use of different induction systems. Unlike pAAV, the pMC HDI induction system was primarily developed to address cccDNA *in vivo* [17]. As previously described [35], HBeAg secretion and cccDNA formation may be correlated; if so, significantly higher HBeAg levels should be found when using minicircle constructs. However, the point mutation of the START codon of the polymerase adversely affected the viral replication cycle. Consequently, the formation of new cccDNAs [36] resulted in similar

if not lower HBeAg-levels during the experiment. Nevertheless, HBeAg persistence is variable even among CHB patients and thus not a definitive CHB marker [37].

In conclusion, the C3H/HeN mouse strain is more suitable than C57Bl/6 for developing a long-term *in vivo* model reflecting CHB. Based on the pAAV/1.2HBV-A-associated HBsAg-levels, in contrast to pMC/1.0HBV-D-pre-S-associated HBsAg-levels, we believe that the pAAV induction system provides more suitable experimental paradigm for various immunopathology studies aimed at assessing the efficacy and safety of novel therapeutic approaches requiring robust yet simple *in vivo* testing. Notwithstanding previously published mouse models, we firmly believe that the persistence of HBsAg levels in our mouse model using pAAV/1.2HBV-A with a T2308C point mutation in the polymerase START codon could last much longer than 20 weeks. Thanks to the T2308C [17] point mutation of the polymerase START codon and the resulting lack of virion progeny; such *in vivo* testing can be routinely performed in a BSL2 animal facility. Our model provides several advantages, including its accessibility, convenience, and affordability.

#### **Conflict of interest**

There is no conflict of interest.

#### **Acknowledgements**

This research was funded by the OP RDE Project entitled “Chemical biology for drugging undruggable targets” Chem-BioDrug. No. CZ.02.1.01/0.0/0.0/16\_019/0000729. The authors thank Dr. Carlos V. Melo for editing the manuscript.

#### **References**

1. Sunbul M. Hepatitis B virus genotypes: Global distribution and clinical importance. *World J Gastroenterol.* 2014;20(18):5427-5434.
2. World Health Organization. *Global Hepatitis Report, 2017.*; 2017.
3. Krajden M, McNabb G, Petric M. The laboratory diagnosis of hepatitis B virus. *Canadian Journal of Infectious Diseases and Medical Microbiology.* 2005;16(2):65-72.
4. Ha HL, Shin HJ, Feitelson MA, Yu DY. Oxidative stress and antioxidants in hepatic pathogenesis. *World J Gastroenterol.* 2010;16(48):6035-6043.

5. Liu L, Yang F. Application of modified mesenchymal stem cells transplantation in the treatment of liver injury. *Physiol Res.* 2021;70(3):327-343.
6. Farghali H, Kgalalelo Kemelo M, Wojnarová L, Kutinová Canová N. In vitro and in vivo experimental hepatotoxic models in liver research: applications to the assessment of potential hepatoprotective drugs. *Physiol Res.* 2016;65(Suppl 4):S417-S425.
7. Akbar SMF, Al Mahtab M, Aguilar JC, Yoshida O, Khan S, Penton E, Gerardo GN, Hiasa Y. The Safety and Efficacy of a Therapeutic Vaccine for Chronic Hepatitis B: A Follow-Up Study of Phase III Clinical Trial. *Vaccines (Basel).* 2022;10(1).
8. Leowattana W, Leowattana T. Chronic hepatitis B: New potential therapeutic drugs target. *World J Virol.* 2022;11(1):57.
9. Liu T, Sun Q, Gu J, Cen S, Zhang Q. Characterization of the tenofovir resistance-associated mutations in the hepatitis B virus isolates across genotypes A to D. *Antiviral Res.* 2022;203:105348.
10. Wieland SF. The Chimpanzee Model for Hepatitis B Virus Infection. *Cold Spring Harb Perspect Med.* 2015;5(6):a021469-a021469.
11. Summers J, Smolec JM, Snyder R. A virus similar to human hepatitis B virus associated with hepatitis and hepatoma in woodchucks. *Proc Natl Acad Sci U S A.* 1978;75(9):4533.
12. Mason WS, Seal G, Summers J. Virus of Pekin ducks with structural and biological relatedness to human hepatitis B virus. *J Virol.* 1980;36(3):829.
13. Marion PL, Oshiro LS, Regnery DC, Scullard GH, Robinson WS. A virus in Beechey ground squirrels that is related to hepatitis B virus of humans. *Proc Natl Acad Sci U S A.* 1980;77(5):2941.
14. Guidotti LG, Matzke B, Schaller H, Chisari F V. High-level hepatitis B virus replication in transgenic mice. *J Virol.* 1995;69(10):6158-6169.
15. Grompe M, Al-Dhalimy M, Finegold M, Ou CN, Burlingame T, Kennaway NG, Soriano P. Loss of fumarylacetoacetate hydrolase is responsible for the neonatal hepatic dysfunction phenotype of lethal albino mice. *Genes Dev.* 1993;7(12A):2298-2307.
16. Wu LL, Wang HY, Chen PJ. Hydrodynamic HBV Transfection Mouse Model. *Methods in Molecular Biology.* 2017;1540:227-235.
17. Yan Z, Zeng J, Yu Y, Xiang K, Hu H, Zhou X, Gu L, Wang L, Zhao J, Young JAT, Gao L. HBVcircle: A novel tool to investigate hepatitis B virus covalently closed circular DNA. *J Hepatol.* 2017;66(6):1149-1157.
18. Ortega-Prieto AM, Cherry C, Gunn H, Dorner M. In Vivo Model Systems for Hepatitis B Virus Research. *ACS Infect Dis.* 2019;5(5):688-702.
19. Milich DR, Leroux-Roels GG. Immunogenetics of the response to HBsAg vaccination. *Autoimmun Rev.* 2003;2(5):248-257.
20. Peng XH, Ren XN, Chen LX, Shi BS, Xu CH, Fang Z, Liu X, Chen JL, Zhang XN, Hu YW, Zhou XH. High persistence rate of hepatitis B virus in a hydrodynamic injection-based transfection model in C3H/HeN mice. *World J Gastroenterol.* 2015;21(12):3527-3536.

21. Santantonio T, Jung MC, Pastore G, Angarano G, Günther S, Will H. Familial clustering of HBV pre-C and pre-S mutants. *J Hepatol.* 1997;26(2):221-227.
22. Huang LR, Wu HL, Chen PJ, Chen DS. An immunocompetent mouse model for the tolerance of human chronic hepatitis B virus infection. *Proc Natl Acad Sci U S A.* 2006;103(47):17862-17867.
23. Wang D, Tai PWL, Gao G. Adeno-associated virus vector as a platform for gene therapy delivery. *Nat Rev Drug Discov.* 2019;18(5):358-378.
24. Guo X, Chen P, Hou X, Xu W, Wang D, Wang TY, Zhang L, Zheng G, Gao ZL, He CY, Zhou B, Chen ZY. The recombinant cccDNA produced using minicircle technology mimicked HBV genome in structure and function closely. *Scientific Reports* 2016 6:1. 2016;6(1):1-10.
25. Wang L, Cao M, Wei QL, Zhao ZH, Xiang Q, Wang HJ, Zhang HT, Lai GQ. A new model mimicking persistent HBV e antigen-negative infection using covalently closed circular DNA in immunocompetent mice. *PLoS One.* 2017;12(4):e0175992.
26. Chou HH, Chien WH, Wu LL, Cheng CH, Chung CH, Horng JH, Ni YH, Tseng HT, Wu D, Lu X, Wang HY, Chen PJ, Chen DS, Cheng CH, Chung CH, Performed XL, Wrote DSC. Age-related immune clearance of hepatitis B virus infection requires the establishment of gut microbiota. *PNAS.* 2015;112(7).
27. Li L, Li S, Zhou Y, Yang L, Zhou D, Yang Y, Lu M, Yang D, Song J. The dose of HBV genome contained plasmid has a great impact on HBV persistence in hydrodynamic injection mouse model. *Viral J.* 2017;14(1):1-12.
28. Suda T, Liu D. Hydrodynamic Delivery. *Adv Genet.* 2015;89:89-111.
29. Sun Y, Qi Y, Peng B, Li W. NTCF-Reconstituted In Vitro HBV Infection System. *Methods in Molecular Biology.* 2017;1540:1-14.
30. Du Y, Broering R, Li X, Zhang X, Liu J, Yang D, Lu M. In Vivo Mouse Models for Hepatitis B Virus Infection and Their Application. *Front Immunol.* 2021;12:4578.
31. Řezáčová P, Pokorná J, Brynda J, Kožišek M, Cígler P, Lepšík M, Fanfrlík J, Řezáč J, Šašková KG, Siegllová I, Plešek J, Šícha V, Grüner B, Oberwinkler H, Sedláček J, Kräusslich HG, Hobza P, Král V, Konvalinka J. Design of HIV protease inhibitors based on inorganic polyhedral metallocarboranes. *J Med Chem.* 2009;52(22):7132-7141.
32. Kao JH. Diagnosis of hepatitis B virus infection through serological and virological markers. <http://dx.doi.org/10.1586/1747412424553>. 2014;2(4):553-562.
33. Kramvis A. Genotypes and genetic variability of hepatitis B virus. *Intervirology.* 2014;57(3-4):141-150.
34. Sengupta S, Rehman S, Durgapal H, Acharya SK, Panda SK. Role of surface promoter mutations in hepatitis B surface antigen production and secretion in occult hepatitis B virus infection. *J Med Virol.* 2007;79(3):220-228.
35. Zhou T, Guo H, Guo JT, Cuconati A, Mehta A, Block TM. Hepatitis B virus e antigen production is dependent upon covalently closed circular (ccc) DNA in HepAD38 cell cultures and may serve as a cccDNA surrogate in antiviral screening assays. *Antiviral Res.* 2006;72(2):116-124.

36. Levrero M, Pollicino T, Petersen J, Belloni L, Raimondo G, Dandri M. Control of cccDNA function in hepatitis B virus infection. *J Hepatol.* 2009;51(3):581-592.
37. The World Health Organisation. *Guidelines on Hepatitis B and C Testing.* Vol 66.; 2017.

Figures:

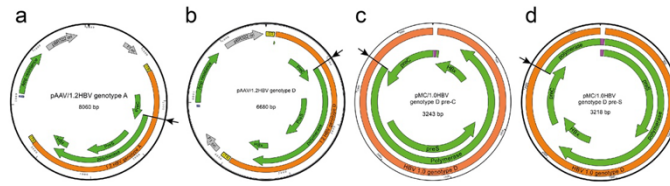


**Fig.1: Plasmid maps:** pAAV/1.2HBV-A (a) and D (b), pMC/1.0HBV-D-pre-C (c) and pre-S (d); mutation T2308C [17] eliminating the START codon of the HBV polymerase pointed as an arrow; the orange represents the HBV sequence; green represents open reading frames encoding the polymerase, HBx = HBV X protein, pre-C region encoding HBeAg and HBcAg, pre-S domain encoding 3 forms of HBsAg; grey represents the bacterial origin of replication; yellow represents inverted terminal repeats from AAV2 virus; blue represents promoter, and purple represents the ATT recombination site (resulting from a minicircle preparation from the parental plasmid [17]).



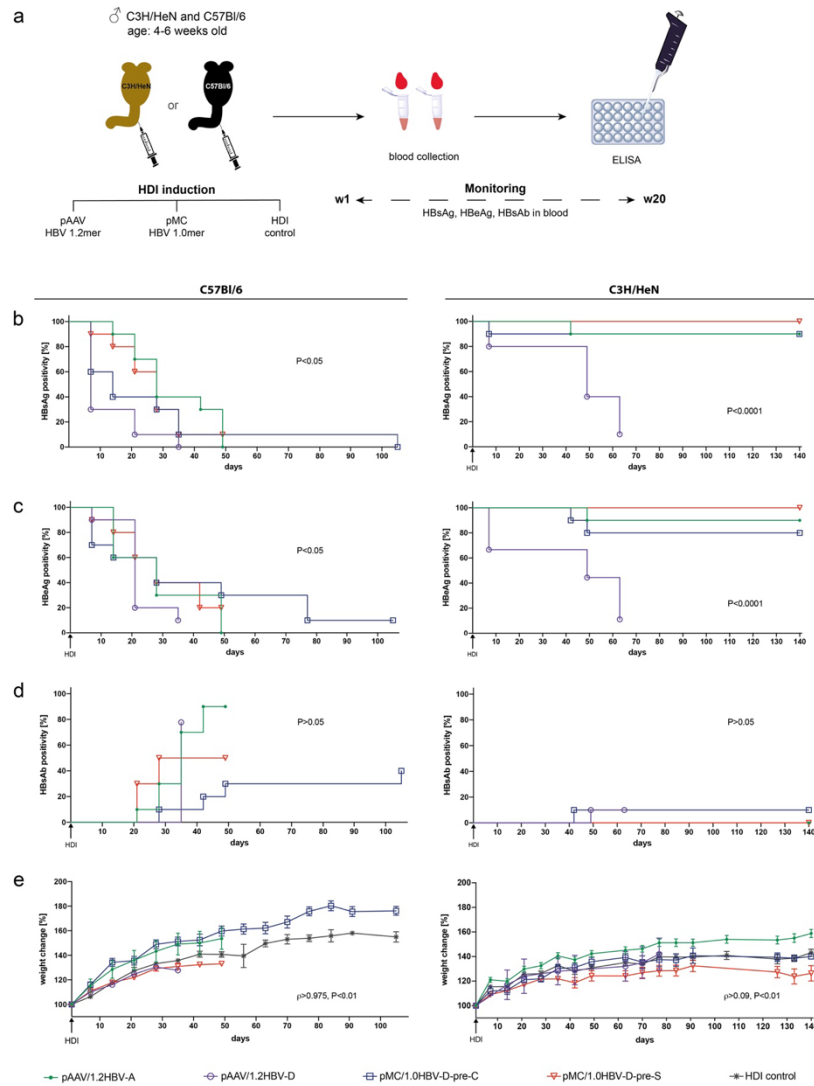


**Fig.2: CHB in vivo model establishment and characterisation in C57Bl/6 and C3H/HeN mice:** (a) scheme of the experiment and continuous monitoring of HBsAg (b), HBeAg (c) and HBsAb (d) blood levels; the positivity proportions of all induction systems (pAAV/1.2HBV-A and D, pMC/1.0HBV-D-pre-C and pre-S) are shown as Kaplan-Meier curves and compared using the Log-rank test. (b, c, d) n=5-20 mice/group. (e) Weight as stratified by induction system groups for both mouse strains, data were analysed using Spearman correlation test,  $\rho$  expressing Spearman's rank correlation coefficient. Data expressed as mean value per group  $\pm$  SEM. n=5-20 mice/group.

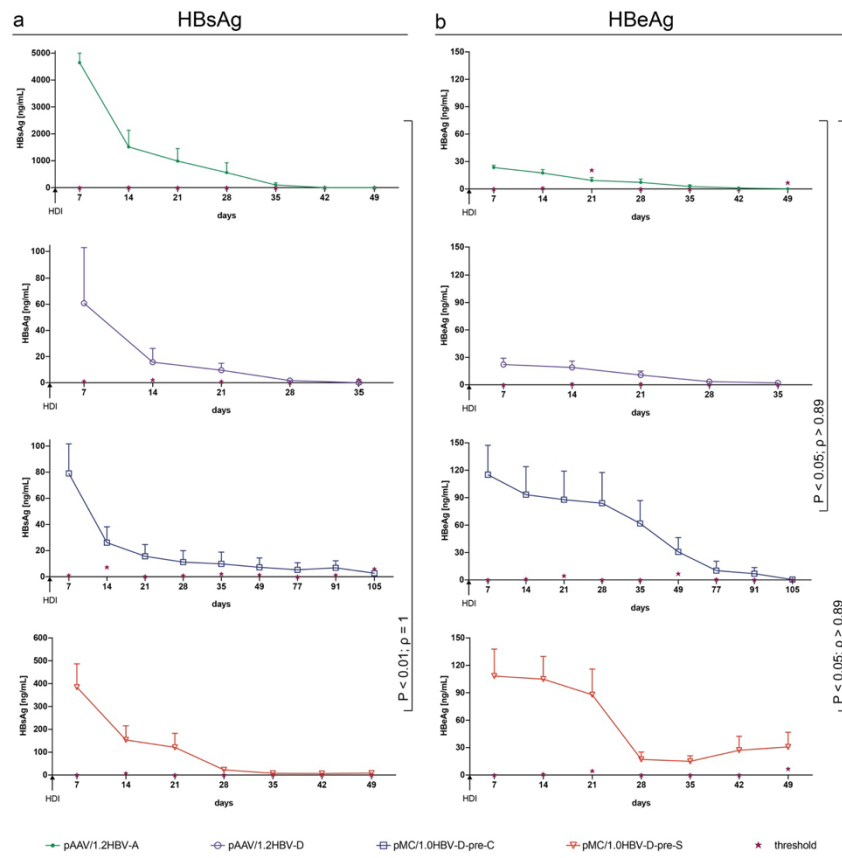


**Fig.3: HBV marker levels in CB7Bl/6 mice:** HBsAg (a) and HBeAg (b) were monitored in animals hydrodynamically injected with plasmid constructs. Data were compared using the Spearman correlation test; unless otherwise stated,  $P > 0.05$ ,  $\rho$  expressing Spearman's rank correlation coefficient. Data were expressed as mean  $\pm$  SEM per group. (a, b)  $n = 5-20$  mice/group

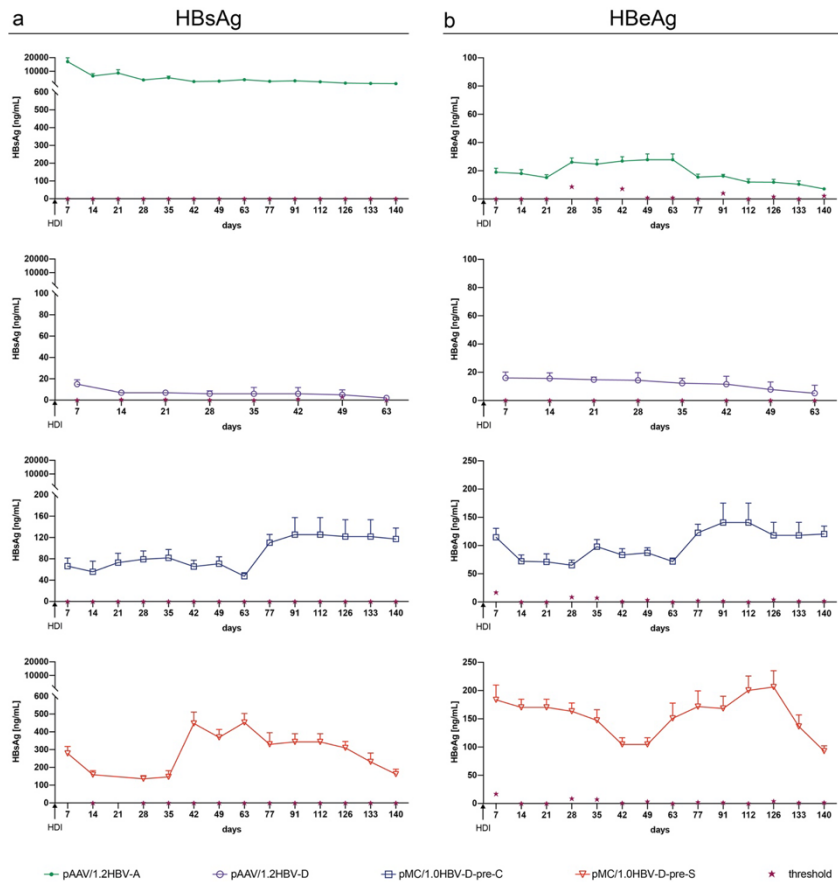


**Fig.4: HBV marker levels in C3H/HeN mice:** HBsAg (a) and HBeAg (b) were monitored in animals hydrodynamically injected with plasmids. Data were compared using the Spearman correlation test (all data were nonsignificant (ns) =  $P > 0.05$ ). Data were expressed as mean  $\pm$  SEM per group. (a, b)  $n=5-20$  mice/group

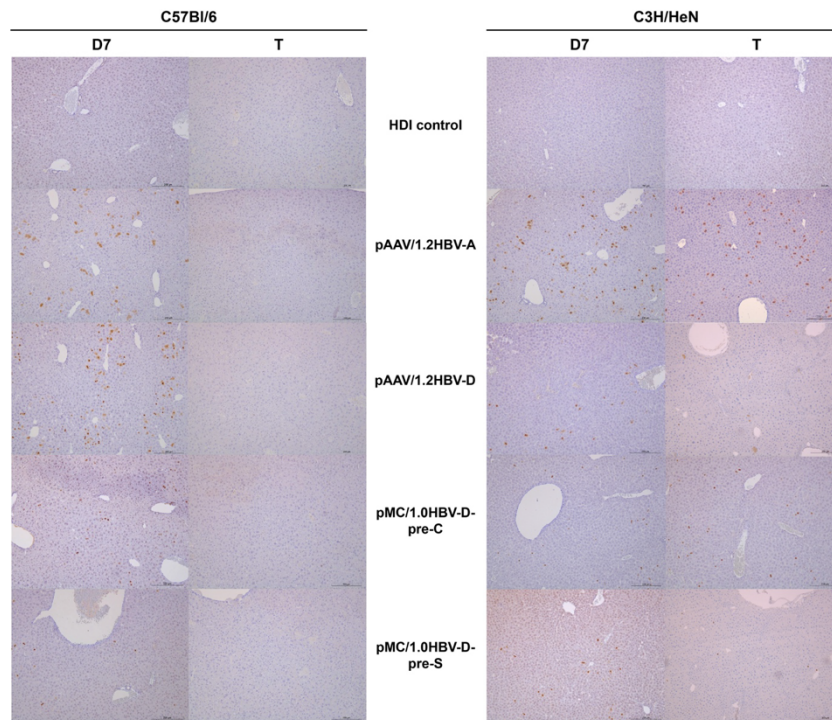


**Fig.5: HBcAg expression in liver sections of C57Bl/6 and C3H/HeN mice detected by immunohistochemistry:** HBcAg detected on day 7 (D7) post HDI and at the terminal point of the experiment (T; C57Bl/6: D35 pAAV/1.2HBV-D, D49 pAAV/1.2HBV-A and pMC/1.0HBV-D-pre-S, D105 pMC/1.0HBV-D-pre-C; C3H/HeN: D62 pAAV/1.2HBV-D, D140 pAAV/1.2HBV-A, pMC/1.0HBV-D-pre-C and pMC/1.0HBV-D-pre-S); representative results of HBcAg (brown spots) per induction system group.

**8.5. Supplement S5: Multiparametric Flow Cytometry-based  
Immunophenotyping of Mouse Liver Immune Cells**





*Vanekova, L., Polidarova, M. P., Veverka, V., Birkus, G., & Brazdova, A. (2022). Multiparametric Flow Cytometry-Based Immunophenotyping of Mouse Liver Immune Cells. Methods and protocols, 5(5), 70. <https://doi.org/10.3390/mps5050070>*

My contribution:

Methodology development and validation, data analysis, manuscript preparation.

Protocol

# Multiparametric Flow Cytometry-Based Immunophenotyping of Mouse Liver Immune Cells

Lenka Vanekova <sup>1,2</sup> , Marketa Pimkova Polidarova <sup>1</sup> , Vaclav Veverka <sup>1,2</sup> , Gabriel Birkus <sup>1</sup> and Andrea Brazdova <sup>1,\*</sup> 

<sup>1</sup> Institute of Organic Chemistry and Biochemistry of the Czech Academy of Sciences, Flemingovo namesti 542/2, 160 00 Prague, Czech Republic

<sup>2</sup> Department of Cell Biology, Faculty of Science, Charles University, Vinicna 7, 128 00 Prague, Czech Republic

\* Correspondence: andrea.brazdova@uochb.cas.cz; Tel.: +420-220-183-173

**Abstract:** The liver is a complex organ that governs many types of metabolisms, including energy metabolism and other cellular processes. The liver also plays a crucial role in important functions in immunity, and the activity of liver tissue-associated immunity affects the outcome of many liver pathologies. A thorough characterization of the liver immune microenvironment may contribute to a better understanding of immune signaling, the mechanisms of specific immune responses, and even to improved predictions about therapy outcomes. In this paper, we present an optimized, simple, and rapid protocol to characterize the liver-associated immune cell milieu. We believe that the most suitable technique for obtaining a complex immune cell suspension and for removing contaminating blood cells is to perform mouse liver perfusion, using only phosphate buffer saline. Combining an enzymatic digestion and a mechanical dissociation of liver tissue, followed by cell purification, improves downstream applications. This combination is an essential prerequisite for immune cell determination and characterization. We then demonstrate a flow cytometry-based multiparametric immunophenotyping along with a gating strategy to detect and quantify liver endothelial cells, T cells (helper and cytotoxic), B cells, NK cells, NKT cells, neutrophils, monocytes (subsets included), dendritic cells (subsets included), macrophages and Kupffer cells.

**Keywords:** flow cytometry; immunophenotyping; mouse liver; PBS-based liver perfusion; non-parenchymal cells



**Citation:** Vanekova, L.; Pimkova Polidarova, M.; Veverka, V.; Birkus, G.; Brazdova, A. Multiparametric Flow Cytometry-Based Immunophenotyping of Mouse Liver Immune Cells. *Methods Protoc.* **2022**, *5*, 70. <https://doi.org/10.3390/mps5050070>

Academic Editor: Derek Davies

Received: 4 August 2022

Accepted: 1 September 2022

Published: 3 September 2022

**Publisher's Note:** MDPI stays neutral with regard to jurisdictional claims in published maps and institutional affiliations.



**Copyright:** © 2022 by the authors. Licensee MDPI, Basel, Switzerland. This article is an open access article distributed under the terms and conditions of the Creative Commons Attribution (CC BY) license (<https://creativecommons.org/licenses/by/4.0/>).

## 1. Introduction

The liver is a complex organ, consisting of multiple cell types. The majority of them, 60–80%, are the parenchymal cells—hepatocytes. The remaining cells form a heterogeneous population of non-parenchymal cells (NPC), primarily composed of liver endothelial cells (LEC), hepatic stellate cells (HSC) and immune cells [1–3]. Intrahepatic immune cells are the most prominent component (up to 50%) of NPC [4], consisting of T cells (both cluster of differentiation (CD) 8+ and CD4+), B cells, natural killer (NK) and natural killer T (NKT) cells, neutrophils, monocytes and various subtypes of dendritic cells (DCs) and macrophages [2,3,5]. The relative composition of the liver immune cells varies depending on the physiologic conditions and species, e.g., the NKT cells are more abundant in the liver of mice than humans [2]. Liver immune cell composition differs from lymphoid organs or blood, as the liver is enriched with CD4+ T cells, NK, NKT and gamma delta ( $\gamma\delta$ ) T cells [2,6]. In general, liver is mostly tolerogenic organ, which is important to prevent inflammatory responses to diet and intestinal microflora [7]. As such, NPC actively contribute to the immune tolerance [7], e.g., hepatocytes, Kupffer cells (KC) and LEC induce anergy of T cells [8,9]. In addition, sinusoidal LEC (LSEC) produce lectin called LSECtin that triggers CD8+ T cell tolerance [10]. Moreover, KC secrete the anti-inflammatory cytokine interleukin 10 (IL10) [11], and the liver-resident NK cells can suppress T cells via interaction with immune check-point pathways [12]. Under certain pathological conditions

such as infection, an inflammatory disorder, or cancer, the liver immune cell distribution or function may change. This can lead to a potential imbalance and alteration of immune cell crosstalk [1,2,5,13,14]. To better understand various pathologies affecting the liver, the resident/infiltrating immune populations need to be isolated, immunophenotyped and quantified. The goal is to obtain a single cell suspension of high yield, while still preserving antigen/epitope profiles (minimum epitope degradation) and retaining cell viability for subsequent downstream applications [4,15–21]. In order to avoid cross-contamination of the liver residing in immune subsets from those found in the blood, the *in situ* perfusion of the liver is performed via the vena cava or the portal vein [22]. The next crucial step is the proper processing of the liver tissue. The tissue dissociation can be performed either by a mechanical disruption, by an enzymatic digestion using a collagenase, or a combination of both approaches [21–23]. For liver immune cell phenotyping, the hepatocytes need to be removed from the obtained homogenate, as they may interfere with later downstream immune profiling [18,19]. The cell suspension can be further purified, either by multiple centrifugation steps [3,18] or by purification through a Percoll or Iodixanol density gradient [4,18–21,23]. However, this procedure is time and material consuming. In addition, the harsh conditions of the purification methods may also affect the viability and/or function of cells intended for any downstream application. After the isolation of NPC, the cells can be further analyzed and/or cultivated. Although several studies have focused on the characterization of a single or a few populations, such as macrophages [24], KC [18,19], LEC [17,18,22] or NK cells [16], we and others [21,25] aim to analyze multiple immune populations. Several immunophenotyping methods are available. Conventional or spectral flow cytometry is often used for various immunophenotyping [26,27]. Different approaches are cytometry by time-of-flight (CyTOF), in which mass spectrometry analysis of single cells labeled with isotope-conjugated markers is used [15], or automated parallel RNA single-cell sequencing combining fluorescence-activated cell sorting techniques [28] and massive multiplexing RNA sequencing [29]. Although CyTOF and an automated massively parallel single-cell RNA sequencing approach allow analysis of more than 20 colors in one panel, the costs and instrumental setup, both make it rarely available in regular academic laboratory conditions.

In the presented protocol, we describe a robust yet low-cost, fast, effective, practical, and straightforward procedure for the isolation of mouse liver NPC that relies on a mouse liver dissociation kit from Miltenyi Biotec [30]. Moreover, we present a thorough immunophenotyping protocol using conventional flow cytometry that allows for the detection and quantification of various immune populations in one single sample. To specifically analyze hepatic immune microenvironment avoiding red blood cell contamination, the procedure consists of liver perfusion with PBS, liver tissue dissociation by combining mechanical disruption and enzymatic digestion, followed by the purification of cells and immunophenotyping. We address a multiparametric flow cytometry analysis, valuable for both regular and large-scale screenings, including a gating strategy to detect and quantify LEC, T cells (helper and cytotoxic), B cells, NK cells, NKT cells, neutrophils, monocytes (reparative and inflammatory), DCs (including their subsets), macrophages and KC. The method can be useful in research focusing on the characterization of the liver immune milieu in mouse models of human pathologies, or in studies of the liver immune response to different treatments. This method could also be valuable for regular small as well as large-scale screenings, e.g., a preclinical evaluation of drug efficacy.

## 2. Experimental Design

### 2.1. Materials

1. Debris removal solution (Miltenyi Biotec, Bergisch Gladbach, Germany; Cat. no.: 130-109-398; store protected from light at 4 °C, do not freeze)
2. DMEM High Glucose w/stable glutamine, w/sodium pyruvate (Biowest, Riverside, MO, USA; Cat. no.: L0103-500; store protected from light at 4 °C, do not freeze)

3. Aerrane (Isoflurane UPC, Baxter, Deerfield, IL, USA; Cat. no.: FDG9623; store protected from light at room temperature (RT))
4. Liver dissociation kit, mouse (Miltenyi Biotec, Bergisch Gladbach, Germany; Cat. no.: 130-105-807; individual components store at 4 °C, reconstituted components store for max. 6 months at −20 °C, avoid freeze/thaw cycles)
5. Phosphate buffered saline w/o calcium, w/o magnesium (Biowest, Riverside, MO, USA; Cat. no.: P0750; store at 4 °C)
6. Red blood cell lysis buffer (RBL; store at RT; see Reagent Setup)
7. Trypan blue solution (Sigma-Aldrich, Burlington, MA, USA; Cat. no.: T8154, store at RT)
8. Fixation buffer (BD Biosciences, Franklin Lakes, NJ, USA; Cat. no.: 554655, store protected from light at 4 °C, do not freeze), optional reagent
9. Flow cytometry (FC) staining buffer (store for max. 1 month at 4 °C, do not freeze; see Reagent Setup)
10. Fluorescently labeled antibodies for FC purposes (see Table 1; store protected from light at 4 °C)

## 2.2. Equipment

- 25 mL tissue sample vessel (Carl Roth, Karlsruhe, Germany; Cat. no.: AYX2.1)
- Blunt dissecting scissors (VWR<sup>®</sup>, Radnor, PA, USA; Cat. no.: HAMMHSB120-14)
- Cotton pads (Batist Medical a.s., Cerveny Kostelec, Czech Republic; Cat. no.: 5670)
- Dry bath incubator (Major Science, Saratoga, CA, USA; Cat. no.: MD-02N)
- 15 mL conical centrifuge tubes (VWR<sup>®</sup>, Radnor, PA, USA; Cat. no.: 525-1084)
- 1.5 mL microcentrifuge tubes (VWR<sup>®</sup>, Radnor, PA, USA; Cat. no.: 89000-028)
- Forceps with round blade (VWR<sup>®</sup>, Radnor, PA, USA; Cat. no.: 232-0106)
- Forceps with straight blade (VWR<sup>®</sup>, Radnor, PA, USA; Cat. no.: BSNC00DSA)
- gentleMACS C-tube (Miltenyi Biotec, Bergisch Gladbach, Germany; Cat. no.: 130-093-237)
- gentleMACS Octo dissociator with heaters (Miltenyi Biotec, Bergisch Gladbach, Germany; Cat. no.: 130-096-427)
- Ismatec IPC pump (Ismatec, Wertheim, Germany; Cat. no.: ISM 930)
- Luna-II automated cell counter (Logos Biosystems, Anyang-si, Gyeonggi-do, Korea; Cat. no.: L40002)
- Cell counting slides (Logos Biosystems, Anyang-si, Gyeonggi-do, Korea; Cat. no.: L12003)
- MACS SmartStrainer, 100 µm (Miltenyi Biotec, Bergisch Gladbach, Germany; Cat. no.: 130-098-463)
- Neo Delta Ven T cannula 24G (Delta Med, Viadana, Lombardia, Italy; Cat. no.: 3113122)
- R540 Enhanced Anesthesia Machine (RWD, Baltimore, MD, USA; Cat. no.: R540IE)
- Refrigerated centrifuge with swinging buckets (ThermoFisher Scientific, Waltham, MA, USA; Cat. no.: 15253457)
- Sharp scissors (VWR<sup>®</sup>, Radnor, PA, USA; Cat. no.: 233-1104)
- Extension tubes (Gama group, Ceske Budejovice, Czech Republic; Cat. no.: 606301-ND)
- Pump tubing (Tygon<sup>®</sup>, Ismatec, Wertheim, Germany; Cat. no.: ISMCSC0024T, ISMCSC0048T)
- Tweezers (VWR<sup>®</sup>, Radnor, PA, USA; Cat. no.: 229-0374)
- Water bath (Polysciences, Warrington, PA, USA; Cat. no.: WBE20A12E)
- BD LSRFortessa flow cytometer (BD Biosciences, Franklin Lakes, NJ, USA) or any multiparametric flow cytometer with at least 13-fluorescence detectors)

## 2.3. Software

- Diva software (Becton Dickinson, Franklin Lakes, NJ, USA, v8.0.1. or later, BD FACS-Diva™ Software [www.bdbiosciences.com](http://www.bdbiosciences.com), accessed on 4 August 2022) or any equivalent
- FlowJo analysis software (BD Biosciences, Franklin Lakes, NJ, USA, v10 or later, [www.bdbiosciences.com](http://www.bdbiosciences.com), accessed on 4 August 2022) or any equivalent





**Table 1.** Materials for immunophenotyping.

Cell Staining (cat. no.)	Clone	Dilution	Isotype Controls (cat. no.)	Manufacturer	Staining Buffer	FC Compensations	
rat anti-mouse CD3 BV605 (564009)	17A2	1/100	BV605 Rat IgG2b, $\kappa$ (563145)	BD Biosciences	FC		
rat anti-mouse CD4 BV421(562891)	GK1.5	1/50	BV421 Rat IgG2b, $\kappa$ (562603)	BD Biosciences	FC		
rat anti-mouse CD8 BV510 (563068)	53-6.8	1/50	BV510 Rat IgG2a, $\kappa$ (562952)	BD Biosciences	FC		
rat anti-mouse CD11b APC-R700 (564985)	M1/71	1/100	APC-R700 Rat IgG2b, $\kappa$ (564984)	BD Biosciences	FC		
hamster anti-mouse CD11c PE-CF594 (565591)	N418	1/50	PE-CF594 Hamster IgG2, $\lambda$ 1	BD Biosciences	FC	CompBead Anti-Rat and Anti-Hamster Ig $\kappa$ /Negative Control Compensation Particles Set (552845)	
rat anti-mouse CD19 BUV395 (563557)	1D3	1/100	BUV395 Rat IgG2a, $\kappa$ (563556)	BD Biosciences	FC		
rat anti-mouse Ly-6C PE (560592)	AL-22	1/50	PE Rat IgM, $\kappa$ (553943)	BD Biosciences	FC		
rat anti-mouse Ly-6G APC (560599)	1A8	1/50	APC Rat IgG2a $\kappa$ (553932)	BD Biosciences	FC		
rat anti-mouse CD45 PerCP (561047)	30-F11	1/100	PerCP Rat IgG2b, $\kappa$ (552991)	BD Biosciences	FC		
rat anti-mouse CD49b FITC (553857)	DX5	1/100	FITC Rat IgM, $\kappa$ (553942)	BD Biosciences	FC		
rat anti-mouse CD31 BUV496 (741084)	390	1/100	BUV496 Rat IgG2a, $\kappa$ (564663)	BD Biosciences	FC		
rat anti-mouse F4/80 BV650 (743282)	T45-2342	1/50	BV650 Rat IgG2a, $\kappa$ (563236)	BD Biosciences	FC		
live/dead marker Zombie NIR (423106)	n/a *	1/200	n/a *	Biolegend	PBS		cells

NOTE: working concentrations of either FC antibodies or related isotype controls were identical. \* n/a: not applicable.

### 3. Procedure

**Note:** In this protocol (Figures 1–3), we perform a PBS-based perfusion via portal vein using C3H/HeN mice. However, the same method can be applied on any mouse strain. We process the mouse liver by combining a mechanical disruption and an enzymatic digestion. NPC are then purified based on a gradient centrifugation.

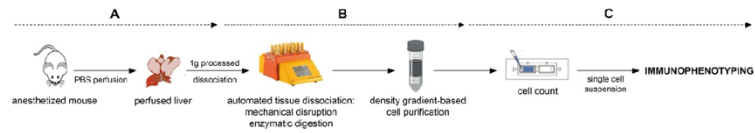


**Figure 1.** Workflow as a schematic description. (A) in vivo manipulation part. (B) liver processing. (C) downstream procedure.

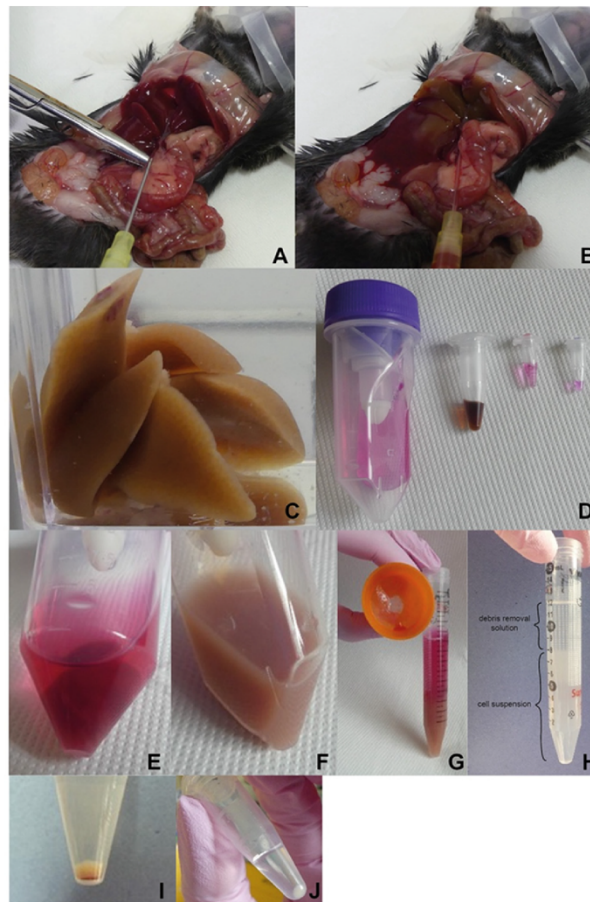


**Figure 2.** Illustrated work procedure. (A) Uncovered and stretched portal vein to perform perfusion.

(B) Gradual liver perfusion. (C) Perfused liver. (D) Material preparation for dissociation. C-tube with cell culture medium, dissolved particular components of the liver dissociation kit (all Miltenyi Biotec, described from the left). (E) Liver placed into C-tube with the dissociation mix. (F) Liver homogenate after dissociation. (G) Filtrate of dissociated tissue. (H) Density gradient-based cell purification (layer of debris removal solution on top of the cell suspension; before centrifugation). (I) Obtained cells contaminated with leftover of red blood cells. (J) Final NPC yield after the removal of red blood cells.

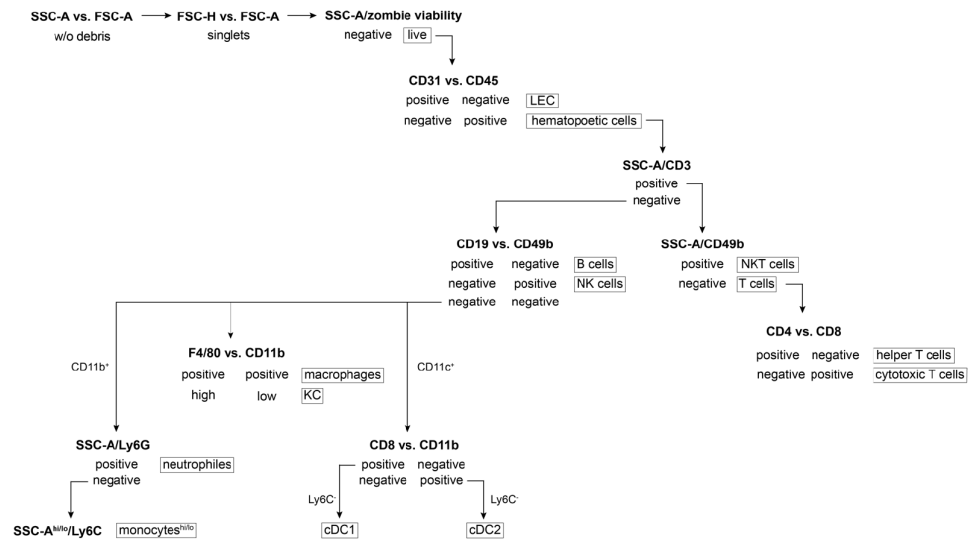


**Figure 3.** Schema of gating strategy for flow cytometry data acquisition. SSC-A: side scatter-area; FSC-A/H: forward scatter-area/height; hi/lo: high/low population.

### 3.1. Liver Perfusion

1. Set up of instruments: prime peristaltic pump with tempered PBS, set the flow rate to 2.5 mL/min.
2. Anesthetize a mouse using 2–5% isoflurane in air or oxygen mixture until the deep loss of sensitivity.
3. Place the fully anesthetized mouse to a supine position in a breathing mask, attach paws to the pad to stretch the mouse.
4. Disinfect the abdomen with 70% ethanol. Lift the skin with tweezers. Using blunt dissecting scissors, cut the skin and peritoneum horizontally in the lower abdomen. Continue with a lateral cut on both sides of the abdomen, up to the lower rib cage.
  - ▲ **CRITICAL STEP** Continuously observe breathing rate to be low and deep without any sign of choking. Be sure not to cut any of the organs or diaphragm.
5. Use forceps to grab the abdominal skin and peritoneum and roll the skin up to the rib cage to reveal the abdominal cavity. Move intestines to the side to expose the portal vein.
  - ▲ **CRITICAL STEP** For optimal procedure, no bleeding should occur.
6. Straighten the vein. Place the needle of the cannula in parallel to the portal vein with the bevel up (Figure 2A). Inject the lower part of the vein with the cannula needle, then pull out the needle from the cannula, and move the polymer part further into the

vein. A blood backflow should be visible. **Note:** It is not necessary to immobilize the cannula by a vein ligation.

7. Adjust the pump flow rate to 2.5 mL/min, ensure there are no bubbles in the tubing, place the tubing into the cannula, cut one kidney, and immobilize the tubing onto the pad.
  - ▲ **CRITICAL STEP** Observe an immediate liver color change as a proof of correct perfusion setting (Figure 2B).
8. Wash the liver with 30–40 mL of PBS until the liver completely lightens and no blood appears in the wash volume.
9. Remove the cannula and turn off the pump. Carefully remove the gallbladder and harvest the liver into 50 mL sample vial with PBS (Figure 2C).
10. **OPTIONAL STEP** Carefully remove the gallbladder to prevent bile contamination of the liver; if contaminated, thoroughly wash the liver with PBS.

### 3.2. Liver Dissociation

**Note:** The protocol below does not differ from the manufacturer's instructions (liver dissociation kit from Miltenyi Biotec [30]).

1. Cut off 1 g of liver tissue (weight should not exceed 1.2 g of tissue per one dissociation [30]).
2. Wash the liver with preheated cell medium and place it into C-tube with liver dissociation mix (according to the manufacturer's instruction). After attaching C-tube onto the dissociator with heater, launch a 37C\_m\_LIDK\_1 program predefined by the manufacturer (Figure 2D,E).
  - ▲ **CRITICAL STEP** Aliquoted components should be thawed right before use, repeated freeze-thaw cycles should be strictly avoided.
3. Detach C-tube from the dissociator when the program terminates. Gently resuspend obtained liver homogenate and filter it through a pre-wetted 100 µm cell strainer into a 15 mL falcon tube. To avoid loss of cells within the C-tube, wash the tube and strainer with 5 mL of cell culture medium (Figure 2F,G).
4. Centrifuge the homogenate sample for 10 min at 300× g, RT. Discard supernatant and resuspend the pellet in PBS (RT).

### 3.3. Liver Homogenate Processing to Prepare Single Cell Suspension

5. Centrifuge the obtained cell suspension for 10 min at 300× g, 4 °C and discard the supernatant.
6. Resuspend the pellet in pre-cooled PBS, add the debris removal solution and overlay gently with the pre-cooled PBS (according to the manufacturer's instruction).
  - ▲ **CRITICAL STEP** Observe phase formation to control the step (Figure 2H).
7. Centrifuge for 10 min at 3000× g, 4 °C.
  - ▲ **CRITICAL STEP** Reduce the centrifugation break as well as acceleration rate (level 4 out of 9 applied on centrifuge used in this protocol), 3 phases have to be well defined.
8. Aspirate the two upper phases and add up to 15 mL of pre-cooled PBS, mix the suspension by gentle inverting the tubes.
9. Centrifuge for 10 min at 1000× g, 4 °C and discard the supernatant (Figure 2I).
10. Resuspend pellet in 1 mL of RBL to remove remaining red blood cells and incubate for 5 min at RT.
11. Fill the tube with PBS, mix the suspension by gentle inverting the tube.
12. Centrifuge for 5 min at 500× g, RT and discard the supernatant (Figure 2J).
13. **OPTIONAL STEP** Repeat the steps C.10–C.12 if pelleted cells are still contaminated with red blood cells, eventually platelets.
14. Resuspend the pellet in at least 1 mL of PBS to count the cells.

15. Use any cell counter to determine cell concentration, viability on the basis of Trypan blue exclusion, size distribution and clustering.
16. **OPTIONAL STEP** Using the LUNA cell counter, follow the steps below (17–19).
17. Prepare a 1:1 mixture of cells and Trypan blue (10  $\mu$ L + 10  $\mu$ L) to determine the cell count (concentration), viability, distribution, and clustering. Apply 10  $\mu$ L of the mixture into a cell counting slide chamber, wait until the equilibrium is established.
18. Set the counting protocol to the following settings: dilution factor 2, min. cell size 3  $\mu$ m, max. cell size 30  $\mu$ m, size gating 3–30  $\mu$ m, live cell sensitivity 7, roundness 60%, declustering level medium.
19. Apply the loaded protocol on a sample, verify the autofocus and count the cells, verify the gating strategy of the program (Figure 4).

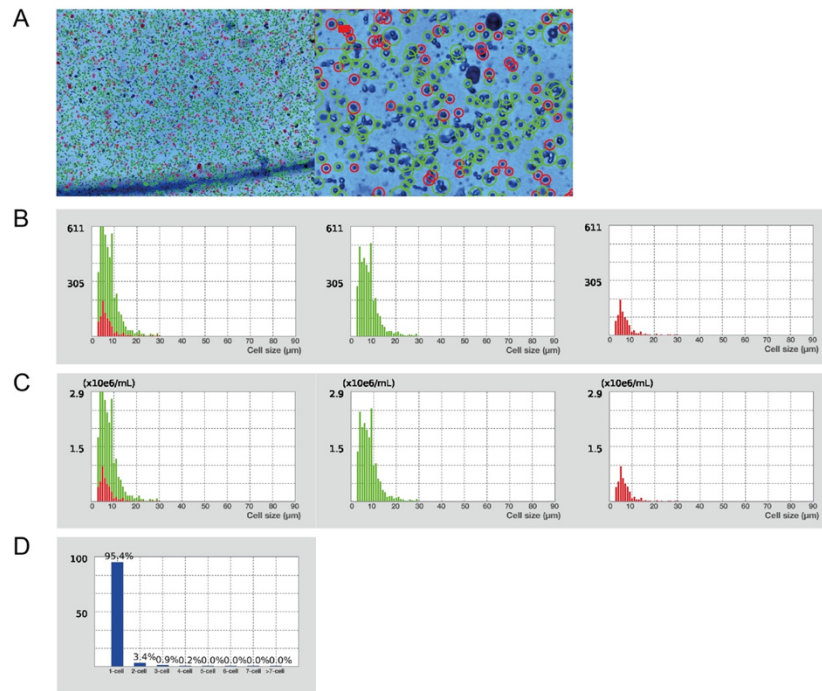


**Figure 4.** Characteristics of the obtained single cell suspension. (A) Evaluation of cell viability and total cell concentration (Trypan Blue stain, 1 $\times$  and 4 $\times$  magnification in Luna cell counter). Green circles represent live cells (82%); red circles dead cells (18%). Total yield of  $2.2 \times 10^7$  live cells/mL from 1 g of liver tissue. (B) Cell size distribution by cell number. Green histograms represent live cells; red histograms represent dead cells. (C) Cell size distribution by cell concentration. Green histograms—live cells; red histograms—dead cells. (D) Cell cluster map.

### 3.4. FC Based Immunophenotyping

**Note:** Type of samples: immunophenotyping samples, unstained control, antibody isotype controls, fluorescence minus one (FMO) controls, positive control for live/dead marker (dead cells), single stained controls for compensation matrix (set up using compensation beads).

1. Centrifuge the obtained cell suspension for 10 min at  $300\times g$ ,  $4\text{ }^{\circ}\text{C}$  and discard the supernatant. Wash with an excessive volume of PBS and centrifuge for 5 min at  $500\times g$ , RT. Discard the supernatant.
2. Resuspend cells in 40  $\mu\text{L}$  of PBS.
3. To distinguish live and dead cells, add the live/dead Zombie NIR marker at a pre-determined dilution (Table 1) and incubate for 20 min at RT, avoid light. **Note:** Any other viability dye can be used. The used Zombie viability kit is a fixable (paraformaldehyde or methanol), an amine-reactive fluorescent dye that is non-permeant to live cells.
4. In parallel, prepare a positive control of dead cells by boiling  $0.3\text{--}0.5\times 10^6$  cells in 40  $\mu\text{L}$  PBS for 5 min at  $65\text{ }^{\circ}\text{C}$ , cool the sample down to RT, perform staining as in D.3 step. This sample is also used as a single stain control to create a compensation matrix.
5. Wash the cells by adding 150  $\mu\text{L}$  of PBS (RT) and centrifuge for 5 min at  $500\times g$ , RT. Discard the supernatant.
6. Perform specific staining by resuspending the pellets in 40  $\mu\text{L}$  of FC staining buffer (see Reagent Setup), incubate with the staining antibody mixture or relevant isotype controls at a pre-determined concentration (Table 1) for 30 min at  $4\text{ }^{\circ}\text{C}$ , avoid light.
7. Wash the cells by adding 150  $\mu\text{L}$  of FC buffer and centrifuge for 5 min at  $500\times g$ , RT, discard the supernatant.
8. **OPTIONAL STEP** Fix the cells by resuspending the pellets in 80  $\mu\text{L}$  of Fixation buffer, incubate for 15–45 min at RT, avoid light; wash the cells by adding 150  $\mu\text{L}$  of FC buffer and centrifuge for 5 min at  $500\times g$ , RT, discard the supernatant.
9. Resuspend the cells in 250  $\mu\text{L}$  of FC buffer and transfer cell suspension into a FC tube through its cell strainer snap cap. Samples without the fixation step are intended for immediate analysis; however, fixed samples can be stored at  $4\text{ }^{\circ}\text{C}$  for up to one week and then assayed.
10. For a compensation matrix set up, prepare single stained samples using a drop of both types of compensation beads (anti-rat/hamster and negative particle set, Table 1) into 30  $\mu\text{L}$  of FC buffer (1 drop is approximately of 50  $\mu\text{L}$  equivalent). Perform staining directly in FC tubes to minimize potential losses.
11. Add the specific staining antibody in the same dilution as for the immunophenotyping (count sample volume as a composition: 50  $\mu\text{L}$  drop of specific + 50  $\mu\text{L}$  negative beads + 30  $\mu\text{L}$  of FC buffer), incubate under the same conditions as in step 6.
12. Wash the beads by adding 2 mL of FC buffer and centrifuge for 10 min at  $200\times g$ , RT, discard the supernatant.
13. Resuspend the pelleted beads in 250  $\mu\text{L}$  of FC buffer, vortex thoroughly.
14. Launch a calibration procedure at the flow cytometer, create the compensation matrix using the unstained and single stained samples, and calculate the compensations.
15. **OPTIONAL STEP** If required, define the acquisition mode in terms of cells or beads used for the compensation set up depending on the flow cytometer available.
16. Formulate the gating strategy (Figure 3) to monitor cell subsets of interest, respect subset hierarchy and marker exclusivity.
17. Run samples for the immunophenotyping purposes by gating on a rare population (either KC or neutrophils).
18. Acquire and record data by collecting at least 10,000 events of the population of interest.
19. **OPTIONAL STEP** If necessary, record the same sample several times by gating on various immune populations to then easily define and characterize any population.
20. Export fsc files to evaluate the data in FlowJo software or any equivalent.

### 3.5. Data Analysis

1. Start the gating strategy first by the debris exclusion, looking at forward and side scatter, followed by a doublet and dead cell exclusion.

2. Gate the particular immune population by exclusion of non-desired cells and the selection of those specific cells (Table 2, Figures 3 and 5). **Note:** Zombie viability dye is permeant only to cells with compromised membranes, therefore a negative population needs to be gated as live subset.
3. **OPTIONAL STEP** To quantify individual populations and their subsets, export the frequency of various subsets as a percentage in either the live cells or the parent population regarding the data representation.

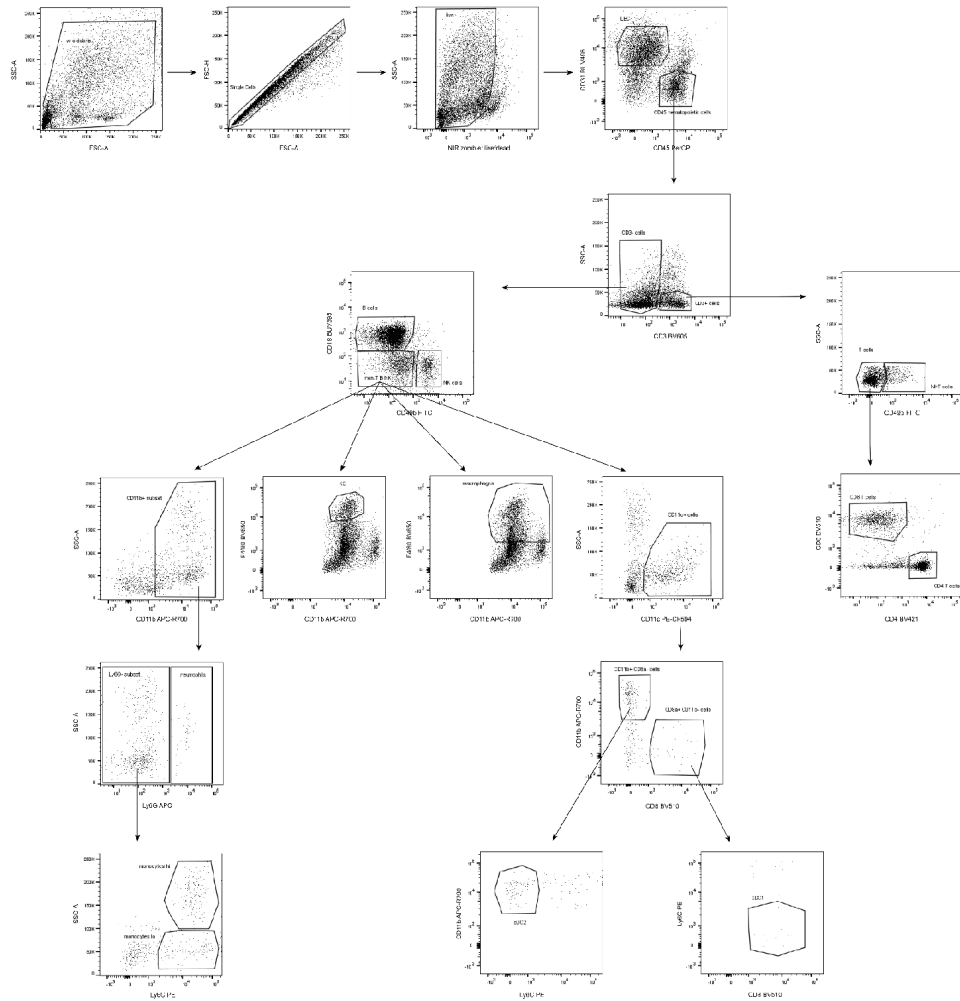


Figure 5. Illustration of gating strategy for individual immune populations. (Shown images represent a composition of three independent measurements).



**Table 2.** Phenotypes of particular immune populations.

Immune Population	Immunophenotype
liver endothelial cells	CD31+ CD45–
hematopoietic cells (leukocytes)	CD31– CD45+
T cells	CD31– CD45+ CD3+ CD49b–
helper T cells	CD31– CD45+ CD3+ CD49b– CD4+ CD8–
cytotoxic T cells	CD31– CD45+ CD3+ CD49b– CD4– CD8+
B cells	CD31– CD45+ CD3– CD49b– CD19+
NK cells	CD31– CD45+ CD3– CD49b+
NKT cells	CD31– CD45+ CD3+ CD49b+
neutrophils	CD31– CD45+ CD3– CD19– CD49b– CD11b+ Ly6G+
reparative monocytes	CD31– CD45+ CD3– CD19– CD49b– CD11b+ Ly6G– Ly6C <sup>lo</sup>
inflammatory monocytes	CD31– CD45+ CD3– CD19– CD49b– CD11b+ Ly6G– Ly6C <sup>hi</sup>
CD8 cDC1	CD31– CD45+ CD3– CD19– CD49b– CD11c+ CD8+ CD11b– Ly6C–
CD11b cDC2	CD31– CD45+ CD3– CD19– CD49b– CD11c+ CD8– CD11b+ Ly6C–
KC	CD31– CD45+ CD3– CD19– CD49b– CD11blo F4/80hi
macrophages	CD31– CD45+ CD3– CD19– CD49b– CD11b+ F4/80+

#### 4. Expected Results and Discussion

The key to a successful isolation and characterization of liver immune cells is an effective PBS-based liver perfusion. The perfusion via the liver portal vein can be technically challenging, considering the relative size of the vein (internal radius about 0.12 cm [31]). Here, the critical step is the selection of the correct size and length of the cannula. In this protocol, we recommend using a 24G cannula without wings and a safety lock, 19 mm length and 0.74 mm external catheter to achieve a stable and continuous perfusion. The next important step is the portal vein stretching (e.g., with forceps as shown in Figure 2A), thanks to which the vein is more visible, accessible, and easily injectable. Then, during the perfusion, the PBS flow needs to be continuous to avoid blockage in terms of bumps around the vein, liver, pancreas, stomach, and no PBS leakage should occur. The sign of correct perfusion is an immediate and gradual color change of the liver from dark red, through brown and pinkish, to beige. Overall, the liver becomes blanched and slightly swollen. In the case of limited areas of re-coloring, the cannula should be slightly moved backwards and forwards, and/or the liver can be smoothly and gently rolled over with a wet cotton pad to free a potentially blocked PBS flow.

If the protease-based perfusion of the liver alters cell surface markers on immune cells [4], a thorough optimization process would be required, unlike the simple PBS-based technique used in this protocol. The PBS-based perfusion allows removing immune cells present in blood, and it is faster and technically not as challenging as the enzymatic perfusion [22]. In addition, the PBS-based perfusion is compatible with the immunohistopathology analysis. The detailed identification and potential quantification of specific subsets relies on one in time combination of a mechanical disruption and an enzymatic digestion of the liver tissue, optimized by Miltenyi Biotec [30]. In order to avoid incomplete tissue dissociation, it is important not to exceed the maximum weight of 1.2 g of a tissue per cell isolation. Inappropriate temperature settings or an incorrect order of individual protocol steps would provide potentially misleading data.

To obtain high quality flow cytometry data, it is also essential to remove cell debris and the remaining hepatocytes from samples, as this detritus can create an irrelevant background as well as interfering autofluorescence during the sample acquisition. For further FC staining of NPC, knowledge of the cell concentration and viability is mandatory. For this purpose, we have chosen the LUNA cell counter to simplify the workflow, to focus on reproducibility, and to determine the cluster map (Figure 4). The typical yield of NPC

from one 1 g of liver tissue has been more than  $20 \times 10^6$  cells, yet it may differ based on the mouse strain used and the age of the mouse [14,32,33]. This protocol is optimized to produce not only a high number of cells with viability more than 80% (Figure 4A), but also to obtain a single cell suspension (more than 95% of single cells, (Figure 4D)). Nevertheless, a slow and harsh workflow and/or inappropriate cell processing can rapidly decrease the viability of cells and may also negatively affect the FC data as antigen/epitope may degrade. Unlike Medina-Montano, et al. [34], we believe that combination of liver perfusion and mechanical disruption with enzymatic digestion is mandatory to obtain exclusively hepatic immune microenvironment thus avoiding blood specific immune cell contamination. Using a multiparametric flow cytometry-based phenotyping requires a precise compensation matrix due to the high spillover signals. To determine the undesirable autofluorescent character of tissue and to correctly quantify cells, an unstained sample is required. This issue can be overcome by using spectral flow cytometer as it measures full range of emission spectrum of each fluorochrome across all lasers [27] or CyTOF-based technique which uses unique isotope-conjugated markers without need of compensation [15]. However, different sets of controls such as single stain controls need to be used. Regarding the basic immunophenotype determination as well as the particular quantification, it is crucial to define a proper gating and a non-specific antibody binding, thanks to the FMO and antibody isotype controls. The so-called isoclonic antibody control could be an alternative to the antibody isotype controls, as it is based on the staining with the excess of an identical, yet unlabeled antibody related to the specific immune marker. However, we present the use of a relevant isotype control.

The gating strategy for the presented multicolor FC panel (Figures 3 and 5) is based on the gradual elimination of unwanted populations and further identification of targeted subsets. The additional combination of immune profiling can expand the obtained datasets. The introduced FC panel (Table 1) is not limited by the determination of basic populations as it can be extended to particular (sub)phenotypes of NK or NKT subsets, e.g., cytotoxic CD8+ subpopulations. In the presented gating strategy, we show the simple approach of gating the inflammatory (or classical) Ly6C<sup>high</sup> monocytes and reparative (also called non-classical or patrolling) Ly6C<sup>low</sup> monocytes in order to monitor the overall changes of many immune subsets. However, recent studies describe multiple subsets of monocytes with distinct functions [35]. As such, if monocytes were the center of focus, a monocyte-specific panel should be designed. In addition, although neutrophils are characterized as Ly6G+, which is their distinguishing feature, they also express Ly6C [36]. However, the low Ly6C expression characterizes the myeloid-derived suppressor cells of neutrophil origin [37]. These alternative gating strategies can provide supplementary information on ongoing immune reactions such as inflammation, immunosuppression [38], and even tumor immune responses [39]. Accordingly, the gating of functional cells could be a useful approach in therapeutic studies (cancer, autoimmune diseases, etc.). Concerning data exportation and interpretation, the frequency of cell population in live cells can be used for monitoring the changes of immune subset ratios in various pathophysiological conditions [40]. In addition, the frequency of parent population is suitable for monitoring the expression of a particular marker within the population of interest.

In addition to the FC-based immunophenotyping, the quality control of isolated cells could be verified by functional assays. For example, *in vitro* lipopolysaccharide (LPS) treatment induces tumor necrosis factor alpha (TNF $\alpha$ ) production by KC [18]. Alternatively, other functional analyses can be applied for KC, HSC or LSEC [41] or any other population of interest.

Taken all together, our complete protocol allows a highly effective and comprehensive progression in liver immune research and in the understanding of various pathologies.

## 5. Reagents Setup

1. RBL buffer
  - a. 0.1 mM EDTA
  - b. 12 mM NaHCO<sub>3</sub>
  - c. 155 mM NH<sub>4</sub>Cl
  - d. Store at RT, no contamination should appear.
2. FC staining buffer
  - a. 0.5% BSA (*w/v*)
  - b. 2 mM EDTA
  - c. Prepare a solution in 1x PBS. Store at 4 °C up to 1 month without any preservative such as 0.02% (*v/v*) thimerosal or 0.02–0.05% (*w/v*) sodium azide.

**Author Contributions:** Conceptualization, A.B.; methodology, L.V. and M.P.P.; validation, L.V., M.P.P., V.V., G.B. and A.B.; data analysis, L.V., M.P.P. and A.B.; writing—original draft preparation, L.V., M.P.P. and A.B.; writing—review and editing, V.V., G.B. and A.B.; funding acquisition, G.B. All authors have read and agreed to the published version of the manuscript.

**Funding:** The work and the APC were funded by Gilead Sciences, Inc. and OP RDE Project “Chemical biology for drugging undruggable targets” Chem-BioDrug, No. CZ.02.1.01/0.0/0.0/16\_019/0000729.

**Institutional Review Board Statement:** The animal study protocol was approved by the Institutional Review Board and Ethics Committee of the Institute of Organic Chemistry and Biochemistry of the Czech Academy of Sciences and the Czech Academy of Sciences (protocol code CAS 76/2019, 12/8/2019).

**Data Availability Statement:** Not applicable.

**Acknowledgments:** Our special thanks belong to Tamara Jenkins for the editing of our manuscript.

**Conflicts of Interest:** The authors declare that this study was partly funded from Gilead Sciences, Inc. This funder was not involved in the study design, collection, analysis, interpretation of data, the writing of this article or the decision to submit it for publication.

## References

1. Bogdanos, D.P.; Gao, B.; Gershwin, M.E. Liver Immunology. *Compr. Physiol.* **2013**, *3*, 567–598. [[CrossRef](#)] [[PubMed](#)]
2. Heymann, F.; Tacke, F. Immunology in the Liver—From Homeostasis to Disease. *Nat. Rev. Gastroenterol. Hepatol.* **2016**, *13*, 88–110. [[CrossRef](#)] [[PubMed](#)]
3. Freitas-Lopes, M.A.; Mafra, K.; David, B.A.; Carvalho-Gontijo, R.; Menezes, G.B. Differential Location and Distribution of Hepatic Immune Cells. *Cells* **2017**, *6*, 48. [[CrossRef](#)] [[PubMed](#)]
4. Blom, K.G.; Qazi, M.R.; Matos, J.B.N.; Nelson, B.D.; DePierre, J.W.; Abedi-Valugerdi, M. Isolation of Murine Intrahepatic Immune Cells Employing a Modified Procedure for Mechanical Disruption and Functional Characterization of the B, T and Natural Killer T Cells Obtained. *Clin. Exp. Immunol.* **2009**, *155*, 320–329. [[CrossRef](#)] [[PubMed](#)]
5. Tacke, F.; Zimmermann, H.W. Macrophage Heterogeneity in Liver Injury and Fibrosis. *J. Hepatol.* **2014**, *60*, 1090–1096. [[CrossRef](#)] [[PubMed](#)]
6. Klugewitz, K.; Adams, D.H.; Emoto, M.; Eulenburg, K.; Hamann, A. The Composition of Intrahepatic Lymphocytes: Shaped by Selective Recruitment? *Trends Immunol.* **2004**, *25*, 590–594. [[CrossRef](#)]
7. Lian, Z.-X.; Li, L. The Liver as a Lymphoid Organ. In *Liver Immunology*, 3rd ed.; Gershwin, M.E., Vierling, J.M., Tanaka, A., Manns, M.P., Eds.; Springer International Publishing: Cham, Switzerland, 2020; pp. 17–33. ISBN 978-3-030-51709-0.
8. Kuiper, A.; Gehring, A.J.; Isogawa, M. Mechanisms of HBV Immune Evasion. *Antivir. Res.* **2020**, *179*, 104816. [[CrossRef](#)]
9. You, Q.; Cheng, L.; Kedl, R.M.; Ju, C. Mechanism of T Cell Tolerance Induction by Murine Hepatic Kupffer Cells. *Hepatology* **2008**, *48*, 978–990. [[CrossRef](#)]
10. Diehl, L.; Schurich, A.; Grochtmann, R.; Hegenbarth, S.; Chen, L.; Knolle, P.A. Tolerogenic Maturation of Liver Sinusoidal Endothelial Cells Promotes B7-Homolog 1-Dependent CD8+ T Cell Tolerance. *Hepatology* **2008**, *47*, 296–305. [[CrossRef](#)]
11. Xu, L.; Yin, W.; Sun, R.; Wei, H.; Tian, Z. Kupffer Cell-Derived IL-10 Plays a Key Role in Maintaining Humoral Immune Tolerance in Hepatitis B Virus-Persistent Mice. *Hepatology* **2014**, *59*, 443–452. [[CrossRef](#)]
12. Zhou, J.; Peng, H.; Li, K.; Qu, K.; Wang, B.; Wu, Y.; Ye, L.; Dong, Z.; Wei, H.; Sun, R.; et al. Liver-Resident NK Cells Control Antiviral Activity of Hepatic T Cells via the PD-1-PD-L1 Axis. *Immunity* **2019**, *50*, 403–417.e4. [[CrossRef](#)] [[PubMed](#)]
13. Zheng, M.; Tian, Z. Liver-Mediated Adaptive Immune Tolerance. *Front. Immunol.* **2019**, *10*, 2525. [[CrossRef](#)]

14. Wu, L.; Peng, W.-H.; Wu, H.-L.; Miaw, S.-C.; Yeh, S.-H.; Yang, H.-C.; Liao, P.-H.; Lin, J.-S.; Chen, Y.; Hong, Y.-T.; et al. Lymphocyte Antigen 6 Complex, Locus C+ Monocytes and Kupffer Cells Orchestrate Liver Immune Responses against Hepatitis B Virus in Mice. *Hepatology* **2019**, *69*, 2364–2380. [CrossRef] [PubMed]
15. David, B.A.; Rubino, S.; Moreira, T.G.; Freitas-Lopes, M.A.; Araújo, A.M.; Paul, N.E.; Rezende, R.M.; Menezes, G.B. Isolation and High-Dimensional Phenotyping of Gastrointestinal Immune Cells. *Immunology* **2017**, *151*, 56–70. [CrossRef]
16. Fang, X.; Du, P.; Liu, Y.; Tang, J. Efficient Isolation of Mouse Liver NKT Cells by Perfusion. *PLoS ONE* **2010**, *5*, e10288. [CrossRef]
17. Finlon, J.M.; Burchill, M.A.; Tamburini, B.A.J. Digestion of the Murine Liver for a Flow Cytometric Analysis of Lymphatic Endothelial Cells. *J. Vis. Exp.* **2019**, *143*, e58621. [CrossRef]
18. Li, P.; Li, J.; Li, M.; Gong, J.; He, K. An Efficient Method to Isolate and Culture Mouse Kupffer Cells. *Immunol. Lett.* **2014**, *158*, 52–56. [CrossRef] [PubMed]
19. Lynch, R.W.; Hawley, C.A.; Pellicoro, A.; Bain, C.C.; Iredale, J.P.; Jenkins, S.J. An Efficient Method to Isolate Kupffer Cells Eliminating Endothelial Cell Contamination and Selective Bias. *J. Leukoc. Biol.* **2018**, *104*, 579–586. [CrossRef]
20. Shi, W.; Wang, Y.; Zhang, C.; Jin, H.; Zeng, Z.; Wei, L.; Tian, Y.; Zhang, D.; Sun, G. Isolation and Purification of Immune Cells from the Liver. *Int. Immunopharmacol.* **2020**, *85*, 106632. [CrossRef]
21. Mohar, I.; Bremel, K.J.; Murray, S.A.; Ebrahimkhani, M.R.; Crispe, I.N. Isolation of Non-Parenchymal Cells from the Mouse Liver. In *Malaria Vaccines. Methods in Molecular Biology*; Vaughan, A., Ed.; Humana Press: New York, NY, USA, 2015; Volume 1325, pp. 3–17. ISBN 9781493928149.
22. Cabral, F.; Miller, C.M.; Kudrna, K.M.; Hass, B.E.; Daubendiek, J.G.; Kellar, B.M.; Harris, E.N. Purification of Hepatocytes and Sinusoidal Endothelial Cells from Mouse Liver Perfusion. *J. Vis. Exp.* **2018**, *132*, 56993. [CrossRef]
23. Aparicio-Vergara, M.; Tencerova, M.; Morgantini, C.; Barreby, E.; Aouadi, M. Isolation of Kupffer Cells and Hepatocytes from a Single Mouse Liver. In *Alpha-1 Antitrypsin Deficiency. Methods in Molecular Biology*; Borel, F., Mueller, C., Eds.; Humana Press: New York, NY, USA, 2017; Volume 1639, pp. 161–171. ISBN 9781493971633.
24. Sulen, A. Liver Macrophage Isolation by Flow Cytometry Sorting. In *Kupffer Cells*; Aouadi, M., Azzimato, V., Eds.; Humana Press: New York, NY, USA, 2020; Volume 2164, pp. 15–20. ISBN 9781071607046.
25. Wei, C.; Ni, C.; Song, T.; Liu, Y.; Yang, X.; Zheng, Z.; Jia, Y.; Yuan, Y.; Guan, K.; Xu, Y.; et al. The Hepatitis B Virus X Protein Disrupts Innate Immunity by Downregulating Mitochondrial Antiviral Signaling Protein. *J. Immunol.* **2010**, *185*, 1158–1168. [CrossRef] [PubMed]
26. Gondois-Rey, F.; Granjeaud, S.; Kieu, S.L.T.; Herrera, D.; Hirsch, I.; Olive, D. Multiparametric Cytometry for Exploration of Complex Cellular Dynamics. *Cytom. Part A* **2012**, *81*, 332–342. [CrossRef] [PubMed]
27. Ferrer-Font, L.; Pellefigues, C.; Mayer, J.U.; Small, S.J.; Jaimes, M.C.; Price, K.M. Panel Design and Optimization for High-Dimensional Immunophenotyping Assays Using Spectral Flow Cytometry. *Curr. Protoc. Cytom.* **2020**, *92*, e70. [CrossRef]
28. Giladi, A.; Paul, F.; Herzog, Y.; Lubling, Y.; Weiner, A.; Yofe, I.; Jaitin, D.; Cabezas-Wallscheid, N.; Dress, R.J.; Ginhoux, F.; et al. Single-Cell Characterization of Haematopoietic Progenitors and Their Trajectories in Homeostasis and Perturbed Haematopoiesis. *Nat. Cell Biol.* **2018**, *20*, 836–846. [CrossRef] [PubMed]
29. Jaitin, D.A.; Kenigsberg, E.; Keren-Shaul, H.; Elefant, N.; Paul, F.; Zaretsky, I.; Mildner, A.; Cohen, N.; Jung, S.; Tanay, A.; et al. Massively Parallel Single-Cell RNA-Seq for Marker-Free Decomposition of Tissues into Cell Types. *Science* **2014**, *343*, 776–779. [CrossRef]
30. Miltenyi Biotec Liver Dissociation Kit Mouse Protocol. Available online: <https://www.miltenyibiotec.com/US-en/products/liver-dissociation-kit-mouse.html?countryRedirected=1#gref> (accessed on 17 February 2021).
31. Choi, W.-M.; Eun, H.S.; Lee, Y.-S.; Kim, S.J.; Kim, M.-H.; Lee, J.-H.; Shim, Y.-R.; Kim, H.-H.; Kim, Y.E.; Yi, H.-S.; et al. Experimental Applications of In Situ Liver Perfusion Machinery for the Study of Liver Disease. *Mol. Cells* **2019**, *42*, 45–55. [CrossRef] [PubMed]
32. Rogers, A.B. Stress of Strains: Inbred Mice in Liver Research. *Gene Expr.* **2018**, *19*, 61–67. [CrossRef]
33. Sellers, R.S.; Clifford, C.B.; Treuting, P.M.; Brayton, C. Immunological Variation between Inbred Laboratory Mouse Strains: Points to Consider in Phenotyping Genetically Immunomodified Mice. *Vet. Pathol.* **2012**, *49*, 32–43. [CrossRef]
34. Medina-Montano, C.; Cacicedo, M.L.; Svensson, M.; Limeres, M.J.; Zeyn, Y.; Chaves-Giraldo, J.E.; Röhrig, N.; Grabbe, S.; Gehring, S.; Bros, M. Enrichment Methods for Murine Liver Non-Parenchymal Cells Differentially Affect Their Immunophenotype and Responsiveness towards Stimulation. *Int. J. Mol. Sci.* **2022**, *23*, 6543. [CrossRef]
35. Canè, S.; Ugel, S.; Trovato, R.; Marigo, I.; De Sanctis, F.; Sartoris, S.; Bronte, V. The Endless Saga of Monocyte Diversity. *Front. Immunol.* **2019**, *10*, 1786. [CrossRef]
36. Lee, P.Y.; Wang, J.-X.; Parisini, E.; Dascher, C.C.; Nigrovic, P.A. Ly6 Family Proteins in Neutrophil Biology. *J. Leukoc. Biol.* **2013**, *94*, 585–594. [CrossRef] [PubMed]
37. Deniset, J.F.; Kubes, P. Neutrophil Heterogeneity: Bona Fide Subsets or Polarization States? *J. Leukoc. Biol.* **2018**, *103*, 829–838. [CrossRef] [PubMed]
38. Wang, C.; Liu, X.; Li, Z.; Chai, Y.; Jiang, Y.; Wang, Q.; Ji, Y.; Zhu, Z.; Wan, Y.; Yuan, Z.; et al. CD8+NKT-like Cells Regulate the Immune Response by Killing Antigen-Bearing DCs. *Sci. Rep.* **2015**, *5*, 14124. [CrossRef]
39. Li, Z.; Wu, Y.; Wang, C.; Zhang, M. Mouse CD8+NKT-like Cells Exert Dual Cytotoxicity against Mouse Tumor Cells and Myeloid-Derived Suppressor Cells. *Cancer Immunol. Immunother.* **2019**, *68*, 1303–1315. [CrossRef] [PubMed]

40. Pimkova Polidarova, M.; Brehova, P.; Dejmek, M.; Birkus, G.; Brazdova, A. STING Agonist-Mediated Cytokine Secretion Is Accompanied by Monocyte Apoptosis. *ACS Infect. Dis.* **2022**, *8*, 463–471. [[CrossRef](#)] [[PubMed](#)]
41. Pfeiffer, E.; Kegel, V.; Zeilinger, K.; Hengstler, J.G.; Nüssler, A.K.; Seehofer, D.; Damm, G. Featured Article: Isolation, Characterization, and Cultivation of Human Hepatocytes and Non-Parenchymal Liver Cells. *Exp. Biol. Med.* **2015**, *240*, 645–656. [[CrossRef](#)]